VOL. 648 NO. 1 OCTOBER 1, 1993

including
FACSS Symposium on Size-Exclusion Chromatography, Philadelphia, PA, September 20–25, 1992

JOURNAL OF CHROMATOGRAPHY

INCLUDING ELECTROPHORESIS AND OTHER SEPARATION METHODS

ELSEVIER

JOURNAL OF CHROMATOGRAPHY

INCLUDING ELECTROPHORESIS AND OTHER SEPARATION METHODS

Scope. The *Journal of Chromatography* publishes papers on all aspects of **chromatography, electrophoresis** and related methods. Contributions consist mainly of research papers dealing with chromatographic theory, instrumental developments and their applications. The section *Biomedical Applications*, which is under separate editorship, deals with the following aspects: developments in and applications of chromatographic and electrophoretic techniques related to clinical diagnosis or alterations during medical treatment; screening and profiling of body fluids or tissues related to the analysis of active substances and to metabolic disorders; drug level monitoring and pharmacokinetic studies; clinical toxicology; forensic medicine; veterinary medicine; occupational medicine; results from basic medical research with direct consequences in clinical practice. In *Symposium volumes*, which are under separate editorship, proceedings of symposia on chromatography, electrophoresis and related methods are published.

Submission of Papers. The preferred medium of submission is on disk with accompanying manuscript (see *Electronic manuscripts* in the Instructions to Authors, which can be obtained from the publisher, Elsevier Science Publishers B.V., P.O. Box 330, 1000 AH Amsterdam, Netherlands). Manuscripts (in English; *four* copies are required) should be submitted to: Editorial Office of *Journal of Chromatography*, P.O. Box 681, 1000 AR Amsterdam, Netherlands, Telefax (+31-20) 5862 304, or to: The Editor of *Journal of Chromatography, Biomedical Applications*, P.O. Box 681, 1000 AR Amsterdam, Netherlands. Review articles are invited or proposed in writing to the Editors who welcome suggestions for subjects. An outline of the proposed review should first be forwarded to the Editors for preliminary discussion prior to preparation. Submission of an article is understood to imply that the article is original and unpublished and is not being considered for publication elsewhere. For copyright regulations, see below.

Publication. The *Journal of Chromatography* (incl. *Biomedical Applications*) has 40 volumes in 1993. The subscription prices for 1993 are:

J. Chromatogr. (incl. *Cum. Indexes, Vols. 601–650*) + *Biomed. Appl.* (Vols. 612–651):
Dfl. 8520.00 plus Dfl. 1320.00 (p.p.h.) (total *ca.* US$ 5466.75)

J. Chromatogr. (incl. *Cum Indexes, Vols. 601–650*) only (Vols. 623–651):
Dfl. 7047.00 plus Dfl. 957.00 (p.p.h.) (total *ca.* US$ 4446.75)

Biomed. Appl. only (Vols. 612–622):
Dfl. 2783.00 plus Dfl. 363.00 (p.p.h.) (total *ca.* US$ 1747.75).

Subscription Orders. The Dutch guilder price is definitive. The US$ price is subject to exchange-rate fluctuations and is given as a guide. Subscriptions are accepted on a prepaid basis only, unless different terms have been previously agreed upon. Subscriptions orders can be entered only by calender year (Jan.–Dec.) and should be sent to Elsevier Science Publishers, Journal Department, P.O. Box 211, 1000 AE Amsterdam, Netherlands, Tel. (+31-20) 5803 642, Telefax (+31-20) 5803 598, or to your usual subscription agent. Postage and handling charges include surface delivery except to the following countries where air delivery via SAL (Surface Air Lift) mail is ensured: Argentina, Australia, Brazil, Canada, China, Hong Kong, India, Israel, Japan*, Malaysia, Mexico, New Zealand, Pakistan, Singapore, South Africa, South Korea, Taiwan, Thailand, USA. *For Japan air delivery (SAL) requires 25% additional charge of the normal postage and handling charge. For all other countries airmail rates are available upon request. Claims for missing issues must be made within six months of our publication (mailing) date, otherwise such claims cannot be honoured free of charge. Back volumes of the *Journal of Chromatography* (Vols. 1–611) are available at Dfl. 230.00 (plus postage). Customers in the USA and Canada wishing information on this and other Elsevier journals, please contact Journal Information Center, Elsevier Science Publishing Co. Inc., 655 Avenue of the Americas, New York, NY 10010, USA, Tel. (+1-212) 633 3750, Telefax (+1-212) 633 3764.

Abstracts/Contents Lists published in Analytical Abstracts, Biochemical Abstracts, Biological Abstracts, Chemical Abstracts, Chemical Titles, Chromatography Abstracts, Current Awareness in Biological Sciences (CABS), Current Contents/Life Sciences, Current Contents/Physical, Chemical & Earth Sciences, Deep-Sea Research/Part B: Oceanographic Literature Review, Excerpta Medica, Index Medicus, Mass Spectrometry Bulletin, PASCAL-CNRS, Referativnyi Zhurnal, Research Alert and Science Citation Index.

US Mailing Notice. *Journal of Chromatography* (ISSN 0021-9673) is published weekly (total 52 issues) by Elsevier Science Publishers (Sara Burgerhartstraat 25, P.O. Box 211, 1000 AE Amsterdam, Netherlands). Annual subscription price in the USA US$ 4446.75 (subject to change), including air speed delivery. Second class postage paid at Jamaica, NY 11431. **USA POSTMASTERS:** Send address changes to *Journal of Chromatography*, Publications Expediting, Inc., 200 Meacham Avenue, Elmont, NY 11003. Airfreight and mailing in the USA by Publications Expediting.

See inside back cover for Publication Schedule, Information for Authors and information on Advertisements.

0021-9673/93/$06.00

Printed in the Netherlands

VOL. 648, NO. 1 JOURNAL OF CHROMATOGRAPHY OCTOBER 1, 1993

CONTENTS

(Abstracts/Contents Lists published in Analytical Abstracts, Biochemical Abstracts, Biological Abstracts, Chemical Abstracts, Chemical Titles, Chromatography Abstracts, Current Awareness in Biological Sciences (CABS), Current Contents/Life Sciences, Current Contents/Physical, Chemical & Earth Sciences, Deep-Sea Research/Part B: Oceanographic Literature Review, Excerpta Medica, Index Medicus, Mass Spectrometry Bulletin, PASCAL-CNRS, Referativnyi Zhurnal, Research Alert and Science Citation Index)

FACSS SYMPOSIUM ON SIZE-EXCLUSION CHROMATOGRAPHY, PHILADELPHIA, PA, SEPTEMBER 20–25, 1992

REGULAR PAPERS

Column Liquid Chromatography

(Continued overleaf)

Contents (continued)

SHORT COMMUNICATIONS

Chromatography of Mycotoxins

Techniques and Applications

edited by **V. Betina**

Journal of Chromatography Library Volume 54

This work comprises two parts, Part A: Techniques and Part B: Applications. In Part A the most important principles of sample preparation, extraction, clean-up, and of established and prospective chromatographic techniques are discussed in relation to mycotoxins. In Part B the most important data, scattered in the literature, on thin-layer, liquid, and gas chromatography of mycotoxins have been compiled. Mycotoxins are mostly arranged according to families, such as aflatoxins, trichothecenes, lactones etc. Chromatography of individual important mycotoxins and multi-mycotoxin chromatographic analyses are also included. Applications are presented in three chapters devoted to thin-layer, liquid, and gas chromatography of mycotoxins.

Contents:

1993 xiv + 440 pages
Price: US $ 180.00 / Dfl. 315.00
ISBN 0-444-81521-X

ORDER INFORMATION

For USA and Canada
ELSEVIER SCIENCE PUBLISHERS
Judy Weislogel,
P.O. Box 945
Madison Square Station,
New York, NY 10160-0757
Fax: (212) 633 3880

In all other countries
ELSEVIER SCIENCE PUBLISHERS
P.O. Box 211,
1000 AE Amsterdam
The Netherlands
Fax: (+31-20) 5803 705

US$ prices are valid only for the USA & Canada and are subject to exchange rate fluctuations; in all other countries the Dutch guilder price (Dfl.) is definitive. Customers in the European Community should add the appropriate VAT rate applicable in their country to the price(s). Books are sent postfree if prepaid.

ELSEVIER
SCIENCE PUBLISHERS

JOURNAL OF CHROMATOGRAPHY

VOL. 648 (1993)

JOURNAL of CHROMATOGRAPHY

INCLUDING ELECTROPHORESIS AND OTHER SEPARATION METHODS

ELSEVIER

AMSTERDAM — LONDON — NEW YORK — TOKYO

J. Chromatogr., Vol. 648 (1993)

0021-9673/93/$06.00

Printed in the Netherlands

SYMPOSIUM ISSUE

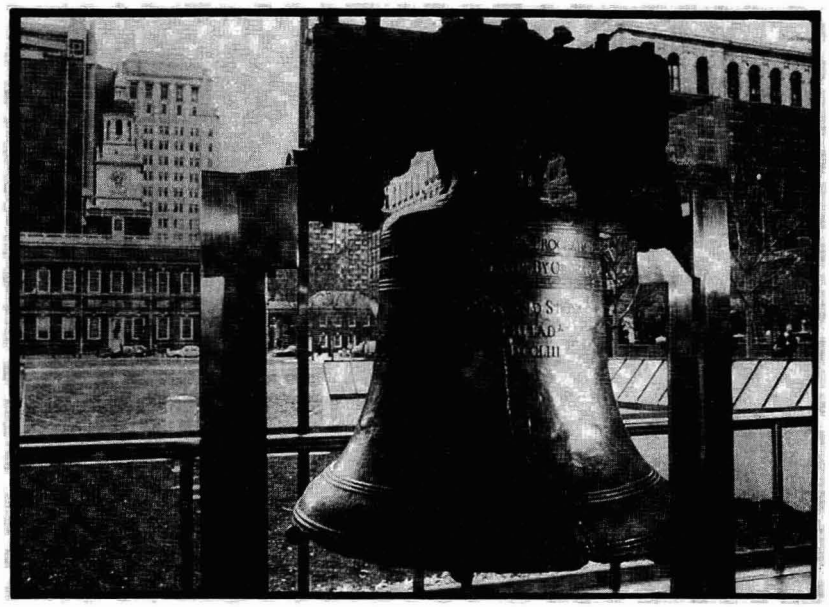

FACSS SYMPOSIUM ON SIZE-EXCLUSION CHROMATOGRAPHY

Philadelphia, PA (USA), September 20–25, 1992

SYMPOSIUM VOLUMES

Guest Editors

P.L. DUBIN
(Indianapolis, IN, USA)

M. POTSCHKA
(Vienna, Austria)

CONTENTS

Journal of Chromatography, 648 (1993) 1
Elsevier Science Publishers B.V., Amsterdam

CHROM. 25 501

Foreword

Liquid chromatography has established itself as an indispensable analytical tool and its technological development has entered a phase of consolidation. Excellent equipment is available and the rate at which improvements are introduced is bound to decline. Application development continues to be largely a matter of trial-and-error, while the field of fundamental studies is all but exhausted.

The present symposium, entitled *Advances in Size-Exclusion Chromatography* (SEC), took place at the *19th Annual Meeting of the Federation of Analytical Chemistry and Spectroscopy Societies* in Philadelphia on September 22nd 1992. In SEC, which accounts for some 15% of chromatographic applications at a rising trend, a notable number of issues are poorly understood. Some of them are of direct relevance to other types of chromatography, in particular to the field of ion-exchange chromatography. Besides purification, a prime goal of SEC is the determination of polymer sizes, which relies on accurate understanding of the physical mechanisms involved. The renewed debate of various aspects of this "universal calibration problem" has apparently resolved less than it has rendered uncertain, and many researchers have responded to this by shifting away from column calibration to on-line specialty detectors, which are capable of absolute determinations of intrinsic viscosity, radius of gyration, molecular mass, etc. Even so, the problem of errors due to shear degradation of high-molecular-mass polymers remains, and the direct detector approach is not without technical problems either.

A prominent problem in both SEC and ion-exchange chromatography is the mechanism of charge interactions between polyelectrolyte solutes and the matrix walls, which inevitably are charged; Edwards and Dubin (page 3) present new data on this problem. Three papers address various aspects and limitations of on-line light scattering detectors. Hagel (page 19) comments on SEC peak capacity and calibration stratagems and compares the reliability of column calibration with that of size-sensitive detectors; DeGroot and Hamre (page 33) document polymer shear degradation and microgel formation; and Wyatt (page 27) demonstrates that a multi-angle light scattering detector may measure polymer size (radius of gyration in this case) even below the concentration detection limit of a differential refractive index detector (a single-angle detector yields molecular mass only in combination with a differential refractive index detector). As much as column calibration tells about a sample's polymer structure it reveals about the structural topology of the porous material itself; this is a central aspect of the paper by Vilenchick *et al.* (page 9), who introduce a novel porous alumina matrix. The preeminent problem of universal calibration, albeit understood enough to be of practical use, is the unresolved contradictions between theory(ies) and experiment; in the first part of a treatise on the mechanism of size-exclusion chromatography, Potschka (page 41) investigates the properties of transport processes in porous materials. Unfortunately, several other participants of the symposium where unable to submit their contribution for publication.

As symposium chairman, I wish to thank Paul Dubin, who organized the symposium, John Dorsey, FACSS section chair for chromatography, Barry Lavine, FACSS program chair, and the Federation of Analytical Chemistry and Spectroscopy Societies and its sponsoring affiliates. It was a pleasure to be in the Delaware Valley, which has made substantial contributions to chromatography, and in Philadelphia in particular.

Vienna (Austria) Martin Potschka

Journal of Chromatography, 648 (1993) 3–7
Elsevier Science Publishers B.V., Amsterdam

CHROMSYMP. 2757

pH effects on non-ideal protein size-exclusion chromatography on Superose 6

Shun L. Edwards[☆] and Paul L. Dubin*

Department of Chemistry, Indiana University–Purdue University at Indianapolis, 1125 East 38th Street, Indianapolis, IN 46205-2810 (USA)

ABSTRACT

The retention behavior of five globular proteins (ribonuclease, lysozyme, β-lactoglobulin, serum albumin, γ-globulin) was determined on Superose 6 in low ionic strength (0.02–0.04 *M*) mobile phases of high, intermediate and low pH (10.0, 7.0, 4.3). Quantitative assessments of attractive or repulsive solute-packing interactions were made by comparing the chromatographic partition coefficient to the value obtained for non-interacting spherical solutes on the same column. The dependence of this "non-ideal" adsorption or exclusion on net protein charge is complex, but not very sensitive to protein type. The results suggests that on size-exclusion chromatography packings that behave as weak cation-exchange resins the electrostatic solute-packing interaction is not governed by a highly localized set of a few charged sites.

INTRODUCTION

Ion-exchange chromatography (IEC) is a key tool in the analysis and preparative separation of peptides and proteins (see, for example, ref. 1). There is a considerable divergence of viewpoints about the fundamental nature of protein-substrate interactions in IEC. At one extreme, it has been proposed that a well-defined, localized set of charged amino acid groups on a protein react in a stoichiometric manner with a complementary set of fixed charges on the packing, releasing an identical number Z (*e.g.* three or four) of small ions [2]. This classical ion-exchange model attributes the effect of ionic strength (which always diminishes the capacity factor k') to a mass-action equilibrium in which the small ions with charge opposite to the fixed charges on the packing play the role of "displacer ions" [3]. Applying to this concept the treatment of Boardman and Partridge [4], Drager and Regnier [5] obtained a linear dependence of ln k' on ln M (where M, the molarity of the displacer ion, is the ionic strength for univalent electrolyte mobile phases) with a slope of Z. Linear plots in support of this model were reported for β-lactoglobulin on Mono-Q, a strong anion-exchange resin [2].

A completely different point of view results if the attractive force between protein and packing is considered to be the result of relatively long-range, spatially averaged interactions between two surface of opposite charge [6]. The role of the small ions is then via Debye–Hückel screening, and the dependence of k' on ionic strength (I) is quite different [7]. In support of this viewpoint, we note the result of Haggerty and Lenhoff [8] who found excellent correlation between k' and the protein mean surface potential, calculated using the molecular modeling software program Delphi [9]. From this perspective, a quasi-global protein charge, not a local one, controls interaction, and no complementary ion-pairing is envisioned. The treatment of Ståhlberg [6] follows similar lines, and explicitly states

* Corresponding author.
☆ Present address: Eli Lilly and Company, Indianapolis, IN 46285, USA.

0021-9673/93/$06.00

that the charge distribution of packing and protein are likely to be asymmetric, and thus inimical to the stoichiometry central to the Regnier model. Given this disparity of viewpoints, it would seem prudent to understand the phrase "ion-exchange chromatography", as applied to proteins, as meaning "chromatography of proteins on a column packed with a support that can operate as an ion-exchange resin", thus recognizing that the mechanism for protein retardation on such a column may or may not partake of the same stoichiometric features as controls the separation of small ions.

Since the preceding treatments predict different dependences of k' on I, one would expect that experiment should cast a decisive vote. However, the practical range of I in ion-exchange chromatography is quite limited because the strength of the interactions under typical conditions precludes the use of low ionic strength mobile phase. Data obtained in a narrow range of I cannot reveal departures from proposed expressions for $k'(I)$, especially for semi-logarithmic or double-logarithmic relations. (It should be noted that in one study where the ionic strength was varied over several orders of magnitude [10] the log–log dependence of k' on I predicted by Regnier was observed only within limited ranges of I.) Weak ion-exchange resins which can easily be operated over a wide range of I are not in common use. However, virtually all aqueous size-exclusion chromatography (SEC) packings, based on silica or on cross-linked hydrophilic polymers, carry some negative charge at neutral or basic pH [11], and are in this sense weak ion-exchange resins. The dependence of retention time on I can thus be examined over several decades of I.

One difficulty that arises in the use of SEC data to test theories of IEC is the choice of the proper reference compound for the determination of relative peak retention. All theories will lead to the fraction of protein in the bound state, and hence its migration velocity v relative to an unretained solute, *i.e.* $k' = (v_0/v)^{-1} = t/t_0$. But in SEC one conventionally measures the elution volume relative to a solute too big to enter the pores, *i.e.*

$$K_{SEC} = (V_e - V_0)/(V_t - V_0) \quad (1)$$

where V_e is the observed elution volume, V_0 that of the aforementioned large solute, and V_t the elution volume of a compound similar in size to the solvent. However, V_0 does not correspond to the unretained solute embodied in k', and the dependence of K_{SEC} on I would mix together size and interaction effects. The unretained solute with retention time t_0 must be a non-interacting solute of the same size as the analyte in question. Recently, we have established [12] that the dependence of K_{SEC} on solute radius R is coincident for pullulans (non-ionic flexible chain polymers) [13], ficolls (non-ionic, densely branched, quasi-spheres) [14] and carboxylated starburst dendrimers [15] (compact dendritic species with negative surface charge), on Superose 6 in neutral pH, $I > 0.2$ mobile phase. That the combined K_{SEC} *vs.* R plot for these solutes represents the behavior of non-interacting spheres is supported by the observation that data for several proteins obtained at $I > 0.2$ also fall on this curve, particularly when the mobile phase pH is close to the protein pI. Thus, comparisons of protein retention to the value predicted from this "ideal" curve facilitates the analysis of coulombic interaction effects on protein chromatography.

In the current work we present limited results for a number of globular proteins under conditions of rather low ionic strength ($0.02 < I < 0.04$) and over a range of pH (4.3–10). Under these conditions, the protein pI values may be above or below the pH, and the charge on the packing, due to sulfate and/or carboxylic acid groups [16], also may vary with pH. In contradistinction to the IEC studies mentioned above, the results are obtained both in the repulsive (pH > pI) as well as the attractive (pH < pI) regimes. The deviation in K_{SEC} from that for the "ideal" sphere of identical R is observed as a function of I and pH. The results constitute a "range-finding" study in that the number of ionic strengths examined are too small to provide a test of the theories mentioned above. However, the insights obtained set the stage for more detailed examinations.

TABLE I

CHARACTERISTICS OF PROTEINS USED IN THIS STUDY

Protein[a]	Source	MW	p*I*	R_S (nm)[b]	R_η (nm)[b]
Ribonuclease (R-5503)	Bovine pancreas	13 700	9.0	1.75	1.90
Lysozyme (L-6876)	Egg white	14 000	11.0	1.85	2.0
β-Lactoglobulin (L-2506)	Bovine milk	35 000	5.2	2.7	2.65
Albumin (A-7906)	Bovine serum	66 000	4.9	3.5	3.4
γ-Globulin (G-5009)	Bovine	150 000	7.0	5.6	–

[a] All from Sigma, except γ-globulin also supplied by CalBiochem.
[b] Literature sources for R_S and R_η as cited in ref. 12.

EXPERIMENTAL

Materials

Table I lists the proteins employed in this study, along with their MW, isoelectric point, and Stokes radius and viscosity radius, where available. In the subsequent analyses we use the average of the Stokes radius R_S and the viscosity radius R_η, although it should be noted that the differences between these are too small to significantly affect our interpretation of the results. All buffers and salts were reagent grade, from Sigma, Mallinckrodt, Fisher or Aldrich.

Methods

Size-exclusion chromatography. SEC was carried out on a prepacked Superose 6 HR 10/30 column, which had a column efficiency of 3800–4600 plates/m throughout most of these studies. The HPLC instrument was a Beckmann System Gold, equipped with a Beckman Model 156 refractive index detector or a Waters R401 differential refractive index detector, along with the UV detector supplied with the instrument. Solvent was delivered with a Beckmann 110 B pump and an Altex 210A valve with either a 20-, 50- or 100-μl loop. A Rheodyne 0.2-μm precolumn filter was placed in-line to protect the column. Flow-rates were measured and found to be constant within ±0.5% by weighing of collected eluent. Sample preparation was accomplished by shaking or tumbling for 1–2 h. The concentrations of all polymers and proteins were in the range 2–5 mg/ml, except for concentration effect studies. Samples were filtered through 0.45-μm Gelman filters before injection. K_{SEC} was determined according to eqn. 1 with V_0 determined from the retention of either $2 \cdot 10^6$ MW dextran or $4 \cdot 10^6$ MW poly(ethyleneoxide) as 6.50 ml, and V_t determined from the retention of dextrose as 19.98 ml.

RESULTS AND DISCUSSION

In order to examine effects of both ionic strength and pH, we obtained protein retention data at four sets of conditions: pH 7.0, $I = 0.02$ *M*; pH 7.0, $I = 0.04$ *M*; pH 4.3, $I = 0.03$ *M*, and pH 10.0, $I = 0.02$ *M*. The results are presented in Fig. 1A for pH 7.0, and Fig. 1B for pH 4.3 and

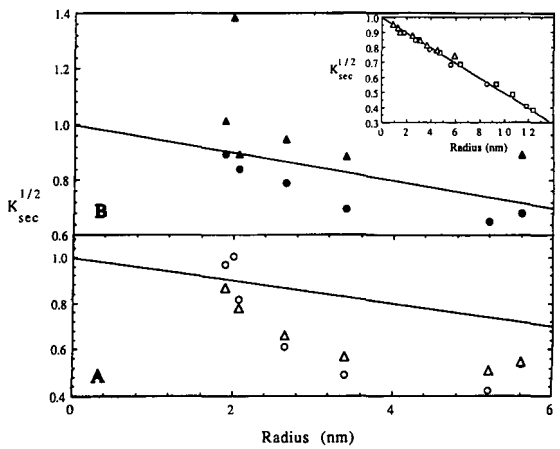

Fig. 1. Dependence of $K_{SEC}^{1/2}$ on protein radius, on Superose 6, in various buffers. A: (△) pH 7.0, $I = 0.04$ *M*; (○) pH 7.0, $I = 0.02$ *M*. B: (▲) pH 4.3, $I = 0.02$ *M*; (●) pH 10.0, $I = 0.03$ *M*. Insert shows the "ideal curve" generated from data for pullulan (○), ficolls (□) and dendrimers (△) (see ref. 12) corresponding to the solid lines in A and B.

10.0. The data are presented as $K_{SEC}^{1/2}$ *vs.* R, since this linearizes the "ideal curve" obtained for the non-interacting spherical solutes, which is shown as the solid line in Fig. 1A and B, and as the insert. In this treatment, we consider R as a static parameter, unaffected by pH, for the following reasons: (a) limited quasi-elastic light scattering studies for bovine serum albumin (BSA), RNAse and lysozyme, reported elsewhere [17] show no measurable dimensional change for these proteins over the pH range 4–10; (b) the magnitude of the changes in retention are large compared with the expected dimensional change from partial unfolding. It is evident that all the proteins of this study exhibit adsorption (positive deviations from the "ideal" line) for pH 4.3, and nearly all show repulsion at pH 10.0. (We will comment on the pH 7.0 results later). The variation in the extent of deviation from the "ideal" line clearly depends on the individual pI values. Potschka has described these deviations in terms of the horizontal displacements, *i.e.* ΔR, and for SEC in the repulsive range attributes the negative values of ΔR to the electrical double layer around the protein [18]. We follow the same procedure, although we note that (a) there is no compelling reason to assign all of the measured "ΔR" to the protein, as opposed to the electrical double layer near the substrate (ionic strength effects on the repulsive term may be viewed as a diminution in effective pore volume [18,19] with as much justification as an increase in effective solute size [20]); and (b) ΔR has no physical meaning in the case of attraction. Nevertheless, the horizontal displacements of the protein data from the "ideal" curve in Fig. 1A and B provide a good quantitative measure of the magnitude of the non-ideal interaction.

It is not *a priori* evident that the non-ideal contribution is purely coulombic. In this case we should expect considerable variation among the different proteins when ΔR is analyzed on the basis of net charge. Fig. 2 shows the dependence of ΔR on the net protein charge, obtained from published titration data [21–23]. Note that $\Delta R < 0$ refers to repulsion, and $\Delta R > 0$ to attraction. The following conclusions may be reached. (i) As can be seen from pH 7.0 data, higher ionic strengths lead to more nearly ideal behavior, but the effect is more pronounced in the repulsion regime; this finding is supported by results obtained for catalase, apoferritin and thyroglobulin at pH 7.0 [24] (not included in the present paper because titration curves needed for net charge values are not available). (ii) With the exception of a single result for BSA at pH 7.0, data obtained for the five different proteins do not deviate excessively from a common curve (broken line). (iii) The common curve is strongly asymmetric with respect to Z: small positive increments in Z at pH $<$ pI produce large changes in ΔR; comparable changes in ΔR in the repulsive regime require much larger absolute increments in $|-Z|$. It could be argued, correctly, that Fig. 2 fails to represent the packing charge, which is changing along with Z, as pH falls. However, the effect of diminishing pH as one progresses in the positive direction from $Z = 0$ should be a decrease in packing charge; nevertheless, ΔR rises rapidly in the range $0 < Z < 12$.

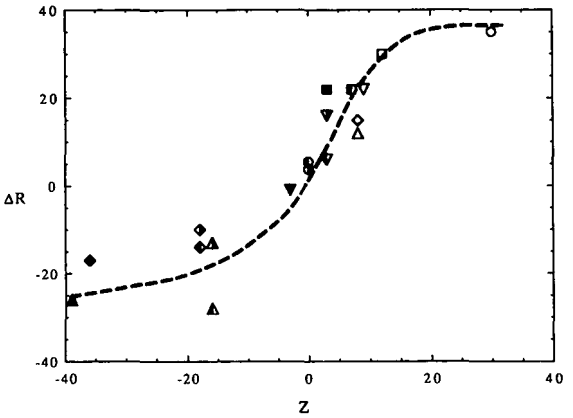

Fig. 2. Data from Fig. 1 plotted as ΔR *vs.* Z, where ΔR is the horizontal separation between the "ideal curve" and the datum (such that positive ΔR corresponds to late elution, or attraction, and negative ΔR to early elution or repulsion) and Z is the net protein charge. In pH 4.3, $I = 0.03$ M eluent: □ = lysozyme; ▽ = RNAse; △ = BSA; ◇ = β-lactoglobulin; ○ = γ-globulin. In pH 7.0, $I = 0.02$ M eluent; ◧ = lysozyme; ▼ = RNAse; ▲ = BSA; ◆ = β-lactoglobulin; ◐ = γ-globulin. In pH 7.0, $I = 0.04$ M eluent: ▼ = RNAse; ▲ = BSA; ◆ = β-lactoglobulin; ◑ = γ-globulin. In pH 10, $I = 0.03$ M eluent: ■ = lysozyme; ▼ = RNAse; ▲ = BSA; ◆ = β-lactoglobulin.

The observation of a common curve, even with some strong individual departures, suggests that both repulsive and attractive forces are

primarily coulombic, and —to a first approximation— more strongly influenced by net protein charge than local charge. It is indisputable that retention on strongly charged columns is often governed by "charge patches", *i.e.* proteins may show strong retention on the "wrong side" of their p*I* values [2], but this appears to be less the case for electrostatic attraction on weakly charged SEC columns. A reasonable hypothesis is that the lower charge density of the SEC column results in a less steep minimum in the orientational energy of "bound" protein, and that the greater orientational mobility of the "bound" protein means that more charged groups may make some contribution to interaction with the packing.

Last, we discuss the asymmetry of Fig. 2, *i.e.* the apparently stronger effect of change in Z on ΔR in the attractive regime. Two possibilities may be considered. The first involves fundamental differences between attractive and repulsive forces, the latter being inherently more long-range. Repulsive interactions may sample the total population of charges on a protein to a greater extent that attractive ones. The effect of a single positive charge on attractive interaction with the anionic packing may thus be greater than the effect of one additional negative charge on the repulsion, because the orientation of the protein at the packing surface is more likely to favor the proximity of the former, and diminish the proximity of the latter. The second consideration is packing charge, which changes along with pH to the extent that the Superose ionophores are carboxylic acid. For acidic proteins, such as BSA, diminution in the pH below p*I* should produce compensating effects, inasmuch as the protein charge (positive) increases while the packing charge diminishes. For highly basic proteins, for which p*I* is well above pK_a of any weak acid packing ionophores, such effects are expected to be negligible in the vicinity of $Z = 0$. A prerequisite to further analysis along these lines is the titration curve of Superose 6, which is one of the objectives of ongoing work.

ACKNOWLEDGEMENT

This work was supported by Grant CHE-9021484 from the National Science Foundation.

REFERENCES

1 K. Gooding and F. Regnier (Editors), *High Performance Liquid Chromatography of Biological Macromolecules: Methods and Applications*, Marcel Dekker, New York, 1988.
2 W. Kopaciewicz, M.A. Rounds, J. Fausnaugh and F.E. Regnier, *J. Chromatogr.*, 266 (1983) 3.
3 M.A. Rounds and F.E. Regnier, *J. Chromatogr.*, 283 (1984) 37.
4 N.K. Boardman and S.M. Partridge, *Biochem. J.*, 59 (1955) 543.
5 R.R. Drager and F.E. Regnier, *J. Chromatogr.*, 359 (1986) 147.
6 J. Ståhlberg, *J. Chromatogr.*, 356 (1986) 231.
7 J. Ståhlberg, B. Jönsson and Cs. Horváth, *Anal. Chem.*, 63 (1991) 1867.
8 L. Haggerty and A.M. Lenhoff, *J. Phys. Chem.*, 95 (1991) 1472.
9 M.K. Gilson, K.A. Sharp and B.H. Honig, *J. Comput. Chem.*, 9 (1987) 327.
10 V. Lesins and E. Ruckenstein, *Colloid Polym. Sci.*, 266 (1988) 1187.
11 P.L. Dubin, in P.L. Dubin (Editor), *Aqueous Size-Exclusion Chromatography*, Elsevier, Amsterdam, 1988, Ch. 5.
12 P.L. Dubin, S.L. Edwards, M.S. Mehta and D. Tomalia, *J. Chromatogr.*, 635 (1993) 51.
13 T. Kato, T. Okamoto, T. Tokuya and A. Takahashi, *Biopolymers*, 21 (1982) 1623.
14 T.C. Laurent and K.A. Granath, *Biochim. Biophys. Acta*, 136 (1967) 199.
15 D.A. Tomalia, R.M. Naylor and W.A. Goddard, III, *Angew. Chem., Int. Ed. Engl.*, 29 (1990) 138.
16 T. Andersson, M. Carlsson, L. Hagel, P.-A. Pernemalm and J.-A. Hanson, *J. Chromatogr.*, 326 (1985) 33.
17 J.M. Park, B.B. Muhoberac, P.L. Dubin and J. Xia, *Macromolecules*, 25 (1992) 290.
18 M. Potschka, *J. Chromatogr.*, 441 (1988) 239.
19 M.G. Styring, C.J. Davison, C. Price and C.J. Booth, *J. Chem. Soc., Faraday Trans. 1*, 80 (1984) 3051.
20 P.L. Dubin, C.M. Speck and J.I. Kaplan, *Anal. Chem.*, 60 (1988) 895.
21 C. Tanford, *J. Am. Chem. Soc.*, 72 (1950) 441.
22 C. Tanford and M.L. Wagner, *J. Am. Chem. Soc.*, 76 (1954) 3331.
23 C. Tanford and J.D. Hauenstein, *J. Am. Chem. Soc.*, 78 (1956) 5287.
24 S.L. Edwards, *Thesis*, Purdue University, Indianapolis, IN, 1992.

Journal of Chromatography, 648 (1993) 9–17
Elsevier Science Publishers B.V., Amsterdam

CHROMSYMP. 2847

Macromolecular porosimetry

Lev Z. Vilenchik, Jawed Asrar, Roger C. Ayotte, Leo Ternorutsky and Christopher J. Hardiman*

Monsanto Chemical Co., Mail Zone Q1A, 800 N. Lindbergh Boulevard, St. Louis, MO 63167 (USA)

ABSTRACT

A new method for the determination of pore size distribution in porous materials has been developed. The method is based on measuring the probability of solubilized macromolecules to penetrate the pore space of a solid substrate. In the absence of any interaction between the macromolecules and the matrix of the porous material, the value of the probability is determined only by ratio of sizes of the macromolecules and the pores. A special software package was developed for slit, cylindrical, and mixed pores.

INTRODUCTION

Porous structure is one of the most important characteristics of numerous materials. Several analytical methods are available to investigate pore size characteristics including mercury porosimetry [1], adsorption of the vapour of inert solvents [2], and small-angle X-ray scattering [3].

The first two methods can be used only for porous materials in the desolvated state. Small-angle X-ray scattering is used to study the structure of polymer materials in the swollen state. This method is complex regarding both the performance of the experiment and the interpretation of results and is therefore seldom used in investigations of porous materials. The porosimetric patterns obtained by these methods usually differ.

The method of macromolecular porosimetry can serve as a universal method for determination of pore structure. It is particularly efficacious for the porosimetry of sorbents used in the chromatography of polymers, since the pore size distribution determined by the aid of this method corresponds to the chromatographic distribution of the macromolecules.

The first attempts to determine pore sizes of porous materials by means of the macromolecular porosimetry were made in the early 1970s [4–6]. A number of different approaches to verify this method have been proposed [7–21]. The most advanced from them has been developed in ref. 20, where the authors could reduce the problem of solving of the integral equation to a simple algebraic equation. However, their approach is valid only for hard spherical macromolecules. In this paper we report further development of the porosimetry method using a special approach for the modeling of flexible chain macromolecules. We have also developed a special software package and two different experimental methods for the determination of pore size distribution in porous materials.

THEORY

Solubilized macromolecules are used as specific probes in the method of macromolecular porosimetry. Unlike solutions of low-molecular-mass substances, a polymer solution is a kind of "double" statistical ensemble. On the one hand,

* Corresponding author.

0021-9673/93/$06.00

it is an ensemble consisting of macromolecules as structural elements. On the other hand, each macromolecule can be considered as a statistical ensemble of elementary segments. Each of these ensembles obeys the laws of thermodynamics and statistical physics with all the ensuing consequences. For example, the concepts of thermodynamic potentials, free energy, entropy, etc. can be used to characterize both the state of the whole polymer solution and that of the individual macromolecules [22]. The interdependence between the changes in the state of the macromolecules and the solution as a whole leads to relationships that have not been observed in the behavior of the solutions of low-molecular-mass substances in the porous medium.

In the absence of any adsorption interaction between macromolecules and the matrix of the porous medium, reliable expressions for the distribution coefficient (K_d) value for macromolecules with different shapes are known [23]. The K_d expressions for spherical macromolecules (proteins, ficols) have recently been validated experimentally [24]. It is possible to write these expressions using only one equation with different meanings for the pore shape parameter [23]:

$$K_d = (1 - R/r)^q \quad (1)$$

where $q = 1$, 2 or 3 for spherical, cylindrical and split pores respectively.

For the slit case we should take into account the existence of wedge-shaped pores; the model used to account for the varying angle of pore walls must be an average of all angles present in the specific porous material being investigated (see Fig. 1). For example, if for the wedge-shaped pores the variation of the angle ranges from 60 to 90° then we replaced eqn. 1 with

$$K_d = 1 - (R/r)(6/\pi)\int_{\pi/3}^{\pi/2} (1/\sin x)\,dx$$
$$= 1 - R/(r_{av}/1.05) \quad (2)$$

where r_{av} corresponds to the average pore radius for the usual slit model, and r is the average effective pore radius taking into account the slope between pore walls

$$r = r_{av}/1.05 \quad (3)$$

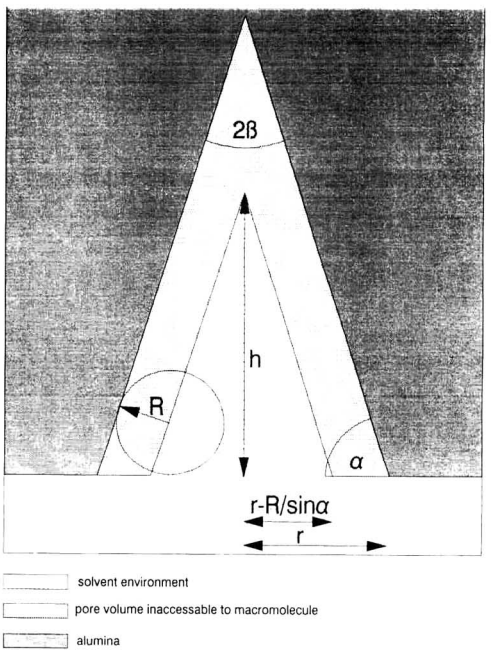

Fig. 1. Model of wedge-shaped macropore in Unisphere alumina.

Flexible-chain macromolecules do not have a definite form and size. Their conformations are changing continuously, and we can observe only some average states. For such kind of macromolecules the coefficient of distribution between free solution and a porous medium is determined by changing the number of macromolecular conformation when a macromolecule may enter into a pore of the medium [25]. However, it was possible to obtain the expression for K_d of these macromolecules only without taking into account an interaction of macromolecular segments with the solvent. Perhaps, it is a reason why theoretical and experimental data are in poor agreement [25].

Meanwhile, it was shown [26] that distribution of flexible-chain macromolecules between free solution and porous medium is determined by ratio of their hydrodynamic radius $\langle R_h \rangle$ and pore radius r. The $\langle R_h \rangle$ value is an average characteristic of the macromolecule. It is equal to the radius of an equivalent hydrodynamic sphere which behaves itself like the macromole-

cule during the interphase transition. In principle, we can assign to each macromolecular conformation an equivalent sphere [8]. Then, for all conformations we will have an ensemble of such equivalent spheres with radii R_h. Averaging according to this ensemble gives us $\langle R_h \rangle$ value for the macromolecule. We can suggest, that the distribution R_h values in this ensemble obeys Gauss' law

$$G(R_h) = 4\pi(2\pi\langle R_h^2\rangle)^{-3/2} R_h^2 \exp(-3R_h^2/2\langle R_h^2\rangle) \quad (4)$$

where $\langle R_h^2 \rangle$ is the mean square sphere radius of the ensemble of the equivalent spheres.

Now, we can use eqn. 1 to calculate K_d value for each sphere from the ensemble $G(R_h)$ in eqn. 4. Averaging according to all spheres of the ensemble has to give the observing value for the coefficient of distribution. Taking into account that any porous material has a distribution of pore sizes $P(r)$, we must average the K_d expression according to the pore size distribution. As a result, we obtain

$$K_d(\langle R_h \rangle) = \int_0^\infty P(r) \int (1 - R_h/r)^q G(R_h)\, dR_h\, dr \quad (5)$$

Eqn. 5 shows that we can calculate the K_d value for a macromolecule with an average size of hydrodynamic radius $\langle R_h \rangle$ if the pore size distribution $P(r)$ and the shape of the pores are known.

It is possible also to solve a reverse problem: to calculate the pore size distribution $P(r)$ from eqn. 5 using known value for distribution coefficient $K_d(\langle R_h \rangle)$. We can use for this goal different kinds of macromolecules: proteins, ficols, or flexible-chain coils with known R_h values. However, in each particular case we should apply the function $G(R_h)$ in a different expression. For flexible-chain macromolecules this is the function G from eqn. 4; for proteins this is a delta function, for ficols this is a special distribution. This is the basis for the new porosimetric method: macromolecular porosimetry, in which solubilized macromolecules are used as specific probes to determine pore size distribution in any porous medium.

EXPERIMENTAL

To measure the distribution coefficient K_d of macromolecules between a free solution and a porous medium being investigated we can use two different types of experiment: batch (static) mode and chromatographic (dynamic) mode.

Static experiment

A known amount of the porous medium being investigated is placed into test tube and is flooded by a macromolecular solution with known concentration. The solution penetrates into the pore space of the medium and distributes between two phases of the system (free volume and pores) owing to a tendency towards thermodynamic equilibrium. As a result, the concentration of macromolecules in free volume became to be less than in primary solution. This decreasing of the concentration is a function of the ratio pore and macromolecules sizes, pore size distribution, and shapes of the pores.

If we use C_0 as the concentration of our primary solution, then C_1 and C_2 are the concentrations in the free volume and porous space of the medium after setting of the thermodynamic equilibrium. We will call C_1 the concentration of a secondary solution. Now we can write

$$V_0C_0 = V_1C_1 + V_2C_2 \quad (6)$$

where V_0 is a primary volume of the solution, V_1 is a volume of the free solution, and V_2 is pore volume.

It is true that

$$V_0 = V_1 + V_2 \quad (7)$$

Now, using the standard definition for the K_d value, we can rewrite eqn. 6 as

$$K_d = C_2/C_1 = X(V_0/V_2) - V_1/V_2 \quad (8)$$

where

$$X = C_0/C_1 \quad (9)$$

To determine ratios V_0/V_2 and V_1/V_2 we can use the following phenomenon: the distribution coefficient for the largest macromolecules is equal to zero if pores of the medium being investigated are not available for the macromolecules because of their sizes.

$$K_d = 0 = X_0(V_0/V_2) - V_1/V_2 \quad (10)$$

where X_0 is the ratio (eqn. 9) for the macromolecules with $K_d = 0$. We have from eqn. 10

$$V_1/V_0 = X_0 \quad (11)$$

Combining eqns. 7 and 11 we can obtain

$$V_2/V_0 = 1 - X_0 \quad (12)$$

Now we can rewrite eqn. 8

$$K_d = (X - X_0)/(1 - X_0) \quad (13)$$

To determine the values X_0 and X we should measure the concentrations C_1 of the biggest macromolecules (with $K_d = 0$) and different other macromolecules into the free volume of our test tube. Knowledge of the primary concentrations C_0 led us to calculate the X_0 and X values according to eqn. 9. The easiest way to measure C_0/C_1 values is the injection of the primary and secondary solutions into a chromatographic column and carrying out a size-exclusion chromatographic (SEC) experiment. Since the area under the SEC chromatogram is proportional to the concentration, the ratio of these areas for primary and secondary solutions gives X and X_0 values.

Dynamic experiment

In this experimental mode a chromatographic column is packed with porous material to be investigated. Then solutions of different macromolecules have to run through this column in the SEC mode. Known standard procedure allow us to determine very easily the distribution coefficients for these macromolecules:

$$K_d = (t - t_0)/(t_1 - t_0) \quad (14)$$

where t is the retention time for macromolecules with given size, t_0 is the retention time for largest macromolecules with $K_d = 0$, and t_1 is retention time for low molecular weight substances with $K_d = 1$.

RESULTS

Silica gel G, Nucleosil 100, and the blend of 60% silica gel G and 40% Nucleosil 100 were investigated by means of the static experiment.

TABLE I

EXPERIMENTAL K_d VALUES FOR SILICA GEL G, NUCLEOSIL 100, AND BLEND FOR DIFFERENT MOLECULAR MASS POLYSTYRENES

M	K_d		
	Silica gel G	Nucleosil 100	Blend
580	0.677	0.767	0.715
2 450	0.497	0.647	0.560
9 200	0.150	0.332	0.115
22 000	0.074	0.169	0.225
66 000	0.009	0.030	0.018
170 000	0.003	0.009	0.004
333 000	0.001	0.002	0.001
3 040 000	0.000	0.000	0.000

Polystyrene standards were used as macromolecular probes. Tetrahydrofuran was chosen as the solvent. Table I shows the distribution coefficients for polystyrene standards with different molecular masses.

The software which was developed in this work, allowed us to calculate on the basis of eqn. 5 a pore size distribution $P(r)$ for each of these porous materials. The distributions for silica gel G and Nucleosil 100 were sought as triangles (*i.e.* the coordinates of their tops). We attempted to achieve the best coincides between experimental values of the distribution coefficients of macromolecules with different molecular weights and K_d value calculated via eqn. 5 using the cylindrical pore model (the value of q equals 1).

Finally, for silica gel G we have obtained P(r) function with the following parameters: the left top on the base line of the triangle has coordinate $r = 15$ Å; right top: $r = 35$ Å; and top at maximum: 30 Å. The corresponding coordinates for Nucleosil 100 are 35, 55 and 50 Å, respectively. For the pore size distribution of these a blend of these porous materials we have obtained a superposition of these two triangles (Fig. 2).

A dynamic mode for pore size determinating was used for new sorbent for SEC: Unisphere alumina (Al_2O_3) (Biotage, Charlottesville, VA, USA) [27–29]. This is a new modification of the old known alumina particles. Unisphere alumina particles look like crystals extending radially

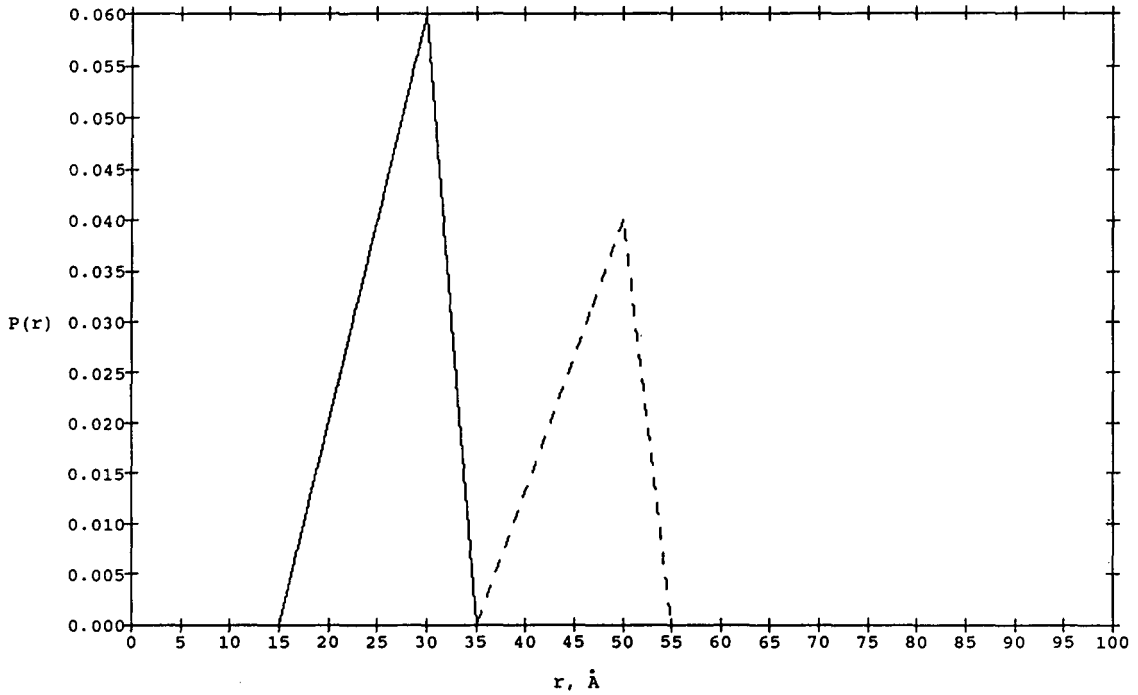

Fig. 2. Pore size distribution for silica gel G (——) and Nucleosil 100 (- - -).

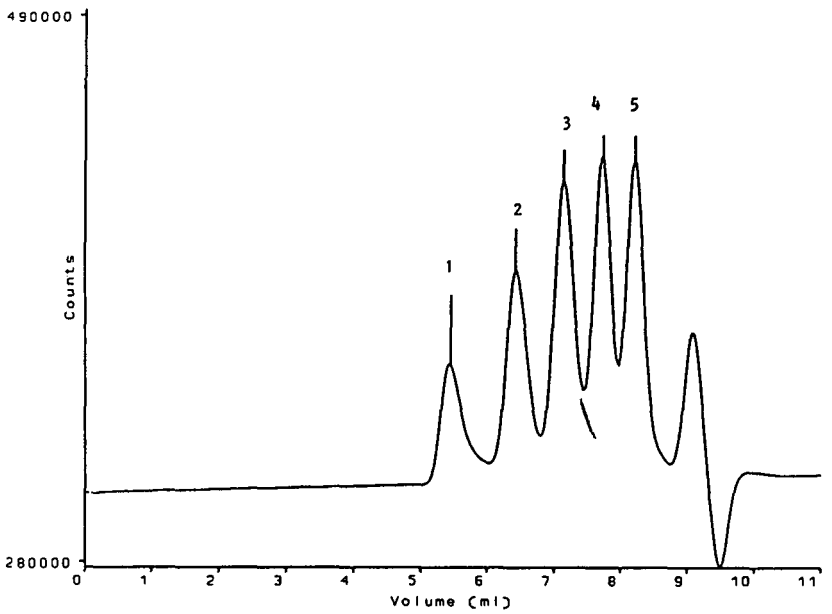

Fig. 3. Typical SEC chromatogram for polystyrene mixture on column packed with Unisphere alumina. Polystyrene standard mixture M_r $8.5 \cdot 10^6$ (peak 1), $1.03 \cdot 10^6$ (2), $1.56 \cdot 10^5$ (3), $2.85 \cdot 10^4$ (4) and $3.25 \cdot 10^3$ (5).

outward from a central core *i.e.* giving wedge-shaped macropores. Each individual plate also contains micropores whose shape is largely cylindrical. Thus the Unisphere alumina particles have a bimodal pore size distribution (PSD). It is known that sorbents with this type of PSD may give good separation of macromolecules ranging from oligomers to high polymers [30].

To check the sensitivity of the macromolecular porosimetry method to small changes of PSD, three different modifications of the Unisphere alumina have been investigated. Two are coated with different amounts of polysiloxane and one is not coated. The chromatographic columns have been packed with these different alumina particles. Each column has been installed in a liquid chromatograph employing tetrahydrofuran as mobile phase. Different mixtures, containing different polystyrene standards, were evaluated using these columns. Thus a total of seventeen polystyrene standards from a molecular mass of 580 to $8.5 \cdot 10^6$ plus toluene, were used. Fig. 3 shows a typical chromatogram from one of these experiments with a polystyrene mixture containing five standards. Molecular mass (M) calibration curves were determined for the alumina columns, and appear in Fig. 4. The retention volume V_0 of the polystyrene standard with M = 8 500 000 was taken to be the exclusion volume of the column, and the retention volume V_t of toluene was also taken to be the total volume of the column. The K_d for the standards was determined according to the eqn. 14, where retention times t_0 and t_1 correspond to the values V_0 and V_t. Table II shows the experimental and theoretical values (according to eqns. 14 and 5, respectively) for the coefficient of distribution K_d for all the polystyrene standards used in the experiment for each of the three chromatographic columns (coated and uncoated). A plot of K_d *versus* log polystyrene molecular mass for all three columns appears in Fig. 5. There is significant differentiation in the low-molecular-mass range only. For polymer molecular mass greater than 10^6 the coefficients of distribution are all similar. The addition of polysiloxane coating

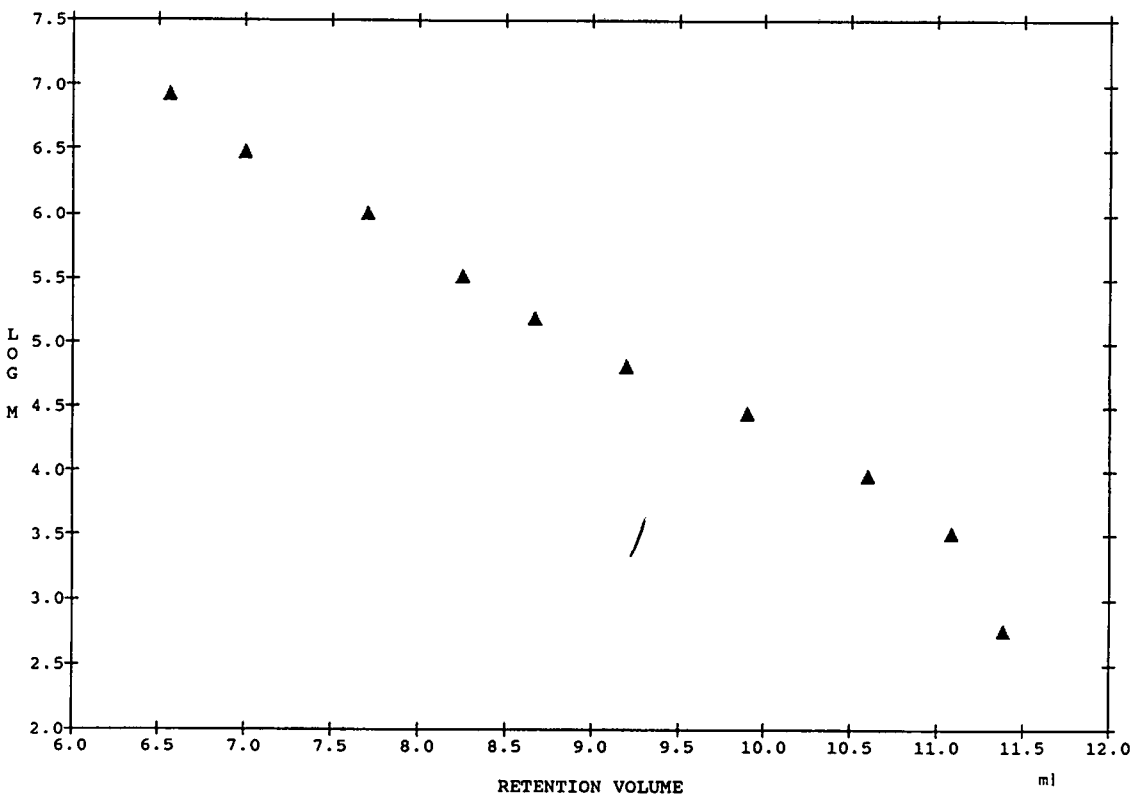

Fig. 4. Calibration of column packed with Unisphere alumina.

TABLE II

EXPERIMENTAL AND CALCULATED K_d VALUES FOR THREE DIFFERENT MODIFICATIONS OF UNISPHERE ALUMINA FOR POLYSTYRENES OF DIFFERENT MOLECULAR MASS

exp = Experimental; calc = calculated; Al = alumina; +15% and +20% = +15% siloxane and +20% siloxane, respectively.

Log M	$\langle R_h \rangle$	K_d(exp), Al	K_d(calc), Al	K_d(exp), Al + 15%	K_d(calc), Al + 15%	K_d(exp), Al + 20%	K_d(calc), Al + 20%
2.76	6.2	0.95	0.95	0.89	0.89	0.87	0.85
3.23	10.3	0.92	0.91	0.80	0.83	0.76	0.77
3.39	12.3	0.91	0.89	0.78	0.80	0.73	0.73
3.51	14.1	0.90	0.88	0.76	0.78	0.70	0.71
3.96	23.1	0.80	0.81	0.70	0.69	0.60	0.60
4.06	26.3	0.77	0.78	0.68	0.67	0.57	0.58
4.34	37.9	0.69	0.70	0.62	0.61	0.52	0.52
4.46	44	0.66	0.67	0.60	0.59	0.50	0.50
4.56	49	0.62	0.64	0.59	0.58	0.48	0.49
4.82	71	0.53	0.55	0.53	0.53	0.44	0.44
5.19	116	0.45	0.44	0.45	0.46	0.38	0.38
5.23	122	0.44	0.43	0.44	0.45	0.37	0.37
5.52	178	0.37	0.36	0.37	0.38	0.32	0.31
5.57	189	0.36	0.35	0.36	0.37	0.30	0.30
6.01	341	0.23	0.23	0.23	0.23	0.20	0.19
6.47	621	0.1	0.11	0.10	0.10	0.09	0.08
6.93	1137	0.02	0.03	0.02	0.03	0.02	0.02

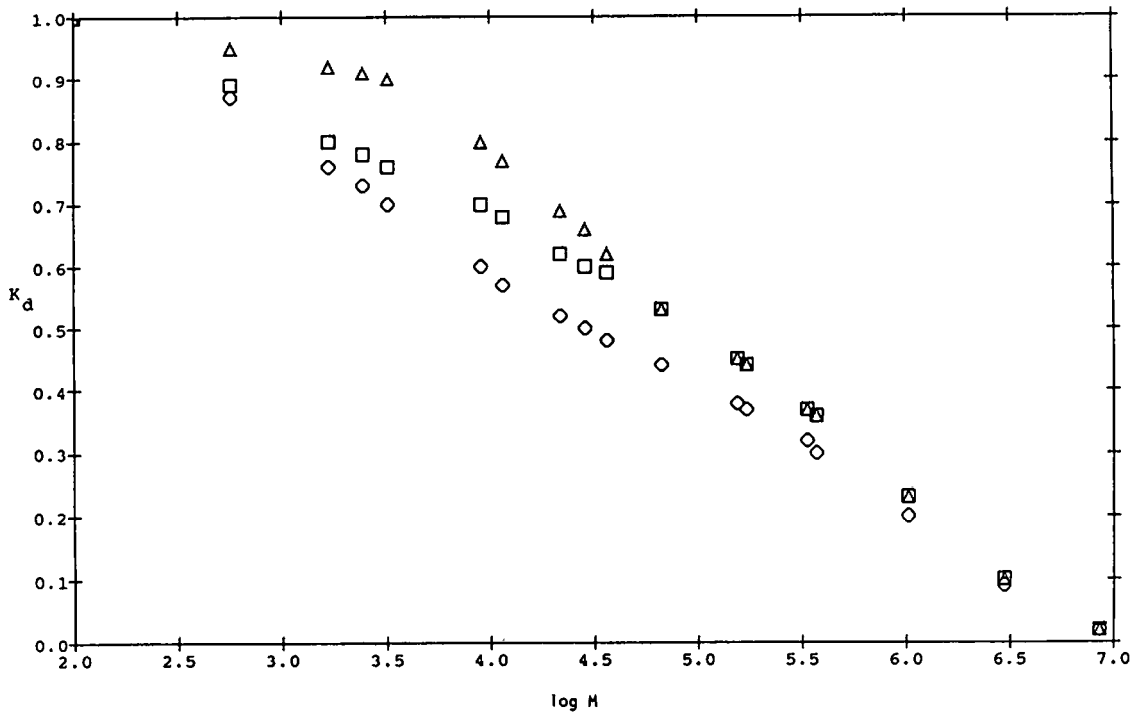

Fig. 5. Distribution coefficient of polystyrene *versus* log M for three different modifications of Unisphere alumina. △ = Unisphere; □ = Unisphere + 15% siloxane; ◇ = Unisphere + 20% siloxane.

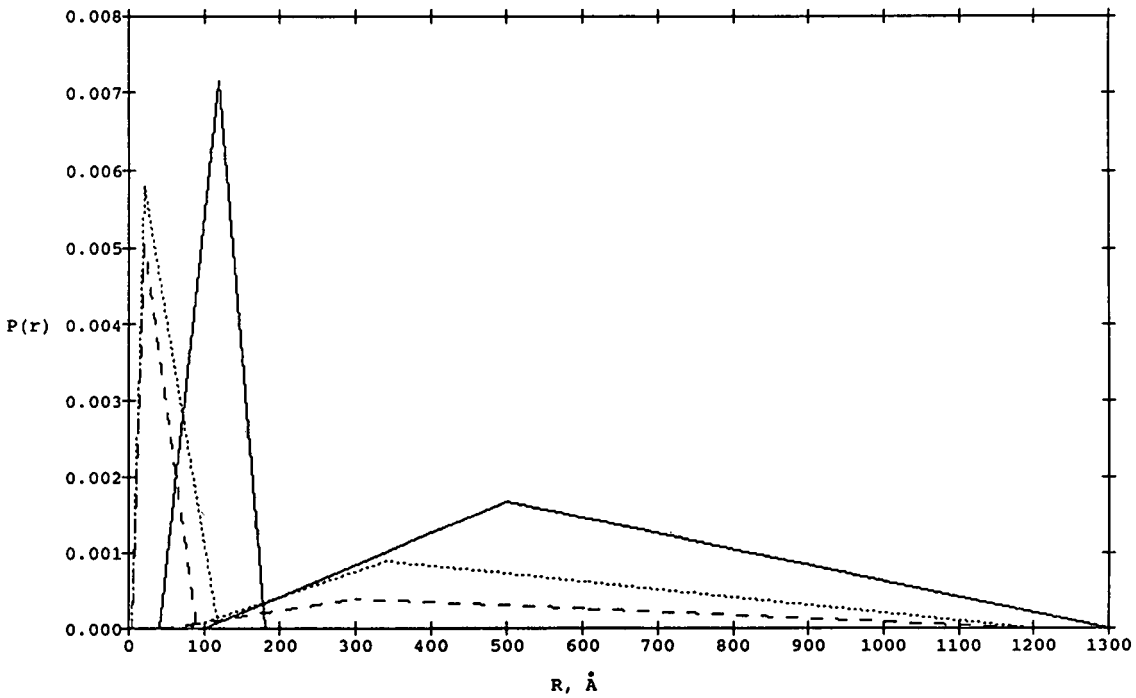

Fig. 6. Pore size distribution for three different modifications of Unisphere alumina. —— = Unisphere; - - - = Unisphere + 15% siloxane; – – – = Unisphere + 20% siloxane.

does not significantly affect distribution coefficient for macromolecules of $M \geqslant 10^6$.

The theoretical values for the coefficients of distribution were obtained by means of the same computer program which was used to calculate PSD for the blend of silica gel G and Nucleosil 100. All the data are shown in Table II. The functions of the distribution of the pore sizes were chosen to give the best coincidence of the theoretical and experimental K_d for all seventeen polystyrene standards. It was found that these functions are bimodal distributions. For the mode of distribution with small pore size we used cylindrical model and for the large pore size mode we used a wedge-shaped model with angle averaging as described in eqn. 2. The key parameters that define these functions are the upper and lower limits of each mode of distribution, their maxima, and the relative fraction of the two modes. We have obtained the distribution functions for the three materials as shown in Fig. 6. As this figure shows, each mode of the distribution represents approximately equal fractions of the total pore volume. After coating with polysiloxane, due to the resulting change in the net pore size distribution, the K_d coefficients for low-molecular-mass polystyrenes significantly decrease while for high molecular mass only a minor decrease is observed. Presumably the loss of pore volume in the small pore size mode is due to pore filling by the coating.

Comparison of these results with data obtained via BET shows a good coincidence for small pore size (Fig. 7). Unfortunately the BET method is unable to determine the distribution of pore sizes over the total range of large PSD.

CONCLUSIONS

It is possible to use macromolecules as probes, in either a static or dynamic mode, to determine pore size distribution of porous solids. The distribution of these macromolecular probes between the pore space and the interparticle space is a function of molecular size relative to the pore size, shape, and distribution thereof. The approaches developed in this and earlier work [4–21] are the basis of a new porosimetric method.

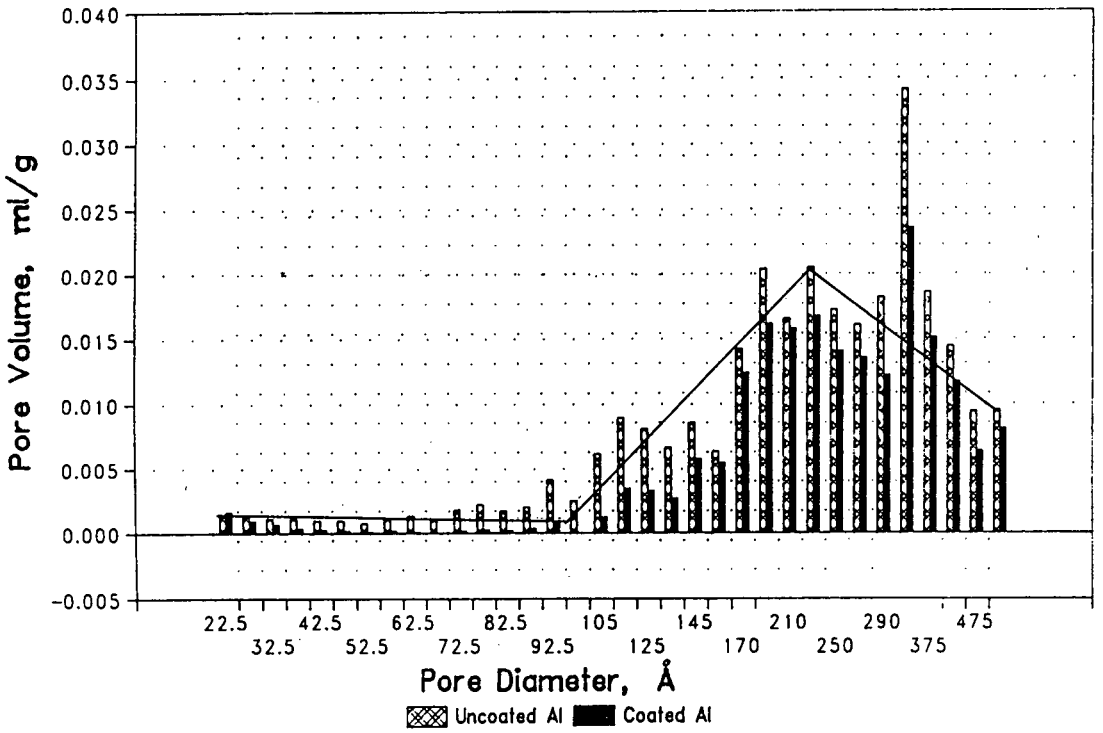

Fig. 7. Pore volume distribution for Unisphere alumina from desorption isotherm data.

REFERENCES

1 H. Ritter and L. Drake, *Ind. Eng. Anal. Ed.*, 17 (1945) 782.
2 S. Brunauer, P.H. Emmett and E. Teller, *J. Anal. Chem. Soc.*, 60 (1938) 309.
3 E.A. Poray-Koschic and V.N. Fillipovich, *Methody Issledovaniya Structury Vysocodispersnykh i Poristykh Tel*, Academy of Sciences of the USSR, Moscow, 1958, p. 7.
4 L.Z. Vilenchik, presented at the *1st International Conference on Absorption Problems USSR, Leningrad, 1971.*
5 L.Z. Vilenchik, *Kinetika i Dynamika Fizicheskoi Adsorbsii*, Nauka, Moscow, 1973, p. 229.
6 L.Z. Vilenchik, *Thesis*, Leningrad Polytechnical University, Leningrad, 1974.
7 D.H. Freeman and I.C. Poinescu, *Anal. Chem.*, 49 (1977) 1183.
8 B.G. Belenkii and L.Z. Vilenchik, *Chromatography of Polymers*, Khimia, Moscow, 1978, p. 184.
9 I. Halász and K. Martin, *Chem. Int. Ed.*, 17 (1978) 901.
10 W. Werner and I. Halász, *J. Chromatogr. Sci.*, 18 (1980) 277.
11 R. Niclov, W. Werner and I. Halász, *J. Chromatogr. Sci.*, 18 (1980) 207.
12 L.Z. Vilenchik, O.I. Kurenbin, T.P. Zhymakina and B.G. Belenkii, *Dokl. Akad. Nauk. USSR*, 250 (1980) 381.
13 D.H. Friman and S.B. Shram, *Anal. Chem.*, 53 (1981) 1235.
14 L. Anderson, *J. Chromatogr.*, 216 (1981) 23.
15 S. Kuga, *J. Chromatogr.*, 206 (1981) 449.
16 L.Z. Vilenchik, O.I. Kurenbin, T.P. Zhmakina, B.G. Belenkii and V.S. Jurchenko, *Zh. Fiz. Khim.*, 55 (1981) 182.
17 T. Crispin and I. Halász, *J. Chromatogr.*, 239 (1982) 351.
18 B.G. Belenkii and L.Z. Vilenchik, *Modern Liquid Chromatography of Macromolecules*, Elsevier, Amsterdam, 1983, p. 318.
19 B. Gelleri and M. Sernetz, *Anal. Chem. Acta*, 163 (1984) 17.
20 J.H. Knox and H.P. Scott, *J. Chromatogr.*, 316 (1984) 311.
21 K. Jerabek, *Anal. Chem.*, 57 (1985) 1595.
22 P.J. Flory, *Principles of Polymer Chemistry*, Cornell Univ. Press, New York, 1953.
23 J.C. Giddings, E. Kucera, C. Russel and M. Myers, *J. Phys. Chem.*, 78 (1968) 397.
24 S. Hussein, M. Mehta, J. Kaplan and P. Dubin, *Anal. Chem.*, 63 (1991) 1132.
25 E. Casassa, *J. Polym. Sci.*, B5 (1967) 773.
26 H. Benoit, V. Grubisic, P. Rempp, D. Decker and J.G. Zilliox, *J. Chim. Phys. Chim. Biol.*, 63 (1966) 1507.
27 R.B. Wilhelmy, *US Pat.*, 4 822 593 (1989); 4 900 537 (1990).
28 L.F. Wieserman, K. Wefers, K. Cross and E.S. Martin, *US Pat.*, 5 037 795 (1991).
29 L.Z. Vilenchik, R.C. Ayotte, J. Asrar and C.J. Hardiman, *US Pat.*, 5 190 658 (1993).
30 W.W. Yau, J.J. Kirkland and D.D. Bly, *Modern Size Exclusion Chromatography*, Wiley, New York, 1979, Ch. 4.

Journal of Chromatography, 648 (1993) 19–25
Elsevier Science Publishers B.V., Amsterdam

CHROMSYMP. 2826

Size-exclusion chromatography in an analytical perspective

Lars Hagel

R&D Department, Pharmacia LKB Biotechnology AB, S-751 82 Uppsala (Sweden)

ABSTRACT

Modern media for size-exclusion chromatography combine maximum selectivity with high plate count to resolve solutes differing in molecular mass by as little as 20%. Separations of solutes differing in molecular mass by only 10% will be very hard to accomplish even for rod-shaped molecules. The reduced column lengths and porosity of small-particle-sized media unfortunately reduces the inherent resolving power to the same order as traditional columns but with a substantial reduction in analysis time. The use of well-calibrated columns for obtaining estimates of molecular mass yields a precision close to that of absolute methods. The simplicity and accuracy of the integral calibration method using a sample of broad molecular mass distribution makes this procedure very suitable for manual calibration of size-exclusion columns.

The objective of analytical size-exclusion chromatography is to separate components of different size well enough to permit their quantitative and/or qualitative determination. The purpose of this communication is to review the present status of size-exclusion chromatography as a tool for analytical characterization of macromolecules.

SEPARATION OF COMPONENTS

Separation is achieved by passing the sample through a porous support. The degree of separation may be quantified by the resolution between peaks. The resolution is a function of the distance between peaks and the width of the peaks. The peak-to-peak distance, or selectivity, is determined by the number and dimension(s) of the pores and is thus set by the characteristics of the gel medium. The width of peaks is influenced by the particle size of the medium. The resolution is also affected by experimental parameters such as column length, eluent velocity and solvent viscosity.

The maximum selectivity of size-exclusion gel media is obtained by using single pore size supports. For such a support it may be shown that the separation range covers approximately one decade in solute radius [1]. Owing to the different relationships between molecular mass and size for solutes of different shape the selectivity for one decade in size will correspond to one, two and three decades in mass for rods, flexible coils and spheres, respectively [2]. Some traditional media for aqueous SEC display such high selectivity (*e.g.* Sephadex and Bio-Gel). Porous glass also yields high selectivity owing to the narrow pore size distribution introduced by the manufacturing process [1]. One example of a modern medium constructed to give high selectivity is porous silica microspheres, where the pore dimension is given by the space between solid silica sub-microspheres of uniform size [3]. A novel medium for aqueous size-exclusion chromatography combines the rigidity of a macroreticular gel with the selectivity of the microreticular gel by the incorporation of dextran into a cross-linked agarose skeleton. The selectivity, as shown in Fig. 1, is close to maximal. This type of medium is preferentially used for separations where differences in solute size are minute. One such example is the analysis of

0021-9673/93/$06.00

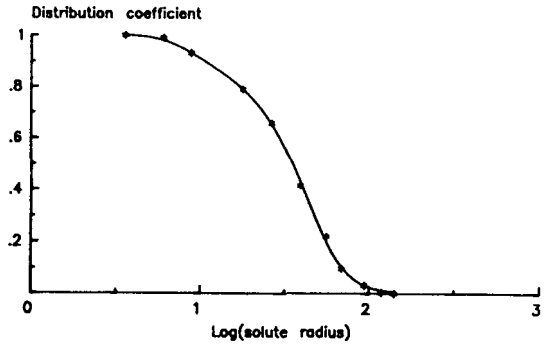

Fig. 1. Selectivity of Superdex 200 for dextrans. Narrow fractions of dextran were run through a column of Superdex 200 prep grade, 62 × 2.6 cm I.D. using a fast protein liquid chromatography system. The molecular mass corresponding to peak elution volume was converted to solute radius through $R_h = 0.271M^{0.498}$ (ref. 1). (Raw data used by courtesy of ref. 4.)

multimeric forms of important biomacromolecules, as illustrated by Fig. 2.

The theoretical limit of resolution, R_s, in size-exclusion chromatography may be inferred from the resolution equation [5]:

$$R_s = 1/4 \cdot \log(M_1/M_2) \cdot N^{1/2} \cdot [-\mathrm{d}(K_D)/\mathrm{d}(\log M)]/(V_0/V_p + K_D) \quad (1)$$

where M_1 is the molecular mass of species 1, K_D is the distribution coefficient, $\mathrm{d}(K_D)/\mathrm{d}(\log M)$ is the molecular mass selectivity of the medium, V_0 is the void volume of the column, V_p is the pore volume of the gel bed and N is the average plate number of the two solutes. The plate number of the solutes may be calculated by using the assumption that the separation is carried out at optimum eluent velocity where peak widths are fairly constant [6]. Inserting $\sigma = \sigma_t$ and $V_R = V_t[1 + V_p/V_t(K_D - 1)]$ in the formula $N = (V_R/\sigma)^2$ and realizing that the maximal plate count is obtained for small solutes, *i.e.* $N_{max} = (V_t/\sigma_t)^2$, eqn. 1 can be rearranged to:

$$\log(M_1/M_2) = 4R_s(V_0/V_p + 1)(N_{max})^{-1/2} \cdot 1/[-\mathrm{d}(K_D)/\mathrm{d}(\log M)] \quad (2)$$

where the first term accounts for the required resolution, the second term is a function of the pore volume of the support, the third term expresses the maximal plate count of the column and the last term reflects the pore size distribution of the media.

The maximal size selectivity of a support is obtained at the inflexion point of the selectivity curve, which is given by the distribution coefficient as a function of the logarithm of solute radius, R. The inflexion point is obtained at $R = r/2$, where r is the pore radius of the support [1]. Using a cylindrical pore model it can be

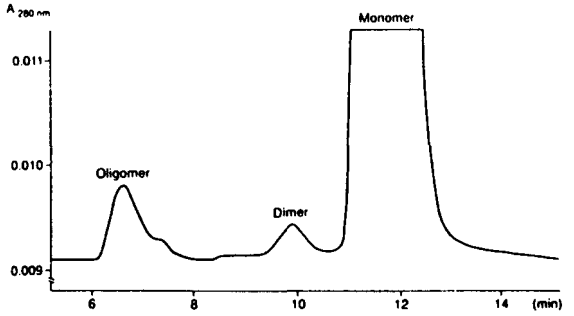

Fig. 2. Analytical size-exclusion chromatography for determination of aggregates in preparations of recombinant human growth hormone (rhGH). The sample, 0.05 ml of rhGH, was applied to Superdex 75 HR 10/30, 30 × 1 cm I.D., and eluted at 1 ml/min with 0.05 *M* sodium dihydrogenphosphate in 0.1 *M* sodium sulphate, pH 7.3. An enlarged section of the original chromatogram is shown. (Courtesy of B. Pavlu, Kabi-Pharmacia Peptide Hormones, and H. Lundström, Pharmacia.)

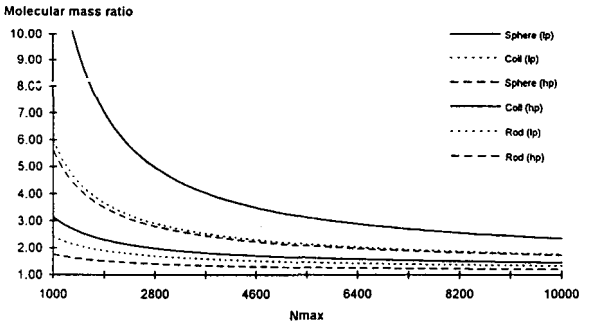

Fig. 3. Resolvability of size-exclusion chromatography. The molecular mass ratio needed for complete resolution of solutes, *i.e.* $R_s = 1.5$ as a function of column plate number is given for various solute shapes and column permeabilities. Curves plotted in order as given by the explanation. Permeability, V_p/V_0, is for low-porous media (lp) = 0.75 and high-porous media (hp) = 2.0. Calculated from eqn. 2.

shown that the inflexion point for a single pore size support is given by [1]:

$$|d(K_D)/d(\log R)|_{max} = \ln(10)/2 = 1.15 \quad (3)$$

In terms of molecular mass the maximal selectivity will equal 1.15 for rods, 1.15/2 for flexible coils and 1.15/3 for spheres. The selectivity for proteins is frequently reported to exceed 0.38. This is probably because the shape of globular proteins is ellipsoidal and may not be approximated by spheres.

The resolvability, *i.e.* the ability to completely resolve solutes of different sizes, as a function of plate number of different solute shapes and media pore volumes is shown in Figs. 3 and 4. As illustrated in Fig. 3 most media, including traditional ones, will separate solutes differing a decade in molecular mass. Also noticeable is the large influence of the pore fraction, V_p/V_0, of the media on the resolvability. The maximal resolvability that can be expected from size-exclusion chromatography is shown by Fig. 4. Whereas a separation of dimer from monomer may be expected from a 30-cm column packed with a 10-μm bead, typically yielding $N_{max} = 10000$ (see Fig. 2), separation of proteins differing in molecular mass by less than 20% will be difficult also with columns of extreme plate numbers. The limit for rod-shaped molecules, such as DNA, seems to be in the vicinity of 10%. Thus, if the molecular mass of solutes of similar shape differs by less than 10%, separation by some principle other than size should be explored.

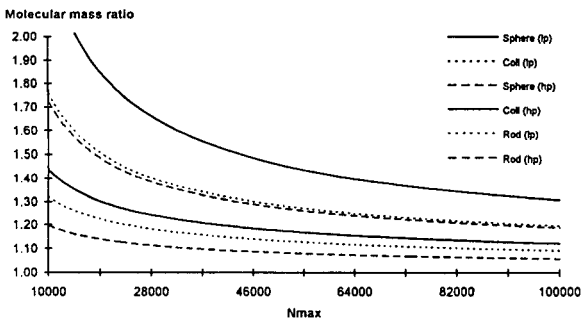

Fig. 4. Resolvability of size-exclusion chromatography using columns of extreme plate counts. Conditions as given in the legend to Fig. 3.

It is important to note that high selectivity yields a low separation range and this is not always desired. For instance, when analysing molecular mass distributions, a separation range covering the complete size range of solute species is required to yield accurate information. It may also be noted that the decrease in column length and pore fraction of modern microparticulate media for size-exclusion chromatography results in lower peak capacity, *i.e.* resolvability, than expected from plate count data. A comparison of peak capacities of different media–column combinations shows a maximum of thirteen completely resolved peaks for both modern and traditional columns [6]. However, the latter type of columns may be operated very fast without too much loss in resolvability as compared with traditional media.

DETERMINATION OF SOLUTE SIZE

The size of solutes may be determined either by using a calibrated system or by employing a size-specific detector. In the first case the column is calibrated with the aid of standards of known size and preferably of the same geometry as the solute to be characterized. Such systems have been utilized for many years for the characterization of molecular mass distributions of polymers. The systems have proven to be very reliable and the major contribution to variability stems from inaccuracy in the data for the calibration samples [7]. The accuracy of the calibration is verified by running reference samples. The reference materials are characterized by an absolute method, *e.g.* light scattering, and the small variability of this technique over an extended period of time is illustrated in Fig. 5. Corresponding data for some different calibrated column systems are shown in Fig. 6. It can be concluded that the variability of the two methods is of the same order of magnitude, *i.e.* displaying a relative standard deviation of approximately 2%, illustrating that size-exclusion chromatography yields data of high precision.

The calibration procedure of the column may be very tedious, involving running a large number of samples, plotting an estimate of the molecular mass *versus* elution volume and then

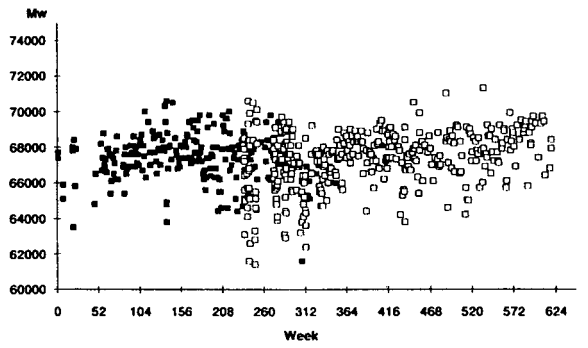

Fig. 5. Weight-average molecular mass, M_w, for a control dextran as determined by light scattering over a period of 12 years. Filled squares represent data obtained with Sofica 2; number of data, $n = 223$, mean value, $x = 67431$, and standard deviation, $s = 1337$. Open squares represents data obtained with KMX-6; $n = 361$, $x = 67253$ and $s = 1621$. (Raw data used by courtesy of ref. 8.)

fitting a high-degree polynomial or another function to the data points. The procedure requires the use of a computer for convenient handling of the calculations. The use of high-degree polynomials for curve fitting may introduce unexpected variations of the curve, especially at the extremes of the calibration range.

Recently, Hagel and Andersson [9] illustrated the use of the integral calibration method for a rapid, simple and accurate calibration of columns in solute size. In this method, the entire distribution is used for calibration, thus providing a very large number of data points, which obviates

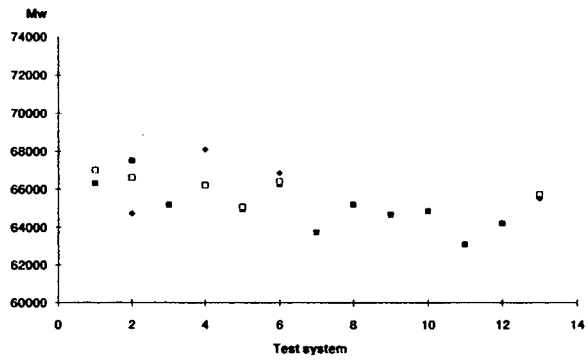

Fig. 6. Weight-average molecular mass, M_w, for a control dextran as determined by size-exclusion chromatography. The same sample as used in Fig. 5 was analysed using different gels and columns yielding $x = 65824$, $s = 1337$ with $n = 25$. (Raw data used by courtesy of ref. 8.)

the need for any curve-fitting procedure. Furthermore, by selecting a calibration substance of sufficiently broad molecular mass distribution, the separation range of interest may be calibrated from a single run. The prerequisite is that the molecular mass distribution of the calibration substance must be accurately known. The method, as applied for determination of solute size of proteins using dextran as calibration sample, is illustrated in Fig. 7. The sample was run on the column to be calibrated (Superose 6), and the cumulative weight fraction of eluted material was calculated simply by reading the response from the recorder chart at successive intervals and normalizing the data, as shown in Fig. 7a. The molecular mass corresponding to each slice of cumulative area was calculated from the known molecular mass distribution of the sample (Fig. 7b) and plotted as a function of retention volume (Fig. 7c). Finally, the molecular mass was transferred to viscosity (hydrodynamic) radius by using the relationship $R_h = 0.271M^{0.498}$ (ref. 1), to yield the final calibration curve in solute size (Fig. 7d). This type of calibration is useful for estimation of size of globular proteins [10–12], and the applicability is illustrated by the evaluation of apparent size of some proteins as compared with literature data in Table I. The accuracy of this simple procedure is in this case better than 5%. Furthermore, peak molecular mass for narrow dextran fractions is in excellent agreement with the nominal data given by the manufacturer. Thus, for many investigations the very simple and time-saving integral calibration method yields sufficient accuracy and precision for the determination of molecular mass of dextran and apparent solute size of globular proteins. As pointed out by Yau *et al.* [13], the method yields less precise calibration in the extremes of the size distribution of the calibration sample owing to column band broadening and experimental imprecision. However, by choosing a sample of broad size distribution a sufficient size range is easily covered, *i.e.* the dextran used in this case yields a calibration range form 2.7 to 11.5 nm.

In case the column is used for obtaining molecular mass distributions, the band broadening of the column will influence the experimentally determined estimates. Models for correc-

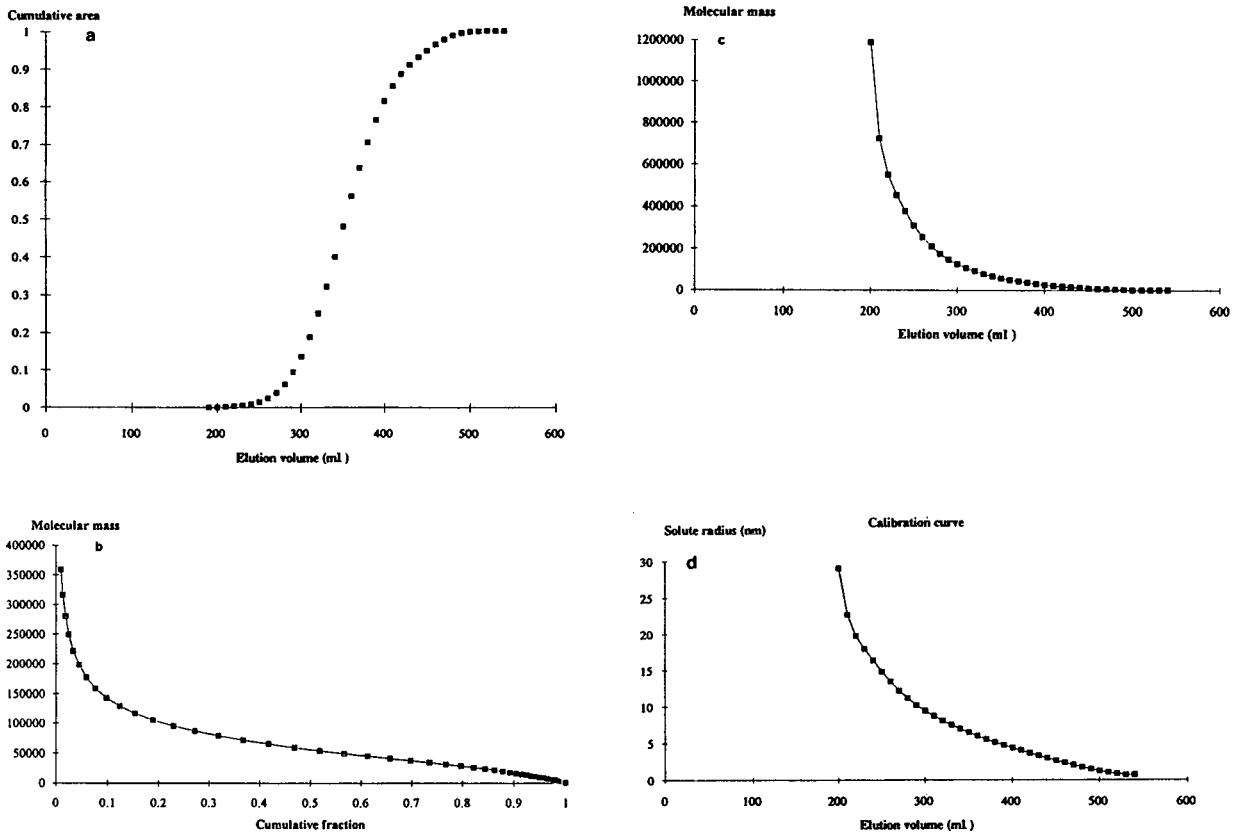

Fig. 7. Illustration of the integral calibration method using dextran of broad molecular mass distribution. (a) The dextran sample with $M_w = 70\,450$ and number-average molecular mass, $M_n = 27\,650$ was chromatographed on Superose 6 packed in a 315 × 16 mm I.D. column and eluted at 1 ml/min using 0.25 M sodium chloride. The cumulative area was calculated from the peak height at 36 successive elution volumes and plotted. (b) The molecular mass distribution as obtained using a carefully calibrated gel filtration column. (c) The resulting calibration curve from data in Fig. 7a and b. (d) The calibration curve in viscosity radius of dextran using the relationship $R_h = 0.271 \cdot M^{0.498}$ (ref. 1). From ref. 9.

tion of band broadening often assume that the extent of band broadening is constant over the entire separation range. However, in reality band broadening may vary quite considerably, especially at high eluent velocity, where non-equilibrium effects cause large broadening of solute bands of higher molecular mass [6]. Application of band-broadening corrections have therefore been questioned, and some authors have found that correction procedures introduce errors rather than eliminate them [14,15]. The band-broadening effect may be minimized by operating the column at optimal eluent velocity where band broadening is minimal [5]. Using the equations proposed by Yau *et al.* [16], it may be calculated that the error in experimental molecular mass is +1 to +2% for the weight average and −1 to −2% for the number average when analysing samples on 10-, 30- or 100-μm medium packed in 25-, 50- or 100-cm-long columns, respectively (the larger errors are obtained for the larger particle sizes). The interstitial eluent velocity required may be estimated from $u = 65K_D D_m/d_p$, where D_m is the diffusion coefficient of the solute and d_p is the average particle size of the gel medium [5]. Band broadening will influence the molecular mass estimates, as outlined above, if the column is calibrated using the molecular mass corresponding to the peak apex (*i.e.* since the position of the peak is not affected by the band broadening). The effect of band broadening may in some cases be compensated

TABLE I

ESTIMATION OF MOLECULAR MASS AND SOLUTE RADIUS

Note that data in parentheses are for solutes eluted outside the recommended calibration range (see text for explanation).

Solute	Measured		Nominal		
	$M_{dextran}$	R_h(nm)[a]	M_{peak} [b]	R_{St}(nm)[c]	R_h(nm)[d]
Dextran	195 300	11.7	196 300		
Dextran	191 500	11.6	196 300		
Dextran	66 880	6.8	66 700		
Dextran	19 310	3.7	21 400		
Dextran	(7230	2.3)	9980		
Thyroglobulin	102 619	8.4		8.1, 8.5	8.3
Ferritin	47 890	5.8		5.9	6.1
Bovine serum albumin	19 305	3.7		3.6	3.6
Myoglobin	(5914	2.0)			2.0
Cytochrome *c*	(4452	1.8)		1.7	1.6

[a] Measured $R_h = 0.271 \cdot (M_{dextran})^{0.498}$, from ref. 1.
[b] Nominal data from the manufacturer's literature for dextrans (Pharmacosmos).
[c] Stokes radii from ref. 10.
[d] Viscosity radii from ref. 11.

for in the calibration procedure by using an iterative procedure, such as the one described by Nilsson and Nilsson [17], where the calibration is adjusted to yield conventionally true values of weight-average molar mass. For samples of similar polydispersity a correct estimate of the weight average will then be obtained. However, the experimental number-average molecular mass will, in theory, always be smaller than the true value. In both cases it may be expected that the molecular mass distribution will be somewhat broader than the true distribution. In most cases the effect from band broadening will be very small, especially for samples of large polydispersity [15], as also illustrated by the accuracy of the integral calibration procedure in Table I.

The use of size-sensitive detectors coupled on-line with size-exclusion columns has gained increased popularity. In this case the column is solely used for fractionation of the solutes into sufficiently narrow fraction slices for the operation of the detectors. Advantages are that column calibration is not necessary for most studies and that useful information is obtained even in the case of non-ideal size-exclusion chromatography. Detection principles used are based upon classical principles such as light scattering and viscosimetry and may be regarded as a refinement of earlier used batch procedures. Of these principles, the use of light scattering at several angles using laser light sources seems to be very promising for yielding data related to solute size and conformation. The high sensitivity for solutes of large size also makes light-scattering detectors suitable for the detection of very small amounts of aggregates in samples for which detectors ordinarily used, *e.g.* UV or refractive index, show low response. A third principle for determination of molecular mass that is becoming feasible is the interfacing of microcolumns for size-exclusion chromatography with mass spectrometers. However, most of these detectors are rather sophisticated and only suitable for research purposes, and there is still a need for inexpensive and user-friendly detectors suitable for routine laboratory use.

CONCLUSIONS

Resolvability of size-exclusion chromatography seems to be close to 20% with respect to difference in molecular mass of spherical solutes

and somewhat better, *i.e.* down to 10% difference in molecular mass, for rod-shaped molecules.

Use of multiple detection principles on-line with the column yields valuable information about solute size, shape and branching. Detectors suitable for routine purposes will be very useful for detection of aggregates and also for revealing solute–matrix interactions.

The traditional way of working, through use of calibrated columns for determination of apparent size, is still dominant and my be employed also by laboratories lacking facilities for data acquisition and computing by using the simple integral calibration procedure with broad standard(s) of known molecular mass distribution(s).

ACKNOWLEDGEMENT

Parts of this work were presented at the *11th International Symposium on HPLC of Proteins, Peptides and Polynucleotides, Washington DC, October 20–23, 1991.*

APPENDIX

Derivation of eqn. 2 from eqn. 1 is done in the following way:

$$R_s = 1/4 \cdot \log (M_1/M_2) \cdot N^{1/2} \cdot [-\mathrm{d}(K_D)/\mathrm{d}(\log M)]/(V_0/V_p + K_D) \quad (1)$$

Using the following relationships;

$N = (V_R/\sigma)^2$ (according to the definition of N)

$\sigma = \sigma_t$ (at optimal conditions, see ref. 6)

$$V_R = V_0 + K_D V_p = V_t(V_0 + K_D V_p)/V_t$$
$$= V_t(V_0 + K_D V_p)/(V_0 + V_p)$$
$$= V_t(V_0/V_p + K_D)/(V_0/V_p + 1)$$

yields

$$N^{1/2} = (V_R/\sigma_t) = (V_t/\sigma_t)(V_0/V_p + K_D)/(V_0/V_p + 1)$$
$$= (N_{max})^{1/2} \cdot (V_0/V_p + K_D)/(V_0/V_p + 1)$$

where $N_{max} = (V_t/\sigma_t)^2$ is the maximal plate count for a small solute (*i.e.* the nominal plate count stated by the manufacturer). Eqn. 1 is thus given by:

$$R_s = 1/4 \cdot \log (M_1/M_2) \cdot (N_{max})^{1/2} \cdot (V_0/V_p + K_D)/(V_0/V_p + 1) \cdot [-\mathrm{d}(K_D)/\mathrm{d}(\log M)]/(V_0/V_p + K_D)$$
$$= 1/4 \cdot \log (M_1/M_2) \cdot (N_{max})^{1/2} \cdot 1/(V_0/V_p + 1)[-\mathrm{d}(K_D)/\mathrm{d}(\log M)]$$

which rearranged yields

$$\log (M_1/M_2) = 4R_s(V_0/V_p + 1)(N_{max})^{-1/2} \cdot 1/[-\mathrm{d}(K_D)/\mathrm{d}(\log M)] \quad (2)$$

REFERENCES

1 L. Hagel, in P. Dubin (Editor), *Aqueous Size-Exclusion Chromatography*, Elsevier, Amsterdam, 1988, Ch. 5.
2 W.W. Yau, J.J. Kirkland and D.D. Bly, *Modern Size-Exclusion Liquid Chromatography*, Wiley, New York, 1979, p. 116.
3 J.J. Kirkland, *J. Chromatogr.*, 125 (1976) 231–250.
4 T. Andersson, Pharmacia LKB Biotechnology, personal communication, 1992.
5 L. Hagel, in J.-C. Janson and L. Rydén (Editors), *Protein Purification, Methods for High Resolution Protein Separation and Analysis*, VCH, Deerfield Beach, FL, 1989, Ch. 3.
6 L. Hagel, *J. Chromatogr.*, 591 (1992) 47–54.
7 L. Andersson, *J. Chromatogr.*, 325 (1985) 37.
8 K. Nilsson and A.-C. Johansson, Kabi-Pharmacia, personal communication, 1992.
9 L. Hagel and T. Andersson, presented at the *11th International Symposium on HPLC of Proteins, Peptides and Polynucleotides, Washington DC, October 20–23, 1991*, paper 214.
10 R.P. Frigon, J.K. Leypoldt, S. Uyeji and L.W. Hendersson, *Anal. Chem.*, 55 (1983) 1349.
11 P.L. Dubin and J.M. Principi, *Macromolecules*, 22 (1989) 1891.
12 M. Potschka, *Anal. Biochem.*, 162 (1987) 47.
13 W.W. Yau, J.J. Kirkland and D.D. Bly, *Modern Size-Exclusion Liquid Chromatography*, Wiley, New York, 1979, p. 297.
14 L.H. Tung, *J. Appl. Polym. Sci.*, 10 (1966) 1271.
15 E.M. Sörvik, *J. Appl. Polym. Sci.*, 21 (1977) 2769.
16 W.W. Yau, J.J. Kirkland and D.D. Bly, *Modern Size-Exclusion Liquid Chromatography*, Wiley, New York, 1979, p. 106.
17 G. Nilsson and K. Nilsson, *J. Chromatogr.*, 101 (1974) 137.

Journal of Chromatography, 648 (1993) 27–32
Elsevier Science Publishers B.V., Amsterdam

CHROMSYMP. 2823

Mean square radius of molecules and secondary instrumental broadening

Philip J. Wyatt

Wyatt Technology Corporation, 802 East Cota Street, P.O. Box 3003, Santa Barbara, CA 93130-3003 (USA)

ABSTRACT

In a chromatographic separation such as size-exclusion chromatography, the concentrations of the injected molecules are generally so low by the time they reach the light-scattering (LS) detector that terms involving the second virial coefficient may be neglected in the equations which relate the measured Rayleigh excess ratio to the derived molecular weights and sizes. For sufficiently large molecules (root mean square radius greater than about 10 nm for 633 nm incident light wavelength), the root mean square radius may be calculated independently of the molecular concentration from the Rayleigh ratios measured as a function of scattering angle. Precise measurements of the root mean square radius are presented for some nearly monodisperse polystyrene standards. These measurements confirm that the eluting molecules have a nearly constant size over a relatively broad range of elution volumes, yet the corresponding mass values are not constant. This inconsistency is shown to be due to a secondary instrumental broadening (IB) of the sample which occurs primarily in the refractive index detector which follows the LS detector. This secondary IB, which may be calculated from the distorted mass *versus* elution volume curves, is shown to vary with molecular mass.

Consider the following equation [1] which is based on the Rayleigh–Gans–Debye (RGD) approximation [2] in the limit of vanishingly small molecular concentrations, c, and which forms the basis for the interpretation of light scattering measurements made from solutions of macromolecules of weight-average molecular mass M_w.

$$\frac{K^*c}{R(\theta)} \approx \frac{1}{M_w P(\theta)} + 2A_2c \tag{1}$$

The left-hand side of eqn. 1 represents the quantities measured and the right-hand side includes the unknown quantities to be determined by means of a least squares fit to the experimental data. In particular, $R(\theta)$ is the excess Rayleigh ratio,

$$R(\theta) = f_{geom}[I(\theta) - I_S(\theta)]/I_0 \tag{2}$$

where $I(\theta)$ is the intensity of light scattered by the solution into the solid angle subtended by the detector at the scattering angle θ, $I_S(\theta)$ is the corresponding quantity for the pure solvent, I_0 is the incident intensity, and f_{geom} is an absolute calibration constant that is a function of the scattering geometry, the structure of the (scattering) cell containing the solution, and the refractive indices of the solvent and scattering cell. The physical constant K^* for vertically polarized incident light is given by

$$K^* = 4\pi^2(dn/dc)^2 n_0^2/(N_A\lambda_0^4) \tag{3}$$

where n_0 is the solvent refractive index, N_A is Avogadro's number, λ_0 is the vacuum wavelength of the incident light, and dn/dc is the refractive index increment. The second virial coefficient is A_2. The scattering function, $P(\theta)$, is a function of the half scattering angle $\theta/2$ and the mean square radius, $\langle r_g^2 \rangle$:

$$P(\theta) = 1 - \left(\frac{4\pi n_0 \sin\theta/2}{\lambda_0}\right)^2 \langle r_g^2 \rangle /3 + \alpha_2 \sin^4\theta/2 - \cdots \tag{4}$$

0021-9673/93/$06.00

where

$$\langle r_g^2 \rangle = \frac{1}{M} \int r^2 \, dm \qquad (5)$$

and α_2 and higher order coefficients [3,4] in this $\sin^2 \theta/2$ series are constants dependent on the structure of the molecules. Note that the integral of eqn. 5 is the *definition* of the mean square radius. The integration (or summation) is taken over all mass elements dm of a molecule of mass M at a distance r from the molecule's center of gravity. The mean square radius is not the same as the so-called hydrodynamic radius.

At the very low concentrations typical of high-performance size-exclusion chromatography (HPSEC), the determination of the mean square radius [5] from the recorded light scattering data as a function of angle is easily shown to be independent of the concentration, c, the refractive index increment, dn/dc, and the weight-average molecular mass, M_w. Note that at such low concentrations when $2M_wA_2c << 1$, eqn. 1 reduces to the simple form

$$\frac{R(\theta)}{K^*} = McP(\theta), \qquad (6)$$

i.e. $P(\theta)$ is directly proportional to $R(\theta)$ and the results of ref. 5 follow. (This is true even for the case of heterogeneous co-polymers as long as only one molecular species is present in each detected eluting fraction. If more than a single species is present in any fraction, then they must all have approximately the same refractive index increment, dn/dc). Indeed, the mean square radius may always be determined even for elution regions where there is no differential refractive index (DRI) detector signal. All that is required is that the light scattering signals at the various detectors (angles) be sufficiently strong so that the coefficient of the term linear in $\sin^2 \theta/2$ of eqn. 4 may be determined [5].

Fig. 1 illustrates an excellent example of a strong light scattering signal without a corresponding DRI signal. In the foreground is the DRI signal (marked at the right with the small symbol *ri*) as a function of elution volume while the excess Rayleigh ratios, $R(\theta)$, at the different angles collected by the DAWN detector (Wyatt Technology Corporation, Santa Barbara, CA, USA), are shown behind, also as a function of elution volume. The sample was comprised of a set of biopolymers (in an aqueous buffered solution) used for calibration purposes in HPSEC measurements. At the smallest elution is seen the light scattering signature of a very large aggregate which produces no DRI signal. The z-average root mean square radius for this peak is over 64 nm and easily calculated independently of the concentration, dn/dc, and M_w values.

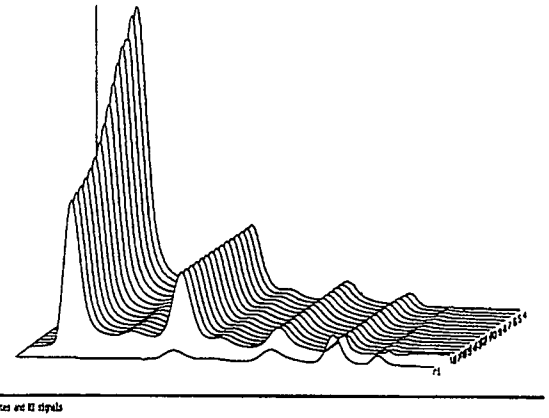

Fig. 1. Rayleigh excess ratio as a function of scattering angle (detector) from a set of biopolymers showing the presence of a large aggregate whose corresponding DRI signal is negligible. This fraction, which yields a very intense and steep variation of scattered light intensity, is shown at the smallest elution volume to the left of the figure.

A great number of papers have been written [6–10] concerning so-called band broadening or instrumental broadening (IB) effects and the corrections to the measured data required to recover the correct mass distribution present in the separated sample. Although by far the greatest broadening occurs within the columns, a smaller, secondary broadening may occur in the mass detector that follows them. With a light-scattering (LS) detector inserted between the columns and the mass detector, the broadening that occurs within the column will not affect the derived weight-average molecular masses as long as the concentration at each eluting slice is known as it reaches the LS detector. Unfortunately, the concentration variation itself may be distorted by the secondary instrumental broadening that occurs *after* the LS detector.

The slight distortions in concentration profiles

that are due to the large DRI dead volumes, tubing mismatches, and other flaws in the subsequent chromatographic are rarely important when measuring polymers of relatively broad distribution. Such secondary distortions, however, become very important for extremely narrow standards such as those used frequently for system calibration for conventional HPSEC. Perhaps of more immediate importance are protein applications where even the slightest instrumental band broadening can yield unreasonable molecular distributions for species known to be monodisperse.

What has been developed here is the ability to measure the secondary IB effects *directly* without disturbing the measurement by introducing an additional detector. It may be reasoned that the secondary broadening caused by a DRI detector may be measured easily by placing two such detectors in sequence. Such an arrangement permits only a determination of the *difference* of the DRI response profile which, in turn, requires a somewhat complex deconvolution to extract the functional form of the net broadening of a single detector. Most DRI detectors, furthermore, have very large diameter tubing after their detection cell (to reduce back pressure) which would affect secondary IB were it not (usually) the last element of the HPSEC system. Using very narrow standards whose root mean square radii are accurately measurable, a light scattering detector can be used to determine most of the broadening of the sample that occurs in the region between the columns and the end of the DRI detector cell, as will be shown presently. For the measurements reported here, only about 17% of the volume contributing to the secondary IB is in the LS detector itself. This will have a small effect on the derived secondary IB which is due primarily to the large volume of tubing often required by the DRI detector to maintain thermal stability.

Fig. 2 presents the excess Rayleigh ratio as a function of detector (angle) measured with a DAWN light scattering detector ($\lambda = 632.8$ nm) from a sample of three polystyrene standards (Pressure Chemical Co., Pittsburgh, PA, USA; lot numbers 30121, 50912 and 80317) separated using two mixed-bed Shodex (Showa Denko, Tokyo, Japan) KF 80M columns at a tetrahydrofuran flow-rate of 1.0 ml/min. Shown in the foreground is the RI signal from a Waters 410 detector, suitably corrected for a volume delay of 173 ml. (This delay volume is made up of approximately 30 μl from DAWN instrument, 11 μl from the tubing connecting the DAWN to the Waters 410 and a dead volume in the Waters 410 from the inlet to the end of the DRI cell of 133 μl. Although the actual cell volume of the Waters 410 is given by the manufacturer as 56 μl, a large tubing dead volume is needed to assure good temperature stability, especially at high flow-rates.) The signals from some detectors have been dropped because of noise. Fig. 3

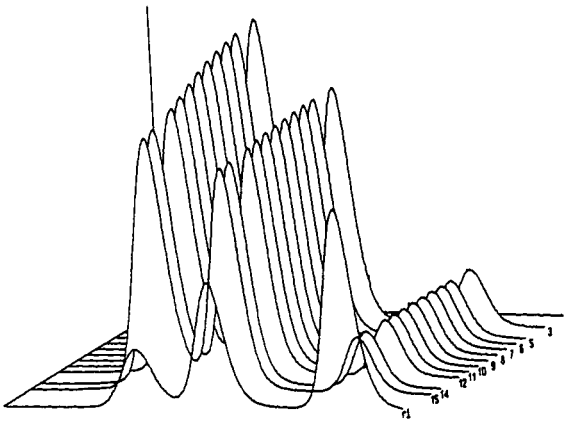

Fig. 2. Rayleigh excess ratio as a function of scattering angle (detector) from three polystyrene standards and contrasted with the corresponding signal from the RI detector, shown in the foreground.

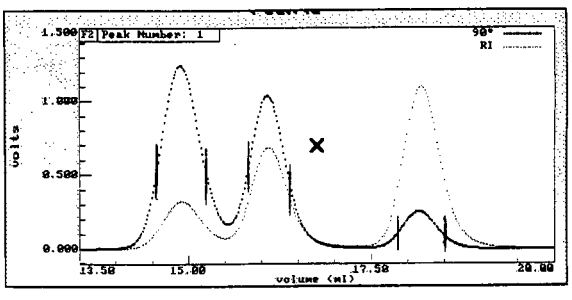

Fig. 3. Light scattering signal from the detector at 90° from Fig. 1 overlaid with the signal from the DRI detector and corrected for the delay volume between the DRI and DAWN instruments. The central region of each peak corresponding approximately to the full width at half maximum is indicated by each pair of vertical bars.

shows the 90° light-scattering signal (DAWN detector 11) overlaid with the DRI signal which is corrected for the 173-μl delay volume. The central regions of each peak, defined approximately as the peak full width at half maximum, are clearly indicated by the vertical bars. The three corresponding weight average molecular masses for these regions as marked are 606 000, 217 000 and 31 300, respectively. The corresponding masses mixed and injected in a 100-μl loop were $9.5 \cdot 10^{-2}$, $1.7 \cdot 10^{-1}$ and $2.7 \cdot 10^{-1}$ mg, respectively.

Table I presents the software (ASTRA, Wyatt) generated light-scattering characteristics of the three narrow regions delineated in Fig. 3. These include the number-, weight- and z-average molecular masses (M_n, M_w and M_z), the corresponding weighted root mean square radii r_{g-n}, r_{g-w} and r_{g-z} and finally the sample polydispersity defined as the ratio M_w/M_n. The columns used for the separation were not optimal as evident from the overlap seen in Fig. 3 between the two larger samples. Nevertheless, the small sample *fractions* delineated in Fig. 3 may have considerably smaller polydispersities than the corresponding *total* samples.

Fig. 4 shows the root mean square radius as a function of elution volume for the three regions selected. Note that for the smallest, 30 000, fraction, the size cannot be clearly derived since it is below the limits of resolution for the 632.8-nm laser wavelength used. Figs. 5 and 6 present, respectively, the corresponding mass variations for the two largest fractions based on calculation by eqn. 1 with the concentration profile generated by the inline DRI detector. Since the root mean square radii for these fractions are *constant*, the corresponding masses also *must be constant*. Thus any deviation from mass constancy must be due entirely to a distortion of the concentration profile at the DRI detector due to secondary broadening effects.

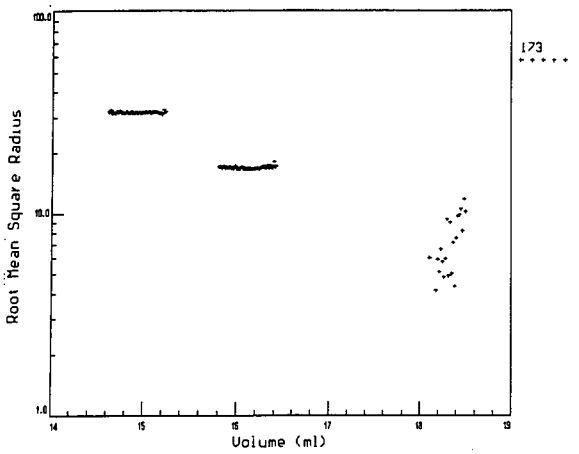

Fig. 4. Root mean square radius *versus* elution volume for the three regions indicated in Fig. 2.

If the weight-average molecular mass at a slice

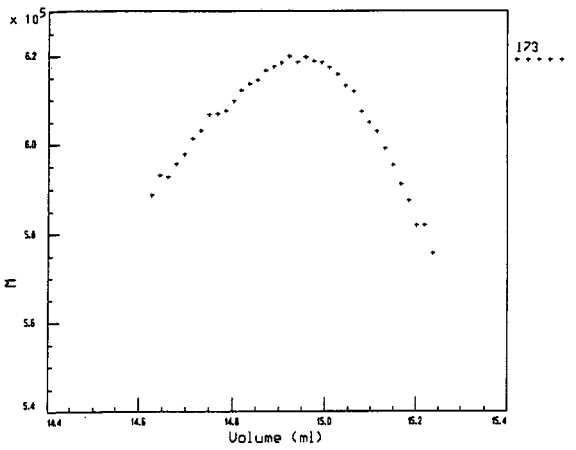

Fig. 5. Apparent mass variation with elution volume for the 606 000 fraction of Fig. 2.

TABLE I

MOLECULAR MOMENTS FROM LIGHT SCATTERING

Peak	M_n	M_w	M_z	r_{g-n}	r_{g-w}	r_{g-z}	M_w/M_n
1	605 870	606 120	606 360	31.7	31.7	31.7	1.0004
2	216 450	216 550	216 650	16.9	16.9	16.9	1.0005
3	31 271	31 297	31 321	6.9	6.9	6.9	1.0008

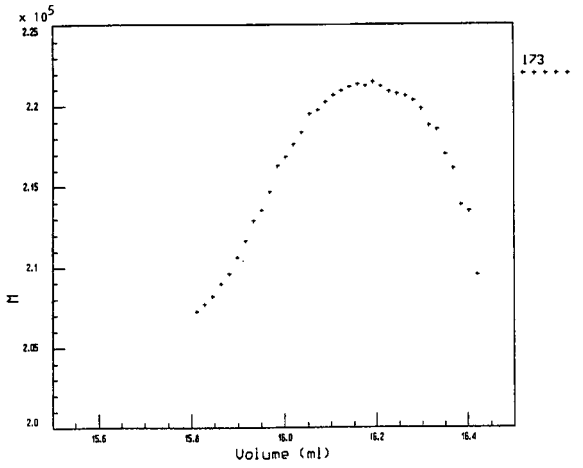

Fig. 6. Apparent mass variation with elution volume for the 217 000 fraction of Fig. 2.

i is given by M_i and the corresponding concentration is c_i, then we have immediately the relationship between the erroneously calculated mass M'_i and the secondary IB distorted concentration, c'_i, as

$$\frac{M'_i}{M_i} = \frac{c_i}{c'_i} = \rho \tag{7}$$

However, since M_i must be constant ($=M$, say) at each slice in the region (since the $\langle r_g^2 \rangle$ values are constant), the corrected concentration c_i for each region where the eluting mass is constant is given simply by

$$c_i = \rho c'_i = c'_i M'_i / M \tag{8}$$

The weight-average molecular mass of the monodisperse sample, M_w, may be determined independently of the HPSEC-derived value (assumed to be slightly in error due to secondary IB) by performing an off-line Zimm [1] plot analysis of the unseparated sample. Thus the secondary instrumental broadening may be measured directly by means of effectively monodisperse standards whose root mean square radii may be determined accurately to be constant over a reasonable range of elution volumes. As pointed out for Gugliotta *et al.* [10] for the case of low-angle light scattering (a subset of the more general form discussed here), the response for a strictly monodisperse sample is proportional to the product of the concentration and molecular mass. Since the molecular mass is constant, the recorded concentration response is directly proportional to the standard spreading function, g(t), *i.e.*

$$g(t) \propto c'_i = c'(t) \tag{9}$$

Although Alba and Meira [11] state that truly monodisperse synthetic polymers are "... impossible to obtain ...", the measurements reported here of size monodispersity, confirm that for selected eluting regions, such monodispersity is small enough to permit the deduction of secondary IB. For example, even with the mass variations shown in Figs. 4 and 5, the corresponding polydispersities (M_w/M_n) are calculated to be 1.0004 and 1.0005, respectively. Introducing a constant mass for each of these fractions reduces the corresponding polydispersities to 1.0000 and 1.0001, respectively. The latter deviation from unity is due entirely to the slight experimental uncertainties. The apparently small uncorrected values have been discussed above.

Although no measure of the mean square radius of the smaller 31 300 fraction is possible, the calculated polydispersity shown in Table I suggests that it too may be quite monodisperse. On this basis, it is instructive to examine the dilution factors ρ for all three mass fractions as a function of $t - t_0$, where t_0 corresponds to the time at which the peak concentration is detected (in seconds) at the DRI detector. These are shown in the abbreviated Table II. (The data were collected every second and only every third point is shown. These data have been smoothed by replacing each value with a three-point average including the values of its two adjacent slices.) At a flow-rate of 1 ml/min, each second corresponds to approximately 16.7 μl. Some rather interesting observations may be made from these results. The dilution factors (secondary IB factors, ρ) are not symmetric (probably due to tailing effects in the intervening volumes); they are a function of molecular mass, but do not appear to vary monotonically with molecular mass; and this latter variation most probably depends on the geometry of the various

TABLE II

DILUTION FACTORS FOR THREE MASS FRACTIONS

$t - t_0$	$\rho_{606\,000}$	$\rho_{217\,000}$	$\rho_{31\,300}$
−15	0.9661	0.9584	0.9382
−12	0.9796	0.9619	0.9636
−9	0.9911	0.9727	0.9842
−6	1.0015	0.9870	0.9945
−3	1.0095	1.0016	1.0100
0	1.0167	1.0121	1.0137
3	1.0211	1.0189	1.0230
6	1.0212	1.0216	1.0247
9	1.0154	1.0215	1.0253
12	1.0032	1.0184	1.0204
15	0.9883	1.0115	1.0083
18	0.9681	0.9961	0.9905

"dead volumes" involved. It is important to stress further than the secondary IB effects measured here are *extremely* small; probably much smaller than might even be noticed since the polydispersities shown in Table I were calculated from the *uncorrected* data and these are in themselves far less than the values quoted by the manufacturer as "less than 1.06". The manufacturer's values are based on HPSEC calibrations and refer to the entire peaks, not just the small central regions selected in this paper. The extremely small secondary IB effects measured here augur well for the future, since much greater secondary IB effects are easily introduced by adding more dead volume introducing tubing of sharply varying crosssections, or permitting kinks or burrs within the tubing. The sensitivity of the technique is very great, though only applicable to molecules sufficiently large so that their mean square radii may be determined accurately.

The thesis proposed in this paper, that uniformity of the derived mean square radius allows one to conclude that the selected sample has a similarly monodisperse mass distribution should prove to be extremely important for examining explicitly the form of secondary instrumental broadening (without the introduction of any major assumptions) as a function of molecular mass, flow-rate, column structure, the volume delay between columns and detectors, and the dead volume of the detectors themselves. Alba and Meira are certainly correct when they state that truly monodisperse synthetic polymers are impossible to obtain. However, the ability to examine *nearly* monodisperse fractions of HPSEC-separated "narrow" standards has been shown to permit the detection and quantification of secondary IB effects that are in themselves extremely small. As mentioned earlier, the applications of the technique to proteins will be the most important. The secondary broadening that occurs after the LS detection may be probed by proteins of known narrow distributions even if they are too small to confirm such mondispersity by means of measurements of the corresponding mean square radius.

ACKNOWLEDGEMENTS

The skillful experimental measurements of Lena Nilsson and Janet Howie are gratefully acknowledged. The contributions of Dr. Louis Papazian and Dr. David Shortt to the analytical interpretations presented in this paper are appreciated.

REFERENCES

1 B.H. Zimm, *J. Chem. Phys.*, 16 (1948) 1093.
2 H.C. van de Hulst, *Light Scattering by Small Particles*, Dover, New York, 1981.
3 P. Debye, *J. Phys. Colloid Chem.*, 51 (1947) 18.
4 P.F. Mijnlieff and D.J. Coumou, *J. Colloid Interface Sci.*, 27 (1968) 553.
5 P.J. Wyatt, *Anal. Chim. Acta*, 272 (1993) 1.
6 L.H. Tung, *J. Appl. Polym. Sci.*, 10 (1966) 375.
7 L.H. Tung, *J. Appl. Polym. Sci.*, 13 (1969) 775.
8 K.S. Chang and Y.M. Huang, *J. Appl. Polym. Sci.*, 16 (1972) 329.
9 T. Ishige, S.-I. Lee and A.E. Hamielec, *J. Appl. Polym. Sci.*, 15 (1971) 1607.
10 L.M. Gugliotta, J.R. Vega and G.R. Meira, *J. Liq. Chromatogr.*, 17 (1990) 1671.
11 D. Alba and G.R. Meira, *J. Liq. Chromatogr.*, 9 (1986) 1141.

Journal of Chromatography, 648 (1993) 33–39
Elsevier Science Publishers B.V., Amsterdam

CHROMSYMP. 2789

Characterization of high-molecular-mass polyethylenes by gel permeation chromatography–low-angle laser-light scattering

A. Willem deGroot* and Wayne J. Hamre

Polyolefins Research, B-3833 Building, Dow USA Texas Operations, 2301 Brazosport Boulevard, Freeport, TX 77541-3257 (USA)

ABSTRACT

Gel permeation chromatography–low-angle laser-light scattering (GPC–LALLS) has been applied to the analysis of high-molecular-mass polyolefins. It was found that changing the particle size of the column packing from 10 to approximately 50 μm resulted in an increase in the molecular mass of NBS 1476 of from 100 000 to 195 000. It was also found that changing the flow-rate from 1.0 to 0.1 ml/min resulted in an increase in the molecular mass of the same sample of from 195 000 to 280 000 for the large particle size gel columns. Increases were also seen with commercial low-density samples when changing these same conditions, but the increases were not as large in magnitude. A change in the frit size on the columns did not seem to have an effect on the measured molecular masses of the NBS 1476 samples. Another finding in this study was that slurry high-density polyethylene samples which previously had been very difficult to characterize using GPC–LALLS gave much higher molecular masses which were much more reproducible when characterized using the large particle size columns with low flow-rates.

INTRODUCTION

Since its development as a practical technique [1–3], classical wide-angle light scattering has proven to be a very powerful tool for the polymer chemist studying polyethylene. The technique can give absolute mass-average molecular masses, second virial coefficients and radii of gyration of dissolved polyethylene in solution [4,5]. Its main limitation is its difficulty of use and the fact that it does not give any information on the polydispersity of the sample. Conversely, gel permeation chromatography (GPC) is generally much easier to use and gives an approximation of all the molecular mass averages [6,7]. The disadvantages of this technique are that it requires calibration and it is capable of only giving an apparent molecular mass for polyethylenes with long chain branching, *i.e.*, low-density polyethylenes. In theory then, the combination of these two polymer characterization tools should result in a very powerful technique which should give *z*-average, mass-average, and number average molecular masses without calibration. With the advent of a low-angle laser-light scattering instrument (LALLS) it is now possible to combine the two techniques [8–11] and this has been applied to the analysis of polyolefins [12–14]. It has also been reported that the combination of these two characterization methods can be used to determine the level of long chain branching in low-density polyethylenes [15–17].

We have observed many difficulties over the last few years in our attempts to characterize the molecular mass of higher-molecular-mass polyethylene resins using GPC–LALLS. These include poor reproducibility of both the LALLS and the differential refractive index (DRI) detec-

* Corresponding author.

tor responses, spiking in the LALLS detector response, partial plugging represented by increases in the pressure transducer response, and lack of correlation with rheological data. All of these results seem to suggest that the polymer is having difficulty passing through the GPC column due to resistance in the frits, in the gel itself, or perhaps in the post-column filter. Another example of the difficulty in characterizing high-molecular-mass polyethylene can be found in the literature on National Bureau of Standards (NBS) 1476 polyethylene standard. The value obtained typically for the mass-average molecular mass using static light scattering has been around 215 000 g/mol [4,12,13], but the value obtained with GPC–LALLS is generally reported to be around 100 000 g/mol [12,13]. There are currently three theories in the literature which attempt to explain this phenomenon. One states that there is a small amount of high-molecular-mass polymer in NBS 1476 which is filtered out [4,12]. A second theory states that the small amount of high-molecular-mass polymer in NBS 1476 is diluted to such an extent that it is undetectable by the LALLS detector [13]. The third theory states that there is shear degradation during the GPC experiment [13]. Indeed, there are several references in the literature concerning shear degradation during the GPC experiment [18–21], one of which involves shear degradation of polyolefins [22].

In an effort to determine the exact cause of these difficulties in characterizing high-molecular-mass polyethylenes a detailed program was begun to evaluate GPC columns with different frit sizes and particle sizes. This report was written to discuss the initial findings of this study.

MATERIALS AND METHODS

The LALLS measurements were made using a Chromatix Model KMX-6 low-angle laser-light scattering instrument. This instrument incorporates a He–Ne laser source with a wavelength of 632.8 nm. The GPC system used was the Waters Model 150-C GPC/ALC. Molecular masses were calculated using laboratory-written software. The mass average molecular masses reported were determined using the method proposed first by Martin [23].

TABLE I

DESCRIPTION OF THE RESINS USED IN THIS STUDY

Resin	MI[a]	Density	Description
NBS 1475	2.07	0.9784	High-density polyethylene
NBS 1476	1.19	0.9312	Low-density polyethylene
LDPE-A	8.0	0.916	Low-density polyethylene
LDPE-B	4.2	0.924	Low-density polyethylene
LLDPE-A	1.0	0.92	Linear low-density polyethylene
HMW-HDPE	0.2	0.965	High-molecular-mass high-density polyethylene

[a] Melt indices were determined using the standard ASTM melt index test [24].

The solutions for study by GPC–LALLS were prepared by dissolving the samples in 1,2,4-trichlorobenzene (TCB) for at least 3 h at 160°C. All samples were prepared on a mass-to-mass basis using 1.304 g/ml for the density of TCB at 145°C. Butylated hydroxytoluene was used as a free radical scavenger and its concentration was 250 ppm (w/w).

The samples used are listed in Table I. Three sets of GPC columns were donated by Polymer Labs., one set was donated by Waters, and one set was purchased from Phenomenex. All column sets consisted of three columns. The exclusion limit of all the columns tested was approximately molecular mass $10 \cdot 10^6$ using polystyrene. These columns are described in more detail in Table II.

DISCUSSION

One of the first big challenges in characterizing polyethylenes by GPC–LALLS is to get from the point where the LALLS detector response has very few spikes. There are several keys to getting to this point. First, the column set being used must not be shedding particles. It helps tremendously to have a 0.5-μm filter in place after the column set to aid in this. However, often this is not enough and a new column set must be

TABLE II

DESCRIPTION OF GPC COLUMNS USED IN THIS STUDY

Column manufacturer	Particle size (μm)	Column type	Frit size (μm)
Polymer Labs.[a]	10	Mixed bed	3
Polymer Labs.[a]	20	Mixed bed	5
Polymer Labs.[a]	20	Mixed bed	10
Phenomenex[b]	20	Individual pore sizes 10^6, 10^5, 10^4 Å	10
Waters' Styragel[c]	30–60	Individual pore sizes 10^5, 10^6 Å	10

[a] Three columns 300 × 7.5 mm in size.
[b] Three columns 300 × 7.8 mm in size.
[c] Three columns 300 × 7.8 mm in size.

"bled" of particles for several weeks. (The length of time seems to be related to particle size with the larger particle size gel taking less time). Second, there must not be any cold spots in the system which can cause polymer to crystallize. Finally, the sample must be completely dissolved. These steps are somewhat different than those necessary to obtain good static light scattering data. This requires well filtered solutions and extremely clean glassware. In GPC–LALLS it appears that the columns themselves act as a very efficient filtration system and alleviate the necessity of cleaning glassware and often even filtering the samples.

Another big challenge in characterizing polyethylene is data interpretation. The LALLS detector often detects small amounts of polymer, sometimes referred to as microgel, which is not detected by the DRI detector. This is because the LALLS detector response is proportional to both the mass-average molecular mass and the concentration, whereas the DRI detector response is only proportional to the concentration. An example of this is shown in Fig. 1. Here one can see that there is a small amount of polyethylene which is not "seen" by the DRI detector, but gives a very strong response from the LALLS photomultiplier tube. This indicates that the polymer is very low in concentration, but very high in molecular mass. If one were to use the standard calculations to calculate the molecular mass of this sample, *i.e.*, see eqn. 1 below, the mass-average molecular mass would be under predicted because the DRI detector response has returned to baseline where there is still a LALLS detector response.

$$\frac{Kc_i}{R_{\theta i}} = \frac{1}{M_{wi}} + 2A_{2i}c_i \tag{1}$$

In equation 1 above, K is the optical constant defined in eqn. 2 below, c_i is the concentration at each elution volume, $R_{\theta i}$ is Rayleigh's ratio at each elution volume, M_{wi} is the mass-average molecular mass of the sample at each elution volume, and A_{2i} is the second virial coefficient at each elution volume.

$$K = \frac{2\pi^2 n^2}{\lambda^4 N_A} \cdot \left(\frac{dn}{dc}\right)^2 (1 + \cos^2\theta) \tag{2}$$

In eqn. 2 π has its normal value, n is the refractive index of the solution, λ is the wavelength of light, N_A is Avogadro's number, (dn/dc) is the refractive index increment, and θ is the

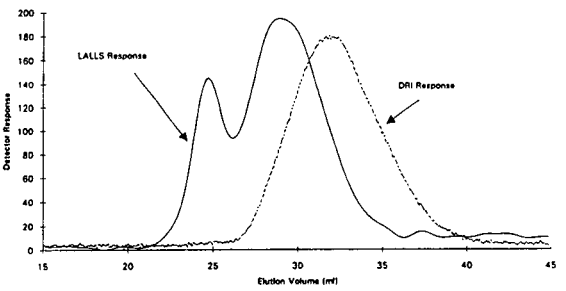

Fig. 1. DRI and LALLS detector responses for NBS 1476.

angle of the measurement. In low-angle laser-light scattering θ is typically less than 10 and $(1 + \cos^2 \theta)$ reduces to a value of two.

The molecular mass calculated from eqn. 1 for the data in Fig. 1 is 105 000 g/mol. This value is obviously low since at several of the early elution volumes the concentration is zero. A way to get a better approximation of the mass-average molecular mass of this sample is to use the method first described by Martin [23] (eqn. 3 below). In this method the total area of the LALLS detector response and the total concentration are used. The value obtained for the data in Fig. 1 by this method is 122 000 g/mol. Although the value here is higher it is still much lower than the value found for static light scattering for NBS 1476.

$$M_w = \frac{k_c}{Kk_{LS}} \cdot \frac{\text{total peak area of the LALLS signal}}{\text{total peak area of the DRI signal}} \quad (3)$$

Here k_c is the proportionality constant between the signal of the DRI detector and the concentration, k_{LS} is the similar constant for the LALLS detector signal, and K is defined in eqn. 2 above. A potential disadvantage of this equation is that the second virial coefficient cannot be used since the concentration is not calculated at each elution volume. This is not a problem for polyethylene, however, since the value of the second virial coefficient in TCB is so low [12].

Another problem which we have experienced is specific to high-molecular-mass, high-density polyethylenes (HMW-HDPEs). This problem is best described as a lack of reproducibility and a large amount of spiking as shown in Fig. 2 and Table III. Fig. 2 shows the LALLS detector response for a typical HMW-HDPE sample run using the Polymer Labs.' 10-μm columns and a 1.0 ml/min flow-rate. As can be seen, there is a tremendous amount of spiking present. The data in Table III were calculated using the area under the LALLS detector response for 5 samples run back to back. These data may actually be a little misleading, since they were smoothed and de-spiked before being reduced.

To address this problem, we began a study to evaluate several different column particle sizes and frit sizes to determine if the problems we were seeing with HMW-HDPEs were a result of shear degradation in the columns. Table I describes the samples used, Table II describes the columns used and Tables IV–VIII show the results of a flow-rate study using each of the column sets.

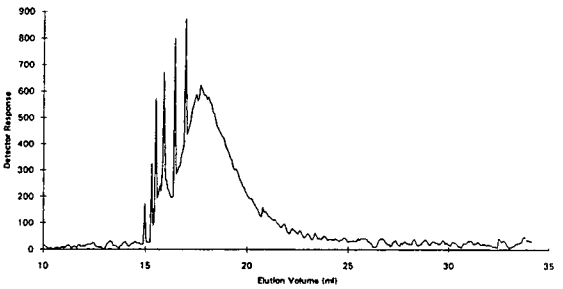

Fig. 2. LALLS detector response for HMW-HDPEs. Polymer Labs.' 10-μm columns, 1.0 ml/min flow-rate.

NBS 1475 was used as a standard to show that the instrument was operating properly. As indi-

TABLE III

GPC–LALLS REPRODUCIBILITY STUDY OF HMW-HDPE RESIN USING POLYMER LABS.' 10-μm COLUMNS AND A 1.0 ml/min FLOW-RATE

Run	M_w
1	$2.36 \cdot 10^5$
2	$2.84 \cdot 10^5$
3	$2.56 \cdot 10^5$
4	$2.70 \cdot 10^5$
5	$2.50 \cdot 10^5$
R.S.D. (%)	7.1

TABLE IV

GPC–LALLS RESULTS ON THE POLYMER LABS.' 10-μm GPC COLUMNS

Resin	M_w		
	1.0 ml/min	0.2 ml/min	0.1 ml/min
NBS 1475	$5.4 \cdot 10^4$	$5.33 \cdot 10^4$	$5.67 \cdot 10^4$
NBS 1476	$1.01 \cdot 10^5$	$1.34 \cdot 10^5$	$1.4 \cdot 10^5$
LDPE-A	$4.62 \cdot 10^5$	–	$4.77 \cdot 10^5$
LDPE-B	$2.7 \cdot 10^5$	–	$2.91 \cdot 10^5$
LLDPE-A	$1.25 \cdot 10^5$	–	$1.33 \cdot 10^5$

TABLE V

GPC–LALLS RESULTS ON POLYMER LABS.' 20-μm PARTICLE SIZE COLUMNS WITH 10-μm FRITS

Resin	M_w		
	1.0 ml/min	0.2 ml/min	0.1 ml/min
NBS 1475	$5.18 \cdot 10^4$	$5.21 \cdot 10^4$	$5.27 \cdot 10^4$
NBS 1476	$1.17 \cdot 10^5$	$1.58 \cdot 10^5$	$1.99 \cdot 10^5$
LDPE-A	$5.41 \cdot 10^5$	$5.51 \cdot 10^5$	$5.85 \cdot 10^5$
LDPE-B	$2.95 \cdot 10^5$	$3.05 \cdot 10^5$	$3.19 \cdot 10^5$
LLDPE-A	$1.25 \cdot 10^5$	$1.27 \cdot 10^5$	$1.23 \cdot 10^5$

TABLE VI

GPC–LALLS RESULTS ON POLYMER LABS.' 20-μm PARTICLE SIZE COLUMNS WITH 5-μm FRITS

Sample	M_w		
	1.0 ml/min	0.2 ml/min	0.1 ml/min
NBS 1475	$5.55 \cdot 10^4$	$5.43 \cdot 10^4$	–
NBS 1476	$1.20 \cdot 10^5$	$1.65 \cdot 10^5$	–

TABLE VII

GPC–LALLS RESULTS ON PHENOMENEX 20-μm PARTICLE SIZE COLUMNS WITH A 10-μm FRIT

Sample	M_w		
	1.0 ml/min	0.2 ml/min	0.1 ml/min
NBS 1475	$5.2 \cdot 10^4$	–	–
NBS 1476	$1.09 \cdot 10^5$	–	–

TABLE VIII

GPC–LALLS RESULTS FOR THE WATERS STYRAGEL COLUMNS

Resin	M_w		
	1.0 ml/min	0.2 ml/min	0.1 ml/min
NBS 1475	$6.1 \cdot 10^4$	$5.38 \cdot 10^4$	$5.7 \cdot 10^4$
NBS 1476	$1.95 \cdot 10^5$	$2.07 \cdot 10^5$	$2.77 \cdot 10^5$
LDPE-A	$6{:}32 \cdot 10^5$	$6.17 \cdot 10^5$	$6.25 \cdot 10^5$
LDPE-B	$3.64 \cdot 10^5$	$3.41 \cdot 10^5$	$3.55 \cdot 10^5$
LLDPE-A	$1.44 \cdot 10^5$	$1.37 \cdot 10^5$	$1.45 \cdot 10^5$

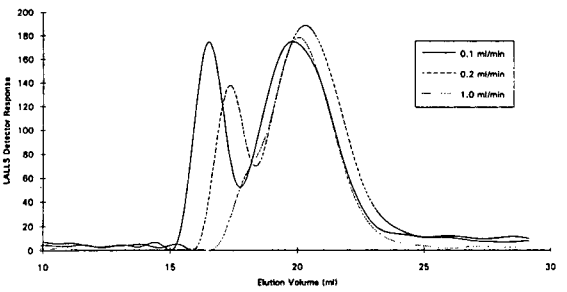

Fig. 3. LALLS detector response for NBS 1476. Polymer Labs.' 10-μm columns.

cated in Tables IV–VIII, the mass-average molecular mass of NBS 1475 was consistently around 55 000 g/mol and was independent of the flow-rate or column set used. Conversely, the molecular mass of NBS 1476 varied dramatically with flow-rate and particle size of the column packing. This is shown in Figs. 3–5 and Tables IV, V and VIII. These data strongly suggest that NBS 1476 is shear degraded as it passes through the GPC columns, since the molecular mass is dependent on both particle size and flow-rate. Interestingly, in Fig. 5 there is an extra peak in the LALLS detector response around an elution volume of 11 ml. This is most likely totally excluded polymer. At the lower flow-rates this very-high-molecular-mass polymer has more time to diffuse into and out of void spaces and is retained a little, thus the peak does not appear at the lower flow-rates. It probably does not appear in the other smaller particle size column sets because it is shear degraded down to a smaller size.

Another interesting finding of this study was

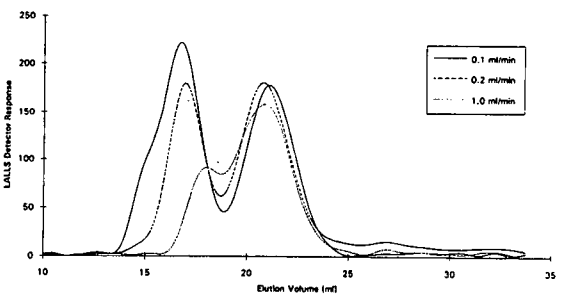

Fig. 4. LALLS detector response for NBS 1476. Polymer Labs.' 20-μm columns.

that the mass-average molecular mass of NBS 1476 was up around 280 000 g/mol. This is higher than had been found before. However, Stejskal *et al.* [4] found a molecular mass of 254 000 g/mol and suggested that the molecular mass could be higher because of errors which occur in extrapolating to zero concentration and angle in the Zimm plot.

Frit size did not seem to make a difference. This is demonstrated by comparing the molecular mass of NBS 1476 determined using the Polymer Labs.' 20-μm columns with 5- and 10-μm frit sizes. This seems reasonable since the post-column filter size is much smaller, *i.e.*, 0.5 *versus* 5 and 10 μm.

We also investigated two commercial low-density products and a linear-low-density product to determine if the molecular mass of these resins was affected by flow-rate. These samples are described in Table I and the molecular mass data are shown in Tables IV, V and VIII. The values show that varying the flow-rate had very little effect on the molecular mass of the LLDPE resin. There was an effect on the two LDPEs, however, it was much smaller than the effect on NBS 1476. The most likely explanation for this phenomenon is that these samples did not contain the small amount of very-high-molecular-mass polymer which NBS 1476 contains. It is this very-high-molecular-mass polymer or microgel which is sensitive to the shear degradation.

Another interesting finding of this flow-rate and particle size study was that the spiking found typically for HMW-HDPE resins disappeared when the flow-rate was at 0.2 ml/min or less. This finding was very exciting and allowed us to greatly improve the reproducibility of our molecular mass characterization of these resins. The results of a reproducibility study for the same sample shown in Fig. 2 and Table III are shown in Table IX. An overlay of the LALLS detector responses are shown in Fig. 6. As indicated in Table IX, the data at the lower flow-rates with the larger particle size columns is much more reproducible and the molecular masses are much higher. In the past spiking has been attributed to incomplete dissolution of HMW-HDPEs even though dissolution is carried out well above the melting point of the polymer [25]. The data here indicates that the spiking may be attributed to a chromatographic phenomenon, perhaps polarization as described by Giddings [19]. The polarization effect could cause high molecular mass polymer to concentrate and thus come out of solution.

The results of this study indicate that there is severe shear degradation occurring during the passage of NBS 1476 through smaller particle size GPC columns. This finding successfully

TABLE IX

GPC–LALLS REPRODUCIBILITY STUDY USING WATERS' STYRAGEL COLUMNS WITH 0.1 ml/min FLOW-RATE

Run	M_w
1	$1.60 \cdot 10^6$
2	$1.57 \cdot 10^6$
3	$1.55 \cdot 10^6$
4	$1.63 \cdot 10^6$
5	$1.64 \cdot 10^6$
R.S.D. (%)	2.4

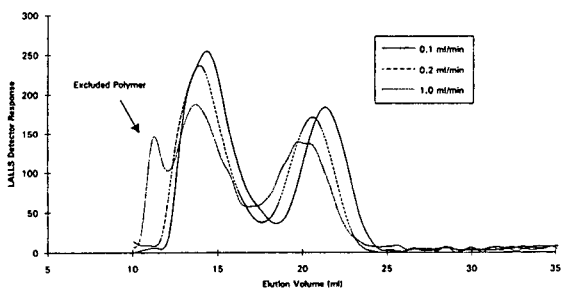

Fig. 5. LALLS detector response for NBS 1476. Waters' Styragel columns.

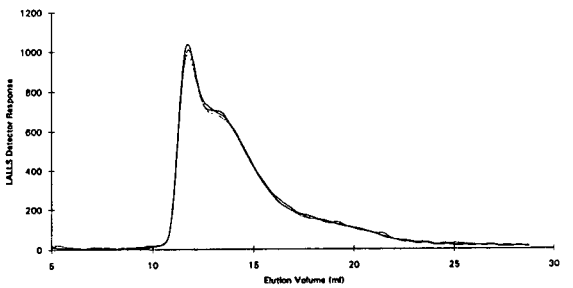

Fig. 6. LALLS detector response for HMW-HDPE. Waters' Styragel columns, 0.1 ml/min flow-rate.

explains the discrepancy which has existed in the literature for several years between the molecular mass of NBS 1476 determined using the GPC–LALLS technique and the molecular mass determined using static light scattering. This finding will also allow us to determine more accurate molecular masses for higher-molecular-mass polyethylenes. Finally, a method was developed which allows us to characterize the molecular mass of HMW-HDPEs.

ACKNOWLEDGEMENTS

The authors would like to thank Dr. John McConville and Dr. Elizabeth Meehan of Polymer Laboratories and Mr. Joe Arsenault of Waters for their donation of the column sets used in this study.

REFERENCES

1 P. Kratochvil, *Introduction to Classical Light Scattering from Polymer Solutions*, Elsevier, Amsterdam, New York, 1987.
2 M.B. Huglin (Editor), *Light Scattering from Polymer Solutions*, Academic Press, London, 1972.
3 K.A. Stacey, *Light-Scattering in Physical Chemistry*, Butterworths, London, 1956.
4 J. Stejskal, J. Horska and P. Kratochvil, *J. Appl. Polym. Sci.*, 27 (1982) 3929.
5 F.W. Billmeyer, *J. Am. Chem. Soc.*, 75 (1953) 6118.
6 W.W. Yau, J.J. Kirkland and D.D. Bly, *Modern Size-Exclusion Liquid Chromatography*, Wiley, New York (1979).
7 B.J. Hunt and S.R. Holding, *Size Exclusion Chromatography*, Blackie, Glasgow, 1989.
8 A.C. Ouano, *J. Chromatogr.*, 118 (1976) 303.
9 A.C. Ouano and W. Kaye, *J. Polym. Sci.*, 12 (1973) 541.
10 T.L. Hjertberg, I. Kulin and E. Sorvik, *Polym. Testing*, 3 (1983) 267.
11 H.G. Barth and S.S. Huang, *ANTEC* (1986) 473.
12 T.B. MacRury and M.L. McConnell, *J. App. Polym. Sci.*, 24 (1979) 651.
13 V. Grinshpun, K.F. O'Driscoll and A. Rudin, *J. Appl. Polym. Sci.*, 29 (1984) 1071.
14 A.W. deGroot, *J. Appl. Polym. Sci: App. Polym. Symp.*, 43 (1989) 85.
15 A. Hamielec, *Pure Appl. Chem.*, 54 (1982) 293.
16 D.E. Axelson and W. C. Knapp, *J. Appl. Polym. Sci.*, 25 (1980) 119.
17 P. Lang and W. Burchard, *Makromol. Chem., Rapid Commun.*, 8 (1987) 451.
18 H.G. Barth and F.J. Carlin, Jr., *J. Liq. Chromatogr.*, 7 (1984) 1717.
19 J.C. Giddings, *Adv. Chromatogr.*, 20 (1982) 217.
20 W.G. Rand and A.K. Mukherji, *J. Polym. Sci.: Polym. Lett. Ed.*, 20 (1982) 501.
21 E.L. Slagowski, L.J. Fetters and D. McIntyre, *Macromolecules*, 7 (1974) 394.
22 J.G. Rooney and G. VerStrate, in J. Cazes (Editor), *Liquid Chromatography of Polymers and Related Materials*, Vol. 3, Marcel Dekker, New York, 1981, p. 207.
23 M. Martin, *Chromatographia*, 15 (1982) 426.
24 American Society for Testing Materials, Philadelphia, PA, method ASTM D-1238.
25 V. Grinshpun, K.F. O'Driscoll and A. Rudin, *Am. Chem. Soc. Symp. Ser.*, 245 (1984) 273.

Journal of Chromatography, 648 (1993) 41–69
Elsevier Science Publishers B.V., Amsterdam

CHROMSYMP. 2871

Mechanism of size-exclusion chromatography

I. Role of convection and obstructed diffusion in size-exclusion chromatography

M. Potschka

Porzellangasse 19/2/9, A-1090 Vienna (Austria)

ABSTRACT

Based on experimental evidence, this paper establishes a proper theory of obstructed diffusion which includes the behaviour of polyelectrolytes at low ionic strength and has relevance far beyond chromatography. In addition, it establishes the role of convection in the chromatographic transport process within the porous matrix, which consequently is totally porous and filled with a slowly moving "stagnant" zone. Convection is a crucial factor for the high resolution of modern HPLC columns and size-exclusion chromatographic analysis of ultra-large polymers would be impossible otherwise. Convection processes in the mobile and stagnant zones, of course, are related and a proper description of eddy dispersion thus facilitates understanding of the process within the pores. The processes of dispersion and retention are demonstrated to be governed by different measures of size which delimits the role of transport processes in the mechanism of retention and provides information on the asymmetry of polymer shape by the same experiment. The comprehensive interpretation of chromatographic dispersion facilitates *a priori* modelling of resolution, improves size distribution analysis via straightforward correction of physical dispersion and certainly enriches our physical intuition.

INTRODUCTION

Transport through porous media is of relevance not only to chromatography, but also to heterogeneous catalysis, photographic processes, membrane separations, enhanced oil recovery, organ cultures, cell biophysics and more. Obstructed diffusion has been observed in all instances and has been studied by a variety of methods. Contrary to widespread presumption, however, a proper quantitative theory remains to be identified. Transport may also occur by convection, which is certainly more complex and less well understood, both experimentally and theoretically.

This paper analyses the factors that determine peak width (dispersion) in size-exclusion chromatography (SEC). The simultaneous contribution of a variety of parameters to dispersion can only be disentangled by varying the experimental conditions. Of the many factors, emphasis will be placed on the mass transfer term C (in Van Deemter's terminology), which describes the hydrodynamic process in the so-called stagnant zone within the porous matrix. Traditionally this process is considered to be entirely due to diffusion, in part because it had been assumed that the porous beads contained dead-end pores, a model still found in many textbooks. The parameters that define this obstructed diffusion then can be deduced in order to clarity the theory of diffusion in restricted spaces. Electron microscopy, however, demonstrates that chromatographic media are totally porous (reviewed in ref. 1). The existence of interconnected flow-through capillaries rather than of dead-end pores provides for the possibility that under certain conditions convection augments, or even domi-

0021-9673/93/$06.00

nates, the mass transport. Unrecognized, derived parameters of obstructed diffusion would be in systematic error. Only very limited experimental evidence is available on the latter problem.

The purpose of this study was to illuminate the role of convective mass transfer for standard SEC operation and properly identify it in order to test unambiguously the theory of obstructed diffusion. The present investigation also addresses and revises the mobile zone term A, whose proper functional form and magnitude are crucial for the analysis of convection and diffusion in the stagnant zone, both because the C-term quantitatively depends on proper values for the other factors, and because it conceptually helps to model the equivalent situation of convection in the so-called stagnant zone.

As analysis depends on a proper account of all factors that contribute to peak dispersion and no up-to-date review is available, the subject is introduced in the Theory section. To document the crucial role of convection, its functional terms are facultatively omitted from data analysis. For the sake of clarity and because of uncertainty about their correctness, convective terms are therefore not even included in the Theory section but are introduced in the second part of the Discussion. The Theory section thus provides a refined but still conventional apparatus that the Results section uses for data analysis. The observed inconsistent variability of apparent obstruction is taken as evidence for the occurrence of convection and clearly documents the magnitudes that properly extended theory will have to account for via convection. The first part of the Discussion then compares the experimental results with previously published data on obstructed diffusion and with its relevant theory. Finally, the second part of the discussion explicitly summarizes the emerging understanding of convection in porous matrices.

THEORY

Hydraulic properties of porous networks

Normal chromatography takes place under flow and diffusive and convective properties are closely related to geometric and hydraulic characteristics. One decisive criterion is the regime of flow that one is dealing with: molecular or continuum, laminar, inertial or turbulent. To this end, the ratio of inertial force to viscous force is crucial. This ratio is called the Reynolds number, Re [2], but its numerical significance depends on the geometric topology involved. If we equate the characteristic length with the bead diameter we obtain for the interstitial volume

$$Re = \frac{d\,(\mu\text{m}) \cdot \rho\,(\text{g/ml})}{100 \cdot \eta\,(\text{cP})} \cdot c\,(\text{cm/s}) = \frac{L\,(\text{cm}) \cdot d\,(\mu\text{m}) \cdot \rho\,(\text{g/ml})}{6000 \cdot V_{\text{void}}\,(\text{ml}) \cdot \eta\,(\text{cP})} \cdot \text{flux}\,(\text{ml/min}) \quad (1)$$

where ρ is the fluid density, η its viscosity and c the actual mean linear fluid velocity in the interstitial space, which should not be confused with the superficial velocity defined for the equivalent empty column. Unfortunately, some workers even interchange the labels for the various possible definitions of velocity (see, e.g., ref. 3). The column parameters are given in Table I.

The use of the total liquid flux in eqn. 1 assumes that flow through the pores contributes a negligible volume. This will be justified below. Under normal operating conditions $Re < 0.01$ and the extremal value that can be reached with say TSK6000PW is $Re = 0.04$. This is well within $Re < 0.1$, which is considered the laminar regime dominated by viscous forces [4]. This is also the region of geometric scaling. Inertial effects are said to become dominant for $Re > 1$ and turbulence starts at *ca.* $10Re$ for packed beds [5] and much later for open-tubular capillaries. The Reynolds number for the pores is always smaller than that of the interstitial volume given above. With liquids one is dealing with the continuum regime, as the mean free path length in liquids is of the order of ångstroms, *i.e.*, much smaller than the dimensions of the pores.

Chromatographic columns contain two sizes of cavities, the interstitial space and the pores proper, in parallel across the same pressure drop. According to the Hagen–Poiseuille equation [6–8], the ratio of the flow-rates is proportional to the square of the ratio of their radii. The radius of the cavity created by spherical

TABLE I

COLUMN PARAMETERS

Property	Symbol and units	TSK6000PW	TSK5000PW	Superose-6	Superose-12
pH stability range	pH	2–12	2–12	1–14	1–14
Maximum back-pressure	Δp_{max} (bar)	5	10	10	20
Shape of beads		Spherical	Spherical	Spherical	Spherical
Bead diameter	d (μm)	25 (±5)[a]	17 (±2)[a]	13 (±2)	10 (±2)
Column length	L (cm)	60	60	30	30
Total column volume	V_{column} (ml)	26.5	26.5	23.6	23.6
Total liquid volume	V_{tot} (ml)	23.0	21.85	21.75	19.5
Interstitial volume	V_{void} (ml)	*ca.* 10[b]	10.2	7.0	7.6
Interstitial porosity	$p_i = \frac{V_{void}}{V_{column}}$	*ca.* 0.38[b]	0.38	0.30	0.32
Bead porosity	$p_b = \frac{V_{tot} - V_{void}}{V_{column} - V_{void}}$	0.87	0.71	0.89	0.74
Tortuosity factor[c]	ξ_1/p_b	1.22	1.71	1.18	1.60
Maximum pore radius[d]	R_{max} (nm)	*ca.* 370	55	27	13
Average pore radius[e]	$R_{1/2}$ (nm)	*ca.* 125	36	25	14
Convective factor	$Cf = \frac{10^6 \cdot [d\ (\mu m)]^2}{9 \cdot [R_{max}\ (nm)]^2} \left(\frac{p_i}{1-p_i}\right)^2$	190	4000	4700	13 000

[a] Note that TSK-PW columns are now sold with modified specifications [145].
[b] Based on similar values for TSK5000PW.
[c] Using eqn. 17 with p_b.
[d] Measured from the minimum size R_{SEC} of solutes that still elute at V_{void} under conditions where interfacial repulsion R_{IF} is a minimum but without correcting for it. The true R_{max} and pore size distribution are therefore larger than suggested by the table.
[e] From ref. 72, with revision.

beads may be approximated from the diameter of the bead as [9,10]

$$r_i = \frac{d}{3} \cdot \frac{p_i}{1-p_i} \quad (2)$$

where p_i is the interstitial porosity and d is the z-average bead diameter. Close random packing is not required. Interstitial porosity is a trivial measure of the quality in packing the column and is independent of bead size. In the literature a value of $p_i = 0.36$ is considered an optimum close random packing of spheres [9,11]. For comparison, hexagonal close packing yields $p_i = 0.26$ [12]. Pore radii are measured chromatographically and typical values are listed in Table I. The ratio of the interstitial flow-rate to the flow-rate inside the pores is thus introduced as the convective factor:

$$Cf = \frac{10^6 \cdot d^2\ (\mu m)}{9 \cdot R_{max}^2\ (nm)} \left(\frac{p_i}{1-p_i}\right)^2 \quad (3)$$

Typical Cf values are listed in Table I. Clearly, most of the liquid flow is due to the interstices between the beads in all instances. This is supported by the observation that the pressure drop Δp is the same for equally sized beads regardless of their pore size [13].

Judged by the Cf values, the liquid of the porous network within the beads is effectively stagnant. This justifies the standard model of SEC in spite of flow-through capillaries, namely a parallel process of flow between the beads and diffusion into a stagnant liquid inside the beads. However, the finite flow that nonetheless is present in the quasi-stagnant zone may augment diffusion via convective transport. The role of convection within the pores is therefore to be judged by comparison with diffusion rates and not with bulk flow. A traditional measure of diffusion rate is the Peclet number, specified below, which assumes a standard three-dimensional random walk. Numerical factors aside,

convection dominates the distribution of solute inside the porous network of the beads whenever the Peclet number *Pe* exceeds the convective factor *Cf*. According to this rationale the dominant mode of solute transport in the so-called stagnant zone is expected to be convection for TSK6000PW but diffusion for Superose-12 (Table I). Fig. 1 illustrates the situation. The onset of convection is most easily recognized by analysing peak dispersion. This analysis, which is presented in the Results section, suggests that convective transport already contributes in the case of Superose-6.

To reduce peak dispersion it is obviously sufficient that the largest pores distribute solute within the bead by convection. The intervening region of smaller pores left by the larger ones forms microbeads with significantly reduced effective bead diameter. It is for this reason that eqn. 3 was based on R_{max} and not on $R_{1/2}$. Recently novel media have been synthesized that contain a mixture of small and ultra-large pores to take advantage of these hydraulic properties. This "perfusion chromatography" [14,15], as it was called, resembles the properties of conventional wide-pore SEC media as discussed above.

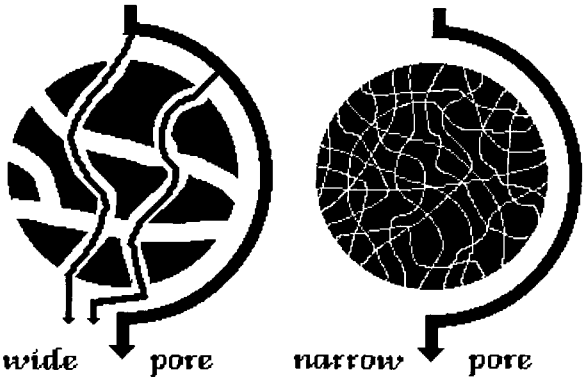

Fig. 1. Schematic diagram of a porous bead as used for packing SEC columns. All types of beads are totally porous and contained well connected flow-through capillaries. In principle there is always some liquid flow through the interior channels of the bead. If these pores are narrow the amount of this flow is insignificant and all of the observed flow of a column passes around the bead. Materials then enter the pores exclusively via diffusion. If the pores are wide some relevant fraction of liquid flow passes through the pores themselves. This provides for convective transport of materials into the beads.

The maximum radius R_{max} of these media (Poros; PerSeptive Biosystems, Cambridge, MA, USA) is only slightly larger than that of TSK6000PW, but $Cf > 40$ for the smallest bead size available.

Van Deemter equation

In the following, extra-column instrumental dispersion will not be dealt with and is assumed to be zero for the experimental data presented. Further, the number of plates is high in all instances. In the limit of geometric scaling, classical dispersion analysis then focuses on the reduced Van Deemter master equation. It has been derived in many different ways both from rate theory and from statistical theory. The reduced plate height h is given as [16]

$$h = \frac{L}{dN} = \frac{10^4}{5.54} \cdot \frac{L\,(\mathrm{cm})}{d\,(\mu\mathrm{m})} \left[\frac{w_h\,(\mathrm{ml})}{V\,(\mathrm{ml})}\right]^2$$

$$= A + \frac{B}{Pe} + CPe + P \qquad (4)$$

where L is the column length, d the diameter of the packing beads, N the number of plates in the column, V the retention volume, w_h the peak width at half-height and Pe a reduced velocity called the Peclet number, which is a measure of the ratio of diffusion time per bead to the flow time across the same distance times a numerical factor [2]. Like the diffusion coefficient, it depends on fluid viscosity and temperature. For water at room temperature (20°C), one obtains

$$Pe = \frac{dc}{D} = 0.777 \cdot \frac{L\,(\mathrm{cm}) \cdot d\,(\mu\mathrm{m})}{V_{void}\,(\mathrm{ml})}$$

$$\cdot \mathrm{flux}\,(\mathrm{ml/min}) \cdot R_s\,(\mathrm{nm}) \qquad (5)$$

where R_s is the diffusional Stokes radius and the other variables are column parameters defined in Table I together with representative numerical examples. A, B, C and P are functions that will be discussed below. If the baseline peak width w, defined at the 4σ level, is used a different numerical factor applies [17]. In the Van Deemter equation, the use of the Peclet number allows data obtained with different-sized solutes, different flow-rates and different columns to be combined into a single master curve. Similarly, the

reduced plate height eliminates trivial column variabilities. Representative experimental Van Deemter plots are presented in the Results section. In the following the functional form of the Van Deemter terms is summarized with due account of diverging views.

P-term

P is a measure of sample polydispersity and depends on the selectivity, *i.e.*, the slope of the calibration graph for retention [18–20]:

$$P = \frac{L}{d} \cdot \frac{\ln\left(\frac{M_w}{M_n}\right)}{V^2} \left(\frac{\partial V}{\partial \ln M}\right)^2$$

$$= 10^4 \left(\frac{1+a}{3}\right)^2 \frac{L\,(\mathrm{cm})}{d\,(\mu\mathrm{m})} \cdot \frac{\frac{M_w}{M_n} - 1}{[V\,(\mathrm{ml})]^2} \left[\frac{\partial V\,(\mathrm{ml})}{\partial \ln R_\eta}\right]^2 \quad (6)$$

where a is the Mark–Houwink exponent. P dominates in eqn. 4 whenever $M_w/M_n > 1.01$ and then obscures the other parameters. Hence essentially monodisperse samples are required for a meaningful analysis of dispersion.

A-term convection

Giddings [21] lists at least four additive factors for eddy dispersion (convective mixing) in the mobile zone, namely, velocity differences at different radial positions within a capillary, velocity differences amongst different nearby channels due to geometric factors, velocity differences in different regions due to variable packing quality and velocity differences at different radial positions of the packed bed column due to flow distortions near the column wall. Originally Van Deemter assumed that the sum of these, called the A_e-term, is a constant whose value depends on the quality of the packing. Huber, Horváth and Giddings then independently established that each convective subprocess is counteracted by diffusion. Giddings famous coupling equation reads [21]

$$A = \sum_i \left(A_i^{-1} + \frac{\omega_i}{Pe}\right)^{-1} \quad (7)$$

where A_i remains a constant characteristic for each subprocess and ω_i is a proportionality constant. The coupling constant for intra-capillary effects is large of the order of $\omega_1 \approx 100$ and causes an extended Pe dependence, whereas all other coupling constants are small and the Pe variation is significant only below $10Pe$. A different form for A was derived by Huber [22]:

$$A = (A_e^{-1} + \omega' Pe^{-k})^{-1} \quad (8)$$

where $k = 0.5$ and A_e was also considered to be a constant. Horváth and Lin [23] derived the same with $k = 0.33$. Knox and co-workers used an empirically determined k ranging from 0.2 to 0.5 [24] or alternatively an unlimitedly growing function [25,26]:

$$A = A_e = A'' Pe^{0.33} \quad (9)$$

with A'' depending on the quality of the column packing. Ideally its value was 0.5–1 but could possibly reach 5 or greater. By just varying the flow-rate at constant solute size, others sometimes found larger exponents [27], as would be expected in certain instances from eqn. 14 discussed below. For infinite diameter columns exponents as low as 0.2 were found [28,29]. Koch and Brady [16,30] presented a theoretical computation, which scales with p_i but whose simplifications are strictly valid only in the limit $p_i \rightarrow 1$. They demonstrated that eddy dispersion will increase unlimitedly with Pe under the assumption of a viscous regime owing to the formation of boundary layers that are inaccessible to convection [16,30]:

$$A_e = 1.5\left(1 + \varepsilon \cdot \frac{V_{column} - V_{void}}{V_{column}} \cdot \ln Pe\right) \quad (10)$$

with the computed value $\varepsilon = 2.2$ for ideally smooth spheres. A rougher surface should have a smaller ε. The factor 1.5 represents the computational situation; in practice, A_e seems to depend on the quality of packing and the complex functional origins of the prefactor are poorly understood. The constant term is equivalent to the sum of the low-coupled convective contributions. A_e also depends on column diameter if the ratio of column diameter to bead diameter is less than 100 [31–33]. More importantly, A_e is a sensitive function of the bead size distribution

and dramatically increases with modestly increasing size heterogeneity [20,34]. Note that the natural logarithm, the cube root and the coupling equation with suitable constants produce similar trends. The logarithmic dependence originates from the boundary conditions and is related to the thickness Δr of the boundary layers formed (eqn. 14). Reanalysis of dispersion data published by Basedow *et al.*[35] for non-porous pieces of broken glass ($p_i = 0.48$) yields $\varepsilon \approx 0.5$ for different-sized solutes at normal flow-rates, albeit the tortuosity was $\xi_i = 2.0$. This margin increases to $\varepsilon \approx 1.0$ if small solutes at varying flow-rates are used instead and demonstrates that the conditions of flow in packed beds are not laminar, *i.e.*, the ln *Pe* dependence in eqn. 10 is an oversimplification. This important result demarcates and identifies the failure of geometric scaling in liquid chromatography. In fact, ε in eqn. 10 becomes a function of flow-rate, namely

$$\varepsilon \propto c^{m-0.33} \approx c^{0.2} \tag{11}$$

according to the data of Basedow *et al.* [35]. In the inertial regime A_e goes through a maximum, which is well explained by the Taylor–Aries theory and was observed experimentally in one case around 30 000 *Pe*, albeit the true determinant is the Reynolds number. At Reynolds numbers $Re > 10$ the A_e-term eventually becomes constant [36].

A-term film transfer

Mass transfer of solute into accessible pores is associated with extra diffusive resistance across a boundary layer at the interphase between the mobile and stagnant zones just as in any membrane diffusion experiment. The added diffusive contribution to the mobile zone mass transfer was estimated by Wakao and Funazkri, who correlated empirical data, as follows (reviewed in ref. 16):

$$A_p = 1.5\left(\frac{V - V_{void}}{V}\right)^2 \frac{V_{void}}{V_{column} - V_{void}} \cdot \frac{Pe^{0.4}}{1 + 9Pe^{-0.6}} \tag{12}$$

Over the range of typical experimental values, the last term roughly corresponds to $Pe^{0.6}$. Typically, a small totally included molecule ($V = V_{tot}$) has $Pe \approx 10$ and $A_p \approx 0.2$. A_p may increase to about 1 in the middle of the separation range and then decreases back to about 0.3 for the largest molecules. It vanishes at the void. Huber [22] reported a similar term but with $A_p \propto Pe^{0.5}$. According to film theory [16,37],

$$A_p = 13 \cdot \frac{V_{tot} - V_{void}}{V_{void}} \cdot \frac{\Delta r}{d} \cdot CPe \tag{13}$$

where Δr is the thickness of the boundary layer, which depends on the effectiveness of convective mixing and decreases with increasing solute size as [38–43]

$$\Delta r \propto \frac{D_{bulk}^{0.33}}{[c(\mathrm{cm/s})]^m} \tag{14}$$

where c is the stirring speed and $m = 0.33$ for laminar flow, $m = 0.50$ for convective conditions and $m = 0.75$ for turbulent flow. Eqn. 14 is related to the Nusselt number. For $m \approx 0.4$, one effectively obtains $A_p \propto Pe^{0.6}$, in agreement with typical experimental values and with eqn. 12. In eqn. 13, C is the Van Deemter coefficient (see, *e.g.*, eqn. 21) and explicitly includes obstructed diffusion which is hidden in the empirical correlation of eqn. 12. As film theory does not quantitatively predict the magnitude of Δr, eqn. 12 was used in subsequent analysis. A_p should be serially added to the other dispersion terms. Note that according to eqn. 14 either ε in eqn. 10 will become a function of flow rate or *Pe* becomes multiplied by a novel term except for laminar conditions. The same holds for A_p in eqn. 12 or 13.

A-term final equation

Most frequently a single coupling term of the sums of various convective and diffusive contributions is used empirically to which the boundary layer resistance is added serially [16,44]:

$$A = \left(A_e^{-1} + \omega \cdot \frac{B}{Pe}\right)^{-1} + A_p \tag{15}$$

where B is the Van Deemter B-term and ω is a proportionality constant that depends on the column diameter. For column diameters in excess of 100 bead diameters, one theory gives a constant $\omega = 0.55$ due to dominant radial diffu-

sion [33]. Judged by experimental data [45], $\omega B \approx 0.5$ and the coupling is only significant for poorly packed columns at low *Pe*. Others claimed a higher experiment derived limiting value of $\omega = 1.2$ [31]. Clearly, the experimental patterns are dominated by the low-coupling events. This is no problem for the present data analysis, which explicitly includes the second coupling region in the form of a *Pe*-dependent A_e (eqn. 10). A_p is taken from eqn. 12 and $\omega B = 0.5$. The appropriateness of eqn. 15 with a single coupling term in the form chosen could not be validated with the available data at $Pe > 10$.

B-term

Excluding adsorption effects, the Van Deemter coefficient for axial diffusion in SEC may be explicitly written as [16]

$$B = 2\left(\xi_i^{-1} + \xi_p^{-1} \cdot \frac{V - V_{void}}{V_{void}} \cdot \frac{D_{pore}}{D_{bulk}}\right) \quad (16)$$

where D_{pore}/D_{bulk} measures the increased friction in confined spaces. The same term appears in the *C*-coefficient and will be discussed below. Earlier treatments ignored the second term in *B*, which is due to diffusional spreading inside the pores (see, *e.g.*, ref. 22). The factor 2 comes from the proportionality between the diffusion coefficient and the mean distance travelled by a random walk. Considering realistic values for the tortuosity ξ (see below), *B* typically equals 2 and is certainly less than 4 for all practical circumstances. Hence the term may be ignored for $Pe > 10$.

Tortuosity

The ratio by which the curved path a particle has to take through a porous network is longer than the linear end-to-end distance is called tortuosity. In the absence of actual measurements one may assume $\xi = 1.5$ and *i* and *p* refer to the interstitial and pore space, respectively. This coincides with the value for minimal surfaces of cubic symmetry [46]. For an unbounded solution, $\xi = 1$ by definition. Theoretically, the tortuosity in a network of cylindrical pores is [47]

$$\xi_1^{-1} = 1 - \frac{2}{3}(1+p)(1-p)^{3/2} \quad (17)$$

where *p* is the porosity. The limiting value for a cylinder with negligible diameter is $\xi = 3.0$ [46]. In addition to an increased path length, the cross-section of real pores is not constant. Its variation leads to constrictions of the flow path and yields an additional geometric factor [21,48]:

$$\xi_2 = \langle A \rangle \left\langle \frac{1}{A} \right\rangle \quad (18)$$

where $\langle A \rangle$ is the average over the local pore cross-section. ξ_2 increases as the ratio of maximum to minimum cross-section increases [49]:

$$\frac{A_{max}}{A_{min}} = \left(\frac{R_{max}}{R_{min}}\right)^2 \approx 1.6(\xi_2)^3 \quad (19)$$

For closely packed beds of spheres one typically finds $\xi_2 \approx 1.3$, which corresponds to almost a fourfold difference between maximum and minimum cross-sections [49]. The interstitial tortuosity is then simply the product $\xi_i = \xi_1 \xi_2$, but the particular values of $\xi_i = 2.4$–2.6 calculated for the columns in Table I are surprisingly high.

In those instances where the pore volume fraction enters the measurement, such as for the stagnant zone mass transfer, the excluded volume term is added to the obstruction factor whilst nominal porosity is added to tortuosity [50]. The empirical tortuosity coefficient should then be considered to be the product of tortuosity in its primary meaning of constriction and of porosity, *i.e.*,

$$\xi_p = \frac{\xi_1 \xi_2}{p_b} \quad (20)$$

Theoretical values of ξ_1/p_b are listed in Table I. In practice, ξ_p is often derived from the intercept of semi-logarithmic obstructed diffusion relationships, which is sensitive to systematic errors. ξ^{-1} is called the intrinsic conductivity but some workers have labelled it tortuosity instead. Tortuosity is a constant for a given porous structure.

C-term

Finally, for a rate-limiting diffusion within the pores, $C = C_d$ and one may write for the mass transfer term between mobile and stagnant zone

[16]

$$C_d = \xi_p \cdot \frac{V - V_{void}}{V^2} \cdot \frac{V_{void}}{30} \cdot \frac{D_{bulk}}{D_{pore}} \quad (21)$$

where the factor 30 assumes conditions close to equilibrium [51]. Far from equilibrium (large C-term), eqn. 21 will underestimate D_{bulk}/D_{pore} [52]. Here $V - V_{void}$ may but need not be equal to the real geometric volume that is sterically accessible to the solute, since energetic differences may exist between the mobile and stationary zones. Adsorption, however, is assumed to be absent. The presence of a stationary zone requires a modified form of eqn. 21. Up to this point no real assumption about the mechanism of transport has been made and the apparent diffusion coefficient in the pores may also include factors of convection. It is only a formal choice to express C in terms of two functions instead of expressing D_{pore} in terms of two functions. Facultative omission of convective terms therefore exclusively modifies parameters of obstructed diffusion in whatever term is used (*e.g.*, eqn. 22) and is uncoupled from the remainder of dispersion analysis.

Obstructed diffusion

Occasionally a simple exponential function was advocated for obstructed diffusion [16,53]:

$$D_{pore} = D_{bulk} \exp\left(-\alpha \cdot \frac{R_s}{R_{1/2}}\right) \quad (22)$$

and the wide variation of empirical data (see Discussion) hardly justifies more than a single adjustable parameter. Further, the present results are well represented in this form. It is inherent in the derivation that the radius of the solute should equal the diffusional Stokes radius R_s. We shall investigate below whether this holds experimentally and will actually modify eqn. 22. The disadvantage of this semi-logarithmic approach is that, according to theory, slopes taken below $R/R_{1/2} < 0.1$ and above $R/R_{1/2} > 0.05$ need to be distinguished.

Theory of obstructed diffusion

Initially many chromatographers considered the ratio $\xi D_{bulk}/D_{pore}$ to be merely a constant independent of solute size (see Discussion) [44], even though related fields dealt with size-dependent functions. Two factors play a role, frictional drag (according to Faxen [54]) and steric hindrance (according to Ferry [55,56]). The observed increase in friction is truly a problem of flow line perturbation in the proximity of obstacles, *i.e.*, a hydrodynamic interaction between object and obstacle which increases drag. It should not be viewed as if objects were enlarged in size as this exceeded the pore size in which they are contained by orders of magnitude. Steric hindrance is related to the partition coefficient of SEC but it is usually assumed to be the sterically excluded volume of cylindrical capillaries $(1 - R/R_{1/2})$ [2] according to the geometric model employed in theory.

Renkin [57] was first to combine both terms. All theories so far have assumed ideal cylindrical geometry of pore radius $R_{1/2}$ or parallel plates, where $R_{1/2}$ is replaced by half the distance between the plates, $z/2$. Rectangular geometry yields different functions [58,59] and will not be considered further here. The simplest approach, further, is limited to calculation of the force exerted on spherical objects in axial-symmetric flow. Following Faxen and Renkin, various improvements in calculating this centreline approximation were made [50,57,60–63]. For aspect ratios $R/R_{1/2} < 0.5$, there is general consensus (see Fig. 2a). The initial semi-logarithmic slope is $\alpha = 4.6$ [64]. The centreline approximation is the most widely used formula in the field. An extended solution, that includes integration over all eccentric positions, but still with simplifying assumptions, has been presented by Famularo in ref. 63. It seems to be largely unknown in the field. It has an initial slope of $\alpha = 5.5$ that bends to $\alpha = 7.4$ for $R/R_{1/2} > 0.05$ (see Fig. 2c). Consequently, the neglect of non-symmetrical terms amounts to an unacceptable error. The gradual transitions towards solution (a) is expected since centreline terms become more dominant as the aspect ratio increases. Brenner and co-workers [65–67] confirmed the initial semi-logarithmic slope of $\alpha = 5.5$. Their computation claims validity for $R/R_{1/2} < 0.1$ but starts to deviate from Famularo above $R/R_{1/2} > 0.05$ in an oscillatory manner (see Fig. 2b). This discrepancy remains to be understood on a computational level be-

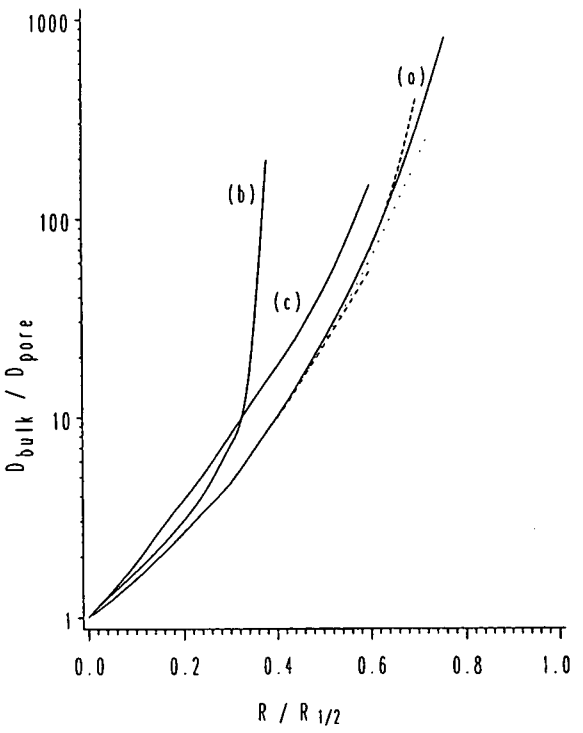

Fig. 2. Theoretical functions for obstructed diffusion in cylindrical tubes with both a drag term and an excluded volume term. (a) Centreline approximations: Faxen and Renkin [57] (lower dashed line), Haberman and Sayre (quoted in ref. 62) (dotted line), Bishop *et al.*, eqn. 12 in ref. 84 (upper dashed line), Paine and Scherr [61] (solid line), all with identical initial slope of $\alpha = 4.6$. (b) Extended solution: Brenner and Gaydos [65], with initial slope of $\alpha = 5.5$. (c) Best solution: Famularo in ref. 63, with initial slope of $\alpha = 5.5$ below $R/R_{1/2} = 0.05$ and with slope of $\alpha = 7.4$ above $R/R_{1/2} = 0.05$.

fore one can be confident that the values of Famularo are correct in all details. There is, however, little reason to doubt the calculation of the initial slope, which thus definitely supersedes the earlier centreline approximation. This is particularly noteworthy, as the initial slope $\alpha = 4.6$ of the pure centreline approximation has already been claimed to be experimentally verified (see Table IV and its discussion). The rapid rise of Brenner and co-workers' slope (Fig. 2b) above $R/R_{1/2} > 0.3$ is a computational artifact [60] and may have misled the formulation of theory for hydrodynamic chromatography (HDC), where friction bends the calibration graphs backwards for large solutes [68]. Experimental HDC data of this kind are better explained in terms of shear deformation [8]. Mavrovouniotis and Brenner have calculated the limiting case of $R/R_{1/2} > 0.9$, which asymptotically approaches infinity [69]. Scaling theory has been applied to the problem of obstructed diffusion of flexible polymers [70] and tests of its applicability have attracted some interest, but the issue is not decided. Some arguments will be raised in the Discussion section. Note that convective obstruction is much less than diffusional obstruction, especially above $R_s/R_{1/2} > 0.5$ [60].

In comparing data on obstructed diffusion, one must keep in mind that some types of measurement besides SEC are independent of the excluded volume term. For them the pure drag term becomes $\alpha = 3.5$ instead of 5.5 for low aspect ratios. The middle range then should more be of the order of $\alpha = 4.5$ and continues to increase instead of remaining a constant $\alpha = 7.4$ over the entire region. Eqn. 22 is therefore a poor representation of frictional drag variation alone.

Summary

With few exceptions, the *C*-term of the Van Deemter equation for SEC has been exclusively analysed as a diffusion problem. All data on obstructed diffusion obtained from SEC thus lack consideration of convective mass transport, and most were superficial in their treatment of mobile zone factors. To document the role of convection in a model-independent manner, experimental dispersion data are initially analysed with a combination of eqns. 4, 5, 10, 12, 15, 16, 21 and 22. Eqn. 22 eventually will be replaced by eqn. 29 in the Results section. Convective transport modifies D_{pore} and application of eqn. 22 or 29 alone consequently leads to superficially low apparent α values. In this manner the occurrence of convection is easily recognized. Subsequent complete analysis (which is deferred to the second part of the Discussion) then will add eqn. 31 to the above list and test the validity of various proposed theories for C_c (eqns. 30, 33, 36 and 37) with the constraint that the α value should become universal.

EXPERIMENTAL

The instrument, materials and procedures were the same as reported previously [1,71,72]. Peak widths were measured manually off the charts. All reported measurements and theory pertain to the regime of infinite dilution with samples eluting independent of the presence of other components in the case of mixtures. Experience shows that injection volumes should be small and samples to be injected in SEC should not exceed

$$c_{inj} < 0.1[\eta]^{-1} \quad (23)$$

where according to Simha

$$c^* \approx [\eta]^{-1} \quad (24)$$

is called the overlap concentration [70]. For rigid spheres, such as globular proteins, this limit concentration of the dilute solution regime c^* roughly corresponds to the solubility limit. Further, $I \geq 0.002$ M is a lower useful limit for SEC studies since, for the requirement of infinite dilution, the polymer should not contribute significantly to the ionic strength of the eluent:

$$I_{polymer} \approx \frac{n(n+1)}{2} \cdot \frac{c_{inj}\ (mg/ml)}{M} << I \quad (25)$$

where n is the net charge of the polymer. Solute concentrations in excess of eqn. 25 induce concentration gradients of the support electrolyte that increasingly distort the elution profiles. For measurement of peak dispersion it is particularly important that the solvent of the sample and the eluent are identical.

It has been verified that none of the samples studied here changes its structure over the range of solvent conditions employed. Hence no aggregation, dissociation or denaturation takes place and consequently R_s and R_η, each corresponding to conditions of infinite dilution, remain the same. For coiled polyelectrolytes whose intramolecular forces induced continuous structure changes at varying ionic strength, the hydrodynamic constants appropriate for the particular single condition that was studied in their case were used.

Column parameters are given in Table I. Based on these data and the Hagen–Poiseuille equation, the manufacturer of TSK-PW (Toso-Haas, Tonda, Japan) recommends not to exceed 1.2 ml/min and that of Superose (Pharmacia–LKB, Uppsala, Sweden) specifies 1.5 ml/min. Experiments were performed at different flow-rates, not exceeding 0.5 ml/min, at room temperature. Table II shows typical calibration data that relate molecular size to retention volumes. Typically retention volumes and solute sizes are correlated in a semi-logarithmic fashion without recurrence to any particular model of pore geometry. This makes the analysis independent of V_{tot}, whose proper assessment is disputable. In fact, none of the dispersion analysis depends on V_{tot} either.

TABLE II

REFERENCE DATA AND ELUTION VOLUMES ON SUPEROSE-12

Sample[e]	R_s (nm)	R_{SEC}[a] (nm)	Superose-12 V (ml)[b]
TMV	49	62	7.60 (void)
TBSV	17.2		7.80
Phage MS2	13.9		7.80
DNA (195 bp)	9.3	12.6	8.22
NF200TP+[c]	8.9	11.7	8.50
Thyroglobulin	8.6		9.08
β-Galactosidase	6.86		10.48
Apoferritin	6.06		10.72
Immunoglobulin G	5.23		11.77
Alcohol dehydrogenase	4.55		12.30
Alkaline phosphatase	3.30		13.18
Ovalbumin	2.83		13.65
Calmodulin	2.10		14.10
Myoglobin (horse)	1.91		15.28
Vitamin B_{12}[d]	0.75		19.50

[a] Missing values are for spherical particles where $R_{SEC} = R_s$.
[b] I = 200 mM; pH = 8.0; 10 mM Tris–HCl–194 mM NaCl.
[c] Proteolytic fragment of neurofilament NF200, phosphorylated form.
[d] Used to estimate V_{tot}; however, ^2H_2O elutes about 1 ml later.
[e] TMV = tobacco mosaic virus; TBSV = tomato bushy stunt virus.

RESULTS

Operational parameters

All of the data were obtained with essentially Gaussian peaks. The asymmetry was actually

1.1–1.2 for all Peclet numbers and substances. Fig. 3 demonstrates that the peak width w_h and the reduced plate heights depend on the loading concentration and also vary with the age and status of a column. It is therefore crucial that the stability of performance be checked during a series of axial dispersion measurements. High values of h, observed after cleaning the column, may gradually return to normal lower values. Disturbance of the gel bed on changing the entrance frits (a standard operational option for Superose columns), however, may lead to permanent loss of performance. The latter is easily checked in glass columns with coloured substances. Back-flushing usually leads to a recoverable loss of performance. Fig. 3 also shows that plate heights depend on loading concentration. To guarantee comparable experimental conditions, all subsequent data were taken at loads between 1 and 100 μg, where concentration has no influence and the signal-to-noise ratio is still acceptable. Injection volumes were 10–100 μl.

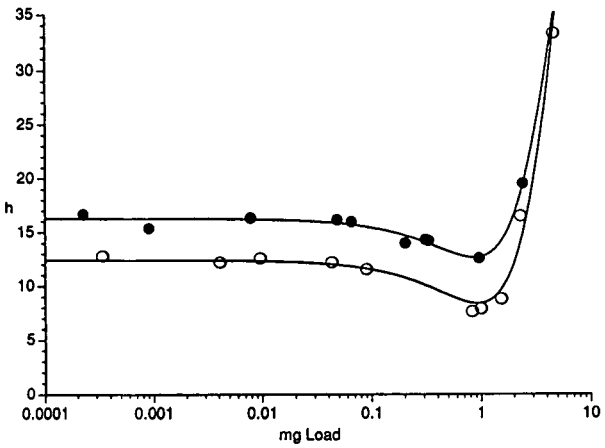

Fig. 3. Dependence of the reduced plate height h on sample load. Here sample load is defined as injection concentration times injection volume. Superose-12 in 10 mM Tris–HCl–94 mM NaCl (pH 8.0, $I = 100$ mM); flow-rate, 0.4 ml/min; room temperature. Sample, ovalbumin. Two series of measurements at different times but with the same column and conditions resulted in different magnitudes of axial dispersion. ● = Earlier series of measurements; ○ = later series of measurements. Both series employed an injection volume of 100 μl. The loading capacity is *ca.* 2 mg. Viscous fingering was clearly discernible above 10 mg (corresponding to an injection concentration of $c^*/3$).

Proteins are normally monodisperse and thus ideally suited for the analysis of dispersion. Among the exceptions is immunoglobulin, which is polyclonal and is known to contain a mixture of similar sizes of different molecules of variable isoelectric points. Fig. 4 shows that the peak width of immunoglobulin is higher than those of other similar-sized proteins. This is in agreement with the previous statement that even minor

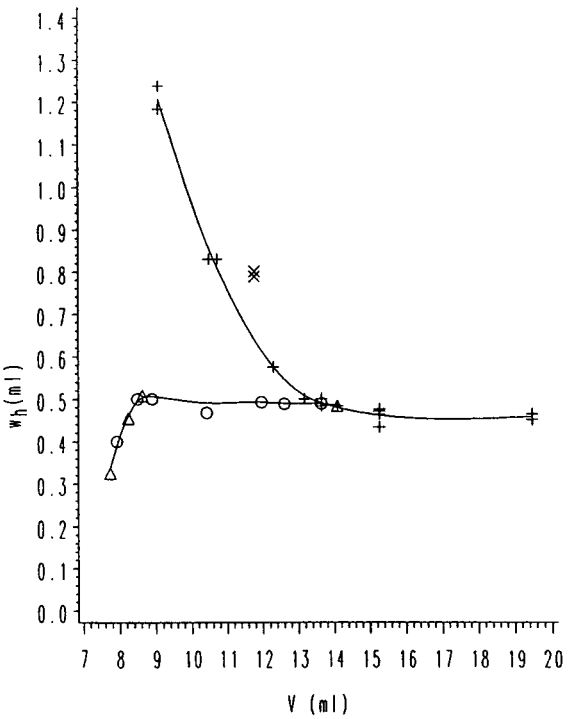

Fig. 4. Axial dispersion for different solutes and conditions on Superose-12 at a flow-rate of 0.5 ml/min, room temperature, buffered aqueous solutions with supporting electrolyte. Shown is the peak width as a function of elution volume. Upper curve: different proteins at $I = 200$ mM, pH 8.0. From left to right: thyroglobulin, β-galactosidase, apoferritin, alcohol dehydrogenase, alkaline phosphatase, ovalbumin, calmodulin, myoglobin, vitamin B_{12} (+), immunoglobulin G (×). Vertically corresponding marks are repetitive measurements on the same protein. Note that immunoglobulin G, measured under identical conditions, is off the graph because it is heterogeneous. Lower curve: eluents of different ionic strength ranging from $I = 3$ to 200 mM (the lowest value corresponding to the left-most points) at pH 8.0: ○ = ovalbumin; △ = calmodulin. Even though the retention of these samples corresponds to large proteins owing to interfacial repulsion, their peak widths are much smaller [*cf.*, condition (upper curve)].

polydispersity obscures the dynamic aspects of peak dispersion. This behaviour of immunoglobulin has been found reproducibly under all conditions studied and immunoglobulin was therefore excluded from further dispersion analysis. A similar observation regarding immunoglobulin heterogeneity was reported previously [73].

In addition, it was observed that aged samples of glycoproteins sometimes gave increased peak widths without notable changes in retention volume. In this event a new sample was employed and the old data were rejected. Any extra pressure drop due to column clogging usually also increased the peak width. Mismatch of the eluent between the column and injected solution also tends to increase the peak width. This may actually be one of the reasons for the poor data quality in Fig. 5, which shows one of the earliest data sets acquired.

Eddy contribution to peak dispersion

Fig. 5 presents data obtained at a single flow-rate with one particular column (TSK6000PW) with different-sized solutes. Peclet numbers can therefore be viewed as a function of diffusional Stokes radius. Regardless of the details of interpretation it is obvious that the presented data below $Pe < 100$ are unaffected by the C-term. On the other hand, data above $Pe > 10$ are unaffected by the B-term of eqn. 4, albeit the B-term couples into eqn. 15. This middle region is thus dominated by the A-term. It is reasonably fitted by the original eqn. 10 with $\varepsilon = 2.2$. However a detailed numerical non-linear least-squares fit reduces it to $\varepsilon = 1.7$. The fitting function actually shown is of course that of eqn. 15 in all instances. As no measurements were conducted at low Peclet numbers, one cannot distinguish between eqns. 15 and 8, nor could the functional form of B (eqn. 16) be tested.

The same analysis was performed with a different column, Superose-12, and is shown in Fig. 6. Again, different-sized solutes at a single flow-rate are plotted. The C-term extends to lower Pe and it is more difficult to view the A-term alone. However, it is clear that eddy dispersion is decisively less than predicted by theory. The *ad hoc* hypothesis of an adjustable ε gives a reasonable fit with $\varepsilon \approx 0.6 \pm 0.2$. The

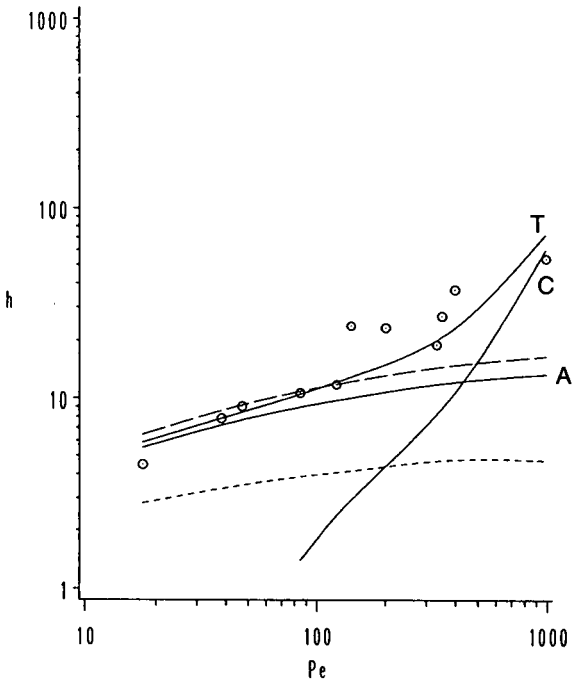

Fig. 5. Van Deemter plot of axial dispersion showing the reduced plate height h as a function of Peclet number Pe. TSK6000PW column 1; eluent, sodium borate (pH 8.25, $I = 4$ mM) in water; flow-rate, 0.2 ml/min; room temperature. Different proteins and viruses (from left to right): vitamin B_{12}, cytochrome c, carbonic anhydrase, bovine serum albumin, catalase, apoferritin, thyroglobulin, phage Qβ, turnip yellow mosaic virus (TYMV), tomato bushy stunt virus (TBSV), tobacco mosaic virus (TMV). Best theoretical representation was obtained from simultaneous fitting of the various theoretical contributions to peak dispersion (for the parameter obtained see Table III). Total dispersion (T) is the sum of an A-term with $\varepsilon = 1.7$ (A) and a C-term (C). For comparison a hypothetical A-term with $\varepsilon = 2.2$ (long dashed line) and $\varepsilon = 0.3$ (short dashed line) are also shown.

compensatory mutual dependence of the three variables is indicated in Table III, which also summarizes the parameters for several other data sets, whose graphical presentation would be repetitious.

Because of the high precision of the data, the parameters for Superose-6 are particularly stable and well determined (Table III). With $\varepsilon \approx 0.5$, the eddy dispersion is similar to, if not even lower than, that for Superose-12. Data for TSK5000PW, on the other hand, are comparable to those for TSK6000PW. It should be noted, however, that a fresh TSK6000PW column yielded a significantly lower ε than the column shown in Fig. 5 (Table III). The deterioration of

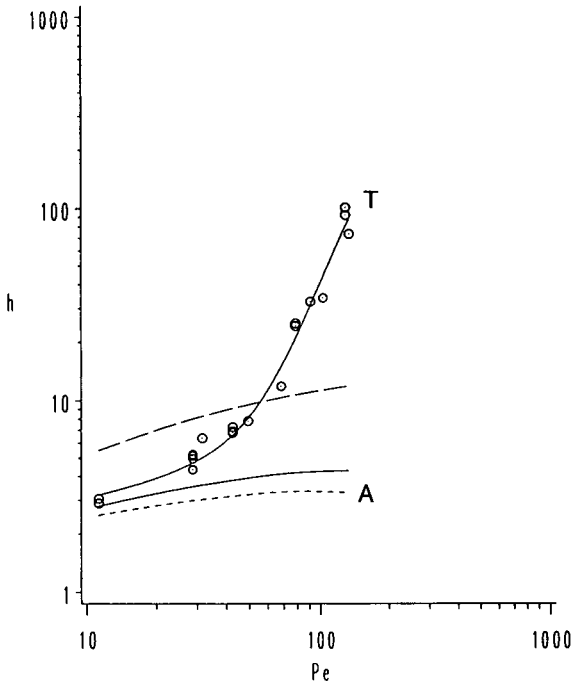

Fig. 6. Van Deemter plot of axial dispersion showing the reduced plate height h as a function of Peclet number Pe. Superose-12; eluent, Tris–HCl–NaCl (pH 8.0, $I = 200$ mM) in water; flow-rate, 0.5 ml/min; room temperature. Same proteins as in Fig. 4 (upper curve) plus a proteolytic fragment of neurofilament protein NF200, which is located near thyroglobulin. Vertically corresponding points are multiple determinations of the same protein. The best theoretical representation was obtained from simultaneous fitting the various theoretical contributions to peak dispersion (for the parameters obtained, see Table III). Total dispersion (T) is the sum of an A-term with $\varepsilon = 0.57$ (flat A) and a C-term (not shown). For comparison, a hypothetical A-term with $\varepsilon = 2.2$ (long dashed line) and $\varepsilon = 0.3$ (short dashed line) are also shown.

columns may therefore be far more limiting for the analysis of dispersion than it is for retention. In any case, eddy dispersion is worse on TSK-PW than Superose. Figs. 5 and 6 include a comparative tracing with $\varepsilon = 0.3$ as the lower limit, corresponding to the data of Basedow *et al.* [35] if the tortuosity difference is neglected. Otherwise Basedow's data actually yield $\varepsilon = 0.5$ and thus match the present Superose data. As the difference between the two series of measurements in Fig. 3 is presumably due to the ε value in eqn. 10, its repeated empirical validation is crucial. Variation of ε does not seem to be related to porosity as a criterion of packing quality as far as eqn. 10 is concerned and a novel parameter of "packing quality" may need to be introduced. Koch and Brady [30] stated that ε depends on the nature of the microstructure. Their value of $\varepsilon = 2.2$ is for ideally smooth spheres. A rougher surface should have a smaller ε. Heterogeneity of the bead sizes, on the other hand, increases A_e [20,34]. Whether this explains the higher values for TSK-PW remains open to speculation.

Hindered transport in the stagnant zone

Once the A-term is known, the experimental values for the C-term may be calculated from the data. However, as they still contain trivial column parameters, it is better to calculate directly the term $\xi_p D_{bulk}/D_{pore}$. This has been done in Fig. 7 for the data for Superose-12. Fig. 7 establishes an exponential size dependence and

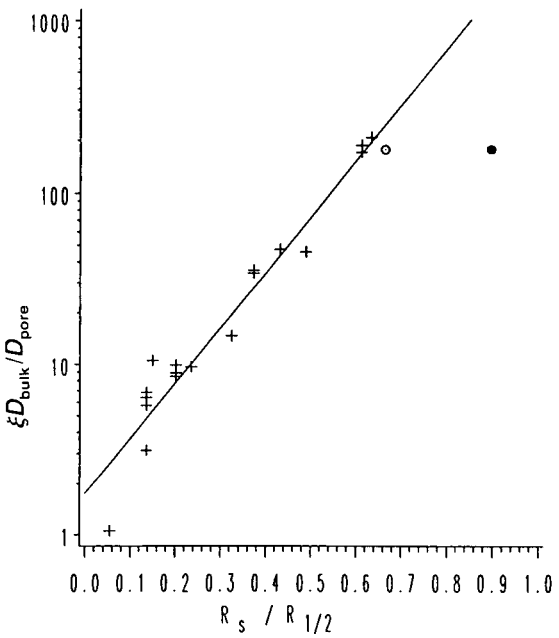

Fig. 7. Obstructed diffusion on Superose-12 in buffered aqueous solution with supporting electrolyte at a flow-rate of 0.5 ml/min at high ionic strength. The various sized proteins are the same as shown in Fig. 6 (+). A 195 bp DNA sample is shown with a diffusional Stokes radius R_s (○) and with a retention radius based on a comparison with proteins, R_{SEC} (●). Data were calculated from experimental values of reduced plate height minus the best-fit A-term, and further divided by the various additional factors of the C-term according to theory. The slope of the semi-logarithmic dependence of obstruction ($\xi D_{bulk}/D_{pore}$) *vs.* aspect ratio ($R/R_{1/2}$) is $\alpha = 7.4$.

TABLE III

PARAMETER FIT OF PEAK DISPERSION

Column	Flow-rate (ml/min)	I (M)	Type of radius in pore	Parameter[a]		
				ε	ξ_p	α
Superose-12	0.500	0.200	Stokes radius R_s	0.57	1.75	7.4
			Stokes radius R_s	0.38	1.90	7.3[b]
			Stokes radius R_s	0.92[b]	1.05	8.3
Superose-12	0.500	0.003–0.2	Calibrated radius R_R	0.92	1.75	7.4
Superose-6	0.250	0.100	Stokes radius R_s	0.52	1.45	5.6
			Stokes radius R_s	0.48	1.55	5.5[b]
Superose-6	0.500	0.214	Stokes radius R_s	0.55	1.50	5.6
TSK5000PW	0.150	0.214	Stokes radius R_s	2.0		
TSK6000PW, column 1	0.200	0.0041	Stokes radius R_s	1.7	1.75[b]	3.5
			Calibrated radius R_R	1.7	1.75[b]	2.0
TSK6000PW, column 2	0.167	0.06 or 0.2	Stokes radius R_s	1.26	1.60	1.0
			Stokes radius R_s	1.26[b]	1.17	2.0[b]

[a] Parameters of eqn. 10 together with eqn. 15, of eqn. 21 and of eqn. 29.
[b] Parameters forced to the specified value whereas the others were optimized.

validates the choice made with eqn. 22. In the case of major convective effects this kind of plot should lead to a plateau value; a minor contribution, however, would simply decrease the slope compared with the universal value proper for obstructed diffusion. Without involving theory, one may simply compare the semi-logarithmic slopes of different columns with varying Cf parameters to survey empirically the occurrence of convection. Exponential relationships were obtained in all instances. Instead of graphical analysis, a simultaneous numerical fit of the raw data was subsequently performed for the various columns and conditions and the resulting α values are given in Table III. The huge differences between the columns studied clearly demonstrates the occurrence of convective but the phenomenological level cannot immediately decide whether the largest observed value, $\alpha = 7.4$, corresponds to pure diffusion or whether ideal obstructed diffusion in the particular geometric network is still larger. Pre-empting the detailed theoretical interpretation of the second part of the discussion section we may record here that Superose-12 at the flow-rate studied safely operates in a purely diffusive regime and $\alpha = 7.4$ is the empirical reference value that is to be compared against theories of obstructed diffusion. Similarly, one may then test the various available theories for the process of convection with the intent of floating all of the apparent α values to a true value of $\alpha = 7.4$.

The observed apparent α values obviously depend crucially on the aspect ratio $R/R_{1/2}$ in eqn. 22. By theory one deals with a diffusion process and R_s would seem to be the obvious choice for the solute radius. This choice is even less critical for the spherical proteins chosen in this investigation as solid spheres ideally have $R_\eta = R_s$. Concerning the pore radius, the choice of average exclusion radius $R_{1/2}$ is certainly a simplification as each solute samples all pore sizes each with different degree of obstruction and larger solutes also preferentially sense larger pores. Alternatively, one could have used individual retention data directly to determine a sliding average cylinder aspect ratio

$$\frac{R_\eta}{R_{1/2}} = 1 - \left(\frac{V - V_{void}}{V_{tot} - V_{void}}\right)^{1/2} \quad (26)$$

If it is correct that retention is defined by a different size criterion, as is implied in eqn. 26 and demonstrated in the next section, this procedure of course fails to provide appropriate aspect ratios $R_s/R_{1/2}$ once $R_\eta \neq R_s$. Reanalysis of the spherical proteins in Fig. 7 in this manner yields $\xi_p = 1.1$ and $\alpha = 7.5$ compared with $\xi_p = 1.7$ and $\alpha = 7.4$ from Table III and ensures the robustness of analysis. The exact match of the Superose-12 data with one of the theories of obstructed diffusion (Famularo) that predicts $\alpha = 7.4$ for ideal monodisperse cylinders should none the less be considered coincidental. In this regard one should note that the pore radii used in analysis had been determined out of context in a publication prior to this investigation and unintentional bias in data handling is hopefully limited by the fact that empirical analysis was completed before the author became aware of the work of Famularo [63] and Rodrigues [141].

Determination of Stokes radii from peak dispersion

Dispersion theory was put forward to argue that retention should be described by diffusional Stokes radii. Peak retention, however, is clearly not determined by R_s but by a term which is R_η or very similar to it most of the time [71,74]. If dispersion is determined by diffusional Stokes radii, as it should be, a difference between retention and dispersion size should be observable with asymmetric molecules and this would establish directly that different kind of processes are involved. At non-vanishing concentrations the situation becomes more complicated as hydrodynamic parameters are concentration dependent. Flexible polymers then diffuse faster inside confinements than solid spheres of equal bulk Stokes radius (see Discussion). The latter was suggested to be true for deformable coiled polymers even at infinite dilute conditions if $R/R_{1/2} > 0.4$. It was then natural to test the SEC dispersion of asymmetric molecules.

Fig. 7 shows that a DNA sample [195 base pairs (bp)] almost matches the protein curve if plotted in terms of its Stokes radius. A more extensive study of DNA restriction fragments, however, indicated a minor tendency towards a smaller peak width w_h than proteins of supposedly same diffusional Stokes radius (unpublished data). While the latter were measured at loads not exceeding 3 μg and in the verified absence of concentration effects on retention volumes, it was not excluded that concentration still had effects on peak width. Overall correlation in terms of Stokes radii is fairly good. The same sample plotted with its chromatographic retention radius R_{SEC} is off the calibration (Fig. 7). In quantitative terms the latter is rejected with a 5σ standard deviation. Hence molecules of different asymmetry but equal retention have different peak widths, as retention is not determined by diffusional Stokes radii. Fig. 7 also contains a coiled protein, a neurofilament fragment designated NF200TP+. It fits well with its Stokes radius determined by quasi-elastic light scattering [74]. In terms of R_{SEC} (not shown), it would be off by a 3σ standard deviation. Both DNA and NF200TP+ are stiff coils and asymmetric. Synthetic chain polymers, however, are usually heterogeneous and thus not well suited for the present analysis. The observations clearly indicate that transport processes do not determine the mechanism of retention.

These examples suggest the means by which R_s may be approximately determined from chromatographic experiments simultaneously with another size measure (the viscosity radius R_η) obtained from retention information. Analysis of both retention and dispersion can be used to decide whether an unknown sample is chain-like with a large ratio of contour length to diameter or has an asymmetric shape. The largest handicap at present is the precision of the data. With the present 1σ variance of 30%, only highly asymmetric samples such as DNA are easily identified.

Ionic strength effects of dispersion

It is well known that the elution of polyelectrolyte samples depends on ionic strength [1,72]. In contrast, only two publications have so far addressed the role of ionic strength on the magnitude of obstructed diffusion [75,76]. The following is the first analysis of the ionic strength dependence of chromatographic peak dispersion. Fig. 4 shows the primary data used for Fig. 6, namely the w_h values as a function of retention

volume for proteins at 200 mM ionic strength on Superose-12 at one given flow rate (0.5 ml/min). If the ionic strength is decreased all of these samples elute earlier. This ionic strength variation is shown in Fig. 4 for two proteins, ovalbumin and calmodulin. Close to the void volume, the peak width drastically decreases but the other peak widths are approximately constant regardless of ionic strength and thus retention volume. Beyond doubt there is some significant difference between a sample at low ionic strength that elutes at this position mainly for reasons of interfacial repulsion, and another one at high ionic strength that elutes at the same volume position mainly because of its large bulk hydrodynamic size.

A w_h plot is somewhat deceiving, however. In contrast to w_h, h does increase with decreasing elution volume since h depends on V^{-2} in eqn. 4. Similarly, C (eqn. 21) depends strongly on retention volume. The A-term, however, almost remains unaffected. It thus becomes straightforward to compute $\xi_p D_{bulk}/D_{pore}$ as a function of ionic strength for a single protein. Surprisingly, this value is not at all a constant, which one might have expected as bulk diffusion coefficients of native proteins hardly change with ionic strength as long as these proteins do not aggregate, dissociate or denature (none of which applies here). Clearly, then, the diffusion rate inside the pores depends on ionic strength. One must therefore somehow define a generalized radius parameter to quantify the data.

At this point recurrence is made to published models of retention [1,72,77]. There are two strategies to use, a reduced pore size or an increased solute size. The truth is, of course, that it is a mutual effect. However, the charge effect on retention depends strongly on solute size, such that the effective reduced pore size would be different for each sample [1]. It therefore makes more sense to tag it to an increased solute term. Quantitatively one then equates the retention volume at low ionic strength to a single effective size R_R that is calibrated via the known sizes at high ionic strength (where R_{IF} is assumed to be negligible). For the sake of terminology it must be added that R_R differs from R_s, R_η and R_{SEC} in principle. Briefly,

$$R_R = R_{SEC} + R_{IF} \quad (27)$$

with $R_{SEC} \geq R_\eta$. For solid rigid objects, R_{SEC} is independent of ionic strength. The dimension of flexible polymers, on the other hand, changes with ionic strength even at infinite dilution under bulk conditions, which causes a variation of R_{SEC} besides the interfacial layer term R_{IF}. R_{IF} encompasses the increase in size due to mutual interfacial repulsion and was discussed in detail previously [1,72,77]. It ideally converges to zero for high ionic strength, even though the influence from hydration forces remains. The R_{IF} term in chromatography is equivalent to the well known concentration effects in bulk solution. Even though solute–solute interactions are eliminated by the experimental conditions of infinite dilution there always remains a finite "concentration" of walls, without which there would not be any SEC effect.

One may therefore presume that a similar effect occurs in transport through confined spaces. In the previous section it was demonstrated that the effective molecular size of retention and dispersion are different except for solid spherical objects. The latter, however, is the case with ovalbumin and calmodulin and for them $R_D = R_R$ since $R_s = R_\eta$. In general terms, the effective size in diffusive dispersion is then

$$R_D = \beta R_s + R_{IF} \quad (28)$$

The complicating introduction of a parameter β is necessary to handle flexible polymer chains. For compact spherical objects, non-deformable rods and stiff coils, $\beta = 1$, as was demonstrated in the preceding section. For flexible polymers such as polystyrene or dextran, $\beta < 1$ at finite concentration and $\beta = 1$ at infinite dilution as long as $R/R_{1/2} < 0.4$ (see Discussion). Note that bulk diffusion coefficients of solid rigid objects, and hence R_s, virtually do not depend on ionic strength once minute amounts of support electrolyte are present [78]. With the parameter R_D at hand to describe the diffusional size inside the pores, where it differs from bulk, one may now quantify the ionic strength variation in a manner similar to regular high ionic strength data. This is done in Fig. 8, which shows $\xi_p D_{bulk}/D_{pore}$ at variable ionic strength as a function of R_R

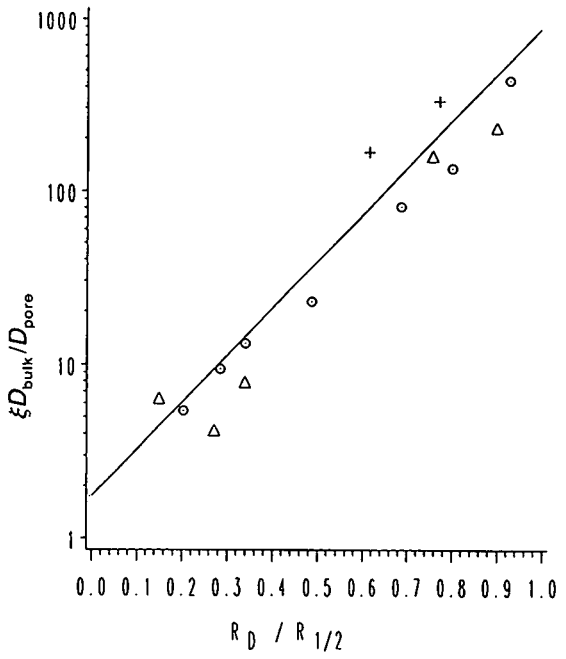

Fig. 8. Obstructed diffusion on Superose-12 at variable low ionic strength. Buffered aqueous solution with supporting electrolyte at a flow-rate of 0.5 ml/min. The aspect ratio is calculated from reference solute sizes matched by their elution volume to include contributions from interfacial repulsion. Lowest ionic strength data are right-most, highest ionic strength data left-most. Data are based on Fig. 4 plus some additional data and were analysed according to theory. ○ = Ovalbumin; △ = calmodulin; + = thyroglobulin.

($= R_D$). The data follow the same type of exponential function according to eqn. 22. Their slope ($\alpha = 6.2$) is, however, lower than that at high ionic strength using the same column ($\alpha = 7.4$). This leads to the following *ad hoc* assumption:

$$D_{pore} = D_{bulk} \cdot \frac{R_D}{R_s} \cdot \exp\left(-\alpha \cdot \frac{R_D}{R_{1/2}}\right) \qquad (29)$$

which is meant to replace eqn. 22. For $R_D = R_s$, eqn. 29 becomes trivially identical with eqn. 22. Note that eqn. 29 may fail if eqn. 25 no longer holds. Via eqn. 29, one obtains for Superose-12 $\alpha = 7.4$ even at low ionic strength. The magnitude of frictional obstruction, expressed in the term α, thus becomes truly independent of the extent of interfacial repulsion (R_{IF} in eqn. 28). The concept of an increased sample size R_{IF}, or of decreased pore size, with decrease in ionic strength, thus shows up both in retention and in dispersion. However, retention and dispersion measure different rotational averages of the solute shape, as demonstrated above, at least as long as convection does not dominate dispersion.

At this point one should reconsider the difference of peak widths for samples of identical retention but different ionic strength (Fig. 4). According to the presented analysis, *C*-terms vary little with ionic strength. The observed large difference in Fig. 4 is therefore due to the Peclet term with which *C* becomes multiplied. This Peclet term refers to mass transport in the interstitial volume and is therefore calculated with bulk diffusion coefficients and R_s. These differ for different-sized samples even though their size R_R inside the pore may be equal.

DISCUSSION

Obstructed diffusion

Obstructed diffusion in SEC is due to four factors: tortuosity, constriction and porosity in the geometry of the porous matrix (collectively just called tortuosity) and frictional drag between a diffusing object and obstructing walls. Flexible polymers are deformed by this frictional drag and their obstructed diffusion becomes an intricate subject of polymer physics. The present data represent the first comprehensive study of obstruction with native globular proteins, ideally applicable to the basic hydrodynamic theories of solid spherical objects.

Tortuosity. Tortuosities of the stagnant zone were calculated from the intercept of plots such as Fig. 7 or obtained directly from global numerical fit of dispersion data (eqn. 4). A value of $\xi_p = 1.5$–1.8 was found for all conditions studied (Table III), but according to Fig. 2c the true tortuosity is 7% larger. Compared with the respective tortuosity factors (Table I), this magnitude implies a significant role of channel constriction (eqn. 19) with a ratio of maximum to minimum radius of *ca.* 2. Tortuosity determined in this manner is, however, extremely sensitive to uncertainties of the aspect ratio $R_s/R_{1/2}$, whereas α values are not, and the accuracy in deriving the pore size variation is therefore limited. Whether Superose-12 exhibits a pore

size variation of at least 1.5 or rather is monodisperse cylindrical must therefore remain undecided. For reticular porous glass of porosity $p_i = 0.48$ a factor of 3 difference was found between microscopic mean radii and mercury porosimetry, which measures minimum radii [79]. A factor of 2 difference was found between mercury porosimetry and radii determined from the volume-to-surface ratio [80]. Others have found smaller ratios for similar glasses [81]. Note that the size dependence of porosity is explicitly treated in the outlined theories for the α term whereas the size dependence of constriction [48,82] is not.

The observed values of tortuosity agree with most of the values reported in the literature (Table IV) and excessive deviations rather indicate systematic experimental difficulties. Particularly values of $\xi_p < 0.93$ are theoretically impossible. Many times problems are obvious, *e.g.*, large values of tortuosity in conjunction with the lack of a dependence on the aspect ratio $R_s/R_{1/2}$, *i.e.*, $\alpha = 0$, amongst the early studies owing to large scatter of data that obscures any size dependence that might have been present. Note that the notion of size-independent D_{pore}/D_{bulk} values [44] persisted in the field of chromatography until about 1983 in spite of theoretical predictions to the contrary and even evidence in related fields (Table IV).

TABLE IV

OBSTRUCTED DIFFUSION

Matrix	Sample[a]	Range of $R_D/R_{1/2}$	Tortuosity, ξ_p	Drag, $\alpha\beta$	Method[b]	Ref.
Frictional drag						
Vycor glass	Linear polystyrene	0.0–1.0	3	0[c]	ND	81
CPG glass	Linear polystyrene	0.0–0.1	1.3	2	QLS	85
CPG glass	Linear polystyrene	0.0–0.2	1.3	2.7	QLS	84
Porous glass	Linear polystyrene	0.0–0.4	1.4	4.1	ND	113
CPG glass	Linear polystyrene	0.1–0.8	1.0	3.4	QLS	67
CPG glass	Star polyisoprene	0.0–0.1	1.3	1.75	QLS	67
CPG glass	Star polyisoprene	0.0–0.1	1.3	3.3	QLS	67
Sephadex	Dextran	0.4–0.7	1.0	2.3	FRAP	110
Sephadex	OM	*ca.* 0.0	1.5	n.a.	ND	100
Porous glass	Water, OM	0.0–0.5	1.7	*ca.* 4	NMR	102
Silica–alumina catalyst	OM	0.1–0.5	2	4.6	ND	50
Vycor glass	OM (dye)	*ca.* 0.5[d]	2.7[c]	*ca.* 6.2	FRS	93
Parallel plates	Latex spheres	0.0–0.1		3.3	QLS	90
Sepharose 4B	Proteins	0.1	1.75 (1.55)	2.1 (3.7[c])	ND	101
Amylose gels	Proteins	0.1–0.4	1.2	1.0	QLS	107
Vycor glass	Proteins	0.0–0.2	2	7.0	ND	81
Frictional drag plus excluded volume						
CPG glass	Linear polystyrene	0.0–0.4	6	0[c]	SEC	48
VITX glass	Linear polystyrene	0.0–0.4	6 (±2)	0[c]	SEC	82
Silica	Linear polystyrene	0.1–0.5	3 (6)	2.3 (1.8)	SEC	95
LiChrospher	Linear polystyrene	0.1–0.8 (0.4)	2 (1)	3 (8)	SEC	19
Hypersil	Linear polystyrene	0.0–0.7 (0.3)[e]	6	1 (3.5)[e]	SEC	18
TSK-G6000H6	Linear polystyrene	0.0–0.6 (0.8)[e]	4	3 (2)[e]	SEC	82
Porasil	Linear polystyrene	0.2–0.9	1.4	2.6[f]	SEC	37
Nuclepore membrane	Linear polystyrene	0.0–0.7	1.0	8.5	SDB	92
Etched mica membrane	Linear polystyrene (high M)	0.0–0.5	1.0	7.6	SD	103
Etched mica membrane	Linear polystyrene (low M)	0.0–0.5	1.0	5.5	SD	105
Etch polycarbonate membrane	Linear polystyrene	0.1–0.6 (0.9)	–	6.3	SD	98,99
Nuclepore membrane	Linear polyisoprene	0.1–0.5	0.7	6.0	SD	87
Nuclepore membrane	Star polyisoprene	0.1–0.5	1.7	6.0	SD	87
Nuclepore membrane	Dextran	0.0–0.1	1.0	0[c]	SD	86
Nuclepore membrane	Dextran	0.1–1.0	0.7	3.6	SD	86
Nuclepore membrane	Dextran	0.3–0.7	0.4	3.4–5.3	SD	94

TABLE IV *(continued)*

Matrix	Sample[a]	Range of $R_D/R_{1/2}$	Tortuosity, ξ_p	Drag, $\alpha\beta$	Method[b]	Ref.
TSK2000/3000SW	Dextran	0.0–0.8	2.9	4.3	SEC	106
Nuclepore membrane	Ficoll	0.0–0.3	1.0	4.4	SD	86
Nuclepore membrane	Ficoll	0.2–0.7	0.6	7.0	SD	86
Nuclepore membrane	Ficoll sulphate	0.0–0.2	0.5 (1.0)	8.4 (4.0)	SD	76
Etched mica membrane	Asphaltenes	0.0–0.8	–	3.9	SD	64
Collodion membrane	OM			>3.3	SD	109
Collodion membrane	OM (sucrose)	0.0–0.2	1	6.2	SD	108
Etched mica membrane	OM (porphyrins)	0.0–0.2	1	5.0	SD	105
Etched mica membrane	OM	0.0–0.2	1	4.6	SD	38
Etched mica membrane	OM	0.2–0.4	1	7.0	SD	38
Etched polycarbonate membrane	OM (inulin)	0.0–0.1	1	8.9	SDB	88
Kidney glomeruli	OM	0.0–0.2 (0.5)	–	4.6	SDB	58
Capillary circulation of perfused hind legs	OM, proteins	0.0–0.6	–	6.7	SDB	111
Cellulose membrane	OM	0.2–0.3	–	4.5	SDB	57
Cellophane membrane	OM	0.1–0.2	–	6.3	SDB	57
Cellophane membrane	OM, proteins, dextran	0.0–1.0	2.0–2.7	–[g]	SD	91
Etched mica membrane	Latex spheres	0.0–0.4	1.0	*ca.* 7.0[h]	SD	75
Nuclepore membrane	Latex spheres	0.1–0.8	1.0	2.5	SDB	89
Millipore membrane	Latex spheres	0.1–0.4	0.08	3.2	SDB	114,128
PSM-800 silica	Silica sol	0.2	*ca.* 2	*ca.* 7	SEC	104
Etched mica membrane	Proteins	0.0–0.4	1	8.2	SD	115,116
Nuclepore membrane	Proteins	0.0 (0.4)–0.8	–	*ca.* 1.0 (2.0)	SDB	96
Agarose gels	Proteins	0.1–0.2	1.0	4.0	SDB	83
Agarose gels	Proteins	0.2–0.5	0.6	*ca.* 7.0	SDB	83
Zorbax-GF250,450	Proteins	0.2–0.5	–	3.1	SEC	97
LiChrosorb diol	Proteins	0.0–0.4	4.2	3.8	SEC	62
LiChrospher silica	Proteins	0.0–1.0	1.9	3.5	SEC	117
TSK-250SW	Proetins	0.1–0.4	1.0	3.5	SEC	73
TSK2000/3000SW	Proteins	0.0–0.8	2.9 (2.0)	4.3 (5.3)	SEC	106
TSK2000SW	Proteins	0.5	*ca.* 2	*ca.* 7	SEC	112
TSK3000SW	Proteins	0.4	*ca.* 1.5	*ca.* 7	SEC	112
TSK-6000PW	Proteins	0.1–0.4 (0.2)[e]	1.6	1.0 (3.0)[e]	SEC	This study
TSK-6000PW	DNA	0.1–0.4 (0.2)[e]	1.5	1.0 (3.0)[e]	SEC	This study
Superose-6	Proteins	0.0–0.6	1.5	5.6 (6.0)[e]	SEC	This study
Superose-12	Proteins	0.0–0.9	1.7	7.4 (7.4)[e]	SEC	This study

[a] OM = Non-polymeric organic molecules.

[b] QLS = quasi-elastic light scattering within the porous material; FRAP = fluorescence recovery after photobleaching within the porous material; NMR = nuclear magnetic resonance; FRS = forced Rayleigh scattering; ND = non-steady state (transient) diffusion with infinite reservoir; SD = steady-state diffusion with finite reservoir, boundary layer effects absent or corrected; SDB = steady-state diffusion with finite reservoir, boundary layer effects non-corrected, which may significantly underestimate α; SEC = dispersion in chromatography (non-steady state diffusion with finite reservoir), α-term may be decreased by convection.

[c] Large scatter in the data prevented detailed assessment. Numerical fit was forced to listed value in order to obtain the complimentary tortuosity (respective drag).

[d] The molecular size given in the original article disagrees with the diffusion coefficients reported in the same article; still, the dye may be adsorbed.

[e] Values in parentheses are for maximum (R_{max}) instead of average pore size ($R_{1/2}$).

[f] Convection explicitly treated in separate term.

[g] Large effect (order of 7 probable) but pore size unknown. Note that exponential relationship is obtained for all data if Stokes radius is used instead of the author's definition of a characteristic radius.

[h] Electrostatic repulsion not corrected with eqn. 29 but by the original authors using certain quantitative energetic assumptions.

Drag and excluded volumes. The present data confirm the applicability of an exponential representation of obstructed diffusion but the observed magnitudes expressed in terms of a coefficient α do not coincide for the different columns studied. These differences are believed to be due to convective transport and the second part of the discussion will elaborate how inclusion of convection theory is able to make all data converge to $\alpha = 7.4$ as the value proper for

obstructed diffusion. This value coincides with the theoretical calculations for cylindrical pores by Bean.

A comparison of this result with the abundant literature on obstructed diffusion [18,19,37,38, 48,50,57,58,62,64,67,73,75,76,81–117] shows that the scatter amongst different studies is almost unacceptable even for methods such as quasi-elastic light scattering or diffusion cell measurements that need not worry about convection (Table IV). Most would probably have opted for the centreline approximation. Interestingly, there is a trend to larger α values in more recent studies. In retrospect, various sources of error must be held responsible for the observed irreproducibility, namely concentration effects, the specific nature of flexible polymers, incorrect or lack of correction for boundary layer resistance, problems of pore size and shape, influence of ionic strength, adsorption and convection. Experiments may have also failed in trivial respects, *e.g.*, proper sampling rate and angle in quasi-elastic light scattering or residual flow (ultrafiltration) in diffusion cell measurements. The remainder of the discussion summarily addresses these problems without possibly passing judgement in all individual cases. Future studies will need to include far more experimental controls to avoid perpetuating this dismal status of affairs.

Preface to Table IV. The earliest experimental study to correlate steady-state diffusion with the aspect ratio of pores in copper hexacyanoferrate(II) precipitation membranes was only qualitative [118]. This is also true of some early chromatographic studies that exemplified the role of diffusion for the mechanism of SEC [119,120]. Many subsequent studies only provided raw data that here are interpreted for the first time. Of those publications that provide theoretical interpretations, only four applied an exponential relationship [50,64,89,91]. For the present comparison, literature data were uniformly reanalysed in terms of eqn. 29 with $R_D = R_s$ except for identified cases of low ionic strength. In some uncertain cases alternative fitting pairs of ξ and α have been included. Since many data are suspected to include concentration effects, Table IV formally lists the product of α times β. Table IV is divided into two sections. First come the methods that are independent of the volume of measurement, such as quasi-elastic light scattering, and therefore measure pure frictional drag, ideally $3.5 \leqslant \alpha \leqslant 4.5$ at least up to $R_s/R_{1/2} \leqslant 0.5$. Current technical limitations prevent measurement by quasi-elastic light scattering at low concentration. Second, there are those methods which for certain boundary conditions [50] also require an excluded volume term; here ideally $5.5 < \alpha \leqslant 7.4$ for solid spheres up to $R_s/R_{1/2} \leqslant 0.6$. Chromatographic dispersion measurements represent a transient diffusion with a finite reservoir and belong to the latter category. Below $R_s/R_{1/2} < 0.1$ the magnitude of obstruction is too small to be reliably measured by SEC and has insignificant weight in wider data sets. All SEC data therefore should yield $\alpha = 7.4$ for diffusion proper. Diffusion cell measurements could in principle provide accurate measurements of the initial slope at low aspect ratios, but none have so far convincingly established the break point which is expected at $R/R_{1/2} = 0.05$ by Famularo and at $R/R_{1/2} = 0.2$ by the centreline approximation (Renkin and others).

Boundary layer resistance. In conventional diffusion measurements across a membrane, a boundary layer of depleted concentration forms whose magnitude depends on the efficiency of stirring and on the pore density. Boundary layer resistance further decreases diffusion rates, more for small than for larger solutes. Hence uncorrected data tend to show decreased values of α and increased tortuosity. While the effect is dramatic for the data of Conlon and Craven [89], it is present also with those of Ackers and Steere [83], which at low aspect ratios superficially fitted to theories with centreline approximation that are now known to underestimate obstruction. Deviations observed in diffusion cell measurements seem to be largely due to insufficient corrections for boundary layers.

For the SEC data in this study, the contribution from boundary layer effects has been explicitly treated with eqn. 12; other studies may, however, have neglected this term and some failed to correct for any of the A-term. Consequently low α-values for SEC in Table IV by themselves do not prove that convective mass transfer did occur.

Flexible polymers. Flexible chain polymers (polystyrene, polyisoprene, dextran) yield lower values of $\beta < 1$ in most studies (Table IV and ref. 121); some, however, find $\beta \approx 1$ at low enough concentrations [87,92,98,99]. Highly branched chain-polymers (Ficoll, star polymers) approach the behaviour for solid spheres (latex, proteins, small molecules), where $\beta = 1$, even at higher concentrations. The present study demonstrates that at least under conditions close to infinite dilution, DNA and asymmetric proteins also approach the behaviour of solid spheres in terms of their equivalent Stokes radii. Values of $\beta < 1$ may be an artifact of sample polydispersity [103]. In addition, values of $\beta < 1$ are expected whenever the polymer is free-draining [94]. Values of $\beta < 1$ have also been rationalized as a truncation of the configurational distribution by sterically excluding the most expanded polymer conformations, which will shift average diffusion coefficients to larger values. Quantitative agreement between theory [62] and experimental polystyrene data [37] was claimed (note that the legend to Fig. 7 in ref. 62 specifies R_G where clearly R_s was used to plot the polystyrene data of ref. 37); in this regard, see also ref. 122. Finally, a complicated theory of flexible chains becoming deformed or even reptating through the pores was advanced [70], but whether they actually reptate is disputed [84,123]. The deformation to a one-dimensional chain is entropically so unfavourable that it requires large driving forces to make the chain enter the pore at all. At infinite dilution such forces may be found in electrophoresis or in ultrafiltration at sufficiently high shear rates (cf., refs. 8 and 124), but not by diffusion. Under infinitely dilute conditions ample evidence is available [1,71] that universal calibration in terms of R_η describes SEC retention with few exceptions that suggest earlier elution as opposed to delayed retention predicted for reptation. However, in semi-dilute solution chain polymers are already deformed and then preferentially enter the pore space where they might reptate [125]. Hence the magnitude of obstruction decreases strongly with increasing concentration of flexible polymers [92,98,99,126]. In fact, a recent theory concluded that $\beta = 1$ for $R/R_{1/2} < 0.4$ as long as flexible polymers are at infinite dilution [69,122]. For higher aspect ratios drag was suspected to deform polymers and enhance transport even at infinite dilution; according to different sets of experiments, however, this ought to happen without increasing retention volumes. One conclusion from this analysis is that concentration effects are significant in the process of kidney glomerular filtration (see ref. 127). Current estimates of the term $\alpha\beta$ for polystyrenes at infinite dilution correspond well with the results of the present study with compact spheres as well as to the theory of Famularo without any need to invoke special partitioning effects (*cf.*, refs. 103 and 122).

Proper choice of pore size. Obstructed diffusion theory depends on pore shape. Even though track-etched mica contains extremely well defined pores, their shape is rhomboidal and obstructed diffusion has not yet been calculated for this case. The observed pattern of α values, which have been defined with equivalent cylindrical pore radii (which different workers have even done in different ways), is not much different from, say, track-etched polycarbonate membranes (Nuclepore), which contain smooth cylindrical pores of fairly monodisperse size.

What values of pore size should be used for polydisperse porous networks? Table IV is based on average values $R_{1/2}$ whenever such data were available, but some workers only reported aspect ratios and may have used other criteria. Further, large solutes probe pores above average size and *vice versa* such that constant mean $R_{1/2}$ may underestimate α. The worst case correction replaces $R_{1/2}$ by R_{max} (Table I). The data from the present study clearly demonstrate that even after such a correction a significant difference remains between the different columns from this study that needs to be explained via convection (Table IV). The uncertainty regarding proper aspect ratios, however, limits quantitative tests of the theory of convection.

Obstructed diffusion of polyelectrolytes at low ionic strength. For the reanalysis of literature data, proper R_D values and eqn. 29 were used at low ionic strength. The only exception is a study of latex as a function of ionic strength [75], which did not provide proper R_{IF} values and consequently could not be analysed in terms of eqn. 29. The non-electrostatic term used by the

workers, which they indirectly based on theoretical assumptions, was included in Table IV. In some instances, effects of ionic strength may have gone unnoticed. In particular, all measurements of latex spheres may have been conducted at insufficient ionic strength and low α values may in part be due to neglect of R_{IF}. Once eqn. 25 no longer holds, ion mobilities further couple in and accelerate diffusion of the macromolecular polyelectrolyte (see also refs. 114 and 128). The present study is the first to relate quantitatively obstructed diffusion that includes a significant contribution from electrostatic interfacial repulsion with independent experimental evidence about their magnitude. The constant α values for Superose-12 at low ionic strength up to $R_D/R_{1/2} < 0.9$ unfortunately cannot be compared with less disputable conditions of high ionic strength which for Superose-12 only reach up to $R_s/R_{1/2} < 0.6$. Most other data on obstructed diffusion do not exceed this margin either.

The demonstration of charge-related effects on size, and thus on aspect ratio, points to a fundamental issue that has already been exemplified for the retention problem at SEC [1]. If hydration forces of significant extent exist, and it is likely that they do, even high ionic strength data will be affected by R_{IF} terms and the concept of size relevant to transport processes in confined spaces may need general revision.

Adsorption. The rate of equilibration in chromatographic beads with solutes was often found to be biphasic, possibly owing to a slower adsorption process [79,120]. Adsorption of molecules delays their migration and thus superficially increases the degree of obstruction. Studied together with non-adsorbing solutes, adsorbing solutes have often been identified and excluded (*e.g.* refs. 50, 102). Other obvious cases were retrogradly excluded (*e.g.*, ref. 129). The questionable data in ref. 94, whatever the reason, seem to have been superseded by ref. 86. Excessively large values of tortuosity may derive from preferential adsorption of the smaller solutes. Small opposite tends that result in superficially increased α values are, however, difficult to identify. While all other sources of error underestimate α, the largest observed values are not automatically the correct ones due to the possibility of adsorption.

One-sided obstruction. The restricted diffusion close to a wall but open to bulk solution on the other side was studied by photon correlation spectroscopy from an evanescent wave [130]. Excess frictional drag is lower than in cavities of parallel plates with same centreline distance, as expected.

Concentrated solutions. It should be mentioned that much earlier an exponential obstruction factor had been derived for the transport of compact objects through concentrated solutions of chain polymers [131,132]. The relationship between polymer concentration and "pore size" unfortunately remains subject to assumptions and it is difficult to arrive at conclusions regarding the magnitude of α. The hydrodynamics of porous matrices undoubtedly provide valuable insight into the properties of concentrated solutions. These, however, are still more complicated [123].

Convective mass transport

As early as 1969 it was reported that axial dispersion is less than predicted by the Van Deemter equation [133], but no reason was given and data were not well analysed. Judged by the results of this study, however, their claim is feasible for their experimental conditions. Later, another study claimed flow through the pores but did not present data [134]. As they were operating at $Cf = 200$ they indeed should have observed convection. Around 1978–82 several studies involved convective mass transport in gas chromatography and SEC, which will now be discussed in more detail with notation adapted to the present style. Intra-pore convection theory seems to have been rederived since [14,135].

First study. Rate-limiting convection may be described by an effective diffusion coefficient according to Taylor–Aries theory. Its convective term $c^2R_{1/2}^2/D$ (c = linear flow-rate, D = three-dimensional diffusion coefficient, $R_{1/2}$ = pore radius) is additive to diffusion proper and leads to the following expression with a numerical factor based on a cylindrical cross-section [136]:

$$C_c = \frac{\xi_p}{69\,500} \cdot \frac{(V - V_{void})}{V^2} \cdot \frac{(V_{column} - V_{void})^2}{V_{void}} \frac{D_{pore}}{D_{bulk}} \left(\frac{c_{p,eluent}}{c_{p,solute}}\right)^2 \frac{Cf^3}{Pe^2} \quad (30)$$

where c_p is the mean linear velocity of solute or eluent inside the pores and the ratio accounts for effects of hydrodynamic chromatography which include the role of excess drag on convection. Cf is the convective factor defined in eqn. 3. Since diffusion and convection are parallel processes, the final C-term is

$$C^{-1} = C_d^{-1} + C_c^{-1} \quad (31)$$

Equal contributions of convection and diffusion are predicted for

$$Pe = \frac{1}{25} \cdot \frac{D_{pore}}{D_{bulk}} \cdot \frac{c_{p,eluent}}{c_{p,solute}} \cdot Cf^{3/2} \quad (32)$$

where $p_i = 0.34$ was assumed. According to this derivation, convection plays a role at much lower Peclet numbers than initially guessed upon introducing the convective factor term. Owing to the D_{pore}/D_{bulk} term and Pe^{-2} dependence in eqn. 30, convection does not lead to a plateau value but to a pronounced maximum around equality of convection and diffusion followed by a rapid decrease for higher Pe. Such a decrease has been predicted independently for turbulent open capillary flow [137], but the derivation does not apply to low Reynolds numbers. Grüneberg and Klein [138] rejected the Taylor–Aries approach as an artifact of inappropriate assumptions.

Second study. Grüneberg and Klein [138] calculated a term for rate-limiting convection at low Reynolds numbers from random walk theory which is valid as long as the porous zone is still stagnant ($Cf \gg 1$):

$$C_c = l\xi_p \cdot \frac{(V - V_{void})}{V^2} \cdot V_{void} \cdot \frac{c_{p,eluent}}{c_{p,solute}} \frac{Cf}{Pe} \quad (33)$$

where $l = 2$. The same equation but with a numerical factor $l = 3$ was later obtained by Gibbs and Lightfoot [135]. Eqn. 33 replaces eqn. 30 and is used in conjunction with eqn. 31. In their original theory ($l = 2$), equal contributions of convection and diffusion are predicted for

$$Pe = 60 \cdot \frac{D_{pore}}{D_{bulk}} \cdot \frac{c_{p,eluent}}{c_{p,solute}} \cdot Cf \quad (34)$$

where the numerical factor has been modified to account for a tortuosity factor which their original derivation omitted from an equation equivalent to eqn. 21. Accordingly, onset of convection is much later. It eventually leads to a plateau whereas the earlier treatment had predicted a maximum.

However, their own data seem to contradict their theory. On VITX porous glass at $Cf = 5600$ they claimed to observe unusually small C terms compared with VITX glass with smaller pores and thus larger Cf. The reduced plate height h increases linearly with increasing Peclet number and does not (yet) reach a plateau. They claimed to find convection two orders of magnitude larger than predicted by eqn. 33. However, their analysis is flawed and ignores frictional drag which potentially could explain their experimental observations.

Third study. The major novelty of the approach of Rodrigues *et al.* [139] is a complex non-additive coupling between diffusion and convection that replaces eqn. 31 and thus diverges from the additivity theorem of dispersion. Carta *et al.* [140] and Rodrigues *et al.* [141] have adapted this treatment to spherical geometry. Their analysis is equivalent to eqns. 31 and 33 if l is made a variable function of the intra-pore Peclet number λ:

$$\lambda^{-1} = 6 \cdot \frac{D_{pore}}{D_{bulk}} \cdot \frac{c_{p,eluent}}{c_{p,solute}} \cdot \frac{Cf}{Pe} \quad (35)$$

$$\frac{1}{l} = \frac{5}{3}\left(\frac{1}{\tanh \lambda} - \frac{1}{\lambda}\right)^{-1} - \frac{5}{\lambda} \quad (36)$$

According to eqn. 36, one obtains for $\lambda = 1$ $l = 3$, for $\lambda >> 1$ $l = 0.6$ and for $\lambda << 1$ $l = +\infty$; for $\lambda > 10$ the plateau region is reached where $l < 0.7$ and h remains constant with increasing Pe. Rodrigues *et al.*'s equation does not consider the role of inaccessible boundary layers for convection and corresponds in this regard to Van Deemter's original assumption of a constant value for the A-term.

Fourth study. Van Kreveld and Van den Hoed [37] employed an equation similar to eqn. 33 but

based on an effective diffusion whose convective term equals c times a coefficient Cf', which replaces Cf in eqn. 33 and which they adjusted numerically. For Porasil with narrow pores ($R_{1/2} = 13$ nm, $Cf = 5 \times 10^6$, $d = 125$ μm), they observed the onset on convection around $Pe > 10^4$ for polystyrene in the size range $R_s = 3$–12 nm. They reported a plateau in line with eqn. 33 and contradicting eqn. 30. This plateau depends on polystyrene size and their data may be interpreted as

$$Cf' = \frac{240}{l} \cdot \frac{d\ (\mu\text{m})}{R_s\ (\text{nm})} \cdot \frac{c_{p,\text{solute}}}{c_{p,\text{eluent}}} \qquad (37)$$

Hence onset of convection is a factor 500 earlier than predicted by Rodrigues *et al.*, *i.e.*, eqn. 33 with $l = 0.6$ together with eqn. 31, and worse for larger l values. This is in the trend of the claims by Grüneberg and Klein. For the sake of completeness it must be added that the data of Van Kreveld and van den Hoed were obtained at elevated Reynolds numbers, $Re \approx 0.3$–3, *i.e.*, above normal laminar conditions of SEC operation. In fact, one expects $Cf \propto c^{-1}$ in the inertial regime ($Re > 1$) [142]. The numerical factor in eqn. 37 certainly decreases with increasing pore size but no data are available in this regard.

Fifth study. Kirkland [104] claimed intra-pore convection in SEC and refers to Van Kreveld and Van den Hoed but omits quantitative analysis. His data for the PSM-800 silica matrix ($R_{1/2} = 24$ nm, $Cf = 5000$, $d = 6$ μm) exhibit two regimes for the C-term but no plateau. At low flow-rates the C-term crudely corresponds to $\alpha \approx 7$, if the convective term is omitted and falls between the present data for Superose-6 and Superose-12, as would have been expected from the column parameters. At flow-rates above 1 ml/min h continues to increase linearly with increasing Pe but at a decreased rate corresponding to an apparent value of $\alpha \approx 1$, if convective terms are omitted. The same slope is observed for the PSM-500 silica matrix ($R_{1/2} \approx 8$ nm, $Cf = 80\,000$, $d = 7.7$ μm) above 0.2 ml/min. In this instance the initial regime has not been carefully measured but the magnitude of h suggests that it also occurs. Both data sets belong to the low Reynolds number regime ($Re < 0.1$), albeit not as low as in the present study. The slope of $\alpha \approx 1$ implies that the onset of convection is a factor 300 earlier than predicted by Rodrigues *et al.* (eqn. 33) with $l = 0.6$ and corresponds fairly well with eqn. 37. Considering what has been said about eddy dispersion in the mobile zone (A_e-term), these results may not be surprising, except that they are much larger than the Pe variation of A_e. A qualitative picture, however, is emerging: Kirkland's low flow-rate regime corresponds to the conditions and results of the present study; Kirkland's high flow-rate regime corresponds to the initial part of the data of Van Kreveld and Van den Hoed before the onset of their plateau.

Sixth study. Rokushika *et al.* [112] presented dispersion data without interpretation and remarked on their irregularity. For TSK2000SW ($R_{max} \approx 5$ nm, $d = 10$ μm, $Cf \approx 200\,000$) at $Re < 0.03$, their data show a dependency of α on flow-rate, from $\alpha \approx 7$ at 0.1 ml/min to $\alpha \approx 6$ at 3 ml/min. These conditions correspond to $\lambda < 0.01$ and therefore lack convective contributions completely according to Rodrigues *et al.* They are, however, consistent with the second domain of Van Kreveld and Van den Hoed and Kirkland and agree semi-quantitatively with Cf' from eqn. 37. Interestingly, the onset of this effect is later for TSK3000SW.

Seventh study. Afeyan *et al.* [14] recently analysed POROS material ($Cf \approx 90$, $d = 20$ μm) ate $Re < 0.3$ and proposed a theory of convection that is identical with that of Grüneberg and Klein ($l = 2$) without applying it to their data. Judgement is difficult because the paper does not report all the information needed for analysis, but the plateau observed in the range $\lambda = 3$–8 may agree with Rodrigues *et al.* ($l = 0.6$) even though a value as low as $l = 0.2$ cannot be excluded. Lack of a second regime may simply be due to the fact that for such wide-pore material $Cf' > Cf$ rather than the opposite and thus never comes to play.

Shell model. A completely different explanation for a decrease of the C-term with increasing flow rate was put forward by Kubín [143]. He assumed that penetration of the beads is limited to an outer shell of variable thickness because there is insufficient time to establish equilibrium throughout the bead. Others have used Kubín's

model to explain their experimental observation of a decrease of the C-term with increasing flow rate [144]. Owing to limitations of space a thorough discussion of this matter is deferred to a forthcoming second part of this series ("The role of transport processes and non-equilibrium in size-exclusion chromatography"). The predictions of Kubín's particular model are, however, briefly compared with the results of this investigation.

This study. Kubín's shell model predicts a maximum around $R/R_{1/2} \approx 0.5$ for the Superose-12 data shown in Fig. 7. In this regard Kubín's model is phenomenologically indistinguishable from the Taylor–Aries theory (first study). At the same time the Kubín model underestimates the effect for TSK6000PW if it alone had to explain the low value of α that is observed in this instance. In order to explain fully the observed dispersion data, convective mass transport must therefore occur.

According to the presented Taylor–Aries theory (see First study) (eqn. 30), Superose-12 data should belong to the diffusive regime. For Superose-6 eqn. 32 predicts a maximum around 100 *Pe*, which is just above the range of measurement. The reported α value should undoubtedly be biased by convection. Finally, TSK6000PW should be entirely in the convective regime. Clearly, no maximum is observed (see Fig. 5) and neither is a plateau. The functional form of eqn. 30 must therefore be doubted.

According to the data of Van Kreveld and Van den Hoed (see Fourth study), the TSK6000PW column would operate in the plateau of convection, which is not borne out by the data. It must be emphasized that according to eqn. 37 even Superose-12, with the same pore size and even smaller beads, should be subject to convective contributions.

The random walk model (see Second study) (eqn. 33 with $l = 2$) predicts that Superose-12 operates in the diffusive regime. Since all data were taken at $\lambda < 0.3$, Rodrigues *et al.*'s analysis (see Third study) claims $l > 10$ and safely excludes convective terms. In analogy with Rokushika *et al.*'s data (see Sixth study), the second convective domain is not yet manifest for Superose-12 at 0.5 ml/min flux. The Superose-12 data consequently represent pure effects of obstructed diffusion. Superose-6 exhibits a slight contribution from convection. The data represent a range $\lambda = 1$–8, which corresponds to $l = 0.8$–3 according to Rodrigues *et al.* (see Third study) and is difficult to distinguish from the random walk models. The apparent α values for TSK6000PW are significantly decreased but the plateau region lies outside the range of measurement. The available data represent a range of $\lambda = 3$–30 which corresponds to $l = 0.6$–1.2. According to the data of Afeyan *et al.* (see Seventh study) one would not expect much of a second domain for this column. Explicit account of convection increases α to a value around 7 and demonstrates that this magnitude is the true value for diffusive mass transfer of solid spheres in all porous matrices. A value of $l = 2$ is clearly insufficient in this regard and gives preference to Rodrigues *et al.*'s equation (eqns. 33, 35, 36). The large scatter of this particular data set and the wide pore size distribution of TSK6000PW, however, preclude a decisive validation of the details of Rodrigues *et al.*'s equation.

The experimental data in this investigation are based on different solutes run at the same flow-rate. Future study of their flow-rate dependence is expected to resolve the undecided quantitative issue. It is obvious, however, that Rodrigues *et al.*'s analysis does not predict the observation of a second domain of dramatically increased convection. In part this should be related to the neglected Peclet number, Reynolds number and geometric dependence (see A_e-term in Theory section). The observed magnitude and phenomenology (Cf' term), however, is clearly not understood. The cumulative empirical evidence, however, is consistent and leaves no doubt about the crucial influence of convection not only for novel wide pore materials but even for traditional SEC situations.

CONCLUSIONS

Of all theoretical considerations of obstructed diffusion, the numerical results of Famularo come closest to experimental truth and their use is strongly recommended. His calculations are well represented by a logarithmic one-parameter

function for obstructed diffusion in those instances where excluded volume and drag effects occur together, such as in SEC. The parameter then is $\alpha = 7.4$ except for the very initial slope of $\alpha = 5.5$. Drag effects alone are not well represented in this manner. Geometrically simple membrane pores and complex porous networks of variable cross-section behave similarly as far as data quality permits a conclusion. Advanced theoretical efforts in complex geometry are desirable, however, as much as experimental consolidation. The centreline approximation is clearly erroneous and many of its widespread applications, particularly in the field of biological porosimetry, will need to be revised. There is reasonably good evidence that, in the limit of infinite low sample concentration, obstructed diffusion correlates with the diffusional Stokes radius of infinite dilution plus extra interfacial terms due to the finite "concentration" of the pore walls. Deviations to smaller sizes are artifacts of finite sample concentrations, at least for aspect ratios of $R/R_{1/2} < 0.4$. The obstructed diffusion of polyelectrolytes at low ionic strength is fully explained by the role of interfactial effects analogous to their role in SEC retention. As different sizes are derived by retention and dispersion for asymmetric molecular shapes, the mechanism of retention is not determined by transport processes.

Convective mass transport within the stagnant zone occurs in most SEC studies. SEC of large polymers is only feasible because convection substantially improves resolution. Of all theories of convection, the equation of Rodrigues *et al.* comes closest to experimental evidence, but does not explain the occurrence of the manifold increased convection at higher than standard flow-rates that was observed in two other studies and is currently not understood. Consequently, ultra-rapid separations are feasible even with narrow-pore materials without ever exceeding a reduced plate high of $h \approx 100$, which may be sufficient for some process control applications. For those who so far have remained sceptical about the existence of flow-through capillaries in chromatographic matrices, the demonstration of convection also provides evidence for this totally porous nature of the materials. Further, the so-called "stagnant" zone moves slowly through the beads, even though the flow is Cf times less than in the mobile zone.

Analysis of Van Deemter's A-term suggests that the assumption of laminar flow in the mobile zone is invalid. Comparison of different chromatographic columns yields a variation of the A-term by a factor of 3, the origins of which remain to be established. Such variation was formerly attributed to the quality of the column packing and is not explained by the role that theory gives to the porosity parameter. A proper physical description of convection and diffusion in the mobile zone is obviously intimately helpful in formulating the equivalent problem of stagnant zone mass transfer. The theory now seems fit for accurate predictions of reduced plate heights and thus enables *a priori* optimization of resolution and correction of physical dispersion in size distribution analysis. A refined understanding of the mechanism of chromatographic dispersion helps in comprehending the geometric topology of packed beds and porous materials and of its hydrodynamics.

SYMBOLS

a	Mark–Houwink exponent
c	interstitial linear velocity
c_p	intra-pore linear velocity
c^*	overlap concentration
c_{inj}	concentration of the injected sample
d	bead diameter
flux	volumetric flow-rate
h	reduced plate height
k	adjustable parameter in A-term
l	constant or variable factor in C_c
m	exponent that measures fluid conditions
n	net charge of polymer
p	porosity [of the interstitial (p_i) or bead (p_b) zone]
w_h	peak width at half-height
A	Van Deemter term A
A_e	term for eddy dispersion
A_p	term for film resistance of trans-zone transfer
$\langle A \rangle$	average cross-sectional area of a pore

A_{max} maximum cross-sectional area of a pore
A_{min} minimum cross-sectional area of a pore
B Van Deemter term B
C Van Deemter term C
C_c convective contribution to mass transfer term
C_d diffusive contribution to mass transfer term
Cf convective factor
D diffusion coefficient [in bulk solution (D_{bulk}) or in confined pore space (D_{pore})]
I ionic strength
L column length
M generic molecular mass
M_n number-average molecular mass
M_w mass-average molecular mass
N number of plates
P Van Deemter-like term of sample polydispersity
Pe Peclet number (of mobile zone)
R generic radius
R_R effective radius of retention in SEC
R_D effective radius of dispersion in SEC
R_{IF} interfacial contribution to the effective radius
R_{SEC} equivalent shape radius of core body as part of R_R
R_s bulk diffusional Stokes radius at infinite dilution
R_η bulk viscosity radius at infinite dilution
R_{max} maximum pore radius
R_{min} minimum pore radius
$R_{1/2}$ average pore radius
Re Reynolds number
V retention volume
V_{column} total volume of the empty column
V_{tot} total liquid volume of the filled column
V_{void} interstitial volume
Δp back-pressure
Δr film thickness

Greek letters

α key factor in obstructed diffusion
β concentration dependent size compression factor
η solution viscosity
$[\eta]$ intrinsic viscosity
λ Peclet number (of stagnant zone)
ρ density
σ standard deviation
ξ tortuosity [of the interstitial (ξ_i) or pore (ξ_p) zone]
ε adjustable parameter in A_e
$\omega, \omega', \omega_i$ proportionality constants in A-term

REFERENCES

1 M. Potschka, *Macromolecules*, 24 (1991) 5023.
2 R.C. Weast and M.J. Astle (editors), *CRC Handbook of Chemistry and Physics*, CRC Press, West Palm Beach, FL, 59th ed., 1979.
3 M.A. Stadalius, B.F.D. Ghrist and L.R. Snyder, *J. Chromatogr.*, 387 (1987) 21.
4 A.E. Scheidegger, *The Physics of Flow Through Porous Media*, Macmillan, New York, 1957.
5 T.H. Gouw and R.E. Jentoft, in T.H. Gouw (Editor), *Guide to Modern Methods of Instrumental Analysis*, Wiley, New York, 1972, p. 43.
6 R.M. Webber, J.L. Anderson and M.S. Jhon, *Macromolecules*, 23 (1990) 1026.
7 A.A. Zick and G.M. Homsy, *J. Fluid Mech.*, 115 (1982) 13.
8 M. Potschka, *J. Polym. Sci.*, submitted for publication.
9 D.M. Smith and D.G. Huizenga, *J. Phys. Chem.*, 89 (1985) 2394.
10 G. Stegeman, J.C. Kraak and H. Poppe, *J. Chromatogr.*, 550 (1991) 721.
11 D.P. Haughey and G.S.G. Beveridge, *Can J. Chem. Eng.*, 47 (1969) 130.
12 W.J. Moore, *Physical Chemistry*, Prentice-Hall, Englewood Cliffs, NJ, 1972, p. 863.
13 J.H. Aubert and M. Tirrell, *Rheol. Acta*, 19 (1980) 452.
14 N.B. Afeyan, N.F. Gordon, I. Mazsaroff, L. Varady, S.P. Fulton, Y.B. Yang and F.E. Regnier, *J. Chromatogr.*, 519 (1990) 1.
15 N.B. Afeyan, N.F. Gordon, S.P. Fulton and F.E. Regnier, in R.H. Angeletti (Editor), *Techniques in Protein Chemistry*, Vol. 3, Academic Press, San Diego, 1992, p. 135.
16 S.G. Weber and P.W. Carr, in: P.R. Brown and R.A. Hartwick (Editors), *High Performance Liquid Chromatography* (*Chemical Analysis*, Vol. 98), Wiley, New York, 1989, p. 1.
17 B.A. Bidlingmeyer and F.V. Warren, *Anal. Chem.*, 56 (1984) 1583A.
18 J.H. Knox and F. McLennan, *J. Chromatogr.*, 185 (1979) 289.
19 O. Chiantore and M. Guaita, *J. Liq. Chromatogr.*, 5 (1982) 643.
20 J.V. Dawkins and G. Yeadon, *J. Chromatogr.*, 188 (1980) 333.

21 J.C. Giddings, *Dynamics of Chromatography, Part 1*, Wiley, New York, 1965.
22 J.F.K. Huber, *Fresenius' Z. Anal. Chem.*, 277 (1975) 341.
23 C. Horváth and H. Lin, *J. Chromatogr.*, 126 (1976) 401.
24 J.H. Knox, *J. Chromatogr. Sci.*, 17 (1977) 352.
25 P.A. Bristow and J.H. Knox, *Chromatographia*, 10 (1977) 279.
26 G.J. Kennedy and J.H. Knox, *J. Chromatogr. Sci.*, 10 (1972) 549.
27 J.L. Waters, J.N. Little and D.F. Horgan, *J. Chromatogr.*, 7 (1969) 293.
28 J.H. Knox and J.F. Parcher, *Anal. Chem.*, 41 (1969) 1599.
29 J.H. Knox, G.R. Laird and P.A. Raven, *J. Chromatogr.*, 122 (1976) 129.
30 D.L. Koch and J.F. Brady, *J. Fluid Mech.*, 154 (1985) 399.
31 C.L. de Ligny, *J. Chromatogr.*, 49 (1970) 393.
32 G.E. Fleig and F. Rodriguez, *Chem. Eng. Commun.*, 13 (1982) 219.
33 R.N. Kelley and F.W. Billmeyer, Jr., *Anal. Chem.*, 41 (1969) 874.
34 A.J. de Vries, M. LePage, R. Beau and C.L. Guillemin, *Anal. Chem.*, 39 (1967) 935.
35 A.M. Basedow, K.H. Ebert, H.J. Ederer and E. Fosshag, *J. Chromatogr.*, 192 (1980) 259.
36 D.S. Horne, J.H. Knox and L. McLaren, *Sep. Sci.*, 1 (1966) 531.
37 M.E. van Kreveld and N. van den Hoed, *J. Chromatogr.*, 149 (1978) 71.
38 R.E. Beck and J.S. Schultz, *Biochem. Biophys. Acta*, 255 (1972) 273.
39 D.M. Malone and J.L. Anderson, *AIChE J.*, 23 (1977) 177.
40 C.K. Colton and K.A. Smith, *AIChE J.*, 18 (1972) 958.
41 A.A. Kozinski and E.N. Lightfoot, *AIChE J.*, 18 (1972) 1030.
42 M.P. Bohrer, *Ind. Eng. Chem., Fundam.*, 22 (1983) 72.
43 B.D. Mitchell and W.M. Deen, *J. Colloid Interface Sci.*, 113 (1986) 132.
44 J.C. Giddings and K.L. Mallik, *Anal. Chem.*, 38 (1966) 997.
45 W. Heitz and J. Čoupek, *J. Chromatogr.*, 36 (1968) 290.
46 D.M. Andersson and H. Wennerström, *J. Phys. Chem.*, 94 (1990) 8683.
47 L.M. Pismen, *Chem. Eng. Sci.*, 29 (1974) 1227.
48 J.C. Giddings, L.M. Bowman, Jr. and M.N. Myers, *Macromolecules*, 10 (1977) 443.
49 J. van Brakel and P.M. Heertjes, *Int. J. Heat Mass Transfer*, 17 (1974) 1093.
50 C.N. Satterfield, C.K. Colton and W.H. Pitcher, Jr., *AIChE J.*, 19 (1973) 628.
51 E. Glueckauf, *Trans. Faraday Soc.*, 51 (1955) 1540.
52 A.M. Lenhoff, *J. Chromatogr.*, 384 (1987) 285.
53 W.W. Yau, J.J. Kirkland and D.D. Bly, *Modern Size-Exclusion Liquid Chromatography*, Wiley, New York, 1979.
54 H. Faxen, *Anal. Phys.*, 68 (1922) 89.
55 J.D. Ferry, *Chem. Rev.*, 18 (1936) 373.
56 J.D. Ferry, *J. Gen. Physiol.*, 20 (1936) 95.
57 E.M. Renkin, *J. Gen. Physiol.*, 38 (1954) 225.
58 J.R. Pappenheimer, E.M. Renkin and L.M. Borrero, *Am. J. Physiol.*, 167 (1951) 13.
59 A.J. Hurd, R.C. Mocklev and W.J. O'Sullivan, in W.T. Mayo, Jr. and A.E. Smart (Editors), *Proceedings of the 4th International Conference on Photon Correlation Techniques in Fluid Mechanics*, Joint Institute for Aeronautics and Acoustics, Stanford University, Stanford, CT, 1980, pp. 22-1–22-10.
60 J.L. Anderson and J.A. Quinn, *Biophys. J.*, 14 (1974) 130.
61 P.L. Paine and P. Scherr, *Biophys. J.*, 15 (1975) 1087.
62 V.G. Maltsev, B.G. Belen'kii and T.M. Zimina, *J. Chromatogr.*, 292 (1984) 137.
63 C.P. Bean, in G. Eisenman (Editor), *Membranes: a Series of Advances*, Vol. 1, Marcel Dekker, New York, 1972, p. 1.
64 R.E. Baltus and J.L. Anderson, *Chem. Eng. Sci.*, 38 (1983) 1959.
65 H. Brenner and L. Gaydos, *J. Colloid Interface Sci.*, 58 (1977) 312.
66 J. Happel and H. Brenner, *Low Reynolds Number Hydrodynamics*, Prentice-Hall, Englewood Cliffs, NJ, 1965.
67 N. Easwar, K.H. Langley and F.E. Karasz, *Macromolecules*, 23 (1990) 738.
68 R. Tijssen, J. Bos and M.E. van Kreveld, *Anal. Chem.*, 58 (1986) 3036.
69 W.M. Deen, *AIChE J.*, 33 (1987) 1409.
70 P.G. de Gennes, *Scaling Concepts in Polymer Physics*, Cornell University Press, Ithaca, NY, 1979.
71 M. Potschka, *Anal. Biochem.*, 162 (1987) 47.
72 M. Potschka, *J. Chromatogr.*, 441 (1988) 239.
73 Q.C. Meng, Y.-F. Chen, L.J. Delucas and S. Oparil, *J. Chromatogr.*, 445 (1988) 29.
74 M. Potschka, P. Timmins, K. Weber and N. Geisler, in preparation.
75 D.M. Malone and J.L. Anderson, *Chem. Eng. Sci.*, 33 (1978) 1429.
76 W.M. Deen and F.G. Smith, III, *J. Membr. Sci.*, 12 (1982) 217.
77 M. Potschka, *J. Chromatogr.*, 587 (1991) 276.
78 D.L. Edmark, *J. Chem. Phys.*, 62 (1975) 4197.
79 W. Haller, *J. Chromatogr.*, 32 (1968) 676.
80 C.N. Satterfield, C.K. Colton, B. de Turckheim and T.M. Copeland, *AIChE J.*, 24 (1978) 937.
81 C.K. Colton, C.N. Satterfield and C.J. Lai, *AIChE J.*, 21 (1975) 289.
82 J. Klein and M. Grüneberg, *Macromolecules*, 14 (1981) 1411.
83 G.K. Ackers and R.L. Steere, *Biochim. Biophys. Acta*, 59 (1962) 137.
84 M.T. Bishop, K.H. Langley and F.E. Karasz, *Macromolecules*, 22 (1989) 1220.
85 M.T. Bishop, K.H. Langley and F.E. Karasz, *Phys. Rev. Lett.*, 57 (1986) 1741.

86 M.P. Bohrer, G.D. Patterson and P.J. Carroll, *Macromolecules*, 17 (1984) 1170.
87 M.P. Bohrer, L.J. Fetters, N. Grizzuti, D.S. Pearson and M.V. Tirrell, *Macromolecules*, 20 (1987) 1827.
88 J.T. van Bruggen, J.D. Boyett, A.L. Van Bueren and W.R. Galey, *J. Gen. Physiol.*, 63 (1974) 639.
89 T. Conlon and B. Craven, *Aust. J. Chem.*, 25 (1972) 695.
90 P.G. Cummins and E. Staples, *J. Phys. E*, 14 (1981) 1171.
91 C.K. Colton, K.A. Smith, E.W. Merrill and P.C. Farrell, *J. Biomed. Mater. Res.*, 5 (1971) 459.
92 D.S. Cannell and F. Rondelez, *Macromolecules*, 13 (1980) 1599.
93 W.D. Dozier, J.M. Drake and J. Klafter, *Phys. Rev. Lett.*, 56 (1986) 197.
94 W.M. Deen, M.P. Bohrer and N.B. Epstein, *AIChE J.*, 27 (1981) 952.
95 J.V. Dawkins and G. Yeadon, *J. Chromatogr.*, 206 (1981) 215.
96 E. Fuchs and G. Gorin, *Biochem. Biophys. Res. Commun.*, 5 (1961) 196.
97 B.F.D. Ghrist, M.A. Stadalius and L.R. Snyder, *J. Chromatogr.*, 387 (1987) 1.
98 G. Guillot, L. Léger and F. Rondelez, *Macromolecules*, 18 (1985) 2531.
99 G. Guillot, *Macromolecules*, 20 (1987) 2600.
100 S.B. Horowitz and I.R. Fenickel, *J. Phys. Chem.*, 68 (1964) 3378.
101 W. Korthäuer, B. Gelleri and M. Sernetz, *Ann. N.Y. Acad. Sci.*, 501 (1987) 517.
102 J. Kärger, J. Lenzher, H. Pfeifer, H. Schwabe, W. Heyer, F. Janowski, F. Walf, S.P. and Z. Danov, *J. Am. Ceram. Soc.*, 66 (1983) 69.
103 I.A. Kathawalla and J.L. Anderson, *Ind. Eng. Chem. Res.*, 27 (1988) 866.
104 J.J. Kirkland, *J. Chromatogr.*, 185 (1979) 273.
105 I.A. Kathawalla, J.L. Anderson and J.S. Lindsey, *Macromolecules*, 22 (1989) 1215.
106 J.K. Leypoldt, R.P. Frigon and L.W. Henderson, *J. Appl. Polym. Sci.*, 29 (1984) 3533.
107 V.M. Leloup, P. Colonna and S.G. Ring, *Macromolecules*, 23 (1990) 862.
108 E. Manegold, *Kolloid Z.*, 49 (1929) 372.
109 L. Michaelis, *Kolloid Z.*, 62 (1933) 2.
110 E. Poitevin and P. Wahl, *Biophys. Chem.*, 31 (1988) 247.
111 J.R. Pappenheimer, *Physiol. Rev.*, 33 (1953) 387.
112 S. Rokushika, T. Ohkawa and H. Hatano, *J. Chromatogr.*, 176 (1979) 456.
113 M.B. Tennikov, B.G. Belen'ky, V.V. Nesterov and J.D. Ananyeva, *Colloid. J. USSR*, 41 (1979) 526 (Engl.), 603 (Russ.).
114 B.M. Uzelac and E.L. Cussler, *J. Colloid Interface Sci.*, 32 (1970) 487.
115 J.H. Wong, *Ph.D. Thesis*, University of Pennsylvania, 1976.
116 J.H. Wong and J.A. Quinn, in M. Kerker (Editor), *Colloid and Interface Science*, Vol. 5, Academic Press, New York, 1976, p. 169.
117 R.R. Walters, *J. Chromatogr.*, 249 (1982) 19.
118 R. Collander, *Kolloid-Beih.*, 19 (1924) 72.
119 Z. Grubisic-Gallot and H. Benoit, *J. Chromatogr. Sci.*, 9 (1971) 262.
120 P. Fasella, G.G. Hammes and P.R. Schimmel, *Biochim. Biophys. Acta*, 103 (1965) 708.
121 J.S. Schultz, R. Valentine and C.Y. Choi, *J. Gen. Physiol.*, 73 (1979) 49.
122 M.G. Davidson and W.M. Deen, *J. Membr. Sci.*, 35 (1988) 167.
123 G.D.J. Phillies, *Macromolecules*, 19 (1986) 2367.
124 T.D. Long and J.L. Anderson, *J. Polym. Sci., Polym. Phys. Ed.*, 23 (1985) 191.
125 Q.T. Nguyen and J. Néel, *J. Membr. Sci.*, 14 (1983) 111.
126 G. Guillot, *Macromolecules*, 20 (1987) 2606.
127 M.P. Bohrer, W.M. Deen, C.R. Robertson, J.L. Troy and B.M. Bremmer, *J. Gen. Physiol.*, 74 (1979) 583.
128 J.L. Anderson and J.A. Quinn, *J. Colloid Interface Sci.*, 40 (1972) 273.
129 B. Prasher and Y.H. Ma, *AIChE J.*, 23 (1977) 303.
130 K.H. Lan, N. Ostrowsky and D. Sornette, *Phys. Rev. Lett.*, 57 (1986) 17.
131 A.G. Ogston, B.N. Preston, J.D. Wells and J. McK. Snowden, *Proc. R. Soc. London, Ser. A*, 333 (1973) 297.
132 R.I. Cukier, *Macromolecules*, 17 (1984) 252.
133 J.N. Little, J.L. Waters, K.J. Bombaugh and W.J. Pauplis, *J. Polym. Sci., Part A-2*, 7 (1969) 1775.
134 D.J. Nagy, C.A. Silebi and A.J. McHugh, *J. Appl. Polym. Sci.*, 26 (1981) 1567.
135 S.J. Gibbs and E.N. Lightfoot, *Ind. Eng. Chem., Fundam.*, 490 (1986) 25.
136 E.A. Di Marzio and C.M. Guttman, *J. Chromatogr.*, 55 (1971) 83.
137 V. Pretorius and T.W. Smuts, *Anal. Chem.*, 38 (1966) 274.
138 M. Grüneberg and J. Klein, *Macromolecules*, 14 (1981) 1415.
139 A.E. Rodrigues, B.J. Ahn and A. Zoulalian, *AIChE J.*, 28 (1982) 541.
140 G. Carta, M. Gregory, D. Kirwan and H. Massaldi, *Sep. Technol.*, 2 (1992) 62.
141 A.E. Rodrigues, J.C. Lopes, Z.P. Lu, J.M. Loureiro and M.M. Dias, *J. Chromatogr.*, 590 (1992) 93.
142 C.L. Prince, V. Bringi and M.L. Shuler, *Biotechnol. Prog.*, 7 (1991) 195.
143 M. Kubín, *J. Chromatogr.*, 108 (1975) 1.
144 A.E. Hamielec and S. Singh, *J. Liq. Chromatogr.*, 1 (1978) 187.
145 T. Hashimoto, *J. Chromatogr.*, 544 (1991) 249.

Journal of Chromatography, 648 (1993) 71–77
Elsevier Science Publishers B.V., Amsterdam

CHROM. 25 315

Dimethoxyphenylpropyl bonded silica phase for higher fullerenes separation by high-performance liquid chromatography

Kiyokatsu Jinno*, Hatsuichi Ohta, Yoshihiro Saito, Takashi Uemura, Hideo Nagashima and Kenji Itoh

School of Materials Science, Toyohashi University of Technology, Toyohashi 441 (Japan)

Yung-Lin Chen, Gary Luehr and Jim Archer☆

J&W Scientific, Folsom, CA 95630-4714 (USA)

John C. Fetzer and Wilton R. Biggs

Chevron Research and Technology Company, Richmond, CA 94802 (USA)

(First received March 19th, 1993; revised manuscript received May 18th, 1993)

ABSTRACT

Fullerenes were separated using three chemically bonded phases, dimethoxyphenylpropyl (DMP), monomeric octadecyl and polymeric octadecyl modified silicas (ODS), with *n*-hexane as the mobile phase. DMP and the monomeric ODS are the best choices for the separation of C_{60} and C_{70} compounds, while DMP is the only phase that has high temperature stability while maintaining the resolution. For the separation of higher fullerenes, DMP offers faster analysis at higher temperatures while maintaining its high resolution, whereas ODS phases cannot provide similar run times while offering the same resolution. In conclusion, DMP is the most suitable and promising stationary phase for fullerenes analysis because of the short run time and its superior separation efficiency.

INTRODUCTION

Since the existence of all-carbon molecules such as C_{60} and C_{70} was confirmed in 1985, there have been many publications dealing with the separation and analysis of these compounds, called fullerenes, using various analytical techniques [1–18]. The unique properties and structures of these molecules have been widely studied, and now studies on their usefulness in materials science fields are the driving force that attract many scientists to this field of chemistry. In order to further scientific investigations of fullerenes, chromatographic separation techniques are required to separate and purify these molecules. High-performance liquid chromatography (HPLC) is probably the best method one can choose for this application.

Although novel stationary phases based on nitrophenyl groups have proved to be useful for C_{60} and C_{70} separation and a few are now commercially available [19–21], a basic approach to optimize separation systems for higher ful-

* Corresponding author.
☆ Present address: Sandoz Argo, Inc., Palo Alto, CA 94304, USA.

0021-9673/93/$06.00

lerenes is still urgently required. Studies of the separation of C_{60} and C_{70} using multi-legged biphenyl bonded phase (BP) [22], commercially available octadecyl silica (ODS) phases (polymeric and monomeric phases) [23–26] and a novel dimethoxyphenylpropyl silica bonded phase (DMP) [27] have been previously conducted in our laboratory. The separation of higher fullerenes such as C_{76}, C_{78} and C_{84} with ODS phases was also reported in previous papers [25,26]. These investigations indicated that there is still potential for further studies to obtain higher selectivity with the above-mentioned stationary phases using their characteristic chromatographic properties. In this communication, we describe an approach to enhance the selectivity of separation with varying column temperature in order to get better resolution for C_{60}, C_{70} and other higher fullerenes using various stationary phases, especially DMP phase.

EXPERIMENTAL

The HPLC system used consisted of a Tosoh CCPE pump (Tokyo, Japan), a Hewlett-Packard 1040 A photodiode array detector (Yokogawa Analytical Systems, Musashino, Japan) controlled by an HP 9000 computer, and a Rheodyne 7520 injector (Cotati, CA, USA) with 20-μl loop volume for injection. The column temperature was controlled by a Tosoh RE-8000 oven at temperatures between 30 and 80°C and by a LAB-Thermo Model LH-1000E (Toyo Seisakusho, Tokyo, Japan) at temperatures lower than 30°C. Separation columns evaluated herein were as follows: Develosil ODS-5 (monomeric type, 5 μm, Nomura Chemicals, Seto, Japan), 250 mm × 4.6 mm I.D.; Wakosil II 5C18AR (polymeric type, 5 μm, Wako Chemicals, Tokyo, Japan), 250 mm × 4.6 mm I.D.; and DMP (monomeric type, 5 μm, laboratory made), 150 mm × 4.6 mm I.D. In this work, DMP was used as the primary stationary phase and others were used as references for the comparison of the chromatographic performance for fullerenes separations, since it has been found previously [27] that DMP is very promising stationary phase for fullerenes separation (C_{60} and C_{70}). The mobile phase was *n*-hexane at a flow-rate of 1 ml/min.

Carbon soot was produced by a common arc discharge in an inert gas environment. The soot was extracted with toluene in order to obtain the C_{60} and C_{70} fraction and the residue was extracted with 1,2,4-trichlorobenzene to get highly concentrated higher fullerenes [25]. The solution was then evaporated to dryness and then redissolved in toluene for use as the test sample for the injection.

RESULTS AND DISCUSSION

Separation of C_{60} and C_{70}

In general, in HPLC, high temperature results in lower retention and high resolution. However, Pirkle and Welch [19] reported an unusual temperature dependence of their special column (the so-called Pirkle column) for C_{60} and C_{70} separation, *i.e.* higher temperature causes higher retention and high resolution. In this work, therefore, the first step was to separate C_{60} and C_{70} with various stationary phases and varying column temperature. In Fig. 1, the separation factors for C_{60} and C_{70} are plotted against temperature. With the polymeric ODS phase, the separation factors changed drastically with the column temperature: decreasing the temperature increased selectivity. Low temperature makes it possible to separate both fullerenes with low retention and resolution. At temperatures greater than 40°C, the same separation cannot be achieved because of very low retention and co-elution of C_{60} and C_{70}. This means that polymeric ODS is not suitable for separating C_{60} and C_{70} even at low column temperatures, because the retentions of two fullerenes are very short and the separation efficiency is very sensitive to small changes in temperature. With the monomeric ODS phase, the change in the separation factors with temperature is not as drastic as found when using the polymeric ODS phase, but the tendency for the selectivity to increase at lower temperatures is clearly seen. From the practical point of view, the monomeric phase is preferable to the polymeric, although at low temperatures the polymeric ODS phase can offer much higher separation factors than the monomeric ODS. Actual

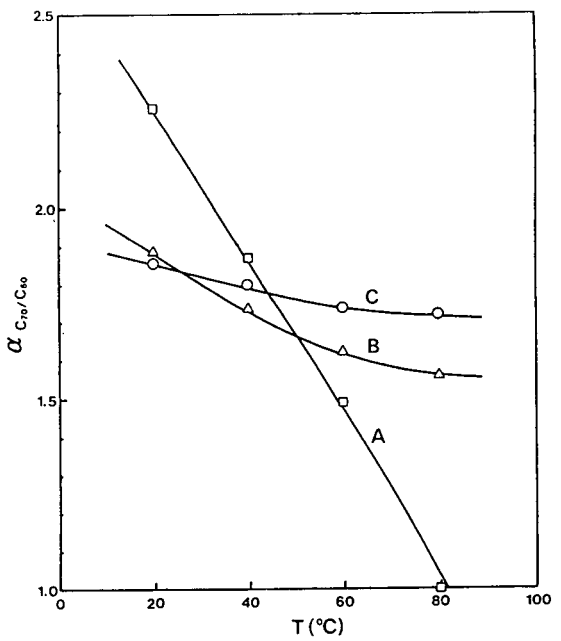

Fig. 1. Relationships between separation factors (α) for C_{60} and C_{70} with four different stationary phases and column temperature. (A) Polymeric ODS; (B) monomeric ODS; (C) DMP.

retention values with the polymeric phase are always lower than those with the monomeric, and this fact demonstrates that the monomeric material is the better stationary phase for fullerenes separations. As previously reported by Pirkle and Welch [19] different retention mechanisms are affected to varying degrees by temperature change. With the DMP phase, the temperature dependency is very minimal, not as low as the Pirkle column, but the lowest temperature dependency of the three phases studied.

Higher fullerenes separation

In our previous work [26], polymeric and monomeric ODS phases with toluene–acetonitrile as the mobile phase were evaluated for the separation of higher fullerenes such as C_{76}, C_{78}, C_{82} and C_{84}. Interesting results were obtained in that work: the elution order of C_{76} and one of three isomers of C_{78}, *i.e.*, C_{78}–C_{2v}, with the monomeric phase was reversed by using the polymeric phase. Also, the elution order of C_{82} and C_{84} with the monomeric ODS was reversed when compared with the polymeric phase, *i.e.*, the order with the latter is C_{84} then C_{82}. These differences in the elution characteristics of the monomeric and the polymeric phases can be explained by the molecular planarity recognition capability of the phases, as discussed in our previous paper [26]. Here we will compare three stationary phases with *n*-hexane as the mobile phase in determining elution orders and temperature dependence as it relates to the retention of higher fullerenes.

In Fig. 2, the temperature dependency of the separation of higher fullerenes with the DMP phase is demonstrated. The results clearly show that with this phase the elution characteristics of fullerene isomers do not change dramatically even at different column temperatures. Increasing the temperature only allows faster analysis with similar resolution for those higher fullerenes. The thermal stability of the separation with the DMP phase is apparently seen in the results. For comparison, the chromatograms obtained with the monomeric and the polymeric ODS phases are summarized in Figs. 3 and 4, respectively. The elution behaviours with both ODS phases show higher temperature dependency than is the case with the DMP phase. The polymeric phase shows a drastic elution change with temperature. Even at 20°C, the temperature which offers the highest resolution with the polymeric ODS, only partial separation was realized for higher fullerenes. This means that the polymeric phase is very poor for separation of the higher fullerenes with *n*-hexane as the mobile phase. With the monomeric phase the resolution is a little better. At 20°C with the monomeric ODS, only three major peaks which range from C_{76} to C_{84} in the chromatogram appear, and these peaks merge into two major peaks at 80°C. Therefore, the monomeric phase is better than the polymeric phase but neither is good for higher fullerenes separations.

Two important and conclusive facts are obtained from the experimental results: (1) the resolution of higher fullerenes with the DMP phase is better than with other phases using *n*-hexane as the mobile phase and (2) increasing the temperature with the DMP phase results in slightly faster analysis without loss of resolution. It is clear that the DMP phase is the best

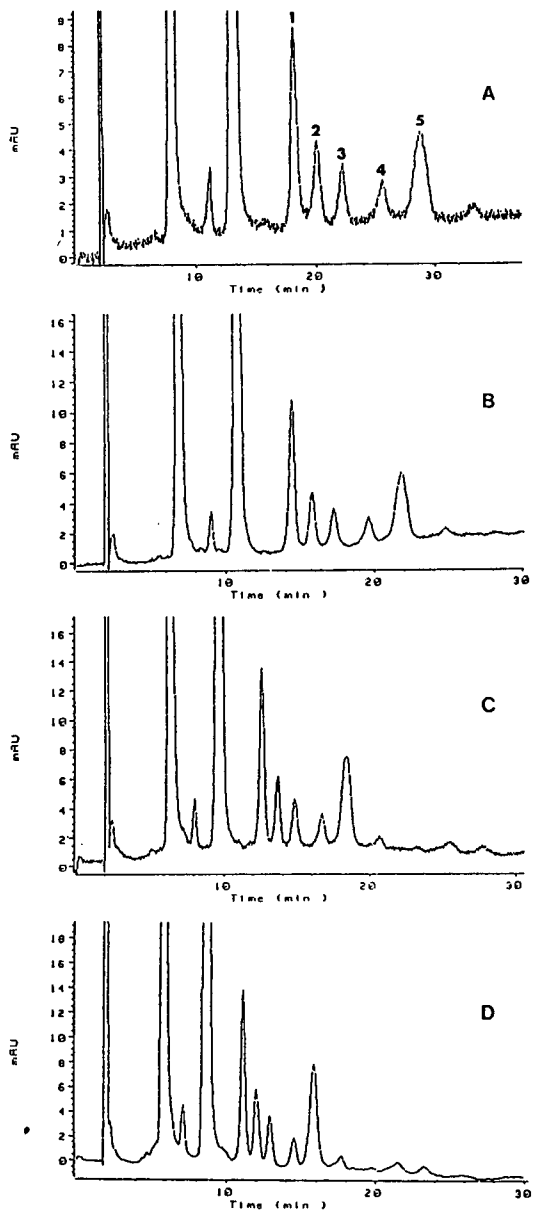

Fig. 2. Separations of higher fullerenes with the DMP phase at different temperatures. (A) 20°C; (B) 40°C; (C) 60°C; and (D) 80°C. Peak assignments are described in the caption of Fig. 5.

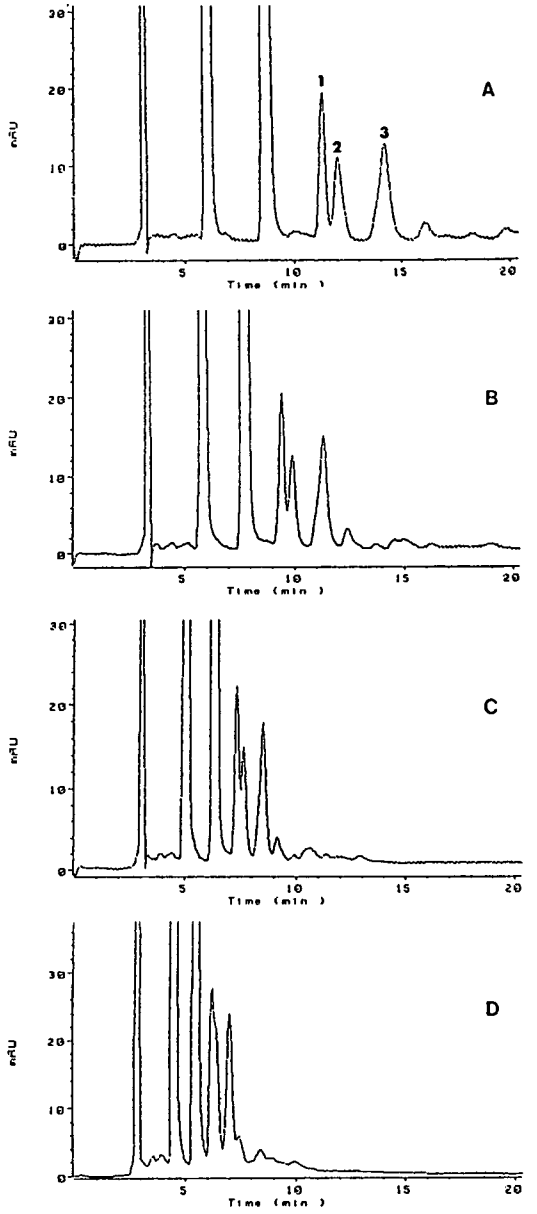

Fig. 3. Separations of higher fullerenes with the monomeric ODS phase. (A) 20°C; (B) 40°C; (C) 60°C; and (D) 80°C. Peak assignments are given in the text.

stationary phase for the separation of isomers of higher fullerenes.

UV–Vis spectra obtained by the separation with the DMP phase reveal that the elution order of higher fullerenes is C_{76} (peak 1 in Fig. 2), C_{78}–C_{2v} + C_{78}–D_3 (peak 2), C_{78}–$C_{2v'}$ (peak 3), C_{82} (peak 4) and C_{84} (peak 5), as seen in those spectra summarized in Fig. 5. This order is different from those with ODS phases when toluene–acetonitrile was used as the mobile phase [26], *i.e.*, with the monomeric phase the order is C_{76}, C_{78}–$C_{2v'}$, C_{78}–C_{2v} + C_{78}–D_3, C_{82} and C_{84}, and with the polymeric phase it is

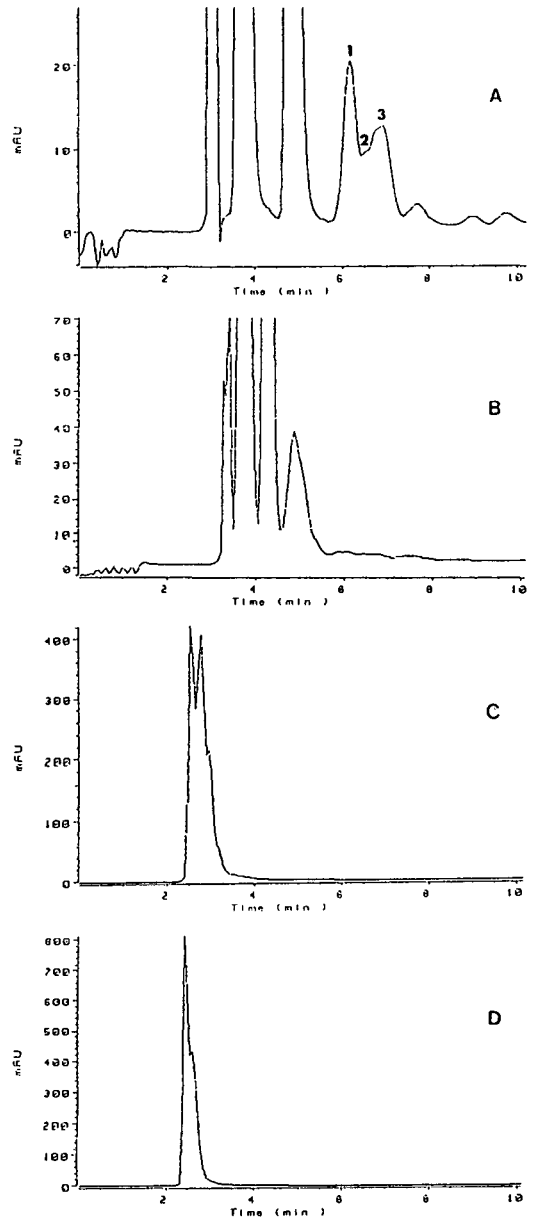

Fig. 4. Separations of higher fullerenes with the polymeric ODS phase. (A) 20°C; (B) 40°C; (C) 60°C; and (D) 80°C. Peak assignments are given in the text.

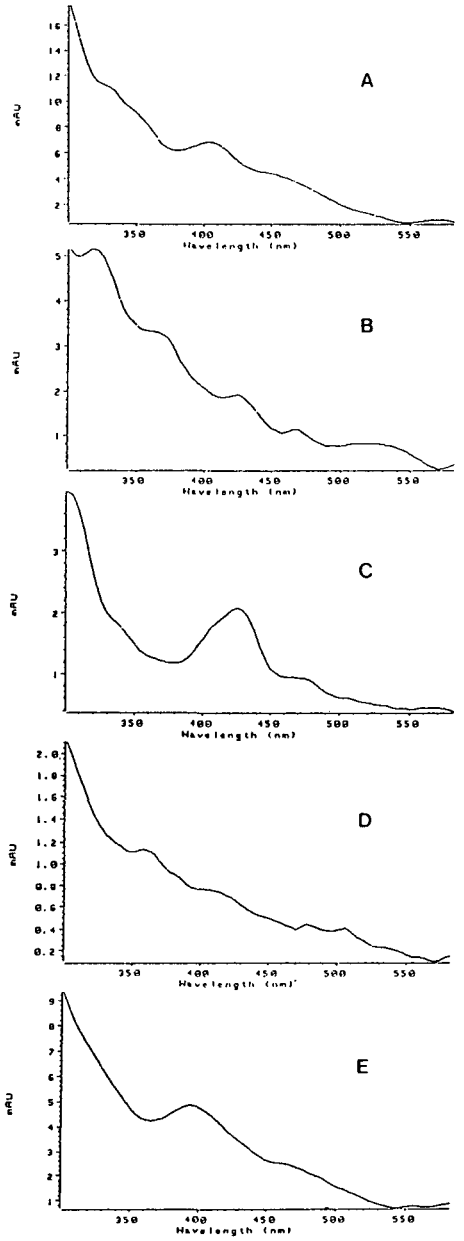

Fig. 5. UV–Vis spectra of the peaks in the chromatograms shown in Fig. 2. (A) Peak 1; (B) peak 2; (C) peak 3; (D) peak 4; and (E) peak 5. By careful examination the spectra can be assigned as follows: (A) C_{76}; (B) C_{78}–C_{2v} + C_{78}–D_3; (C) C_{78}–$C_{2v'}$; (D) C_{82}; (E) C_{84}.

C_{78}–$C_{2v'}$, C_{76}, C_{78}–C_{2v}, C_{78}–D_3 and C_{84} + C_{82}. With *n*-hexane as the mobile phase, the order with the polymeric phase is not clearly seen because of low resolution for these fullerenes. By measuring spectra at several points from 6 to 8 min of the chromatogram obtained at 20°C, it was determined that the order was similar to that with the toluene–acetonitrile mobile phase. Peak 1 in Fig. 4 is C_{78}–$C_{2v'}$ + C_{76}, peak 2 is C_{78}–C_{2v} and peak 3 includes C_{84}, C_{78}–D_3 and C_{82}. With

the monomeric phase the order is also similar to the case with the toluene–acetonitrile mobile phase, although with *n*-hexane even at 20°C three isomers of C_{78} elute together and C_{82} makes a little shoulder at the left side of the C_{84} peak. This means that the peak assignments in Fig. 3 are as follows: peak 1 is C_{76}, peak 2 is three C_{78} isomers in the order C_{78}–$C_{2v'}$, C_{78}–C_{2v} and C_{78}–D_3, and peak 3 is $C_{82} + C_{84}$. In conclusion, it has been found that the elution order of the higher fullerenes from C_{76} to C_{84} is very different with different stationary phases. This is a very important finding and indicates that HPLC separations can be used not only to isolate and purify fullerenes, but also to identify their size and shape. The different order seen for C_{78}–$C_{2v'}$ and C_{2v} isomers is caused by the cavity-like shape of the DMP phase, which might be much better suited to catch $C_{2v'}$ isomer than C_{2v} isomer because the former is a little bulkier than the latter. The polymeric ODS phase, which has the largest molecular planarity recognition capability, retains $C_{2v'}$ less than even C_{76}, and these small differences of shape and structure of the higher fullerenes isomers can be recognized by different types of stationary phases in HPLC. This indicates that HPLC separations are performed under molecular level interactions such as solute–stationary phase interaction. If one can choose a series of appropriate stationary phases and determine the elution order of unknown fullerene isomers, the shape and size of those molecules can be predicted by systematic HPLC analyses. For fullerenes higher than C_{84} this approach is very promising if one can combine LC–MS technique to determine the isomers' molecular masses [28,29]. This research is under way in our laboratory using the stationary phases mentioned in this work in addition to other different types which can offer different selectivity, such as liquid-crystal bonded phases [30–32].

ACKNOWLEDGEMENT

The kind donation of a UV–Vis photodiode array detector system by Yokogawa Analytical Systems Inc. is acknowledged.

REFERENCES

1 R. Taylor, J.P. Hare, A.K. Abdul-Sada and H.W. Kroto, *J. Chem. Soc., Chem. Commun.*, (1990) 1423.
2 J.R. Heath, S.C. O'Brien, Q. Zhang, Y. Liu, R.F. Curl, H.W. Kroto and R.E. Smalley, *J. Am. Chem. Soc.*, 107 (1985) 7779.
3 R.D. Johnson, G. Meijer and D.S. Bethune, *J. Am. Chem., Soc.*, 112 (1990) 8983.
4 R.D. Johnson, G. Meijer, J.R. Salem and D.S. Bethune, *J. Am. Chem. Soc.*, 113 (1991) 3619.
5 C.S. Yannoni, R.D. Johnson, G. Meijer, D.S. Bethune and J.R. Salem, *J. Phys. Chem.*, 95 (1991) 9.
6 P.-M. Allemand, A. Koch and F. Wudl, *J. Am. Chem. Soc.*, 113 (1991) 1050.
7 C.I. Frum, R. Engleman Jr., H.G. Hedderich, P.F. Bernath, L.D. Lamb and D.R. Huffman, *Chem. Phys. Lett.*, 176 (1991) 504.
8 J.P. Hare, T.J. Dennis, H.W. Kroto, R. Taylor, A.W. Allaf, S. Balm and D.R.M. Walton, *J. Chem. Phys., Chem. Commun.*, (1991) 412.
9 D.S. Bethune, G. Meijer, W.C. Tang and H.J. Rosen, *Chem. Phys. Lett.*, 174 (1990) 219.
10 S.C. O'Brien, J.R. Heath, R.F. Curl and R.E. Smalley, *J. Chem. Phys.*, 88 (1988) 220.
11 J.B. Howard, J.T. McKinnon, Y. Makarovsky, A.L. Lafleur and M.E. Johoson, *Nature*, 352 (1991) 139.
12 D.R. Luffer and K.H. Schram, *Rapid Commun. Mass Spectrom.*, 4 (1990) 552.
13 H. Ajie, M.M. Alvarez, S.J. Anz, R.D. Beck, F. Diederich, K. Fostiropoulos, D.R. Huffman, W. Kratschmer, Y. Rubin, K.E. Schriver, D. Sensharma and R.L. Whetten, *J. Phys. Chem.*, 94 (1990) 8630.
14 D.M. Cox, S. Behal, M. Disko, S.M. Gorun, M. Greaney, C.S. Hsu, E.B. Kollin, J. Miller, J. Robbins, W. Robbins, R.D. Sherwood and P. Tindall, *J. Am. Chem. Soc.*, 113 (1991) 2940.
15 D.S. Bethune, G. Meijer, W.C. Tang, H.J. Rosen, W.G. Golden, H. Seki, C.A. Brown and M.S. de Vries, *Chem. Phys. Lett.*, 179 (1991) 181.
16 W.A. Scrivens, P.V. Bedworth and J.M. Tour, *J. Am. Chem. Soc.*, 114 (1992) 7917.
17 M.S. Meier and J.P. Selegue, *J. Am. Chem. Soc.* 57 (1992) 1924.
18 Y. Cui, S.T. Lee, S.V. Olesik, W. Flory and M. Mearini, *J. Chromatogr.*, 625 (1992) 131.
19 W.H. Pirkle and C.J. Welch, *J. Org. Chem.*, 56 (1991) 6973.
20 C.J. Welch and W.H. Pirkle, *J. Chromatogr.*, 609 (1992) 89.
21 K. Kimata, K. Hosoya, T. Araki and N. Tanaka, *J. Org. Chem.*, 58 (1993) 282.
22 K. Jinno, K. Yamamoto, T. Ueda, H. Nagashima, K. Itoh, J.C. Fetzer and W.R. Biggs, *J. Chromatogr.*, 594 (1992) 105.
23 J.C. Fetzer and E.J. Gallegos, *Poly. Arom. Comp.*, 2 (1992) 245.

24 R.C. Klute, H.C. Dorn and H.M. McNair, *J. Chromatogr. Sci.*, 30 (1992) 438.
25 K. Jinno, T. Uemura, H. Nagashima and K. Itoh, *Chromatographia*, 35 (1993) 38.
26 K. Jinno, T. Uemura, H. Ohta, H. Nagashima and K. Itoh, *Anal. Chem.*, (1993) in press.
27 K. Jinno, Y. Saito, Y.-L. Chen, G. Luehr, J. Archer, J.C. Fetzer and W.R. Biggs, *J. Microcolumn Sep.*, 5 (1993) 135.
28 K. Jinno, T. Uemura, H. Nagashima and K. Itoh, *J. High Resolut. Chromatogr.*, 15 (1992) 627.
29 J.F. Anacleto, R.K. Boyd and M.A. Quilliam, *J. High Resolut Chromatogr.* 16 (1993) 85.
30 J.J. Pesek and T. Cash, *Chromatographia*, 27 (1989) 559.
31 K. Jinno, H. Mae, Y. Saito, J.J. Pesek, J.C. Fetzer and W.R. Biggs, *J. Microcolumn Sep.*, 3 (1991) 417.
32 K. Jinno, Y. Saito, R. Malhan nee Chopra, J.J. Pesek, J.C. Fetzer and W.R. Biggs, *J. Chromatogr.*, 557 (1991) 459.

Journal of Chromatography, 648 (1993) 79–90
Elsevier Science Publishers B.V., Amsterdam

CHROM. 25 359

Optimization of pressure-flow limits, strength, intraparticle transport and dynamic capacity by hydrogel solids content and bead size in cellulose immunosorbents

Jeffrey A. Kaster

Department of Chemical Engineering, Virginia Polytechnic Institute and State University, 133 Randolph Hall, Blacksburg, VA 24061 (USA)

Willer de Oliveira and Wolfgang G. Glasser

Department of Wood Science and Forest Products, Virginia Polytechnic Institute and State University, 133 Randolph Hall, Blacksburg, VA 24061 (USA)

William H. Velander*

Department of Chemical Engineering, Virginia Polytechnic Institute and State University, 133 Randolph Hall, Blacksburg, VA 24061 (USA)

(First received October 23rd, 1992; revised manuscript received April 15th, 1993)

ABSTRACT

The design of existing beaded adsorbent materials for column-mode protein purification has emphasized the impact of diffusional transport phenomena upon adsorbent capacity. A design model is presented here that optimizes molecular accessibility of proteins relative to the mechanical stability at low operating pressures by manipulation of size and solids content for uncross-linked cellulose beads. Cellulose beads of several different sizes ranging from about 250 to 1000 μm diameter and having different solids contents were evaluated. Solids content of greater than about 9% cellulose greatly reduced the permeability of large proteins such as thyroglobulin and β-amylase into the beaded matrix at bead contacting times of about 5 and 50 s. Furthermore, the amount of permeation at 3% solids content by thyroglobulin at bead contacting times of about 5 s was about tenfold larger than predicted by diffusion models using the binary diffusivity in a purely aqueous continuum. The utility of a low solids content, large bead cellulose support was shown with immobilized IgG (M_r 155 kDa) capturing recombinant human Protein C (M_r 62 kDa). A 1000 μm diameter beaded cellulose immunosorbent having 3% solids content gave equivalent capacity to a 140 μm diameter beaded, cross-linked agarose support containing 4% solids. In contrast to the smaller diameter, cross-linked beaded agarose, the low solids content beaded cellulose benefitted from greater physical stability due to more optimal pressure-flow characteristics imparted by large bead size.

INTRODUCTION

The chromatographic behavior of packed columns of rigid particles has been well detailed. However, these studies have tended to emphasize the high-pressure liquid chromatography (HPLC) family of very small particles (10 to 50 μm diameter) and have not been well extended to softer hydrogel supports composed of cellulose or agarose derivatives. Soft hydrogel sup-

* Corresponding author.

0021-9673/93/$06.00

ports have been most successfully applied to the immunopurification of large molecules like human plasma proteins such as Protein C (M_r 62 kDa) [1]. The utility of immunosorbents for large scale purifications and the effects of the immobilization chemistry upon antigen binding activity are discussed elsewhere [2]. We discuss here the material aspects of beaded cellulose hydrogels that affect the design of immunosorbents so as to maintain dynamic capacity at high flow rates while generating minimal pressure drop across a column.

The mechanical stability of currently available beaded hydrogels supports is limited at the pressure drops created by high fluid velocities [3]. Immunosorbents commonly consist of cross-linked agarose, cellulose, or synthetic polymer hydrogels with a bead diameter of about 60 to 200 μm and solids contents of less than about 9% (w/w) [4]. Many small agarose or cellulose beaded supports begin to deform at about 4 kPa/cm bed or less followed by an exponential increase in the pressure drop across the column [5]. Furthermore, the velocity at which small bead hydrogel supports crush is inversely proportional to the column diameter [6]. Thus, the strength of hydrogel supports cannot be simply scaled for industrial affinity purification of proteins by increasing the column diameter while holding the bed depth constant [7]. At low fluid velocities, these hydrogels behave roughly as predicted by classical chromatographic theory that has been applied to more rigid HPLC-type supports [8,9].

The processing rates of most chromatographic supports are also limited by the fluid contacting time over which intraparticle diffusional transport can occur. Past hydrogel designs have prioritized a minimization of the path length through which the protein of interest must diffuse in order to be adsorbed. Diffusional transport is particularly slow for proteins, as most have binary diffusion coefficients in water on the order of 10^{-7} cm^2/s or less [10]. The binary diffusion coefficient for proteins in hydrogel support materials would necessarily decrease as the solids content of the hydrogel is increased and diffusional transport becomes hindered.

While the path length for diffusional transport is shortened by decreasing particle size, viscous form drag increases due to an increase in the surface area exposed to flow per volume of support. Therefore, the pressure drop at a given fluid velocity is increased as particle size is decreased. This effect has been well correlated for flow in packed beds of rigid spheres using "Darcy's Law" type expressions such as the Ergun correlation [11]. Thus, the diametrically opposed phenomena of bead penetration and viscous form drag require an optimization of dynamic adsorbent capacity *vs.* throughput at pressure drops that can be supported by the adsorbent and ancillary column equipment. We present here a design model for hydrogel-based immunosorbents that seeks to optimize intraparticle protein transport, physical strength, pressure-flow characteristics, and dynamic capacity by manipulation of bead size and solids content in the particle. Immunosorbents made from cellulose beads are used to evaluate the model and some comparisons to commercially available cross-linked agaroses are made.

EXPERIMENTAL

Cellulose chromatographic supports

Cellulose beads (VPI beads) were produced by regeneration of pure cellulose (Whatman) having a degree of polymerization of about 180–200 [12]. The cellulose was dissolved in a chaotropic, saturated solution of LiCl (9%, w/w) in dimethyl acetamide (DMAC) and the residual insolubles were removed by filtration [13]. Dissolved cellulose concentrations of 0.5–3.3% (w/w) were used. Typically, a batch size of about 0.1–1 l of beads was made by atomization of the cellulose solution into twice the volume of an azeotropic mixture of isopropanol and water or 90% by volume aqueous methanol. A 20 gauge needle was used as an atomizing nozzle. An air jet placed at the tip of the atomizing nozzle was used to disrupt the bead as it emerged from the atomizer. Bead size was varied by adjusting the air jet and cellulose solution flow rate. A single needle could produce up to one l of beads per hour. Extraction of the chaotropic LiCl–DMAC solvent by the aqueous alcohol was achieved by incubation for several hours at room tempera-

ture. This resulted in the regeneration or precipitation of the cellulose as a beaded hydrogel. The beads were then washed in a column mode with 10 bed volumes of water. The solids content of the water-washed cellulose beads was determined by weight loss upon freeze drying of beads that were lightly blotted to remove excess water. Bead size was measured by photomicroscopy of random samples of 15–20 beads. Cellulose beads with diameters less than 250 μm and solids contents ranging from 6 to 13% were kindly provided by SCHZ Lovosice.

Pressure drop

The pressure drop across a column of beaded support was measured at various flow rates. Beads were packed as an aqueous slurry into a 15×1.0 cm column (C10–20, Pharmacia). Degassed deionized water was pumped through the column at various flow rates using a Rainin HPX HPLC pump with a 2070 kPa back-pressure valve in line before the column to maintain pressure on the pump. A KM 5007 I.S. digital pressure gauge (Kane-May) was attached by a three-way valve above the column. The column was first consolidated for a minimum of 30 min at a flow rate that gave a pressure drop of at least 3.4 kPa across the column. The flow rate was then increased incrementally with a minimum of 5 min allowed for the pressure drop across the column to come to equilibrium. The pressure drop was assumed to be asymptotically stable when the change in pressure was less than 0.34 kPa/min. We have defined pressure exponentiation as a greater than 250 kPa change in pressure drop across the column at a set flow rate after exhibiting a stable pressure profile (less than 0.34 kPa change per min) at the previous flow rate.

Permeation studies

Solute permeation in underivatized cellulose beads was studied by elution behavior of single component solutions of dextran, several large proteins and tryptophan (Sigma) relative to that obtained for 0.269 μm latex beads. The elution profiles as detected at 280 nm were studied at two bead contacting times. The chromatographies were run using degassed deionized water for the latex beads and degassed Tris-buffered saline solution (pH 7.0) for the proteins. The permeation studies were run using two flow rates: 0.1 ml/min (0.127 cm/min) and 1.0 ml/min (1.27 cm/min). The void volume of the column was determined using Nanosphere 0.269 ± 0.007 μm polystyrene latex microspheres (Duke Scientific) diluted 1:10 with deionized water.

Cellulose bead activation

Cellulose beads were activated with CNBr by a modification of the method of Porath *et al.* [14]. The beads were blotted to remove excess water, weighed, and 5.0 g were placed in a 40-ml beaker with 5 ml of cold 5 *M* potassium phosphate buffer. The beads and buffer were stirred for 10 min while kept at 0–5°C in an ice bath. CNBr solution (2 ml of 0.1 g/ml CNBr in deionized water) was then added dropwise over 2 min with continuous gentle stirring. The reaction was allowed to continue for an additional 8 min with constant stirring. The reaction was stopped by decanting the beads into a filter and washing with 1 l of 0.1 *M* $NaHCO_3$. Beads were immediately transferred to a 20-ml sample bottle (Wheaton polyethylene scintillation vial, Cole-Parmer) for antibody immobilization.

Immunoglobulin immobilization to CNBr activated beads

A murine anti-human protein C monoclonal antibody, 7D7B10-Mab (American Red Cross), was bound to cellulose or agarose beads by placing 5 mg of 7D7B10-Mab in 2.5 ml coupling buffer (0.1 *M* $NaHCO_3$–0.5 *M* NaCl, pH 8.3) with 5.0 g (preactivated weight) of CNBr activated beads in a 20-ml sample bottle. The immobilization reaction was run overnight at 0–4°C using a turntable agitator. The beads were then washed with two 5-ml deionized water washes to remove free immunoglobulin and unreacted active sites were blocked with 10% ethanolamine in 1 *M* $NaHCO_3$ pH 8.3 for a minimum of 4 h at 0–4°C. The immobilization step was terminated with three alternating washes in 0.05 *M* Na acetate–0.5 *M* NaCl, pH 4.0 and 0.05 *M* Tris–0.5 *M* NaCl, pH 8.0. Beads were stored in TBS pH 7.0 at 0–4°C. The

amount of antibody immobilized was determined by ELISA using the method in refs. 2 and 15.

Column configuration

7D7B10-Mab cellulose or agarose immunosorbent beads (5 ml) were packed into a C10–20 jacketed column (Pharmacia) cooled to 2–6°C with a recirculating cold water bath. Two Rainin HPX pump modules with 100 ml/min pump heads were used for buffer delivery. A 2070 kPa pressure regulator was placed in line upstream of the column to maintain back pressure on the pumps. Protein C-rich feeds were pumped through a Masterflex pump (Cole-Parmer) with a 7013 head for low flow rates (2.5 and 5.0 ml/min) and a 7016 head for high flow rates (10, 20, 40, and 80 ml/min). The pumps and column were connected with low pressure fittings including a three-way valve for preventing back flow into the feed line. Protein content of the column effluent was measured by absorbance at 280 nm with a Knauer Variable Wavelength Monitor UV detector and by ELISA of effluent fractions. A 0.4 mm path length preparative flow cell was used for the 2.5 and 5.0 ml/min runs and a high flow rate variable path length flow cell (Sonntek) was used for all other runs. Buffer delivery and data collection was controlled through Rainin's Dynamax system using a Macintosh Plus computer.

Binding and elution of PC

Recombinant Protein C (rhPC) feed stock was prepared by diluting precentrifuged transgenic pig milk whey–50 m*M* EDTA containing 1 g/l rhPC with degassed 0.1 *M* NaCl, 0.05 *M* Tris, 0.025 *M* EDTA, pH 7.0 (TBS 25 m*M* EDTA) in the ratio: one part whey to three parts TBS 25 m*M* EDTA [16]. The diluted whey was centrifuged for 15 min at 3400 *g* and then gravity filtered to remove precipitates. Diluted clarified whey was stored at 0–4°C for up to 12 h before loading onto the column. During each run, the 7D7B10 cellulose or agarose immunosorbent columns were loaded with 200 ml of the diluted transgenic pig milk whey. The metal dependence of Protein C binding to 7D7B10-Mab (binding of Protein C by 7D7B10-Mab occurs only in the absence of calcium ions) was used to facilitate the elution of the protein from the antibody column [17]. The immunosorbent columns were washed with 18 column volumes of TBS 5 m*M* EDTA after the loading of the whey. The Protein C was eluted with TBS 25 m*M* $CaCl_2$ and 5-ml samples were collected from the start of the elution step. The column was regenerated with successive washes of 4 *M* NaCl, 2 *M* NaSCN, and TBS 5 m*M* EDTA.

Protein C assay

Protein C was assayed using sandwich ELISA with 7D7B10 anti PC Mab as the capturing antibody as described in references 2 and 15.

THEORETICAL

The time that a packet of fluid is in contact with any one bead is defined as the bead contacting time. This bead contacting time is calculated from the bead diameter d_b and the superficial velocity v as follows:

$$t_b = \frac{d_b}{v} \tag{1}$$

The bead contacting time is used to estimate the approximate time available for a species to penetrate the bead.

The analytical equations for diffusion into a sphere have been solved [18]. For this work, the solution for the volume average concentration throughout the sphere has been used as a benchmark to determine the extent of diffusion into the bead assuming that all transport within the bead is diffusive. The analytical solution for the volume average concentration in the bead with the boundary conditions that the concentration at $t = 0$ is $c_0 = 0$ and that the concentration at the surface is c_b for all $t > 0$ is given as:

$$c_{av} = c_b - \frac{6c_b}{\pi^2} \sum_{n=1}^{\infty} \frac{1}{n^2} e^{-D_{PW} n^2 \pi^2 t / R^2} \tag{2}$$

The height equivalent to a theoretical plate (HETP) was calculated from peak width measurements by the standard equation using the half height width:

$$\mathrm{HETP} = \frac{L}{5.545\left(\frac{t_R}{w_h}\right)^2} \tag{3}$$

This equation holds for peaks that are relatively Gaussian [19]. The experimental HETPs were compared to estimated values for HETP given by the correlations of Mikes [20] and Johnson and Stevenson [21].

RESULTS

The amount of cellulose in beads made by regeneration into aqueous alcohol was linearly dependent upon the dissolved cellulose concentration in LiCl–DMAC as shown in Fig. 1. At constant dissolved cellulose concentration, the solids content of the beads was essentially independent of bead size for diameters in the ranges of 1.0–1.8 mm and 0.6–0.8 mm. The standard error ranged from 0.05–0.2% and was calculated for a minimum of three measurements of solids content.

Fig. 2a and b presents the pressure drop *vs.* linear velocities obtained by column mode operation in a 15 × 1.0 cm packed bed for VPI beads of the present work and various commercially available beaded agaroses. Fig. 2a gives pressure drop *vs.* linear velocities obtained by column mode operation for VPI beads of different solids content having a size of about 600–700 μm diameter. Pressure exponentiation occurs for beads containing 1% solids at superficial velocities greater than about 15 cm/min (Fig. 2a; curve 1). Pressure exponentiation occurs for beads containing 1.2% solids at superficial velocities of greater than about 40 cm/min (Fig. 2a; curve 2). Pressure exponentiation occurs for beads containing 1.9% solids at superficial velocities of greater than about 70 cm/min (Fig. 2a; curve 3). Beads containing 3.2% solids did not exhibit a

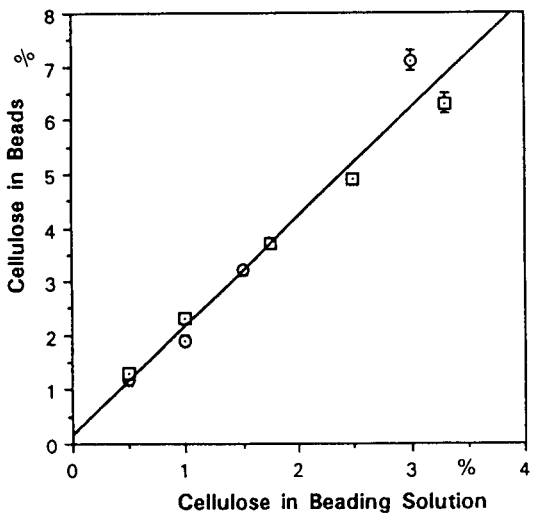

Fig. 1. Mass percent cellulose in beads as a function of solution concentration. □ = Large beads, 1.0–1.8 mm in diameter; ○ = small beads, 0.6–0.8 mm in diameter.

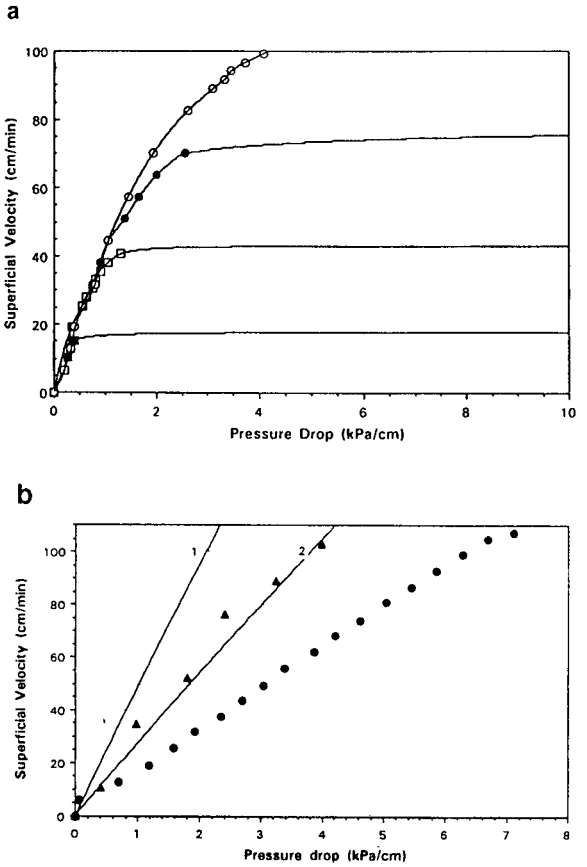

Fig. 2. (a) The effects of solids content on the pressure drop curve. VPI cellulose beads in a 15.0 × 1.0 cm column. (1) ■ = 600 μm diameter beads, 0.9% solids (w/w); (2) □ = 700 μm diameter beads, 1.2% solids; (3) ● = 800 μm diameter beads, 1.9% solids; (4) ○ = 700 μm diameter beads, 3.2% solids. (b) Pressure drops across columns of nominal 300 μm beads. Experimental results plotted in comparison to the theoretical results of the Ergun equation [11]. ● = Sepharose 6MB (250 ± 40 μm diameter cross-linked agarose beads, 9% solids), ▲ = VPI cellulose beads (340 ± 40 μm diameter cellulose beads, 9% solids); (1) theoretical 250 μm diameter beads, (2) theoretical 340 μm diameter beads.

pressure exponentiation at flow rates up to 100 cm/min (Fig. 2a; curve 4).

Fig. 2b compares the observed pressure-flow behavior of uncross-linked 9% cellulose (300–380 μm diameter) and cross-linked 9% agarose (250–300 μm diameter) with the predicted pressure-flow behavior of idealized rigid spheres having diameters of 340 μm (Fig. 2b, curve 1) and 250 μm (Fig. 2b, curve 2). No pressure exponentiation at velocities up to about 100 cm/min was seen for either bead. The Ergun equation [11], a semi-empirical prediction of pressure drop as a function of flow rate for rigid spheres, shows that both cellulose and cross-linked agarose yield more pressure drop than that predicted for rigid spheres of the same size.

Fig. 3 plots the crushing velocity, percent solids content and bead size from the above data for VPI beads and Perloza cellulose beads (SCHZ Lovosice). We term the crushing velocity as the superficial velocity (ml flow/min/cm^2 bed area or cm/min) at which the pressure drop across the column exponentiates. Low crushing velocities (about 5–10 cm/min in a 15 cm column) are seen in beads with solids content less than about 6% (w/w) and with size smaller than about 200 μm in diameter.

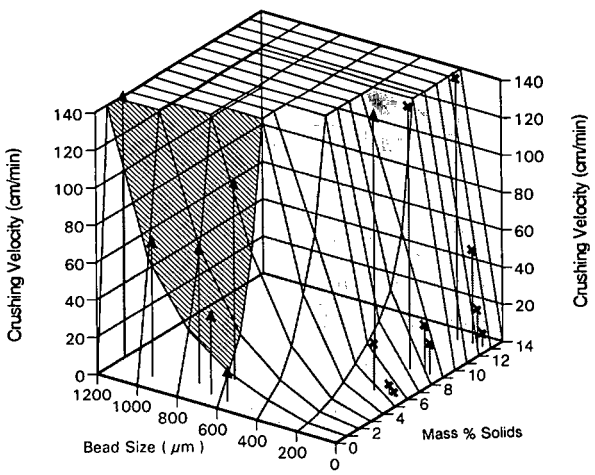

Fig. 3. Relationship between bead size, composition, and crushing velocity. × = Cellulose beads of less than 200 μm, courtesy of SCHZ Lovosice; ▲ = cellulose beads of present work. Dark shaded area = projected crushing velocity as a function of bead size and weight percent solids; hatched area = approximate projected surface defining the performance and composition of VPI beads; lightly shaded area = approximate projected surface defining the performance and composition of commercially available beads.

Fig. 4A, B, C, and D presents permeation chromatography done on underivatized cellulose beads ($\approx$1000 μm) at superficial velocities of 0.12 cm/min ($t_b \approx 50$ s) and 1.2 cm/min ($t_b \approx 5$ s). Cellulose beads with solids contents of 3%, 4%, 6%, and 9% with average diameters of about 1000 μm were studied. As indicated by a sharp elution peak of 0.269 μm diameter latex polymer spheres, void volumes ranged from 0.40–0.45 column volumes for all beads analyzed (Fig. 4A, B, C, and D; panel a). The void volumes did not vary with linear velocity. For any of the biochemical species evaluated in these permeation experiments; after about 1.5 column volumes, no absorbance was detected in the subsequent 10 column volumes.

Permeation experiments using blue dextran (M_r 2 000 kDa) in 3% cellulose beads gave an elution profile at 0.12 cm/min having two maxima with about 80% of the O.D. 280 nm centered at about 0.5 column volumes with the remainder being more broadly centered at about 1.0 column volumes (Fig. 4A; panel b). The elution profile for blue dextran at 1.2 cm/min gave a single maximum at about 0.5 column volumes (Fig. 4B; panel b). Thyroglobulin (M_r 669 kDa) also gave a bimodal elution pattern, but greater than 80% of the protein was centered about 1.0 column volumes with the remainder centered at about 0.45 column volumes for the 0.12 cm/min trial (Fig. 4A; panel c). A shift to about 50% of the absorbance at 280 nm centered at about 0.5 column volumes occurred at a superficial velocity of 1.2 cm/min for thyroglobulin. β-amylase (M_r 200 kDa) gave a broad elution peak with a maximum at 1.0 column volumes at 0.12 cm/min which shifted to about 0.75 column volumes at 1.2 cm/min. Tryptophan gave an elution peak centered about 1.0 column volumes at both velocities with a slight peak broadening occurring at 1.2 cm/min. Permeation experiments using cellulose beads of 4.8% and 6% solids content showed similar results with full penetration of small and intermediate species but excluding the blue dextran (data not shown).

Permeation experiments of blue dextran,

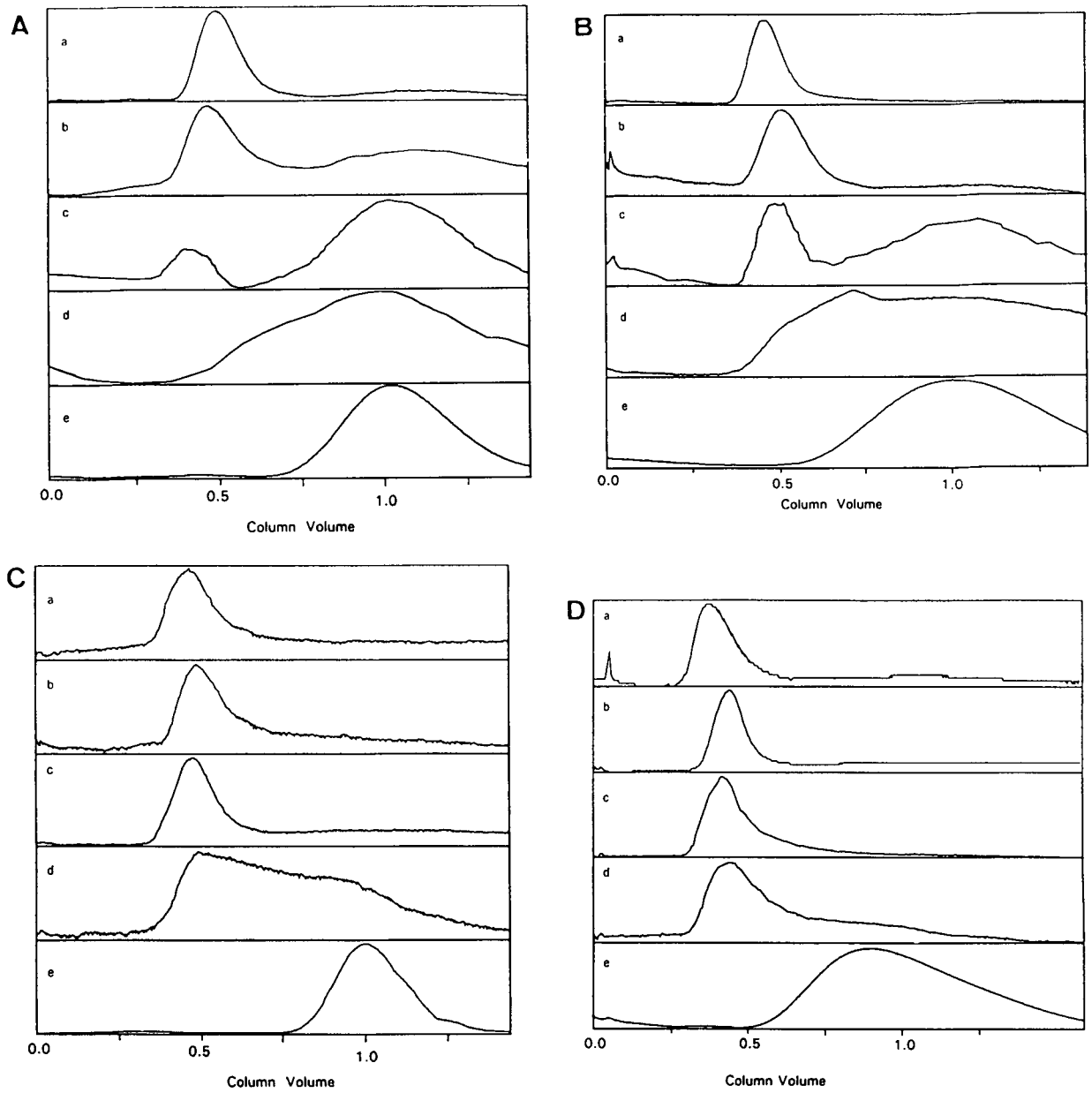

Fig. 4. Gel permeation chromatography on 3% (1 mm) cellulose beads (A, B) and 9% (0.8 mm) cellulose beads (C,D). Column: 35.4 × 1.0 cm. (A) superficial velocity, 0.12 cm/min, bead contacting time, 47 s. (B) Superficial velocity, 1.2 cm/min, bead contacting time, 5 s. (C) Superficial velocity, 0.12 cm/min, bead contacting time, 40 s. (D) Superficial velocity, 1.2 cm/min, bead contacting time, 4 s. a = Nanosphere 0.269 μm microspheres; b = blue dextran, molecular mass 2 000 000; c = thyroglobulin, molecular mass 669 000; d = β-amylase, molecular mass 200 000; e = tryptophan, molecular mass 204.

thyroglobulin, and β-amylase in 9% cellulose beads gave similar elution profiles at both 0.12 cm/min and 1.2 cm/min (Fig. 4C and 4D; panels b, c and d, respectively). The elution profile for the above large molecular mass species gave a single maximum at about 0.5–0.6 column vol-

TABLE I

RESIDENCE TIMES IN IMMUNOAFFINITY EXPERIMENTS

Support material	Bound antibody	Superficial velocity (cm/min)	Column residence time (s)	Bead contacting time [a] (s)	Eluted antigen binding efficiency (%)
3% Cellulose beads[b]	7D7B10	3.2	124	1.9	17 ± 5
		6.4	62	1.0	17 ± 3
		12.7	31	0.5	13 ± 2
		25.5	16	0.2	12 ± 1
		50.9	8	0.1	8 ± 1
		101.9	4	0.06	3 ± 3
4% Cross-linked agarose beads[c]	7D7B10	3.2	106	0.3	19 ± 1

[a] Bead contacting time calculated as column residence time × the ratio of the bead size to the column length.
[b] ≈1000 μm diameter beads.
[c] ≈140 μm diameter beads.

umes. In contrast, tryptophan gave an elution peak centered about 1.0 column volumes at both velocities with a slight peak broadening occurring at 1.2 cm/min (Fig. 4C and 4D; panel e).

The results of immunoaffinity adsorption experiments using cross-linked agarose and uncross-linked cellulose beads in a column loading and elution mode are listed in Table I. The column loading of the target protein was done at the same superficial velocity as the elution of product in each set of experiments. Both supports contained approximately 1 mg of immobilized Mab per ml hydrogel. Column residence and bead contacting times are given in Table I for each set of experiments. At column residence times of about 60 s or greater ($t_b \geq 1$ s), the amount of Protein C captured and eluted by the immobilized monoclonal antibody on 3% cellulose beads (≈1000 μm in diameter) was similar to that measured for the same antibody immobilized on the cross-linked 4% agarose beads (≈140 μm in diameter) column ($t_b = 0.3$ s). The capacity of the cellulose and agarose immunosorbents decreased significantly at t_b of about 0.5 s or less.

DISCUSSION

Fig. 5a combines the gross exclusion criteria of cellulose beads reported in the literature (with solids content greater than about 6%) with data obtained here for the VPI beads. We have here defined exclusion as greater than 80% of peak area at O.D. 280 nm appearing in the void volume at a linear velocity of about 1.2 cm/min or less (the void volume being taken as 0.40–0.45 column volumes). The data from Fig. 5a suggests the design criteria shown in Fig. 5b for the production of useful beaded cellulose sorption materials for protein purification. We have applied these criteria to the design of immunosorbents for the efficient capture of human Protein C (M_r 62 kDa) by an IgG class Mab (M_r 155 kDa). Larger proteins like thyroglobulin (M_r 669 kDa) and β-amylase (M_r 200 kDa) were also shown to permeate beads having 3% solids content.

The transport phenomena affected by changes in particle size and solids content are opposing in their impact upon chromatographic throughput and adsorbent capacity. Thus, when taken together, the data presented above suggest an optimization process illustrated in Fig. 5b. A "window of acceptable support characteristics" for a soft hydrogel is defined by the opposing effects of molecular accessibility, mechanical strength in a flow field, and the percentage of solids in the hydrogel. The lower limit for solids content at any given bead size is determined by the mechanical strength of the hydrogel as manifested by crushing velocity at a given bed depth. A minimum solids content of the gel at a given bead size might be chosen such that the crushing velocity is several-fold higher than the desired

a

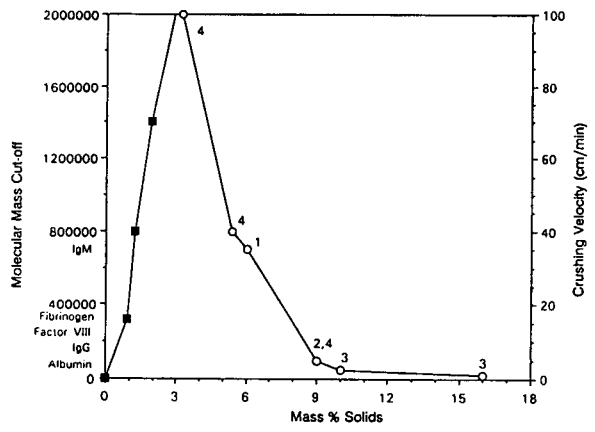

b

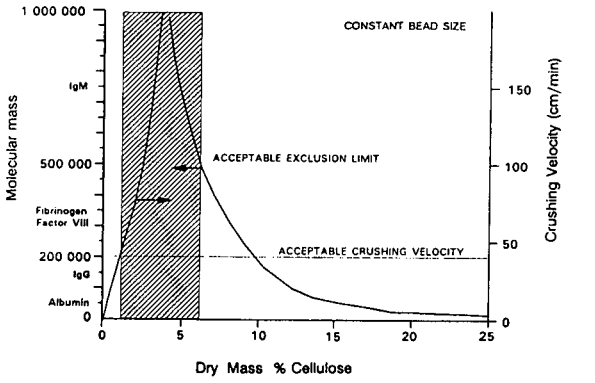

Fig. 5. (a) Data summary of molecular exclusion (greater than 90% excluded) and crushing velocity of various cellulose supports. ■ = Crushing velocity of VPI cellulose beads, ○ = molecular mass exclusion limit of various cellulose beads. 1 = Perloza cellulose beads; 2 = Kuga [23]; 3 = Peska *et al.* [24]; 4 = VPI cellulose beads. (b) Design characteristics for cellulose supports.

maximum operating superficial velocity. Because intraparticle transport is usually rate limiting, an estimate of the bead contacting time (t_b) can be used to determine a suitable operating velocity.

We have included a broad range of bead sizes as an important dimension of support characteristics. Fig. 3 shows the nonlinear relationship between crushing velocity, bead size, and solids content of cellulose hydrogels. It is noted that the least desirable matrices from the consideration of strength under flow are those that combine small bead size and low solids content.

The remaining variable not presented in Fig. 3 is dynamic capacity. Therefore, the 1000 μm diameter beads having 3% solids were evaluated for immunosorptive capacity since they possessed both molecular accessibility and sufficient physical strength under the flows which would exceed that needed for small or large-scale immunopurification processing. At a t_b of about 1 s, large cellulose beads exhibited immunosorptive efficiencies similar to 140 μm diameter agarose beads, as shown in Table I. Efficiency calculations are based upon an assumption of two antigens captured and eluted per immobilized antibody. Relative to the small cross-linked agarose immunosorbent, the cellulose immunosorbent could operate at shorter column residence times since faster flow rates could be sustained without risk of crushing. The fast throughput of the cellulose media occurred at a greatly decreased pressure drop due to increased bead size. Our analysis also included a comparison of cellulose beads of similar size to available agaroses. Because the strength of cellulose beads was similar to that of cross-linked agarose of a similar size and solids content, some of the design rationale developed here for larger cellulose beads may be applicable to the design of large bead agaroses used for immunosorbents. At the same low Mab densities used here, the dynamic capacity of both cellulose and agarose beads may be due to Mab immobilized near the surface. However, the cellulose beads gave similar capacities with eightfold less surface area per volume than the agarose beads. In addition, the peak widths seen in the immunoaffinity experiments were significantly smaller than would be predicted by the diffusion based, semi-empirical correlations of Mikes [20] and Johnson and Stevenson [21]. As shown in Table II, the experimental HETP (eqn. 3) for the cellulose immunosorbent was predicted to be 130 cm for a 1000 μm bead while the actual HETPs measured were about 0.4–0.9 cm. The experimental HETP for agarose beads with equivalent immunosorbent capacity was found to be about that of the cellulose. In the case of the small agarose beads, the HETP calculated by the above correlations agreed well with the experimental values.

We have attempted to grossly characterize the

TABLE II

HEIGHT EQUIVALENT TO A THEORETICAL PLATE: EXPERIMENTAL RESULTS *VS.* THEORY

Beaded material	System	Particle diameter (mm)	Superficial velocity (cm/min)	Experimental HETP[a] (cm)	Calculated HETP Johnson and Stevenson[b] (cm)	Calculated HETP Mikes[c] (cm)
Sepharose CL-4B (Agarose)	Immunoaffinity	0.14	2.5	0.4	0.6	0.7
VPI (Cellulose)	Immunoaffinity	1.2	13	0.4–0.9	132	134
	Gel permeation	1.2	0.13	0.9	0.5	0.5
	Tryptophan		1.3	1.8	2.8	3.2
	Gel permeation	1.2	0.13	1.0	5.2	6.1
	Thyroglobulin		1.3	0.9	49	58

[a] Calculated from eqn. 3.
[b] Ref. 21.
[c] Ref. 20.

transport of large and small molecules into the underivatized cellulose bead containing 91–97% water. The structure of these low solids content cellulose beads is likely stabilized by dispersed regions that have a high degree of hydrogen bonding. Preliminary studies of bead morphology by photomicroscopic evaluation of 10 μm cross-sections infiltrated with polymeric fixative indicate a homogeneous distribution of solids content in underivatized and derivatized cellulose beads (data not shown). In addition, no visible changes in bead appearance such as size or shape occurred as a result of Mab derivatization. We therefore studied the intraparticle transport from permeation experiments on underivatized beads to help understand the transport phenomena in Mab derivatized beads. The cost of Mab in making large columns of immunosorbents prevented us from doing permeation experiments on the immunosorbent columns proper.

The 3–9% range of solids contents studied here was chosen in an attempt to identify a transition of hydrogel structure from a very sparse density of low diffusional resistance to sufficient density to sterically encumber diffusional transport of proteins. We hypothesize that the transition regime for transport of proteins would consist of three experimentally identifiable modes of intraparticle transport phenomena. First, in approaching the limit of an aqueous continuum at very low solids content, a mixture of convective and diffusive modes of intraparticle transport would be expected to occur for even large molecules such as proteins. This would be a transport regime that would be faster than that predicted from diffusion alone. Second, a perturbation to slightly higher solids content would be expected to dampen out intraparticle convection and result in diffusion being the dominant mode of intraparticle transport. This intermediate solids content would not be expected to exert significant steric hindrance to diffusing proteins. Third, at still higher solids content, a transition to significant steric exclusion resulting from a higher density of gel structure would prevent diffusional transport of large proteins into the interior of the bead.

For cases where the solids content is low enough to eliminate the effects of steric exclusion, an estimate of the penetration solely by diffusion can be made by analytical solution [22]. Additional correlations that incorporate the effect of diffusion have been developed to describe chromatographic performance such as elution peak width [20,21]. The discussion below makes comparisons of estimates of intraparticle diffusional transport from both the analytical solution of diffusion into an aqueous sphere and predictions of peak width using chromatographic performance correlations.

The binary diffusion coefficient of tryptophan

TABLE III

EXTENT OF DIFFUSION IN GEL PERMEATION EXPERIMENTS BY THE ANALYTICAL SOLUTION

Species	Molecular mass	$D_{PW} \times 10^6$ cm^2/s	Extent of diffusion ($c_{av}/c_\infty \times 100$)			
			$t = 4$ s, $d_b = 0.8$ mm	$t = 5$ s, $d_b = 1$ mm	$t = 40$ s, $d_b = 0.8$ mm	$t = 50$ s, $d_b = 1$ mm
Tryptophan	204	5.0	34.1	30.9	82.2	77.0
β-Amylase	200 000	0.4	10.4	9.3	30.9	27.9
Thyroglobulin	669 000	0.26	8.4	7.6	25.3	22.9
Blue dextran	2 000 000	0.0583	4.0	3.6	12.5	11.2
Nanospheres 0.269 μm	N.A.	0.0126	1.9	1.7	5.9	5.3

in water is approximately twenty times larger than that of thyroglobulin [10]. Table III provides an estimate of the percentage of the equilibrium volume average concentration (c_{av}/c_b, eqn. 2) that could be achieved in the bead at the various bead contacting times (t_b, eqn. 1) estimated for the permeation data presented here. Permeation of tryptophan should have occurred to about 80% of equilibrium ($c_{av}/c_b = 0.8$) at $t_b = 50$ s and only about 30% of the equilibrium value ($c_{av}/c_b = 0.3$) should have been reached at $t_b = 5$ s. Thus, permeation could have occurred if the diffusion coefficient in the bead were the same as that of a purely aqueous continuum. The experimental HETPs for tryptophan at $v = 0.13$ and 1.3 cm/min were similar to that predicted by the diffusion based HETPs calculated by the methods of Mikes [20] and Johnson and Stevenson [21]. In summary, the gel permeation behavior of tryptophan in particles having 3–9% solids content is well described by diffusional transport in a homogeneous aqueous media.

The degree of permeation by large proteins such as thyroglobulin into 3% beads having 1000 μm average diameter at about 50 or 5 s bead contacting times was significantly more than would have been predicted by a purely diffusive transport. We have estimated that thyroglobulin should have permeated these beads to less than 25% of equilibrium ($c_{av}/c_b = 0.25$) at $t_b = 50$ s or to less than 8% of equilibrium ($c_{av}/c_b = 0.08$) at $t_b = 5$ s (Table III). The experimental HETP from the thyroglobulin permeation in 3% cellulose beads at $t_b = 50$ s was about 1.0 cm while the predicted HETP was about 5–6 cm. Furthermore, the experimental HETP at $t_b = 5$ s was about 0.9 cm as compared to the predicted HETP of 49–58 cm (Table II). Some of the bimodal aspects of the elution profile of thyroglobulin may be due to aggregation or nonspecific adsorption to the cellulose. Beads having 9% solids content appeared to exclude both blue dextran and thyroglobulin at $t_b = 40$ and 4 s. The elution behavior of β-amylase at $t_b = 40$ s was similar for both 3% and 9% cellulose beads. However, β-amylase did not appear to significantly permeate at $t_b = 4$ s in 9% cellulose beads. Thus, the β-amylase permeation behavior in 9% cellulose beads may be indicative of a gel structure that imparts significant hindrance to diffusion of large proteins. The lack of permeation by blue dextran in 9% cellulose beads of this work is similar to those reported by Kuga [23] and Peska *et al.* [24] which used cellulose beads having bead diameters less than about 200 μm. The rapid intraparticle transport of large proteins in the 3% cellulose beads observed in these studies may be evidence of an intraparticle transport regime having both convection and diffusion.

CONCLUSIONS

Using the above design rationale, we have developed large bead cellulose immunoaffinity sorbents which have equivalent capacity and

immunosorbent efficiency (utilization of coupled antibody) to that of smaller beaded hydrogel immunosorbents. It appears that beads of 3% solids content show some characteristics of enhanced intraparticle mass transfer over that explainable by unhindered diffusion. We are currently elucidating the dynamic immunosorbent capacity of beaded cellulose hydrogels derivatized with higher loadings of Mab to determine the extent of penetration of the immobilized IgG into the cellulose beads.

ACKNOWLEDGEMENTS

We thank professors L. Wang, S. Cramer and C.F. Ivory for their valuable comments. Special thanks to K. Van Cott for his help and comments in the editing process. This work was partially funded by National Science Foundation Grants BCS-9011098 and CBT-8803036 to W.H.V.

SYMBOLS

c_0	initial concentration of protein in bead (mg ml^{-1})
c_b	bulk fluid protein concentration (mg ml^{-1})
c_{av}	volume average concentration of protein in bead (mg ml^{-1})
CV	dimensionless throughput "column volume" ($= vt / L$)
d_b	diameter of bead (cm)
D_{PW}	diffusion coefficient of the protein through water ($cm^2\ s^{-1}$)
HETP	height equivalent to a theoretical plate (cm)
L	length of the column (cm)
M_r	molecular mass (kDa)
R	radius of bead (cm)
t	time (s)
t_b	bead contacting time ($= d_b/v$) (s)
t_R	retention time of a protein in the column (s)
v	superficial velocity of the bulk fluid through the column (cm s^{-1})
w_h	peak width measured at half the height of the peak (s)

REFERENCES

1 W.H. Velander, T. Morcol, D.B. Clark, D. Gee and W.N. Drohan, *Adv. Appl. Biotechnol.*, 11 (1990) 11–27.
2 C.L. Orthner, F.A. Highsmith, J. Tharakan, R.D. Madurawe, T. Morcol and W.H. Velander, *J. Chromatogr.*, 558 (1991) 55–70.
3 S.L. Fowell and H.A. Chase, *J. Biotechnol.*, 4 (1986) 1–13.
4 K. Kang, D. Ryu, W.N. Drohan and C.L. Orthner, *Biotechnol. Bioeng.*, 39 (1992) 1086–1092.
5 L.F. Chen and G.T. Tsao, *Biotechnol. Bioeng.*, 18 (1976) 1507–1516.
6 S. Katoh, *Trends Biotechnol.*, 5 (1987) 328–331.
7 Y.D. Clonis, *Bio/Technology*, 5 (1987) 1290–1293.
8 F.H. Arnold, W.H. Blanch and C.R. Wilke, *Chem. Eng. J.*, 30 (1985) B9–B23.
9 F.H. Arnold, W.H. Blanch and C.R. Wilke, *Chem. Eng. J.*, 30 (1985) B25–B36.
10 M.T. Tyn and T.W. Gusek, *Biotechnol. Bioeng.*, 35 (1990) 327–338.
11 R.E. Treybal, *Mass-Transfer Operations,* McGraw-Hill, 3rd ed., 1980, p. 200.
12 W.H. Velander, J.A. Kaster and W.G. Glasser, *US Pat. Appl.*, 07/496 314.
13 C.L. McCormick and D.K. Lichatowich, *J. Polym. Sci., Polym. Lett. Ed.*, 17 (1979) 479–484.
14 J. Porath, K. Aspberg, H. Drevin and R. Axen, *J. Chromatogr.*, 86 (1986) 53–56.
15 W.H. Velander, A. Subramanian, R. Madurawe and C.L. Orthner, *Biotechnol. Bioeng.*, 39 (1992) 1013–1023.
16 W.H. Velander, A. Subramanian, A.W. Degener, T. Morcol, J.L. Johnson, T.D. Wilkins, F.C. Gwazdauskas, R.M. Akers, H. Lubon and W.N. Drohan, *ACS Proceedings of the Meeting: Harnessing Biotechnology for the 21st Century,* 1992.
17 W.H. Velander, R.D. Madurawe, C.L. Orthner, J.P. Tharakan, A.H. Ralston, D.K. Strickland and W.N. Drohan, *Biotechnol. Prog.*, 5(3) (1989) 119–125.
18 H.S. Carslaw and J.C. Jaeger, *Conduction of Heat in Solids,* Oxford University Press, Oxford, 2nd ed., 1978, pp. 233–237.
19 R.W. Yost, L.S. Ettre and R.D. Conlon, *Practical Liquid Chromatography: An Introduction,* Perkin Elmer, 1980, pp. 38–41.
20 O. Mikes in Z. Deyl, K. Macek and J. Janak (Editors), *Liquid Column Chromatography: A Survey of Modern Techniques and Applications*, Elsevier, 1975, pp. 82–83.
21 E.L. Johnson and R. Stevenson, *Basic Liquid Chromatography*, Varian, Palo Alto, CA, 1978, pp. 15–31.
22 J.R. Welty, C.E. Wicks, R.E. Wilson, *Fundamentals of Momentum, Heat, and Mass Transfer*, John Wiley and Sons, New York, 2nd ed., 1976, pp. 561–569, 711–725.
23 S. Kuga, *J. Chromatogr.*, 195 (1980) 221–230.
24 J. Peska, J. Stamberg, J. Hradil and M. Ilavsky, *J. Chromatogr.*, 125 (1976) 455–469.

Journal of Chromatography, 648 (1993) 91–99
Elsevier Science Publishers B.V., Amsterdam

CHROM. 25 363

Peptidyl methyl ketones as ligands in affinity chromatography of serine and cysteine proteinases

K. Peters* and S. Fittkau

Institute of Physiological Chemistry, Medical Faculty of the Martin Luther University Halle–Wittenberg, Hollystrasse 1, 06114 Halle/Saale (Germany)

A. Steinert

Chemical Laboratory Dr. Wessling GmbH & Co. KG, Köthener Strasse 33a, 06118 Halle/Saale (Germany)

D. Ströhl

Institute of Analytical Chemistry, Department of Chemistry, Martin-Luther-University Halle–Wittenberg, Weinbergweg 16, 06120 Halle/Saale (Germany)

(Received May 13th, 1993)

ABSTRACT

Peptidyl methyl ketones are reversible inhibitors of serine and cysteine proteinases and can be employed as ligands in affinity chromatography. Serine proteinases of the subtilisin family may be purified using the tripeptidyl methyl ketone $-Ala_2-PheCH_3$ as ligand, whereas for papain, the best-known cysteine proteinase, both the $-Ala_2-PheCH_3$ and the $-Phe-AlaCH_3$ ligands are efficient. Complete elution of affinity-bound proteinases with isopropanol was demonstrated by investigations with thermitase, a subtilisin-type serine proteinase, which was ^{14}C labelled. Bound proteinases with different affinity for a defined ligand may be consecutively eluted using increasing concentrations of isopropanol in the elution buffer, as was shown, for example, with a mixture of thermitase and subtilisin DY. The quality of the lyophilized affinity-purified thermitase is similar to that of thermitase preparations purified by isoelectric focusing and adsorption on porous glass bodies. The affinity of thermitase for the immobilized $-Ala_2-PheCH_3$ ligand linked to Divicell via an ε-aminocaproic acid (Aca) spacer is about two orders of magnitude lower than its affinity for the soluble inhibitor benzyloxycarbonyl–$Ala_2-PheCH_3$ and one order of magnitude lower than its affinity for Ac–Aca–$Ala_2-PheCH_3$. In comparison with affinity gels made with commercial CH-Sepharose 4B, the Divicell gels possess higher concentrations of ligands and have a higher stability.

INTRODUCTION

Peptidyl methyl ketones are potent reversible inhibitors of serine and cysteine proteases [1–5]. They are easy to synthesize, they have a higher chemical stability than other reversible peptide inhibitors (*e.g.* aldehydes) and their amino acid sequence may be adapted to the specificity of a defined enzyme. In an earlier paper [6] we introduced peptidyl methyl ketones as a new type of ligands in affinity chromatography of serine proteases. However, a number of questions remained unanswered (for instance the completeness of the enzyme elution, the long-term stability of the gels and the inhibition constant of the immobilized peptidyl methyl ketone are unknown).

In this work, the properties of the affinity gel Divicell–Aca–$Ala_2-PheCH_3$ (Aca = ε-aminocaproic acid) are discussed in comparison with

* Corresponding author.

0021-9673/93/$06.00

the Sepharose 4B–Aca–Ala_2–$PheCH_3$ gel. Adsorption and desorption studies on both affinity gels were performed with the enzymes α-chymotrypsin, the subtilisins Carlsberg, BPN′ and DY and thermitase, as well as proteinase K.

Divicell, a macroporous bead cellulose with excellent flow parameters, was tested as support of affinity gels since it seems to possess some advantages in comparison with Sepharose 4B [7,8]. The inhibition constant (K_i) of the immobilized tripeptidyl methyl ketone –Ala_2–$PheCH_3$ in its reaction with thermitase was estimated and compared with the K_i values for the reaction of thermitase with the soluble inhibitors Z–Ala_2–$PheCH_3$ (Z = benzyloxycarbonyl) and Ac–Aca–Ala_2–$PheCH_3$. This last inhibitor should simulate the molecular structure of the spacer–tripeptidyl methyl ketone part of the affinity gel.

The completeness of the elution of the bound enzyme in the presence of isopropanol was examined by affinity chromatographic studies with ^{14}C-labelled acetyl-thermitase.

The separation of two related proteinases from a mixture by stepwise elution with increasing isopropanol concentration from the affinity gel Divicell–Aca–Ala_2–$PheCH_3$ was performed with a model mixture of pure subtilisin DY and pure thermitase.

Later, the paper describes the use of Divicell–Aca–Ala_2–$PheCH_3$ for the purification of thermitase from a crude extract. Considering the specificity of the cysteine proteinase papain, the affinity gels Divicell–Aca–Phe–$AlaCH_3$ and Divicell–β-Ala–Phe–$AlaCH_3$ were synthesized and adsorption and desorption studies on these gels were undertaken with papain.

EXPERIMENTAL

Inhibitors

Z–Ala_2–$PheCH_3$ was prepared according to Fittkau and Jahreis [1]. Ac–AcaOH was synthesized from ε-aminocaproic acid via H-AcaOMe × HCl and Ac–AcaOMe. Direct reaction of ε-aminocaproic acid with anhydrous acetic acid in pyridine as solvent produced by-products that could not be eliminated.

H–AcaOMe × HCl was obtained from the reaction of ε-aminocaproic acid with thionyl-chloride in water-free methanol [9] (yield, 97%; m.p. of the white needles 120–123°C; TLC, $CHCl_3$–CH_3OH, 9:1).

H–AcaOMe × HCl was acetylated in the presence of triethylamine with an excess of acetic anhydride. A light-brown oil was obtained which could not be induced to crystallize (yield, 40%; TLC, $CHCl_3$–CH_3OH, 9:1).

Ac–AcaOMe was saponified with 1 *M* NaOH within a few minutes to give white crystals of Ac–AcaOH (yield, 59%; m.p. 101–104°C; TLC, $CHCl_3$–CH_3OH, 9:1).

Ac–AcaOH was coupled with H–Ala_2–$PheCH_3$ × HCl using the mixed anhydride method to give a white powder of the tetrapeptidyl methyl ketone Ac–Aca–Ala_2–$PheCH_3$ [yield, 77%; m.p. 197–200°C; TLC, $CHCl_3$–CH_3OH, 5:1; CH_3OH–CH_3COOH–water, 2:1:2 (1% in ethyl acetate); $[\alpha]_D^{25}$ −23.6° (1% in ethyl acetate); HPLC RP-8 LiChrospher (Merck); elemental analysis for $C_{24}H_{36}N_4O_5$: C found 62.05 (calculated 62.59), H 7.88 (7.88), N 11.99 (12.16), O 18.08 (17.37)].

The purity of all intermediate compounds was controlled by TLC, by the melting point and by the optical activity; all final products were additionally characterized by elemental analysis, HPLC (RP-8 column, acetonitrile–water–0.1% trifluoroacetic acid system) and ^{1}H NMR spectroscopy. All compounds were purified to homogeneity.

In the case of Z–Ala_2–$PheCH_3$ and Ac–Aca–Ala_2–$PheCH_3$ two-dimensional ^{1}H COSY (correlated spectroscopy) spectra were also recorded using a Varian Unity 500 spectrometer (USA). The spectra were recorded in 256 experiments and a matrix of 256 × 2000 data points. As an example, the COSY spectrum of Ac–Aca–Ala_2–$PheCH_3$ is given in Fig. 1.

In order to distinguish between the ^{1}H signals of both alanine residues in the compounds Z–Ala_2–$PheCH_3$ and Ac–Aca–Ala_2–$PheCH_3$ NOE (nuclear Overhauser effect) difference spectra were recorded. The NOE experiments were performed with samples degassed repeatedly (five freeze–pump-through cycles). In all experiments the temperature was 25°C. The following proton chemical shifts with respect to internal tetramethylsilane were found for the three final products.

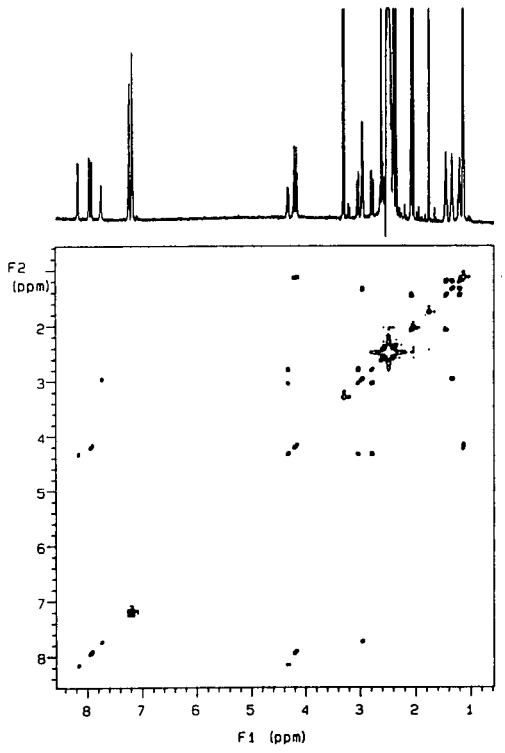

Fig. 1. Two-dimensional correlated 500-MHz proton NMR spectrum of Ac–Aca–Ala_2–$PheCH_3$ in [$^2H_6$]DMSO (15.8 mg/ml). A contour plot is shown, the one-dimensional spectrum on the diagonal, and the off-diagonal cross-peaks occur at the intersection of chemical shifts of two J-coupled spins. The one-dimensional ^1H NMR spectrum is shown at the top of the contour.

Z–Ala(2)–Ala(1)–$PheCH_3$. $PheCOCH_3$ (2.04 ppm); Phe (CαH 4.34; CβH 2.79 and 3.06; C_6H_5 7.16–7.25; NH 8.21); Ala(1) (CαH 4.22; CβH 1.16; NH 7.95); Ala(2) (CαH 4.03; CβH 1.16; NH 7.45); Z (CH_2 5.00; C_6H_5 7.33).

Ac–Aca–Ala(2)–Ala(1)–$PheCH_3$. $PheCOCH_3$ (2.04 ppm); Phe (CαH 4.33; CβH 2.79 and 3.04; C_6H_5 7.16–7.26; NH 8.16); Ala(1) (CαH 4.14–4.24; CβH 1.12–1.15; NH 7.97); Ala(2) (CαH 4.14–4.24; CβH 1.12–1.15; NH 7.93); Aca (CαH 2.07; CβH 1.42–1.48; CγH 1.31–1.37; CδH 1.18–1.23; CεH 2.94–2.99; NH 7.75); Ac (CH_3 1.76).

Z–Phe–$AlaCH_3$. $AlaCOCH_3$ (1.98 ppm); Ala (CαH 4.23; CβH 1.75; NH 8.42); Phe (CαH 4.26; CβH 2.74 and 2.99; C_6H_5 7.14–7.33; NH 7.54); Z (CH_2 4.93; C_6H_5 7.29).

Affinity gels

Divicell activated with 5-norbornene-2,3-dicarboximido carbonochloridate (30–34 μmol of activated OH groups per ml of gel) was a gift from Dr. H.-F. Boeden (Central Institute of Molecular Biology, Berlin, Germany) and Dr. R. Müller (Leipziger Arzneimittelwerke, Leipzig, Germany). It was suspended in 0.1 *M* sodium tetraborate buffer, pH 8.0, and coupled with ε-aminocaproic acid and β-alanine with stirring overnight. The amino acids were added in 30- or 25-fold molar excess, respectively, to the activated groups of the support [10]. Residual activated hydroxyl groups were bound with 1 *M* ethanolamine.

Titration of Divicell–AcaOH and Divicell–β-AlaOH was performed with 0.9 *M* NaOH in a TTT 2 pH-stat autotitrator (Radiometer, Copenhagen, Denmark). Concentrations between 17 and 21 μmol of carboxyl groups per ml of sedimented Divicell–AcaOH (depending on the charge) and 15 μmol of carboxyl groups per ml of Divicell–β-AlaOH were determined. In contrast, for commercial CH-Sepharose 4B (Pharmacia, Uppsala, Sweden) 13 μmol of carboxyl groups per ml of gel were titrated.

The N-terminal free peptidyl methyl ketone hydrochlorides were coupled to the support–spacer conjugate with an excess of N-ethyl-N′-(3-dimethylamino-)propyl carbodiimide × HCl (Serva, Heidelberg, Germany) at pH 4.5–5.0 with stirring overnight at room temperature. The peptidyl component was added in a three- to six-fold molar excess compared with the spacer carbonyl groups. For instance, 11 ml of Divicell–AcaOH containing 231 μmol of carboxyl groups were coupled with 237 mg (= 693 μmol) of H–Ala_2–$PheCH_3$ × HCl freshly prepared from Z–Ala_2–$PheCH_3$ in 20 ml of water, pH 4.7, in the presence of 228 mg (= 1.19 mmol) of carbodiimide hydrochloride. Residual carboxyl groups were blocked with 1 *M* ethanolamine in the presence of carbodiimide.

The affinity gels were characterized by amino acid analysis with an Analysator 339 (Microtechno, Prague, Czech Republic) after total hydrolysis (boiling for 24 h with 6 *M* HCl under reflux). The amino acid compositions of the affinity gels are summarized in the following.

Sepharose 4B–Aca–Ala_2–$PheCH_3$. Aca 8.6 μmol per ml of gel (100%); Ala (2) 6.0 (70%); $PheCH_3$ 5.4 (63%); ethanolamine not determined.

Divicell–Aca–Ala_2–$PheCH_3$. Aca 14.1 μmol per ml of gel (100%); Ala (2) 8.4 (60%); $PheCH_3$ 8.6 (61%); ethanolamine 0.9 (6%).

Divicell–Aca–Phe–$AlaCH_3$. Aca 17.0 μmol per ml of gel

(100%); Phe 8.0 (47%); $AlaCH_3$ 7.4 (44%); ethanolamine 3.4 (20%).

Divicell–β-Ala–Phe–$AlaCH_3$. β-Ala 10.8 μmol per ml of gel (100%); Phe 4.0 (37%); $AlaCH_3$ 4.0 (37%); ethanolamine 2.3 (21%).

All gels were stored at 4°C in 0.1 *M* phosphate buffer, pH 6.0, containing 0.5 or 1.0 *M* NaCl and 0.02% NaN_3.

Substrates

Suc–Ala_2–PhepNA (Suc = succinyl; pNA = *para*-nitroanilide), a chromogenic substrate of serine proteinases with chymotryptic specificity, and Z–Phe–ArgNMec (NMec = N-methylcoumaryl amide), a cysteine proteinase substrate with a fluorescent end group after hydrolysis, were both synthesized in our laboratory according to the method of Brömme and co-workers [4,11].

Enzymes

Thermitase as a crude preparation and purified by adsorption on porous glass bodies was obtained from Dr. U. Kettmann (Institute of Physiological Chemistry, Martin Luther University Halle-Wittenberg, Halle, Germany). Thermitase purified by isoelectric focusing was a gift from Dr. W.E. Höhne (Institute of Biochemistry, Humboldt University Berlin, Germany). The subtilisins Carlsberg, Novo and DY were gifts from Professor N.C. Genov (Institute of Organic Chemistry, Bulgarian Academy of Sciences, Sofia, Bulgaria). α-Chymotrypsin and papain (crystal suspension) were purchased from Boehringer (Mannheim, Germany). Active site titrations were carried out with *trans*-cinnamoylimidazol according to Schonbaum *et al.* [12] on a Shimadzu UV 300 spectrophotometer (Japan).

The enzymatic activity of the serine proteinases against Suc–Ala_2–PhepNA in 0.1 *M* Tris–HCl buffer, pH 8.2, was recorded with an Eppendorf photometer (Germany). The activity of papain against Z–Phe–ArgNMec in 0.1 *M* Tris–HCl buffer, pH 7.5, was monitored on a Perkin-Elmer 1000 M fluorimeter (Germany).

The preparation of ^{14}C-labelled thermitase was performed as follows. A 2.5-mg aliquot of thermitase was dissolved in 500 μl of 0.1 *M* phosphate buffer (pH 7.5, 0.5 *M* NaCl) containing a 1.54-fold excess of Z–Ala_2–$PheCH_3$ and 1% (v/v) dimethyl sulphoxide (DMSO). At intervals of 10 min, three 1-μl aliquots (total: 32 μmol with a radioactivity of about 13.5 MBq) of ^{14}C-labelled acetic anhydride were added. The pH was adjusted to 7.5–7.6 with 0.92 *M* NaOH. After addition of the last aliquot of acetic anhydride the solution was allowed to react for 1 h at room temperature. In order to separate the acetylated enzyme from acetic acid, peptidyl methyl ketone and DMSO, gel filtration on Sephadex G-25 column (Pharmacia) was performed (column 43 × 1.2 cm; 0.1 *M* phosphate buffer, pH 7.5, 0.5 *M* NaCl; flow-rate 9 ml/h). A 100-μl volume of the fraction that contained the highest concentration of acetylated protein was directly applied to the affinity gel Divicell–Aca–Ala_2–$PheCH_3$ (column 3.5 × 0.7 cm) equilibrated with 0.1 *M* Tris–HCl buffer, pH 7.5, 0.5 m*M* calcium acetate.

Affinity chromatography

Simple binding and retention studies were carried out with pure enzymes and gel volumes between 1.1 and 1.4 ml (column length 4.0–16.0 cm, diameter 0.4–0.7 cm).

For the determination of the binding capacities and the K_i value of the immobilized tripeptidyl methyl ketone –Ala_2–$PheCH_3$, a small column containing 60 μl of affinity gel (1.30 × 0.25 cm) was used. The gels were equilibrated with 0.1 *M* Tris–HCl buffer, pH 7.8, 0.5 m*M* Ca^{2+}, before applying the enzymes. After loading 1.0–1.2 mg of enzyme dissolved in 200 μl of the buffer described above, the gels were washed with buffer containing 0.5 *M* then 1 *M* NaCl to break down and to determine non-specific adsorptions of the protein.

In order to elute the enzymes different amounts of isopropanol (10–50%, v/v) were added to the buffer. The flow-rate was adjusted to 2–3 ml/h.

The adsorption properties of the unmodified matrix as well as of the affinity gels against non-specific proteins were tested with haemoglobin.

The preparation of thermitase from prepurified crude material is described in the legend to Fig. 3. The fractions containing the purified

enzyme were combined and desalted by ultrafiltration in an Amicon cell (USA) with a YM 10 membrane. After this procedure thermitase was lyophilized.

All investigations using pure enzymes were performed at room temperature. The preparation of thermitase from crude material was performed at 4°C.

Kinetic parameters

The K_i values of the soluble inhibitors were determined as described by Fittkau *et al.* [2].

The K_i for the reaction of the tripeptidyl methyl ketone $-Ala_2-PheCH_3$ immobilized on Divicell via Aca with thermitase was estimated by modified frontal analysis [13]. A concentrated thermitase solution (3.0 mg/ml) with a defined activity was continuously applied to a column containing 60 μl of affinity gel until the enzymatic activity in the eluate was the same as the activity of the applied solution and remained constant.

RESULTS AND DISCUSSION

For the subtilisins Carlsberg and DY, thermitase and proteinase K a strong adsorption on both affinity gels, Sepharose 4B–Aca–Ala_2–$PheCH_3$ and Divicell–Aca–Ala_2–$PheCH_3$, was obtained. Subtilisin BPN′ and α-chymotrypsin were retained by the Divicell gel much more than by the Sepharose affinity gel, but in the case of α-chymotrypsin not enough to use Divicell–Ala_2–$PheCH_3$ for purification procedures.

Desorption of the bound enzymes could be achieved as described by Stepanov *et al.* [14] and Van den Burg *et al.* [15] by addition of isopropanol to the mobile phase. The amounts of isopropanol needed for a complete and sharp elution of the different proteinases correlate with the inhibition constants of the soluble inhibitor of these enzymes, Z–Ala_2–$PheCH_3$ [3]. The lower the K_i value, the more isopropanol is necessary. For instance, to elute subtilisin BPN′ ($K_i = 1.3 \cdot 10^{-4}$ M) from the gel Divicell–Aca–Ala_2–$PheCH_3$ 10% (v/v) isopropanol in the elution buffer is sufficient, but for the elution of thermitase ($K_i = 3.0 \cdot 10^{-7}$ M) at least 35% (v/v) isopropanol is needed. The other subtilisins as well as proteinase K, possessing inhibition constants between both these K_i values, are eluted sharply with isopropanol concentrations of 15–25% (v/v). Therefore, a 1:1 molar model mixture of pure subtilisin DY and pure thermitase could be separated by stepwise elution from the affinity gel Divicell–Aca–Ala_2–$PheCH_3$ using buffers containing 15% and 35% (v/v) isopropanol, respectively (see Fig. 2). However, since 15% isopropanol in the elution buffer causes a desorption of small amounts of thermitase, the eluted subtilisin DY is contaminated with it.

Using the Sepharose gel, in general lower isopropanol concentrations in the elution buffer are sufficient to elute the different enzymes, indicating weaker enzyme–ligand interactions [6]. The recovery of the enzymatic activity after affinity chromatography amounted in all cases to more than 85%.

The use of isopropanol as eluent has the advantage of enzyme stabilization. The enzymatic activity decreases rapidly with increasing isopropanol concentration. Autolysis is suppressed [15]. However, this inactivation is completely reversible as it could be shown after dilution of the alcohol to be less than 1% (v/v). Treating thermitase with a higher concentration of isopropanol even induces an increase in activi-

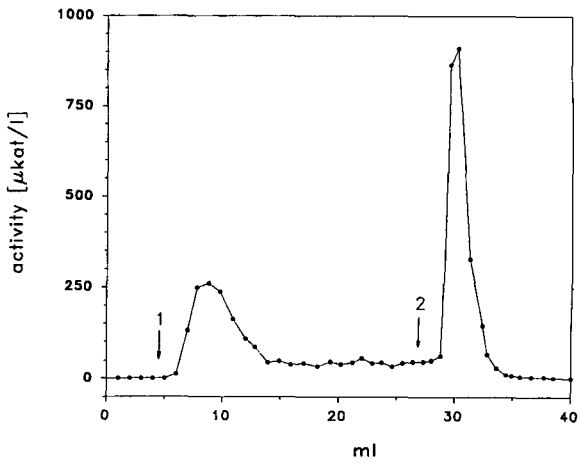

Fig. 2. Stepwise elution of subtilisin DY and thermitase from the affinity gel Divicell–Aca–Ala_2–$PheCH_3$. Conditions: 0.1 M Tris–HCl buffer, pH 7.8, 0.5 mM Ca^{2+}, 1 M NaCl, (1) 10% (v/v) and (2) 35% (v/v) isopropanol. Substrate: Suc–Ala_2–PhepNA. Column: 4.5 × 0.6 cm. Flow-rate: 3 ml/h.

ty after dilution [6]. In order to prove the completeness of elution, pure thermitase dissolved in buffer was acetylated with ^{14}C-labelled acetic anhydride in the presence of an excess of Z–Ala_2–$PheCH_3$. The peptidyl methyl ketone reversibly inhibits more than 99% of the enzyme activity and in this way prevents acetylation of active-site amino acid residues.

The inhibitor and the excess of acetylating reagent were eliminated by gel filtration on a Sephadex G-25 gel before applying 100 μl of the most radioactive protein fraction to an affinity column filled with Divicell–Aca–Ala_2–$PheCH_3$. Only 17% of the applied radioactivity appeared with the front; however, no enzymatic activity against Suc–Ala_2–PhepNA could be determined in these fractions. In the fractions containing 40% (v/v) isopropanol, 74% of the radioactivity and all the enzymatic activity appeared. Altogether, a recovery of 93% radioactivity and 87% enzymatic activity could be observed.

These investigations indicate that thermitase and —because of the recovery of enzymatic activity of between 85% and 95% in experiments with the other mentioned proteases— related enzymes could be completely eluted from affinity gels with peptidyl methyl ketone ligands by addition of isopropanol to the eluent.

In order to test the behaviour of an inert protein at the affinity gels Divicell- or Sepharose 4B–Aca–Ala_2–$PheCH_3$ haemoglobin was applied to the affinity columns. In neither case could any retention be observed. Therefore, haemoglobin could be used to determine the dead volume of a column system.

The pure support materials also retain neither haemoglobin nor the subtilisin proteinases.

The binding capacities of Sepharose 4B- and Divicell–Aca–Ala_2–$PheCH_3$ were estimated with thermitase. Whereas for the Sepharose gel a capacity of 1.7 μmol of enzyme per ml of sedimented gel was determined, for the Divicell gel a maximal adsorption of 1.4 μmol of enzyme per ml gel was found.

Considering the real concentrations of ligands, only about 28% and 17%, respectively, of the present ligands are able to bind active enzyme molecules. The difference in the binding capacities between the two gels can only be explained by steric effects.

When the Sepharose affinity gel was used more than 20–25 times (well below the capacity limit), changes in the adsorption and desorption properties were observed. The basic enzymatic activity measured in the eluate during the washing procedure —which is due to the equilibrium between bound and free enzyme and, in general, very low for tight-binding proteases— increases, and lower isopropanol concentrations in the elution buffer are sufficient for elution. The same effects could be observed if Sepharose 4B–Aca–Ala_2–$PheCH_3$ was stored at 4°C for 10 months. In this case, the capacity decreased by more than 40% [6].

In comparison, the gel Divicell–Aca–Ala_2–$PheCH_3$ seems to be much more stable than the Sepharose gel. Storage for more than 2 years and use far below the capacity limit does not cause changes in the gel properties.

One reason for the higher stability of the Divicell gel is the type of bonding between support and spacer. The Aca in the Divicell gel is bound to the support via urethane bonding, which is much more stable than the isourea bonding found in commercial CH-Sepharose [8]. Incubation of the affinity gel Sepharose 4B–Ala_2–$PheCH_3$ with a more concentrated enzyme solution for 2 days leads to the hydrolysis of the bonds between the two alanine residues and between spacer and ligand found with amino acid analysis [6].

The experiment that was performed to determine the binding capacity of the affinity gel Divicell–Aca–Ala_2–$PheCH_3$ was also used to estimate the inhibition constant, K_i, of the immobilized tripeptidyl methyl ketone according to the equation:

$$K_i = c_E c_I / c_{EI}$$

Under conditions of saturation c_E is equal to the enzyme concentration of the applied solution, c_{Eo}, c_{EI} is given by the binding capacity of the gel and c_I corresponds to the concentration of uncomplexed ligands involved in the equilibrium between free and bound enzyme.

The concentration of the free ligands could not be determined from the experiments but should be much lower than the difference between the total concentration of ligands and the concentration of the ligands complexed with enzyme,

because not all ligands are accessible to the enzyme molecules. Steric hindrance should be taken into account.

Therefore, K_i was calculated for a range of c_I from 1% to 13% of the total ligand concentration assuming that only 18–30% of immobilized ligands are able to interact with the enzyme. With a total ligand concentration of 8.5 μmol per ml of gel, an enzyme concentration $c_{Eo} = 7.8 \cdot 10^{-5}$ *M* in the interstitial volume of the gel and a maximal adsorption of 1.4 μmol of thermitase per ml of gel, a K_i value between 0.4 and $6 \cdot 10^{-5}$ *M* was found. In comparison, the K_i of the soluble thermitase inhibitor Z–Ala_2–$PheCH_3$ amounted to $3.0 \cdot 10^{-7}$ *M* [3]. Since this value takes into account the hydrophobic interactions of the benzyloxycarbonyl residue with the protein, the inhibitor Ac–Aca–Ala_2–$PheCH_3$ was synthesized to simulate the structure of the spacer-bound tripeptidyl methyl ketone better than the Z–Ala_2–$PheCH_3$ inhibitor.

In the case of thermitase, the K_i for Ac–Aca–Ala_2–$PheCH_3$ was determined to be $1.7 \cdot 10^{-6}$ *M*, which is about one order of magnitude greater than for the Z-protected inhibitor and about one order of magnitude smaller than for the immobilized peptidyl methyl ketone. It can be concluded that the kinetic constants of soluble peptidyl methyl ketones, and especially of inhibitors that contain the spacer at the N-terminus, are important in determining optimal ligands for affinity chromatography, although the conformational structure of the inhibitor may change during immobilization.

The affinity gel Divicell–Aca–Ala_2–$PheCH_3$ was used to purify thermitase in one step from a crude preparation. A concentrate of the culture medium of *Thermoactinomyces vulgaris* was prepurified by gel filtration on Sephadex G-75 and then directly applied to a column containing the affinity gel. After washing, the pure enzyme could be eluted with a sharp peak by adding 40% (v/v) isopropanol to the buffer. The elution diagram is shown in Fig. 3. After ultrafiltration and lyophilization the enzyme was characterized by sodium dodecyl sulphate–polyacrylamide gel electrophoresis (SDS-PAGE), protein spectrum, specific activity against Suc–Ala_2–PhepNA and active site titration with *trans*-cinnamoylimidazol. Similar results can be obtained if thermitase is purified with Sepharose–Aca–Ala_2–$PheCH_3$ [6].

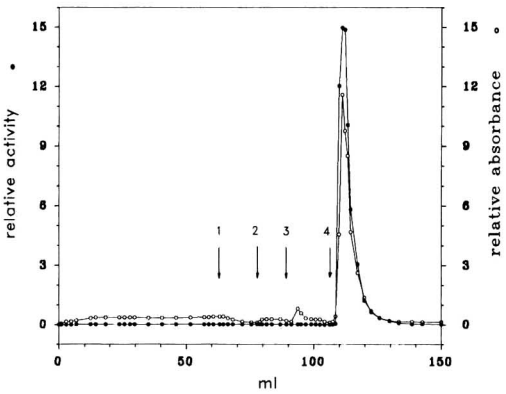

Fig. 3. Chromatography of thermitase on a column filled with the affinity gel Divicell–Aca–Ala_2–$PheCH_3$. Relative absorbance at 280 nm (○) = absorbance of the eluate/absorbance of the applied solution; relative activity (●) = activity of the eluate/activity of the applied solution. Conditions: Sephadex G-75 prepurified thermitase in 65 ml of 0.1 *M* ammonium acetate, pH 7.5, 0.5 m*M* Ca^{2+}. Arrows indicate the change of eluent: 1 = 0.1 *M* ammonium acetate, pH 7.5, 0.5 m*M* Ca^{2+}; 2 = 0.1 *M* Tris–HCl buffer, pH 7.8, 0.5 m*M* Ca^{2+}; 3 = 0.1 *M* Tris–HCl buffer, pH 7.8, 0.5 m*M* Ca^{2+}, 1 *M* NaCl; 4 = 0.1 *M* Tris–HCl buffer, pH 7.8, 0.5 m*M* Ca^{2+}, 1 *M* NaCl, 40% (v/v) isopropanol. Substrate: Suc–Ala_2–PhepNA. Column: 5.0 × 0.6 cm. Flow-rate: 12 ml/h (1 and 2), 5 ml/h (3).

Comparisons with thermitase fractions purified by isoelectric focusing [16] and adsorption on porous glass bodies [17] indicated that thermitase purified by affinity chromatography with the –Ala_2-$PheCH_3$ ligand as described has the same quality as the other preparations, for instance the electropherograms are almost the same for all enzyme charges (Fig. 4).

Specific activities between 1.40 and 1.98 μkat/mg and active amounts of total protein between 75% and 93% were determined for all thermitase fractions independently of their method of purification.

Peptidyl methyl ketones are effective inhibitors not only of serine proteinases but also of cysteine proteinases [4,5]. Inhibition constants in the micromolar range [4] lead to the assumption that peptidyl methyl ketones are also available as ligands in affinity chromatography of cysteine proteinases.

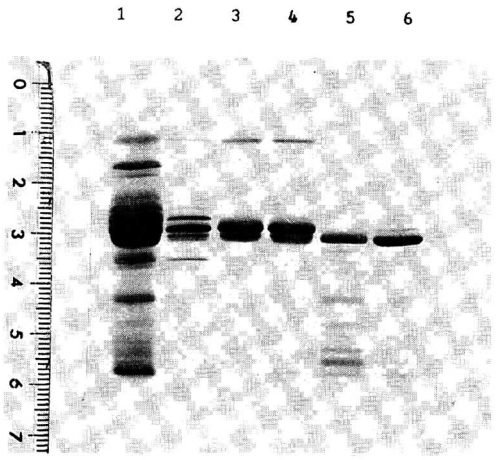

Fig. 4. SDS-polyacrylamide gel electrophoresis of thermitase. Collecting gel: 4.5% PAA, pH 6.8. Separation gel: 15.0% PAA, pH 8.8. Current: 40 mA, 2 h. In order to prevent autolysis during the boiling with SDS, thermitase was denatured with 20% trichloroacetic acid (1–4) and incubated at room temperature for 90 min with an eight-fold excess of the irreversible inhibitor Z–Ala_2–$PheCH_2Cl$ (5 and 6), respectively, before treatment with SDS. Lanes: 1 = Crude extract; 2 = after gel filtration on Sephadex G-75; 3 and 5 = after isoelectric focusing; 4 and 6 = after affinity chromatography with Divicell–Aca–Ala_2–$PheCH_3$.

Since papain, the best-known cysteine proteinase, possesses a specificity for substrates and inhibitors with aromatic amino residues in P_2 and relatively small amino acid residues in P_1 [18], the affinity gels Divicell–Aca–Phe–$AlaCH_3$ and Divicell–β-Ala-Phe–$AlaCH_3$ were synthesized and tested for papain binding.

Regardless of the spacer length, both gels adsorb papain strongly. In both cases the proteinase could only be eluted sharply with 50% (v/v) isopropanol in the elution buffer. However, papain also binds to Sepharose 4B- and Divicell–Aca–Ala_2–$PheCH_3$, but for elution an isopropanol concentration of only 30% and 40% (v/v), respectively, is sufficient. The lower isopropanol concentration in the latter experiments indicates weaker interactions between papain and the tripeptidyl methyl ketone ligand than between papain and the ligand –Phe–$AlaCH_3$. The recovery of enzymatic activity was 70–80% in all experiments.

Summarizing all investigations, it can be concluded that peptidyl methyl ketones are in general useful as ligands in affinity chromatography of serine and cysteine proteinases. The separation may be specified by adapting the amino acid sequence of the ligand to the specificity of the enzyme, which should be purified. Elution may be performed by use of an organic solvent that reduces autolysis of the proteases but influences the activity only reversibly. Because of its higher stability and higher ligand concentrations Divicell should be preferred over Sepharose as a support of the affinity gel.

ACKNOWLEDGEMENTS

We are grateful to Dr. H.-F. Boeden and Dr. R. Müller for donating activated Divicell, Professor Dr. N.C. Genov, Dr. U. Kettmann and Dr. W.E. Höhne for donating the enzyme preparations and D. Pauli, E.-M. Kötters and G. Rascher for excellent technical assistance.

REFERENCES

1 S. Fittkau and G. Jahreis, *J. Prakt. Chem.*, 326 (1984) 48–53.
2 S. Fittkau, K. Smalla and D. Pauli, *Biomed. Biochim. Acta*, 43 (1984) 887–899.
3 K. Peters, D. Pauli, H. Hache, R.N. Boteva, N.C. Genov and S. Fittkau, *Curr. Microbiol.*, 18 (1989) 171–177.
4 D. Brömme, B. Bartels, H. Kirschke and S. Fittkau, *J. Enzyme Inhib.*, 3 (1989) 13–21.
5 D.H. Rich, in A.J. Barrett and G. Salvesen (Editors), *Proteinase Inhibitors*, Elsevier, Amsterdam, 1986, pp. 153–178.
6 K. Peters and S. Fittkau, *Biomed. Biochim. Acta*, 49 (1990) 173–178.
7 H.-F. Boeden, K. Pommerening, M. Becker, C. Rupprich, M. Holtzhauer, F. Loth, R. Müller and D. Bertram, *J. Chromatogr.*, 552 (1991) 389–414.
8 M. Baeseler, H.-F. Boeden, R. Koelsch and J. Lasch, *J. Chromatogr.*, 589 (1992) 93–100.
9 M. Brenner and W. Huber, *Helv. Chim. Acta*, 36 (1953) 1109–1115.
10 W. Büttner, M. Becker, C. Rupprich, H.-F. Boeden, P. Henklein, F. Loth and H. Dautzenberg, *Biotechnol. Bioeng.*, 33 (1989) 26–31.
11 D. Brömme and S. Fittkau, *Biomed. Biochim. Acta*, 44 (1985) 1089–1094.
12 G.R. Schonbaum, P. Zerner and M.L. Bender, *J. Biol. Chem.*, 236 (1961) 2930–2935.
13 J. Turkova, *Affinity Chromatography*, Elsevier, Amsterdam, 1978, pp. 41–44.

14 V.M. Stepanov, L.P. Revina, S.T. Abramov, A.Y. Strongin and U. Behnke, *J. Appl. Biochem.*, 2 (1980) 342–345.
15 B. van den Burg, V.G.H. Eijsink, B.K. Stulp and G. Venema, *J. Biochem. Biophys. Methods*, 18 (1989) 209–220.
16 C. Frömmel, G. Hausdorf, W.E. Höhne, U. Behnke and H. Ruttloff, *Acta Biol. Med. Ger.*, 37 (1978) 1193–12022.
17 R. Kleine, U. Rothe, U. Kettmann and H. Schelle, in V. Turk and L. Vitale (Editors), *Proteinases and Their Inhibitors*, Pergamon Press, Oxford, 1981, pp. 201–211.
18 B. Ashbóth, Z. Majer and L. Polgár, *FEBS Lett.*, 233 (1988) 339–341.

Journal of Chromatography, 648 (1993) 101–109
Elsevier Science Publishers B.V., Amsterdam

CHROM. 25 285

Chromatographic investigation of the slowly interconverting atropisomers of hindered naphthamides

William H. Pirkle*, Christopher J. Welch☆ and Andrew J. Zych

School of Chemical Sciences, University of Illinois, Urbana, IL 61801 (USA)

(First received February 8th, 1993; revised manuscript received May 11th, 1993)

ABSTRACT

Chromatographic separation of the stereoisomers of a series of racemic N,N-disubstituted-2-methyl-1-naphthylenecarboxamide atropisomers using several recently developed chiral stationary phases is reported. Separation factors in excess of three are obtained in the best cases, allowing for convenient separation and investigation of the kinetics of stereoisomer interconversion. Examples of deracemization as well as an apparent cog wheel rotational process are also reported.

INTRODUCTION

The chromatographic separation of interconverting species has been a subject of considerable interest to chromatographers for quite some time. A theoretical treatment of the subject was given by Keller and Giddings in 1960 [1], with an expanded treatment provided by Horváth and co-workers in 1984 [2]. Just as nuclear magnetic resonance spectroscopy has proven useful in monitoring kinetic processes on the "NMR time scale", Mannschreck has illustrated the utility of HPLC in the study of kinetic processes occurring on the much slower "HPLC time scale" [3]. Mannschreck as well as others have reported on the liquid chromatographic separation of interconverting enantiomers, [4–9] while Schurig and co-workers have carried out similar studies using gas chromatography [10–12]. Recently, the liquid chromatographic separation of interconverting diastereomers containing proline residues has received considerable attention, [13–16] some of these compounds possessing significant activity as angiotensin converting enzyme (ACE) inhibitors.

The chromatographic separation of the enantiomers of compound **1a**, (Fig. 1) was described by Mannschreck and co-workers [4], who determined an energy barrier to enantiomer interconversion of 100.4 kJ/mol at 25.3°C in

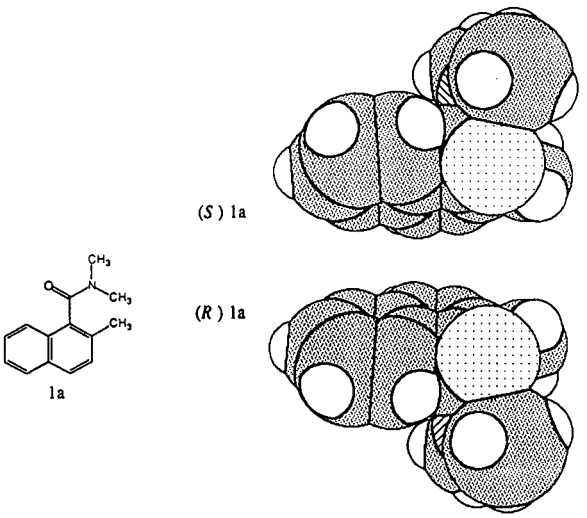

Fig. 1. Enantiomeric forms of compound **1a**.

* Corresponding author.
☆ Present address: Regis Chemical Company, 8210 Austin Avenue, Morton Grove, IL 60053, USA.

0021-9673/93/$06.00

dioxane, which corresponds to an interconversion half-life of about 6 h. The two enantiomeric forms of **1a** are chiral owing to restricted rotation about the $C_{(carbonyl)}-C_{(aryl)}$ bond. These molecules adopt a conformation in which the plane of the carboxamide system is approximately perpendicular to the plane of the aromatic system, the β-methyl group serving as a steric impediment to enantiomer interconversion.

Our interest in these amides initially stemmed from considerations of their chromatographic behavior on a type of chiral stationary phase (CSPs 4–6, Fig. 3) developed recently in our laboratory. We have advanced a model to account for the separation of the enantiomers of naproxen and related 2-aryl-propionic acids on these CSPs [17,18]. This model suggests that the enantiomers of **1a** and similar analytes might also be separated using this type of CSP. As with naproxen, compound **1a** also possesses an electron-rich conjugated π system with a proximate hydrogen bond acceptor situated out of the plane of the π system.

To test this hypothesis, compounds **1a–j** (Fig. 2) were prepared and their chromatographic properties were studied using a series of CSPs

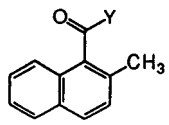

1

compound	Y	compound	Y
1a	N(Me)Me	1f	pyrrolidine
1b	N(Et)Et	1g	piperidine
1c	N(allyl)allyl	1h	hexamethyleneimine
1d	N(*n*-hexyl)*n*-hexyl	1i	morpholine
1e	N(*n*-octyl)*n*-octyl	1j	methyl N *n*-butyl

Fig. 2. N,N-2-methyl-1-naphthylenecarboxamide analytes.

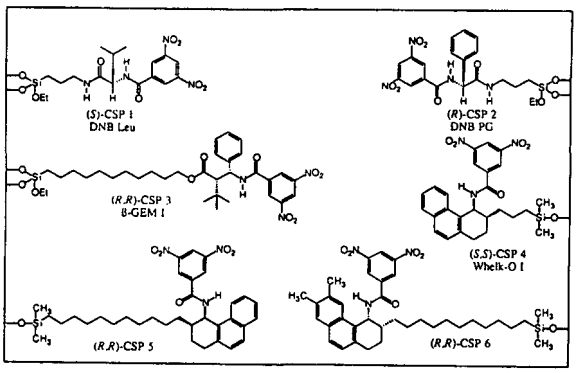

Fig. 3. π-Acidic CSPs used in the study.

(Fig. 3) developed in our laboratory. The commercial versions of CSPs 1–3 were used. The data reported for CSP 4 were collected using the prototype which, generally speaking, shows less enantioselectivity and efficiency than the newly developed "Whelk-O 1" commercial version (Regis).

MATERIALS AND METHODS

Apparatus

Chromatographic analysis was performed using a Rainin Rabbit HP solvent delivery system, a Rainin pressure monitor, a Rheodyne Model 7125 injector with a 20-μl sample loop, a Milton Roy UV monitor (254 nm) and an Altex C-R1A integrating recorder. Signs of optical rotation were determined using an Autopol III Automatic Polarimeter as an inline chromatography detector. ^{1}H NMR spectra were recorded on a Varian XL 200 FT NMR spectrometer.

Materials

All chemicals used were of reagent grade quality and were used without further purification. Chromatography solvents were EM Science HPLC grade. CSPs 1, 2, and 3 were obtained from Regis Chemical Company, Morton Grove, IL (USA). CSPs 4 and 5 were described previously [17,18]. CSP 6 will be described in a forthcoming publication.

Methods

All chromatographic experiments were conducted at a flow-rate of 2 ml/min at ambient

temperature. Column void time was determined by injection of tri-*tert.*-butyl benzene [19]. ^{1}H NMR chemical shifts are reported in ppm (δ) relative to tetramethylsilane.

Synthesis of analytes **1a–j** involved initial preparation of 2-methyl-1-naphthoyl chloride (method of Adams and Binder [20]), followed by reaction with the appropriate amine in a two-phase system consisting of dichloromethane and 1 *M* NaOH. Following an extractive workup and purification by flash chromatography on a silica support, compounds **1a–j** were all satisfactorily characterized by ^{1}H NMR.

RESULTS AND DISCUSSION

Data pertinent to the chromatographic separation of the enantiomers of analytes **1a–i** on CSPs 1–6 are shown in Table I. All of the π-acidic CSPs examined in the study provide some degree of separation for the enantiomers of at least some of analytes **1a–i**. The greatest separation factors (α's) are provided by CSPs 4 and 6, which also show the greatest enantioselectivity in the separation of naproxen enantiomers. The amino acid-derived CSPs 1 and 2 display but moderate enantioselectivities for these analytes, with the β-amino acid-derived CSP 3 [21] performing somewhat better. Retention, indicated by the capacity factor (k_1') for the first-eluted enantiomer, is greatest on CSPs containing aromatic substituents at the stereogenic center. This suggests that face-to-edge $\pi-\pi$ interaction, invoked to account for separation of the enantiomers of naproxen and related analytes on these CSPs, [17,18] may be important in the case of analytes **1a–i** as well.

The molecular interactions responsible for chiral recognition of analytes **1a–i** on the π-acidic CSPs 1–6 are believed to be similar to those proposed for the separation of naproxen enantiomers on these CSPs [17,18]. Fig. 4 depicts a schematic representation of what is believed to be the more stable diastereomeric adsorbate formed between the more strongly retained enantiomer of **1a** and each of the CSPs 1–4

For the DNB Leu CSP (CSP 1), access of analytes to the two faces of the planar π-acidic dinitrobenzamide ring system is presumed to be governed by the steric bulk of the isobutyl side chain. Approaching from the more sterically accessible side, the (*S*) enantiomer of compound **1a** can undergo simultaneous $\pi-\pi$ interaction and hydrogen bonding interactions with the CSP to a greater extent than can the (*R*) enantiomer (Fig. 4a).

A rationale based on steric approach might

TABLE I

CHROMATOGRAPHIC SEPARATION OF THE ENANTIOMERS OF ANALYTES **1a–i** USING CSPs 1–6

Conditions: mobile phase, 20% 2-propanol in hexane; flow-rate, 2.00 ml/min; temperature, ambient; void time determined by injection of tri-*tert.*-butylbenzene; k_1' = capacity factor for initially eluted enantiomer; α = separation factor.

Compound	CSP 1 DNB Leu		CSP 2 DNB PG		CSP 3 β-GEM I		CSP 4		CSP 5		CSP 6	
	k_1'	α	k_1'	α	k_1'	α	k_1'	α	k_1'	α	k_1'	α
1a	2.82	1.17	7.96	1.07	6.93	1.62	4.91	2.21	3.93	1.74	3.67	2.24
1b	1.80	1.11	4.47	1.08	4.57	1.68	3.29	2.46	2.53	1.91	2.42	2.34
1c	1.46	1.10	3.56	1.08	3.70	1.63	3.23	2.66	–	–	2.29	2.53
1d	0.98	1.00	1.90	1.09	2.82	1.93	2.05	3.00	1.40	2.31	1.46	2.86
1e	0.80	1.00	1.57	1.09	2.42	1.92	1.71	3.09	1.21	2.41	1.27	2.91
1f	3.35	1.00	7.56	1.10	7.18	1.68	5.11	2.04	3.78	1.61	3.94	2.01
1g	4.51	1.14	10.3	1.10	8.29	1.59	6.24	2.63	4.76	2.02	4.41	2.63
1h	3.46	1.09	6.34	1.00	6.12	1.47	4.46	2.08	3.36	1.65	3.30	2.08
1i	6.37	1.18	13.8	1.05	7.59	1.61	7.95	2.43	5.50	1.92	5.79	2.45

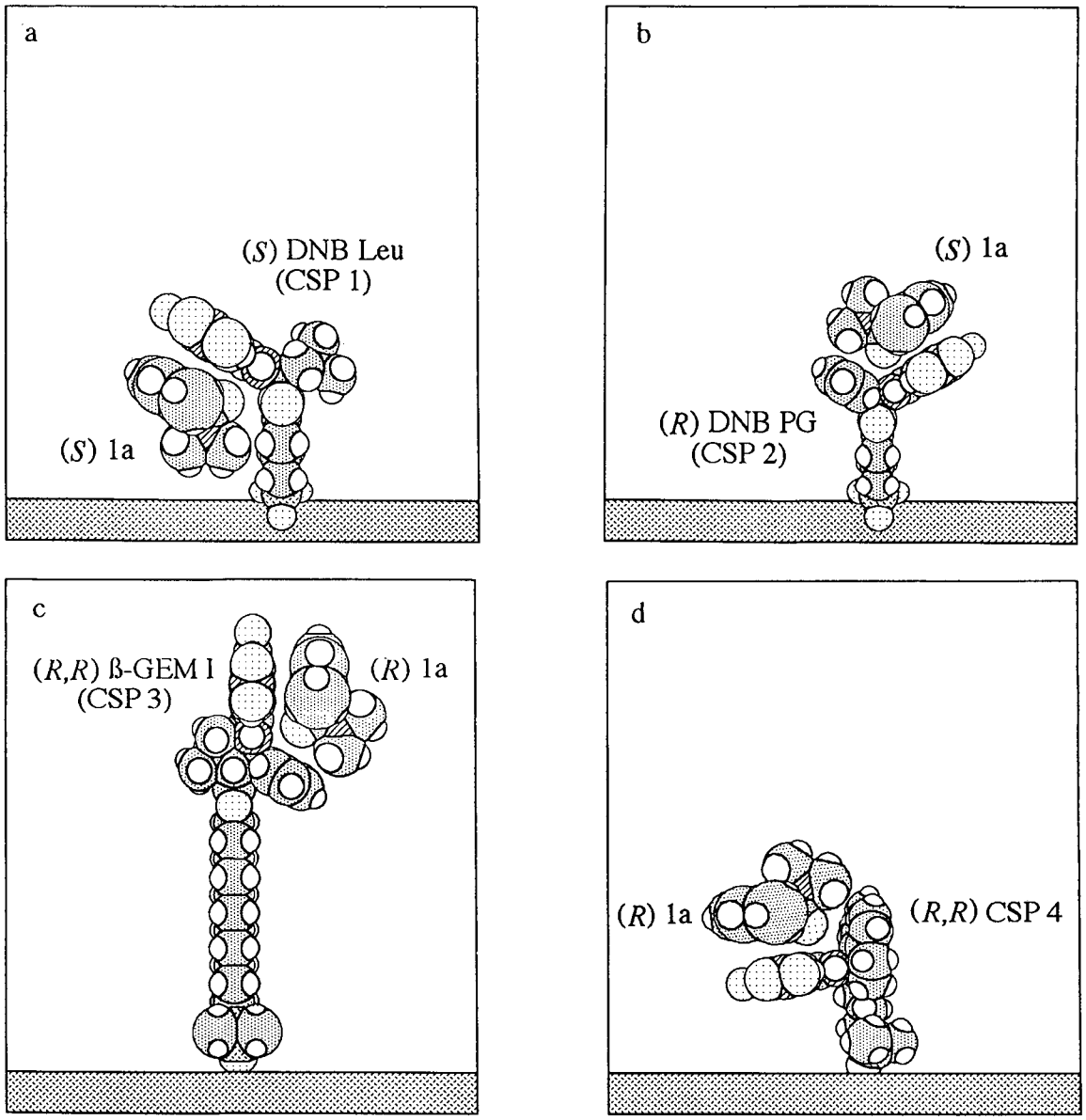

Fig. 4. Schematic representation of chiral recognition rationale for separation of the enantiomers of **1a** on several π-acidic CSPs.

lead one to predict preferential retention of the (*R*) enantiomer of **1a** by the (*R*)-DNB PG CSP (CSP 2), however, recent studies suggest that the phenyl ring at the stereogenic center of this CSP may be involved in beneficial face-to-edge $\pi-\pi$ interaction with analytes which approach the dinitrobenzamide system from the side of the phenyl substituent. To the extent that such face-to-edge $\pi-\pi$ complexation is important, retention of the (*S*) enantiomer of **1a** on the (*R*)-DNB PG CSP is expected (Fig. 4b).

The β-GEM I CSP (CSP 3) is similar to the DNB PG CSP in that it also bears an aromatic substituent at the stereogenic center. Furthermore, this β-amino acid-derived CSP 3 contains a second stereogenic center bearing a *tert.*-butyl substituent which may be useful in restricting access to the face of the dinitrobenzamide system

opposite the phenyl substituent. The (*R*)-β-GEM I CSP is therefore expected to selectively retain the (*R*) enantiomer of **1a**, which can more readily approach from the side of the phenyl substituent (Fig 4c). It should be pointed out that while the "shapes" of CSPs 2 and 3 appear to be effectively "enantiomeric" in Fig. 4, a priority inversion in the Cahn, Ingold, Prelog stereochemistry nomenclature system [22] assigns an (*R*) absolute configuration to CSP 2 and an (*R*,*R*) absolute configuration to CSP 3.

CSP 4 and the closely related CSPs 5 and 6 (Fig. 3) were designed specifically to better utilize the face-to-edge $\pi-\pi$ interactions which are believed to be important in the DNB PG and β GEM I CSPs. These CSPs contain an aromatic substituent at the stereogenic center which is held in a conformation favorable for simultaneous face-to-face and face-to-edge $\pi-\pi$ interactions with the analyte. In addition, the tether connecting the selector to the silica support may serve to restrict access to the "undesired" face of the dinitrobenzamide system. (*S*,*S*) CSP 4 is thus expected to selectively retain the (*S*) enantiomer of **1a** (Fig. 4d).

The sign of the optical rotation at 589 nm was determined for each enantiomer using a polarimetric detector. Table II shows the sign of rotation for the more retained enantiomer of analyte **1a** on each of the CSPs used in the study as well as the absolute configuration assigned to the more retained enantiomer using the model illustrated in Fig. 4. All of the models proposed to account for enantioselective recognition of **1a** by the various CSPs assign the (*S*) absolute configuration to the levorotatory enantiomer and the (*R*) absolute configuration to the dextrorotatory enantiomer. Moreover, the circular dichroism spectra of the enantiomers of **1a** are similar to those of the configurationally related enantiomers of several alkyl 2-methyl-naphthyl ketones [23].

TABLE II

ELUTION ORDERS FOR COMPOUND **1a** ON CSPs 1–6

Column	Rotation [a]	Assigned [b]
(*S*)-CSP 1	(−)	(*S*)
(*R*)-CSP 2	(−)	(*S*)
(*R*,*R*)-CSP 3	(+)	(*R*)
(*S*,*S*)-CSP 4	(−)	(*S*)
(*R*,*R*)-CSP 5	(+)	(*R*)
(*R*,*R*)-CSP 6	(+)	(*R*)

[a] Sign of rotation of the more retained enantiomer of analyte **1a**.

[b] Absolute configuration of the more retained enantiomer of analyte **1a** based upon the model illustrated in Fig. 4.

Interconverting enantiomers offer some interesting possibilities in chiral recognition and separation studies. In one study, the enantiomers of analyte **1a** were preparatively resolved using an analytical size (25 cm × 4.6 mm I.D.) β-GEM I column (CSP 3). The reversion of a single enantiomer of **1a** to the racemate was monitored, and the rate of enantiomerization was determined to be in 0.023/h ($t_{1/2}$, 15.1 h; solvent, 20% 2-propanol in hexane; temperature, 25°C), a finding which is close to the value of 0.058/h determined for this compound by Mannschreck at 25.3°C in dioxane [4].

When one enantiomer of a racemic solution is preferentially adsorbed by a CSP, an excess of the opposite enantiomer exists in solution. When a pathway for enantiomer interconversion is introduced, this solution excess will become "racemized" leading to a net enrichment in the more retained enantiomer. In a study of the deracemization of **1a**, a racemic solution was pumped onto a β-GEM I column using 20% 2-propanol in hexane as a mobile phase. The column was then removed from the HPLC system, column end plugs were inserted, and the column was allowed to stand at room temperature of a period of one week. The column was then eluted with 5% methanol in dichloromethane, the effluent showing an enrichment in the more strongly retained enantiomer. Analogous solution studies using the soluble β-GEM I selector result in enrichment of the more strongly complexed enantiomer. The extent of enrichment increases when larger ratios of chiral selector to analyte are used, the limiting enantiomeric ratio (1.68:1) approximating the separation factor obtained when the racemate is chromatographed on the β-GEM I CSP ($\alpha = 1.62$). This kind of experiment finds a close analogy in earlier studies of the deracemization of a π-

acidic analyte in the presence of a chiral π-basic selector [24].

When amide **1j** is chromatographed on CSP 4, four stereoisomers are found to be present. This indicates that rotation about the $C_{(carbonyl)}$–$N_{(amide)}$ bond as well as the $C_{(aryl)}$–$C_{(carbonyl)}$ bond is slow on the HPLC time scale (Fig. 5).

The *E* and *Z* amide rotamers of **1j** were separated by chromatography on silica gel. Fig. 6 shows ^{1}H NMR spectra of the mixture of diastereomers (i), and the high (ii) and low (iii) R_F bands obtained from separation by preparative

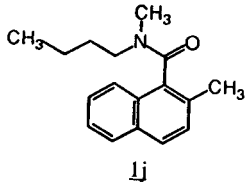

1j

Fig. 5. Chromatographic separation of the stereoisomers of **1j**. Conditions: CSP, (*R*,*R*)-CSP 4; mobile phase, 20% 2-propanol in hexane: flow-rate, 2.0 ml/min; ambient temperature.

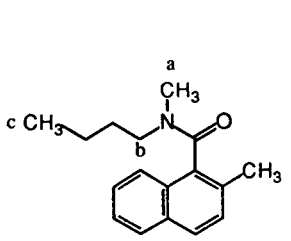

E diastereomer

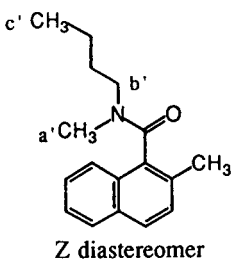

Z diastereomer

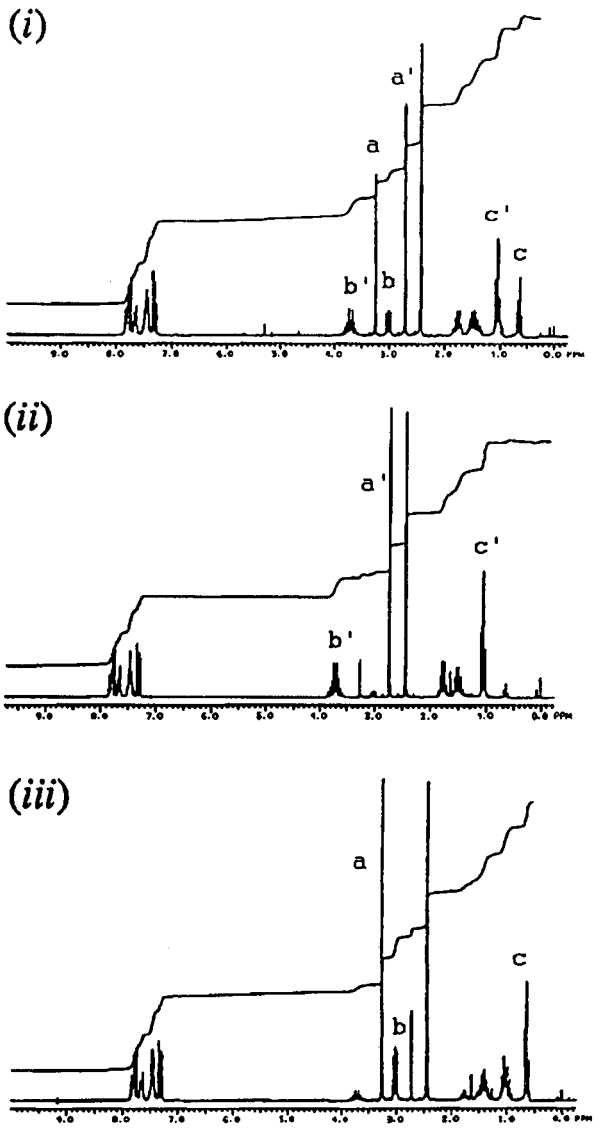

Fig. 6. 200 MHz ^{1}H NMR spectra (C^2HCl_3) of: (i) mixture of *E* and *Z* diastereomers before chromatographic fractionation; (ii) high R_F band from preparative TLC separation, assigned as *Z* rotamer; (iii) low R_F band from preparative TLC separation, assigned as *E* rotamer.

TLC (2% methanol in dichloromethane). Analysis of molecular models suggests that it is the *Z* amide rotamer which should have the signal for the amide methyl group (protons a′) in the furthest upfield position, this group being strongly shielded by the naphthyl ring. The corresponding methyl group of the *E* rotamer (protons a) is positioned close to the lone pair of the carbonyl oxygen and would accordingly be expected to occur at a relatively downfield position. Similarly the signal from the α-methylene protons of the *E* rotamer (protons b) are found upfield of the corresponding signals in the *Z* rotamer (protons b′).

Based on these arguments, the high R_F band from the preparative TLC separation contains the *Z* rotamer, while the low R_F band contains the *E* rotamer. Interestingly, even the butyl C-methyls (protons c, c′) show chemical shift differences which are consistent with this assignment, the *E* rotamer methyl resonance (proton c) occurring at the more upfield position.

Fig. 7 depicts chromatograms obtained when the two fractions from the preparative TLC separation were evaluated on (*R*,*R*) CSP 4. The stereoisomers giving rise to the first and third peaks are assigned as the enantiomers of the *Z* diastereomer, whereas those giving rise to the second and fourth peaks are assigned as arising from the *E* diastereomer. Based upon the model depicted in Fig. 4d, the four stereoisomers resolved upon (*R*,*R*) CSP 4 are assigned, in the order of their elution, as: *Z*-(*R*); *E*-(*R*); *Z*-(*S*); *E*-(*S*).

Preparative separation of a sample of **1j** on (*R*,*R*) CSP 4 afforded a sample which was highly enriched in the *Z*-(*R*) isomer. The equilibration of this enriched sample to the racemic mixture of diastereomers was monitored to determine interconversion rates for the C–N and C–C bond rotations. A schematic diagram of the possibilities for interconversion of the four species is shown in Fig. 8. Conversion of the *Z*-(*R*) to the *E*-(*R*) isomer is an amide bond rotation process which requires a single $C_{(carbonyl)}$–$N_{(amide)}$ bond rotation. Conversion of the *Z*-(*R*) to the *Z*-(*S*) isomer is an enantiomer interconversion process and requires a single $C_{(aryl)}$–$C_{(carbonyl)}$ bond rotation. Conversion of the *Z*-(*R*) to the *E*-(*S*)

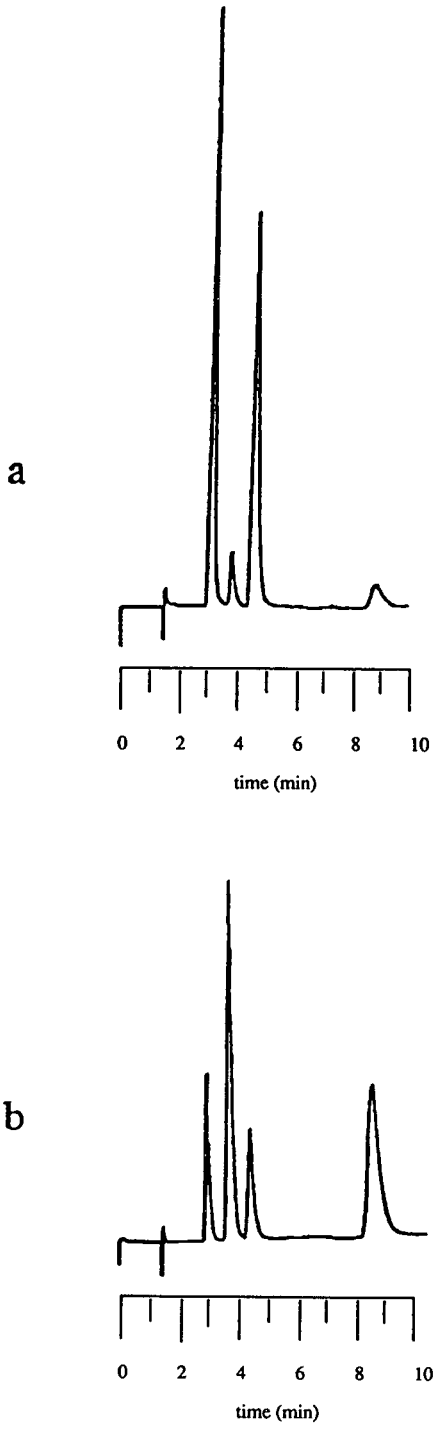

Fig. 7. Chromatographic separation of the enantiomers of the preparatively separated diastereomers of **1j**. (a) High R_F fraction; (b) low R_F fraction. Conditions: CSP, (*R*,*R*)-CSP 4; mobile phase, 20% 2-propanol in hexane; flow-rate, 2.0 ml/min; ambient temperature.

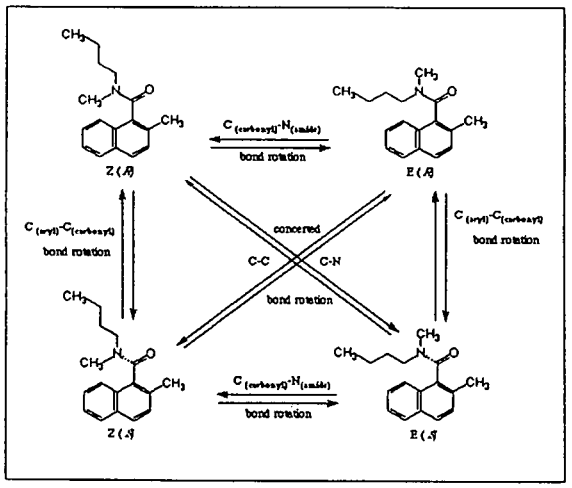

Fig. 8. Schematic representation of the interconversion of the four stereoisomers of analyte **1j**.

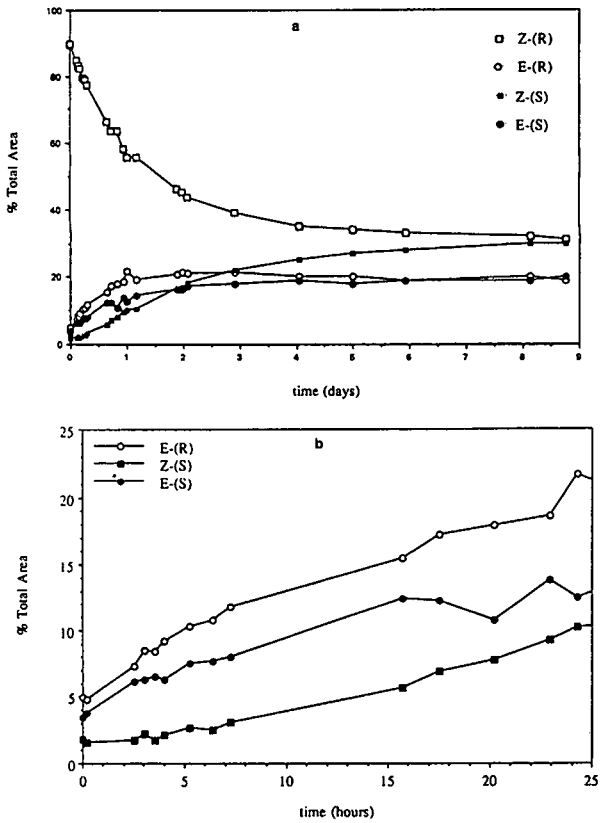

Fig. 9. (a) Time course for the equilibration at room temperature in 20% 2-propanol in hexane of the preparatively enriched *Z*-(*R*) isomer with the other stereoisomers of **1j** to afford a racemic mixture of diastereomers. (b) Expanded view of initial data showing the unexpectedly rapid formation of the *E*-(*S*) isomer.

isomer requires both a $C_{(carbonyl)}$–$N_{(amide)}$ bond rotation and a $C_{(aryl)}$–$C_{(carbonyl)}$ bond rotation. We therefore expected to see the formation of the *E*-(*S*) isomer only after significant amounts of the *E*-(*R*) and *Z*-(*S*) isomers had been formed.

Fig. 9 shows the results of this study in which the equilibration of the *Z*-(*R*) isomer to afford a racemic mixture of diastereomers was monitored by HPLC. Interestingly, the rate of $C_{(carbonyl)}$–$N_{(amide)}$ rotation is seen to be quite slow, on an order with the $C_{(aryl)}$–$C_{(carbonyl)}$ bond rotation rate, as evidenced by the rate of appearance of the *E*-(*R*) isomer. Quite unexpectedly, the rate of formation of the *E*-(*S*) isomer is even greater than the rate of formation of the *Z*-(*S*) isomer. This result can only be explained by the contribution of a concerted $C_{(carbonyl)}$–$N_{(amide)}$ and $C_{(aryl)}$–$C_{(carbonyl)}$ bond rotation, represented by the diagonals in Fig. 8. This situation, reminiscent of "dynamic gearing" described by Mislow and others [25], will be the subject of future studies.

CONCLUSION

The enantiomers of a number of axially chiral aromatic carboxamide analytes are conveniently separated using several π-acidic chiral stationary phases, the recently described CSP IV affording the better separations. Rationales accounting for the observed enantiomer separations on all of the CSPs used in the study have been advanced. Signs of optical rotation for the retained enantiomers on all of these CSPs are consistent with the proposed models, and absolute configuration of the enantiomers of these analytes have been tentatively assigned on this basis. The use of these CSPs to monitor rates of stereoisomer interconversion and to afford deracemization have been demonstrated. Amide **1j** has been shown to exist as a mixture of four slowly interconverting stereoisomers, all separable by HPLC. The rate at which the *Z*-(*R*) form equilibrates with other rotameric forms was followed, the data suggesting that concerted $C_{(aryl)}$–$C_{(carbonyl)}$ and $C_{(carbonyl)}$–$N_{(amide)}$ bond rotations may be important in the interconversion of the rotamers of hindered naphthamides.

ACKNOWLEDGEMENTS

This work was supported by funds from the National Science Foundation and a gift of HPLC solvents from E.M. Science. CJW was supported by a Department of Education Advanced Opportunities in Chemistry Graduate Fellowship.

REFERENCES

1 R.A. Keller and J.C. Giddings, *J. Chromatogr.*, 3 (1960) 205.
2 W.R. Melander, H.J. Lin, J. Jacobson and Cs. Horváth, *J. Phys. Chem.*, 88 (1984) 4527.
3 A. Mannschreck, H. Zinner and N. Pustet, *Chimia*, 43 (1989) 165.
4 M.A. Cuyegkeng and A. Mannschreck, *Chem. Ber.*, 120 (1987) 803.
5 A. Mannschreck and L. Kießl, *Chromatographia*, 28 (1989) 263.
6 A. Mannschreck, E. Hartmann, H. Buchner and D. Andert, *Tetrahedron. Lett.*, 28 (1987) 3479.
7 M. Pütmann, F. Oesch, L.W. Robertson and A. Mannschreck, *Chemosphere*, 15 (1986) 2061.
8 J. Vorkapi-Furac, M. Mintas, T. Burgemeister and A. Mannschreck, *J. Chem. Soc., Perkin Trans. II*, (1989) 713.
9 J. Veciana and M.I. Crespo, *Angew. Chem. Int. Ed. Engl.*, 30 (1991) 74.
10 V. Schurig, W. Bürkle, A. Zlatkis and C.F. Poole, *Naturwissenschaften*, 66 (1979) 423.
11 V. Schurig and W. Bürkle, *J. Am. Chem. Soc.*, 104 (1982) 7573.
12 W. Bürkle, H. Karfunkel and V. Schurig, *J. Chromatogr.*, 288 (1984) 1.
13 J. Jacobson, W. Melander, G. Vaisnys and Cs. Horváth, *J. Phys. Chem.*, 88 (1984) 4536.
14 R. Hanai and A. Wada, *J. Chromatogr.*, 394 (1987) 273.
15 S. Gustafsson, B.M. Eriksson and I. Nilsson, *J. Chromatogr.*, 506 (1990) 75.
16 T.V. Alfredson, *J. Chromatogr.*, 507 (1990) 277.
17 W.H. Pirkle, C.J. Welch and B. Lamm, *J. Org. Chem.*, 57 (1992) 3854.
18 W.H. Pirkle and C.J. Welch, *J. Liq. Chromatogr.*, 15 (1992) 1947.
19 W.H. Pirkle and C.J. Welch, *J. Liq. Chromatogr.*, 14 (1991) 1.
20 R. Adams and L.O. Binder, *J. Am. Chem. Soc.*, 63 (1941) 2773.
21 W.H. Pirkle and J.E. McCune, *J. Chromatogr.*, 441 (1988) 311.
22 R.S. Cahn, C. Ingold and V. Prelog, *Angew. Chem. Int. Ed. Engl.*, 5 (1966) 385.
23 D. Casarini, L. Lunazzi, F. Pasquali, F. Gasparrini and C. Villani, *J. Am. Chem. Soc.*, 114 (1992) 6521.
24 W.H. Pirkle and D.S. Reno, *J. Am. Chem. Soc.*, 109 (1987) 7189.
25 H. Iwamura and K. Mislow, *Acc. Chem. Res.*, 21 (1988) 175.

Journal of Chromatography, 648 (1993) 111–118
Elsevier Science Publishers B.V., Amsterdam

CHROM. 25 272

Determination of malonaldehyde by coupled high-performance liquid chromatography–spectrofluorimetry after derivatization with luminarin 3

Falaye Traoré*, Robert Farinotti and Georges Mahuzier

Laboratoire de Chimie Analytique II, Méthodologie Bioanalytique, Faculté des Sciences Pharmaceutiques et Biologiques de l'Université Paris-Sud, 5 rue Jean-Baptiste Clément, 92290 Chatenay-Malabry (France)

(First received December 14th, 1992; revised manuscript received May 6th, 1993)

ABSTRACT

A high-performance liquid chromatographic method with fluorescence detection is described for the specific determination of free malonaldehyde (MDA). Malonaldehyde was labelled with luminarin 3 in acetate buffer (pH 4.0) at room temperature in the dark. An aliquot of the reaction mixture was injected on to an octadecyl-bonded column using acetonitrile–imidazole buffer (30:70, v/v) as the mobile phase. The eluate was monitored with a fluorescence detector at 395 nm (excitation) and 500 nm (emission). A linear calibration graph was established between 7.2 and 90 ng/ml of MDA and the limit of quantification (LOQ) was lower than 7 ng/ml of MDA. The precision was characterized by R.S.D.s of 11% at 7.2 ng/ml and 2% at 90 ng/ml. The structure of the derivative was confirmed as the 5-hydroxy-2-pyrazoline form. UV absorbance and corrected fluorescence spectral data and quantum yields of the luminarin 3 derivative of malonaldehyde are presented.

INTRODUCTION

Several methods have been developed to determine the amount of malonaldehyde (MDA) formed by lipid peroxidation either *in vivo* or *in vitro*. The most common method MDA is based on spectrophotometric or spectrofluorimetric measurement of the condensation product formed from MDA and 2-thiobarbituric acid (4,6-dihydroxy-2-thiopyrimidine) (TBA) [1,2]. This method is not specific for MDA and often overestimates MDA levels [2–10]. Some workers have proposed more selective methods based on the chromatographic separation of MDA: in its free form [3,4]; derivatized with TBA [5,11,12] or its derivatives such as 1,3-diethyl- [6,7] or 1,3-dimethyl-, 1-methyl-, 1,3-diphenyl- and 1-phenyl-TBA [6]; derivatized with dansylhydrazine (DNSH) [8], 2-hydrazinobenzothiazole (HBT) [9], 2,4-dinitrophenylhydrazine (DNPH) [13–15], pentafluorophenylhydrazine (PFPH) [16], *p*-nitrophenylhydrazine (NPH) [17] or N-methylhydrazine (NMH) [18]; and based on the formation of a fluorescent compound derived from 1,4-dihydropyridine 3,5-dicarbaldehydes, produced by a condensation reaction of malonaldehyde, aliphatic amines and aliphatic aldehydes in neutral medium (Hantzsch reaction) [10].

Reactions of MDA with TBA, DNSH, HBT or DNPH require hot and or acidic conditions. A major drawback of these methods from a biochemical point of view is the artifactual generation of MDA from the biological materials that can be induced under the strongly acidic conditions and elevated temperatures required for the formation of the derivatives. It is therefore

* Corresponding author.

0021-9673/93/$06.00

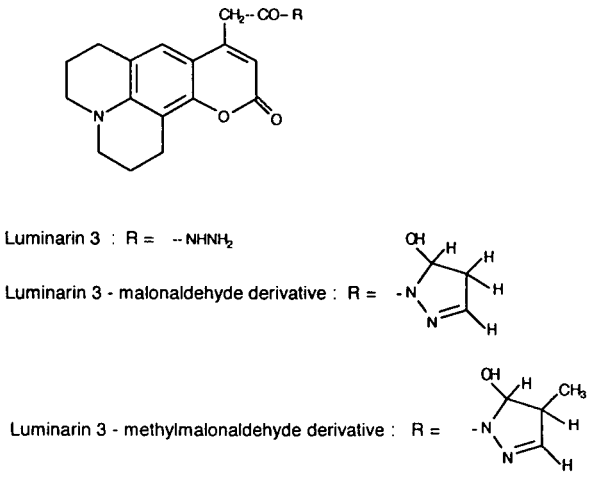

Fig. 1. Structures of luminarin 3 and its derivatives.

uncertain what proportion of the determined MDA was originally present in the sample in the free state and what proportion might have been bound or generated from precursors. Therefore, mild derivatization conditions are required for the reliable determination of free MDA.

We used the derivatizing agent luminarin 3 (Fig. 1) for the determination of low concentrations of MDA under mild conditions. Owing to its quinolizinocoumarin nucleus, luminarin 3 is a useful fluorescent and chemiluminescent label [19–21], and its hydrazine group reacts easily with carbonyl compounds, permitting the derivatization of MDA at room temperature in acetate buffer (pH 4.0).

As chemiluminescence detection requires a postcolumn reaction system with one or two additional pumps, fluorescence detection was preferred. This method is sensitive and specific for the determination of free MDA.

EXPERIMENTAL

Reagents

All reagents and solvents were of analytical-reagent grade. Luminarin 3 and 2-methyl-1,1,3,3-tetraethoxypropane (MeTEP) were obtained from Eurobio-Seratec (Les Ulis, France) and 1,1,3,3-tetraethoxypropane (TEP), imidazole and 2,4-pentanedione (acetylacetone) from Aldrich-Chemie (Steinheim, Germany). Quinine sulphate and silica gel (0.04–0.063 mm) were purchased from Merck (Darmstadt, Germany).

Standard malonaldehyde solution

A stock standard solution of MDA was prepared by acidic hydrolysis of TEP, assuming 100% conversion of TEP into MDA [15]. A 0.245-ml volume of TEP was placed into a brown 100-ml graduated flask, diluted to volume with 1% (w/v) sulphuric acid, mixed thoroughly and kept in the dark at room temperature for 2 h. This solution contains 10 m*M* MDA and can be stored at −20°C for several months. It was used to prepare a calibration graph in the range 7.2–90 ng/ml after dilution with 100 m*M* acetate buffer (pH 4.0). The calibration graph was constructed by plotting the peak-height ratio of the luminarin 3 derivative of MDA to standard luminarin 3–methylmalonaldehyde against MDA concentration.

The absorbance of 100 μM MDA solution in 1% sulphuric acid at λ_{max} (245 nm) was measured to verify the molar absorption coefficient and hence the purity of the solution.

Standard luminarin 3 solution

A 10 m*M* solution of luminarin 3 in dimethyl sulphoxide (DMSO) was prepared. This solution can be stored for several months at −20°C.

Standard luminarin 3–malonaldehyde solution

A standard solution of luminarin 3–malonaldehyde (L3–MDA) was obtained from the reaction of MDA and luminarin 3. When incubated at room temperature and stirred for 30 min, the reaction mixture was composed of 100 ml of a standard solution of MDA (72 mg, 1 mmol) and 10 ml of 100 m*M* luminarin 3 solution in DMSO (313 mg, 1 mmol). Sodium hydrogencarbonate (2.5 g) was added and the mixture was stirred gently until the acid had been neutralized (pH 7.0). The mixture was then extracted with 200 ml of dichloromethane. The extract was dried with anhydrous magnesium sulphate, filtered and evaporated to dryness under vacuum.

The residue was dissolved in 5 ml of dichloro-

methane and purified chromatographically on silica gel 60 (0.04–0.063 mm) using an elution gradient of 0 to 40% tetrahydrofuran in dichloromethane. The eluate was evaporated under vacuum and the residue was dried in a desiccator to give a yellow powder, yield 72.3%. Elemental analysis: calculated for $C_{20}H_{21}N_3O_4$, C 65.40, H 5.72, N 11.44; found, C 65.41, H 5.81, N 11.40%.

The structure of L3–MDA was also confirmed by ^1H and ^{13}C NMR spectroscopy (data not shown). The electron impact mass spectrum was characterized by ions at *m/z* (relative abundance, %) 367 (19.09), 349 (5.54), 282 (8.77), 281 (8.72), 256 (9.02), 255 (48.96), 254 (20.53), 227 (10.87), 226 (17.13), 68 (100.00), 67 (13.05) and 44 (34.98).

L3–MDA was prepared as a 10 m*M* solution in DMSO. This solution can be stored for several months at −20°C.

Standard solution of luminarin 3–methylmalonaldehyde (internal standard)

Luminarin 3–methylmalonaldehyde (L3–MeMDA) was synthesized as described above from MeMDA prepared by hydrolysis of 2-methyl-1,1,3,3-tetraethoxypropane in 1% sulphuric acid for 2 h at room temperature.

L3–MeMDA was obtained in the form of yellowish brown needles, yield 53%. Elemental analysis: calculated for $C_{21}H_{23}N_3O_4$, C 66.14, H 6.04, N 11.02; found, C 66.06, H 6.18, N 10.97%.

The structure of this compound was confirmed by ^1H and ^{13}C NMR spectroscopy (data not shown) and its electron impact mass spectrum was characterized by ions at *m/z* (relative abundance, %) 381 (29.74), 363 (11.42), 282 (17.49), 281 (20.52), 256 (11.75), 255 (65.34), 254 (28.84), 227 (14.42), 226 (23.09), 82 (85.99), 81 (100.00), 57 (26.76), 56 (5.99), 55 (17.25), 54 (36.92), 44 (30.62) and 43 (12.02).

A 17 μM solution of L3–MeMDA was prepared: 38.1 mg of L3–MeMDA were placed in a test-tube and 4 ml of DMSO were added to obtain a 25 m*M* stock solution. This solution was diluted with the same solvent to obtain the desired concentration.

10 mM imidazole buffer solution (pH 7.0)

The pH of the solution was adjusted with concentrated nitric acid.

Acidified acetylacetone solution

A 1 *M* solution of acetylacetone in 1% sulphuric acid was prepared extemporaneously.

Apparatus

High-performance liquid chromatographic (HPLC) analysis was performed with a Chromatem 380 pump (Touzart-Matignon, Vitry sur Seine, France), equipped with a Rheodyne (Cotati, CA, USA) Model 7125 injector with a 20-μl sample loop and a Waters (Milford, MA, USA) Model 420-C fluorescence HPLC monitor. The data were processed in a Shimadzu C-R5A integrator (Touzart et Matignon). For the verification of the purity of L3–MDA and L3–MeMDA standards, a Shimadzu SPD-6A UV detector was connected to the outlet of fluorescence detector. The signal from each detector was recorded on a double-trace integrator. Corrected fluorescence and absorbance spectra were measured with a Perkin-Elmer (St. Quentin en Yvelines, France) Model LS 50 luminescence spectrometer and a Shimadzu Model UV-2100 UV–Vis recording spectrophotometer (Touzart et Matignon), respectively, in 1-cm quartz cells. Spectral band widths of 5 and 10 nm were used for the excitation and emission monochromators, respectively. Electron impact and chemical ionization mass spectra were measured on a Nermag R-1010-C mass spectrometer (Delsi-Nermag, Argenteuil, France). ^1H and ^{13}C NMR spectra were recorded on a Bruker (Bruker, Wissous, France) AC 200-MHz NMR spectrometer using [$^2H_6$]dimethyl sulphoxide as solvent and tetramethylsilane (TMS) as reference.

Chromatographic conditions

Chromatographic separation was performed using a 5-μm Nucleosil C_{18} column (150 × 4.6 mm I.D.) (Beckman, Les Ulis, France). The mobile phase was an isocratic mixture of acetonitrile and 10 m*M* imidazole buffer (pH 7.0) (30:70, v/v) at a flow-rate of 1.5 ml/min at room temperature. Filters of 395 and 500 nm were used for excitation and emission, respectively.

The absence of coumarinic contaminants in L3–MDA and L3–MeMDA standards was checked by means of liquid chromatography with fluorescence and UV detection on a 5-μm Nucleosil silica column (250 × 4.6 mm I.D.) (Interchim, Montluçon, France) using ethyl acetate–diisopropyl ether (90:10, v/v) as the mobile phase at a flow-rate of 1.5 ml/min. The UV detector wavelength was set at 360 nm; 360- and 440-nm filters were used for excitation and emission, respectively, in fluorimetric detection.

Fluorescence and absorbance measurements

Fluorescence quantum yields were determined with reference to quinine hydrogen sulphate in 0.05 *M* sulphuric acid, according to Parker and Rees [22]. Quantum yields were measured at room temperature without deoxygenation. The intrinsic fluorescence sensitivity was expressed by the equation $IFS = \phi\varepsilon/H$, where ϕ is the quantum yield, H is the half band width (cm^{-1}) and ε is the molar absorptivity ($l\ mol^{-1}\ cm^{-1}$) [23].

Derivatization procedure

A 200-μl volume of 100 m*M* acetate buffer solution (pH 4.0) containing malonaldehyde was mixed with 10 μl of 10 m*M* luminarin 3 solution and 10 μl of 17 μ*M* L3–MeMDA (internal standard) in a glass test-tube. The mixture was protected from light and kept at room temperature for 30 min for the optimum formation of the luminarin 3–MDA derivative. Then 10 μl of acidified 1 *M* acetylacetone solution were added to the mixture to react with excess reagent. After 5 min, an aliquot of the reaction mixture was injected on to the HPLC column.

RESULTS AND DISCUSSION

Condensation of luminarin 3 with malonaldehyde and methylmalonaldehyde. Characterization of the derivatives

The condensation reaction of luminarin 3 with dicarbonyl compounds may involve one or two luminarin 3 molecules. When one molecule is involved, a ring formation reaction may take place, producing a pyrazole or 5-hydroxy-2-pyrazoline derivative.

MDA and MeMDA react with luminarin 3, a nucleophilic reagent, in acidic medium to form the derivatives shown in Fig. 1. The identity and purity of the luminarin 3 derivatives of malonaldehyde and methylmalonaldehyde were confirmed by elemental analysis, mass spectrometry (MS), ^{1}H and ^{13}C NMR spectroscopy and HPLC analysis. The results demonstrated that the condensation reaction between luminarin 3, MDA and MeMDA is equimolar and that 5-hydroxy-2-pyrazoline derivatives are formed.

The purity of the L3–MDA and L3–MeMDA standards was determined to be >99% by HPLC on Nucleosil silica (normal-phase) and Nucleosil ODS (reversed-phase) columns with both UV and fluorescence detection. The luminarin 3 derivative of MDA showed a single peak in both chromatographic systems. The luminarin 3 derivative of MeMDA showed two peaks in normal-phase chromatography. However, when a reversed-phase system with acetonitrile was used, only a single peak was obtained. These two peaks were confirmed to be the *threo* (70%) and *erythro* (30%) isomers by NMR spectroscopy.

The electronic impact mass spectra of L3–MDA and L3–MeMDA show fragmentation patterns consistent with the proposed structures. The evidence for the 5-hydroxy-2-pyrazoline form was that L3–MDA and L3–MeMDA showed a parent ion at m/z 367 and 381, respectively, with additional ions at m/z 349 and 363, respectively, corresponding to $[M-18]^{+\bullet}$. These ions result from the loss of hydroxyl and hydrogen from the 5- and 4-positions of the pyrazoline ring, respectively. The most abundant ions were at m/z 68 and 81, respectively. These ions correspond to the loss of a pyrazole ring, which appears, with the gain of a hydrogen atom and itself, respectively, from ions at m/z $[M-18]^{+\bullet}$. The remainder of the molecule appears in the form of carboxyl fragments (at m/z 282 or 281) which lose CO to give the fragment at m/z 255. This latter species fragments further, by the ejection of CO from the lactone ring and a hydrogen atom, to give the fragment at m/z 226.

Choice of optimum conditions for derivatization

The reaction of MDA ($pK = 4.46$) with luminarin 3 proceeded at room temperature under weakly acidic conditions (pH 4.0). In

order to confirm that the present procedure is specific for free MDA, 100 μM of TEP, a precursor of MDA, was treated at pH 1.0, 2.0, 3.0, 4.0, 5.0 and 6.0 and at temperatures of 25 and 50°C. The amount of MDA formed was determined from the absorbance at 245 nm. This study showed (Fig. 2) that the best yields for conversion of TEP to MDA were obtained by incubation at 50°C. At pH 1.0, whatever the temperature, we observed 100% transformation of TEP into MDA. At pH 3.0, 60% of MDA was formed at 50°C in 60 min, whereas at 25°C and pH 3.0 or 4.0 no MDA was formed after 120 min. This phenomenon has been observed previously by Kawai *et al.* [17]. These results demonstrate that the present procedure is specific for free (genuine) MDA.

The procedure reported in a previous paper [19] required strongly acidic conditions (0.1 M H_2SO_4) for the formation of luminarin 3 derivatives. Under these conditions MDA precursors are hydrolysed to give MDA. Accordingly, the determination of free MDA and that generated from its precursors could be obtained from the difference between MDA levels prior to and after acid hydrolysis.

Concerning the derivatization of MDA by luminarin 3, the influence of the reaction time and luminarin 3 concentration on the peak-height ratio of L3–MDA to L3–MeMDA was also studied. The peak-height ratios were almost constant after about 30 min and over the range of luminarin 3 concentrations investigated (0.05–0.5 μmol). The other important factor for analytical application is the thermal stability of the luminarin 3–MDA derivative. To prevent degradation of the product, the reaction temperature should not exceed room temperature (25°C) [19]. Under these conditions the luminarin 3–MDA derivative was stable for at least 24 h. These experiments indicated that the optimum conditions were those used in the derivatization procedure described above.

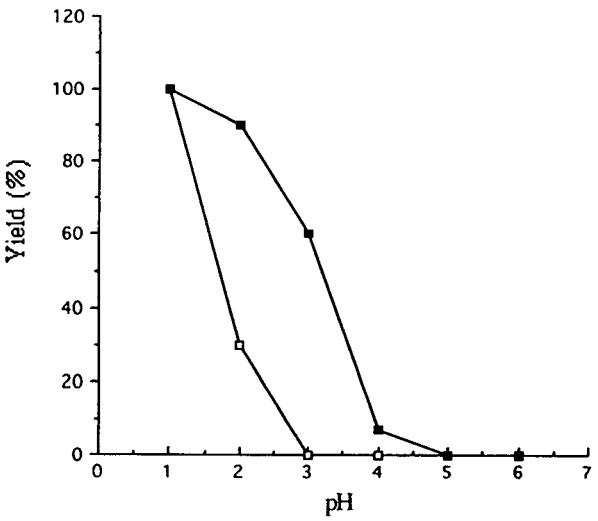

Fig. 2. Effect of pH on hydrolysis of TEP (0.1 μmol/ml), (□) at 25°C for 120 min and (■) at 50°C for 60 min. Formation of MDA was determined by UV spectrophotometry at 245 nm.

Liquid chromatography

The selected chromatographic conditions were used to separate luminarin 3 from its derivatives with MDA, MeMDA and acetylacetone. The mobile phase components, acetonitrile and imidazole buffer, were chosen for their ability to

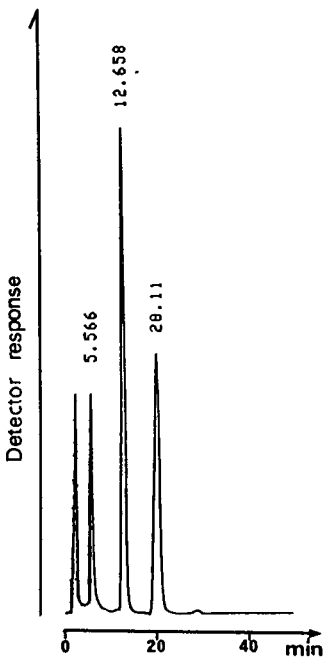

Fig. 3. Elution profile of a mixture of standard solutions of luminarin 3 (at 5.6 min) and luminarin 3 derivatives of MDA (at 12.7 min) and MeMDA (at 20.1 min) in reaction mixture (8 mV full-scale). A 15-pmol amount of each derivative was injected on to the column. For other details, see text.

promote peroxyoxalate chemiluminescence detection as reported by Tod and co-workers [20,21] for other luminarin derivatives. Fig. 3 shows typical chromatograms of a mixture of standard solutions of luminarin 3, luminarin 3–MDA and MeMDA derivatives. Their retention times were 5.6, 12.5 and 20.1 min, respectively. The luminarin 3–MDA derivative was well separated from the reagent and internal standard. For this separation of pure standards, the limit of detection was evaluated as the concentration that gave a signal-to-noise ratio of 3. A limit of detection of 0.45 ng/ml (0.125 pmol per injection) was found for L3–MDA, which is lower than values given in the literature for other HPLC methods [3–6,10,13,14]. It should be noted that derivatization with DNSH [8] and NMH [18] can give similar detection limits. Beljean-Leymarie and Bruna [9] used a gas chromatographic (GC) method after derivatization of MDA with HBT and reported a detection limit of 0.04 pmol per injection. Although the method is highly sensitive for MDA, it requires hot and acidic conditions for more efficient formation of the derivative. To our knowledge, only the GC method developed by Tomita *et al.* [16] gives a higher sensitivity than the present method.

In practice, when the derivatization was performed on smaller amounts of MDA, the unreacted reagent seriously interfered with the detection of the luminarin 3–MDA derivative. To reduce this interference we added an excess of acetylacetone which, under these conditions, reacts with most of the excess of luminarin 3. This reaction gives two (additional) products,

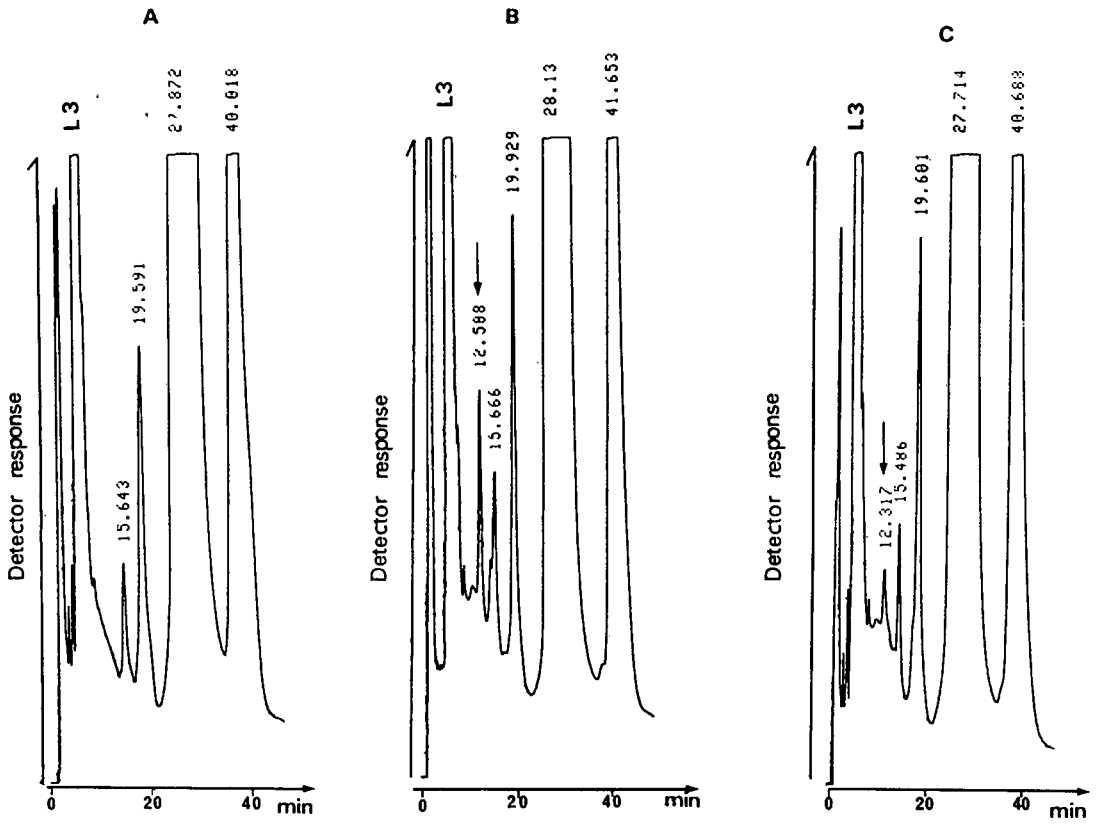

Fig. 4. Separation of luminarin 3–MDA derivative with fluorescence detection. (A) Blank; (B) chromatogram of the reaction mixture when 36 ng/ml of MDA were derivatized (4 mV full-scale); (C) chromatogram of the reaction mixture when 7.2 ng/ml of MDA were derivatized (4 mV full-scale). Numbers on peaks indicate retention times in minutes. For other details, see text.

TABLE I

UV ABSORPTION AND FLUORESCENCE DATA FOR LUMINARIN 3–MDA IN ACETONITRILE AND ACETONITRILE–10 m*M* IMIDAZOLE BUFFER (pH 7.0)

Acetonitrile concentration (%)	λ_{ex} (nm)	λ_{em} (nm)	ε^a (l mol^{-1} cm^{-1})	ϕ^b	IFS^c
0	401	502	22 952	0.39	3.85
30	402	495	28 072	0.39	4.34
50	399	491	28 682	0.51	5.63
70	399	485	28 976	0.51	5.60
100	394	464	32 139	0.71	8.55

[a] Molar absorptivity.
[b] Quantum yield.
[c] Intrinsic fluorescence sensitivity.

with peaks at 28.4 and 40.7 min, which were proved to be the pyrazole and monohydrazone forms of the luminarin 3–acetylacetone derivative, respectively (by liquid chromatography–mass spectrometry; data not shown). Fig. 4 shows the chromatograms of the reaction mixture obtained with (A) a blank acetate buffer solution and (B and C) standard solutions of MDA [(B) 36 and (C) 7.2 ng/ml]. Although these chromatograms are complex, experiments with spiked plasma samples displayed no additional peaks (different reaction conditions; data not shown). Therefore, owing to the good selectivity of the reagent, further inferences are not be expected.

Calibration graphs constructed for MDA with L3–MeMDA as internal standard ($n = 6$) were linear in the range 7.2–90 ng/ml, corresponding to 1.74–21.74 pmol of injected MDA derivative. The regression line was described by the following equation:

ratio of peak heights = 0.0129 · concentration (ng/ml) + 0.0270 ($r^2 = 0.999$)

The intra-run relative standard deviations were 10.6% for 7.2 ng/ml, 7.3% for 18 ng/ml, 5.6% for 36 ng/ml, 2.4% for 72 ng/ml and 1.8% for 90 ng/ml of MDA ($n = 6$). Hence the limit of quantification, *i.e.*, the lowest concentration that can be determined with an R.S.D. of less than 15%, was lower than 7 ng/ml (Fig. 4C).

Spectral properties

The influence of mobile phase composition on the absorbance and fluorescence properties of the luminarin 3–MDA derivative was studied.

As shown in Table I, whereas the position of the excitation maxima varied little with the composition of the solvent, the emission maxima showed a marked bathochromic effect with increased polarity of the acetonitrile–imidazole buffer mixture. This is due to the effect of the increased dipole–dipole interaction between the slightly polarized state of the molecule and the solvent characteristic of a $\pi \rightarrow \pi^*$ fluorescence emission.

Variations in the intensity of fluorescence of the luminarin 3–MDA derivative with the acetonitrile content of the mobile phase were studied by determining the relative quantum yields and intrinsic fluorescence sensitivity. These parameters doubled when the acetonitrile content in the mobile phase increased from 0 to 100%. Hence the whole composition range of mobile phases is compatible with highly sensitive detection.

CONCLUSIONS

Owing to its nucleophilic and fluorescence properties and the stability of its derivatives, luminarin 3 is a suitable derivatization reagent for the sensitive and selective HPLC with fluorescence detection of MDA. The method allows

the determination of small amounts of MDA with mild conditions of derivatization, without the formation of interfering by-products. In addition, the derivatization reagent and chromatographic conditions permit chemiluminescence detection.

The limiting factor with respect to the sensitivity of the present method was not detection but derivatization. In future work, acetylacetone could be replaced with a more efficient scavenger to remove all remaining luminarin 3. Even so, the limit of detection was well below that of other HPLC methods and its limit of quantification should allow the precise determination of free MDA in biological fluids. One example given in the literature is the concentration of MDA in normal human urine, which is in the range 10–60 ng/ml [16]. In several instances, the MDA concentration in urine has been shown to be correlated with lipid peroxidation processes following exposure to certain xenobiotics [14,15].

ACKNOWLEDGEMENT

We thank Dr. Martin Czok, Laboratoire de Chimie Analytique I et d'Electrochimie Organique, Université Paris-Sud, Châtenay-Malabry, France, for helpful discussions and assistance with the manuscript.

REFERENCES

1 T. Hirayama, S. Miura, M. Araki, Y. Takeo and T. Watanabe, *J. Assoc. Off. Anal. Chem.*, 73 (1990) 590.
2 M.J. Richard, B. Portal, J. Meo, C. Coudray, A. Hadjian and A. Favier, *Clin. Chem.*, 38 (1992) 704.
3 W.A. Behrens and R. Madère, *Lipids*, 26 (1991) 232.
4 C. Largillière and S.B. Mélancon, *Anal. Biochem.*, 170 (1988) 123.
5 M.J. Richard, P. Guiraud, J. Meo and A. Favier, *J. Chromatogr.*, 577 (1992) 9.
6 K. Nakashima, T. Ando, T. Nakamizo and S. Akiyama, *Chem. Pharm. Bull.*, 33 (1985) 5380.
7 J. Therasse and F. Lemonnier, *J. Chromatogr.*, 413 (1987) 237.
8 T. Hirayama, N. Yamada, M. Noharaa and S. Fukui, *J. Assoc. Off. Anal. Chem.*, 66 (1983) 304.
9 M. Beljean-Leymarie and E. Bruna, *Anal. Biochem.*, 173 (1988) 174.
10 K. Kikugawa, T. Kato and A. Iwata, *Anal. Biochem.*, 174 (1988) 512.
11 G. Lepage, G. Munoz, J. Champagne and C.C. Roy, *Anal. Biochem.*, 197 (1991) 277.
12 M.A. Carbonneau, E. Peuchant, D. Sess, P. Canioni and M. Clerc, *Clin. Chem.*, 37 (1991) 1423.
13 S. Kawai, M. Tomita and K. Kasashima, *J. Chromatogr.*, 495 (1989) 235.
14 M.A. Shara, P.H. Dickson, D. Bagchi and S.J. Stohs, *J. Chromatogr.*, 576 (1992) 221.
15 T. Ekström, P. Garberg, B. Egestad and J. Högberg, *Chem.-Biol. Interact.*, 66 (1988) 177.
16 M. Tomita, T. Okuyama, Y. Hatta and S. Kawai, *J. Chromatogr.*, 526 (1990) 174.
17 S. Kawai, T. Fuchiwaki, M. Tomita and T. Higashi, *J. Chromatogr.*, 514 (1990) 29.
18 H. Tamura and T. Shibamoto, *Lipids*, 26 (1991) 170.
19 F. Traoré, M. Tod, J. Chalom, R. Farinotti and G. Mahuzier, *Anal. Chim. Acta*, 269 (1992) 211.
20 M. Tod, J.-Y. Legendre, J. Chalom, H. Kouwatli, M. Poulou, R. Farinotti and G. Mahuzier, *J. Chromatogr.*, 594 (1992) 386.
21 M. Tod, M. Prevot, J. Chalom, R. Farinotti and G. Mahuzier, *J. Chromatogr.*, 542 (1991) 295.
22 C.A. Parker and W.T. Rees, *Analyst*, 85 (1960) 587.
23 J.B.F. Lloyd, *J. Chromatogr.*, 178 (1979) 249.

Journal of Chromatography, 648 (1993) 119–129
Elsevier Science Publishers B.V., Amsterdam

CHROM. 25 351

Methods for the determination of the enantiomeric purity of the C_3-synthons glycidol (2,3-epoxy-1-propanol) and solketal [2,2-dimethyl-4-(hydroxymethyl)-1,3-dioxolane]

Arie Geerlof, J. Bert A. van Tol, Jaap A. Jongejan and Johannis A. Duine*

Department of Microbiology and Enzymology, Delft University of Technology, Julianalaan 67, 2628 BC Delft (Netherlands)

(First received February 9th, 1993; revised manuscript received May 25th, 1993)

ABSTRACT

Accurate and reliable methods are presented for the determination of enantiomeric excess values of glycidol (2,3-epoxy-1-propanol), glycidyl esters, solketal [2,2-dimethyl-4-(hydroxymethyl)-1,3-dioxolane], homologous 1,3-dioxolane alcohols and substituted primary propanols in biological samples. One method consists of derivatization of the samples with 2,3,4,6-tetra-O-acetyl-β-glucopyranosyl isothiocyanate, followed by separation of the resulting diastereomers on a non-chiral reversed-phase (C_{18}) HPLC column. The second method uses direct injection of (aqueous) samples on to capillary GC columns coated with chiral stationary phases (2,3,6-tri-O-methyl-β- or a 2,3,6-tri-O-trifluoroacetyl-γ-cyclodextrin). The advantages and disadvantages of both methods are discussed.

INTRODUCTION

The enantiomers of glycidol (2,3-epoxy-1-propanol) and solketal [2,2-dimethyl-4-(hydroxymethyl)-1,3-dioxolane] have been advocated as attractive building blocks for the synthesis of homochiral pharmaceuticals and other specialty chemicals [1–4]. Since we have embarked on studies on the application of enzymes in kinetic resolution of these C_3-synthons [5–7], the changing ratio of the enantiomers had to be followed. This required methods that were able to determine the ratio from the start (racemic mixture) to the end (enantiomerically pure), that is, from an enantiomeric excess (e.e.) of 50 to 100%, in a reliable and accurate way. It should be stressed that in this context the sensitivity of the methods for the compound as such is of less importance.

Bioconversions are frequently carried out with either crude cellular material or with a small amount of purified enzyme in aqueous buffers. Hence, under these conditions, direct measurements of optical rotation in the medium are not reliable. Moreover, the determination of enantiomeric purity by NMR measurements in the presence of chiral shift reagents failed, because of instability of the products under these conditions. On the other hand, chromatographic methods could circumvent these restrictions if satisfactory accuracy and sensitivity could be achieved. A strategy frequently used in the analysis of racemic alcohols is to prepare diastereomers, *e.g.*, by using Mosher's acid [α-methoxy-α-(trifluoromethyl)phenylacetic acid (MTPA)], and to separate the diastereomeric products by (non-chiral) GC or HPLC. Commercially available MTPA, however, is only 97.9–

* Corresponding author.

0021-9673/93/$06.00

99.8% pure and kinetic enrichment of one of the enantiomers has been reported [8]. Further, racemization can be expected under the acidic conditions, as observed here (see below) for trifluoroacetic anhydride. Hence, other derivatization methods seemed necessary to attain the high accuracy required.

Based on the derivatization procedure with 2,3,4,6-tetra-O-acetyl-β-glucopyranosyl isothiocyanate (TAGIT) described by Gal [9], diastereomers were prepared from glycidyl butyrate and they could be separated by HPLC (as reported in a preliminary communication by Philippi *et al.* [10]). Hence, it seemed worthwhile to investigate the reliability and accuracy of the method for glycidyl esters and glycidol, assuming that the derivatization proceeds as indicated in Fig. 1. To explore the scope of the method, other C_3-synthons and some homologous 1,3-dioxolane compounds with varying distance between the asymmetric carbon atoms were also investigated. For this derivatization, a modified route was devised, as indicated in Fig. 2.

Direct methods for the separation of enantiomers have been reported. König *et al.* [11] investigated trifluoroacetyl derivatives of epoxy alcohols (including glycidol) using GC with peralkylated α-cyclodextrins as a chiral stationary phase. Using α-, β- or γ-cyclodextrin stationary phases, many racemic compounds, including the trifluoroacetyl esters of glycidol and solketal, could be resolved [12]. Dougherty *et al.* [13] were able to separate glycidol without derivatization applying aqueous samples to a GC column with a permethyl-O-hydroxypropyl-α-

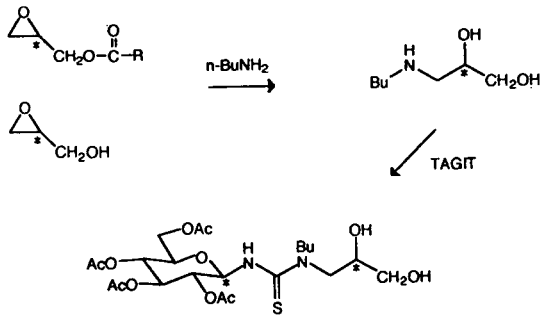

Fig. 1. Conversion of glycidol and glycidyl esters into their diastereomers with TAGIT.

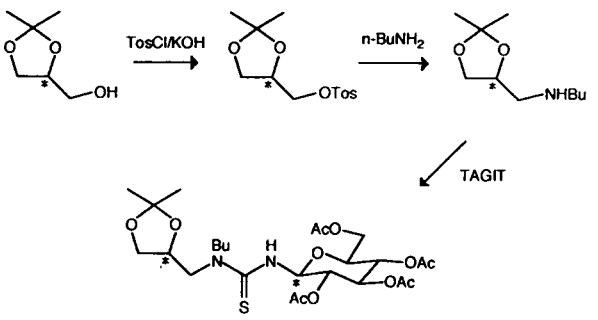

Fig. 2. Conversion of solketal into its diastereomers with TAGIT.

cyclodextrin stationary phase. As the latter strategy is very attractive for the analysis of samples resulting from biological conversions, GC on derivatized β- and γ-cyclodextrin stationary phases was also investigated for the separation of the enantiomers of glycidol, solketal and selected homologues.

EXPERIMENTAL

Chemicals

(*R*,*S*)-Glycidol, (*R*,*S*)-2-butanol, (*R*,*S*)-2-octanol, (*R*,*S*)-2,3-dibromo-1-propanol, (*R*,*S*)-2,3-dichloro-1-propanol, (*R*,*S*)-2-methyl-1-butanol and trifluoroacetic anhydride were purchased from Merck, (*R*)-(+)- and (*S*)-(−)-glycidol, (*R*)-(−)- and (*S*)-(+)-3-bromo-2-methyl-1-propanol, (*R*,*S*)-2-phenyl-1-propanol and (*R*,*S*)-glycerol formal from Aldrich, (*R*,*S*)-, (*R*)-(−)- and (*S*)-(+)-solketal, (*R*)-(−)- and (*S*)-(+)-2-butanol from Janssen Chimica, 2,3,4,6-tetra-O-acetyl-β-glucopyranosyl isothiocyanate (TAGIT), (*R*)-(−)- and (*S*)-(+)-2-octanol and (*R*,*S*)-3-buten-2-ol from Fluka and methanol (HPLC grade) from Rathburn; (*R*,*S*)- and (*R*)-(−)-glycidyl butyrate were gifts from Andeno. All other chemicals were of analytical-reagent grade (Merck).

Other glycidyl and solketyl esters [14], the homologous 1,3-dioxolane alcohols [15] and (*S*)-(−)- and (*R*)-(+)-2,3-O-isopropylidene glyceraldehyde (solketylaldehyde) [16,17] were synthesized according to the literature. The compounds had a chemical purity of 93–99.5%, as established by GC and ^{1}H NMR.

HPLC

Derivatization of glycidol and glycidyl esters. An aqueous sample, containing at least 5 mg of glycidol, was saturated with NaCl and extracted twice with an equal amount of dichloromethane. Samples containing a glycidyl ester were also extracted twice with dichloromethane. The extracts were dried with $MgSO_4$ and the solvent evaporated under reduced pressure. The residue was dissolved in 1 ml of *n*-butylamine and the solution was transferred into a 3-ml sample vial (Waters). The vial was tightly capped (PTFE septum) and heated in an oil-bath at 100°C for 1 h. Subsequently, the cap was removed to allow the residual amine to evaporate. The residue was stored overnight under reduced pressure in a desiccator over P_2O_5 to remove the last traces of the amine. The oily residue was dissolved in 200 μl of acetonitrile and 25 μl of this solution were mixed with 50 μl of acetonitrile containing 1 mg of TAGIT. After standing at room temperature for 5 min, a 5-μl sample of the mixture was injected into the HPLC system.

Derivatization of solketal and homologous 1,3-dioxolane alcohols. An aqueous sample, containing at least 1 mg of solketal or related alcohol, was extracted twice with an equal amount of dichloromethane. The combined extracts were dried with $MgSO_4$ and the solvent was evaporated under reduced pressure. The residue was dissolved in 10 ml of dry diethyl ether and the solution was transferred into a 50-ml flask. *p*-Toluenesulphonyl chloride (75 mg) and powdered KOH (500 mg) were added to the stirred solution at room temperature. After 15 min the mixture was poured into 20 ml of diethyl ether–water (3:1, v/v). After shaking, the organic layer was separated, washed twice with water and dried with $MgSO_4$. The solvent was removed by evaporation under reduced pressure. The residue was dissolved in 2 ml of *n*-butylamine and placed in a 3-ml sample vial (Waters). The vial was tightly capped (PTFE septum) and the solution was heated in an oil-bath at 100°C for 1 h and then poured into 20 ml of a diethyl ether–water (3:1, v/v). After shaking, the organic layer was separated, washed four times with water and dried with $MgSO_4$. The solvent was removed by evaporation under reduced pressure. The residue was dissolved in 0.5 ml of acetonitrile and 25 μl of this solution were added to 50 μl of acetonitrile containing 1 mg of TAGIT. After standing at room temperature for 5 min, 10 μl of this solution were injected into the HPLC-system.

Chromatography of the derivatives. The HPLC system consisted of a pump (Waters Model 510), an injector (Rheodyne Model 7125), a UV detector (Waters Lambda Max Model 480), an integrator (Waters data module) and a reversed-phase column (Waters Nova-Pak C_{18}, 100 × 8 mm I.D., particle size 4 μm). The column was eluted with aqueous methanol (compositions are given in Table I) at a constant flow-rate of 1.0 ml/min at room temperature. The eluent was monitored at 260 nm.

Preparation and identification of the diastereomers

Diastereomers of glycidol [N'-butyl-N'-(R,S)-2',3'-dihydroxypropyl(2,3,4,6-tetra-O-acetyl-β-D-glucopyranosyl)thiourea]. An 11-mg amount of racemic glycidol was derivatized as described above. The residue was dissolved in 250 μl of acetonitrile and 62 mg of TAGIT were added. After standing at room temperature for 60 min, the diastereomers were isolated by HPLC, as indicated above. The eluent was removed by evaporation under reduced pressure and the residues were stored overnight under reduced pressure in a desiccator over P_2O_5. ^{1}H NMR (400 MHz) was performed using a Varian VXR-400 S spectrometer. Well resolved spectra were obtained. From a comparison of the spectra of several 1-acylglycerol derivatives, the corresponding 2,3-epoxy-1-propanyl esters and the free alcohol, the presence of the 2,3-dihydroxy-1-propyl group could be deduced. The results are in agreement with the structure indicated in Fig. 1 and in line with that what could be predicted with analogous cases [9].

^{1}H NMR ($C^2H_3O^2H$): δ 5.90 (s, 1 H, glucose H-1α, J = 9.3 Hz), 5.33 (dd, 1 H, glucose H-3α, J = 9.3 Hz, J = 9.5 Hz), 5.12 (dd, 1 H, glucose H-2β, J = 9.5 Hz, J = 9.5 Hz), 5.03 (dd, 1 H, glucose H-4β, J = 9.7 Hz, J = 9.9 Hz), 4.20 (m, 1 H, NH), 4.31 (dd, 1 H, glucose H-6a, J = 12.3

TABLE I

CHROMATOGRAPHIC PARAMETERS ON A REVERSED-PHASE C_{18} HPLC COLUMN OF THE DIASTEREOMERS OBTAINED WITH TAGIT DERIVATIZATION OF GLYCIDOL, GLYCIDYL BUTYRATE, SOLKETAL, HOMOLOGOUS 1,3-DIOXOLANE ALCOHOLS AND SOME OTHER ALCOHOLS

α = Separation factor = $(t_2 - t_0)/(t_1 - t_0)$; R = resolution = $2(t_2 - t_1)/(W_1 + W_2)$, where W is the peak width. NR = Not resolved. The identity of the peaks (indicated with R or S, in parentheses) was derived from the results obtained with authentic compounds.

Compound	Mobile phase methanol–water (v/v)	Retention times of the diastereomers		α	R
		t_1 (min)	t_2 (min)		
Glycidol	50:50	29.3 (*R*)	31.7 (*S*)	1.09	1.40
Glycidyl butyrate	50:50	29.3 (*S*)	31.7 (*R*)	1.09	1.40
Solketal	58:42	38.3 (*R*)	40.4 (*S*)	1.06	1.01
Compound **1**	60:40	17.0		NR	NR
Compound **3**	60:40	10.8		NR	NR
Compound **4**	80:20	5.9		NR	NR
Compound **5**	60:40	58.6	74.2	[a]	[a]
		76.8	83.0		
Compound **6**	70:30	19.2	21.5	1.13	1.97
Compound **7**	80:20	8.4	9.4	1.15	1.75
Compound **8**	80:20	32.0		NR	NR
2,3-Dibromo-1-propanol	60:40	48.0		NR	NR
2-Butanol	80:20	7.5		NR	NR
2-Methyl-1-butanol	60:40	81.7		NR	NR

[a] Compound **5** consists of four diastereomers. Resolutions of the diastereomers are $R \geq 0.58$ and separation factors $\alpha \geq 1.04$ (which were calculated for peaks 2 and 3).

Hz, $J = 4.4$ Hz), 4.10 (dd, 1 H, glucose H-6b, $J = 12.3$ Hz, $J = 2.2$ Hz), 4.08 (dd, 1 H, glycerol H-1), 3.88 (ddd, 1 H, glucose H-5α, $J = 2.2$ Hz, $J = 4.4$ Hz, $J = 10.1$ Hz), 3.8 (m, 1 H, glycerol H-2), 3.72 (m, 2 H, butyl H-1), 3.66 (m, 1 H, glycerol H-1, $J = 5.1$ Hz, $J = 7$ Hz), 3.55 (dd, 2 H, glycerol H-3, $J = 5.1$ Hz), 2.03 (s, 3 H, acetyl), 2.01 (s, 3 H, acetyl), 2.00 (s, 3 H, acetyl), 1.98 (s, 3 H, acetyl), 1.64 (m, 2 H, butyl H-2, $J = 7$ Hz), 1.33 (m, 2 H, butyl H-3, $J = 7.3$ Hz, $J = 7$ Hz), 0.96 (t, 3 H, butyl H-4, $J = 7.3$ Hz).

Diastereomers of solketal {N'-butyl-N'-[(R,S)-2',2'-dimethyl-1',3'-dioxolan-4'-yl]methyl(2,3,-4,6-tetra-O-acetyl-β-D-glucopyranosyl)thiourea}. A 14-mg amount of racemic solketal was derivatized with 45 mg of TAGIT and the diastereomers produced were isolated as described above. Well resolved ^{1}H NMR spectra of the diastereomers were obtained. The presence of the (2,2-dimethyl-1,3-dioxolan-4-yl)methyl moiety could be deduced from the similarity of the chemical shifts and the coupling constants observed for the diastereomers and the free alcohol. The results are in agreement with the structure indicated in Fig. 2.

^{1}H NMR ($C^2H_3O^2H$): δ 5.97 (s, 1 H, glucose H-1α, $J = 9.1$ Hz), 5.35 (dd, 1 H, glucose H-3α, $J = 9.5$ Hz, $J = 9.5$ Hz), 5.18 (dd, 1 H, glucose H-2β), 5.03 (dd, 1 H, glucose H-4β, $J = 9.7$ Hz, $J = 10.0$ Hz), 4.40 (m, 1 H, dioxolane H-4), 4.32 (dd, 1 H, glucose H-6a, $J = 12.3$ Hz, $J = 4.2$ Hz), 4.11 (dd, 1 H, glucose H-6b, $J = 12.3$ Hz, $J = 2.4$ Hz), 4.10 (dd, 1 H, dioxolane H-5, $J = 8.3$ Hz, $J = 6.0$ Hz), 3.91 (ddd, 1 H, glucose H-5α, $J = 2.4$ Hz, $J = 4.2$ Hz, $J = 10.1$ Hz), 3.75 (m, 2 H, butyl H-1), 3.65 (dd, 1 H, dioxolane H-5, $J = 8.3$ Hz, $J = 7.3$ Hz), 3.63 (dd, 2 H, dioxolane H-4'),

2.02 (s, 3 H, acetyl), 2.01 (s, 3 H, acetyl), 2.00 (s, 3 H, acetyl), 1.99 (s, 3 H, acetyl), 1.59 (m, 2 H, butyl H-2, $J = 7$ Hz), 1.47 (s, 3 H, dioxolane H-2′), 1.33 (s, 3 H, dioxolane H-2″), 1.33 (m, 2 H, butyl H-3, $J = 7.3$ Hz, $J = 7$ Hz), 0.95 (t, 3 H, butyl H-4, $J = 7.3$ Hz).

Gas chromatography

Direct analysis. An aqueous sample (1 ml), containing *ca.* 1.0 mg of the compound to be determined, could be used directly for analysis (0.2–1.0 μl injected) or via extraction with 3.0 ml of dichloromethane. The dichloromethane extract was dried with $MgSO_4$ and the solvent was evaporated with a stream of nitrogen until a residue of *ca.* 50 μl remained.

Derivatization of the samples. An aqueous sample was extracted as described above. The dichloromethane extract was dried with $MgSO_4$ and the solvent was evaporated with a stream of nitrogen. For derivatization, the residue was dissolved in 0.5 ml of dry diethyl ether and 100 μl of trifluoroacetic anhydride (TFAA) were added. After standing at room temperature for 30 min, the excess of TFAA, the trifluoroacetic acid produced and the solvent were removed with a stream of nitrogen and the residue was dissolved in 50 μl of dichloromethane.

Chromatography of the compounds and derivatives. Chromatography was performed with a Hewlett-Packard Model 5890 Series II gas chromatograph with a split injector, a flame ionization detector and an integrator (Hewlett-Packard 3365 Chemstation). The apparatus was equipped with a CP-cyclodextrin-2,3,6-M-19 capillary column (25 m × 0.25 mm I.D., film thickness 0.25 μm) (Chrompack, Middelburg, Netherlands) or a Chiraldex G-TA capillary column (20 m × 0.25 mm I.D., film thickness 0.125 μm) (Astec, Whippany, NJ, USA). The latter was preceded by a retention gap (2.5 m × 0.32 mm I.D.). Nitrogen was used as the carrier gas and the inlet pressure was 56 kPa for the first and 25 kPa for the second column. A split flow of 100:1 was used. The injector and detector temperatures were kept constant at 200 and 250°C, respectively. The injection volume of the samples was 0.2–1.0 μl.

RESULTS AND DISCUSSION

Reversed-phase HPLC of the diastereomers

Derivatization with TAGIT has been applied to the determination of the enantiomeric purity of α-amino acids [18–20], amphetamines [21], catacholamines [22–24], epoxides [9], amino alcohols [25,26], α-methylamino acids [27] and some pharmaceuticals [28–31]. As reported in a preliminary communication [10], derivatization of glycidyl butyrate with TAGIT, followed by reversed-phase HPLC on a C_{18} column, gave satisfactory resolution for determination of the enantiomeric excess (e.e.) values in the enzymatic hydrolysis of glycidyl butyrate. Therefore, we first attempted to determine the reliability and accuracy of the method for a number of glycidyl esters and glycidol itself.

As the derivatization procedure has to be executed in a water-free system, extraction was required. The extracted glycidol or glycidyl ester appeared to be converted within 1 hour into the corresponding amino alcohol (Fig. 1). Treatment of this with TAGIT gave the diastereomer within 5 min, as judged from analysis by HPLC. Nearly baseline separation [$R = 1.40$; $\alpha = 1.09$ (Table I)] was achieved with HPLC (Fig. 3). Several control experiments in which the presence of protein and phosphate buffers (0.1 *M*, pH 6–8) in the sample was tested were carried out. No

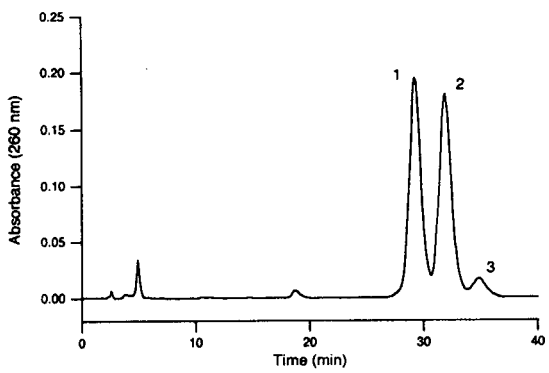

Fig. 3. Chromatogram of TAGIT-derivatized racemic glycidol on a reversed-phase C_{18} HPLC column. The peaks originate from (1) the diastereomer of (*R*)-(+)-glycidol, (2) the diastereomer of (*S*)-(−)-glycidol and (3) *n*-butylamine.

effect was found in samples containing enantiomerically pure (*R*)-(−)-glycidyl butyrate or racemic glycidol, as only one diastereomer and two diastereomers in a 1:1 ratio were found, respectively. This indicates that under the conditions used no racemization or kinetic enrichment occurs and that TAGIT is enantiomerically pure. As the esters and glycidol gave the same products with HPLC, apparently ester hydrolysis occurs and ring opening proceeds in the same way. *n*-Butylamine seemed to be the best choice for the first step in the procedure as isopropylamine, *tert.*-butylamine, pentylamine and both enantiomers of amphetamine gave diastereomers with less adequate separation. Aqueous samples containing glycidol in addition to a glycidyl ester could be analysed by making use of the large differences in solubility in organic solvents. For this purpose the sample was extracted with dichloromethane (no salt was added) and small amounts of glycidol in the organic solvent layer were removed by extraction with water. The water layer from the first extraction could be used for the determination of glycidol.

To determine solketal, the procedure had to be adapted as the compound as such does not react with the amine. Hence solketal was first tosylated and the product was subsequently derivatized with *n*-butylamine (Fig. 2), analogous to the procedure developed by Sowden and Fischer [32] for the synthesis of L-1-amino-2,3-propanediol from (*S*)-(+)-solketal. The amine products reacted readily with TAGIT and the diastereomers formed could be separated (Fig. 4), although the separation parameters [$R = 1.01$; $\alpha = 1.06$ (Table I)] were less satisfactory than for glycidol. Therefore, experiments were performed to check whether the method would be reliable at high e.e. values. In a typical experiment, enantiomerically pure (*S*)-(+)-solketal was deliberately contaminated with 0.25% of the *R*-isomer. It appeared that the experimentally determined e.e. value (99.4 ± 0.2%; six measurements) was very close to the theoretical value (99.5%). As with glycidol, control experiments indicated that no racemization or kinetic enrichment occurs in the procedure developed for solketal.

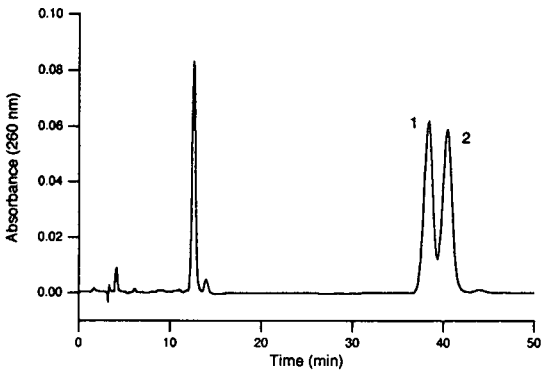

Fig. 4. Chromatogram of TAGIT-derivatized racemic solketal on a reversed-phase C_{18} HPLC column. Peak 1 originates from the diastereomer of (*R*)-(−)-solketal and peak 2 from the diastereomer of (*S*)-(+)-solketal.

To investigate the scope of the method, a number of homologous 1,3-dioxolane compounds (Fig. 5) and 2-butanol, 2-methyl-1-butanol and 2,3-dibromo-1-propanol were subjected to the derivatization procedure developed for solketal. Only the homologous 1,3-dioxolane compounds with the hydroxy group next to the chiral centre at C-4 ($n = 0$; compounds **5**, **6** and **7**) gave diastereomeric products that could be separated. Bulky substituents (R_1 and R_2) as present in compounds **6** and **7** caused an increase in the retention time and a better resolution of the diastereomeric products (Table I). Glycerol formal (compound **1**), which lacks the two methyl groups of solketal at C-2, gave unsatisfactory results. In theory, the introduction of a

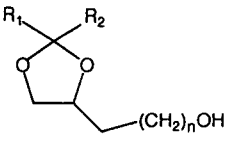

Compound	n	R_1	R_2
1	0	H	H
2	0	CH_3	CH_3
3	1	CH_3	CH_3
4	3	CH_3	CH_3
5	0	CH_3	C_3H_7
6	0	$-(CH_2)_4-$	
7	0	$-(CH_2)_5-$	
8	3	$-(CH_2)_5-$	

Fig. 5. Structures of homologous 1,3-dioxolane alcohols. **1** = 4-(Hydroxymethyl)-1,3-dioxolane (glycerol formal); **2** = 2,2-dimethyl-4-(hydroxymethyl)-1,3-dioxolane (solketal); **3** = 2,2-dimethyl-4-(2-hydroxyethyl)-1,3-dioxolane; **4** = 2,2-dimethyl-4-(4-hydroxybutyl)-1,3-dioxolane; **5** = 2-methyl-2-propyl-4-(hydroxymethyl)-1,3-dioxolane; **6** = 2,2-butylene-4-(hydroxymethyl)-1,3-dioxolane; **7** = 2,2-pentylene-4-(hydroxymethyl)-1,3-dioxolane; **8** = 2,2-pentylene-4-(4-hydroxybutyl)-1,3-dioxolane.

second chiral centre should lead to four different diastereomeric products. Four peaks were indeed present in the chromatogram of compound **5** (second chiral centre at the C-2 atom) in the expected region (Fig. 6). Their assignment has not been carried out. The diastereomers of the homologous 1,3-dioxolane compounds with $n > 0$ (Fig. 5) and of the other alcohols showed no separation on the column used.

For the procedures described here, the samples should contain at least 1 mg of solketal or 5 mg of glycidol and 5–10 μg of the diastereomers were used for HPLC. Hence, substantial improvements could be made with respect to sensitivity, *e.g.*, by improving the yield of extraction (solketal and glycidol show good solubility in water). As our objective was to develop a reliable and sensitive method to determine the ratio of the enantiomers, no attempts were made in this direction.

Gas chromatography on chiral stationary phases

The enantiomeric composition of glycidol- or solketal-containing samples was determined using two commercially available capillary GC columns containing 2,3,6-tri-O-methyl-β-cyclodextrin (β-CD) or 2,3,6-tri-O-trifluoroacetyl-γ-cyclodextrin (γ-CD) as chiral stationary phase. It appeared that aqueous samples of glycidol and solketal could be injected directly on to the capillary columns, giving satisfactory separation

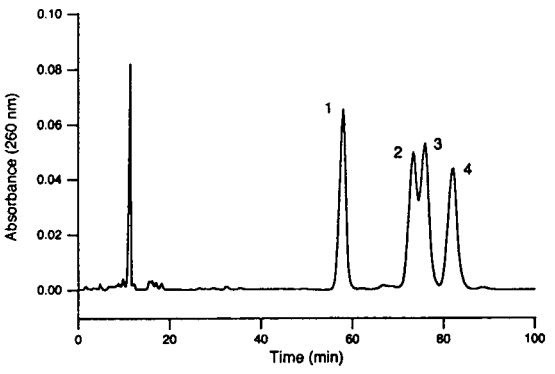

Fig. 6. Chromatogram of TAGIT-derivatized racemic compound **5** [2-methyl-2-propyl-4-(hydroxymethyl)-1,3-dioxolane] on a reversed-phase C_{18} HPLC column. Peaks 1–4 originate from the four diastereomeric products, but their assignment has not been carried out.

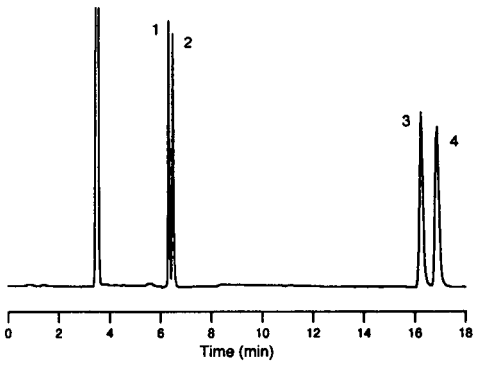

Fig. 7. Chromatogram of racemic glycidol and racemic solketal on a capillary GC column with a 2,3,6-tri-O-trifluoroacetyl-γ-cyclodextrin stationary phase at a column temperature of 90°C. The peaks originate from (1) (*R*)-(+)-glycidol, (2) (*S*)-(−)-glycidol, (3) (*R*)-(−)-solketal and (4) (*S*)-(+)-solketal.

(Fig. 7; Tables II and III), the γ-CD column giving a better separation than the β-CD column. However, to avoid contamination of the system with proteins and buffer compounds (deterioration of the column was observed after *ca.* 50 direct injections), extraction was routinely applied. Owing to their water solubility, samples had to contain *ca.* 1 mg of the compound under these conditions. To check the reliability and accuracy of the method, control experiments were performed. In a typical experiment, to enantiomerically pure (*S*)-solketal 0.25% of the *R*-isomer was added. Experiments on the γ-CD column (six measurements) gave an e.e. value of $99.52 \pm 0.07\%$, very close to the theoretical value of 99.50%.

To investigate which compounds could be determined, racemic mixtures of glycidyl esters, homologous 1,3-dioxolane compounds (Fig. 5), substituted primary propanols and some other alcohols were tested. The enantiomers of most of these compounds could be baseline separated ($R > 1.5$) using the γ-CD column (Table II). The resolution of the glycidyl esters, however, decreased with an increasing chain length of the carboxylic acid moiety. For carboxylic acids longer than C_5 separation was inadequate. Enantiomers of the homologous 1,3-dioxolane alcohols with the hydroxy group close to the chiral centre at C-4 ($n = 0$ and 1; compounds **1**, **3**, **6** and **7**) were all baseline separated. The enantio-

TABLE II

CHROMATOGRAPHIC PARAMETERS ON A CAPILLARY GC COLUMN WITH A CHIRAL (2,3,6-TRI-O-TRIFLUOROACETYL-γ-CYCLODEXTRIN) STATIONARY PHASE OF ENANTIOMERS OF GLYCIDOL, GLYCIDYL ESTERS, SOLKETAL, HOMOLOGOUS 1,3-DIOXOLANE COMPOUNDS AND SOME OTHER ALCOHOLS

Terminology and abbreviations as in Table I.

Compound	Temperature (°C)	Retention times		α	R
		t_1 (min)	t_2 (min)		
Glycidol	80	8.03 (*R*)	8.35 (*S*)	1.068	2.25
Glycidyl acetate	100	9.22	10.0	1.137	5.59
Glycidyl propionate	90	15.8	16.4	1.052	2.33
Glycidyl butyrate	100	14.8 (*R*)	15.1 (*S*)	1.030	1.63
Glycidyl pentanoate	85	47.1	48.0	1.021	1.26
Glycidyl hexanoate	90	65.0	65.8	1.014	0.85
Glycidyl octanoate	120	41.6		NR	NR
Solketal	90	16.2 (*R*)	16.9 (*S*)	1.048	2.34
Compound **1**	90	14.5	15.0	1.046	2.12
Compound **3**	100	17.9	18.4	1.037	1.85
Compound **4**	100	56.0		NR	NR
Compound **5**	100	23.7 [a]	24.9		
Compound **6**	100	45.3	46.8	1.036	1.96
Compound **7**	110	42.8	43.8	1.025	1.45
Compound **8**	150	22.9		NR	NR
Solketyl acetate	70	52.2	53.3	1.022	1.20
Solketyl butyrate	120	>60			
2,3-Dichloro-1-propanol	90	22.7	23.6	1.042	1.40
2,3-Dibromo-1-propanol	110	24.3	25.0	1.034	1.65
3-Bromo-2-methyl-1-propanol	90	22.2 (*R*)	22.8 (*S*)	1.032	1.32
2-Phenyl-1-propanol	100	38.7	40.3	1.045	2.49
2-Butanol	40	6.65 (*S*)	6.85 (*R*)	1.055	1.56
2-Octanol	60	39.8	40.5	1.019	1.15
3-Buten-2-ol	40	6.59	6.73	1.039	1.17

[a] Compound **5** consists of four diastereomers, but only two peaks were observed, with a ratio of 3:1 (peak 1:peak 2).

mers of the homologous 1,3-dioxolane alcohols with $n = 3$ (compounds **4** and **8**) were not resolved. Introduction of a second chiral centre at C-2 (compound **5**) leads theoretically to four diastereomers. However, only two peaks could be detected in the chromatogram. The ratio of the areas of peaks 1 and 2 is 3:1. Hence, the first peak probably represents three diastereomers. The number of compounds that could be determined using the β-CD column appeared to be considerably smaller (Table III). Enantiomers of glycidyl butyrate and of the three primary halopropanols tested were not resolved and in most other instances the chromatographic parameters were significantly below acceptable values. Only the enantiomers of the homologous 1,3-dioxolane compounds could be sufficiently separated, except those of compound **8**. Also, the four diastereomers of compound **5** were not detected. In the chromatogram only three peaks were observed, of which peak 1 may contain two of the diastereomers. The enantiomers of solketylaldehyde, products which are formed from racemic solketal in the conversion with alcohol dehydrogenases [7], gave a baseline separation with a very high resolution ($R = 3.32$).

Alcohols can be derivatized with TFAA prior to the GC analysis to improve their volatility [12,13,33]. To investigate whether this improved the resolution of the alcohols studied here, the

TABLE III

CHROMATOGRAPHIC PARAMETERS ON A CAPILLARY GC COLUMN WITH A CHIRAL (2,3,6-TRI-O-METHYL-β-CYCLODEXTRIN) STATIONARY PHASE OF ENANTIOMERS OF GLYCIDOL, GLYCIDYL BUTYRATE, SOLKETAL, HOMOLOGOUS 1,3-DIOXOLANE COMPOUNDS AND SOME OTHER ALCOHOLS

Terminology and abbreviations as in Table I.

Compound	Temperature (°C)	Retention times		α	R
		t_1 (min)	t_2 (min)		
Glycidol	45	22.1 (*R*)	22.9 (*S*)	1.037	1.52
Glycidyl butyrate	100	15.4		NR	NR
Solketal	95	15.5 (*R*)	15.9 (*S*)	1.028	1.43
Compound **1**	70	38.5	39.7	1.033	1.24
Compound **3**	110	15.4	15.9	1.034	1.47
Compound **4**	120	31.2	31.9	1.023	1.29
Compound **5**	120	13.4 [a]	14.0		
		14.4			
Compound **6**	125	20.0	20.5	1.030	1.54
Compound **7**	125	32.3	33.1	1.026	1.29
Compound **8**	150	52.2		NR	NR
Solketylaldehyde	90	7.18 (*S*)	7.67 (*R*)	1.097	3.32
2,3-Dichloro-1-propanol	100	18.1		NR	NR
2,3-Dibromo-1-propanol	125	17.2		NR	NR
3-Bromo-2-methyl-1-propanol	80	45.1	45.9	1.020	0.43
2-Phenyl-1-propanol	100	46.3	47.4	1.027	1.13
2-Butanol	40	7.16 (*R*)	7.37 (*S*)	1.041	1.16
2-Octanol	70	40.4	41.1	1.020	0.73
3-Buten-2-ol	45	5.70	5.91	1.056	1.21

[a] Compound **5** consists of four diastereomers. Three peaks were observed in a ratio of 2:1:1 (peak 1:peak 2:peak 3).

racemic compounds were derivatized with TFAA and injected on to the β-CD column. In general, the separation of the products could be performed at lower column temperatures and the peaks obtained showed less tailing when compared with the underivatized alcohols. The chromatographic parameters of almost all of the compounds tested improved (Table IV). For instance, the resolution of the enantiomers of solketal increased from $R = 1.43$ to 4.39. Further, the diastereomeric 1,3-dioxolane compound (compound **5**) could be separated into its four diastereomers. Also, the enantiomers of 2,3-dichloro- and 2,3-dibromo-1-propanol could be separated after derivatization. On the other hand, glycidol and glycerol formal (compound **1**) gave only one peak, probably caused by decomposition of the compounds. Further, although the separation seemed feasible for solketal, determination of the optical purity of an (*S*)-(+)-solketal sample (e.e. = 99.1%) resulted in a lower value (e.e. = 98.6%). When a five times higher TFAA concentration and a two times longer derivatization time were used, an even lower e.e. value was found (69.8%). Hence solketal, and probably all homologous 1,3-dioxolane alcohols, are liable to acid racemization during derivatization with TFAA.

Evaluation

Some years ago we managed to determine the e.e. value of glycidyl butyrate in aqueous samples by adapting the TAGIT derivatization method to this compound and separating the diastereomers by HPLC on a reversed-phase column [10]. As shown here, the method has been optimized and proved to be suited for other glycidyl esters and glycidol. As always the same diastereomers were found by HPLC, derivatization proceeds as suggested in Fig. 1, as sup-

TABLE IV

CHROMATOGRAPHIC PARAMETERS ON A CAPILLARY GC COLUMN WITH A CHIRAL (2,3,6-TRI-O-METHYL-β-CYCLODEXTRIN) STATIONARY PHASE OF THE TRIFLUOROACETYL DERIVATIVES OF ENANTIOMERS OF GLYCIDOL, SOLKETAL, HOMOLOGOUS 1,3-DIOXOLANE ALCOHOLS AND SOME OTHER ALCOHOLS

Terminology and abbreviations as in Table I.

Compound	Temperature (°C)	Retention times		α	R
		t_1 (min)	t_2 (min)		
Glycidol	45	16.8		NR	NR
Solketal	100	7.66 (*R*)	8.15 (*S*)	1.090	4.39
Compound **1**	70	20.5		NR	NR
Compound **3**	90	20.1	20.7	1.032	1.53
Compound **4**	110	26.2	27.0	1.033	1.93
Compound **5**	100	18.4	19.0	[a]	[a]
		19.8	21.7		
Compound **6**	125	12.2	12.7	1.049	1.26
Compound **7**	125	19.8	20.8	1.060	1.38
Compound **8**	140	46.6	47.1	1.012	0.65
2,3-Dichloro-1-propanol	90	10.5	10.8	1.031	1.40
2,3-Dibromo-1-propanol	110	12.6	13.0	1.039	2.20
3-Bromo-2-methyl-1-propanol	60	31.2	32.1	1.029	1.10
2-Phenyl-1-propanol	90	31.0	31.6	1.022	1.16
2-Octanol	50	49.5	50.5	1.021	1.00

[a] Compound **5** consists of four diastereomers. Four peaks were obtained with resolutions of $R \geq 1.33$ and separation factors of $\alpha \geq 1.035$.

ported by product identification. Therefore, glycidol and all glycidyl esters can be determined with this method. Control experiments showed that no racemization or kinetic enrichment occurred. As separation of the diastereomers was much better than for solketal, it is estimated that the accuracy at high e.e. values is at least ±0.1%. Modification of the derivatization procedure permitted the determination of solketal and homologous 1,3-dioxolane compounds. Also for these cases it was checked that no detectable racemization or kinetic enrichment occurred. Owing to the lower resolution, the accuracy at high e.e. values of solketal appeared to be ±0.2%.

During the course of our investigations, novel possibilities arose as GC columns with chiral stationary phases became available. The generally adapted strategy for determining racemic alcohols, which is to convert them into esters to obtain good separation characteristics, did not work here as the compounds either decomposed (glycidol) or racemized (solketal). Direct analysis without derivatization appeared to be possible, the γ-CD column being better suited for this than the β-CD column. The high resolution achieved resulted in high accuracies, as illustrated with experiments for solketal at high e.e. values (99.52 ± 0.07%). Despite its convenience, wide range of application and accuracy, the GC method has the disadvantages that the columns are expensive and dedicated to this particular purpose and glycidyl esters from hexanoate on could not be determined. Therefore, the HPLC method is still viable.

ACKNOWLEDGEMENTS

The authors thank Erik Keegstra for the synthesis of the homologous 1,3-dioxolane alcohols, Ir. A. Sinnema (Department of Organic Chemistry, Delft University of Technology) for providing ^{1}H NMR data and Andeno, Venlo, for the gift of racemic and (*R*)-(−)-glycidyl butyrate.

REFERENCES

1 J.M. Klunder, S.Y. Ko and K.B. Sharpless, *J. Org. Chem.*, 51 (1986) 3710–3712.
2 W.L. Nelson and T.R. Burke, *J. Org. Chem.*, 43 (1978) 3641–3645.
3 U. Peters, W. Bankova and P. Welzel, *Tetrahedron*, 43 (1987) 3803–3816.
4 J. Jurczak, S. Pikul and T. Bauer, *Tetrahedron*, 42 (1986) 447–488
5 A. Geerlof, B.W. Groen and J.A. Duine, *Eur. Pat. Appl.*, 90201651.8 (1990).
6 A. Geerlof and J.A. Duine, *Eur. Pat. Appl.*, 91201576.5 (1991).
7 J.B.A. van Tol, A. Geerlof, J.A. Jongejan and J.A. Duine, *Ann N.Y. Acad. Sci.*, 672 (1992) 462–470.
8 W.A. König, K.-S. Nippe and P. Mischnick, *Tetrahedron Lett.*, 31 (1990) 6867–6868.
9 J. Gal, *J. Chromatogr.*, 331 (1985) 349–357.
10 M. Chr. Philippi, J.A. Jongejan and J.A. Duine, in C. Laane, J. Tramper and M.D. Lilly (Editors), *Biocatalysis in Organic Media*, Elsevier, Amsterdam, 1987, pp. 279–284.
11 W.A. König, S. Lutz, G. Wenz, G. Görgen, Ch. Neumann, A. Gäbler and W. Boland, *Angew. Chem.*, 101 (1989) 180–181.
12 W.-Y. Li, H.L. Lin and D.W. Armstrong, *J. Chromatogr.*, 509 (1990) 303–324.
13 W. Dougherty, F. Liotta, D. Mondimore and W. Shum, *Tetrahedron Lett.*, 31 (1990) 4389–4390.
14 N.O.V. Sonntag, *Chem. Rev.*, 52 (1953) 237–416.
15 N.B. Lorette and W.L. Howard, in H.E. Baumgarten (Editor), *Organic Synthesis, Coll. Vol.*, 5 (1973) 5–7.
16 K.E. MaloneyHuss, *Synth. Commun.*, 15 (1985) 273–277.
17 C.R. Schmid, J.D. Bryant, M. Dowlatzedah, J.L. Phillips, D.E. Prather, R.D. Schantz, N.L. Sear and C.S. Vianco, *J. Org. Chem.*, 56 (1991) 4056–4058.
18 N. Nimura, H. Ogura and T. Kinoshita, *J. Chromatogr.*, 202 (1980) 375–379.
19 T. Kinoshita, Y. Kasahara and N. Nimura, *J. Chromatogr.*, 210 (1981) 77–81.
20 N. Nimura, A. Toyama and T. Kinoshita, *J. Chromatogr.*, 316 (1984) 547–552.
21 K.J. Miller, J. Gal and M. Ames, *J. Chromatogr.*, 307 (1984) 335–342.
22 N. Nimura, Y. Kasahara and T. Kinoshita, *J. Chromatogr.*, 213 (1981) 327–330.
23 J. Gal, *J. Chromatogr.*, 307 (1984) 220–223.
24 J.F. Allgire, E.C. Juenge, C.P. Damo, G.M. Sullivan and R.D. Kirchhoefer, *J. Chromatogr.*, 325 (1985) 249–254.
25 A.J. Sedman and J. Gal, *J. Chromatogr.*, 278 (1983) 199–203.
26 J. Gal, *J. Liq. Chromatogr.*, 9 (1986) 673–681.
27 Z. Tian, T. Hrinyo-Pavlina and R.W. Roeske, *J. Chromatogr.*, 541 (1991) 297–302.
28 J. Gal and R.C. Murphy, *J. Liq. Chromatogr.*, 7 (1984) 2307–2314.
29 O. Grech-Bélanger and J. Turgeon, *J. Chromatogr.*, 337 (1985) 172–177.
30 J. Gal, D.M. Desai and S. Meyer-Lehnert, *Chirality*, 2 (1990) 43–51.
31 H. Nishi, N. Fujimura, H. Yamaguchi and T. Fukuyama, *J. Chromatogr.*, 539 (1991) 71–81.
32 J.C. Sowden and H.O.L. Fischer, *J. Am. Chem. Soc.*, 64 (1942) 1291–1293.
33 V. Schurig and H.-P. Nowotny, *Angew. Chem.*, 102 (1990) 969–986.

Journal of Chromatography, 648 (1993) 131–137
Elsevier Science Publishers B.V., Amsterdam

CHROM. 25 355

High-performance liquid chromatography of neutral oligosaccharides on a β-cyclodextrin bonded phase column

Peter J. Simms[☆], Rebecca M. Haines and Kevin B. Hicks*

US Department of Agriculture, Agricultural Research Service, Eastern Regional Research Center, Philadelphia, PA 19118 (USA)

(First received March 9th, 1993; revised manuscript received June 2nd, 1993)

ABSTRACT

A β-cyclodextrin bonded phase HPLC column was used for the separation of neutral oligosaccharides derived from starch, cellulose, pullulan, xylan, inulin, and mannan. Rapid, high-resolution separations resulted when acetonitrile–water mixtures were used as mobile phases. Retention times for oligosaccharides were dependent on both monosaccharide composition and linkage types. Compared to aminoalkyl silica gel phases, commonly used for carbohydrate analysis, the β-cyclodextrin bonded phase appeared to be similar in selectivity and superior in durability. It is anticipated that β-cyclodextrin bonded phase HPLC columns may be useful alternatives to commonly used aminoalkyl-modified silica gels for the separation and analysis of neutral oligosaccharides.

INTRODUCTION

Oligosaccharides, produced from the enzyme or acid catalyzed hydrolysis of polysaccharides, are important compounds both biologically and chemically. Determining the composition and relative quantity of each oligosaccharide present in such hydrolysates has traditionally been a difficult challenge. In recent years, many HPLC methods have been developed for this purpose. Separations of oligosaccharides up to about degree of polymerization (DP) 12 have been obtained on various ion exchange resins [1–5]. Oligosaccharides can also be separated on reversed-phase columns using a simple mobile phase, but the chromatograms are often difficult to interpret because anomers of each oligosaccharide are usually separated [6–8]. Chemically bonded amino-type columns give good resolution of oligosaccharides up to DP 30 [9–12], but these stationary phases can be unstable and degrade rapidly. The development of high-performance anion-exchange chromatography coupled with pulsed amperometric detection (HPAEC–PAD) now allows for the separation of oligosaccharides up to DP 50 and beyond [13,14], as well as the separation of branched oligosaccharides [15,16]. However, specialized equipment is required for these analyses and quantification of oligosaccharides by pulsed amperometric detection is problematic.

In the present study, we examined the use of a β-cyclodextrin bonded phase HPLC column to separate oligosaccharides. Cyclodextrin bonded phase columns have been used primarily for separation of isomers [17–19]. Such separations were accomplished by the formation of transient inclusion complexes between the analytes and the cyclodextrin cavity. Recently [20,21] it has been shown that small molecular mass carbohydrates can be separated on a cyclodextrin

* Corresponding author.
☆ Present address: Greenwich Pharmaceuticals, Horsham, PA 19044-5299, USA.

bonded stationary phase column. We now report on the usefulness of this stationary phase for the separation of neutral oligosaccharides.

EXPERIMENTAL[a]

Materials

A malto-oligosaccharide sample (M250) was obtained from the Grain Processing Corp. (Muscatine, IA, USA). Pullulan and xylan were purchased from Pfanstiehl Laboratories (Waukegan, IL, USA). Mannan hydrolyzates were a gift of Dr. Allan G.W. Bradbury (Kraft General Foods, Tarrytown, NY, USA). Dextrans (mol. mass 70 000) were purchased from Pharmacia (Uppsala, Sweden). Amberlite IRA-94 resin, free-base form, was purchased from Sigma (St. Louis, MO, USA). Cello-oligosaccharides were prepared using a procedure to be published elsewhere. The Amberlite XAD-4 and MB-3 resins were purchased from Rohm and Haas (Philadelphia, PA, USA). All HPLC solvents were purchased from Baxter (Muskegan, MI, USA) and filtered through a 0.45-μm Nylon filter. Water used for HPLC analyses was purified through a Milli-Q filtration system from Millipore (Bedford, MA, USA).

Isolation of inulin oligosaccharides

Inulin oligosaccharides were isolated from Jerusalem artichokes as follows: Jerusalem artichokes (wet mass 500 g) were peeled and then juiced in an Acme Supreme Model 6001 Juicerator lined with Whatman No. 1 filter paper. The juice was collected in a beaker containing 500 ml of washed Amberlite MB-3 resin, and then passed through a glass column packed with an additional 100 ml of the same resin. The column was washed with water and the sample plus the wash were then decolorized by passing them through a glass column containing 200 ml of XAD-4 resin and 50 ml of MB-3 resin. The eluted sample was then evaporated to dryness under reduced pressure. Inulin oligosaccharide standards were purified by HPLC using a preparative-sized (300 × 22 mm I.D.) HPX-42A Ag^+ form column. The details of this purification will be published elsewhere.

Partial acid hydrolyses

Partial acid hydrolyses of dextran, pullulan, and xylan were performed by dissolving the polysaccharide (2 g) in sulfuric acid (0.1 *M*, 25 ml) and refluxing the reaction mixture for one hour with stirring. The reaction was cooled in an ice water bath, and afterwards the sample was passed through a column that contained 30 ml of Amberlite IRA-94 resin. The effluent was diluted with ethanol so that the final concentration was 50:50. The mixture was then centrifuged (10 000 *g*, 20 min) to remove precipitates. The supernatant was then evaporated to dryness under reduced pressure. The resulting sample was used for chromatographic analyses.

Chromatography

β-Cyclodextrin bonded phase columns (Cyclobond I, 250 mm × 4.6 mm I.D.) were purchased from Rainin Instrument (Woburn, MA, USA). According to the manufacturer, Advanced Separation Technologies (Whippany, NJ, USA), the Cyclobond I phase is formed by coupling β-cyclodextrin molecules through a 10 atom spacer arm to 5-μm spherical silica gel particles. The resulting percentage of carbon is approximately 6.5%. The separation column was preceded by a cartridge-type precolumn (Alltech, Deerfield, IL, USA) packed with reversed-phase (C_{18}-bonded) silica gel. The HPLC system used was a Gilson Model 303 dual pump system equipped with a 811 dynamic mixer and a Rheodyne Model 7125 fixed loop (20-μl) injector. Samples were detected with a Waters 401 differential refractometer, and the data were recorded with a Dynamax HPLC Method Manager version 1.2. Oligosaccharide standards were made up at concentrations of approximately 1 to 3 mg/ml by first dissolving pure standards in water, then adding an equal amount of acetonitrile to produce an acetonitrile–water (50:50) solution. Samples were passed through a 0.45-μm Nylon filter prior to injection.

RESULTS AND DISCUSSION

β-Cyclodextrin bonded phase columns have

[a] Reference to a brand or firm name does not constitute endorsement by the US Department of Agriculture over others of a similar nature not mentioned.

been reported [20] to separate sugars in the same way as normal-phase silica gel columns that contain alkylamino, diol, or polyol groups. We have now found that this stationary phase is also useful for separation of larger oligosaccharides. Fig. 1 shows the HPLC separation of two types of gluco-oligosaccharides on this phase using acetonitrile–water eluents. Partial resolution, in ascending order of amylose-derived 1,4-linked (malto-) and dextran-derived 1,6-linked (isomalto-) oligosaccharides up to DP 25 and 15, respectively, was obtained in under 30 min using an acetonitrile–water (65:35) mobile phase (Fig. 1A and B). The resolution between adjacent pairs of oligosaccharides increased slightly up to about DP 12 (Fig. 2) and then gradually decreased (data not shown). Increasing the percentage of acetonitrile to 70% (Fig. 1C and D) increased the retention times of all oligosaccharides, allowed complete separation of early-eluting DP oligomers, and provided increased resolution for all DP pairs between 3 and 12

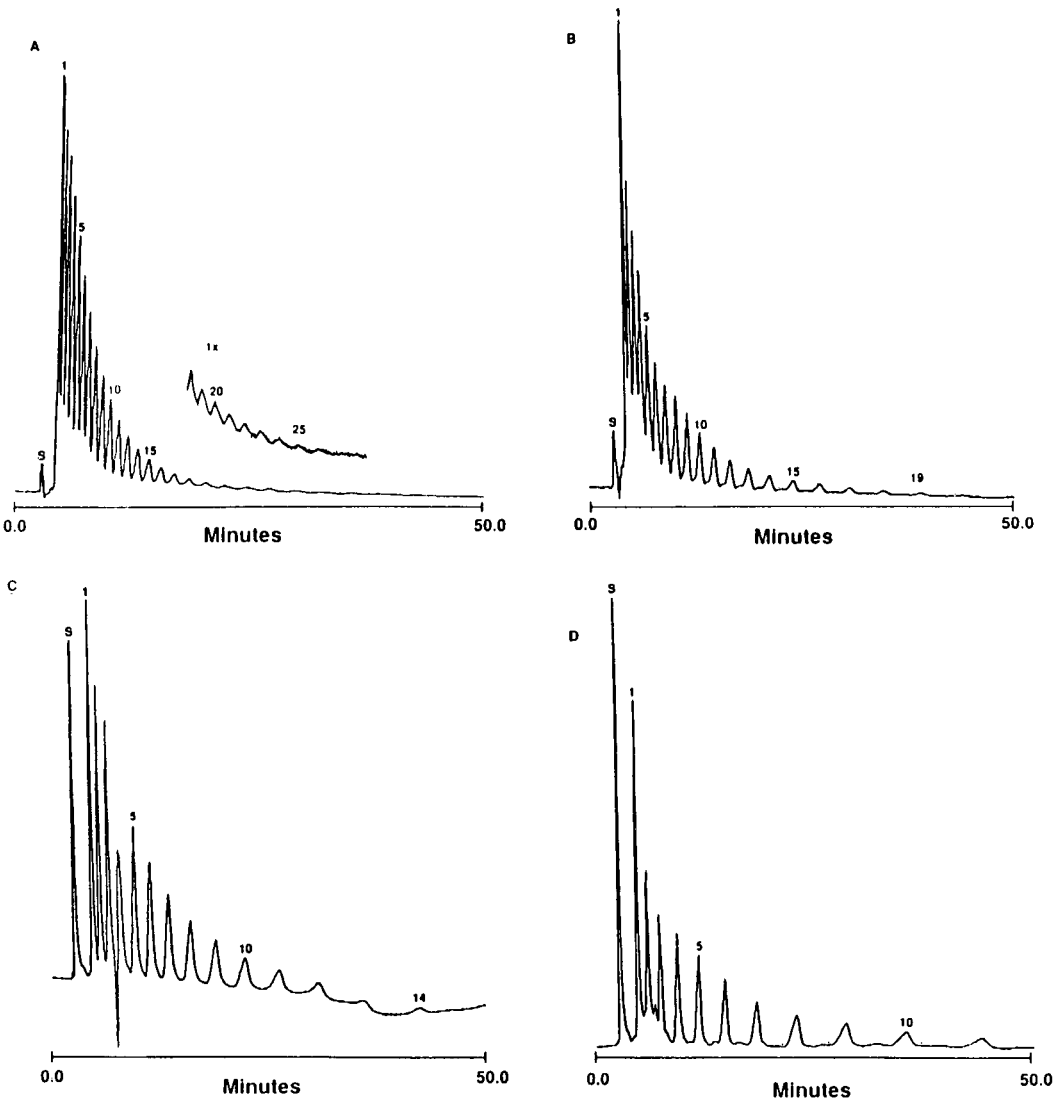

Fig. 1. The HPLC separation of (A) malto- and (B) isomalto-oligosaccharides using an acetonitrile–water (65:35) mobile phase and (C) malto- and (D) isomalto-oligosaccharides using an acetonitrile–water (70:30) mobile phase on a β-cyclodextrin bonded phase column (Cyclobond I, 250 mm × 4.6 mm I.D.). The column was operated at room temperature and 1 ml/min flow-rate with refractive index detection. The numbers above the peaks represent the DP values; S represents the solvent peak.

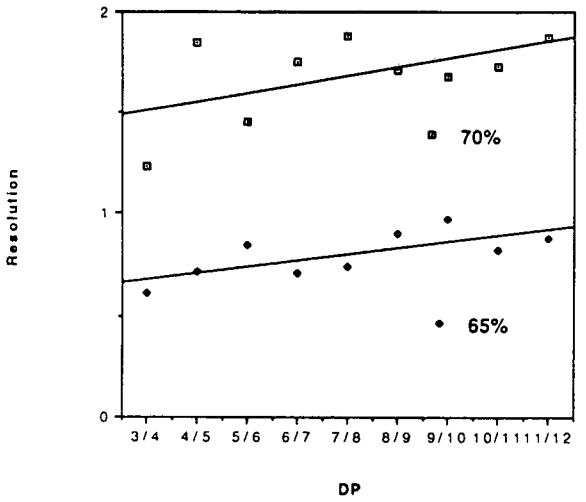

Fig. 2. Resolution values calculated for adjacent peaks of malto-oligosaccharides using mobile phases containing either 65% or 70% acetonitrile. Resolution values were calculated by the following equation, $R = \Delta t/t_w$, where Δt is the distance between adjacent peaks, and t_w is the average width of the peaks at the baseline.

(Fig. 2). At the higher percentage of acetonitrile, however, oligosaccharides above approximately DP 11–14 did not elute within 50 min. At this acetonitrile concentration, it is expected that these larger oligosaccharides would be relatively insoluble and could precipitate onto the stationary phase, eventually leading to decreased column performance.

The difference in retention times between different linkage-classes of gluco-oligosaccharides is readily apparent in Fig. 3. Malto-oligosaccharides generally eluted at shorter retention times than the corresponding isomalto-oligosaccharides. It was possible to resolve similar DP values of isomalto- and malto-oligosaccharides starting at DP 8 with a 70% acetonitrile mobile phase (Fig. 3A). Increasing the percentage of acetonitrile to 75% allowed resolution of oligosaccharides above DP 3 (Fig. 3B).

Pullulan, a mixed-linkage homopolysaccharide composed of α-1,6 linked maltotriose units, was hydrolyzed and the resulting oligosaccharides were analyzed on this stationary phase. The chromatogram (Fig. 4A) was complex and appeared to contain peaks grouped in a unique triplet pattern. The chromatogram obtained with a higher concentration of acetonitrile in the

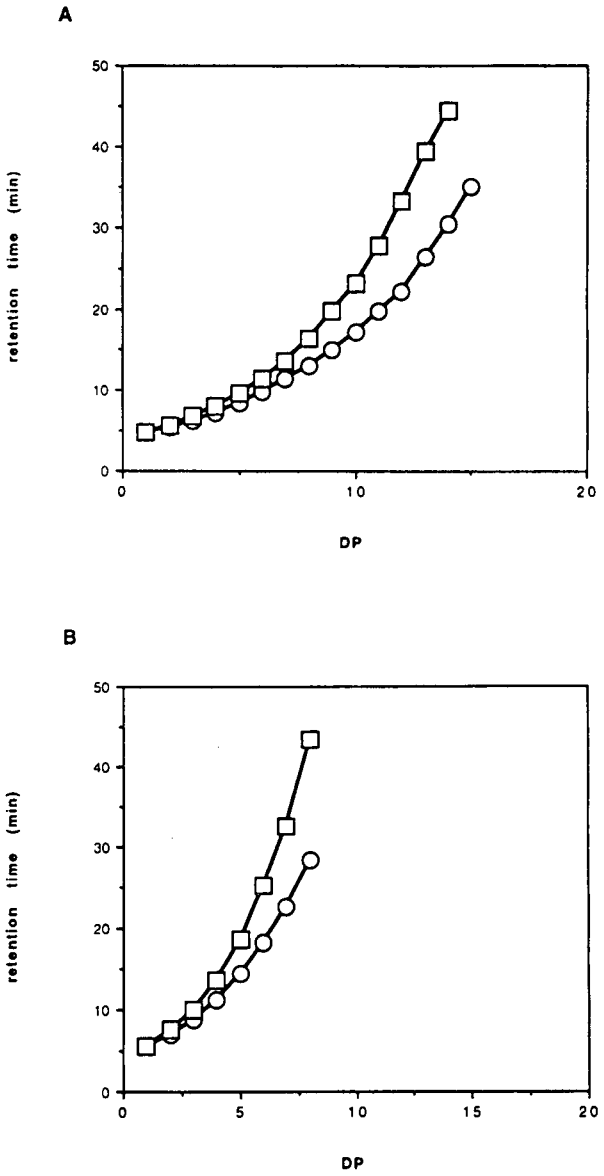

Fig. 3. Graph of retention time *versus* DP for two different classes of gluco-oligosaccharides [(○) malto- and (□) isomalto-series)] on a β-cyclodextrin column with (A) acetonitrile–water (70:30) and (B) acetonitrile–water (75:25) mobile phase. Other conditions as in Fig. 1.

mobile phase resolved some of the former peaks into multiplets (Fig. 4B). These additional, closely eluting peaks are thought to represent oligosaccharides with the same DP value, but with varying combinations of α-1,4 and α-1,6 linkages.

β-1,4 Linked manno- and cello-oligosaccha-

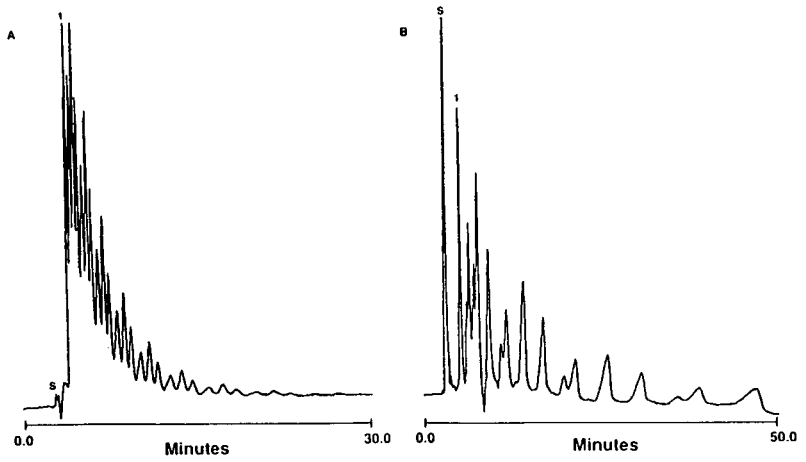

Fig. 4. The separation of pullulan-derived oligosaccharides on the β-cyclodextrin column with an (A) acetonitrile–water (65:35) and (B) acetonitrile–water (70:30) mobile phase. Other conditions as in Fig. 1.

rides from DP 2 to 8 were also readily separated (chromatograms not shown) under similar conditions used for malto-oligosaccharides. Because of the close structural similarity, it was not possible to resolve similar DP isomers of all three classes in the same chromatogram under DP levels of about 7 (Fig. 5).

Inulin-derived oligosaccharides, up to DP 13 ($GlcFru_{12}$), were separated in approximately 20 min using an acetonitrile–water (70:30) mobile phase (Fig. 6A). These oligosaccharides are composed of a sucrose molecule with additional β-1,2 linked fructofuranose units. Better resolution of the early-eluting fructo-oligosaccharides could be obtained with an acetonitrile–water (75:25) mobile phase (Fig. 6B). Under most conditions, the inulin-derived fructo-oligosaccharides eluted earlier than the corresponding manno- and isomalto-oligosaccharides (Fig. 7).

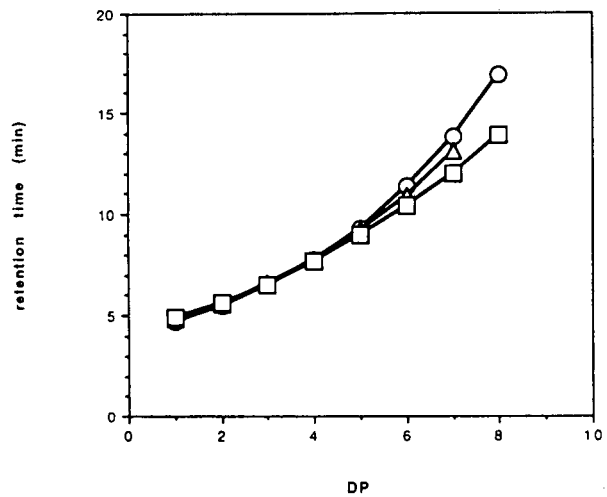

Fig. 5. Dependence of DP on retention time of (○) manno-, (□) malto-, and (△) cello-oligosaccharides on a Cyclobond I column eluted with acetonitrile–water (70:30). Other chromatographic conditions as in Fig. 1.

β-1,4 Linked xylo-oligosaccharides, DP 2–8, were well separated using an acetonitrile–water (80:20) mobile phase (chromatogram not shown). At acetonitrile concentrations lower than 80%, however, DP 2–5 were weakly retained and poorly resolved. The shorter retention times for xylo- *versus* gluco-oligosaccharides would be expected on normal-phase chromatographic systems because the C-5 methylene carbon of the xylopyranose residues results in oligosaccharides that are less polar than the corresponding gluco-oligosaccharides.

The retention times of the fructo- and xylo-oligosaccharides were consistently shorter than the corresponding gluco- and manno-oligosaccharides. These trends are similar to that noticed by Armstrong and Jin [20] for the separation of monosaccharides on this stationary phase. The order of retention for monosaccharides was shown to be pentoses < ketohexoses < aldohexoses. In this report we show that this trend continues for homo-oligosaccharides composed of these monosaccharide units. Thus, the relative

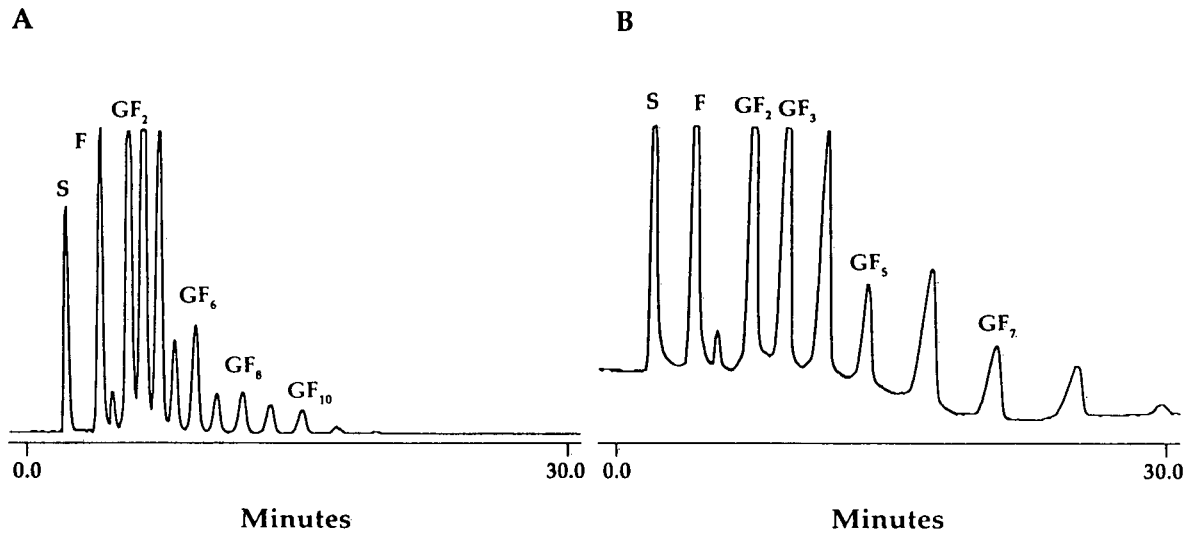

Fig. 6. Separation of inulin-derived oligosaccharide standards using (A) acetonitrile–water (70:30) and (B) acetonitrile–water (75:25). F = fructose, GF_2 = 1-kestose (DP 3), GF_4 = DP 5, etc. Other conditions as in Fig. 1.

retention is: xylose-containing homo-oligosaccharides < those composed of fructose < those composed of glucose or mannose. It is noteworthy that this same order of elution was found when these oligosaccharides were separated on polar alkylamino silica gel stationary phases [21], indicating that the selectivity of these two phases is similar. Alkylamino-type silica gel phases provide excellent selectivity and capacity for carbohydrates, but they are known to have a comparatively short "life" [22]. Diol-modified silica gels [22] and polyamine-bonded vinyl alcohol co-polymer gel columns [15] have been suggested as more durable alternatives. It is not presently known if the Cyclobond I column would be more durable than improved amino-type organic polymer gel columns [15] since they have not been directly compared. The Cyclobond I column is a much more versatile column, however, since it may be also used with different mobile phases, to separate isomeric chiral molecules using an inclusion complexation mode [17–19]. A disadvantage of the diol phases, is that they resolve anomeric forms of reducing sugars, leading to complex chromatographic peaks that are difficult to integrate and quantify. The cyclodextrin stationary phases can be used to resolve anomers, but only under conditions of low temperature (0°C) and with special mobile phases [23]. Under the conditions used in our study, all oligosaccharides eluted with relatively narrow and symmetrical peaks, indicating the absence of anomer resolution. It is not clear why sugar anomers are not separated under these conditions. Perhaps the interaction between the cyclodextrin functionality and the reducing sugar leads to a significant increase in

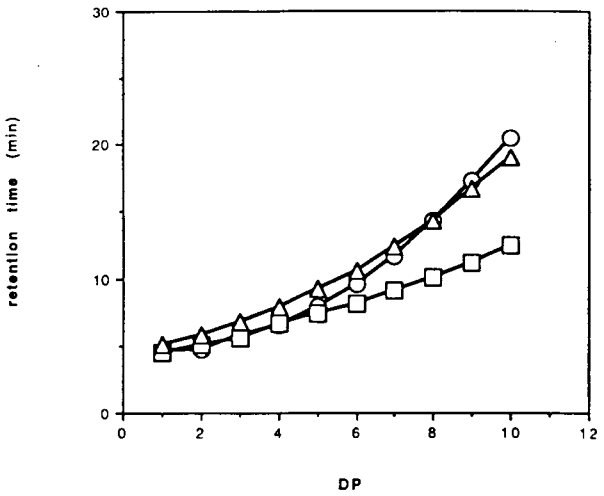

Fig. 7. Retention time *versus* DP for (○) manno-, (□) fructo-, and (△) isomalto-oligosaccharides on the β-cyclodextrin bonded phase column. The analyses were obtained using an acetonitrile–water (70:30) mobile phase. Other conditions as in Fig. 1.

the sugar's mutarotation rate. This action [23] would prevent the separation of the two anomeric forms. It was previously reported [20] that cyclodextrin bonded phases are quite durable for separations of sugars. This was confirmed in this study for larger oligosaccharides; we noted negligible changes in retention times during approximately eight months of heavy use.

CONCLUSION

The β-cyclodextrin bonded phase column was found to be quite useful for the separation of a variety of different neutral oligosaccharides. Retention of oligosaccharides was dependent on both sugar composition and linkage. A normal-phase separation mechanism appeared to be operating since increasing the percentage of acetonitrile, in all cases, led to an increase in oligosaccharide retention times. Because of its selectivity and durability, it is likely that this phase could replace alkylamino-type normal phases for some oligosaccharide applications.

ACKNOWLEDGEMENTS

P.S. thanks the Agricultural Research Service for an Administrator-funded Research Associate fellowship. The authors also thank Drs. A.T. Hotchkiss, Jr. and P.D. Hoagland for helpful discussions during the preparation of this manuscript.

REFERENCES

1 H.D. Scobell and K.M. Brobst, *J. Chromatogr.*, 212 (1981) 51–64.
2 K. Brunt, *J. Chromatogr.*, 246 (1982) 145–151.
3 J. Havlicek and O. Samuelson, *Anal. Chem.*, 47 (1975) 1854–1857.
4 K.B. Hicks and A.T. Hotchkiss, Jr., *J. Chromatogr.*, 441 (1988) 382–386.
5 A.G.J. Voragen, H.A. Schols, M.F. Searle-van Leeuwen, G. Beldman and F.M. Rombouts, *J. Chromatogr.*, 370 (1986) 113–120.
6 L.A.Th. Verhaar, B.F.M. Kuster and H.A. Claessens, *J. Chromatogr.*, 284 (1984) 1–11.
7 G.D. McGinnis, S. Prince and J. Lowrimore, *J. Carbohydr. Chem.*, 5 (1986) 83–97.
8 N.W.H. Cheetham, P. Sirimanne and W.R. Day, *J. Chromatogr.*, 207 (1981) 439–444.
9 F.M. Rabel, A.G. Caputo and E.T. Butts, *J. Chromatogr.*, 126 (1976) 731–740.
10 V. Kahle and K. Tesarik, *J. Chromatogr.*, 191 (1980) 121–128.
11 W.R. Praznik, R.H.F. Beck and E. Nitsch, *J. Chromatogr.*, 303 (1984) 417–421.
12 T. Akiyama, *J. Chromatogr.*, 588 (1991) 53–59.
13 K. Koizumi, Y. Kubota, T. Tanimoto and Y. Okada, *J. Chromatogr.*, 464 (1989) 365–373.
14 A.T. Hotchkiss, Jr. and K.B. Hicks, *Anal. Biochem.*, 184 (1990) 200–206.
15 K. Koizumi, M. Fukuda and S. Hizukuri, *J. Chromatogr.*, 585 (1991) 233–238.
16 R.N. Ammeraal, G.A. Delgado, F.L. Tenbarge and R.B. Friedman, *Carbohydr. Res.*, 215 (1991) 179–192.
17 J.I. Seeman, H.V. Secor, D.W. Armstrong, K.D. Ward and T.J. Ward, *J. Chromatogr.*, 483 (1989) 169–177.
18 D.W. Armstrong and W. Li, *Chromatography*, 2 (1987) 43–48.
19 M. Krause and R. Galensa, *J. Chromatogr.*, 588 (1991) 41–45.
20 D.W. Armstrong and H.L. Jin, *J. Chromatogr.*, 462 (1989) 219–232.
21 Z.L. Nikolov, M.M. Meagher and P.J. Reilly, *J. Chromatogr.*, 321 (1985) 393–399.
22 C. Brons and C. Olieman, *J. Chromatogr.*, 259 (1983) 79–86.
23 D.W. Armstrong and H.L. Jin, *Chirality*, 1 (1989) 27–37.

Journal of Chromatography, 648 (1993) 139–149
Elsevier Science Publishers B.V., Amsterdam

CHROM. 25 360

Identification and determination of individual sophorolipids in fermentation products by gradient elution high-performance liquid chromatography with evaporative light-scattering detection

A.M. Davila, R. Marchal, N. Monin and J.P. Vandecasteele*

Institut Français du Pétrole, 1 et 4 Avenue de Bois-Préau, B.P. 311, 92506 Rueil-Malmaison Cedex (France)

(First received December 29th, 1992; revised manuscript received June 11th, 1993)

ABSTRACT

High-performance liquid chromatography (HPLC) was used for the characterization of sophorolipids, one of the most important types of glycolipid biosurfactants. By using gradient elution with a water–acetonitrile mixture on a reversed-phase (C_{18}) column and evaporative light-scattering detection, resolution of all the important individual sophorolipids present in fermentation products was achieved. In addition to HPLC, a combination of techniques involving selective production by fermentation of sophorolipids, chemical conversions of the products, separation methods and, for identification of lipidic chains of sophorolipids, gas chromatography and mass spectrometry was used. This led to the identification of almost all significant compounds observed in HPLC, including several previously unreported sophorolipids. As a result, a rapid method is now available for investigations of the influence of fermentation conditions on the nature and quantitative distribution of the sophorolipid products obtained.

INTRODUCTION

Among glycolipids, one of the main classes of biosurfactants, sophorose lipids produced from glucose and a lipidic carbon source by yeasts such as *Candida bombicola* have long been the subject of much interest [1,2]. Although the structure of sophorolipids has been studied in detail [1,3–5], much less information is available concerning their production [2], the main point investigated being the relationship between the nature of the lipid carbon source (vegetable oils, fatty acid esters, *n*-alkanes) and the structure of the products formed [6,7]. The production conditions, however, appear to be important both for the yield, which can be fairly high [8], and for composition of the products [6–8].

Analytical difficulties probably account to a large extent for this relative paucity of information, as the sophorolipid mixture produced by fermentation is complex. The purpose of this work was to devise an analytical tool allowing the rapid determination of all quantitatively significant sophorolipid products, in order to be able to follow the progress of fermentation under various conditions. High-performance liquid chromatography (HPLC) with gradient elution was selected for this purpose, detection being achieved with an evaporative light-scattering detector [9–12]. This detector is compatible with gradient elution as its principle makes it independent of the nature of the mobile phase. Further, as its response does not depend on the presence of specific chemical groups, it has been

* Corresponding author.

0021-9673/93/$06.00

shown to be appropriate for the determination of compounds such as lipids [12–18] and surfactants [19]. In the work reported here, HPLC with gradient elution was found in the case of sophorolipids to be a key component in a strategy involving a combination of techniques resulting in identification of individual sophorolipids in a complex mixture.

EXPERIMENTAL

Sophorolipid production

Sophorolipids were produced by *Candida bombicola* CBS 6009 at 25°C in a 4-l laboratory fermenter under conditions of aeration (0.5 v v^{-1} min^{-1}) and of vigorous agitation (800 rpm) produced by a centrifuge propeller. The initial culture medium (2.2 l) had the following mineral composition per litre: 4 g of $(NH_4)_2SO_4$, 1 g of KH_2PO_4, 0.5 g of $MgSO_4 \cdot 7H_2O$ and 5 g of dried cornsteep liquor (Roquette, Lille, France). During the cultures (185 h), the pH of this medium was maintained constant at 3.5 by automatic addition of a 4 *M* NaOH solution. Ethyl esters of rapeseed oil and glucose were the carbon sources. Ethyl esters were fed continuously at a constant rate of 1.75 ml h^{-1} per litre of the initial culture medium. Glucose was added according to two different procedures. In the first, it was supplied in excess from the beginning to the end of the culture by daily additions of 50 g l^{-1} (referred to the initial fermentation volume). Decantation of sophorolipids was triggered by heating the broth for 10 min at 100°C. The lyophilized sophorolipid layer is referred to as sample A. Sample B was prepared according to the second procedure. Glucose (50 g l^{-1}) was added only to the initial medium without any further addition. The broth was centrifuged and the supernatant cleared of cells was then lyophilized. Owing to the different fermentation procedures, widely different sophorolipid compositions were observed in samples A and B.

Chemical conversions of sophorolipids

Catalytic hydrogenation. A 40-mg amount of freeze dried sophorolipids was dissolved in 3 ml of anhydrous methanol. The solution was placed in a 20-ml seal-stoppered tube with 40 mg of a palladium catalyst (5% on $CaCO_3$). The air volume was replaced with hydrogen under 1 bar relative pressure and the sample was incubated with shaking at 60°C for 4 h. At the end of the reaction, the remaining hydrogen was flushed off with nitrogen and the methanol phase was collected and evaporated at room temperature under a stream of nitrogen.

Methylation. Methyl esters of acidic sophorolipids were obtained by incubating at 60°C with shaking for 4 h 40–60 mg of dried sophorolipids and 100 mg of acidic resin (Amberlyst 15; Rohm and Haas, Philadelphia, PA, USA) in 3 ml of methanol. Methanol was then evaporated under a stream of nitrogen. Methanolysis of hydroxy fatty acid moieties (see below) did not take place under these conditions, but with lactonic forms limited ring opening (10–15%) took place. The procedure was used in order to improve the chromatographic resolution of acidic sophorolipids in samples containing small amounts of lactonic forms.

Alkaline hydrolysis. Alkaline hydrolysis of sophorolipids led to the deacetylated acidic structures of the glycolipids. Sophorolipids (100 mg) were dissolved in 10 ml of a mixture of 5 ml of methanol, 5 ml of water and 1.5 g of NaOH and placed in a tube sealed with a PTFE-lined screw-cap. The tube was heated for 30 min in a boiling water-bath. After cooling, the reaction medium was carefully acidified to pH 3.0 by dropwise addition of concentrated H_2SO_4. A 20-ml volume of methanol was added and the mixture was filtered. The clarified filtrate was evaporated under a stream of nitrogen.

Methanolysis. For the determination of the hydroxy fatty acid moieties, sophorolipids (acids and lactones) were cleaved and transesterified in the presence of methanol and H_2SO_4 to yield the methyl esters of hydroxy acids. Amounts of 20–50 mg of sophorolipids were dissolved in a mixture of 2 ml of 1% H_2SO_4 in methanol and 1 ml of toluene containing 2 g l^{-1} of arachidic acid as internal standard. This mixture was poured into a tube that was tightly sealed with a Viton cap (DuPont, Wilmington, DE, USA) and heated for 1 h at 100°C. The resulting hydroxy fatty acid methyl esters were extracted twice with 5 ml of cyclohexane in the presence of 5 ml of 50

g l^{-1} NaCl solution. The cyclohexane phase was cleared by centrifugation and dried under a stream of nitrogen. These conditions gave satisfactory recoveries of hydroxy fatty acid esters for quantitative determination.

Good reproducibility in gas chromatographic (GC) analysis was achieved by silylation of the hydroxy group. Dried methyl ester samples were treated with 0.25 ml of Sylon TP (Supelco, Bellefonte, PA, USA) and 1.75 ml of pyridine at 60°C for 30 min. The silylated hydroxy fatty acid methyl esters were extracted with 10 ml of heptane in the presence of 2 ml of distilled water and the organic layer was used for GC analysis.

Chromatographic procedures

Thin-layer chromatography. Thin-layer chromatography (TLC) was performed on sophorolipids using 20 cm × 20 cm × 1 mm Kiesegel 60 F_{254} plates (Merck, Darmstadt, Germany). The developing solvent was chloroform–methanol–water (65:15:2). Two detection techniques were used: exposure to iodine vapour and vaporization of a solution of α-naphthol in a mixture of sulphuric acid, ethanol and water.

For recovery of the separated products, the spots were scraped off after detection with iodine vapour. The recovered material was placed in a tube and determination was effected using the anthrone reagent [20]. Sophorolipids could also be eluted with the developing solvent for further chromatographic analysis.

Gas chromatography. Methylated and silylated hydroxy fatty acids proceeding from sophorolipid conversion were analysed using a 30 m × 0.32 mm I.D. DB-5 column (J&W Scientific, Folsom, CA, USA) with temperature programming (from 150 to 290°C at 4°C min^{-1}). Identification of these compounds was performed by GC–MS using a 25 m × 0.32 I.D. CP-Sil 8 CB column (Chrompack, Middelburg, Netherlands) under the same chromatographic conditions and an MS 80 mass spectrometer (Kratos, Manchester, UK).

High-performance liquid chromatography. Isocratic HPLC separations of sophorolipids were performed using a two-column system. The first column was an Ultrabase C_{18}, 5 μm (300 mm × 4.6 mm I.D.), from SFCC-Shandon (Eragny, France) and the second was a Lichrosorb 10 RP-8, 5 μm (250 mm × 4.6 mm I.D.), from Chrompack. Elution was performed with acetonitrile–water (70:30, v/v) at a rate of 0.7 ml min^{-1}. HPLC-grade acetonitrile from SDS (Pepin, France) and triply distilled water were used. The instrumentation involved an SP 8875 automatic sampler and an SP 8810 isocratic pump from Spectra-Physics France (Les Ullis, France), an injection valve with a 20-μl sampling loop and an SP 8430 differential refractometric detector from Spectra-Physics.

Gradient elution HPLC separations were performed with a system supplied by Kratos, consisting of a Spectroflow 450 solvent programmer which controlled two Spectroflow 400 pumps. Analytical gradient HPLC was performed using a Hypersil C_{18}, 5 μm (150 mm × 4.6 mm I.D.) column from Interchim (Montluçon, France). The flow-rate was 1 ml min^{-1} and the composition of the acetonitrile–water eluent was programmed from 2 to 70% acetonitrile in 48 min. For sample injection, a Rheodyne Model 7128 valve with a 20-μl sample loop was used. For detection, a DDL 21 evaporative light-scattering (ELS) detector (mass detector) from Cunow (Cergy Saint Christophe, France) was used. For preparative gradient HPLC, a 600-μl sampling loop was used. The column was an Ultrabase C_{18} (250 mm × 10 mm I.D.) from SFCC-Shandon. The flow-rate was 2.5 ml min^{-1} and the composition of the acetonitrile–water eluent was programmed from 50 to 85% acetonitrile in 40 min followed by a 15-min isocratic elution step. Separation was monitored by UV detection (UV 490 spectrophotometer from Waters, Milford, MA, USA) at 210, 233 and 268 nm.

Data acquisition in liquid and gas chromatography was done with an HP 1000/A600 system (Hewlett-Packard, Sunnyvale, CA, USA).

Nuclear magnetic resonance (NMR) spectroscopy

^{1}H and ^{13}C NMR spectroscopy were performed with an MSL 400 spectrometer (Bruker, Karlsruhe, Germany). Trimethylsilane was used as an internal standard. The solvent used was $C^{2}H_{3}O^{2}H$. In ^{13}C NMR, the gate inverse sequence was used. For ^{1}H NMR, one- and two-

dimensional NMR (COSY) techniques were used in chemical group identification.

RESULTS AND DISCUSSION

Production of sophorolipid mixtures with different compositions by varying the fermentation conditions

Sophorolipids present in fermentation broths of *Candida bombicola* are a mixture, the structures of which are presented in Fig. 1. The main structural forms identified are lactones acetylated or not in positions 6′ and 6″ of sophorose and acids acetylated or not in position 6′ of sophorose [5]. Each of these forms constitutes a structural class of compounds. Individual homologous compounds in each class differ in their hydroxy fatty acid moiety, which varies in chain length (ranging mostly from C_{16} to C_{20}), in the number of unsaturations (between 0 and 2) and in the position of the hydroxyl group ($\omega - 1$ or ω). All classes of sophorolipids discussed here are listed in Table I. The shorthand notation adopted to designate classes and individual sophorolipids is also presented.

In a previous study, sophorolipid production from glucose and rapeseed ethyl esters under optimized conditions was described in detail [8]. Further work was devoted to the investigation of the influence of the supply mode of these substrates on the composition of the sophorolipids produced.

The structural classes of the sophorolipid mixtures produced using different fermentations

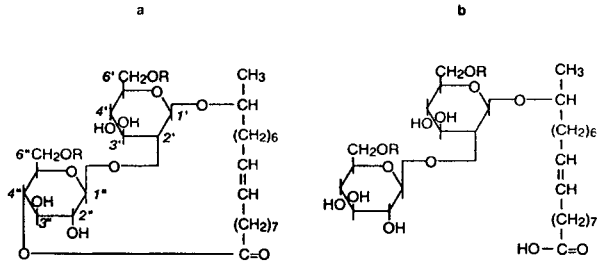

Fig. 1. Structural classes of sophorolipids. Main classes are represented for the case of the usually most abundant individual compound where the constitutive hydroxy fatty acid is 17-hydroxyoctadecenoic acid (17-hydroxyoleic acid). R = H or CH_3CO. (a) 1′,4″-Lactone classes; (b) acid classes.

TABLE I

SOPHOROLIPIDS DISCUSSED AND NOTATION USED

Structural class	Notation used[a]
1′,4″-Lactone 6′6″-diacetate[b]	Sl-4″L6′a6″a
1′,4″-Lactone 6′-monoacetate[c]	Sl-4″L6′a
1′,4″-Lactone 6″-monoacetate[b]	Sl-4″L6″a
1′,4″-Lactone[b]	Sl-4″L
1′,6′-Lactone[b]	Sl-6′L
1′,6″-Lactone[b]	Sl-6″L
Acid 6′6″-diacetate[c]	Sl-A6′a6″a
Acid 6′-monoacetate[b]	Sl-A6′a
Acid 6″-monoacetate[c]	Sl-A6″a
Acid[b]	Sl-A

[a] Notation: Sl, sophorolipid; L, lactone; A, acid; a, acetyl. Methyl ester derivatives, discussed in the text, are denoted mE. Individual sophorolipids are designated by adjunction of the notation for the constituent hydroxy fatty acid, *e.g.*, Sl-(17-OH C_{18}:1) 4″L6′a6″a represents (17-hydroxyoctadecenoic)-1′,4″-lactone 6′,6″-diacetate sophorolipid.

[b] Structures already described in the literature.

[c] Structures detected in this study.

conditions were determined after separation by TLC with reference to the characterization by Asmer *et al.* [5]. The relative compositions of the fermentation mixtures were obtained by scraping off the spots and determination using the anthrone method. Two different procedures of substrate supply allowing strongly preferential production of either lactonic or acidic forms of sophorolipids were developed. As shown in Table II, when glucose was supplied in excess throughout the fermentation, a sophorolipid mixture with a high content in lactonic forms (sample A) was obtained. In contrast, when glucose was only supplied to the culture in the growth phase, acidic forms were largely predominant (sample B). These two samples were used in this work for identification of the various sophorolipid components.

Resolution of sophorolipid classes by HPLC

Separation of the sophorolipid mixtures produced by fermentation was investigated using HPLC with isocratic elution and refractometric detection. After preliminary tests to select a stationary and a mobile phase, the resolution of the main components was obtained with two

TABLE II

RESOLUTION OF THE SOPHOROLIPID MIXTURES FROM FERMENTATIONS A AND B AS DETERMINED BY TLC

Sophorolipid classes			Composition (%)	
TLC spot[a]	R_F	Structure present	Sample A	Sample B
SL-1	0.55	Sl-4″L6′a6″a	51	3
SL-2	0.43	Sl-4″L6″a	3	1
SL-3	0.33	Sl-4″L	18	10
SL-4a, b	0.19	Sl-6′L + Sl-6″L	<1	<1
SL-5 + SL-6	0.10	Sl-A6′a + Sl-A	28	86

[a] Terminology according to Asmer *et al.* [5].

columns in series (a C_{18} and a C_8) and an eluent consisting of acetonitrile–water. Fig. 2 shows the chromatogram obtained for sample A. The lactonic forms were eluted separately at the end of the chromatographic run, but the acidic forms which were eluted ahead were not clearly separated.

In order to improve the separation of the acidic forms, an elution gradient obtained by varying the acetonitrile-to-water ratio was tested. The refractometric detector, which could not be used with gradient elution, was replaced with an ELS detector, which gave satisfactory results.

With gradient elution HPLC, a general strategy for identification of the individual sophorolipids contained in the fermentation mixture was elaborated (Fig. 3). The sophorolipid mixtures were separated into their structural classes by TLC and each isolated class (sample A1) was submitted to gradient HPLC. The elution orders with gradient mode and isocratic mode HPLC were similar. The acidic forms were eluted ahead, followed successively by the non-acetylated lactones and then the monoacetylated and diacetylated lactones. Separation of acetylated and non-acetylated acidic classes in TLC

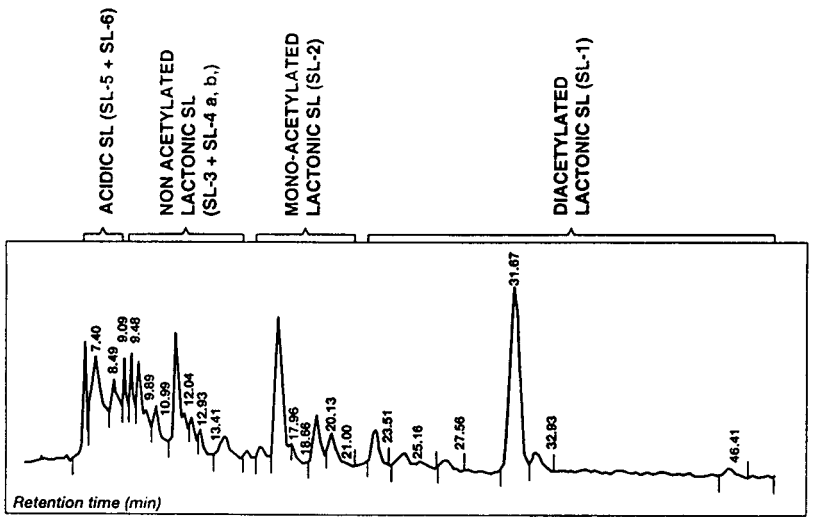

Fig. 2. Separation of a mixture of sophorolipids (sample A) by isocratic HPLC with refractometric detection. For conditions, see Experimental. The locations on the chromatogram of the elution zones for the spots separated in TLC (see Table II) are indicated.

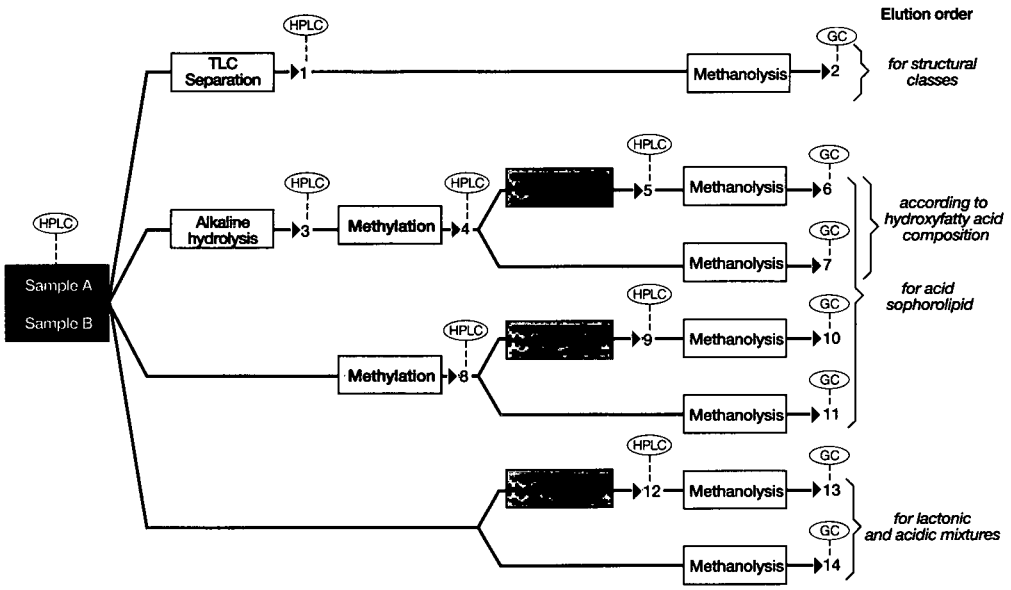

Fig. 3. General strategy for identification of individual sophorolipids. The type of information obtained from the various samples regarding elution order of sophorolipids in HPLC is indicated.

was not clear and therefore their identification in HPLC was ambiguous.

Separation of individual sophorolipids by HPLC: assignment of hydroxy fatty acid moieties

With gradient elution HPLC, it was observed that each class of the mixture isolated by TLC was resolved into several individual components putatively corresponding to homologous sophorolipids varying in their hydroxy acid moieties. The approach adopted to test this hypothesis was to compare on a qualitative and quantitative basis the distribution of sophorolipids obtained in HPLC with that of the corresponding hydroxy fatty acids obtained by GC. For this purpose, a single class, deacylated acidic sophorolipids (Sl-A), which could be obtained in good conditions, was first used (sample A3). It was prepared by alkaline hydrolysis and submitted to HPLC. A sample of Sl-A was also converted into methyl ester derivatives, Sl-mE (sample A4), because methyl esters exhibited a better separation than the corresponding acids in HPLC. Catalytic hydrogenation of the double bonds of the hydroxy fatty acid moieties was then performed on a portion of Sl-mE to yield sample A5. Samples A4 and A5 were submitted to HPLC. For GC analysis, hydroxy fatty acid moieties of samples A4 and A5 were split by methanolysis, yielding samples A7 and A6, respectively. Identification of the hydroxy fatty acids was performed after silylation by coupled GC–MS. The distribution of sophorolipid methyl esters obtained in HPLC (samples A4 and A5) could then be compared with that of the corresponding hydroxy fatty acid methyl esters obtained in GC (samples A7 and A6). Thus the comparison also extended to the effects of catalytic hydrogenation on both types of compounds. Fig. 4 shows that before catalytic hydrogenation the number of compounds was similar according to HPLC or GC. Hydrogenation of the double bonds of hydroxy fatty acids led to analogous changes in the HPLC and GC traces. Assuming the specific responses for all individual sophorolipids to be similar in ELS detection, the relative amounts of sophorolipids were calculated from HPLC and compared with GC data. Table III shows that the distributions of compounds resulting from HPLC and GC determinations could be matched correctly both before and after hydrogenation. Further, the

TABLE III

IDENTIFICATION OF HOMOLOGOUS SOPHOROLIPIDS BY COMPARISON OF THE DISTRIBUTION OF INDIVIDUAL SOPHOROLIPIDS AND OF THEIR CONSTITUTIVE HYDROXY FATTY ACID MOIETIES

Constitutive hydroxy fatty acid	Relative amount before hydrogenation (%)		Relative amount after hydrogenation (%)	
	By GC[a]	By HPLC[c]	By GC[b]	By HPLC[d]
15-OH C_{16}:0	1.7	<1	1.8	1.3
16-OH C_{16}:0	2.2	<1	2.4	2.2
17-OH C_{18}:2	6.3	6.3	–	–
17-OH C_{18}:1	60.6	55.7	–	–
17-OH C_{18}:0	3.2	4.1	69.2	66.7
18-OH C_{18}:2	13.2	18.3	–	–
18-OH C_{18}:1	12.8	15.5	–	–
18-OH C_{18}:0	<0.1	<1	26.6	29.8

[a] Distribution of hydroxy fatty acid methyl esters obtained by methanolysis of deacetylated sophorolipid methyl esters (sample A7).
[b] Similar data for hydrogenated sample (A6).
[c] Distribution of deacetylated sophorolipid methyl esters (sample A4) ordered by matching to the corresponding GC data.
[d] Similar data for hydrogenated sample (A5).

amounts of saturated sophorolipids produced by hydrogenation were globally equal to the sum of the corresponding unsaturated compounds, a similar situation holding also for hydroxy fatty acids. In this way, assignment of a definite hydroxy fatty acid could be done for each individual sophorolipid, thus allowing identification of individual sophorolipid methyl esters.

Influence of the nature of hydroxy fatty acid moieties in HPLC of esters and lactones

Interpretation of Fig. 4 also allows several observations to be made with respect to the influence of the nature of the hydroxy fatty acid moieties on the elution of sophorolipid methyl esters in HPLC. A first point is that sophorolipids were discriminated according to the degree of unsaturtion of their hydroxy fatty acid moieties and that the more saturated the hydroxy acid, the later it was eluted. Moreover, for an identical fatty acid chain, hydroxy acids bearing the hydroxy group on the terminal (ω) carbon were eluted after their homologs bearing the hydroxy group on the subterminal ($\omega - 1$) position. With more concentrated samples a third rule for elution which had priority over the two first ones was observed: it concerned the number of carbons of the fatty acid chain, the lighter compounds being eluted first (data not shown).

The HPLC elution pattern of individual sophorolipids was then investigated for lactones. The main sample used was obtained by crystallization of the lactonic forms (monoacetylated and diacetylated lactones) according to Tulloch *et al.* [4] from a fermentation mixture. The identity of individual sophorolipids was assigned by matching the sophorolipid and corresponding hydroxy fatty acid distributions as in the case of esters. Elution rules related to hydroxy fatty acid moieties established for esters were usually found to apply also to lactonic forms, with a few exceptions that will be discussed later.

Assessment by HPLC of the separation in TLC of lactonic sophorolipids

Identification of individual sophorolipids allowed the separation by TLC of sophorolipids in structural classes to be assessed. The technique of matching the distributions in HPLC and GC of corresponding compounds was again used. The case of acidic structural classes that are not resolved in TLC (see Table II) will not be discussed. Concerning lactonic forms, more peaks were detected in HPLC than in GC

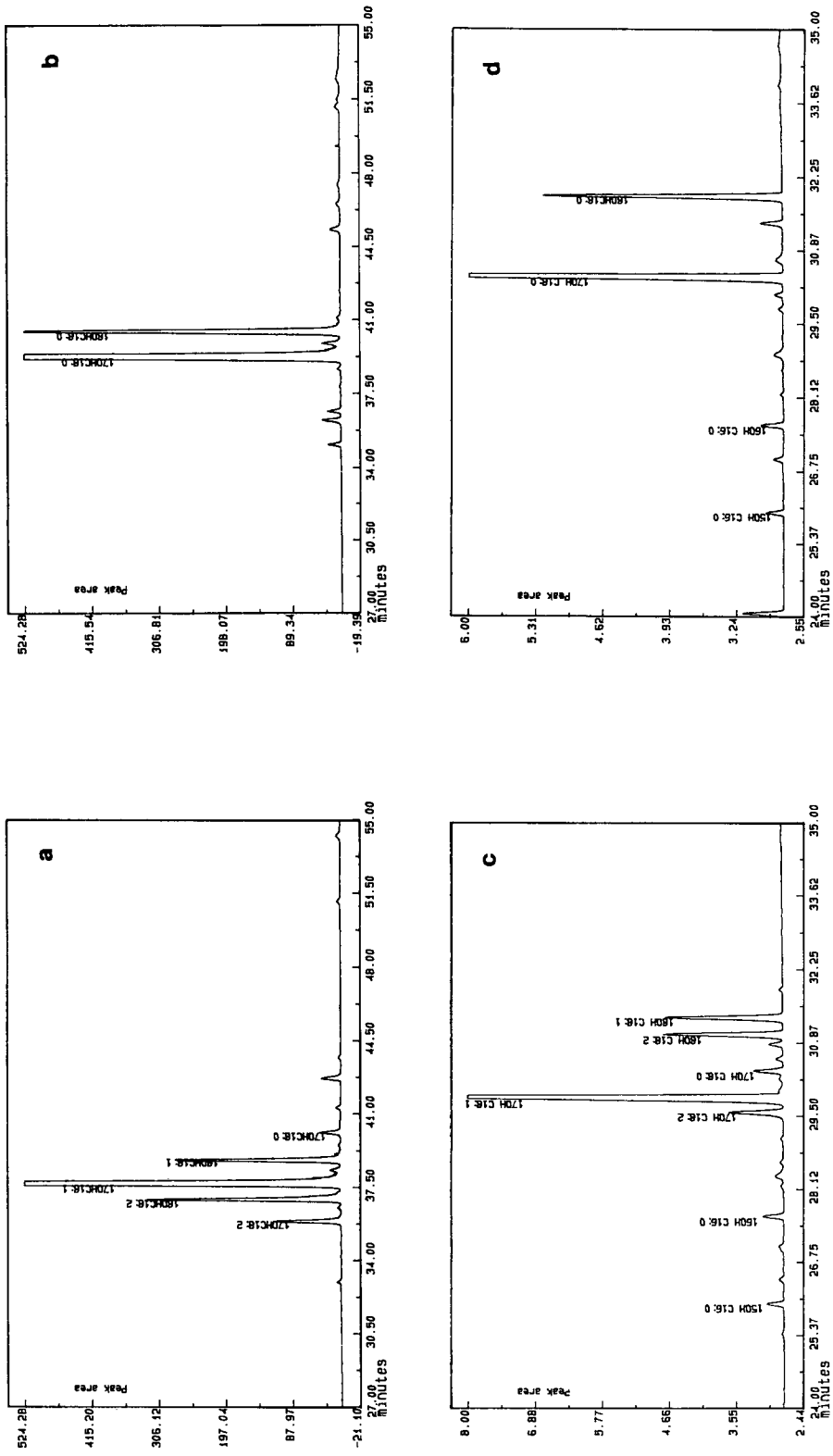

Fig. 4. Identification of homologous sophorolipid methyl esters with different fatty acid compositions. Separation by HPLC of deacetylated sophorolipid methyl esters (Sl-mE). (a) Sample A4; (b) sample A5. Separation by GC of hydroxy acid methyl esters obtained by methanolysis of Sl-mE. (c) Sample A7; (d) sample A6.

analysis for the spots of monoacetylated lactones (SL-2) and non-acetylated lactones (SL-4a, b) (data not shown). This suggested that the separation of classes by TLC was not absolute and that some spots might be constituted by several related classes. For spot SL-4a, b it was found, as already suggested by Asmer *et al.* [5] and indicated in Table II, that it was composed of 1′, 6′ and 1′,6″-lactones (Sl-6′L and Sl-6″L). Further, spot SL-2 appeared here to be constituted of two classes of monoacetylated lactones, two main peaks were observed in HPLC and only one main hydroxy fatty acid (17-OH C_{18}:1) was detected by GC in sophorolipids of SL-2. Therefore, SL-2 was likely to contain, in addition to class Sl-4″L6″a as reported by Asmer *et al.* [5], the related class Sl-4″L6′a. This point was confirmed by kinetic experiments on alkaline hydrolysis under controlled conditions, which showed the disappearance of both sophorolipids at different rates, one of them increasing temporarily (with concomitant hydrolysis of Sl-4″6′a6″a) before decreasing. Structure 4″L6″a, already identified in sophorolipid mixtures and most abundant in our preparation, was tentatively assigned to the most stable class.

Separation of the acidic forms of sophorolipids in HPLC

Sample A and derivatives allowed the identification and characterization of the elution pattern first of esters and then of lactone forms of sophorolipids. A similar study was completed for the acidic forms of sophorolipids using sample B. The deacylated acidic form was prepared (sample B3). To improve the resolution in HPLC, both samples B and B3 were methylated to give samples B8 and B4, respectively. The HPLC traces of these four samples were compared. Table IV shows that acetylated acids were eluted before non-acetylated acids and that the various classes of acetylated sophorolipids were not resolved in HPLC in the case of free acidic sophorolipids. In the present instance, addition of small amounts of acetic acid did not improve the resolution. When acidic forms were methylated (Table IV), the resolution was satisfactory and the elution order was reversed, non-acetylated methyl esters being eluted before acetylated compounds. Three series of peaks corresponding to non-acetylated, monoacetylated and diacetylated forms of acidic sophorolipids were observed after esterification, distributed in a very similar way to those of the corresponding lactones. Two classes of monoacetylated forms were present and their identities (Sl-A6″a and Sl-A6′a) were tentatively assigned by analogy with the elution pattern of lactones.

TABLE IV

ELUTION ORDER OF ACIDIC SOPHOROLIPIDS IN HPLC

HPLC separation was performed on a mixture of predominantly acidic sophorolipids (sample B), deacetylated acidic sophorolipids Sl-A (sample B_3), methyl esters of predominantly acidic sophorolipids (sample B_8) and deacetylated sophorolipid methyl esters Sl-mE (sample B_4).

Individual sophorolipid	Retention time (min)	
	Before methylation	After methylation
Sl-(17-OH C_{18}:1) A	32.9	37.3
Sl-(18-OH C_{18}:1) A	34.0	38.5
Sl-(17-OH C_{18}:1) A6′a	31.8	41.1
Sl-(18-OH C_{18}:1) A6′a	32.3	42.4
Sl-(17-OH C_{18}:1) A6″a	31.8	40.1
Sl-(18-OH C_{18}:1) A6″a	32.3	42.0
Sl-(17-OH C_{18}:1) A6′a6″a	31.8	45.0
Sl-(18-OH C_{18}:1) A6′a6″a	32.3	45.7

Identification of individual sophorolipids was performed as described previously for sample A4 by combining catalytic hydrogenation and quantitative comparison of sophorolipids with the corresponding hydroxy fatty acid methyl esters obtained by methanolysis. For non-esterified acids, the elution order of homologous sophorolipids in each class was found the same as for esters.

Identification of individual sophorolipids in fermentation mixtures

Direct analysis of fermentation mixtures containing both acidic and lactonic forms of sophorolipids was studied. One such case was sample A from which samples A_{12}, A_{13}, A_{14}

were prepared. The HPLC and GC results for these samples confirmed the previous results.

UV detection was also used in HPLC analysis to confirm the location of unsaturated sophorolipids.

The most important compound of sample A, Sl-(17-OH C_{18}:1) 4″L6′a6″a, was isolated by preparative HPLC. ^{13}C and ^{1}H NMR analysis confirmed the identity of sophorose as the sugar moiety and the presence of all chemical groups constituting the molecule and their respective positions [4,21]. It allowed the purity of the sample analysed to be established as 95% (presence of 5% of the 18-OH C_{18}:1 homologue).

A quasi-complete identification of the individual sophorolipids present in fermentation products is presented for sample A in Fig. 5. The most important unknown compound is located in the Sl-4″L6′a6″a class. This compound has not been identified but several lines of evidence suggest it to be a derivative of 17-OH octadecenoate. As it is different from Sl-(17-OH C_{18}:1) 4″L6′a6″a, it is likely to belong to a structural class differing somehow from 4″L6′a6″a. Minor unknown peaks can also be observed in Fig. 5. Some of them can probably be accounted for by the presence of minor hydroxy fatty acids. Fatty acids such as C_{20}:0, C_{20}:1 and C_{22}:1 are present in rapeseed esters and hydroxy fatty acids such as 19-OH C_{20}:O and 19-OH C_{20}:1 have been reported in sophorolipids [2,22,23].

As already indicated, the elution patterns of homologous sophorolipids according to their hydroxy fatty acid moieties observed for esters also held in most instances for lactones and acids. One of the few exceptions can be seen in Fig. 5. Such cases occurred when the elution times for a given class were markedly different from those of the corresponding esters. Here, for class 4″L6′a6″a, 17-OH C_{18}:2 and 18-OH C_{18}:2 sophorolipids were not resolved and were eluted before their 15-OH C_{16}:0 and 16-OH C_{16}:0 homologues.

Finally, the data on the characterization of individual sophorolipids by HPLC obtained from samples of fermentations with rapeseed ethyl esters were also confirmed and extended by similar investigations with samples from fermentations with other lipidic carbon sources such

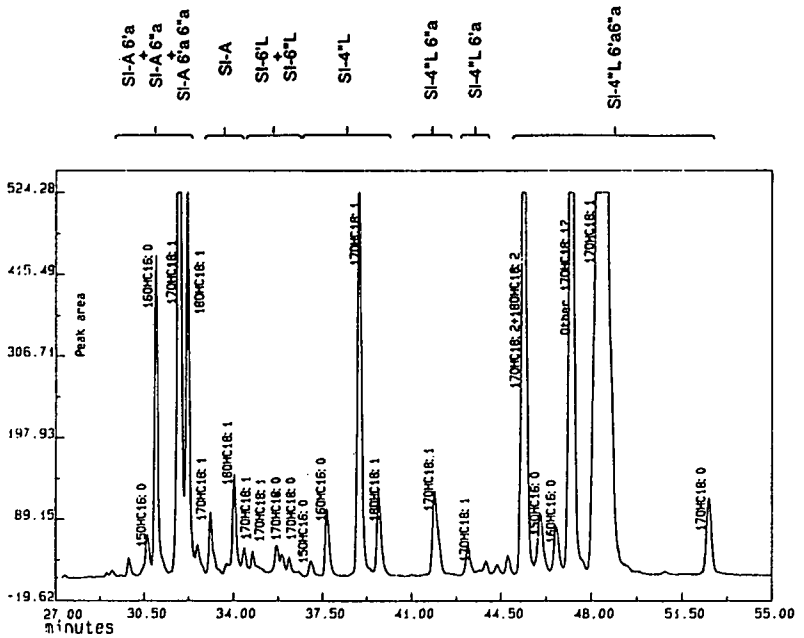

Fig. 5. Elution order in gradient elution HPLC of a mixture of sophorolipids obtained by fermentation (sample A). The identification of structural classes and of individual sophorolipids is presented.

as hexadecane and sunflower oil, which yielded sophorolipids with different hydroxy fatty acid compositions.

CONCLUSIONS

Gradient elution HPLC with ELS detection proved to be a powerful and rapid tool for qualitative and quantitative analysis of sophorolipids, as a single chromatographic analysis of a complex mixture allowed almost all significant individual compounds (over 20) present in the mixture to be identified and determined without prior preparation of the sample.

The ELS detector was found able to detect with excellent sensitivity all sophorolipids present. Within the concentration range utilized, corresponding to injected amounts of 50–400 μg of sophorolipid mixture, linearity of response was observed. The results are in line with the opinion that this detector can be considered as universal for non-volatile compounds [18].

Isolation and direct identification were not done for most of the compounds [only Sl-4″L6′a6″a and Sl-A classes were isolated and structure of the major compound Sl-(17-OH C_{18}:1) 4″L6′a6″a confirmed by NMR]. However, for most other sophorolipids, structure assignment resulted from mutually confirmative lines of evidence and can be conferred a high degree of confidence.

Several sophorolipids classes not yet reported were identified at least tentatively in this study, namely Sl-4″L6′a, Sl-A6″a and Sl-A6′a6″a, and the existence of more of them may be suspected.

The strong dependence of sophorolipid composition on both the nature of the lipidic substrate and on the fermentation conditions has already been mentioned or illustrated here. The technique developed in this study opens up this area to systematic investigation.

ACKNOWLEDGEMENTS

The skilled participation of J. Lemal and C. Sulzer is acknowledged. We thank J.C. Roussel for the NMR analyses and R. Stern and G. Hillion for helpful discussions.

REFERENCES

1 P.A.J. Gorin, J.F.T. Spencer and A.P. Tulloch, *Can. J. Chem.*, 39 (1961) 846.
2 J.F.T. Spencer, D.M. Spencer and A.P. Tulloch, in A.H. Rose (Editor), *Economic Microbiology*, Vol. 3, Academic Press, London and New York, 1979, p. 523.
3 D.F. Jones, *J. Chem. Soc. C*, (1967) 479.
4 A.P. Tulloch, A. Hill and J.F.T. Spencer, *Can. J. Chem.*, 46 (1968) 3337.
5 H.J. Asmer, S. Lang, F. Wagner and V. Vray, *J. Am. Oil Chem. Soc.*, 65 (1988) 1640.
6 D.F. Jones and R. Howe, *J. Chem. Soc. C*, (1968) 2801.
7 V. Klekner, N. Kosaric and Q.H. Zhou, *Biotechnol. Lett.*, 13 (1991) 345.
8 A.-M. Davila, R. Marchal and J.-P. Vandecasteele, *Appl. Microbiol. Biotechnol.*, 38 (1992) 6.
9 T.H. Mourey and L.E. Oppenheimer, *Anal. Chem.*, 56 (1984) 2427.
10 L.E. Oppenheimer and T.E. Mourey, *J. Chromatogr.*, 323 (1985) 297.
11 P.B. Stockwell and B.W. King, *Int. Chromatogr. Lab.*, 7 (1991) 4.
12 A. Stolyhwo, M. Martin and G. Guiochon, *J. Liq. Chromatogr.*, 10 (1987) 1237.
13 A. Stolyhwo, H. Colin and G. Guiochon, *Anal. Chem.*, 57 (1985) 1342.
14 W.W. Christie, *J. Lipid Res.*, 26 (1985) 507.
15 J. Becart, C. Chevalier and J.P. Biesse, *J. High Resolut. Chromatogr.*, 13 (1990) 126.
16 L. Breton, B. Serkiz, J.P. Volland and J. Lepagnol, *J. Chromatogr.*, 497 (1989) 243.
17 T.L. Mounts, S.L. Abidi and K.A. Rennick, *J. Am. Oil Chem. Soc.*, 69 (1992) 438.
18 W.W. Christie, *Rev. Fr. Corps Gras*, 38, No. 516 (1991) p. 155.
19 G.R. Bear, *J. Chromatogr.*, 459 (1988) 91.
20 D. Herbert, P.J. Philips and E. Strange, in J.R. Norris and D.W. Ribbons (Editors), *Methods in Microbiology*, Vol. 5B, Academic Press, London, 1971, p. 209.
21 L. Weber, J. Stach, G. Haufe, R. Hommel and H.-P. Kleber, *Carbohydr. Res.*, 206 (1990) 13.
22 A.P. Tulloch, J.F.T. Spencer and P.A.J. Gorin, *Can. J. Chem.*, 40 (1962) 1326.
23 A.P. Tulloch, in L.A. Wittling (Editor), *Glycolipid Methodology*, American Oil Chemists Society, Champaign, IL, 1976, p. 329.

Journal of Chromatography, 648 (1993) 151–156
Elsevier Science Publishers B.V., Amsterdam

CHROM. 25 343

High-performance liquid chromatography of the photoproducts of nucleic acid components

III☆. Detection of the secondary structure differences in sequence isomeric self-complementary oligonucleotides

V.N. Potaman*, I.P. Chernov and V.V. Demidov

Institute of Molecular Genetics, Russian Academy of Sciences, Moscow 123182 (Russian Federation)

(Received April 19th, 1993)

ABSTRACT

Reversed-phase high-performance liquid chromatography (RP-HPLC) was used to detect differences in the secondary structures of two self-complementary oligodeoxyribonucleotides. The $[d(CCTTTAAAGG)]_2$ duplex assumes an ordinary B-conformation in aqueous solution, while $[d(GGAAATTTCC)]_2$ is known to contain in its central part a stretch of a more rigid B′-form conformation with significantly lowered fluctuational mobility of base pairs. The latter factor causes a marked difference in the amounts of thymine cyclobutane photodimers formed under UV irradiation of corresponding duplexes as revealed by chromatography of two single-stranded oligonucleotides. Increasing the temperature below the duplex melting temperature (stimulation of the B′–B structural transition) results in an increase in photodimer formation that was inhibited in the B′-form. Thus, we demonstrate the usefulness of RP-HPLC for duplex DNA structural studies.

INTRODUCTION

HPLC has been successfully used in preparative and analytical separations of oligonucleotides for more than a decade [1,2]. While many efforts were directed at enhancing selectivity and optimizing separation of nucleic acid constituents, the potential of HPLC for structural studies has not been fully exploited. Except for purity control, a limited number of analytical HPLC applications have been reported. HPLC has been used for the separation of oligonucleotides from their 5′-phosphorylated derivatives [3], sequence isomers of oligonucleotides [4], various tRNAs [5], polynucleotides according to their base composition [6] and single- and double-stranded DNA [7]. Solid-phase hybridization of complementary oligonucleotides on an ion-exchange resin made it possible to follow an equilibrium between single-stranded and duplex forms of short DNAs [8]. Several groups have applied RP-HPLC to photochemical studies of oligonucleotides [9–15]. It has been shown that the formation of pyrimidine photohydrates [10] and photodimers [9,11–15] in oligonucleotides significantly changes their retention on a reversed phase. Modified oligonucleotides can be separated according to the type and sequence

* Corresponding author. Present address: Laboratory of Molecular Genetics, Biology Department, George Mason University, Fairfax, VA 22030, USA.

☆ For Parts I and II, see refs. 9 and 10, respectively.

0021-9673/93/$06.00

position of the pyrimidine photoproduct they contain.

We became interested in whether this last property can be applied to studies of the secondary structures of oligonucleotides. If nucleobase photoreactivity depends on the local structure of the nucleic acid fragment, then the high resolving power of HPLC can be used to locate specific photoproducts and hence the parts of the molecule with different conformations. Studies over the last several years have clearly shown that the duplex form of DNA can contain distinctive local structures that depend on the sequence of the bases. For instance, the $(dA)_n \cdot (dT)_n$ stretches can adopt the B′-form, which is different from the standard B-form [16–26]. This difference is manifested in the helical repeat [27,28], the helical pitch [18] and the width of the major groove [19,29–31]. The ability of short $d(A_nT_n)$ regions to adopt the B′-form depends on the order of bases: 5′-AT-3′ junction (AT step) is well accommodated in the B′-form geometry, while the TA step has a disrupting effect on the B′-form, promoting instead the B-form [17,32,33].

We studied two self-complementary oligonucleotides that contain the same bases but in different sequences. One of them, $[d(CCTTTAAAGG)]_2$ (Fig. 1), is known to assume the standard solution DNA conformation (B-form [16]) with the characteristic fluctuational mobility of constituent bases [17]. The second, $[d(GGAAATTTCC)]_2$, has a mixed structure: several terminal base pairs (bp) have the B-form geometry and at least four central AT bp are included in a stretch of the B′-form [17]. We UV-irradiated double-stranded oligonucleotides under conditions in which $[d(CCTTTAAAGG)]_2$ is in the B-form and $[d(GGAAATTTCC)]_2$ contains the B′-form, and separated the resulting products as single strands. The reduced mobility of bases and hence their reduced probability of adopting a disposition necessary for photoreaction results in a decrease in thymine photodimer yield in the B′-form sequence, as compared with the B-form. Elevated temperature destabilizes the B′-form and shifts the structure to the B-form. This results in an increase in the inner TT photodimer formation that was inhibited in the B′-form.

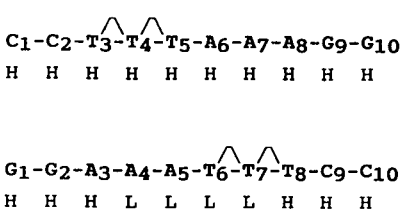

Fig. 1. Sequences of oligodeoxyribonucleotides studied showing high (H) and low (L) probabilities of fluctuational opening of base pairs in the duplexes. The positions of probable thymine dimers are indicated above the sequences by the ∧ symbol.

Our results demonstrate one more important HPLC application. RP-HPLC is able to reveal not only differences in the sequences of nucleic acid fragments (primary structure) but also, combined with photomodification, differences in geometry of spatial arrangement of bases (secondary structure).

EXPERIMENTAL

Materials

Oligonucleotides d(CCTTTAAAGG) and d(GGAAATTTCC) were synthesized by a modified phosphoramidite approach. They were purified by electrophoresis and RP-HPLC, desalted and sequenced. Snake venom phosphodiesterase I (PDE I) was from Pharmacia (Piscataway, NJ, USA). All other chemicals of analytical reagent grade were from various commercial sources.

UV irradiation

Oligonucleotides (25 μM strand concentration, in 150 mM sodium chloride, 15 mM sodium citrate, pH 7.0, without or in the presence of 10 mM acetophenone as a photosensitizer) were irradiated at 302 nm in 1-mm quartz cuvettes in a thermostated cell holder by a TM-36 UV transilluminator (UVP, San Gabriel, CA, USA) at a distance of 2 cm for various periods of time. This irradiation wavelength was chosen to exclude photoreversal of cyclobutadithymines.

Chromatographic conditions

Chromatography was performed on a Jasco LC-800 instrument (Jasco, Tokyo, Japan) using

an 875 UV detector and an 860 CO column oven. Analysis of photomodified samples was accomplished on a Merck LiChrosorb RP-18 (250 × 4 mm) column at 60°C with a 0–30% B gradient, where eluent A was 0.1 *M* ammonium acetate (pH 6.8) and eluent B was 50% methanol in water. The detector signal at 254 nm was fed to a microcomputer to calculate peak areas.

Localization of photodimers

After UV irradiation, oligonucleotides were separated as described and peaks of interest were collected in Eppendorf test tubes. Samples were dried in water and methanol several times in a Speed Vac evaporator to eliminate residual ammonium acetate. The dried material was reconstituted in 40 μl of enzyme reaction buffer (100 m*M* Tris–HCl, pH 8.9, 100 m*M* NaCl, 14 m*M* $MgCl_2$). A 10-μl aliquot of PDE I (0.1 units in the same buffer) was added and the resulting mixture was vortexed and incubated at 37°C for 30 min, after which time it was placed in boiling water for 5 min to inactivate the enzyme. Samples were spun in an Eppendorf microcentrifuge for 10 min and 10- to 40-μl aliquots were separated on a DuPont PEP-RP1 (80 × 6 mm) column at room temperature with a 20 min 0–20% B linear gradient (A, 50 m*M* potassium phosphate, pH 4.9, 5 m*M* tetrabutylammonium dihydrogen sulphate; B, 50% methanol in water). The presence of particular nucleoside-5′-monophosphates cleaved by PDE I from the 3′-end of the oligonucleotides until the enzyme stopped at a photodimer position [9,34] was used to locate photodimers in the sequences (Table I). Cyclobutane types of thymine photodimers were confirmed by acetophenone photosensitization, which promotes the formation of pyrimidine dimers exclusively [34,35].

RESULTS

Experimental doses of UV irradiation were such that no more than one photodimer per duplex was formed (10-20% diminution of the intact oligonucleotide amount). Otherwise, the duplex-destabilizing effect of photodimers and hence the change in oligomer photoreactivity should be considered. Moreover, we expected to obtain largely cyclobutane photodimers, because the yield of non-cyclobutane (6–4) dimers at low doses is several-fold lower than of the cyclobutane dimers [36]. In order to avoid artifacts in analysis of the photoproducts due to probable elution off the column of double- and single-stranded oligonucleotides, chromato-

TABLE I

CLEAVAGE OF NUCLEOSIDE-5′-MONOPHOSPHATES BY PDE I INCUBATED WITH MODIFIED AND UNMODIFIED OLIGONUCLEOTIDES

Aliquots of 10 μl of PDE I (0.1 units in the reaction buffer: 100 m*M* Tris–HCl, pH 8.9, 100 m*M* NaCl, 14 m*M* $MgCl_2$) were incubated at 37°C for 30 min with chromatographically isolated oligonucleotides in a 40-μl total reaction volume. Aliquots of the reaction mixture were separated on a DuPont PEP-RP1 (6 × 80 mm) column at room temperature with a 20 min 0–20% B linear gradient (A, 50 m*M* potassium phosphate, pH 4.9, 5 m*M* tetrabutylammonium dihydrogensulphate; B, 50% methanol in water). Nucleoside-5′-monophosphates were cleaved by PDE I from the 3′-end of the oligonucleotides until the enzyme stopped at a photodimer position. The ∧ symbol indicates positions of dimer formation between two adjacent thymines.

Peaks	Oligomers	Liberated nucleotides			
		AMP	CMP	GMP	TMP
1	d(CC∧TT∧TAAAGG)	+	−	+	+
2	d(CC∧TT∧TAAAGG)	+	−	+	−
3	d(CCTTTAAAGG)	+	+	+	+
4	d(GGAAA∧TT∧CC)	−	+	−	+
5	d(GGAAA∧TT∧CC)	−	+	−	−
6	d(GGAAATTTCC)	+	+	+	+

graphic separations at temperature above the melting point were done. Elevated temperature was additionally justified as it has been found that using the same eluents and gradients it is possible to better resolve some peaks of photoproduct-containing oligonucleotides.

UV irradiation of oligonucleotide duplexes at low temperature resulted in the appearance of several photoproducts. Comparison of photoproducts (Fig. 2a and b) obtained during sensitized photomodification, which promotes formation of almost exclusively cyclobutane TT photodimers [35], with those obtained during direct photomodification (several additional minor peaks, data not shown) allowed us to conclude that in both chromatograms peaks 1 and 2 corresponded to oligonucleotides containing cyclobutane TT photodimers. Further, in all cases we used unsensitized direct photomodification of oligomers to exclude any possible influence of acetophenone on their conformations. The sequence positions of thymine dimers in photomodified oligomers were identified using an exhaustive snake venom phosphodiesterase digestion of oligonucleotides from the 3′-end, which stopped at the photodimer position [34] (Table I). Note that the closer the photodimer is to the 5′-end of oligonucleotide, the greater is the change in retention.

Structural differences between the B-form and mixed-form duplexes clearly manifest themselves in lower yields of photodimers obtained for $[d(GGAAATTTCC)]_2$, as compared with $[d(CCTTTAAAGG)]_2$. More important is the temperature dependence for the yield of the inner T_6T_7 photodimer in $[d(GGAAATTTCC)]_2$. In contrast to other photodimers (Fig. 3), its yield rises more than three-fold with temperature. At higher temperatures, when the duplexes are denatured, all TT photodimers have similar yields. As has been mentioned above, the corresponding T_6T_7 dinucleotide is included in that part of oligonucleotide that is capable of adopting the rigid B′-conformation. Therefore, distinct temperature dependence for the T_6T_7 photodimer at least partly reflects the B′–B form transition.

This assumption is confirmed by the spectrophotometric melting [37]. Both oligonucleo-

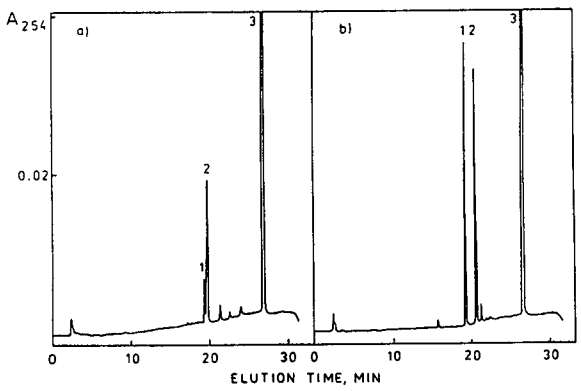

Fig. 2. Chromatograms of oligonucleotides UV-irradiated at 7°C for 10 min in the presence of 10 m*M* acetophenone under conditions in which the double-stranded structures exist. Column: LiChrosorb RP_{18} (250 × 4 mm). Eluents: A, 0.1 *M* ammonium acetate (pH 6.8); B, 50% methanol in water; 0–30% B linear gradient (30 min) at 60°C; flow-rate, 1 ml/min. (a) $[d(GGAAATTTCC)]_2$. Peaks: 1 = d(GGAAA$\widehat{TT}$TCC); 2 = d(GGAAAT$\widehat{TT}$CC); 3 = d(GGAAATTTCC). Unidentified peaks are those of minor photoproducts. (b) $[d(CCTTTAAAGG)]_2$. Peaks: 1 = d(CC$\widehat{TT}$TAAAGG); 2 = d(CCT$\widehat{TT}$AAAGG); 3 = d(CCTTTAAAGG).

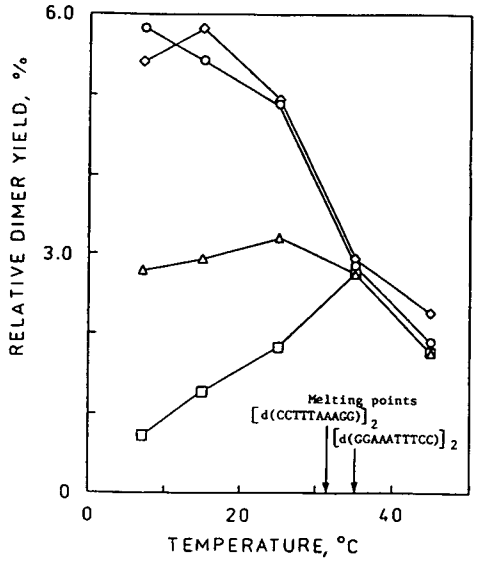

Fig. 3. Temperature dependencies of the photodimer yields (calculated relative to initial amounts of unmodified oligomers) for oligonucleotides in 150 m*M* sodium chloride, 15 m*M* sodium citrate, pH 7.0: □ = d(GGAAA$\widehat{TT}$TCC); △ = d(GGAAAT$\widehat{TT}$CC); ◇ = d(CC$\widehat{TT}$TAAAGG); ○ = d(CCT$\widehat{TT}$AAAGG). Melting points for the duplex form oligonucleotides are indicated by arrows.

tides undergo duplex-coil transitions at 31–35°C. $[d(GGAAATTTCC)]_2$ has also a broad "premelting" interval with a midpoint at about 15°C. Additional evidence of correlation between the B′–B transition and the yield of the T_6T_7 photodimer is provided by the other factor known to destabilize the B′-form but not the B-form, dimethyl sulphoxide (DMSO) [20,21]. DMSO 30% increases the yield of the T_6T_7 photodimer but affects the yields of other photodimers to a lesser extent (data not shown).

DISCUSSION

Several methods were used to study the B′-conformation in poly(dA)–poly(dT) and various oligonucleotides containing $(dA)_n$·$(dT)_n$ stretches. Among them were the UV absorbance, circular dichroism and NMR spectroscopies [17,20,22,33], calorimetry [33], structurally caused changes in electrophoretic mobility [32] and several methods of chemical [25,26] and photochemical [21] probing of nucleic acid duplexes. We used this relatively well-studied problem to ascertain the applicability of chromatographic methods to structural studies of oligonucleotides since we feel that to make the models of molecular structure most reliable, it is desirable to get as much independent evidence from various techniques as possible.

The suitability of liquid chromatography for the structural studies of biological oligomers has been illustrated by the investigations of peptides. Extensive work has been done to calculate the contribution of every constituent amino acid residue to the retention of peptides on a reversed phase [38–40]. Racemization of peptides at practically every peptide bond can be detected using RP mode [41]. Moreover, HPLC is able to reveal kinetic details of *cis–trans* isomerism in proline- and N-methylamino acid-containing peptides [42,43]. Recently, amphipathic α-helix content has been shown to influence peptide retention on RP supports [44].

Yet, application of HPLC to structural studies of nucleic acids is rarer. As far as the spatial structure is concerned, only separation of single- from double-stranded DNA [7], separation of supercoiled, open circular and linear plasmid DNA [45] and on-column hybridization of complementary oligonucleotides [8] can be mentioned. Our results show that it is possible to get more details of double-stranded nucleic acid structure using a combination of HPLC with some other suitable structurally dependent technique of nucleic acid modification (in our case, UV modification at characteristic sites). We have used this approach to study the influence of some cations, including alkali, earth alkali and transition metal ions, on the existence of the B′-form [37]. Since DNA conformations are not restricted to B- and B′-forms and a variety of different site modifications as well as modifying agents can be used, the presented method can be useful for other structural studies of nucleic acid fragments and their complexes with various ligands.

ACKNOWLEDGEMENTS

We are grateful to Dr. V.N. Nezavibatko in whose laboratory this work was carried out. We also thank Drs. O.N. Voloshin, T.N. Bocharova, E.A. Smirnova and M. Ivanovskaya for help during our experiments.

REFERENCES

1 H.J. Fritz, R. Belagaje, E.L. Brown, R.H. Fritz, R.A. Jones, R.G. Lees and H.G. Khorana, *Biochemistry*, 17 (1978) 1257–1267.
2 O. Mikes, *High-Performance Liquid Chromatography of Biopolymers and Biooligomers*, Part B, Elsevier, Amsterdam, 1988, pp. B177–B238.
3 A.M. Delort, R. Derbyshire, A.M. Duplaa, A. Guy, D. Molko and R. Teoule, *J. Chromatogr.*, 283 (1984) 462–467.
4 H. Schott and H. Eckstein, *J. Chromatogr.*, 296 (1984) 363–368.
5 L.W. McLaughlin and R. Bischoff, *J. Chromatogr.*, 418 (1988) 51–72.
6 S. Garcia and J.-P. Liautard, *J. Chromatogr. Sci.*, 21 (1983) 398–404.
7 J.-P. Liautard, *J. Chromatogr.*, 285 (1984) 221–225.
8 M. Guthridge, J. Bertolini and M.T.W. Hearn, *J. Chromatogr.*, 476 (1989) 445–453.
9 V.V. Demidov and V.N. Potaman, *J. Chromatogr.*, 285 (1984) 135–142.
10 V.N. Potaman, T.N. Ulmasov and V.V. Demidov, *J. Chromatogr.*, 329 (1985) 33–42.
11 R.E. Rycyna and J.A. Alderfer, *Biochemistry*, 27 (1988) 3142–3151.

12 R.E. Rycyna, J.C. Wallace, M. Sharma and J.A. Alderfer, *Biochemistry*, 27 (1988) 3152–3163.
13 J.-S. Taylor and I.R. Brockie, *Nucleic Acids Res.*, 16 (1988) 5123–5136.
14 V.V. Demidov, V.N. Potaman and B.S. Kogan, *Nucleic Acids Res.*, 19 (1991) 1947.
15 T. Douki and J. Cadet, *J. Photochem. Photobiol. B: Biol.*, 15 (1992) 199–213.
16 R. Langridge, R.H. Wilson, C.W. Hooper and L.D. Hamilton, *J. Mol. Biol.*, 2 (1960) 19–37.
17 M. Gueron, E. Charretier, J. Hagerhorst, M. Kochoyan, J.L. Leroy and A. Moraillon, in R.H. Sarma and M.H. Sarma (Editors), *Structure and Methods, Vol. 3: DNA and RNA*, Adenine Press, New York, 1990, pp. 113–137.
18 S. Arnott and E. Selsing, *J. Mol. Biol.*, 88 (1974) 509–521.
19 D.G. Alexeev, A.A. Lipanov and I.Y. Skuratovskii, *Nature*, 325 (1987) 821–823.
20 J.E. Herrera and J.B. Chaires, *Biochemistry*, 28 (1989) 1993–2000.
21 V. Lyamichev, *Nucleic Acids Res.*, 19 (1991) 4491–4496.
22 S.S. Chan, K.J. Breslauer, M.E. Hogan, D.J. Kessler, R.H. Austin, J. Ojemann, J.M. Passner and N.C. Wiles, *Biochemistry*, 29 (1990) 6161–6171.
23 J. Sturm, *Biopolymers*, 21 (1982) 1189–1206.
24 J.B. Chaires, *Biochemistry*, 22 (1983) 4204–4211.
25 A.M. Burkhoff and T.D. Tullius, *Cell*, 48 (1987) 935–943.
26 A.M. Burkhoff and T.D. Tullius, *Nature*, 331 (1988) 455–457.
27 L.J. Peck and J.C. Wang, *Nature*, 292 (1981) 375–378.
28 D. Rhodes and A. Klug, *Nature*, 292 (1991) 378–380.
29 H.-S. Park, S. Arnott, R. Chandrasekaran, P.R. Millane and F. Campagnari, *J. Mol. Biol.*, 197 (1987) 513–523.
30 H.C.M. Nelson, J.T. Finch, B.F. Luisi and A. Klug, *Nature*, 330 (1987) 221–226.
31 M. Coll, C.A. Frederick, A.H.-J. Wang and A. Rich, *Proc. Natl. Acad. Sci. U.S.A.*, 84 (1987) 8385–8389.
32 P.J. Hagerman, *Nature*, 321 (1986) 449–450.
33 Y.W. Park and K.J. Breslauer, *Proc. Natl. Acad. Sci. USA*, 88 (1991) 1551–1555.
34 N.K. Kochetkov and E.I. Budowsky (Editors), *Organic Chemistry of Nucleic Acids*, Part B, Plenum Press, London, New York, 1972, pp. 543–618.
35 R.O. Rahn and M.H. Patrick, in S.Y. Wang (Editor) *Photochemistry and Photobiology of Nucleic Acids*, Vol. II, Academic Press, New York, 1976, pp. 97–145.
36 E.C. Friedberg, *DNA Repair*, W.H. Freeman and Co., New York, 1985, pp. 40–54.
37 V.V. Demidov and V.N. Potaman, *Nucleic Acids Res.*, 21 (1993) 2691–2696.
38 J.L. Meek and Z.L. Rosetti, *J. Chromatogr.*, 211 (1981) 209–221.
39 C.A. Browne, H.P.J. Bennett and S. Solomon, *Anal. Biochem.*, 124 (1982) 201–208.
40 T. Sasagawa, T. Okuyama and D.C. Teller, *J. Chromatogr.*, 240 (1982) 329–340.
41 B. Nyasse, B. Bransson and U. Ragnarsson, *Int. J. Peptide Protein Res.*, 36 (1990) 316–319.
42 W.R. Melander, J. Jacobson and Cs. Horváth, *J. Chromatogr.*, 234 (1982) 269–276.
43 M. Lebl, S. Fang and V.J. Hruby, *J. Chromatogr.*, 586 (1991) 145–148.
44 N.E. Zhou, C.T. Mant and R.S. Hodges, *Peptide Res.*, 3 (1990) 8–20.
45 A. Pingoud, A. Fliess and V. Pingoud, in R.W.A. Oliver (Editor), *HPLC of Macromolecules —A Practical Approach*, IRL Press, Oxford, 1989, pp. 183–208.

Journal of Chromatography, 648 (1993) 157–163
Elsevier Science Publishers B.V., Amsterdam

CHROM. 25 353

Optimization of the separation of oligodeoxyribonucleoside phosphoramidates and their characterization by circular dichroism spectroscopy

Akira Murakami*, Yutaka Tamura, Hiroshi Ide and Keisuke Makino

Department of Polymer Science and Engineering, Kyoto Institute of Technology, Matsugasaki, Sakyo-ku, Kyoto 606 (Japan)

(First received December 29th, 1992; revised manuscript received May 28th, 1993)

ABSTRACT

Oligodeoxyribonucleoside phosphoramidates (OPAs) were synthesized via H-phosphonate chemistry. The oxidation of oligodeoxyribonucleoside H-phosphonates was performed in the presence of isopropylamine–carbon tetrachloride (1:4, v/v). Reversed-phase high-performance liquid chromatography was used to separate the diastereoisomers of OPAs for the study of their conformation in solution and their ability to act as antisense molecules. It was found that complete purification of diastereoisomers of OPAs by reversed-phase HPLC could be achieved by a two-step chromatographic approach adopting optimized chromatographic conditions: acetonitrile gradient, column temperature and column length. From the circular dichroism measurements of the tetranucleoside phosphoramidates, it was found that the eight diastereoisomers of the tetranucleotides can be classified into four groups according to their molar ellipticity changes and that the diastereoisomers show different abilities to form hybrids with complementary DNA.

INTRODUCTION

Viral diseases are often fatal in humans because they can rarely be treated by conventional medical care. In particular, infection with human immunodeficiency virus (HIV), completely incurable so far, is rapidly increasing all over the world. One of the most promising treatment approaches is the antisense DNA/RNA method [1,2], in which synthetic oligodeoxyribonucleotides and their analogues are used to bind to the target sequences of DNAs or RNAs and consequently to regulate gene expression in a highly specific manner. To be suitable for trial, there are several requirements in designing the antisense molecules [3]: (1) specificity for the target DNAs or RNAs; (2) stability of the duplex formed with the target DNAs or RNAs; (3) resistance to nucleases; (4) cell membrane permeability; (5) metabolism in body. To satisfy these requirements, modification of the internucleotide phosphate linkages of DNAs or RNAs has been attempted [1,3]. One such group of oligonucleotide analogue is the oligodeoxyribonucleoside phosphoramidates (OPAs) [4]. This type of antisense molecule is resistant to nuclease digestion and is expected to easily penetrate into the cellular membrane because of its high hydrophobicity.

However, when a phosphate linkage of DNA or RNA is modified, the modification results in diastereoisomers, as shown in Fig 1. Therefore, OPAs consist of a number of diastereoisomers. The question arises: Is there a difference in the stability of hybrids between the diastereoisomers and their complementary oligonucleotides [5]? To help answer this question, in the present study, optimization of the reversed-phase HPLC to separate diastereoisomers of di-, tri and tetra-

* Corresponding author.

0021-9673/93/$06.00

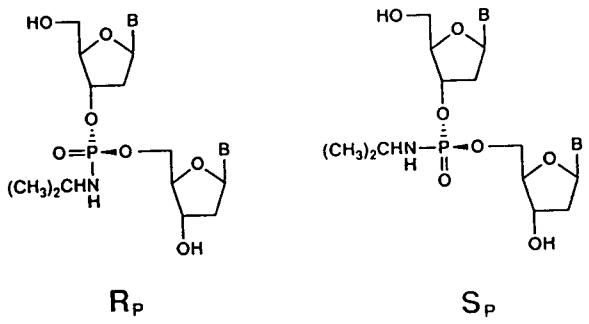

R_P S_P

Fig. 1. R_P and S_P configurations of dinucleoside phosphoramidates.

nucleoside phosphoramidate was explored and the diastereoisomers were characterized by circular dichroism (CD) spectroscopy.

MATERIALS AND METHODS

Reagents

Controlled pore glass was loaded with 35–45 μmol/g of the fully protected nucleoside unit. H-Phosphonate nucleosides were purchased from Milligen/Biosearch (Burlington, CA, USA). HPLC-grade acetonitrile was purchased from J.T. Baker (NJ, USA). Distilled water was purchased from Wako (Osaka, Japan), and further purified with a Millipore Milli-QII system. Other reagents were purchased from Nakalai Tesque (Kyoto, Japan).

Oligodeoxyribonucleotide synthesis

Oligodeoxyribonucleoside phosphodiesters (ODNs) were synthesized at the micromolar scale on a Milligen Cyclon Plus DNA synthesizer (Milligen/Biosearch) via phosphoramidite chemistry [4,6]. Oligodeoxyribonucleoside phosphoramidates (OPAs) were synthesized at the 10 μmol scale in a gas-tight syringe via H-phosphonate chemistry, and the oxidation of oligodeoxyribonucleoside H-phosphonates was carried out in the presence of isopropylamine–carbon tetrachloride (1:4, v/v) [4]. Deprotection of oligodeoxyribonucleotides except for the 5′-dimethoxytrityl (DMT) group was carried out with fresh ammonium hydroxide (28%) at 55°C for 8 h.

Sample preparation for HPLC

The ammonium hydroxide solution (5 ml) containing OPAs was evaporated to one-half of its initial volume, and 0.1 *M* triethylammonium acetate (TEAA, pH 7.0, 2.5 ml) was added. The solution was applied to a C_{18} Sep-Pak cartridge (Waters, Milford, MA, USA). After sequential elution with 0.1 *M* TEAA (pH 7.0) and 0.1 *M* TEAA (pH 7.0)–acetonitrile (85:15), the cartridge was eluted with 0.1 *M* TEAA (pH 7.0)–acetonitrile (50:50). After evaporation to dryness, the residue was dissolved in 0.1 *M* TEAA (pH 7.0)–acetonitrile (70:30) and used for HPLC purification [7].

HPLC separation and purification

Oligonucleotides (ODNs and OPAs) were analysed by reversed-phase HPLC using a Shimadzu LC-6A chromatography system (Shimadzu, Kyoto, Japan). The column temperature was controlled by a CTO-6A column oven (Shimadzu). Reversed-phase columns used were as follows: for the separation of di- and trinucleoside phosphoramidates, a Superspher RP-18(e) (4 μm, 4 × 125 mm, Merck, Darmstadt, Germany); for the separation and the purification of 5′-DMT-dAp(iPr)Tp(iPr)Cp-(iPr)G (iPr = isopropyl), a Superspher RP-18(e) (4 μm, 4 × 250 mm, Merck); for the purification of the diastereoisomers of dAp(iPr)Tp(iPr)Cp-(iPr)G, an ODS-NC_{18} (5 μm, 20 × 250 mm, Shinwa, Kyoto, Japan). The chromatographic conditions are described in the captions to the figures.

Sample preparation for circular dichroism (CD) measurement

Solutions of single strands were prepared by using a buffer consisting of 10 m*M* sodium phosphate, adjusted to pH 7.0, and for hybrids 10 m*M* sodium phosphate and 3 *M* NaCl, adjusted to pH 7.0. Oligonucleotide concentrations were determined spectroscopically by measuring the absorbance at 260 nm. The extinction coefficients for the single-stranded oligodeoxyribonucleotides at 25°C were calculated by the nearest-neighbour approximation [8]. Extinction coefficients in units of $10^{-4}/M^4$/cm at 25°C

are as follows: dApTpCpG, $4.09 \cdot 10^4$; and dAp(iPr)Tp(iPr)Cp(iPr)G, $4.09 \cdot 10^4$.

Single-stranded samples for CD melting studies were prepared at $2.5 \cdot 10^{-5}$ *M* concentration in a buffer containing 10 m*M* sodium phosphate, adjusted to pH 7.0. Hybrid samples for CD melting studies were prepared at $2.5 \cdot 10^{-4}$ *M* concentration in total oligonucleotide strands and annealed in a buffer containing 10 m*M* sodium phosphate, 3.0 *M* NaCl, adjusted to pH 7.0, and incubated at −8°C for 1 h.

Circular dichroism (CD) spectroscopy

CD spectra were recorded using a Jasco Model J-720 spectropolarimeter interfaced with an NEC PC-9801 RX microcomputer. The sample temperature was maintained by placing the sample in a 1 mm or 10 mm path length jacketed cylindrical cell equipped with a Neslab RTE-100 bath circulator. Each spectrum was scanned from 320 to 220 nm, and corresponds to an average of eight scans minus the averaged spectra of the buffer alone. CD melting profiles were recorded by measuring the change in molar ellipticity ([θ]) at 254 nm while the temperature was scanned.

RESULTS AND DISCUSSION

Synthesis of oligodeoxyribonucleoside phosphoramidates

Preparation of OPAs was carried out according to previously reported procedures [4,6] and the averaged coupling yields were estimated to be more than 98% by reversed-phase HPLC.

HPLC separation

In order to characterize the diastereoisomerism of OPAs, dinucleoside phosphoramidates [dAp(iPr)T, dTp(iPr)C and dCp(iPr)G] with a 5′-DMT group were first separated with reversed-phase HPLC [9,10]. The results represented in Fig. 2 show the appearance of two distinct peaks (I and II) and baseline separation in all cases. The two separated peaks correspond to the diastereoisomers due to the phosphoramidate linkage. It was found that the ratios of the yielded diastereoisomers were not equal, as suggested in a previous paper [11]. On the other hand, when the 5′-DMT group was removed by acid treatment, the diastereoisomers of dAp(iPr)T could not be completely separated. It should be noted that, when peak II of dTp(iPr)C, for example, was treated with 80% acetic acid, peaks other than dTp(iPr)C appeared (data not shown). Therefore, it is suggested that the purification of OPAs by reversed-phase HPLC is required to perform the two-step purification, *i.e.* as a first step separation of 5′-DMT-on-OPA and as a second step the separation of 5′-DMT-off-OPA.

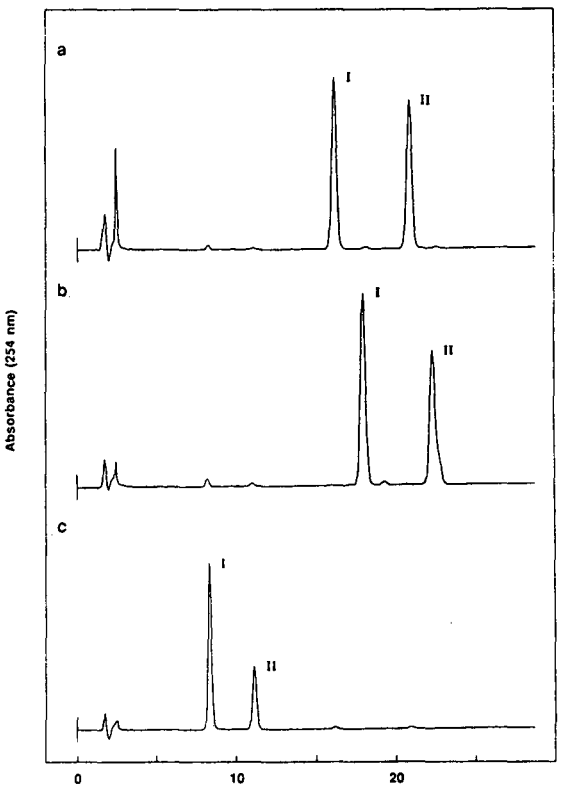

Fig. 2. HPLC analysis of diastereoisomers of (a) 5′-DMT-dAp(iPr)T, (b) 5′-DMT-dTp(iPr)C and (c) 5′-DMT-dCp(iPr)G. Column: Superspher RP-18(e) (4 μm, 4 × 125 mm). Eluents: (A) 0.1 *M* TEAA (pH 7.0) and (B) 0.1 *M* TEAA–acetonitrile (50:50), linear gradient from 75 to 95% B in 40 min. Flow-rate: 0.5 ml/min. Temperature: 30°C. For peak identification, see text.

Under the same conditions, trinucleoside phosphoramidates [dAp(iPr)Tp(iPr)C and dTp(iPr)Cp(iPr)G] with a 5′-DMT group, which consist of four diastereoisomers, were separated.

As depicted in Fig. 3, four distinct, well separated peaks (I, II, III and IV) and baseline separations were achieved in each case. However, when the same chromatographic conditions were applied to the separation of eight diastereoisomers of dAp(iPr)Tp(iPr)Cp(iPr)G with a 5′-DMT group, the eight diastereoisomers could not be separated. For the optimization of the separation, the acetonitrile gradient profile was studied according to the procedure proposed previously [12,13]. The resulting chromatogram is shown in Fig. 4a, indicating that the separation of the diastereoisomers was not complete and that the baseline separation was not achieved. When the same sample was detritylated, six peaks appeared, as shown in Fig. 4b.

To separate all diastereoisomers, improvements in the chromatographic conditions were made by changing the column temperature from 30°C to 40°C (Fig. 5a and b) [14] and the column length from 125 mm to 250 mm (Fig. 5b and c). The chromatograms in Fig. 5 show that the separation was largely improved. However, in spite of such improvement, all eight diastereoisomers could not be separated, and baseline separation was not completely achieved. Based on these results, to isolate all eight diastereoisomers, the following protocol was used. First, the sample with a 5′-DMT group was loaded on a Superspher RP-18(e) column (4 μm, 4 × 250 mm) and the seven peaks, which were designated A to G in order of elution, as shown in Fig. 5c, were fractionated. Subsequently each fraction was treated with 80% acetic acid for detritylation, and applied to the second separa-

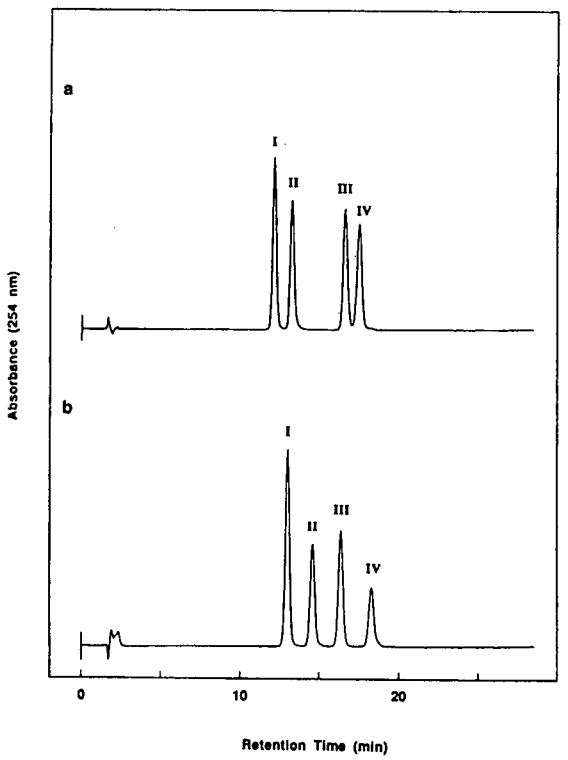

Fig. 3. HPLC analysis of diastereoisomers of (a) 5′-DMT-dAp(iPr)Tp(iPr)C and (b) 5′-DMT-dTp(iPr)Cp(iPr)G. Column: Superspher RP-18(e) (4 μm, 4 × 125 mm). Eluents: (A) 0.1 *M* TEAA (pH 7.0) and (B) 0.1 *M* TEAA–acetonitrile (50:50), linear gradient from 75 to 95% B in 40 min. Flow-rate: 0.5 ml/min. Temperature: 30°C. For peak identification, see text.

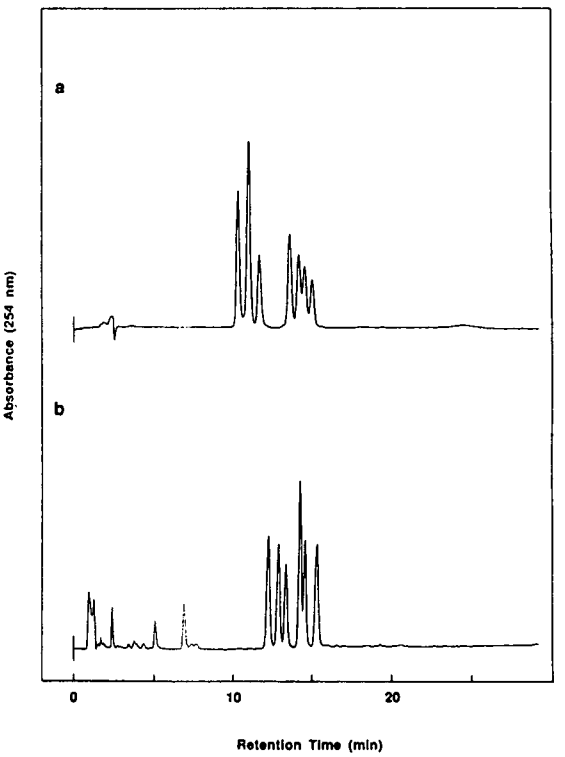

Fig. 4. HPLC analysis of diastereoisomers of (a) 5′-DMT-dAp(iPr)Tp(iPr)Cp(iPr)G, linear gradient from 75 to 95% B in 40 min at a flow-rate of 0.5 ml/min, and (b) dAp(iPr)Tp(iPr)Cp(iPr)G, linear gradient from 35 to 65% B in 30 min at a flow-rate of 1 ml/min. Column: Superspher RP-18(e) (4 μm, 4 × 125 mm). Eluents (A) 0.1 *M* TEAA (pH 7.0) and (B) 0.1 *M* TEAA–acetonitrile (50:50). Temperature: 30°C.

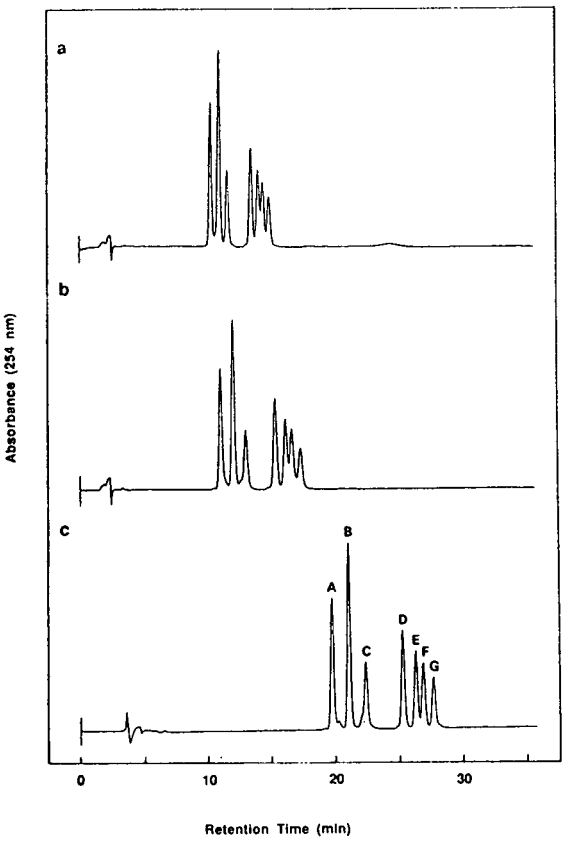

Fig. 5. HPLC analysis of diastereoisomers of (a) 5′-DMT-dAp(iPr)Tp(iPr)Cp(iPr)G on a Superspher RP-18(e) (4 μm, 4 × 125 mm) column and temperature 30°C, (b) 5′-DMT-dAp(iPr)Tp(iPr)Cp(iPr)G on a Superspher RP-18(e) (4 μm, 4 × 125 mm) column and temperature 40°C and (c) 5′-DMT-dAp(iPr)Tp(iPr)Cp(iPr)G on a Superspher RP-18(e) (4 μm, 4 × 250 mm) column and temperature 40°C. Eluents (A) 0.1 *M* TEAA (pH 7.0) and (B) 0.1 *M* TEAA–acetonitrile (50:50), linear gradient from 75 to 95% B in 40 min. Flow-rate: 0.5 ml/min. For peak identification, see text.

tion under the chromatographic conditions set for the detritylated samples. It was found that peak B in Fig. 5 contained two diastereoisomers (B′-1 and B′-2 in Fig. 6). Using this protocol, all eight diastereoisomers could be completely separated, as shown in Fig. 6, in which the peaks corresponding to A to G in Fig. 5c are designated A′ to G′, respectively. The reason why the diastereoisomers could be effectively separated is unclear. One possible explanation of the mechanism could be the effects due to the configuration and conformation of OPAs. The isopropyl moiety introduced into internucleotide linkages is hydrophobic and accounts for the hydrophobicity of OPAs. Also, the direction in which the alkyl moiety points might affect the conformation of OPAs. These effects may together affect the affinity of OPAs for the column packing.

CD measurement

The conformations of the eight diastereoisomers and their hybrids with their complementary ODNs were studied by CD spectroscopy [9,15].

We measured the temperature-dependent CD spectra of ODN (dApTpCpG) and eight diastereoisomers of dAp(iPr)Tp(iPr)Cp(iPr)G. Fig. 7 shows the CD spectra of eight diastereoisomers of dAp(iPr)Tp(iPr)Cp(iPr)G together with their parent ODNs (dApTpCpG) at 20°C. The CD spectra of the diastereoisomers were characteristic of right-handed DNAs and, in comparison with their parent ODNs, the intensities of molar ellipticity were small and different in each diastereoisomer. It was also observed that eight diastereoisomers can be classified into four groups (A′ and B′-1, B′-2 and C′, D′ and F′, E′ and G′).

Fig. 8 shows CD melting curves for the sense ODN (dCpGpApT)–antisense ODN (dApTpCpG) hybrid, the sense ODN–diastereoisomer A′ hybrid and the sense ODN–diastereoisomer G′ hybrid. The melting curve of the sense ODN–diastereoisomer A′ hybrid is similar in shape to that of the sense ODN–Antisense ODN hybrid, but the melting curve of the sense ODN–diastereoisomer G′ hybrid was broader than that of the sense ODN–Antisense ODN hybrid [16]. The shapes of the molar ellipticity *versus* temperature profiles allowed us to measure the transition temperature. The data clearly show that some diastereoisomers showed distinct transition temperatures and that some did not. Though the detailed mechanism is now under investigation, it is considered that alkyl moieties might stabilize or disrupt the hybrid of OPAs with ODNs depending on their configurations.

CONCLUSIONS

It has been found conclusively that diastereoisomers of OPAs up to tetramers can be

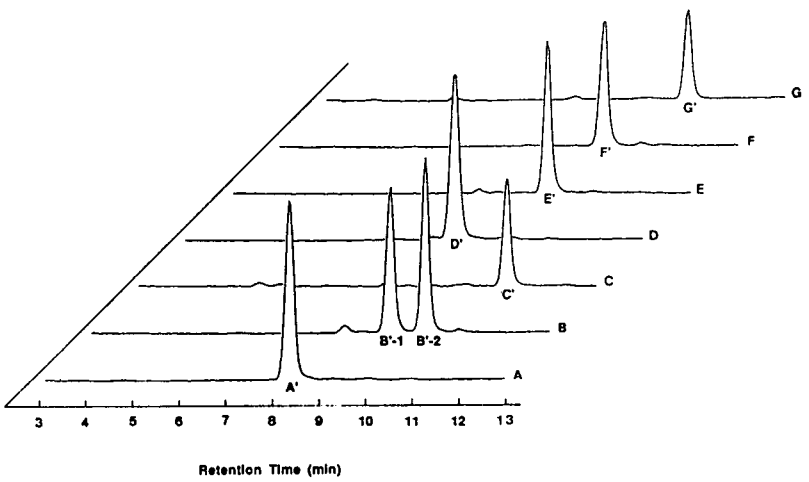

Fig. 6. HPLC analysis of diastereoisomers of d(Ap(iPr)Tp(iPr)Cp(iPr)G). Column: Superspher RP-18(e) (4 μm, 4 × 125 mm). Eluents (A) 0.1 *M* TEAA (pH 7.0) and (B) 0.1 *M* TEAA–acetonitrile (50:50), linear gradient from 35 to 65% B in 30 min. Flow-rate: 1.0 ml/min. Temperature: 40°C. For peak identification, see text.

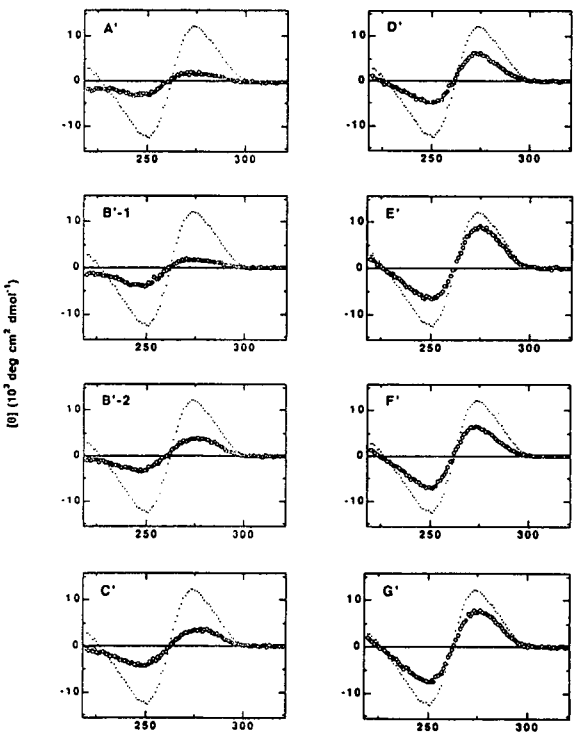

Fig. 7. CD spectra of eight diastereoisomers of dAp(iPr)Tp(iPr)Cp(iPr)G (open circles) and their parent ODN (dApTpCpG) (closed circles) in 10 m*M* sodium phosphate (pH 7.0) at 20°C. The nucleotide concentration is $2.5 \cdot 10^{-5}$ *M*. For peak identification, see text.

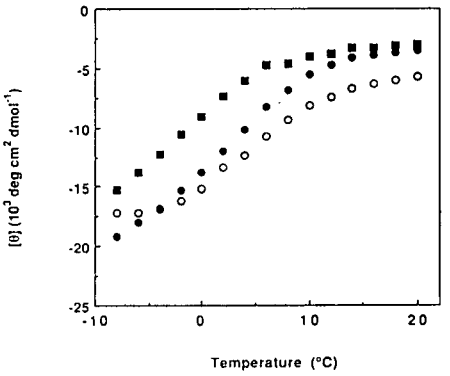

Fig. 8. CD melting curves of sense ODN–antisense ODN hybrid (open circles), sense ODN–diastereoisomer A' hybrid (closed circles), and sense ODN–diastereoisomer G' hybrid (closed squares) in 10 m*M* sodium phosphate (pH 7.0), 3 *M* NaCl. The total nucleotide concentration is $2.5 \cdot 10^{-4}$ *M*.

separated by employing the optimized chromatographic conditions of reversed-phase HPLC. Also, from the CD measurements of the diastereoisomers, it was found that each diastereoisomer shows different conformation in solution and different abilities to form hybrids as antisense DNA.

ACKNOWLEDGEMENTS

We thank Mr. Hidetaka Miyoshi for his technical assistance. This research was partly supported by a Grant-in Aid for Scientific Research

on Priority Areas (032431104) from the Ministry of Education, Science and Culture, Japan.

REFERENCES

1 J.S. Cohen (Editor), *Oligodeoxynucleotides, Antisense Inhibition of Gene Expression*, CRC Press, Boca Raton, FL, 1988.
2 E. Wickstrom (Editor), *Prospects for Antisense Nucleic Acid Therapy of Cancer and AIDS*, Wiley–Liss, New York, 1991.
3 E. Uhlmann and A. Peyman, *Chem. Rev.*, 90 (1990) 543.
4 B. Froehler, P. Ng and M. Matteucci, *Nucleic Acids Res.*, 16 (1988) 4831.
5 W.J. Stec and G. Zon, *J. Chromatogr.*, 326 (1985) 263.
6 T. Tanaka and R.L. Letsinger, *Nucleic Acids Res.*, 10 (1982) 3249.
7 Applied Biosystems, *User Bulletin* 13, Revised, April (1987).
8 D.J. Puglisi and I. Tinoco, Jr., *Methods Enzymol.*, 180 (1989) 304.
9 M. Weinfeld, A.F. Drake, R. Kuroda and D.C. Livingstone, *Anal. Biochem.*, 178 (1989) 93.
10 A.J.J.M. Coenen, L.H.G. Henckens, Y. Mengerink, Sj. van de Wal, P.J.L.M. Quaedflieg, L.H. Koole and E.M. Meijer, *J. Chromatogr.*, 596 (1992) 59.
11 H. Ozaki, M. Kitamura, K. Yamana, A. Murakami and T. Shimidzu, *Bull. Chem. Soc. Jpn.*, 63 (1990) 1929.
12 R.W.A. Oliver (Editor), *HPLC of Macromolecules —A Practical Approach*, Oxford University Press, Oxford, 1989.
13 T. Nambara and N. Ikehara (Editors), *Modern High-Performance Liquid Chromatography*, Hirokawa Publishing Company, Tokyo, 1988, p. 1.
14 C.G. Huber, P.J. Oefner and G.K. Bonn, *J. Chromatogr.*, 599 (1992) 113.
15 G.C. Causley, P.W. Staskus and W. Curtis, *Biopolymers*, 22 (1983) 945.
16 Z.J. Lesnikowski, M. Jaworska and W.J. Stec, *Nucleic Acids Res.*, 18 (1990) 2109.

Journal of Chromatography, 648 (1993) 165–173
Elsevier Science Publishers B.V., Amsterdam

CHROM. 25 322

Multidimensional evaluation of impurity profiles for generic cephalexin and cefaclor antibiotics

B.A. Olsen*, S.W. Baertschi and R.M. Riggin

Lilly Research Laboratories, Eli Lilly and Company, P.O. Box 685, Lafayette, IN 47902 (USA)

(First received February 11th, 1993; revised manuscript received May 14th, 1993)

ABSTRACT

A multidimensional approach is described for characterizing impurities in samples of generic cefaclor and cephalexin antibiotics. High-performance liquid chromatography (HPLC) with gradient elution followed by photodiode array or mass spectrometric detection provides valuable information concerning the nature of impurities observed. Results are presented which demonstrate the utility of these techniques for identifying impurities and distinguishing among process-related impurities, degradation products and formulation excipients. Preparative HPLC isolation and spectroscopic identification of some impurities is also described.

INTRODUCTION

High-performance liquid chromatography (HPLC) is extremely useful for the determination of related substances in cephalosporin antibiotics [1,2]. Related substances are defined as structurally related impurities arising from the manufacturing process or by degradation [3]. Determination of these impurities in bulk drug substances and products is important for quality control and evaluation of samples from different sources. For evaluation of drug quality, it is desirable to determine not only the total amount of related substances, but the nature or identity of these impurities. This is especially important if impurity profiles are qualitatively different between samples. Such differences may be caused by changes in the manufacturing process or a switch in supplier of the bulk drug. Different manufacturing processes may give rise to different process-related impurities, and the treatment of the product during manufacturing and storage by different suppliers may produce a variable profile of degradation products. The "fingerprinting" of drug products using multiple techniques has recently been proposed as a way to monitor and detect such changes [4]. Another aspect of profiling impurities in formulated products such as oral suspensions is the need to distinguish between excipients and impurities.

While HPLC can provide much information regarding impurity profiles, to better meet the needs outlined above, information beyond a single-wavelength absorbance *vs.* time chromatogram is required. Capacity factor data together with ultraviolet–visible spectra from photodiode array (PDA) detection have been used for confirmation of peak identity in toxicological drug screening [5–7], analysis of forensic samples [8–10], drug metabolism studies [11–14] and evaluation of impurities in bulk drugs and formulations [15–18]. Liquid chromatography–mass spectrometry (LC–MS) has also been utilized for positive peak identification and quantification in drug disposition studies [11,19–22] and in confirmation of drug impurity or degradation product identities [23,24]. In this paper, a multi-

* Corresponding author.

0021-9673/93/$06.00

dimensional approach utilizing HPLC with PDA and/or MS detection as tools for drug impurity characterization is described. Preparative HPLC isolation and structural characterization by nuclear magnetic resonance (NMR) spectroscopy is also employed when necessary. The approach is illustrated by examination of impurity profiles for cephalexin and cefaclor bulk drug substance and formulated product from different sources.

EXPERIMENTAL

Reagents

HPLC-grade acetonitrile and methanol were obtained from EM Science (Gibbstown, NJ, USA). Mobile phases were prepared using monobasic sodium phosphate monohydrate, also from EM Science. Water for mobile phase and sample solutions was purified with a Milli-Q system from Millipore (Milford, MA, USA). Samples of bulk and formulated cefaclor were obtained from Eli Lilly & Co. and generic manufacturers.

Apparatus

The chromatographic system consisted of a Model 600E pump (Waters, Bedford, MA, USA) and a Model 728 autoinjector (Alcott, Norcross, GA, USA) with a 20-μl fixed-loop injection valve (Valco, Houston, TX, USA). Single-wavelength detection using a Model 787 UV detector (Applied Biosystems, Ramsey, NJ, USA) set at 220 nm was used for most samples. Single-wavelength chromatograms were recorded using an in-house data acquisition system. When UV spectra of sample components were desired, a Waters Model 990 PDA detector was used in place of the single-wavelength detector. All UV spectra given in the figures were acquired using PDA detection of components after HPLC separation. The amplitude of some spectra has been scaled numerically for ease of comparison in the figures.

The HPLC separation was performed on a 250 mm $\times$ 4.6 mm, 5 μm particle size, YMC-ODS column (YMC, Morris Plains, NJ, USA) using 50 m*M* sodium phosphate, pH 4.0, with a two-stage acetonitrile gradient from 2.25 to 45% [1]. The sample concentration for bulk cephalexin and cefaclor was 5.0 mg/ml. Formulated samples were prepared based on the dosage strength to give concentrations of cephalexin or cefaclor of approximately 5 mg/ml. This concentration provided an injection of 100 μg of antibiotic onto the analytical HPLC column.

The LC–MS experiments were performed with a Beckman System Gold liquid chromatograph (Beckman Instruments, Palo Alto, CA, USA) and a Sciex Model API III mass spectrometer (Sciex, Thornhill, Canada). A heated nebulizer atmospheric chemical ionization source was used for the work described here. The ionspray mode has also been used for similar samples. The mobile phase for LC–MS contained 0.1% acetic acid instead of phosphate buffer. The mobile phase was held at 15% acetonitrile for 15 min followed by a linear ramp to 25% acetonitrile over 10 min. A Beckman Model 168 diode array UV–Vis detector was used between the column and mass spectrometer interface to detect any changes in retention order from the phosphate eluent system. Flow was diverted away from the MS source during elution of the cefaclor peak to reduce cefaclor background in subsequent scans. The source was held at 450°C with nitrogen used as the nebulizer gas at a pressure of 80 p.s.i. (1 p.s.i. = 6894.76 Pa). For these experiments, 200 μl of a 5 mg/ml cefaclor sample solution were injected (1 mg applied to the column).

Preparative isolation

The following conditions were used to isolate impurities from source C cefaclor (see Results and Discussion). The mobile phase for preparative HPLC isolation consisted of a gradient from 25 to 50% solvent B over 18 min after an initial isocratic period (5 min at 25% solvent B). Solvent A consisted of an aqueous solution of 0.1% acetic acid, while solvent B consisted of a mixture of acetonitrile–water–acetic acid (60:40:0.1, v/v/v). The flow-rate was 20 ml/min. A YMC-ODS (250 $\times$ 20 mm, 5 μm particle size) column was used.

The sample was dissolved in 0.025 *M* HCl at a concentration of 10 mg/ml. A total of 40 ml of this solution was injected onto the column for each preparative run (38 preparative runs were made altogether). Three fractions were col-

lected. These fractions were cooled to 0°C immediately upon collection until all 38 preparative runs were completed. The fractions were then frozen and lyophilized to remove solvents. A small aliquot of the remaining solids from each fraction was analyzed by gradient HPLC using the cefaclor-related substances method [1] prior to spectroscopic characterization.

NMR analysis

The NMR spectra were collected on a Bruker 500 MHz NMR system (Bruker Instruments, Billerica, MA, USA) in [$^2H_6$]dimethyl sulfoxide (with a trace of trifluoroacetic acid added to slow down proton exchange and sharpen the resonances), and referenced to internal tetramethylsilane. Carbon–proton correlation assignments were detected using two-dimensional heteronuclear experiments designed to detect correlations due to coupling through one [25] or more than one [26] chemical bond.

RESULTS AND DISCUSSION

Characterization process

To survey the impurities present in cephalexin or cefaclor, a gradient HPLC profile at 220 nm where nearly all related substances will show some absorbance is obtained. This can provide quantitative results for individual and total impurities [1]. Identities of several components may be known from retention time match with known impurities and past experience of which impurities are likely to be present. Matching UV spectra from a PDA detector for a known impurity and a peak of interest with the same retention time provides a strong, if not absolute indication of peak identity.

Most process-related impurities in cephalexin and cefaclor contain an intact 3-cephem nucleus while degradation products do not [1,27]. Therefore, if the spectrum of an unknown component has the characteristic 3-cephem absorbance maximum at about 260–265 nm [28] the component is likely to be a process-related impurity. Other spectral features indicate a degradation product or possibly an excipient in a formulation sample. A sample may be characterized further by obtaining structural information from LC–MS or

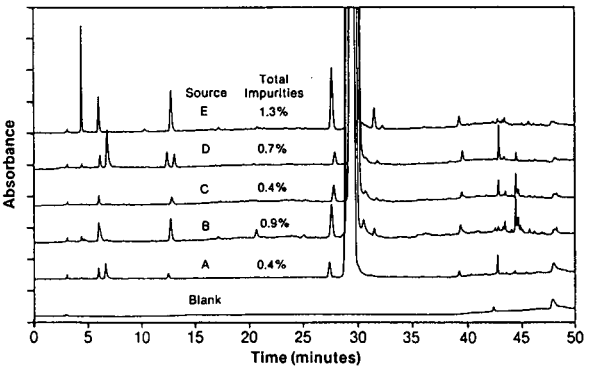

Fig. 1. Impurity profiles of bulk cephalexin from multiple sources. Wavelength 220 nm.

from spectroscopic measurements after preparative HPLC isolation. This can provide absolute identification of previously unknown impurities. This characterization process adjusted for the spectral properties of the compounds being examined could be applied to the analysis of several drugs.

Bulk drug substance analysis

Impurity profiles for bulk cephalexin from several suppliers are shown in Fig. 1. The total level of impurities is comparable among these samples, but there are differences in the individual components present. The chromatogram for the source D sample showed a retention time match with two known impurities, Δ^2-cephalexin (isomer nomenclature follows the cephem ring numbering convention [29]) and N-phenylglycyl cephalexin (Fig. 2). As shown in Fig. 3, the UV

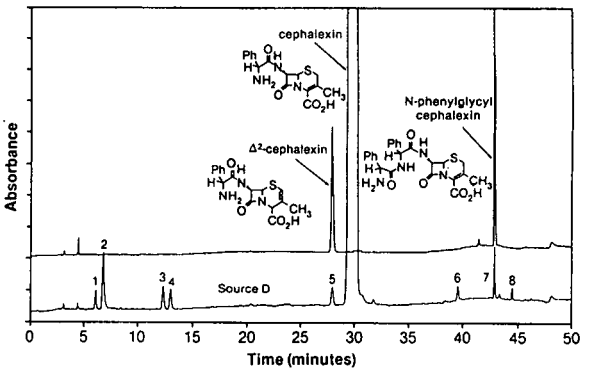

Fig. 2. Retention time comparison of source D cephalexin impurities with Δ^2-cephalexin and N-phenylglycyl cephalexin. Wavelength 220 nm. Approximately 0.4 μg each of Δ^2-cephalexin and N-phenylglycyl cephalexin injected.

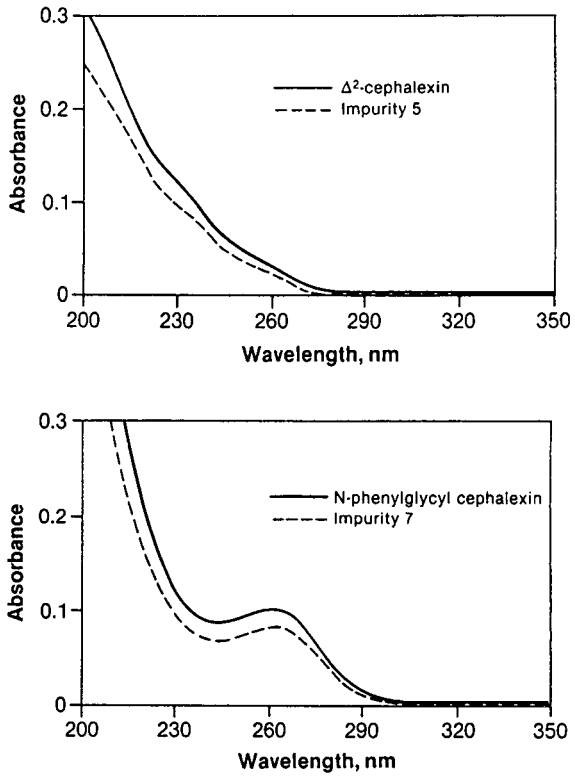

Fig. 3. UV spectra comparison of source D cephalexin impurities with Δ^2-cephalexin and N-phenylglycyl cephalexin.

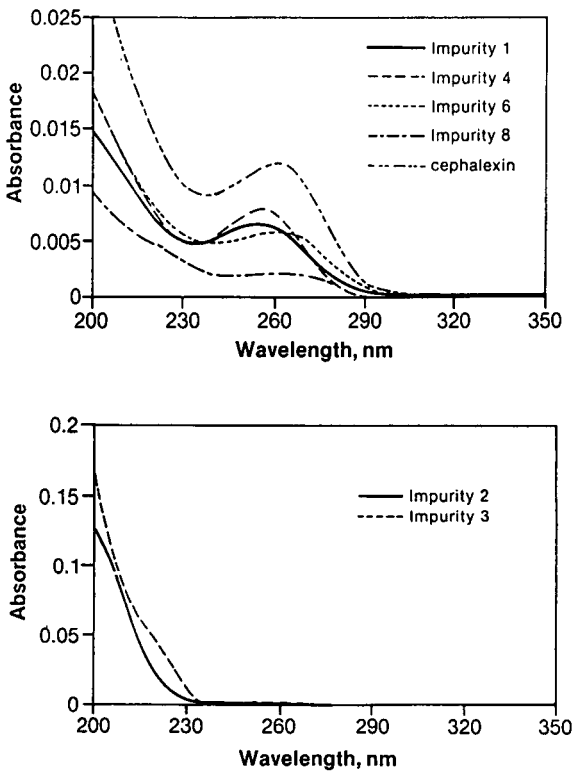

Fig. 4. UV spectra of unknown impurities in source D cephalexin.

spectra for the sample impurities also matched the known impurity spectra, thereby confirming their identities. The Δ^2-isomer is a primary degradation product of cephalexin and has a spectrum much different from that of cephalexin. In contrast, the N-phenylglycyl cephalexin impurity is process-related, resulting from over-acylation during the final synthetic step. Its spectrum is nearly identical to that of cephalexin. Spectra for unknown impurities (Fig. 4) indicated that four are likely to be process-related because of the 3-cephem absorbance band (peaks 1, 4, 6, 8) and two are probably degradation products (peaks 2, 3).

Impurity profiles for bulk cefaclor shown in Fig. 5 revealed three late-eluting impurities in one sample that were not present in the others. These impurities accounted for a large portion of the higher level of total related substances compared to the other samples. The expanded chromatogram in Fig. 6 shows that the retention time of peak 1 matched that of N-phenylglycyl cefaclor (PG-cefaclor) and peak 2 was very close in retention to 2-hydroxy-3-phenylpyrazine (2,3-HPP), a known degradation product. A match of the UV spectra was obtained for PG-cefaclor, but the peak 2 spectrum was much different from

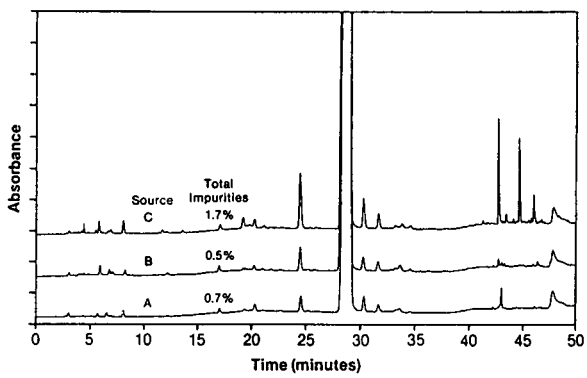

Fig. 5. Impurity profiles of bulk cefaclor from multiple sources. Wavelength 220 nm.

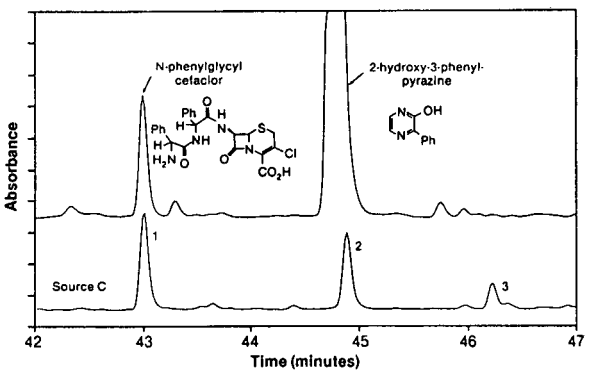

Fig. 6. Expanded chromatogram comparing retention of source C cefaclor impurities with N-phenylglycyl cefaclor and 2-hydroxy-3-phenylpyrazine. Wavelength 220 nm. A 0.6-μg amount of N-phenylglycyl cefaclor and 4 μg 2-hydroxy-3-phenylpyrazine injected.

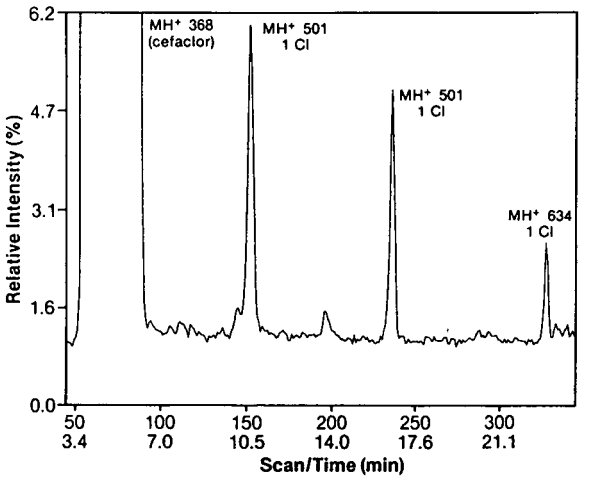

Fig. 8. Total ion current LC–MS chromatogram for late-eluting impurities in source C cefaclor.

that of 2,3-HPP (Fig. 7). Spectra of peaks 2 and 3 were nearly identical to that of PG-cefaclor, suggesting that they were also process-related impurities.

The source C cefaclor sample was analyzed by LC–MS–MS using atmospheric pressure chemical ionization followed by collison-induced dissociation of the molecular ion for fragmentation information. The protonated molecular ions from each peak of the total ion current chromatogram are indicated in Fig. 8 with an example of MS–MS fragmentation data for the first impurity peak shown in Fig. 9. The identification of PG-cefaclor by retention time and UV spectral match was further confirmed by the MH^+ ion at m/z 501 and appropriate fragment ions. Impurity peaks 2 and 3 gave MH^+ ions corresponding to cefaclor plus one and two phenylglycine groups, respectively. Without careful control of

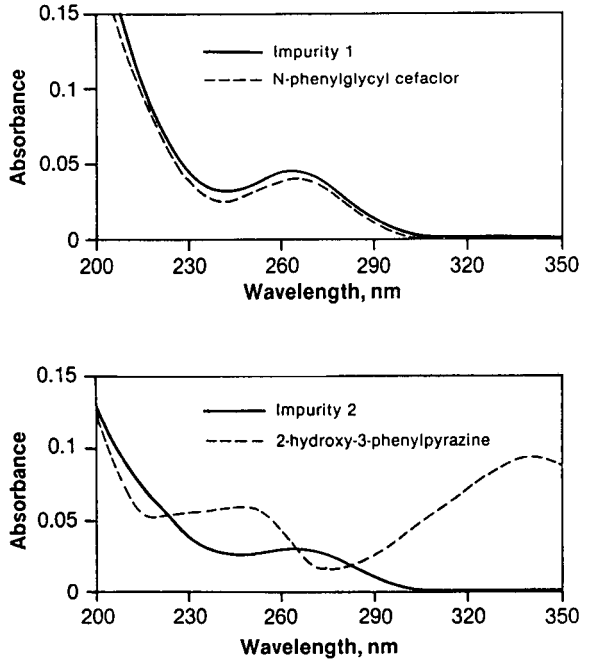

Fig. 7. UV spectra comparison of source C cefaclor impurities with N-phenylglycyl cefaclor and 2-hydroxy-3-phenylpyrazine.

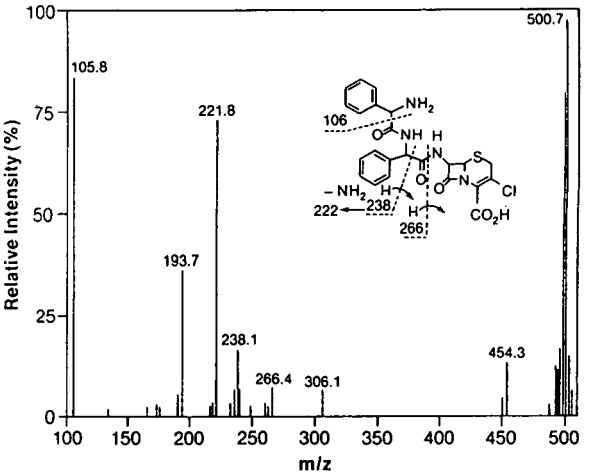

Fig. 9. MS–MS data for impurity 1 in source C cefaclor.

the reaction conditions used to prepare cefaclor, acylation at sites other than the desired 7-amino group on the 3-chloro nucleus may take place. Adding another phenylglycine to the phenylglycine side chain of a cefaclor molecule forms PG-cefaclor. Adding yet another phenylglycine to the side chain gives a compound with a molecular mass corresponding to that observed for impurity 3. During the acylation reaction it may have also been possible to form an acid chloride at the carboxylic acid on the 3-chloro nucleus. This species could then form an amide with phenylglycine in addition to being acylated at the 7-amino position. This compound would have the same molecular mass as PG-cefaclor, but with the extra phenylglycine at a different position. The mass spectral data for impurities 2 and 3 supported the structures given in Fig. 10.

Additional confirmation of the molecular structure of impurity peaks 1–3 was obtained by preparative HPLC isolation and off-line characterization by NMR. Conditions for isolation and NMR analysis are contained in the Experimental section. Chemical shift assignments of the proton and carbon NMR spectra for the three isolated impurites are given in Table I. These data confirm the structures as those given in Fig. 10.

Formulation analysis

The presence of excipients in formulations such as oral suspensions adds the complication of distinguishing peaks due to excipients from those due to impurities. If the excipients in a formulation are known, their retention and UV response under the gradient HPLC conditions can be compared to suspect peaks in the sample. Even

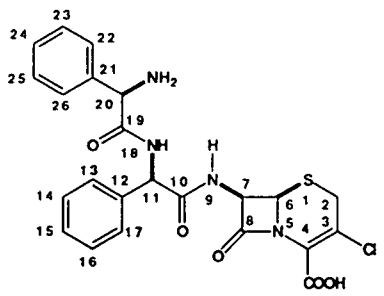

Impurity 1: N-phenylglycyl cefaclor

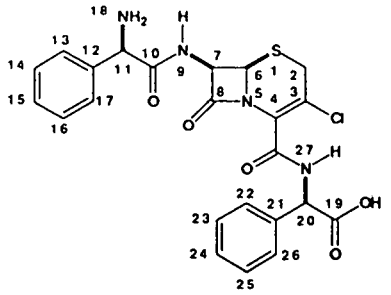

Impurity 2: C-phenylglycyl cefaclor

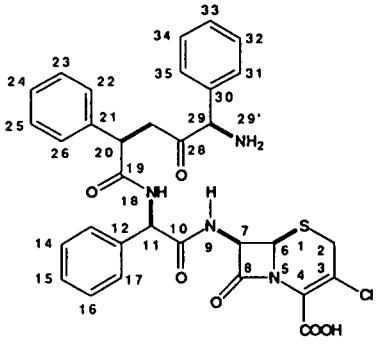

Impurity 3: N,N'-diphenylglycyl cefaclor

Fig. 10. Structures of impurities 1–3 in source C cefaclor.

TABLE I

^1H AND ^{13}C NMR ASSIGNMENTS OF CEFACLOR AND IMPURITIES FROM SOURCE C (IN [$^2H_6$]DIMETHYL SULFOXIDE)

^{13}C first line; ^1H second line; values in ppm *vs.* tetramethylsilane. n.a. = Not assigned; n.m. = not measured; – = not applicable.

Site[a]	Cefaclor	1	2	3
2	30.07	n.m.	29.72	29.88
	3.87, 3.58	3.85, 3.58	3.78, 3.49	3.86, 3.59
2-COOH	161.61	n.m.	159.57	161.57
	–	–	–	–
3	121.03	n.m.	118.03	120.91
	–	–	–	–
4	125.56	n.m.	127.48	125.30
	–	–	–	–
6	57.29	n.m.	57.32	57.33
	5.15	5.07	5.08	5.08
7	58.90	n.m.	58.74	58.58
	5.82	5.69	5.70	5.69
8	163.17	n.m.	162.24	163.69
	–	–	–	–
9	–	n.m.	–	–
	9.64	9.40	9.64	9.33
10	168.45	n.m.	168.57	170.08
	–	–	–	–
11	55.69	n.m.	55.56	55.83
	5.06	5.67	5.04	5.55
12	133.57	n.m.	133.66	137.59
	–	–	–	–
13, 17	128.06	n.m.	n.a.	127.07
	7.54	n.a.	n.a.	7.29
14, 16	128.91	n.m.	n.a.	n.a.
	7.44	n.a.	n.a.	n.a.
15	129.54	n.m.	n.a.	n.a.
	7.44	n.a.	n.a.	n.a.
18	–	–	–	–
	8.78	9.32	8.72	9.06
19	–	n.m.	171.14	168.74
	–	–	–	–
20	–	n.m.	56.45	55.83
	–	5.12	5.48	5.82
21	–	n.m.	137.05	138.07
	–	–	–	–
22, 26	–	n.m.	n.a.	127.31
	–	n.a.	n.a.	7.29
23, 25	–	n.m.	n.a.	n.a.
	–	n.a.	n.a.	n.a.
24	–	n.m.	n.a.	n.a.
	–	n.a.	n.a.	n.a.
27	–	–	–	–
	–	8.63	–	9.20
28	–	–	–	166.79
	–	–	–	–
29	–	–	–	55.16
	–	–	–	5.11

(Continued on p. 172)

TABLE I *(continued)*

Site[a]	Cefaclor	1	2	3
30	–	–	–	133.99
	–	–	–	–
31, 35	–	–	–	127.86
	–	–	–	7.43
32, 34	–	–	–	n.a.
	–	–	–	n.a.
35	–	–	–	n.a.
	–	–	–	n.a.
36	–	–	–	–
	–	–	–	8.60

[a] See Fig. 10 for numbering.

without knowing what excipients were used, their distinctive absorption spectra can often indicate their presence.

Chromatograms for two cefaclor oral suspensions are shown in Fig. 11. An unknown component designated as peak 1 was observed in the source A sample. FD&C Red 40 was listed as a coloring agent on the package insert for this sample and the retention time for this compound matched that of the unknown peak. The UV spectrum of FD&C Red 40 also clearly matched that of the unknown peak (Fig. 12). The large late-eluting component (peak 2) in sample B was identified by retention time and UV spectral match (Fig. 12) as benzoate, a common preservative, even though this ingredient was not listed on the package or package insert. Identification of these peaks as excipients justified not including them as impurities and allowed an

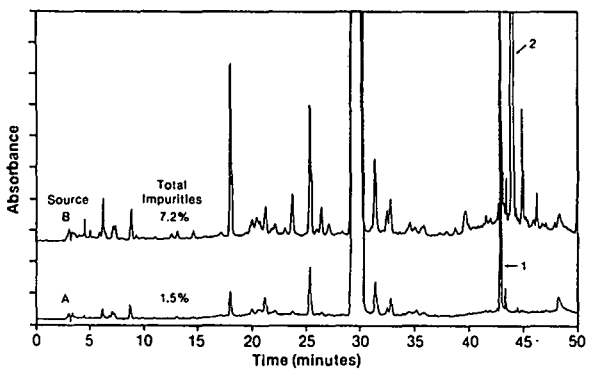

Fig. 11. Impurity profiles of cefaclor oral suspension formulations from two sources. Wavelength 220 nm. UV spectra for unknown peaks 1 and 2 are given in Fig. 12.

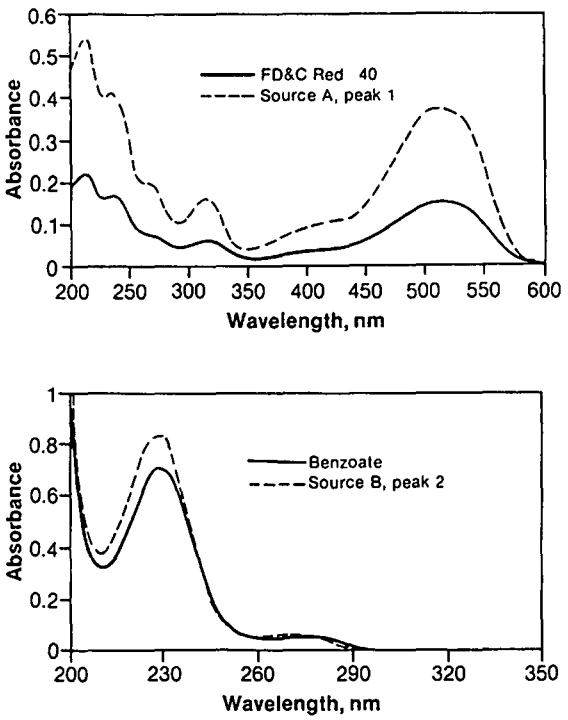

Fig. 12. Comparison of excipient and sample component UV spectra.

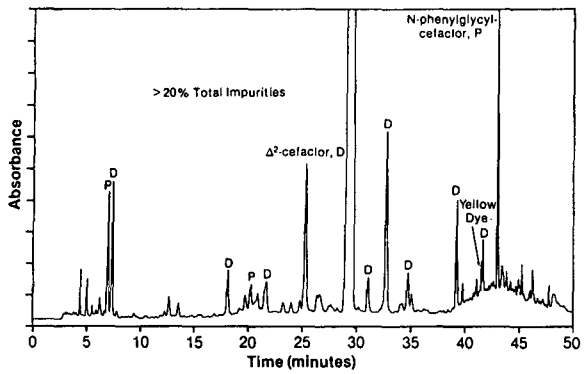

Fig. 13. Impurity profile for cefaclor granule formulation. Wavelength 220 nm. P = Process-related impurity; D = degradation product.

accurate assessment of total impurities in the samples.

Another example of formulation analysis is the impurity profile of a cefaclor granule formulation shown in Fig. 13. Some peaks were identified, while others were characterized as process-related impurities or degradation products as indicated. This example shows the utility of the approach for a sample containing a large number of impurities.

CONCLUSIONS

For HPLC analysis of impurities in cephalexin and cefaclor, PDA detection can be used to confirm impurity identity, provide an indication of whether an impurity is process-related or a degradation product, and distinguish excipients from impurities. LC–MS can also be used to obtain structural information useful in identification of unknowns. While the experimental conditions would change for different products, the general approach used here for cephalexin and cefaclor can be applied to the analysis of many drugs.

ACKNOWLEDGEMENTS

We wish to thank D. Dorman and L. Spangle for providing the NMR spectra and interpretation, J. Occolowitz for assistance with the MS identification and F. Perry for helpful discussions during the course of this work.

REFERENCES

1 L.J. Lorenz, F.N. Bashore and B.A. Olsen, *J. Chromatogr. Sci.*, 30 (1992) 211–216.
2 S. Ting, *J. Assoc. Off. Anal. Chem.*, 71 (1988) 1123–1130.
3 *US Pharmacopeia* XXII, United States Pharmacopeial Convention, Rockville, MD, 1989.
4 T. Layloff, *Pharm. Tech.*, September (1991) 146–148.
5 K. Jinno, M. Hayashida and T. Watanabe, *J. Chromatogr. Sci.*, 28 (1990) 367–373.
6 S.F. Cooper, R. Masse and R. Dugal, *J. Chromatogr.*, 489 (1989) 65–68.
7 D.W. Hill and K.J. Langer, *J. Liq. Chromatogr.*, 10 (1987) 377–409.
8 I.S. Lurie, D.A. Cooper and R.F.X. Klein, *J. Chromatogr.*, 598 (1992) 59–66.
9 I.S. Lurie and K. McGuinness, *J. Liq. Chromatogr.*, 10 (1987) 2189–2204.
10 I.S. Lurie, J.M. Moore, D.A. Cooper and T.C. Kram, *J. Chromatogr.*, 405 (1987) 273–281.
11 S.M. Bjorge and T.F. Woolf, *LC·GC*, 9 (1991) 780–786.
12 M. Binger and P. Workman, *J. Chromatogr.*, 532 (1990) 321–336.
13 B.J. Clark, A.F. Fell, H.P. Scott and D. Westerlund, *J. Chromatogr.*, 286 (1984) 261–273.
14 A.F. Fell, B.J. Clark and H.P. Scott, *J. Chromatogr.*, 297 (1984) 203–214.
15 P. Betto, E. Ciranni-Signoretti and R. Di Fava, *J. Chromatogr.*, 586 (1991) 149–152.
16 E. Owino, B.J. Clark and A.F. Fell, *J. Chromatogr. Sci.*, 29 (1991) 450–456.
17 B.F.H. Drenth, R.T. Ghijsen and R.A. de Zeeuw, *J. Chromatogr.*, 238 (1982) 113–120.
18 R. Baker, *J. Chromatogr.*, 393 (1987) 447–453.
19 J.D. Gilbert, E.L. Hand, A.S. Yuan, T.V. Olah and T.R. Covey, *Biol. Mass Spectrom.*, 21 (1992) 63–68.
20 H. Fouda, M. Nocerini, R. Schneider and C. Gedutis, *J. Am. Soc. Mass Spectrom.*, 2 (1991) 164–167.
21 T.R. Covey, E.D. Lee and J.D. Henion, *Anal. Chem.*, 58 (1986) 2453–2460.
22 T. Wachs, J.C. Conboy, F. Garcia and J.D. Henion, *J. Chromatogr. Sci.*, 29 (1991) 357–366.
23 Th. Becue and M.Broquarie, *J. Chromatogr.*, 557 (1991) 489–494.
24 K.L. Tyczkowska, R.D. Voyksner and A.L. Aronson, *J. Chromatogr.*, 594 (1992) 195–201.
25 A.E. Derome, in J.E. Baldwin (Editor), *Modern NMR Techniques for Chemistry Research (Organic Chemistry Series)*, Pergamon Press, New York, 1987, Ch. 9.
26 G.E. Martin and A.S. Zektzer, *Magn. Reson. Chem.*, 26 (1988) 631–652.
27 B. Mason and J. Tranter, *Anal. Proc.*, 18 (1981) 310–313.
28 P.V. Demarco and R. Nagarajan, in E.H. Flynn (Editor), *Cephalosporins and Penicillins*, Academic Press, New York, 1972, pp. 360–366.
29 E.H. Flynn (Editor), *Cephalosporins and Penicillins*, Academic Press, New York, 1972.

Journal of Chromatography, 648 (1993) 175–181
Elsevier Science Publishers B.V., Amsterdam

CHROM. 25 364

Determination of minor impurities in terazosin hydrochloride by high-performance liquid chromatography

John F. Bauer*, Suzanne K. Krogh, Zui L. Chang and Chun F. Wong

PPD Physical Analytical Chemistry Department, Abbott Laboratories, North Chicago, IL 60064 (USA)

(First received March 10th, 1993; revised manuscript received June 2nd, 1993)

ABSTRACT

Minor impurities in the anti-hypertensive agent terazosin monohydrochloride dihydrate were determined using high-performance liquid chromatography. Manufacturing impurities and degradation products were separated using a reversed-phase system. Detector response was linear for the individual impurities to approximately 0.5 μg/ml which represents 0.05% of the drug concentration. The procedure provides quantitation of impurities to approximately the 0.05% level with precision (relative standard deviations) of ±0.1% to ±1.2% at a level of approximately 0.5%. A variety of reversed-phase columns were evaluated for the assay method with the optimum resolution achieved using a Zorbax Rx-C8 5-μm packing.

INTRODUCTION

Terazosin monohydrochloride dihydrate is an active antihypertensive agent commercially known as Hytrin (**1**).

Chemically the drug substance is 2-(4-[2-tetrahydrofuranylcarbonyl]-1-piperazinyl)-6,7-dimethoxy-4-quinazolinamine monohydrochloride dihydrate. The compound is prepared via a multistep synthesis and therefore the possibility of by-product formation exists. Several of these potential by-products have been identified in bulk terazosin and represent a range of size and polarity (Fig. 1).

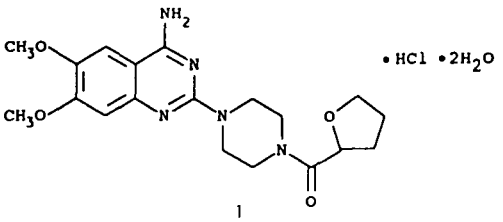

1

The effectiveness of terazosin as an antihypertensive agent is reported elsewhere in the litera-

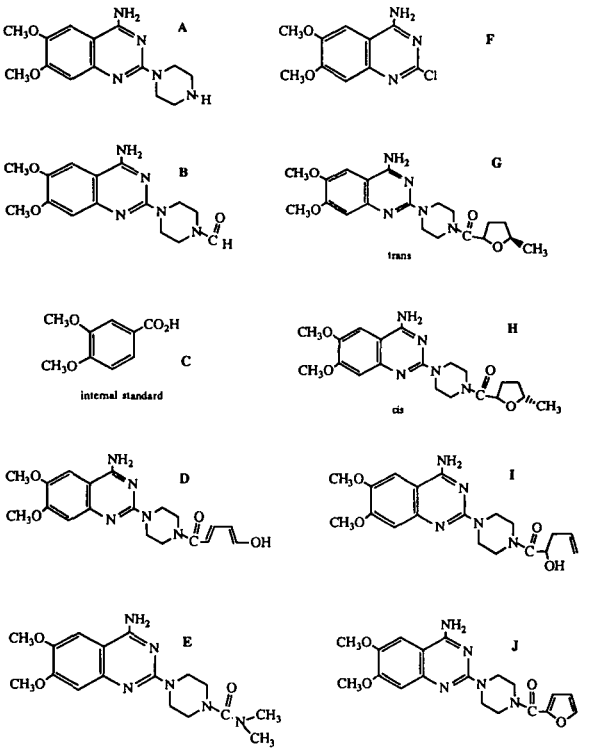

Fig. 1. Potential by-products of terazosin synthesis.

* Corresponding author.

0021-9673/93/$06.00

ture [1–6]. Various HPLC methods have been reported for the determination of terazosin and other quinazolinamines and their metabolites [7–9]. This paper describes the use of HPLC for the quantitation of minor impurities which can occur in terazosin bulk drug. The procedure is used to detect and quantitate potential manufacturing impurities and degradation products. The technique allows the direct determination of these materials without derivatization. In this work a reversed-phase chromatographic column and isocratic elution are used to achieve the required resolution of the drug substance and various impurities. This approach provides reliable quantitation of minor impurities which show marked differences in retention on different stationary phases.

EXPERIMENTAL

Apparatus

The HPLC system consisted of a Spectra-Physics isocratic pump (Spectra-Physics, Santa Clara, CA, USA), an autosampler (Waters, Milford, MA, USA), a variable wavelength ultraviolet detector Spectra 100 (Spectra-Physics) and a Model CR 4A data handling system (Shimadzu, Kyoto, Japan). Chromatographic separations described in the method were made using 5-μm Zorbax Rx C_8 columns measuring 15 cm × 4.6 mm I.D. (Mac Mod, Chadds Ford, PA, USA). Additional columns used included μ-Bondapak C_{18} (10 μm) measuring 30 cm × 3.9 mm I.D. (Waters), Nucleosil C_{18} (5 μm) measuring 15 cm × 4.6 mm I.D. (Macherey-Nagel, Düren, Germany). Bakerbond C_4 wide-pore (5 μm) measuring 25 cm × 4.6 mm I.D. (J.T. Baker, Philipsburg, NJ, USA), Versapak C_{18} (5 μm) measuring 30 cm × 4.0 mm I.D. (Alltech, Deerfield, IL, USA) and a Serva Techsphere C_8 (5 μm) measuring 25 cm × 4.6 mm (Serva Biochemicals, Paramus, NJ, USA).

Prior to use, the components of the eluent were filtered through 0.45-μm nylon membranes (Alltech).

Reagents

Acetonitrile and isopropanol were UV grade, distilled in glass, from Fisher Scientific (Fair Lawn, NJ, USA). 3,4-Dimethoxybenzoic acid, citric acid and sodium citrate dihydrate were reagent grade and were from Aldrich (Milwaukee, WI, USA). A 0.05 *M* solution of sodium citrate and citric acid prepared in deionized water was used in the HPLC eluent (pH = 4.4). All bulk drugs, reference standards and related impurity standards were synthesized at Abbott Laboratories (North Chicago, IL, USA). A 0.2 mg/ml solution of 3,4-dimethoxybenzoic acid in methanol was used as internal standard.

The eluent consisted of 175 ml of acetonitrile, 50 ml of isopropyl alcohol and 1775 ml of 0.05 *M* citrate buffer.

Instrument conditions

Instrument parameters were as follows: flow-rate, 2.0 ml/min; pressure, approximately 1500 p.s.i. (1 p.s.i. = 6894.76 Pa); detector, 254 nm at 0.10 a.u.f.s., attenuation at 16, ambient temperature (*ca.* 22°C) and an injection volume of 50 μl.

Analytical procedure

Terazosin bulk drug samples were prepared by dissolving approximately 100 mg of the drug substance in 100 ml of 90% citrate buffer and 10% acetonitrile containing 10 ml of internal standard solution. Impurity standards for impurities **A**, **F**, **I** and **J** were prepared at a concentration of 0.01 mg/ml (1% level in the same matrix). The amounts of these impurities were determined in the sample by comparing the corresponding peak area ratio (PAR) (*i.e.*, peak area/peak area of internal standard) in the sample and standard preparations. All other impurities were determined by comparing the peak area ratio for the impurity in the sample preparation to that of terazosin at the 1% level.

RESULTS AND DISCUSSION

The HPLC conditions described in the text were developed to resolve the drug substance, manufacturing impurities and the predominant degradation product (impurity **A**). Shown in Fig. 1 are the possible manufacturing impurities identified in the course of this work. Fig. 2 shows the degradation pathway which leads to additional

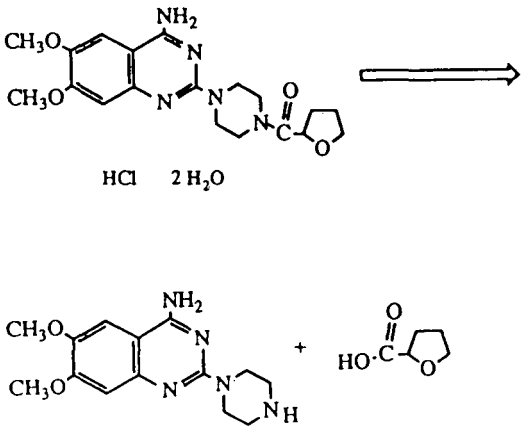

Fig. 2. Hydrolysis degradation pathway of terazosin.

impurity **A** when terazosin is hydrolyzed. These impurities were either isolated and identified by MS and NMR or identified by LC–MS techniques.

The presence of an amine moiety in both terazosin and its impurities required the use of ion-pairing to produce the most symmetrical peak shapes for each of the components. Although gradient elution may be used to resolve these components, a simple isocratic system with ion-pairing was developed that adequately resolves the drug from the early eluting impurities while still eluting the strongly retained impurities within a reasonable time. No single modifier provided optimum resolution of both early and late eluting impurities. Acceptable results were obtained using the ternary system described in the text where a small amount of acetonitrile aids in the resolution of the early eluting components and isopropanol helps to resolve the more strongly retained impurities while maintaining peak symmetry. Although the addition of isopropanol provided better peak shape, the majority of the packings investigated still showed poor resolution for the late eluting peaks (impurities **I** and **J**) which often co-eluted. The Rx-C_8 column, however, differs from the other reversed-phase columns used in that the silanes used are diisopropyl rather than dimethyl. These bulky groups provide steric protection of the siloxane bond and prevent substrate interaction with unprotected silanol groups resulting in a more uniform reversed-phase separation by minimizing interaction with the polar groups on the support. The Rx-C_8 column gave good resolution for all the known impurities including the late eluting components which are separated by six minutes. A detection wavelength of 254 nm provides a very similar response for the impurities and drug substance, providing the best estimate of unknowns quantitated *versus* the drug substance.

TABLE I

PRECISION DATA FOR IMPURITIES ANALYSIS IN BULK TERAZOSIN

Impurity	mg Found			
	Compound **A**	Compound **F**	Compound **I**	Compound **J**
Analyst I				
mg Added	6.45	9.97	9.25	11.23
Equivalent impurity level (%)	0.32	0.50	0.46	0.56
Mean	6.306	10.168	9.282	11.124
S.D.	0.053	0.051	0.011	0.138
R.S.D. (%)	0.84	0.50	0.12	1.24
Analyst II				
mg Added	9.5	12.9	11.3	10.3
Equivalent impurity level (%)	0.48	0.64	0.56	0.52
Mean	9.462	13.064	11.308	10.276
Std. Dev.	0.073	0.116	0.122	0.049
Rel. Std. Dev. %	0.77	0.89	1.08	0.47

Shown in Fig. 3 are typical chromatograms for a mixed standard preparation having individual concentrations for impurities of approximately 100 μg/ml and a typical lot of terazosin spiked with 0.05% of each impurity.

Detector response for terazosin and impurities was linear to approximately 0.5 μg/ml which represents 0.05% of the drug concentration (correlation coefficient >0.9999). Linearity curves of concentration *versus* detector response essentially intersected the origin, allowing the use of one-point calibration for quantitation of known and unknown impurities. Since no lots of terazosin were found which contained all the possible impurities, precision was performed on two artificial mixtures containing the four most frequently occurring impurities at approximately 0.5% each. The study was performed by two analysts on separate days. These data are presented in Table I. As shown the assay precision (R.S.D.) ranged from ±0.12% to ±1.24% for impurities having mean values of 0.32% to 0.64%.

Several alternative reversed-phase packings were evaluated for the determination of terazosin impurities. For this evaluation the

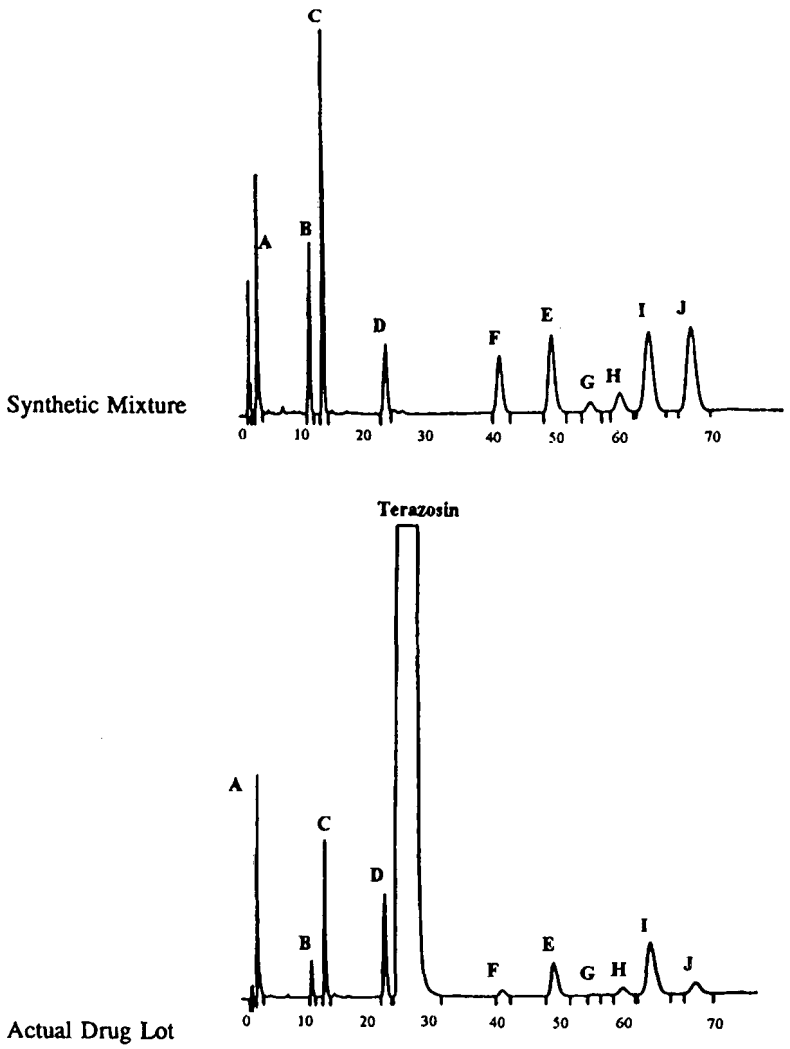

Fig. 3. Chromatograms of synthetic mixture and actual drug lot on Zorbax Rx C_8 column. Numbers indicate time (min).

same eluent was used as described in the experimental. The same synthetic standard mixture shown in Fig. 3 was used for this evaluation. The most discriminating difference in performance between the packings tested [Nucleosil C_{18} (Alltech and Macherey Nagel), Bakerbond C_4, Versapak C_{18}, μ-Bondapak C_{18}, Servo Techsphere C_8 and Zorbax Rx-C_8] was in the resolution of the late eluting peaks (impurities **I** and **J**). Several of the packings showed poor resolution for many of the impurities however, even when acceptable resolution was obtained for the majority of the compounds difficulty was encountered with impurities **I** and **J**. Depending on the column used, this pair of impurities could either co-elute or be resolved completely. Table II presents the corresponding resolution factor for this impurity pair for each packing tested. Fig. 3 and 4 show the HPLC traces.

To determine the reproducibility of the Rx-C_8 packing, a second lot of packing was obtained and evaluated. The separation obtained for terazosin and impurities was identical to the original lot.

The reproducibility of the separation and columns combined with their longevity and good

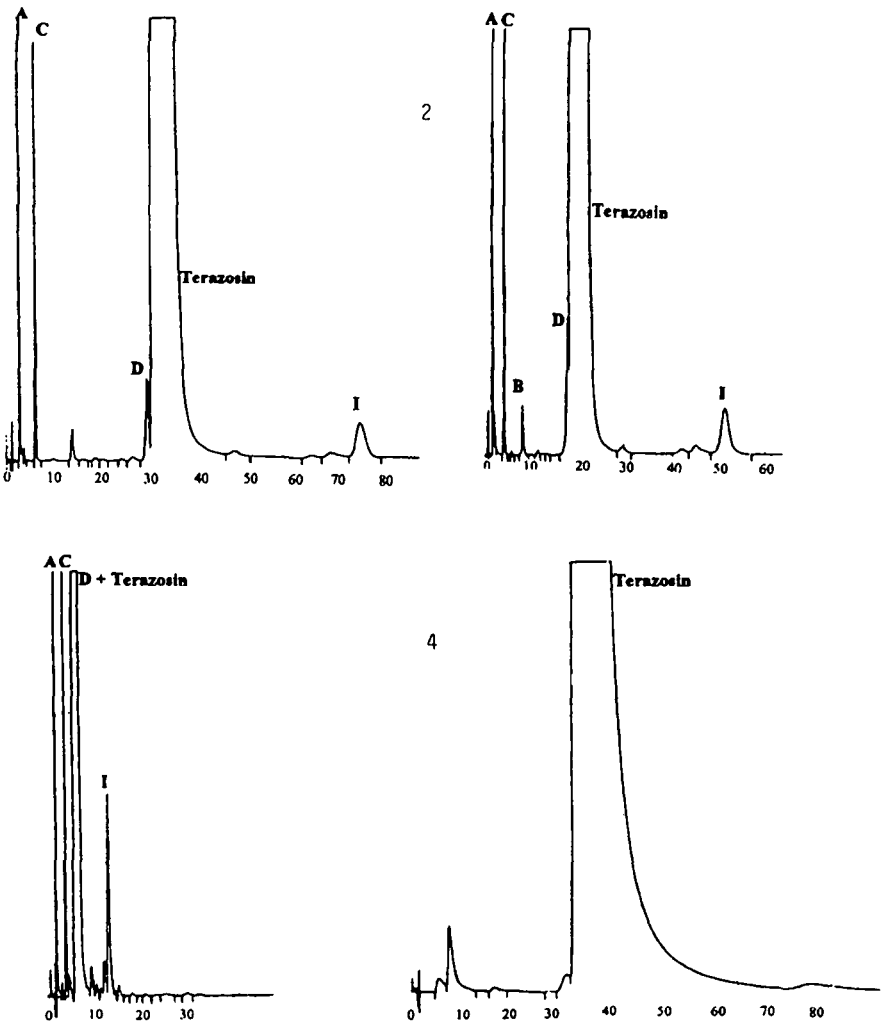

Fig. 4.

(Continued on p. 180)

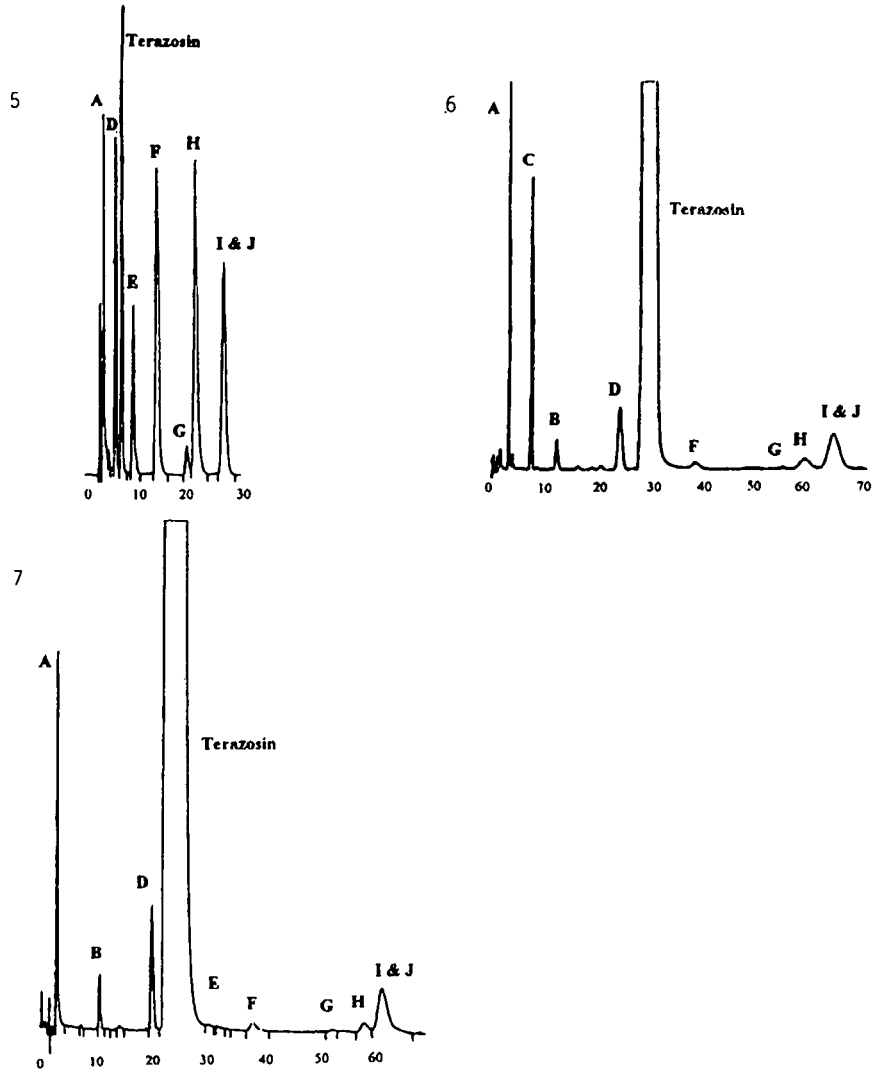

Fig. 4. Chromatograms of synthetic mixture on various packings. 1 = Alltech Nucleosil C_{18}; 2 = Macherey Nagel Nucleosil C_{18}; 3 = Bakerbond C_4; 4 = Versapak C_{18}; 5 = Bakerbond C_8; 6 = Waters μ-Bondapak C_{18}; 7 = Serva Techsphere C_8. Numbers indicate time (min).

TABLE II

PERFORMANCE OF VARIOUS REVERSED-PHASE PACKINGS FOR TERAZOSIN LATE ELUTING IMPURITY SEPARATION

Source	Packing	Column dimension	Resolution factor for impurities I and J
Alltech	Nucleosil C_{18} (5 μm)	15 cm × 4.6 mm	Co-elute
Macherey Nagel	Nucleosil C_{18} (5 μm)	12.5 cm × 4.0 mm	Co-elute
Waters	μ-Bondapak C_{18} (10 μm)	30 cm × 3.9 mm	1
Baker	Bakerbond C_4 (5 μm)	25 cm × 4.6 mm	0.9
Serva	Techsphere C_8 (5 μm)	25 cm × 4.6 mm	Co-elute
Zorbax	Rx C_8 (5 μm)	15 cm × 4.6 mm	2.4

solution stability of the drug make this a rugged determination which is well suited for automation.

ACKNOWLEDGEMENTS

The authors thank Mr. Steve Cepa and Mr. Mike Cirovic for their assistance in the spectral identification of related minor impurities and Ms. Diane Horgen for her assistance in the preparation of this manuscript.

REFERENCES

1 H. Tsuchihashi and T. Nagatomo, *J. Pharmacobio. Dyn.*, 12 (1989) 170–174.
2 T. Nagatomo, A. Tajiri, T. Nakamura and R. Hokibara, Y. Tanaka, J. Aono and H. Tsuchihashi, *Chem. Pharm. Bull.*, 35 (1987) 1629–1632.
3 S. Chrysant, I. Bal, B. Johnson and M. McPherson, *Clin. Cardiol.*, 8/9 (1985) 486–489.
4 R. Graham, *Am. J. Cardiol.*, 53 (1984) 16A–20A.
5 E. Nelson, J. Pool, A. Taylor and J. Mitchell, *Clin. Pharmacol. Ther. (St. Louis)*, 31 (1982) 255.
6 P. Abraham, C. Halstenson, G. Matzke, J. Napier and W. Keane, *Pharmacotherapy (Carlisle, Mass.)*, 5 (1985) 285–289.
7 I. Jane, A. McKinnon and R. Flanagan, *J. Chromatogr.*, 323 (1985) 191–225.
8 R. Bhamra, R. Flanagan and D. Holt, *J. Chromatogr.*, 380 (1986) 216–221.
9 S. Patterson, *J. Chromatogr.*, 311 (1984) 206–212.

Journal of Chromatography, 648 (1993) 183–186
Elsevier Science Publishers B.V., Amsterdam

CHROM. 25 340

Simultaneous extraction and determination of sulfadiazine and trimethoprim in medicated fish feed by high-performance liquid chromatography

V. Hormazabal, I. Steffenak* and M. Yndestad

Department of Food Hygiene, Norwegian College of Veterinary Medicine, P.O. Box 8146-Dep., N-0033 Oslo 1 (Norway)

(First received March 9th, 1993; revised manuscript received May 27th, 1993)

ABSTRACT

A simple and rapid method for the simultaneous extraction and determination of sulfadiazine and trimethoprim in medicated fish feed by HPLC using sulfadimidine as internal standard is presented. The calibration curves were linear in the investigated areas, 1.25–10 mg/g of sulfadiazine and 0.25–2 mg/g trimethoprim. The recovery of sulfadiazine was 96–99%, and the recovery of trimethoprim 100–105%.

INTRODUCTION

Sulfadiazine and trimethoprim are often used in combination in the treatment of fish diseases, being administered by incorporation into the feed at a ratio of 5:1. This drug combination, together with the quinolones oxolinic acid and flumequine, and oxytetracycline, are the most commonly used drugs for this purpose in Norwegian fish farming [1]. In 1991, a total amount of 5679 kg of sulfadiazine–trimethoprim was used.

A number of procedures for the determination of sulfonamides in combination with trimethoprim in biological fluids and pharmaceutical preparations have been described [2–7].

HPLC methods for the determination of sulfadimidine (sulfamethazine) and sulfathiazole in feeds have also been published by Blanchflower and Rice [8], Conway [9], Houglum *et al.* [10], and Smallidge *et al.* [11]. Torel *et al.* [12] have analysed feed premixes containing sodium sulfamethazine, sodium sulfamethoxypyridazine and trimethoprim, but did not give any account of the procedure except for the HPLC conditions. McNally *et al.* [13] have published a method for determination of trimethoprim and sulfadiazine in medicated fish feed. The method is simple but time consuming.

The purpose of the present study was to develop a simple and rapid method for simultaneous determination of sulfadiazine and trimethoprim in fish feed.

MATERIALS AND METHODS

Materials and reagents

The starting point for samples was "clean" fish feed, *i.e.* feed containing no drugs. Sulfadiazine, trimethoprim, and the internal standard sulfadimidine were added to this unmedicated fish feed to prepare standard curves, and for recovery studies. The "real" samples to be analysed were taken from commercial medicated fish feed produced by Skretting (Stavanger, Norway).

All chemicals and solvents were of analytical

* Corresponding author.

0021-9673/93/$06.00

or HPLC grade. Sulfadiazine and trimethoprim were supplied by Sigma. Sulfadimidine (sulfamethazine) (Serva) was used as internal standard.

A standard solution of sulfadiazine was made by dissolving 150 mg sulfadiazine in 50 ml 0.03 *M* sodium hydroxide–ethanol (1:1), and diluting to 150 ml with water. The trimethoprim standard solution was made by dissolving 50 mg trimethoprim in 10 ml 0.02 *M* H_3PO_4–CH_3CN (1:1), and diluting to 50 ml with water, and the standard solution of the internal standard sulfadimidine by dissolving 100 mg sulfadimidine in 5 ml acetone, and diluting to 100 ml with water. All standard solutions were put in an ultrasonic bath for 2 min before they were diluted with water.

Chromatographic conditions

The analyses were performed on a Perkin-Elmer HPLC system, consisting of a Series 400 solvent delivery system, an ISS 100 sampling system equipped with a Lauda RMT6 cooler (14°C) from Messgeräte Werk Lauda (Lauda-Königshafen, Germany), and an LC 235C UV detector (Perkin Elmer, Norwalk, CT, USA). The detector was operated at 270 nm. The integration was carried out using the software programme Omega-2 (Perkin-Elmer) in an Olivetti M 300 PC connected to a Star LC24-10 printer. The analytical column (stainless steel, 25 cm × 4.6 mm I.D.) and guard column (stainless steel, 2.0 cm × 4.6 mm I.D.) were packed with 5-μm particles of Supelcosil-LC-18-DB (Supelco, Bellafonte, PA, USA).

The mobile phase was 0.01 *M* aqueous Na_2HPO_4 pH 2.8–0.1% triethylamine in CH_3CN (79:21) at a flow-rate of 0.9 ml/min. Aliquots of 10 μl were injected onto the column for the determination of sulfadiazine and trimethoprim.

Sample preparation and clean-up

The feed sample, 1 g ground feed, was weighed into a 50-ml centrifuge tube with screw cap (NUNC). Internal standard sulfadimidine (1 ml of 1 mg/ml) and 3 ml 0.7% trichloroacetic acid (TCA) in acetone were added to the sample, which was then mixed well and left in an ultrasonic bath for 10 min at 40°C. The TCA solution was made by mixing 87 g TCA with 13 g water, to 0.7 ml of this solution was added 99.3 ml acetone.

The sample was transferred to a 500-ml volumetric flask. The centrifuge tube was washed and the volumetric flask filled to the mark with 0.01 *M* Na_2HPO_4, pH 3–CH_3CN (80:20). The pH in the Na_2HPO_4 solution was adjusted with 5 *M* H_3PO_4. The sample was well mixed, and an aliquot of 500 μl was filtered through a Costar spin-X centrifuge filter unit (low type) with 0.22-μm cellulose acetate binding by centrifugation for 1 min. Aliquots of 10 μl of the filtrate were injected onto the HPLC.

Calibration curves and recovery studies

The calibration curves for sulfadiazine and trimethoprim were made by spiking feed samples with standard solutions of sulfadiazine and trimethoprim to yield 1.25, 2.5, 5, 7.5 and 10 mg sulfadiazine per gram in feed, and 0.25, 0.5, 1, 1.5, and 2 mg trimethoprim per gram, respectively, in the samples. Duplicate samples were used. The recovery rates were determined by comparing peak height measurements of spiked feed to those of standard solutions. The linearity of the standard curves for sulfadiazine and trimethoprim in feed was tested using peak height ratios.

RESULTS AND DISCUSSION

Chromatograms of clean and spiked samples of fish feed are shown in Fig. 1 for sulfadiazine and trimethoprim. Fig. 2 shows a real (commercial) sample of medicated fish feed containing sulfadiazine and trimethoprim.

The linearity of the standard curves for sulfadiazine and trimethoprim in feed were tested using peak height ratios. The standard curves were linear in the investigated areas, 1.25–10 mg/g for sulfadiazine and 0.25–2 mg/g for trimethoprim. The correlation coefficients were $r = 0.9996$ for sulfadiazine in feed, and $r = 0.9994$ for trimethoprim.

Table I shows the recoveries and repeatabilities for sulfadiazine and trimethoprim from feed. The recovery of sulfadiazine from feed based on peak height varied from 96 to

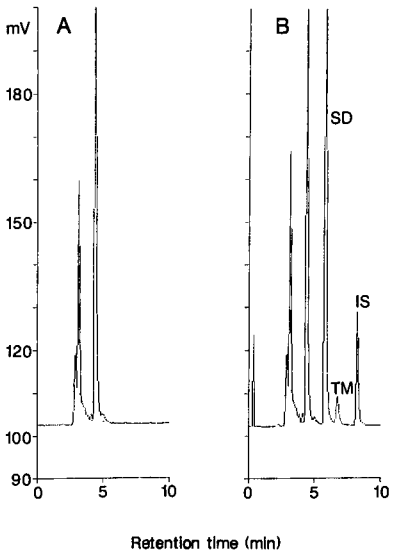

Fig. 1. Chromatograms of extracts from 1 g fish feed for the determination of sulfadiazine (SD) and trimethoprim (TM) with sulfadimidine as internal standard (IS). (A) Unspiked fish feed. (B) Fish feed spiked with 5 mg/g sulfadiazine and 1 mg/g trimethoprim.

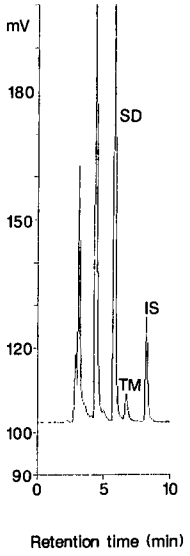

Fig. 2. Chromatogram of extract of 1 g "real" sample of fish feed containing sulfadiazine (SD) and trimethoprim (TM) with sulfadimidine as internal standard. The sample contains 5.0 mg/g sulfadiazine and 1.0 mg/g trimethoprim.

99%, the corresponding figures for trimethoprim being 100 and 105%. The standard deviation (S.D.) varied from 2.2 to 5.8%.

Table II shows the results of analysis of eight parallel samples of fish feed prepared so as to contain 5 mg/g sulfadiazine and 1 mg/g trimethoprim. The samples were found to actually contain 5.12 mg/g sulfadiazine and 1.04 mg/g trimethoprim on average, with an S.D. of 0.12 and 0.01, respectively.

McNally *et al.* [13] have previously published a method for the determination of trimethoprim and sulfadiazine in feed, in which the drugs are extracted with methanol by repeated extractions by slow rotation for 20 min, the procedure being repeated four times. The method is simple though time consuming. The present method is also simple, as well as being rapid and robust, and a large number of samples can easily be dealt with per day.

TABLE I

RECOVERY OF SULFADIAZINE (SDZ) AND TRIMETHOPRIM (TM) FROM FISH FEED

Material	No. of samples	Amount in spiked samples (mg/g)	Recovery (%)			
			SDZ		TM	
			Mean	S.D.	Mean	S.D.
Feed (1 g)	8	1.25	96	3.9		
	8	5.0	99	3.3		
	8	0.25			105	5.8
	8	1.0			100	2.2

TABLE II

ACTUAL CONTENT OF SULFADIAZINE (SDZ) AND TRIMETHOPRIM (TM) IN COMMERCIAL SAMPLES OF MEDICATED FISH FEED

The fish feed was prepared so as to contain 5 mg/g sulfadiazine and 1 mg/g trimethoprim.

Sample No.	Amount in samples (mg/g)	
	SDZ	TM
1	5.05	1.06
2	5.22	1.05
3	5.20	1.04
4	5.25	1.05
5	5.01	1.03
6	5.21	1.04
7	4.93	1.03
8	5.07	1.04
Average	5.12	1.04
S.D.	0.12	0.01

ACKNOWLEDGEMENTS

The study was supported by the Agricultural Research Council of Norway.

REFERENCES

1 I. Nafstad, *Nor. Veterinaertidsskr.*, 104 (1992) 215.
2 V. Ascalone, *J. Chromatogr.*, 224 (1981) 59.
3 R. Ballerini, M. Chinol, A. Stocchi, A. Cambi and M. Ghelardoni, *Farmaco Ed. Prat.*, 35 (1980) 84.
4 L. Essers and H. Korte, *Chemotherapy*, 28 (1982) 247.
5 R. Gochin, I. Kanfer and J.M. Haigh, *J. Chromatogr.*, 223 (1981) 139.
6 O. Spreux-Varoquaux, J.P. Chapalin, P. Cordonnier, C. Advenier, M. Pays and L. Lamine, *J. Chromatogr.*, 274 (1983) 187.
7 A. Weber, K.E. Opheim, G.R. Siber, J.F. Ericson and A.L. Smith, *J. Chromatogr.*, 278 (1983) 337.
8 W.J. Blanchflower and D.A. Rice, *J. Assoc. Off. Anal. Chem.*, 71 (1988) 302.
9 B. Conway, *Analyst*, 113 (1988) 1397.
10 J.E. Houglum, R.D. Larson and R.M. Neal, *J. Assoc. Off. Anal. Chem.*, 71 (1988) 1054.
11 R.L. Smallidge, E.J. Kentzer, K.R. Stringham, E.H. Kim, C. Lehe, R.W. Stringham and E.C. Mundell, *J. Assoc. Off. Anal. Chem.*, 71 (1988) 710.
12 J. Torel, J. Cillard, P. Cillard and M. Vie, *J. Chromatogr.*, 323 (1985) 447.
13 V. McNally, T. Lenehan, M.T. Kelly and M.R. Smyth, *Anal Lett.*, 23 (1990) 2215.

Journal of Chromatography, 648 (1993) 187–190
Elsevier Science Publishers B.V., Amsterdam

CHROM. 25 328

Preparative high-performance liquid chromatographic purification of saffron secondary metabolites

M.R. Castellar, H. Montijano, A. Manjón and J.L. Iborra*

Department of Biochemistry and Molecular Biology B and Immunology, Faculty of Chemistry, University of Murcia, P.O. Box 4021, E-30001 Murcia (Spain)

(First received February 10th, 1993; revised manuscript received May 24th, 1993)

ABSTRACT

A preparative HPLC procedure to isolate picrocrocin, the compound responsible for the taste of saffron and precursor of the aromatic safranal, and the mixture of yellow pigments from a saffron hydroalcoholic extract has been developed. A reversed-phase C_{18} column was employed as the stationary phase. The best separation was obtained with 45% methanol, plus a 90% acetonitrile pulse 3 min after starting the run, as mobile phase. To obtain the highest yield from the system, sample size was increased up to 2 ml of 200 mg ml^{-1} saffron extract; under such conditions a good resolution was obtained and picrocrocin and saffron pigments were separated with a high purification yield and purity.

INTRODUCTION

Saffron is a very high-value spice obtained from dried *Crocus sativus* stigmas. It is mainly employed to provide colour and flavour to foods [1,2]. The most important secondary metabolites in saffron are picrocrocin and crocetin glycosyl esters. Picrocrocin is a colourless bitter glycoside, responsible for the bitter taste of saffron and precursor of safranal, the saffron aromatic. This latter compound can be obtained from picrocrocin by chemical or enzymatic hydrolysis [1,3–6]. In fact, picrocrocin has potential value as a food additive, to provide aroma and flavour. The yellow–red pigments of saffron are a mixture of glycosides derived from the polyene dicarboxylic acid crocetin, in which glucose and gentobiose occur as carbohydrate residues. Of this group of substances the digentobiosyl ester of crocetin, namely crocin, is the most abundant; other crocetin derivatives are designated crocin ester 1 [crocetin (β-D-gentobiosyl)-(β-D-glucosyl) ester] and crocetin ester 2 [crocetin-mono-(β-D-gentobiosyl) ester] [1,3,7,8]. The major components of this mixture of pigments are freely soluble in water, which is an important advantage of the mixture for its use as a colour additive in the food and pharmaceutical industries.

Analytical separation of saffron secondary metabolites by TLC [4,9,10] and HPLC [2,8, 11,12] has been described. All these studies were carried out for analytical purposes, but none of them developed a preparative system for the purification of saffron secondary metabolites. In a previous study in our laboratory, isolation of picrocrocin and pigments by preparative TLC was achieved [13]. Purification results obtained gave a good chromatographic purity and high isolation yield for picrocrocin. However, the operation time was long and the pigments were strongly retained on the support, resulting in a low purification yield. The aim of this work was

* Corresponding author.

0021-9673/93/$06.00

to develop a simple and reproducible method to isolate picrocrocin and the mixture of yellow pigments from saffron by preparative HPLC.

EXPERIMENTAL

Materials

Dried saffron type "Mancha Superior" was purchased from a local supplier and stored in the dark at 4°C. Acetonitrile and methanol of HPLC grade were from Romil. Water was double distilled and filtered through a Millipore system (Milli-Q). All others reagents were analytical grade and were used without further purification.

Sample preparation

Crude extract was obtained from saffron as previously described [13]. Saffron was ground, resuspended in 50% ethanol and stirred; the vegetal tissue residue was discarded after centrifugation. The hydroalcoholic extract obtained was vacuum concentrated, and the aqueous solution obtained was lyophilized and stored at −20°C until use. Samples of extract (from 10 to 200 mg ml^{-1}) were prepared by dissolving the lyophilized extract in water.

Method development

Preparative HPLC analyses were performed on a Shimadzu HPLC system equipped with two LC-8A pumps, injectors for analytical and preparative runs, a UV–Vis spectrophotometric detector (SPD-6AV) with analytical and preparative flow cells, an FCV-100B fraction collector and a C-R4A Chromatopac integrator. Columns used were 25 cm × 0.46 cm I.D. and 25 cm × 2.12 cm I.D. (Supelco) for the analytical-scale (referred to below as the small-scale column) and the preparative-scale assays, respectively, both packed with Supelcosil PL C-18 (12 μm particle size). The standard mobile phase used for preparative separation of picrocrocin and pigments was isocratic 45% methanol, plus a 6-s pulse of 90% acetonitrile 3 min after starting the run. The sample solution was manually injected with a syringe. Flow-rates were 2 and 42 ml min^{-1} and sample sizes 20 μl and 2 ml for small-scale and preparative assays, respectively. Picrocrocin was detected at 250 nm and pigments at 440 nm for small-scale assays. As crocin elution could also be detected at 250 nm, for preparative runs all compounds were monitored at 250 nm. All separations were performed at room temperature.

The identification of saffron secondary metabolites was made by HPLC using commercial crocin and previously purified picrocrocin [13] as standards. Picrocrocin and crocin were quantified using their molar absorptivities in water: $\epsilon_{250} = 10\,100\ M^{-1}\ cm^{-1}$ [2] and $\epsilon_{440} = 133\,750\ M^{-1}\ cm^{-1}$ [14], respectively.

Purity analysis

The purity of purified compounds was determined by analytical HPLC using a Shimadzu LC-6A chromatograph, equipped with a 150 mm × 4 mm I.D. Lichrosolv RP C_{18} (5 μm particle size) column from Merck, an automatic injector (Shimadzu SIL 9A) and a photodiode-array UV–Vis detector (Shimadzu SPD-M6A). The mobile phase employed was a linear gradient of acetonitrile (20% to 55% within 10 min) in water, sample size was 20 μl and flow-rate 1 ml min^{-1}. Purification yield of picrocrocin was determined by the ratio of the amount of picrocrocin injected into the preparative column and that recovered after purification. For the pigments, only identification and quantitation of crocin was possible, so the purification yield of pigments was referred to as crocin yield, after checking that in the purified pigments there were no qualitative changes, that is the peak-area ratios of the different compounds of the pigment mixture were the same before and after the purification process. The chromatographic purity was determined as the percentage of peak area corresponding to each compound with reference to the total area integrated for all peaks in the chromatogram.

RESULTS AND DISCUSSION

A C_{18} stationary phase, previously used for the separation of saffron secondary metabolites by different authors [2,8,11,12], was selected. The most suitable mobile phase was determined

after an analysis employing the small-scale section of the preparative HPLC equipment. Several binary and ternary isocratic solvent systems consisting of combinations of methanol, acetonitrile and water were assayed as eluents. Of these, 50% (v/v) methanol was selected as optimum mobile phase for picrocrocin and pigments separations, obtaining an analysis time shorter than 8 min, with capacity factor (k') values of 1.4, 2.8 and 7.2 for picrocrocin, crocin and crocetin ester 1, respectively. The selectivity coefficients (α) and resolution (R_s) values between picrocrocin and crocin were 2.28 and 3.46, and between crocin and crocetin ester 1, 1.92 and 3.32, respectively.

These separation conditions were applied to the preparative column, keeping constant the linear eluent velocity [15], which meant increasing the flow-rate from 2 to 42 ml min^{-1}. However, it was not possible to elute the components with the same resolution, because the retention time was longer for all the components. Thus, slight changes in the organic solvent concentration of the mobile phase had to be made. With the methanol concentration adjusted to 55%, retention times were 2.1, 3.3 and 5.0 min for picrocrocin, crocin and crocetin ester 1, respectively; the remaining, more hydrophobic, pigments were retained in the column, and their elution with 55% methanol required the operation time to be extended by up to 25 min. Under these conditions it was possible to obtain pure picrocrocin and crocin, which can be used as standards.

A modification of the elution system consisting in a reduction in the methanol concentration from 55% to 45%, which increased the retention time of pigments, and giving a 90% acetonitrile pulse for 6 s 3 min after starting run, to facilitate the elution of all the remaining pigments, was assayed. Thus, picrocrocin was obtained at a retention time of 2.8 min, and all the pigments together, in the same fraction, at 5.2 min. The run was finished after 7 min and initial conditions achieved. Separation between these fractions was about 2 min, which allowed an increase in the amount of injected sample for every run. Fig. 1 shows preparative HPLC chromatograms for this latter system; picrocrocin was peak

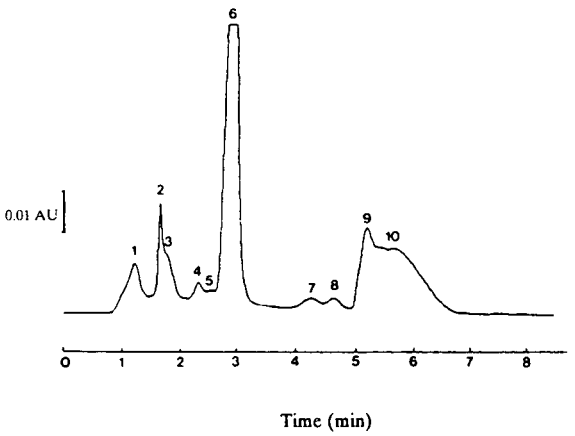

Fig. 1. Chromatograms of preparative separation of 10 mg ml^{-1} saffron extract with 45% methanol, plus a 90% acetonitrile pulse 3 min after starting the run, as the mobile phase (see text for peak identification).

number 6, while pigments were peaks numbers 9 and 10.

To obtain the highest yield of picrocrocin and crocin with the preparative HPLC method developed, the separation was assayed with 2 ml of 10, 50, 100, 150 and 200 mg ml^{-1} saffron extract. According to the detector response, monitored at 250 nm, fractions of picrocrocin and pigments were collected from 2.6 to 3.2 min and from 4.9 to 6.5 min, respectively. These collected fractions were analysed, after concentration, by an analytical HPLC system equipped with a photodiode array UV–Vis detector to determine chromatographic purity. Chromatograms obtained are shown in Fig. 2. Peak numbers 6, 7 and 9 are picrocrocin, crocin and crocetin ester 1, respectively; purified picrocrocin fraction (a) showed only one peak and no other contaminant compounds were detected in significant amounts, while the pigments fraction showed peaks corresponding to crocin and crocetin ester 1 and other yellow pigments derived from crocetin.

Purification yields of 80% and 99% were achieved for picrocrocin and pigments, respectively, and no significant changes in these values were obtained for the different sample sizes assayed. Chromatographic purity for picrocrocin was always over 95%. An increase in picrocrocin purification yield was difficult due to the appearance of a minor yellow pigment, more hydrophilic than crocin, which was eluted slightly

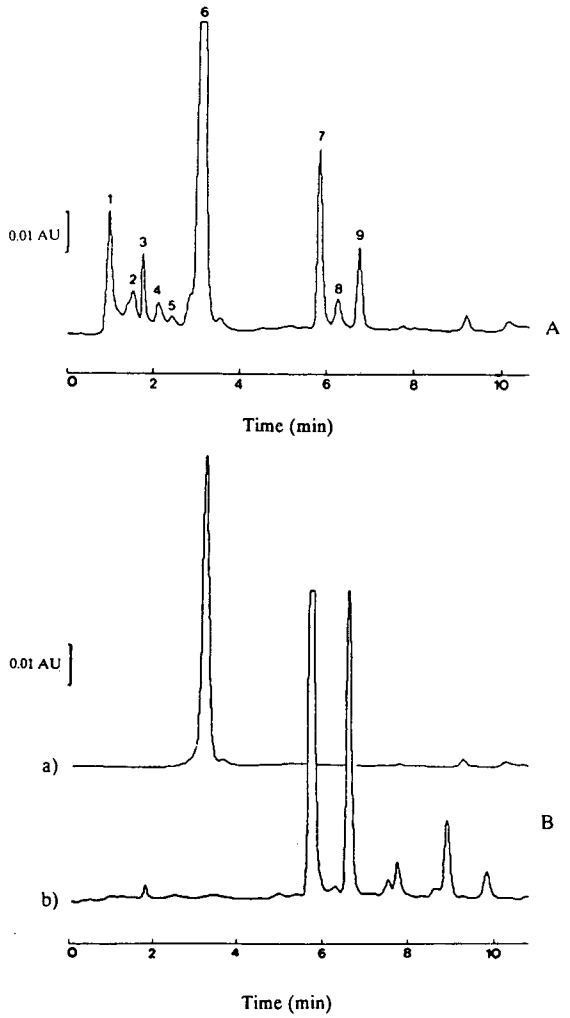

Fig. 2. Analytical HPLC chromatograms before and after the purification process. (A) Saffron extract at 250 nm and (B) picrocrocin fraction at 250 nm (a) and pigments mixture fraction at 440 nm (b) (see text for peak identification).

before picrocrocin. Thus, to maintain a chromatographic purity of 95% the purification yield had to be reduced to 80%. The purified compounds were lyophilized before storage and no degradation was observed after 6 months' storage at −20°C.

Finally, the system employed allows the injection and elution process to be automated. Thus 2 ml of 200 mg ml^{-1} saffron extract could be injected into the column every 8 min, *i.e.* 7.5 runs every hour of continuous operation. This estimation means that 0.51 g h^{-1} picrocrocin could be obtained.

In conclusion, a simple, efficient and reproducible method for the purification picrocrocin and saffron pigments by preparative HPLC has been developed. In addition, the results reported in the present work are a contribution to the possible industrial use of picrocrocin and saffron pigments separately.

ACKNOWLEDGEMENTS

This work was partially supported by Grant No. IN 90-0247 from DGICYT, Spain. M.R.C. is a fellow of DGICYT, Spain.

REFERENCES

1 S.R. Sampathu, S. Shivashankar and Y.S. Lewis, *CRC Crit. Rev. Food Sci. Nutr.*, 20 (1984) 123.
2 H. Himeno and K. Sano, *Agric. Biol. Chem.*, 51 (1987) 2395.
3 C.L. Madan, B.M. Kapur and U.S. Gupta, *Econ. Bot.*, 20 (1966) 377.
4 K. Sano and H. Himeno, *Plant Cell Tissue Organ Cult.*, 11 (1987) 159.
5 J.L. Iborra, M.R. Castellar, J.A. Campillo, M. Cánovas and A. Manjón, *Actas I Congreso Internacional de Tecnología y Desarrollo Alimentarios*, Vol. III, Promociones y Publicaciones Universitarias, Barcelona, 1991, p. 895.
6 J.L. Iborra, M.R. Castellar, M. Cánovas and A. Manjon, *Biotechnol. Lett.*, 14 (1992) 475.
7 H. Pfander and H. Schurtenberger, *Phytochemistry*, 21 (1982) 1039.
8 H. Pfander and M. Rychener, *J. Chromatogr.*, 234 (1982) 443.
9 S. Visvanath, G.A. Ravishankar and L.V. Ventaraman, *Biotechnol. Appl. Biochem.*, 12 (1990) 366.
10 F. Fakhrai and P.K. Evans, *J. Exp. Bot.*, 41 (1990) 47.
11 H. Hori, K. Enomoto and M. Nakaya, *Plant Tissue Cult. Lett.*, 5 (1988) 72.
12 K.S. Sarma, K. Maesato, T. Hara and Y. Sonoda, *J. Exp. Bot.*, 41 (1990) 745.
13 J.L. Iborra, M.R. Castellar, M. Cánovas and A. Manjón, *J.Food Sci.*, 57 (1992) 714.
14 C. Corradi and G. Micheli, *Boll. Chim. Farm.*, 118 (1979) 553.
15 R. Rosset, M. Caude and A. Jardy, *Chromatographies en Phases Liquide et Supercritique*, M. Masson, Paris, 1991, p. 668.

Journal of Chromatography, 648 (1993) 191–197
Elsevier Science Publishers B.V., Amsterdam

CHROM. 25 399

Passive sampling and gas chromatographic determination of low concentrations of reactive hydrocarbons in ambient air with reduction gas detector

Xu-Liang Cao* and C. Nicholas Hewitt

Institute of Environmental and Biological Sciences, Lancaster University, Lancaster LA1 4YQ (UK)

(First received April 14th, 1993; revised manuscript received July 1st, 1993)

ABSTRACT

The use of mercuric oxide reduction gas detection (RGD) for the passive sampling and capillary gas chromatographic determination of low concentrations of volatile organic compounds ($\leq C_6$) in ambient air is described. Sampling times are significantly reduced, compared with those required by the use of a flame ionization detector, due to the high sensitivity of RGD. The RGD signal due to the build-up of artifacts on polymeric sampling matrices during storage has also been investigated for Tenax-TA, Tenax-GR, Carbotrap and Chromosorb 106. The problem is at a minimum with Tenax-TA and GR, is more acute with Carbotrap, and is so severe with Chromosorb 106 that it prevents the use of this material for this application.

INTRODUCTION

Few volatile organic compounds (VOCs) are toxic in their own right at the concentrations found in the ambient atmosphere. Their main contribution to air pollution stems from their atmospheric reactions which lead to the formation of oxidizing species including peroxyacetyl nitrate (PAN), hydrogen peroxide and, especially, ozone [1]. Since the more reactive hydrocarbons (particularly the alkenes) have much higher potentials for tropospheric ozone formation than the non-reactive hydrocarbons (*e.g.*, alkanes) [2], the priority in atmospheric monitoring programmes which focus on photochemical ozone production is the speciation and quantitation of the reactive VOCs. Under some circumstances it would therefore be advantageous to utilize a detection system that has enhanced sensitivity towards alkenes but is relatively insensitive to alkanes and other less reactive VOC species. This would result in a less complex chromatogram from an ambient air sample than is obtained with other universal detectors, for example the flame ionization detector, and so simplify peak identification.

Passive samplers were initially developed for the measurement of time-weighted average personal exposures to airborne contaminants in the workplace. Due to their many advantages over conventional pump samplers [3], passive samplers have also been employed for the monitoring of low concentrations [ppb (v/v) or ppt (v/v) mixing ratios] of organic vapours in ambient air in recent years [4,5]. However a major limitation of their use for this purpose is the increase in the blank signal due to the formation of artifacts on adsorbents during storage and exposure [6]. The long sampling periods necessitated by the very low sampling rates of passive samplers accentuates the problems of contamination and artifact formation. Although blank levels can be minimized by meticulous condition-

* Corresponding author.

0021-9673/93/$06.00

ing of the adsorbing material, artifacts may build up on the unexposed matrix during storage. They may also build up during exposure of the sampler by reaction of ozone with the adsorbent [7], and this may raise detection limits to unacceptable levels. If the resultant blank signal is large relative to the analyte signal or is very variable, passive samplers will not be able to be used directly in rural air sampling. Therefore, sampling time should be as short as possible. This can be achieved by either designing a passive sampler with higher sampling rate or developing much more sensitive detection methods.

Reduction gas detection (RGD) was originally developed for detecting the reducing gases CO and H_2 [8]. It has also been used for the detection of acetaldehyde and acetone [9] and of isoprene (2-methyl-1,3-butadiene) [10]. The response of RGD to a variety of reactive hydrocarbons has been investigated using gas chromatography with packed columns [11]. It was shown that it is considerably more sensitive to alkenes than is flame ionization detection (FID), and has much greater sensitivity to alkenes than alkanes. RGD has also been developed successfully for the capillary gas chromatographic analysis of hydrocarbons up to C_6 with high resolution, but the peak shapes for compounds above C_6 (*e.g.*, benzene, toluene etc.) are extremely broad and severely tailing [12].

Here, the use of RGD for the thermal desorption and capillary gas chromatographic determination of C_2–C_4 alkenes (qualitative) and C_5–C_6 alkenes (quantitative), including isoprene, in ambient air, using a passive sampling technique, is described, together with an assessment of the formation of artifacts on four different commonly used adsorbents.

EXPERIMENTAL

Principles of the reduction gas detector

The principle of operation of the reduction gas detector has been described elsewhere [11–13]. Briefly, it depends upon the reduction of solid mercuric oxide by a reducing gas X on a heated bed:

$$X + HgO\ (solid) \longrightarrow XO + Hg\ (vapour) \quad (1)$$

The resultant mercury vapour concentration is directly proportional to the inlet gas concentration and is quantitatively detected by means of an ultraviolet photometer located immediately downstream of the reaction bed.

Analytical system

Gas chromatographic measurements were made using a Hewlett-Packard 5890 Series II gas chromatograph fitted with a reduction gas detector (RGD-2, Trace Analytical, Menlo Park, CA, USA). The carrier gas used was helium. The capillary column used was a porous-layer open tubular (PLOT) (Al_2O_3/KCl) 50 m × 0.32 mm (Chrompack). A make-up gas line (stainless-steel tube, 1/8 in. I.D.; 1 in. = 2.54 cm) was used to supply helium to the detector to render it compatible with the capillary analytical column. A catalytic combustion filter was used in conjunction with an organic–water vapour trap (molecular sieve) for carrier gas purification. The flow-rate of make-up gas was 25 ml/min. An uncoated fused-silica capillary (15 cm × 0.53 mm) was used as the transfer line between the analytical column and the detector and was connected to the capillary GC column by a low dead-volume glass press-fit connector (Hewlett-Packard).

The exposed passive sampling tubes were thermally desorbed by a Chrompack Thermal Desorption Cold Trap (TCT) Injector, interfaced with the gas chromatograph, using helium carrier gas at a flow-rate through the tube of 35 ml/min. The desorbed analytes were retrapped by a deactivated fused-silica capillary trap (40 cm × 0.53 mm) [14] cooled by liquid nitrogen. After sample concentration, the trap was flash-heated to 220°C at 15°C/s for 1 min, and the trapped vapours injected onto the capillary column in splitless mode. A schematic diagram of the whole TCT–GC–RGD system is shown in Fig. 1.

The GC system was calibrated using a Scotty (Chrompack) 15 ppm (v/v) mixed alkene calibration standard. This was injected into the carrier gas stream by means of a 1 ml gas-tight syringe via the TCT injector, and then carried by

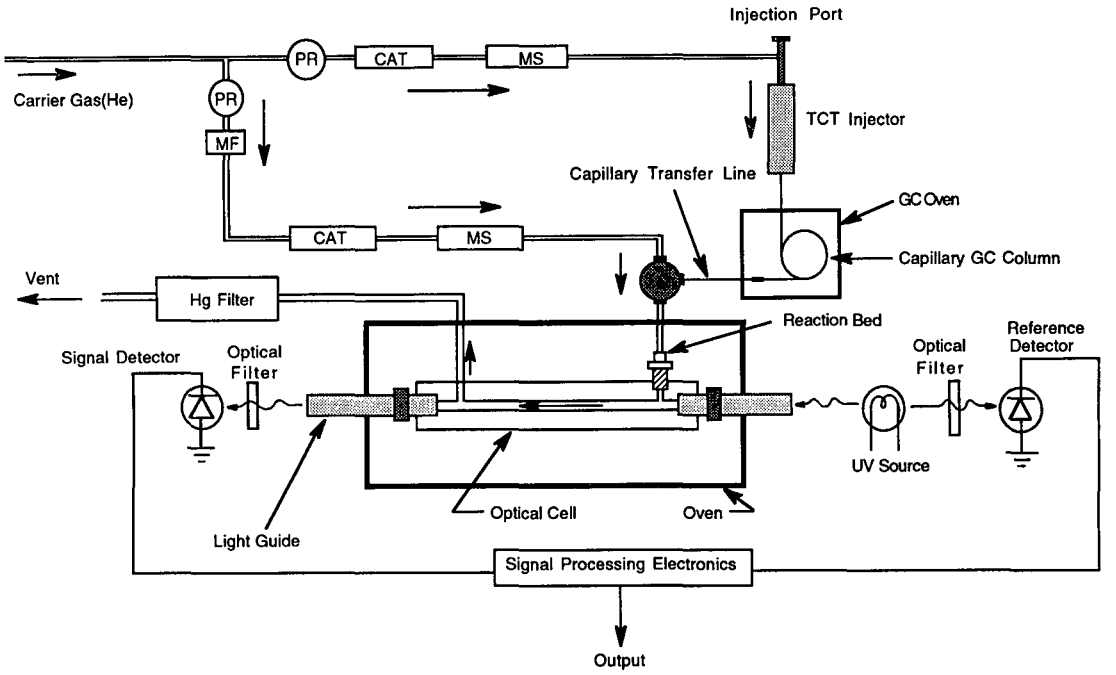

Fig. 1. Schematic diagram for TCT–capillary GC–RGD system. MS = Molecular sieve; CAT = catalytic combustion filter; MF = mass flow regulator; PR = pressure regulator.

helium gas through a heated empty Perkin-Elmer stainless-steel sampling tube to the capillary trap. Peak identification was by means of retention times with quantitation achieved using a VG Minichrom data handling system.

Adsorbents

Four commonly used adsorbents were investigated. Tenax-TA [size 60–80 mesh (284–328 μm), specific surface area 20 m^2/g, Chrompack] is a porous polymer based on 2,6-diphenyl-*p*-phenylene oxide which has been widely used for air sampling. Carbotrap [20–40 mesh (402–568 μm), specific surface area 100 m^2/g, Supelco] is a graphitized carbon black. Tenax-GR (60–80 mesh, specific surface area 20–100 m^2/g, Chrompack) is a new adsorbent which consists of a Tenax matrix filled with 23% graphitized carbon. Its passive sampling performance has been investigated recently [6,15]. Chromosorb 106 (60–80 mesh, specific surface area 800 m^2/g, Chrompack) is a polyaromatic cross-linked resin which can be used for the sampling of more volatile compounds due to its high adsorption capacity.

The diffusion tubes were packed with 0.2 g adsorbent (0.16 g for Tenax-TA), and conditioned for at least 16 h with helium flow at 35 ml/min at the following temperatures: 300°C (Tenax-TA), 320°C (Tenax-GR), 350°C (Carbotrap) and 250°C (Chromosorb 106). It should be mentioned that the low maximum operating temperature (250°C) of Chromosorb 106 necessitates the use of a conditioning time of at least 48 h. The optimum desorption conditions for these adsorbents have been investigated recently [16], and are 250°C for 5 min (Tenax-TA), 260°C for 6 min (Tenax-GR), 280°C for 8 min (Carbotrap), and 220°C for 10 min (Chromosorb 106).

Sampling procedures

Perkin-Elmer stainless-steel diffusion tubes (diameter 4.8 mm, diffusion length 15 mm for tubes with no diffusion cap) packed with different adsorbents were used for the sampling of volatile organic compounds in a rural area in the vicinity of Lancaster, north-west England, during February–March 1993. The relative humidity during sampling varied from 40 to 80%, and the temperature from 2 to 12°C. Swagelok caps were used to seal the conditioned sampling tubes prior

TABLE I

IDEAL UPTAKE RATES OF DIFFERENT HYDROCARBONS FOR PERKIN-ELMER DIFFUSION TUBE

Compounds	Uptake rates [ng/(ppm · min)]
1-Pentene	1.76
Isoprene	1.75
1-Hexene	1.87
Benzene	1.99

to sampling and during storage of exposed tubes prior to analysis. The passive sampling tubes were placed vertically with the open end downwards in a variety of outdoor locations and exposed for about 15 h. The concentrations of organic compounds in air were calculated using the following expression [3]:

$$\text{Analyte concentration (ppm)} = \frac{\text{mass uptake (ng)}}{\text{uptake rate [ng/(ppm · min)]} \times \text{exposure time (min)}} \quad (2)$$

The uptake rate in eqn. 2 was calculated using the following equation [3]

$$\text{Uptake rate [ng/(ppm/min)]} = \frac{DA}{L} \quad (3)$$

where D is the diffusion coefficient in air (cm^2/s), obtainable from the literature [17,18] or calculable for each analyte according to the Hirschfelder method (see ref. 18); A is the cross-sectional area of the diffusion tube (=0.181 cm^2 for Perkin-Elmer diffusion tubes); and L is the diffusion length of the tube. The calculated uptake rates are shown in Table I.

RESULTS AND DISCUSSION

RGD signals resulting from system contamination and the formation of adsorbent artifacts

Passive sampling methods based upon adsorption onto a polymeric matrix and GC analytical systems are both susceptible to contamination problems, giving rise to unwanted detector signals. This was investigated with high-sensitivity RGD by packing sampling tubes with different adsorbents, rigorously conditioning them as for field use and sealing with Swagelok caps. After storage for about 15 h they were thermally desorbed and analysed by the GC–RGD system as described above. The blank chromatograms before and after storage are shown in Figs. 2 and 3, respectively. The RGD response to impurities in the carrier gas and contamination of the TCT–GC system was also determined, and a typical chromatogram is shown in Fig. 2.

It can be seen from Fig. 2 that the high sensitivity of the RGD leads to large blank signals. The response due to system contamination is therefore much larger than that observed using conventional FID [14]. Tenax-TA, Tenax-GR and Carbotrap are seen to be very clean after conditioning, most of the blank signal being due to system contamination rather than being due to the adsorbants themselves, with the exception of the large, broad and tailing benzene peak at a retention time of 17 min. Although the latter part of the chromatogram for Chromosorb

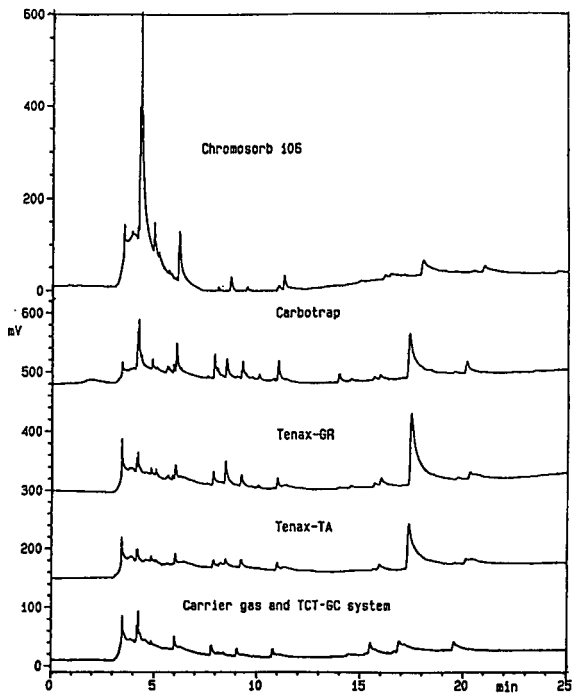

Fig. 2. Chromatograms of blank signals from RGD for different adsorbents before storage. GC conditions: 160°C (8 min) to 180°C at 3°C/min.

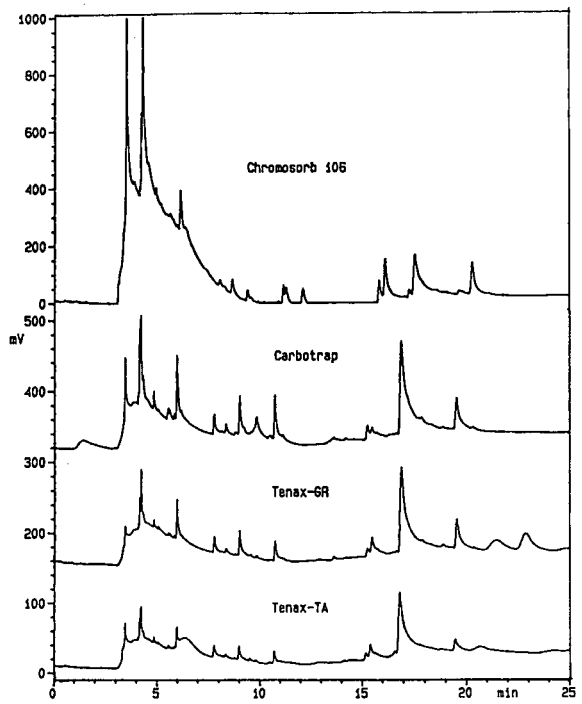

Fig. 3. Chromatograms of blank build-up signals from RGD for different adsorbents after storage for about 15 h. GC conditions: 160°C (8 min) to 180°C at 3°C/min.

106 is relatively clean, there is considerable noise between retention times of 3 and 7 min, and this adsorbent may therefore not be suitable for the sampling and analysis of compounds (C_1–C_4) which elute in this range.

Fig. 3 shows the chromatograms resulting from different adsorbents after storage for 15 h. All four adsorbents showed increased levels of contamination to different extents, with Tenax-TA producing the least noisy signal and Chromosorb 106 (especially in the initial part of the chromatogram) the most. It is unlikely these peaks represent contaminants from ambient air, adsorbed during storage, since the tubes were sealed tightly with Swagelok caps [6]. Rather it seems likely they represent compounds generated within the adsorbents themselves during storage, possibly by degradation of the polymers and low-molecular-weight polymers (by-products) and impurities in the technical-grade reagents used for polymer production, or oxidation of the polymers and the by-products by the residual reactive inorganic gases (*e.g.*, ozone) within the tube. This is less likely since the tubes were purged with helium at high temperatures for 16 h. Such artifact formation processes may be unavoidable, and reduction of the sampling and storage periods to the minimum practicable may be the only way to minimize the problem.

Passive sampling of VOCs in ambient air

Fig. 4 shows representative chromatograms of samples collected with different adsorbents by exposure for about 15 h to ambient air at the same site. The scale differences of the chromatograms should be taken into account when comparing Figs. 2 and 3 with Fig. 4. The amounts of analytes adsorbed onto Tenax-TA are relatively small, compared with the blank build-up signal (shown in Fig. 3), due to the weak adsorption affinity of Tenax-TA for the light hydrocarbons ($\leq C_6$). For Tenax-GR and Carbotrap, the amounts of compounds adsorbed onto the adsor-

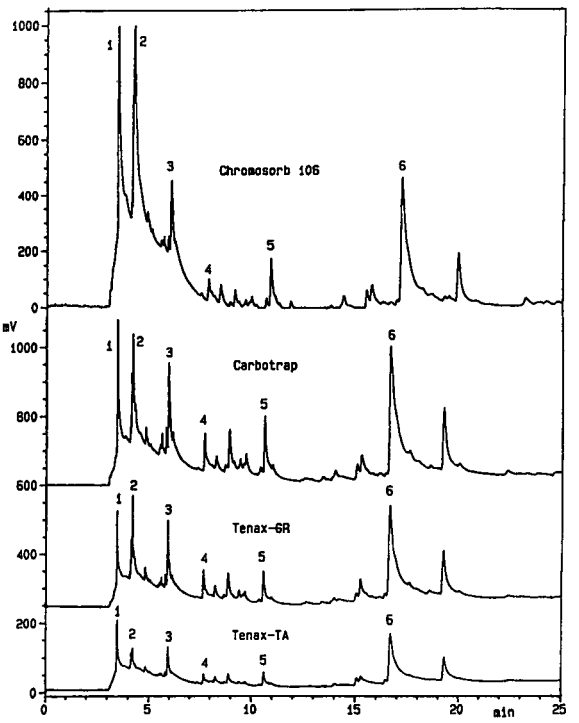

Fig. 4. Chromatograms of passive sampling of VOCs in ambient air for about 15 h for different adsorbents from RGD. GC conditions: 160°C (8 min) to 180°C at 3°C/min. Peaks: 1 = propylene; 2 = 1-butene; 3 = 1-pentene; 4 = isoprene; 5 = 1-hexene; 6 = benzene.

bents are significant compared with their corresponding blank build-up values. In the case of Chromosorb 106, the amounts of most compounds adsorbed are similar to their blank build-up values. Chromosorb 106 and Tenax-TA may therefore not be suitable for this purpose. The other disadvantage of using Chromosorb 106 is that its thermal desorption gives rise to significant amounts of higher-molecular-weight compounds ($\geq C_{10}$) on the GC column to which RGD is sensitive and which must then be removed by lengthy column conditioning.

Because the passive sampling technique may not be suitable for the sampling of very light hydrocarbons ($C \leq 3$) due to their extremely high volatility [19], and the trapping efficiency of the TCT capillary cold trap for very light hydrocarbons ($C \leq 4$) decreases significantly with increasing carrier gas flow-rate [14], propylene and 1-butene were not quantified although they are clearly identifiable in the chromatogram. The concentrations of 1-pentene, isoprene, 1-hexene and benzene in ambient air samples collected on Tenax-GR and Carbotrap were calculated by substracting their corresponding blank signals using eqn. 2 above. The results are summarized in Table II.

It can be seen from Table II that the concentrations of the four selected hydrocarbons vary from as low as 0.03 ppb for isoprene to as high as 1.0 ppb for benzene in the 17 samples collected at this site. The sources of the olefins and benzene in rural air will include vehicle exhaust emissions, fuel leakage and evaporation, solvent evaporation and industrial emissions, with resultant concentrations lower than those observed in urban source areas. Isoprene is the predominant hydrocarbon emitted by a number of deciduous trees and other plant species [20] but its low concentrations may be attributed to the low density of trees in north-west England and to the lack of photosynthetic activity, low temperatures and light intensities prevailing during the sampling periods.

TABLE II

TYPICAL CONCENTRATIONS OF SELECTED POLLUTANTS IN AMBIENT AIR IN NORTH-WEST ENGLAND

Compounds	Concentrations (ppb)		
	n^a	Range	Mean
1-Pentene	18	0.06–0.28	0.16
Isoprene	17	0.03–0.19	0.08
1-Hexene	18	0.04–0.19	0.09
Benzene	17	0.15–1.0	0.41

[a] n = Number of samples.

Comparisons between the chromatograms from RGD with those from FID

Fig. 5 shows the typical GC–FID chromatograms obtained from passive sampling of VOCs in ambient air for Carbotrap and from its blank build-up. Compared with the RGD chromatograms shown in Fig. 4, it can be seen clearly that the chromatograms from RGD looks more simple than those from FID due to the high selectivity of RGD, and many alkanes detected by FID have no or extremely low responses in RGD. Because of the high sensitivity of RGD, the corresponding peaks from the RGD chromatograms are much higher than those from the FID chromatogram, even though the sampling

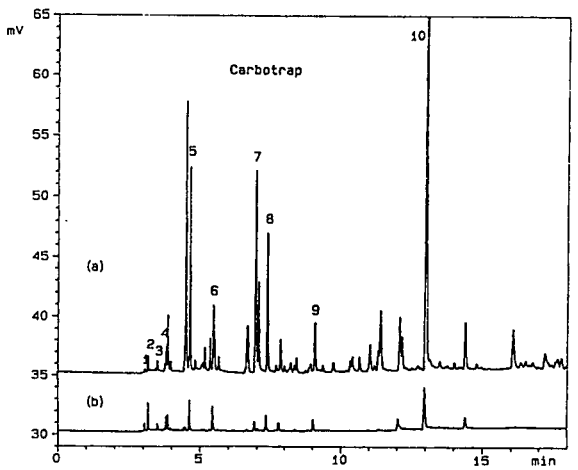

Fig. 5. (a) Chromatogram of passive sampling of VOCs in ambient air for about 4 days for Carbotrap from GC–FID; (b) chromatogram of Carbotrap blank build-up for about 4 days from FID. GC conditions: 160°C (5 min) to 200°C at 5°C/min. Peaks: 1 = propane; 2 = propene; 3 = n-butane; 4 = 1-butene; 5 = n-pentane; 6 = 1-pentene; 7 = isoprene; 8 = n-hexane; 9 = 1-hexene; 10 = benzene.

time for FID is about 8 times longer than for RGD. The present version of RGD was originally designed for use with packed GC columns, not capillary columns, and therefore the peak resolution from RGD is not optimum. This may be improved significantly by designing a micro-RGD system with minimum dead volume.

CONCLUSIONS

RGD is highly sensitive and selective for the analysis of reactive hydrocarbons. Here, its use for the determination of four selected VOCs in rural ambient air, using passive sampling, thermal desorption and capillary GC separation has been demonstrated. Sampling times were significantly reduced compared with those necessary with FID, due to the high sensitivity of the detector. Further development of the use of this detector for capillary GC environmental analysis is certainly warranted.

The RGD responses to the blank signals resulting from the use of four adsorbents (Tenax-TA, Tenax-GR, Carbotrap and Chromosorb 106) have also been investigated. The problem is at a minimum with Tenax-TA and GR, is more acute with Carbotrap, and is so severe with Chromosorb 106 that it prevents the use of this material for this application.

ACKNOWLEDGEMENTS

We would like to thank the Government of China, the British Council and the Natural Environment Research Council for funding. Mr. K. Waterhouse provided invaluable technical assistance. We appreciate the helpful suggestions and critical comments of two anonymous referees.

REFERENCES

1 R.G. Derwent and M.E. Jenkin, *AERE Report R13736*, HMSO, London, 1990.
2 R.G. Derwent and M.E. Jenkin, *Atmos. Environ.*, 25A (1991) 1661–1678.
3 X.-L. Cao and C.N. Hewitt, *Environ. Technol.*, 12 (1991) 1055–1062.
4 M.A. Cohen, P.B. Ryan, Y. Yanagisawa, J.D. Spengler, H. Ozkaynak and P.S. Epstein, *JAPCA*, 39 (1989) 1086–1093.
5 H.C. Shields and C.J. Weschler, *JAPCA*, 37 (1987) 1039–1045.
6 X.-L. Cao and C.N. Hewitt, *J. Chromatogr.*, (1993) in press.
7 X.-L. Cao and C.N. Hewitt, *Environ. Sci. Technol.*, (1993) in press.
8 W.M. Doizaki and M.D. Levitt, *J. Chromatogr.*, 285 (1984) 210–213.
9 D. Ohara and H.B. Singh, *Atmos. Environ.*, 22 (1988) 2613–2615.
10 R. Fall and P. Zimmerman, personal communication.
11 X.-L. Cao, C.N. Hewitt and K.S. Waterhouse, *Anal. Chem.*, (1993) submitted for publication.
12 X.-L. Cao, C.N. Hewitt and K.S. Waterhouse, in P. Sandra and G. Devos (Editors), *Proceedings of the 15th International Symposium on Capillary Chromatography, May 24–28, 1993*, Hüthig, Heidelberg, 1993, pp. 967–972; *J. High Resolut. Chromatogr.*, (1993) submitted for publication.
13 *Reduction Gas Detector (RGD2) Operating Manual*, Trace Analytical, Menlo Park, CA, 1989.
14 X.-L. Cao and C.N. Hewitt, *J. Chromatogr.*, 627 (1992) 219–226.
15 X.-L. Cao and C.N. Hewitt, *Atmos. Environ.*, (1993) in press.
16 X.-L. Cao and C.N. Hewitt, *Chemosphere*, (1993) in press.
17 G.A. Lugg, *Anal. Chem.*, 40 (1968) 1072–1077.
18 K.-H. Pannwitz, *Drager Rev.*, 52 (1984) 1–9.
19 X.-L. Cao, *J. Chromatogr.*, 586 (1991) 161–165.
20 F.C. Fehsenfeld, J. Calvert, R. Fall, P. Goldan, A.B. Guenther, C.N. Hewitt, B. Lamb, S. Liu, M. Trainer, H. Westberg and P. Zimmerman, *Global Biogeochemical Cycles*, 6 (1992) 389–430.

Journal of Chromatography, 648 (1993) 199–211
Elsevier Science Publishers B.V., Amsterdam

CHROM. 25 375

Application of solid-phase microextraction to the headspace gas chromatographic analysis of halogenated volatiles in selected foods

B. Denis Page* and Gladys Lacroix

Health and Welfare Canada, Health Protection Branch, Food Directorate, Bureau of Chemical Safety, Food Research Division, Sir F. Banting Research Centre, Ross Avenue, Ottawa, Ontario K1A 0L2 (Canada)

(First received March 29th, 1993; revised manuscript received June 21st, 1993)

ABSTRACT

Solid-phase microextraction (SPME), with the poly(dimethylsiloxane)-coated silica fiber suspended and equilibrated in the headspace, has been applied to the capillary gas chromatographic (GC) analysis of 33 halogenated volatile contaminants in model aqueous solutions and in foods. With electrolytic conductivity detection, the limits of detection in water ranged from 1.5 μg/kg for vinyl chloride to ≤ 0.005 μg/kg for the tri- to hexachlorobenzenes. Headspace SPME–GC shows a much greater response for the less volatile analytes than those of greater volatility, a procedure complementing headspace GC with gas sampling. In model systems or foods, increasing lipid material decreased the headspace extraction. With 50 mg of lipid, the headspace extraction decreased about 50% for analytes with LODs about 0.1 μg/kg and by $\geq 99.5\%$ for the above chlorobenzenes. Standard addition was used to analyze a variety of beverages and dry foods and to determine the analyte partitions.

INTRODUCTION

Solid-phase microextraction (SPME) is a relatively new sampling technique first described by Belardi and Pawliszyn [1]. Their procedure employs a stationary phase, usually poly(dimethylsiloxane), coated on a fused-silica fiber to extract aqueous samples in completely filled sealed vials. After equilibration between the liquid and the coated fiber, the analytes are thermally desorbed in the injection port of a gas chromatograph, cryofocussed on-column, and separated and detected by established GC procedures. For protection and ease of handling the fiber is attached to a tube which replaces the plunger of a 5-μl positive displacement syringe. The fiber is extended only during sampling or desorption of the analyte.

Pawliszyn and co-workers have conducted extensive studies on SPME including its automation and optimization [2], the dynamics of adsorption [3], the analysis of benzene in water at trace levels [4], aromatic compounds in groundwater [5], and the analysis of caffeine in beverages using an uncoated silica fiber [6]. SPME has been applied to many of the volatile analytes included in the US Environmental Protection Agency Method 624. Some of these studies have recently been summarized and it is reported that a commercial SPME device is forthcoming [7].

In classical headspace gas chromatography (GC), the analyte equilibrates between a liquid and the gas phase in a closed system. At equilibrium, an aliquot of the headspace is taken and analyzed by GC. Apart from the chromatographic detection and separation, the sensitivity attained by headspace GC is dependant on several factors including the vapor pressure of the analyte, the activity coefficient of the analyte in

* Corresponding author.

0021-9673/93/$06.00

the matrix in which it is present [8], as well as the volume of headspace sampled.

In our studies we have extended the classical two-phase headspace GC technique described above to include the SPME fiber coating as a third phase, suspended and equilibrated in the headspace. With the SPME sampling of the headspace, aqueous systems containing dissolved or suspended solids or non-volatile oil can be analyzed. Furthermore, salts may be added to the aqueous phase to increase the partition of volatiles into the headspace.

Using model aqueous systems, our studies compare the classical headspace GC procedure to the proposed headspace SPME–GC combination. The effect of non-polar non-volatile material on the headspace SPME–GC sensitivity in model systems is also studied. Practical application of SPME–headspace GC to a variety of foods, and the matrix effects of the food constituents on the partition into the coated fiber of the SPME device are studied and discussed.

EXPERIMENTAL

Solid-phase microextraction device

The SPME device was constructed as described by Potter and Pawliszyn [4] with minor dimensional modifications using either a Hamilton Model 7105 microliter syringe (Hamilton, Reno, NV, USA) or an SGE Model 5BR-7 microvolume syringe (SGE, Austin, TX, USA) and a 1 or 2 cm length of 100 μm thick poly(dimethylsiloxane)-coated fused-silica optical fiber (FLS100110300, Polymicro Technologies, Tuscon, AZ, USA). The stripped silica end of the coated fiber was cemented into 30 gauge (0.30 mm) stainless-steel tubing for the Hamilton syringe or 28 gauge (0.36 mm) tubing for the SGE syringe using a high-temperature epoxy resin (Epoxy-Patch No. 9340, Dexter, Seabrook, NH, USA). The fiber assembly is held in place in the SGE syringe using a 2×8 mm metric machine screw. After curing overnight the fiber assembly was heated at 250°C in the injector of the GC for 30 min before use. The needle tube with the attached fiber was adjusted so the end of the tube protruded 33 mm beyond the end of the needle when extended and the end of the fiber was 1 cm inside the needle when retracted.

A needle spacer for the Hamilton SPME syringe was fashioned from a 16 or 17 gauge luer tip hypodermic needle cut so the syringe needle protruded about 6 mm when the needle spacer was fitted to the external luer fitting of the syringe. The SGE syringe needle, however, does not have an external luer fitting so a similar spacer was used but did not attach firmly to the syringe. Needle spacers allow reproducible insertion of the needle without over-insertion.

Desorption and chromatography

The desorption of the analytes from fiber and the capillary separation was performed using a Varian Model Vista 6000 GC with cryogenic oven cooling. The GC was equipped with a Hall electrolytic conductivity detector operating in the reductive halogen mode for detection of the halogenated analytes. A disposable electrolyte system (N-Phase, Austin, TX, USA) was used with the detector. An attenuation of $8 \times$ was used for most samples; $2 \times$ was used when estimating sensitivity. The on-column injector of the Varian 6000 GC was replaced by that from a Varian 3400 GC to accommodate 0.53 mm I.D. tubing and further modified (Fig. 1) to permit proper positioning of the fiber for desorption. The glass alignment tube of the injector was

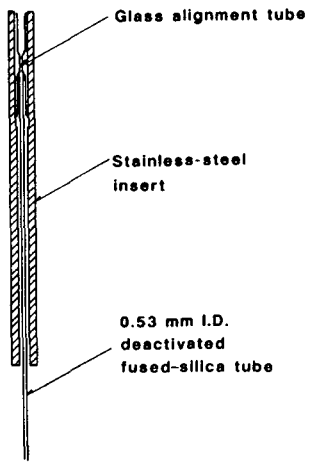

Fig. 1. On-column stainless-steel injector insert and alignment tube for smooth insertion of SPME fiber into 0.53 mm I.D. deactivated fused-silica tubing.

replaced by a 6.5 cm length of 2.1 mm I.D. stainless-steel tubing machined to 4.43 mm O.D. The upper end of the tube was drilled to 2.5 mm I.D. for a depth of 2.3 cm to accommodate a glass 0.53 mm to 0.53 mm press-fit capillary column union (Chromfit, Chromatographic Specialties, Brockville, Ontario, Canada) which acted as an alignment tube for fiber insertion into a 0.5 m × 0.53 mm I.D. piece of deactivated fused-silica tubing for desorption. The constriction in this union is wide enough to permit passage of the fiber assembly. For this purpose the union can also be prepared by carefully drawing out a piece of 2 mm pyrex tubing, cutting to 2 cm in length and fire-polishing the ends. The cap seal of the injector was enlarged to 9.53 mm I.D. to a depth of 6 mm to allow deeper entry of the SGE syringe. The Varian injector needle seal accommodated the SGE syringe but not the Hamilton syringe. For the latter syringe a 9.53 mm diameter HT-9 septum (Alltech, Deerfield, IL, USA) was modified to provide a needle seal using a short piece of 1.5 mm O.D. × 0.3 mm I.D. PTFE tubing flared at one end, inserted through a hole pierced in the center of the septum, and cut off flush. With the fiber assembly adjusted as described above, the syringe end of the fiber will be positioned 2.0 to 2.5 cm into the 0.53 mm deactivated tubing.

The halogenated analytes were separated on a 0.32 m × 30 mm DB-624 (J&W Scientific, Folsom, CA, USA) fused-silica capillary column (1.8-μm film) which was connected to the 0.5 m fused-silica tubing described above using a press-fit capillary column union. The exit of the GC column was connected to the detector by a 0.3 m length of 0.25 mm I.D. deactivated fused-silica tubing which was inserted 3–4 mm into the 0.5 mm I.D. nickel reactor tube. Helium at 2 ml/min (41 cm/s) was used as a carrier gas. The analytes were desorbed from the fiber in the injector by a temperature program from 0 to 250°C at 60°C/min with a 28-min hold. The oven was programmed from − 40°C (2 min hold) for SPME desorption [− 60°C (1.6 min hold) for gas sampling] to 30°C at 50°C/min and then to 250°C at 8°C/min (2 min hold). The detector base was at 250°C and the reactor at 850°C.

Standards

The volatiles determined and studied are listed in Table I. Primary stock solutions of standards were prepared as described by Environmental

TABLE I

VOLATILES STUDIED IN ORDER OF ELUTION AND THEIR REFERENCE NUMBERS

Volatile	No.	Volatile	No.
Vinyl chloride	1	Chlorodibromomethane	18
Methyl bromide	2	1,2-Dibromoethane	19
1,1-Dichloroethylene	3	Chlorobenzene	20
Dichloromethane	4	Bromoform	21
trans-1,2-Dichloroethylene	5	Bromobenzene	22
1,1-Dichloroethane	6	*o*-Chlorotoluene	23
cis-1,2-Dichloroethylene	7	*p*-Chlorotoluene	24
Chloroform	8	*p*-Dichlorobenzene	25
1,1,1-Trichloroethane	9	*o*-Dichlorobenzene	26
Carbon tetrachloride	10	1,2-Dibromo-3-chloropropane	27
1,2-Dichloroethane	11	1,2,4-Trichlorobenzene	28
Trichloroethylene	12	1,2,3-Trichlorobenzene	29
1,2-Dichloropropane	13	1,2,4,5-Tetrachlorobenzene	30
Dibromomethane	14	1,2,3,4-Tetrachlorobenzene	31
Bromodichloromethane	15	Pentachlorobenzene	32
1,1,2-Trichloroethane	16	Hexachlorobenzene	33
Tetrachloroethylene	17		

Protection Agency procedures [9] using chemicals purchased separately to give standards of about 2 mg/ml for each volatile. Hexachlorobenzene was prepared separately in acetone. Secondary standards were prepared by dilution of the primary standard in methanol to give concentrations of 10, 2, 0.4, 0.08, and 0.016 μg/ml for each analyte. Methanol, suitable for trace volatile analysis (Burdick and Jackson, Muskegon, MI, USA) was used to prepare all standards. Liquid chromatographic grade water (Milli-Q system, Millipore, Bedford, MA, USA) was used as required.

Headspace equipment and procedures

For headspace gas analysis and SPME sampling, 30-ml crimp-top headspace vials (actual capacity about 37 ml), 20 mm × 3 mm laminated silicone–PTFE (0.25 mm) septa, and aluminum seals (Supelco, Oakville, Ontario, Canada) were used. PTFE-coated, 25 × 7.5 mm magnetic stirring bars were used for stirring in the vials. The stirring rate was set to give a vortex depth of 1 cm.

The 1-ml headspace gas sampling and injection was conducted using equipment and procedures described previously [10]. The modified injector was used with this needle.

For headspace gas sampling by SPME, the vial septum was prepierced in the center, if required, with a sharp thin probe just before sampling to facilitate insertion of the SPME syringe needle. The needle was inserted so the spacer pushed firmly on the septum surface and the fiber assembly extended so the end of the fiber was about 1 cm above the surface of the liquid. The syringe was clamped in this position and the stirring commenced. After 30 min the fiber assembly was retracted, the syringe needle withdrawn from the septum, the needle inserted into the injector, the fiber extended, and the oven and injector temperature programs started. The fiber was left in place and desorbed for 15 min to ensure total desorption of the least volatile analytes. The procedure for liquid sampling by SPME was only employed with clean water and is the same as described above for SPME sampling of the headspace except that the end of the fiber was positioned about 0.5 cm above the stirring bar.

Studies in model systems

In these studies, unless noted otherwise, stirred vials containing 15 g of water and 6 g of sodium chloride and optimized equilibration times of 30 min and desorption times of 15 min at 250°C were employed. The vials were sealed and spiked through the septum using a 10-μl syringe to give 30 ng of each volatile. The resulting peak areas were either compared to those of another study, to an aqueous standard or to a 1-μl injection of the same volatiles at 1 μg/ml in cold (0°C) 2-pentane.

The relative sensitivity between headspace gas syringe sampling and headspace SPME sampling was studied. The sampled volatiles were either injected or desorbed, respectively, as described previously.

The repeatability of the headspace SPME–GC procedure was studied using six vials each containing 15 g of water, 6 g of sodium chloride and a stirring bar.

The limits of detection (LODs) of the headspace SPME–GC procedure were studied by spiking vials with 3-μl aliquots of standards containing 10, 2, 0.08, 0.04 and 0.016 μg/ml of each analyte.

Vials with no added salt and 25 g of water, required for complete fiber immersion, were used to evaluate the effect of fiber position on the analyte equilibration between the aqueous solution, the headspace gas and the poly(dimethylsiloxane) fiber coating. The SPME fiber was inserted into the spiked water or into the headspace over the water and equilibrated with stirring for 0.75, 1.5 or 3 h.

The effect of dissolved salt on the liquid–gas–solid equilibrium was studied with 6 g of either anhydrous sodium sulfate, sodium chloride or potassium chloride.

The decreases in sensitivity of the headspace SPME procedure were studied using 1.5, 12, 58, and 240 mg of a mixed vegetable oil as representative non-polar lipid food components.

Headspace SPME analysis of beverages and finely divided dry foods

The procedures for obtaining various types of beverage and food samples and their addition to the headspace vials for volatile analysis have been previously described [10–12] and were used in this study.

To analyze beverages, other aqueous samples or finely divided dry foods, three vials, each containing a magnetic stirring bar, 6.0 g of sodium chloride and loosely covered with the laminated silicone–PTFE septum were cooled in a water–ice bath for at least 15 min. For the dry foods, 15 g of water was also added to each vial. The cold liquid (4°C) or dry food (−20°C) samples were opened and, in succession, each vial was tared on a top-loading balance, 15 g aliquots of the liquid or 1.0 g sample of the dry food were added and each vial immediately sealed. After warming to room temperature, the first vial was sampled by headspace SPME for 30 min and analyzed as described above. Halogenated analytes were identified by comparison of retention times to those of external standards. To provide quantitation of any detected GC peaks and to evaluate the matrix effects on the headspace partition of various analytes from a particular sample, the second vial was spiked through the septum using a 10-μl syringe to give 30 ng of each volatile and sampled by headspace SPME as for the first sample. From the increase in peak area of a particular analyte, the concentration of that analyte in the sample can be calculated. When the analyte peak is greater than half that of the enhanced analyte peak (incurred plus added analyte) then quantitation should be conducted by a greater standard addition to the third vial. If the analyte response is too great, smaller, but representative samples of equal weight, can be taken analyzed using appropriate standard additions. Liquids are diluted in the headspace vial with water to give 15 g total liquid. Where the observed matrix effect on the headspace partition for the sample is the same as that for clean water, sample analytes can be quantitated from aqueous external standards.

A limited survey of locally purchased foods and beverages was conducted using headspace SPME–GC to study the analyte partitions and to determine the levels of any incurred chlorinated volatile contaminants.

RESULTS AND DISCUSSION

Headspace SPME–GC equipment

The SPME fiber assemblies were prepared according to Potter and Pawliszyn [4] for use with both the Hamilton and SGE syringes. The SGE syringe, with a blunt 0.63 mm O.D. needle was compatible with the existing Varian injector needle seal. Needle seals were considered preferable to septum injection which could inadvertently introduce pieces of septum into the GC column. For the Hamilton syringe a needle seal was fabricated in-house. All seals and syringes were tested to ensure the absence of leaks as suggested by Potter and Pawliszyn [4]. For best repeatability, the same fiber was used for replicate determinations as even two apparently identical fibers extracted and desorbed slightly different amounts of analytes from over identical solutions. Coated fibers of 2 cm were found to give peaks about twice those of the 1-cm fiber but for convenience and ease of handling, 1-cm fibers were used throughout. The constriction of the press-fit capillary unions used in the injector, permitted facile passage of the 30 gauge fiber assembly of the Hamilton syringe in 8 of 10 unions evaluated yet only 3 of the 10 permitted entry of the 28 gauge tubing required for the SGE syringe.

With on-column cryofocussing, desorption of the SPME fiber or headspace gas injection using the gas-tight syringe in the modified injector gave acceptable chromatograms for all analytes as shown in Fig. 2A and B. Oven cryofocussing, −60°C for the 1-ml headspace injection and −40°C for the desorption, was required to reduce peak broadening of the early eluting peaks. The peak widths were comparable to those obtained from a 1-μl liquid injection in the same injector. No carryover of undesorbed analytes was observed when the fiber was desorbed for a second time. The desorption temperature originally used was 230°C, however, when hexachlorobenzene was later included as one of the

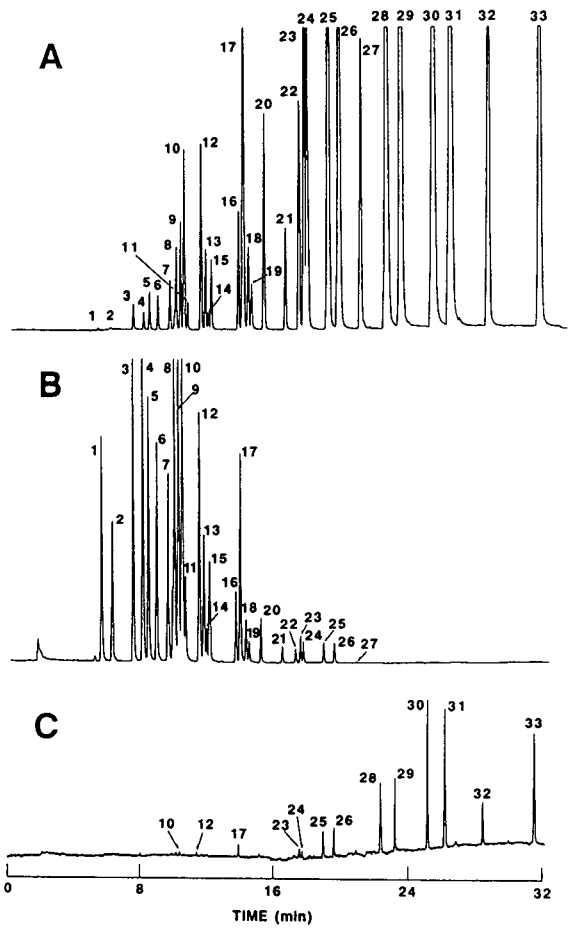

Fig. 2. Chromatograms of: (A) volatiles (2 ng/ml each, peak identities as in Table I) by headspace SPME over 15 ml NaCl saturated water; (B) as in (A) but 1 ml of the headspace injected; (C) as in (A) but at 0.016 ng/ml.

analytes, the desorption temperature was raised to 250°C. This increased temperature also gave complete desorption in 15 min. The equilibration time of the analytes, including hexachlorobenzene, between the liquid, gas and solid phases, when spiked into the liquid and analyzed by headspace SPME was found to be less than 30 min. Thus, when using the same SPME device, samples could be equilibrated and desorbed every 45 min. This turnaround time was only slightly greater than that for the GC.

Because the vial septum consists of a 0.25 mm thick PTFE layer on a silicone backing it was important to evaluate possible analyte adsorption by the silicone once the PTFE layer was pierced. Therefore, five additional punctures were made in the septum with a 20-gauge needle but without needles to plug the punctures. Headspace SPME analysis indicated about a 20% loss attributed to the exposed silicone. Thus, the loss to one puncture would be less than 5% and possibly even less when the SPME needle was in place in the puncture during the headspace SPME sampling.

Table I lists the volatiles studied in our laboratory using the SPME technique. Other halogenated volatiles which may co-elute with or not cleanly separate from those in Table I on the 30-m DB-624 column used in our studies were not included. If required, two possible co-eluting halogenated volatiles may be differentiated using specific detectors or other capillary columns capable of the desired separation.

Our interest in volatile halogenated contaminants concerns their determination in foods and beverages. Arthur *et al.* [7] had demonstrated the application of SPME to volatiles extracted with the coated fiber positioned in water. Our goal was to extend the application of SPME to beverages or to suspensions of dry foods in water. Except for clean water, however, sampling foods or beverages with the SPME fiber positioned in the liquid could possibly transfer non-volatile food material adsorbed by, or adhering to the fiber to the injector and the GC column. Therefore, for food analysis, we chose to evaluate SPME for sampling volatiles in the headspace followed by desorption in the injector and capillary GC separation with electrolytic conductivity detection.

Studies in model systems

The results of the studies in model systems are given in Table II with representative chromatograms presented in Fig. 2. The chromatograms of the analytes desorbed from the coated fiber or injected in 1 ml of headspace gas are shown in Fig. 2A and B, respectively. The percentage of each analyte transferred to the GC for analysis using these two techniques is given in Table II. Because of the different phase volumes, only 1 ml of the total 21.8 ml headspace gas is sampled and determined, yet all of the analyte in the 0.6-μl fiber coating is desorbed and determined.

TABLE II

STUDIES IN MODEL SYSTEMS: HEADSPACE SYRINGE *VS.* HEADSPACE SPME, THE EFFECT OF ADDED SODIUM CHLORIDE, PRECISION (R.S.D.) BY SPME ($n = 6$), LIMIT OF DETECTION (LOD, IN WATER), AND MATRIX EFFECTS OF ADDED NON-POLAR MATERIAL (*VS.* WATER)

No.	% of analyte sampled		% increase with salt by SPME	R.S.D. at 2 μg/kg	LOD (μg/kg)	Matrix effect (% rec. from veg. oil *vs.* water)			
	Syringe	SMPE				1.5 mg	12 mg	58 mg	240 mg
1	1.5	0.02	100	6.1	1.5	100	93.4	100	68.1
2	3.0	0.03	n.d.[a]	8.7	0.75	85.7	92.5	100	56.5
3	4.3	0.36	261	4.2	0.10	105	86.6	67.3	32.0
4	1.8	0.16	300	35	0.10	95.4	96.9	81.2	36.5
5	3.4	0.41	412	4.4	0.10	106	77.1	53.7	23.0
6	2.6	0.40	511	3.6	0.10	107	79.8	54.1	23.3
7	2.2	0.59	638	2.8	0.10	108	74.1	48.0	15.3
8	2.4	0.56	662	4.3	0.05	106	63.9	40.3	17.6
9	3.3	1.2	264	4.4	0.03	87.5	72.8	28.6	10.3
10	3.7	1.5	141	4.7	0.03	98.4	72.2	27.7	9.5
11	2.7	0.35	1160	5.1	0.15	114	75.8	56.0	23.3
12	2.9	1.9	353	4.1	0.02	99.3	59.1	19.4	5.8
13	2.2	1.2	710	3.6	0.05	107	64.1	27.2	7.2
14	0.28	0.24	300	6.1	0.02	114	59.5	40.2	15.0
15	1.5	0.84	843	3.4	0.20	106	57.5	23.4	6.8
16	0.69	1.0	958	4.1	0.07	107	60.2	22.0	5.2
17	2.6	5.7	127	5.8	0.04	85.2	37.8	7.2	2.0
18	0.47	0.97	865	4.8	0.08	99.5	46.8	14.2	3.7
19	0.32	0.80	1050	4.5	0.15	104	51.4	18.3	5.3
20	1.8	6.9	642	3.9	0.02	82.3	25.4	5.0	1.0
21	0.18	1.5	2173	4.9	0.08	94.8	38.0	10.0	2.5
22	0.84	12	1897	3.7	0.02	64.9	13.0	1.9	0.4
23	1.3	16	347	4.8	0.01	56.4	11.3	1.4	0.4
24	1.1	22	395	3.9	0.01	50.8	10.5	1.1	0.4
25	0.49	22	460	4.1	0.005	43.5	7.9	1.1	0.4
26	0.39	26	576	3.7	0.005	43	7.8	1.1	0.4
27	tr.[b]	4.3	1318	3.8	0.03	76.7	19.6	3.8	0.9
28	tr.	46	258	5.3	0.002	22.2	3.8	0.5	0.1
29	–[c]	57	297	4.7	0.002	22.2	3.6	0.5	0.1
30	–	56	121	7.6	0.002	17.2	3.1	0.5	0.2
31	–	72	144	7.7	0.002	17.0	3.7	0.5	0.2
32	–	57	69.7	9.9	0.005	8.1	3.3	0.3	0.2
33	–	n.d.	n.d.	15.2	0.002	2.8	3.0	0.2	0.2

[a] n.d. = Not determined: No. 2, peak detected only when salt added; No. 33 not included in standard.
[b] tr. = Trace level found, $< 3 \times$ baseline noise.
[c] Not detected.

These results relate to the practical sensitivity of each procedure and show the 1-ml headspace gas sampling technique to be progressively more sensitive as the volatility of the analyte, evidenced by earlier GC elution, increases. With SPME, however, as the analyte mass increases, the water solubility (polarity) and analyte volatility decrease, and increasingly more of any analyte that partitions into the headspace from the liquid will be extracted by the non-polar fiber and determined. SPME is progressively more sensitive as the analyte volatility, evidenced by later GC elution, decreases. Thus, headspace gas sampling and headspace SPME can be consid-

ered as complementary headspace sampling procedures.

The adsorption of the analytes with the fiber immersed in the water gave >90% of the peak areas obtained when the fiber was suspended in the headspace for the first 26 volatiles after 0.75 h. The later-eluting 7 volatiles gave 87–25% of the headspace response. Increasing the equilibration time to 1.5 and 3.0 h increased the water sampling to >90% of the headspace response for the first 29 analytes, with the tetra-, penta- and hexachlorobenzenes being found at 75–50%. There was little difference between the 1.5- and 3.0-h results. This study demonstrates that the liquid–solid (fiber in water) equilibration time is slower than the liquid–gas–solid (fiber in headspace) equilibration, even though the analytes are added to the water.

Table II also shows the relative standard deviation for replicate determinations from 15 ml of water containing 30 ng of each target analyte with all values below 10% except for *cis*-1,2-dichloroethylene (No. 4, 35%) and hexachlorobenzene (No. 33, 15.2%). The limit of detection (LOD), defined as 3 × the baseline noise, determined by headspace SPME in a 15-ml solution of water are given in Table II and parallel the percentage of each analyte sampled by headspace SPME as discussed previously. These LODs were extrapolated from several dilute standards with the detector at attenuation 2. Examples of these low detection limits for several of the less volatile analytes are shown in Fig. 2C. The limit of quantitation, defined as 10 × the baseline noise, or about 3 × the LOD, can be calculated from the LOD data.

The effects of aqueous saturation by various salts on the partition of the analytes into the coated fiber showed slightly smaller peaks for the earlier-eluting volatiles with sodium sulfate saturation compared to sodium chloride. The later-eluting volatile peaks were comparable. Potassium chloride gave smaller peaks for all the volatiles. Table II shows increases of the headspace SPME response by factors ranging from about 70 to 2170% when water is saturated with sodium chloride.

The matrix effects of increasing non-volatile non-polar food constituents, represented in Table II by a mixed vegetable oil, are given as the percent recovered compared to water. These reduced recoveries are to be expected, as vegetable oil, present in volumes of about 1.6 to 260 μl, competes with the 0.6-μl SPME fiber coating for the non-polar volatiles. The more volatile analytes are less affected by added oil as they partition significantly into the gas phase in addition to the combined non-polar phases. When large amounts, *e.g.*, 1 g of lipid material, are present, and 30 ng of each analyte are added, then only the first 17 peaks are above the LOD. The effects of proteinaceous material on the partition into the headspace was not studied.

Analytical results for selected foods

Table III reports the halogenated volatiles found in selected waters, fruit juices, fruit drinks, soft drinks and milks. Products to which water from public supplies could have been added, including water itself and the beverages listing water as an ingredient, were found to contain by-products of the water chlorination process, including chloroform (No. 8), bromodichloromethane (No. 15) and chlorodibromomethane (No. 18). Chloroform was found at levels ranging from 0.2 to 14.8 μg/kg. Of these eight samples four also contained bromodichloromethane. The other beverages in Table III, not listing water as an ingredient, were the grapefruit and the apple juice, and the three milks. In these five products, chloroform found was found only at low levels.

Standard addition provides for quantitation but also permits an evaluation of the partition of the target analytes between the SPME fiber and the particular sample matrix (5 g sample aliquot, 10 g water and 6 g of sodium chloride). The effect of non-polar non-volatile sample material parallels that of the vegetable oil noted above for Table II. Apple juice, the cola and ginger ale soft drinks and the cranberry–raspberry drink apparently contain little non-polar material as the analyte partition of all but the last two volatiles are generally >80%. The other juices and drinks, however, contain non-polar volatile and non-volatile material which reduce the partition of the volatiles into the fiber.

Of unique interest is *d*-limonene, a volatile

TABLE III

HALOGENATED VOLATILES IN μg/kg FOUND IN SELECTED BEVERAGES (5 g + 10 g WATER) AND THEIR HEADSPACE SPME PARTITION (%, IN PARENTHESES) COMPARED TO CLEAN WATER (15 ml, 2 μg/kg)

No.	Water[a]		Fruit juice				Soft drink			Fruit drink			Milk, % butterfat		
	Tap	Bottled	Pear	Orange	Apple	Grape-fruit	Orange	Cola	Ginger ale	Citrus	Cranb rasp.	Lemonade	0.1	2.0	3.4
1	–	–	(117)	(85.7)	(111)	(114)	(75.0)	(100)	(100)	(100)	(100)	(109)	(100)	(60.0)	(83.3)
2	–	–	(89.3)	(96.3)	(94.4)	(132)	(78.5)	(75)	(75.0)	(71.5)	(95.2)	(68.7)	(88.0)	(55.2)	(85.7)
3	–	–	(109)	(92.4)	(106)	(109)	(96.8)	(90.4)	(94.0)	(96.6)	(74.4)	(100)	(82.4)	(29.4)	(26.7)
4	–	–	4.6(47.5)	(89.9)	(66.5)	(96.7)	(93.7)	(118)	(116)	(98.5)	(90.4)	(109)	(103)	(66.8)	(66.6)
5	–	–	(104)	(90.1)	(108)	(106)	(103)	(94.0)	(95.8)	(105)	(86.0)	0.49(93.5)	(77.2)	(28.0)	(21.5)
6	–	–	(98.3)	(83.4)	(102)	(98.1)	(94.5)	(86.1)	(91.8)	(91.7)	(82.4)	(95.5)	(81.3)	(28.8)	(23.8)
7	–	–	(95.4)	(84.2)	(102)	(94.3)	(88.9)	(86.7)	(94.4)	(90.7)	(84.9)	(94.8)	(73.2)	(27.0)	(20.1)
8	11.9	1.09	1.2(102)	2.18(86.5)	0.55(108)	(92.3)	2.62(97.7)	10.8(104)	1.56(103)	7.20(128)	14.8(97.0)	0.20(94.2)	0.33(85.5)	1.25(27.9)	(19.5)
9	–	–	(101)	(62.6)	(106)	(86.7)	(91.0)	(73.6)	(86.9)	(87.2)	(67.1)	(95.1)	(62.1)	(12.3)	(8.7)
10	–	–	(97.5)	(68.3)	(108)	(94.5)	(92.6)	(81.2)	(87.1)	(85.5)	(77.5)	(94.2)	(51.7)	(8.6)	(6.3)
11	–	–	(105)	(85.1)	(117)	(88.3)	(86.5)	(97.2)	(103)	(89.6)	(90.2)	(90.2)	(86.5)	(30.7)	(32.2)
12	–	–	(90.6)	(74.7)	(103)	(88.9)	(92.5)	(84.5)	(90.6)	(90.6)	(78.1)	(94.3)	(54.2)	(9.6)	(6.8)
13	–	–	(93.4)	(78.7)	(103)	(87.0)	(85.9)	(86.3)	(94.0)	(89.9)	(83.6)	(91.3)	(67.6)	(16.3)	(10.9)
14	–	–	(91.7)	(79.9)	(112)	(85.5)	(83.3)	(112)	(121)	(87.6)	(88.2)	(84.2)	(61.9)	(25.8)	(20.5)
15	0.53	0.39	1.2(97.1)	0.31(77.4)	(106)	(81.3)	1.72(94.2)	(98)	0.82(108)	(104)	4.7(96.0)	(90.6)	(56.4)	(11.9)	(8.9)
16	–	–	(89.3)	(73.3)	(107)	(77.2)	(81.7)	(91.2)	(103)	(93.8)	(85.7)	(86.4)	(59.4)	(12.2)	(8.3)
17	–	–	(80.0)	(47.7)	(106)	(74.1)	(84.9)	(87.3)	(92.7)	(64.8)	(77.8)	(85.0)	(33.2)	(3.5)	(2.3)
18	–	–	(80.5)	(66.1)	(107)	(73.0)	0.41(87.3)	(96.7)	(113)	(94.8)	1.8(91.7)	(85.6)	(40.8)	(7.7)	(4.9)
19	–	–	(90.1)	(74.8)	(113)	(78.9)	(87.5)	(98.9)	(111)	(101)	(90.0)	(82.8)	(55.6)	(10.4)	(6.6)
20	0.10	–	(69.2)	(49.5)	(102)	(64.8)	(80.0)	(80.3)	(89.8)	(67.4)	(80.5)	0.09(86.0)	(27.1)	(2.7)	(1.5)
21	–	–	(69.2)	(56.9)	(107)	(63.5)	(78.4)	(96.7)	(105)	(92.5)	(87.0)	(83.5)	(30.6)	(5.3)	(3.7)
22	–	–	(46.7)	(32.1)	(105)	(46.1)	(67.8)	(83.3)	(93.4)	(51.6)	(81.2)	(72.0)	(15.5)	(1.0)	(1.4)
23	–	–	(54.8)	(29.5)	(108)	(43.9)	(67.2)	(86.2)	(94.2)	(40.7)	(78.6)	(68.0)	(14.9)	(1.1)	(0.6)
24	–	–	(47.5)	(24.3)	(106)	(40.0)	(60.0)	(82.2)	(90.2)	(39.6)	(78.9)	(61.5)	(12.7)	(0.95)	(0.5)
25	–	–	(39.4)	(22.2)	0.16(103)	(34.6)	(46.6)	(84.1)	(93.7)	(6.3)[b]	(80.6)	(57.8)	(10.8)	(2.5)	(0.5)
26	–	–	0.02(38.6)	(18.9)	(102)	(28.9)	(53.5)	(78.8)	(92.7)	(31.1)	(79.1)	(56.5)	(8.9)	(1.4)	(0.4)
27	–	–	(57.2)	(40.1)	(102)	(51.1)	(67.9)	(90.9)	(98.7)	(68.0)	(85.8)	(70.8)	(22.1)	(2.4)	(1.1)
28	–	–	(23.9)	(9.3)	(111)	(16.1)	(32.4)	(94.8)	(100)	(16.8)	(85.1)	(32.2)	(4.8)	(0.45)	(0.2)
29	–	–	(21.5)	(7.4)	(114)	(13.4)	(30.6)	(88.3)	(98.2)	(15.4)	(82.0)	(31.6)	(3.7)	(0.40)	(0.1)
30	–	–	(15.3)	(4.4)	(121)	(8.6)	(17.2)	(101)	(106)	(7.8)	(89.8)	(18.8)	(2.7)	(0.20)	(0.1)
31	–	–	(12.9)	(3.5)	(123)	(7.1)	(16.3)	(90.7)	(105)	(7.8)	(82.8)	(18.1)	(1.8)	(0.18)	(0.08)
32	–	–	(5.8)	(1.2)	(110)	(2.7)	(7.2)	(71.6)	(101)	(7.5)	(71.2)	(6.7)	(0.7)	(0.13)	(–)[c]
33	–	–	(2.1)	(0.4)	(85)	(0.7)	(3.1)	(34.1)	(65)	(0.8)	(34.3)	(1.4)	(0.2)	(0.17)	(–)

[a] For water 15 g were analyzed. Partition data compared to clean water is 100% and is not reported.
[b] *d*-Limonene coelutes with *p*-dichlorobenzene and interferes its detector response.
[c] Peak not detected, partition not determined.

terpene associated with citrus products, which co-elutes with *p*-dichlorobenzene and disrupts its detection resulting in a small broadened peak for this analyte. To demonstrate that limonene causes this interference, an aqueous saline solution was spiked with 30 ng of each analyte and 1 mg of limonene, an amount chosen to slightly exceed the amount of limonene in 5 ml of processed orange juice [13]. The headspace SPME sampling failed with the Hamilton syringe, however, as the 0.3 mm O.D. fiber coating swelled so that it could not be retracted into the 0.33 mm I.D. protective needle. The SGE syringe, however, with the 0.37 mm I.D. needle readily accommodated the swollen fiber. The fiber swelling was observed with limonene only in model aqueous systems. Swelling was not observed in 5-g orange juice samples, even when spiked with limonene. Apparently non-volatile lipid material in the orange juice reduced the partition of limonene to the fiber. The swelling of the fiber appeared to be limited, as up to 25 mg of limonene in the vial did not restrict the fiber movement in the SGE syringe needle. The analyte capacity of the swollen fiber more than doubles for the more volatile analytes when compared to the unswollen fiber. The adverse chromatographic effects of limonene on the *p*-dichlorobenzene peak noted above were accentuated when limonene was present without juice.

Furthermore, the preceding two peaks were also broadened and not cleanly resolved. These findings with limonene also suggest that competitive adsorption, in which a benign volatile at high concentration may block or displace a target analyte from the fiber, is not an important consideration in headspace SPME.

Headspace SPME chromatograms of an orange juice, a cola soft drink and a fruit drink from Table III containing trihalomethanes are shown in Fig. 3A–C, respectively. There are no interferences evident. With the cola drink (Fig. 3B) there are a number of small peaks eluting between 18 and 30 min which do not correlate with any of the analytes studied. The chromatogram in Fig. 3D shows 15 ml of the blank water used for dilution of the juices, drinks and the milks at an attenuation of 2 × . Except for traces of dichloromethane (No. 4), there are no interferences.

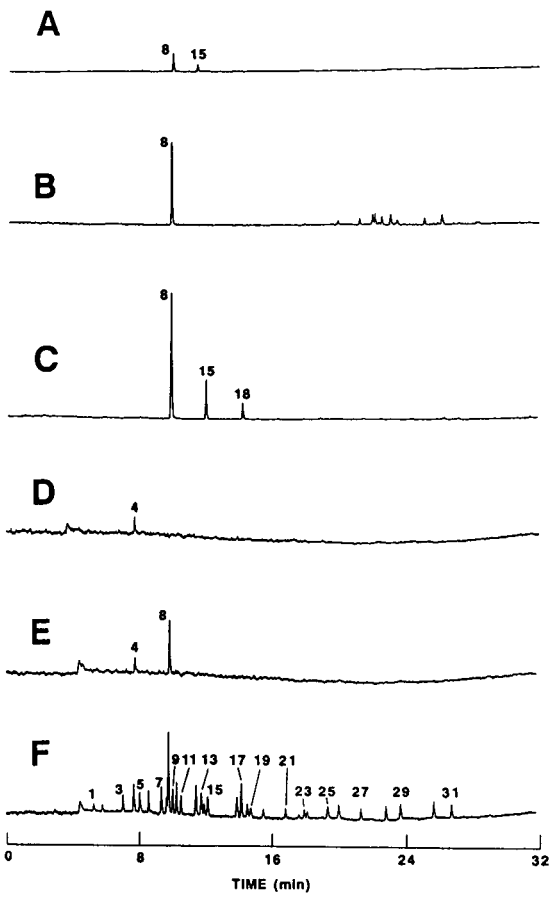

Fig. 3. Chromatograms of beverages, 5 g added to 10 ml of water: (A) orange juice containing chloroform (No. 8) and bromodichloromethane (No. 15); (B) cola soft drink containing No. 8; (C) cranberry–raspberry drink containing Nos. 8, 15 and chlorodibromomethane (No. 18); (D) water blank showing absence of interferences except for dichloromethane (No. 4); (E) 3.4% butter fat milk containing chloroform; and (F) as in (E) spiked at 4 μg/kg milk, only odd analytes numbered, peak identities as in Table I. Attenuation for (A), (B) and (C) 8 × ; others at 2 × .

The headspace SPME responses for the milk samples in Table III are reduced as the concentration of the butterfat increases. Fig. 3E shows the headspace SPME chromatogram at attenuation 2 × from 5 g unspiked 3.4% butterfat (about 170 mg) milk in 10 ml of water. Chloroform (No. 8) at about 9.3 μg/kg is detected in this sample. Fig. 3F shows this milk sample spiked with about 20 ng of each of the 33 analytes studied. An approximate 5-fold reduction of the chloroform response due to the butterfat is noted when Fig. 3F (milk at 2 ×) is compared to Fig. 3B (cola at 8 ×). Only about 10 of the volatiles in Fig. 3F can be considered as greater than the limit of quantitation (LOQ), others are between the LOQ and the LOD, and the volatiles Nos. 32 and 33 are not detected. Although the matrix effect varies considerably for the beverages studied, headspace SPME–GC can still detect and measure volatile contaminants at low μg/kg levels.

Table IV reports similar data to that of Table III for dry, finely divided foods. Most of these foods are reported [14] to contain appreciable lipid material: all-purpose white flour contains about 1.0% fat, the biscuit mix about 13%, the decaffeinated instant coffee 0.2% and the spices in Table IV, 0.5 to 36.3%. Comparable data for the decaffeinated teas and roasted and ground coffees were not available but the fat content of the non-decaffeinated products are 3% (dry weight, green leaf) [15], and 11.9% [16], respectively. In comparing these foods, the % partition from the food–water matrix to the SPME fiber is reduced with increasing food lipid content. Dichloromethane was found in the flour products and in the coffees and teas decaffeinated using dichloromethane. The biscuit mix was found to contain 1,1,1-trichloroethane at about 200 μg/kg. The origin of this contaminant was found to

TABLE IV

HALOGENATED VOLATILES IN μg/kg FOUND IN SELECTED DRY FOODS (1 g + 15 g WATER) AND THEIR HEADSPACE SPME PARTITION (%, IN PARENTHESES) COMPARED TO CLEAN WATER (15 ml, 2 μg/kg)

No.	Flour or flour-based		Decaffeinated teas			Decaffeinated coffees				Spices (% fat) [13]				
	All purpose	Biscuit mix	Brand A (DCM)[b]	Brand B (DCM)	Brand C (N.G.)[b]	Instant (Natural)	R&G[a] Brand A (Natural)	R&G Brand B (DCM)	R&G Brand C (DCM)	Paprika (12.9)	Ground pepper (3.3)	Cinnamon (3.2)	Onion flakes (0.5)	Nutmeg (36.3)
1	(124)	(77.7)	(81.9)[c]	–[c]	–	(100)	(69.0)[c]	–[c]	–	(107)	(88.2)	(87.3)	(100)	(100)
2	(71.6)	(107)	(69.5)	–	–	(107)	(75.3)	–	–	(80.4)	(90.0)	(100)	(75.2)	(85.0)
3	(96.2)	(50.8)	(51.1)	–	–	(83.2)	(24.5)	–	–	(74.7)	(31.6)	(68.0)	(90.2)	(32.7)
4	82.5(97.9)	70.3(10.1)	3.8(79.6)	58.6	13.5	(92.1)	(59.5)	308	76.5	(41.4)	(75.9)	(80.5)	(97.7)	(68.8)
5	(74.5)	(35.9)	(46.2)	–	–	(76.0)	(22.9)	–	–	(44.1)	(30.3)	(53.2)	(92.3)	(29.1)
6	(77.5)	(37.6)	(46.9)	–	–	(81.6)	(25.8)	–	–	(37.4)	(32.8)	(48.5)	(95.7)	(19.4)
7	(87.7)	(28.2)	(35.3)	–	–	(69.8)	(20.4)	–	–	(23.9)	(26.3)	(36.7)	(88.5)	(15.5)
8	(90.9)	(23.7)	(35.2)	–	–	(74.9)	(18.7)	–	–	(21.2)	(24.8)	(35.2)	(96.9)	(15.4)
9	(69.4)	206(15.4)	(31.2)	–	–	(66.3)	(10.0)	–	–	(41.5)	(12.8)	(41.5)	(70.9)	(14.3)
10	(52.1)	(17.0)	(26.1)	–	–	(56.6)	(9.6)	–	–	(40.2)	(9.3)	(37.1)	(62.6)	(14.6)
11	(74.7)	(30.5)	(39.6)	–	–	(65.6)	(26.2)	–	–	(23.7)	(30.4)	(33.0)	(86.7)	(20.4)
12	(52.9)	(9.1)	(23.8)	–	–	(55.3)	(9.1)	–	–	(23.9)	(8.2)	(28.3)	(64.7)	(8.0)
13	(66.9)	(11.9)	(27.3)	–	–	(60.0)	(13.5)	–	–	(14.2)	(18.8)	(29.6)	(80.5)	(8.4)
14	(63.2)	(20.6)	(26.9)	–	–	(54.1)	(17.6)	–	–	(16.3)	(38.9)	(26.6)	(96.6)	(17.4)
15	(44.2)	(9.1)	(20.4)	–	–	(49.8)	(10.9)	–	–	(10.5)	(18.7)	(21.7)	(76.8)	(7.3)
16	(47.2)	(10.4)	(18.4)	–	–	(47.8)	(9.4)	–	–	(8.6)	(12.4)	(16.7)	(70.6)	(5.5)
17	(28.0)	3.9(3.4)	(17.2)	–	–	(34.2)	(5.6)	128	–	(11.6)	(5.4)	(19.9)	(42.5)	(3.5)
18	(35.2)	(6.2)	(12.5)	–	–	(33.1)	(5.9)	–	–	(6.7)	(9.1)	(14.7)	(79.7)	(5.7)
19	(45.0)	(9.4)	(17.1)	–	–	(40.4)	(7.6)	–	–	(7.5)	(10.0)	(17.8)	(92.6)	(9.1)
20	(22.1)	(2.1)	(9.2)	–	–	(23.9)	(2.6)	–	–	(4.1)	(3.8)	(8.2)	(36.5)	(1.5)
21	(22.3)	(3.7)	(8.0)	–	–	(23.6)	(4.3)	–	–	(3.7)	(5.0)	(7.3)	(50.7)	(2.8)
22	(11.3)	(1.0)	(4.4)	–	–	(11.1)	(1.2)	–	–	(2.0)	(1.9)	(2.8)	(23.6)	(0.9)
23	(11.3)	(1.8)	(8.6)	–	–	(11.9)	(1.2)	–	–	(1.9)	(2.1)	(6.3)	(26.3)	(0.7)
24	(10.6)	19.6(0.7)	(7.1)	–	–	(11.9)	(1.1)	–	–	(1.3)	(1.3)	(3.6)	(18.0)	(0.3)
25	2.51(8.8)	31.9(1.4)	(5.3)	–	–	(8.0)	(1.0)	–	–	(1.6)	(1.8)	(3.2)	(15.9)	(0.8)
26	(7.4)	(0.2)	(4.2)	–	–	(6.7)	(0.7)	–	–	(1.3)	(1.4)	(2.4)	(13.7)	(0.4)
27	(17.0)	(1.7)	(5.0)	–	–	(11.7)	(2.2)	–	–	(7.2)	(2.0)	(3.8)	(28.6)	(0.9)
28	(4.2)	(0.2)	(4.6)	–	–	(3.0)	(0.3)	–	–	(0.9)	(0.8)	(1.7)	(6.9)	(0.2)
29	(3.6)	(0.2)	(3.5)	–	–	(2.3)	(0.3)	–	–	(1.1)	(0.7)	(1.3)	(5.5)	???
30	(2.9)	(0.2)	(6.1)	–	–	(1.0)	(0.1)	–	–	(1.7)	(0.6)	(1.8)	(4.5)	(0.2)
31	(2.4)	(0.2)	(4.5)	–	–	(0.8)	(0.1)	–	–	(2.1)	(0.5)	(1.4)	(3.2)	(2.2)
32	(1.1)	(0.2)	(4.8)	–	–	(0.3)	(–)[d]	–	–	(1.7)	(0.4)	(1.3)	(2.2)	(2.3)
33	(0.5)	(0.1)	(4.0)	–	–	(–)	(–)	–	–	(1.6)	(0.3)	(1.2)	(1.2)	(0.4)

[a] R&G = roasted and ground coffee.
[b] Decaffeination agent listed on package: DCM = dichloromethane; N.G. = not given; Natural = naturally decaffeinated (water or carbon dioxide).
[c] Partition data for Brands A averaged from 3 teas or 3 R&G coffees and not reported for other brands.
[d] Peak not detected, partition not determined.

be the paperboard adhesive of the retail package. Using headspace SPME, a small sample of the adhesive suspended in 15 g of water with added salt gave a massive off-scale GC peak for this volatile. Contamination of food by this source was first reported by Page and Charbonneau [17]. Others later reported similar incidents [18,19]. In the limited sampling of dichloromethane-decaffeinated teas and coffees, the levels of dichloromethane found are generally lower than those reported in an earlier survey [20]. Tetrachloroethylene was also found in one of the decaffeinated coffees at 128 μg/kg. Representative chromatograms of 1-g samples of the dry foods are shown in Fig. 4. Chromatograms of the biscuit mix, showing about 200 μg/kg of 1,1,1-trichloroethane (No. 9) and lower levels of other target analytes and a decaffeinated tea, showing 24 μg/kg dichloromethane (No. 4) and a number of unidentified low level responses are shown in Fig. 4A and B, respectively. Chromatograms of a naturally decaffeinated (water process) roasted and ground coffee, demonstrating the absence of halogenated volatiles, and the same coffee spiked with 30 μg/kg of the 33 analyte standard are displayed in Fig. 4C and D,

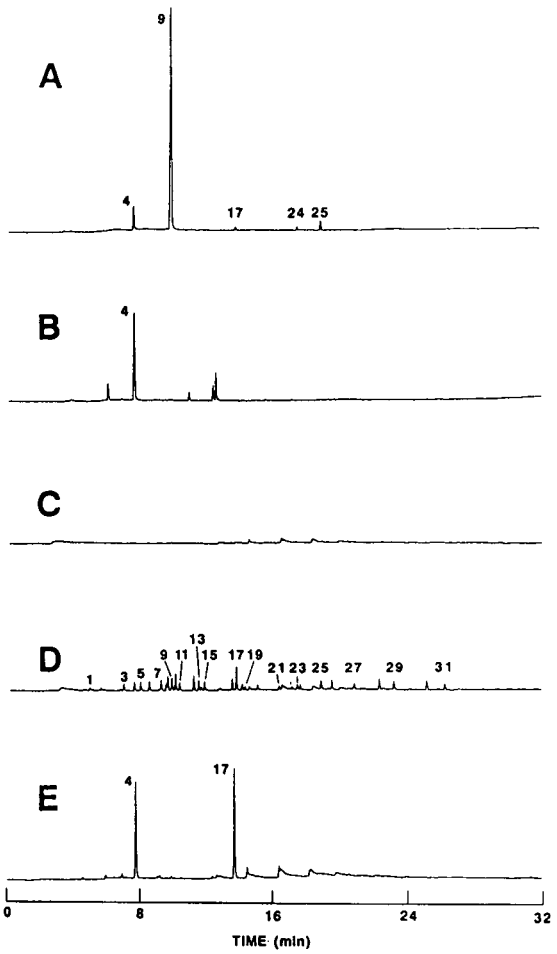

Fig. 4. Chromatograms of dry foods, 1 g added to 15 ml of water: (A) biscuit mix containing dichloromethane (No. 4) and 1,1,1-trichloroethane (No. 9); (B) dichloromethane-decaffeinated tea containing dichloromethane (No. 4); (C) roasted and ground naturally decaffeinated coffee; (D) as in (C) spiked at 30 μg/kg coffee, only odd analytes numbered, peak identities as in Table I; and (E) dichloromethane-decaffeinated roasted and ground coffee containing dichloromethane (No. 4) and tetrachloroethylene (No. 17).

respectively. The latter chromatogram demonstrates the expected reduction in method sensitivity due to the lipid material in the coffee. The last two peaks (Nos. 32 and 33) are not detected at the 30 μg/kg level and the other peaks are at or near the LOD or the LOQ. The final chromatogram (Fig. 4E) shows a dichloromethane-decaffeinated roasted and ground coffee with dichloromethane (No. 4) and tetrachloroethylene (No. 17) residues of about 300 and 130 μg/kg, respectively.

CONCLUSIONS

The application of a previously described SPME device to headspace sampling for capillary GC of a wide range of halogenated volatiles in model systems, water, beverages and finely divided foods is demonstrated. The headspace SPME–GC procedure is simple, robust, inexpensive, and uses existing or easily modified GC injectors. In water, detection of the tri- to hexachlorobenzenes at $\leq$0.005 μg/kg is attained. In water, the much greater response for the less volatile analytes than those of greater volatility complements headspace GC with gas sampling. When headspace SPME is applied to foods, increases in the lipid material markedly reduce the method sensitivity, the decrease being greatest for analytes of least volatility. Standard addition is required for quantitation of foods. Headspace SPME–GC should also be applicable to volatile non-halogenated analytes in similar matrices described above providing a suitable selective GC detector is used.

REFERENCES

1 R.P. Belardi and J.B. Pawliszyn, *Water Pollut. Res. J. Canada*, 23 (1989) 179.
2 C.L. Arthur, L.M. Killam, K.D. Buchholz and J. Pawliszyn, *Anal. Chem.*, 64 (1992) 1960.
3 D. Louch, S. Motlagh and J. Pawliszyn, *Anal. Chem.*, 64 (1992) 1187.
4 D.W. Potter and J. Pawliszyn, *J. Chromotogr.*, 625 (1992) 247.
5 C.L. Arthur, L.M. Killam, S. Motlagh, D.W. Potter and J. Pawliszyn, *Environ. Sci. Technol.*, 26 (1992) 979.
6 S.B. Hawthorne, D.J. Miller, J. Pawliszyn and C.L. Arthur, *J. Chromatogr.*, 603 (1992) 185.
7 C.L. Arthur, D.W. Potter, K.D. Buchholtz, S. Motlagh and J. Pawliszyn, *LC-GC*, 10 (1990) 656.
8 H. Hachenberg and A.P. Schmidt, *Gas Chromatographic Headspace Analysis*, Heyden, London, 1977.
9 Environmental Monitoring Systems Lab., *Methods for the Determination of Organic Compounds in Drinking Water, Report No. EPA/600/4-88/039*, National Technical Information Service, Springfield, VA, USA.
10 B.D. Page and R.J. Avon, *J. Assoc. Off. Anal. Chem.*, 72 (1989) 815.

11 B.D. Page, H.B.S. Conacher, D. Weber and G. Lacroix, *J. Assoc. Off. Anal. Chem. Int.*, 75 (1992) 334.
12 B.D. Page, H.B.S. Conacher, J. Salminen, G.R. Nixon, G. Riedel, B. Mori, J. Gagnon and R. Brousseau, *J. Assoc. Off. Anal. Chem. Int.*, 76 (1993) 26.
13 P.E. Shaw, in H. Maarse (Editor), *Volatile Compounds in Foods and Beverages*, Marcel Dekker, New York, 1991, Ch. 9, p. 305.
14 Health and Welfare Canada, *The Canadian Nutrient File, Ver. 1991*, Supply and Services Canada, Hull, 1991.
15 H. Graham, in M. Grayson (Editor), *Kirk-Othmer Encyclopedia of Chemical Technology*, Vol. 22, Wiley, New York, 1983, p. 631.
16 A. Stefanucci, W.P. Clinton and M. Hamell, in M. Grayson (Editor), *Kirk-Othmer Encyclopedia of Chemical Technology*, Vol. 6, Wiley, New York, 1979, p. 514.
17 B.D. Page and C.F. Charbonneau, *J. Food Safety*, 1 (1977) 129.
18 R.C. Entz and G.W. Diachenko, *Food Addit. Contam.*, 5 (1988) 267.
19 L.J. Miller and A.D. Uhler, *Bull. Environ. Contam. Toxicol.*, 41 (1988) 469.
20 B.D. Page and C.F. Charbonneau, *J. Assoc. Offic. Anal. Chem.*, 67 (1984) 757.

Journal of Chromatography, 648 (1993) 213–219
Elsevier Science Publishers B.V., Amsterdam

CHROM. 25 314

Determination of polychlorinated dibenzo-*p*-dioxins and dibenzofurans in tire fire runoff oil

T.S. Thompson*, T.M. Kolic, J.A. Townsend and R.S. Mercer

Ontario Ministry of the Environment, Dioxin Laboratory, 125 Resources Road, P.O. Box 213, Rexdale, Ontario, M9W 5L1 (Canada)

(First received February 5th, 1993; revised manuscript received May 18th, 1993)

ABSTRACT

Samples of oily runoff resulting from the accidental combustion of automobile tires were analyzed for polychlorinated dibenzo-*p*-dioxins (PCDDs)and polychlorinated dibenzofurans (PCDFs). PCDDs and PCDFs were identified in each of the oil samples studied. The total levels of PCDDs and PCDFs were in the low parts per billion (ppb; 10^{-9} g of PCDDs or PCDFs per g of oil) range. In all of the samples analyzed, the total PCDD concentration was approximately 10 times greater than the total concentration of PCDFs. The most toxic PCDD, 2,3,7,8-T_4CDD, contributed only a small percentage to the overall level of the PCDDs in the oil samples.

INTRODUCTION

The formation of polychlorinated dibenzo-*p*-dioxins (PCDDs) and polychlorinated dibenzofurans (PCDFs) in combustion processes is well documented [1]. Chlorinated PCDDs and PCDFs were first identified as a byproduct of the incineration process when they were discovered in the stack gas and fly ash of three municipal waste incinerators in the Netherlands in the late 1970's [2]. Following this initial report which linked the incineration of refuse as one source of PCDDs and PCDFs, these compounds have since been found in incinerators in North America, Europe, and Japan [3]. In fact, PCDDs and PCDFs have been detected in every municipal waste incinerator tested [4]. Emissions of PCDDs and PCDFs have also been produced from the incineration of hazardous waste [5,6] and sewage sludge [4,7]. The formation of PCDDs and PCDFs from the combustion of chemically treated [8–12] and untreated wood [13,14] has been reported, as well as from the combustion of fossil fuels [10,13,15]. The impact, however, of these sources are not recognized. Marklund *et al.* [16] have reported emissions of PCDDs and PCDFs in automobile exhaust.

In addition to incineration processes, PCDDs and PCDFs have been produced during accidental fires involving PCBs, chlorobenzenes, and other chlorinated transformer and capacitor fluids. Erickson *et al.* studied the formation of PCDDs and PCDFs from the combustion of PCBs, tri- and tetrachlorobenzenes [17,18] and tetrachloroethylene [18]. Addis [19] demonstrated that the combustion of PCB-contaminated dielectric fluids resulted in the formation of a series of PCDFs. There is no evidence to suggest that normal use of electrical equipment will produce either PCDDs or PCDFs. Thermal stress in the presence of oxygen is required for PCDD/PCDF formation.

The first recognized accidental formation of PCDDs and PCDFs from the combustion of

* Corresponding author. Present address: Saskatchewan Health, Environmental Sciences Division, H.E. Robertson Laboratory, 3211 Albert Street, Regina, Saskatchewan, S4S 5W6, Canada.

0021-9673/93/$06.00

chlorinated aromatic compounds in transformer fluid occurred in early 1981 [20]. The office building fire involved approximately 200 gallons (*ca.* 757 l) of transformer fluid which consisted of 65% Aroclor 1254 and 35% tri- and tetrachlorobenzenes. The soot was found to contain levels as high as 2000 ppm of PCDFs and 20 ppm of PCDDs. Other transformer and capacitor fires leading to the formation of PCDDs and PCDFs have been reported in the USA [21].

On February 12, 1990, a large fire broke out at a tire recycling dumpsite located in west central Ontario. Some thirteen million tires were involved in the blaze. The heat of the fire created a black, oily runoff. To minimize contamination of groundwater in the area, this runoff oil was collected for subsequent disposal.

The manufacturing of automobile tires involves the preparation of special polymers. Various different polymers may be used depending upon specific requirements. Chloroprene (2-chloro-1,3-butadiene) rubber is frequently used in tire manufacturing, specifically in the cover-strip, sidewall, and inner-liner portions of passenger automobile tires [22]. During combustion of the chlorine-containing material within the tires, it is possible that chlorinated aromatics would be produced. Samples of the runoff oil were submitted to the Ministry of the Environment's Dioxin Laboratory for analysis of PCDDs and PCDFs. The results of the analyses are presented in this paper.

Our laboratory is set up to routinely analyze for PCDDs and PCDFs in a variety of matrices, of which oil unfortunately is not one. Upon reviewing the literature, there were very few references citing analytical methodologies for the determination of PCDDs and PCDFs in oil or waste oil materials. Two different cleanup methods, which were initially designed for general environmental analysis of PCDDs and PCDFs, were applied to PCB-contaminated waste oil [23]. In one method, the oil sample was fractionated initially using a 50-g alumina column and the resulting fraction containing the PCDDs and PCDFs was subfractionated using a 6-g alumina column. The method yielded poor detection limits (only 100 μg of oil was loaded onto the initial column) and poor recoveries of surrogates and spikes. A more complex procedure employing five liquid–solid partitioning chromatographic columns and a variety of media (sodium sulphate, potassium silicate, silica gel, carbon impregnated glass fibres, sulphuric acid-modified silica gel and alumina) produced much better results. Up to 1 g of oil could be used, thereby lowering detection limits below 10 ppb. Good surrogate and spike recoveries were reported along with relatively little background interference.

Hagenmaier and Brunner [24] developed a procedure for the determination of PCDDs and PCDFs in motor oil samples, including used and recycled oils. Oil samples of 5 g were fractionated using alumina, a mixture of activated, acid- and base-modified silica gels, and finally on Bio-Beads S-X3. Single isomer detection limits were reported to be on the order of 0.05 μg/kg of oil. In a subsequent study involving motor oils and waste oils, a multi-column cleanup procedure was devised for the determination of PCDDs and PCDFs [25]. The method, which involved fractionation on columns containing silica gel, acid- and base-modified silica gels, florisil and alumina, was applicable to 10 g oil samples. Good analyte recoveries and reproducibility were reported. The same group also compared their method to that utilized by Hagenmaier and Brunner. They reported that the two methods produced agreeable results on duplicate samples.

Based upon the results published by the various groups cited, it appears that while there is no simple single-step cleanup procedure available, the use of a variety of chromatographic media will produce extracts amenable to analysis by gas chromatography–mass spectrometry (GC–MS).

EXPERIMENTAL

Chemicals

Silica gel (70–230 mesh) for the open column chromatographic cleanup procedure was obtained from EM Science (Darmstadt, Germany). Basic alumina was purchased from Fisher Scientific (Fair Lawn, NJ, USA). Sulphuric acid (J.T. Baker, Phillipsburg, NJ, USA) and sodium hydroxide pellets (Oxford Labs. of Canada, London, Canada) were used to prepare the acid-

and base-modified silica gel packing materials. Silver nitrate was obtained from Anachemia Chemicals (Mississauga, Canada). The preparation of the packing materials used in the column cleanup is described elsewhere [26]. HPLC-grade water (J.T. Baker) was used in the preparation of the base- and silver nitrate-modified silica gel stationary phases.

PCDD and PCDF standards were purchased from Cambridge Isotope Labs. (Woburn, MA, USA). The calibration standard used for quantitation contained five PCDDs and five PCDFs (one per tetra-, penta-, hexa-, hepta-, and octachloro congener groups) in addition to five $^{13}C_{12}$-labelled PCDDs. The surrogate standard solution used to fortify each sample consisted of the same five isotopically labelled PCDDs present in the calibration standard.

Safety

The work undertaken in this study involves the handling of toxic compounds including 2,3,7,8-T_4CDD and other 2,3,7,8-substituted PCDDs and PCDFs. Similar analyses should only be performed by specially trained personnel experienced in the handling of hazardous chemicals. The compounds studied are potential health hazards and therefore exposure to them should be minimized. Analytical laboratories must establish procedures for the safe handling and disposal of all toxic materials. All staff must be trained in these procedures and all safety measures strictly complied to.

Sample preparation

Approximately 1.5–2 g of oil per sample was weighed into a clean glass vial. Each sample was spiked with 50 μl of the surrogate fortification standard. The oil was diluted with 2–3 ml of hexane and thoroughly mixed. The dilute sample was loaded onto a chromatographic column (30 cm × 1.0 cm I.D.) containing (top to bottom) 44% (w/w) sulphuric acid–silica gel, activated silica gel, 33% (w/w) sodium sulphate–silica gel, activated silica gel, and 10% (w/w) silver nitrate–silica gel. The sample vial was rinsed with three 5-ml aliquots of hexane, each of which was added to the column. The PCDDs and PCDFs were eluted from the silica gel column using a total of 100 ml of hexane. The resulting extract was concentrated to approximately 2 ml and quantitatively transferred to the top of a column (30 cm × 0.6 cm I.D.) containing 5 g of activated basic alumina. A 100-ml portion of hexane was used to initially elute undesired components from the column and was discarded. A second fraction was eluted with 20 ml of a 10:90 (v/v) mixture of carbon tetrachloride–hexane and was discarded. The PCDDs and PCDFs were finally eluted with 30 ml of dichloromethane. Each extract was concentrated and transferred to a small conical glass vial where it was reduced to dryness under a gentle stream of high purity nitrogen gas. The final residue was redissolved with 50 μl of a solution containing 100 pg/μl of $^{13}C_{12}$-labelled H_6CDF in toluene, which is used as an instrumental performance standard.

GC–MS–MS analysis

All PCDD/PCDF analyses were performed using a Finnigan MAT TSQ 70 triple quadrupole mass spectrometer system. A Varian 3400 gas chromatograph was interfaced to the mass spectrometer using a direct capillary inlet. High-resolution GC separations were achieved using a 60-m DB-5 fused-silica capillary column, with an internal diameter of 0.25 mm and a stationary phase film thickness of 0.25 μm (J&W Scientific, Folsom, CA, USA). Ultrahigh purity helium was used as the carrier gas (Matheson Gas Products Canada, Whitby, Canada). A splitless injector system maintained at 300°C was utilized for all GC–MS–MS analyses. The GC oven temperature program was: initial temperature held at 120°C for 1 min; ramped to 250°C at 7.5°C/min; ramped to 300°C at 2.5°C/min and held for 13 min.

The triple quadrupole mass spectrometer was operated in the daughter ion mode using multiple reaction monitoring to achieve the desired selectivity. The first quadrupole region was set to selectively transmit only ions with the mass-to-charge ratio corresponding to the PCDD/PCDF molecular ions. These parent ions undergo collisionally induced dissociation (CID) in the second quadrupole region which is pressurized with approximately 3 mTorr (*ca.* 0.4 Pa) of argon gas. The third quadrupole is set to monitor two daughter ions for each PCDD/PCDF congener

group corresponding to the loss of a COCl group. A third ion corresponding to the loss of two COCl groups is monitored for the confirmation of the tetra- through octachlorinated PCDDs. Polychlorinated diphenylethers (PCPDEs) may rearrange in the mass spectrometer ion source to form PCDF molecular ions and therefore extreme caution must be taken in interpreting mass spectral data. To verify the absence of these interfering PCDPEs, the loss of HCl and Cl_2 from PCDPE molecular ions is also monitored. The ions monitored and those used for quantitation are listed in more detailed discussions of the optimization of MS–MS parameters for the determination of PCDDs and PCDFs [27,28].

RESULTS AND DISCUSSION

Five oil samples were submitted and analyzed for PCDDs and PCDFs. The results of the analyses are summarized in Table I. A large number of isomers were detected in all of the samples analyzed. Isomers from all five PCDD congener groups (tetra- through octachloro) were found to be present in each sample along with tetra-, penta-, and hexachlorinated PCDFs. The total concentration of PCDDs in each sample was approximately one order of magnitude greater than the total level of PCDFs. Although the total T_4CDD concentration was only 2–3 times the total T_4CDF concentration, the remaining PCDD congener groups were found to be present at levels 5–15 times higher than their PCDF counterparts. Similar distributions of isomers were observed for all five samples.

Congener specific analysis of 2,3,7,8-T_4CDD and the remaining 2,3,7,8-substituted PCDDs and PCDFs was performed. The results of the congener specific analyses are summarized in Table II. It should be noted that no single GC column is capable of completely isolating all seventeen 2,3,7,8-substituted PCDDs and PCDFs from the remaining PCDDs and PCDFs. Using the 60-m DB-5 column, congener specificity is only obtained for 2,3,7,8-T_4CDD plus the hepta- and octachlorinated PCDDs and PCDFs. Therefore the concentrations of the other compounds as reported in Table II actually represent the maximum possible concentrations of these

TABLE I

PCDDs AND PCDFs IN TIRE FIRE RUNOFF OIL

All concentrations expressed in parts per trillion (ppt; 10^{-12} g of PCDDs or PCDFs per g of oil). Values have been corrected for recovery of isotopically labelled surrogate standards. Superscripts indicate the number of PCDD or PCDF isomers present.

	Oil sample (sample wt. in g)				
	A (1.5)	B (1.5)	C (1.5)	D (1.6)	E (1.6)
T_4CDDs	1400^{14}	1300^{14}	1100^{14}	950^{14}	1200^{14}
P_5CDDs	2100^{12}	1800^{12}	1500^{12}	1600^{12}	1900^{12}
H_6CDDs	2200^{8}	1900^{7}	1500^{7}	1800^{7}	1900^{7}
H_7CDDs	2000^{2}	1900^{2}	1200^{2}	1400^{2}	1300^{2}
O_8CDD	3700	3200	2700	2500	3300
Total PCDDs	11 400	10 100	8000	8300	9600
T_4CDFs	610^{14}	520^{13}	480^{14}	470^{17}	510^{13}
P_5CDFs	220^{10}	180^{8}	160^{5}	290^{11}	170^{6}
H_6CDFs	140^{3}	120^{3}	56^{1}	250^{5}	53^{2}
H_7CDFs	ND(60)[a]	83^{1}	110^{1}	80^{2}	ND(50)
O_8CDF	ND(40)	34	47	ND(30)	37
Total PCDFs	970	940	850	1100	770

[a] ND = Not detected. Detection limit (in ppt) given in brackets.

TABLE II

TOXIC CONGENER ANALYSIS OF RUNOFF OIL SAMPLES

All concentrations expressed in parts per trillion (ppt; 10^{-12} g of PCDD or PCDF per g of oil). Values have been corrected for recovery of isotopically labelled surrogate standards.

Compound	Concentration in oil samples				
	Oil A	Oil B	Oil C	Oil D	Oil E
2,3,7,8-T_4CDD	53	31	23	30	33
1,2,3,7,8-P_5CDD	170	160	140	140	170
1,2,3,4,7,8-H_6CDD	68	78	30	60	57
1,2,3,6,7,8-H_6CDD	ND(10)[a]	ND(10)	ND(10)	ND(10)	ND(10)
1,2,3,7,8,9-H_6CDD	330	290	130	250	220
1,2,3,4,6,7,8-H_7CDD	950	900	570	670	630
O_8CDD	3700	3200	2700	2500	3300
2,3,7,8-T_4CDF	52	65	69	42	74
2,3,4,7,8-P_5CDF	9.6	12	11	20	12
1,2,3,7,8-P_5CDF	5.5	ND(5)	ND(8)	10	ND(5)
1,2,3,4,7,8-H_6CDF	ND(10)	ND(10)	ND(10)	73	ND(20)
1,2,3,6,7,8-H_6CDF	ND(10)	ND(10)	ND(10)	ND(10)	ND(20)
1,2,3,7,8,9-H_6CDF	ND(10)	ND(10)	ND(10)	ND(10)	ND(20)
2,3,4,6,7,8-H_6CDF	ND(10)	ND(10)	ND(10)	ND(10)	ND(20)
1,2,3,4,6,7,8-H_7CDF	ND(60)	ND(40)	ND(60)	36	ND(50)
1,2,3,4,7,8,9-H_7CDF	ND(50)	ND(30)	ND(60)	ND(30)	ND(40)
O_8CDF	ND(40)	34	47	ND(30)	37

[a] ND = Not detected. Detection limit (in ppt) given in brackets.

compounds. In other words, their true concentrations will be less than the reported values if other co-eluting isomers are present.

The contribution of 2,3,7,8-T_4CDD to the total concentration of T_4CDDs was found to be small for all samples analyzed. In fact, the concentration of 2,3,7,8-T_4CDD was found to range from 2 to 4% of the total T_4CDD concentration. The most toxic pentachlorinated PCDD, 1,2,3,7,8-P_5CDD, was estimated to constitute approximately 9% of the total P_5CDD concentration. Two toxic H_6CDDs, the 1,2,3,4,7,8-H_6CDD and 1,2,3,7,8,9-H_6CDD congeners, were tentatively identified. These two congeners contributed approximately 15% of the total H_6CDD concentration, with the latter about four times more abundant than the former. The 2,3,7,8-substituted H_7CDD was found at concentrations ranging form 570 to 950 ppt, about half of the total H_7CDD concentration in each sample. The O_8CDD congener was the predominant PCDD ranging in concentration from 2500 to 3700 ppt.

Unlike the PCDDs, the concentrations of the PCDF congener groups tended to decrease with increasing degree of chlorination. The T_4CDFs were found to account for between 42 and 66% of the total PCDF concentration. The more highly chlorinated species, the H_7CDFs and the O_8CDF, were present at low ppt levels or were not detected at all. With the exception of one sample, no 2,3,7,8-substituted H_6CDFs or H_7CDFs were identified in the oil samples analyzed. In the case of that one sample, one 2,3,7,8-substituted H_6CDF (1,2,3,4,7,8-H_6CDF) was found at 73 ppt while the 1,2,3,4,6,7,8-H_7CDF was weakly detected at 36 ppt. The highly toxic 2,3,4,7,8-P_5CDF congener was found in all five samples at concentrations ranging from 10 to 20 ppt while the less toxic 1,2,3,7,8-P_5CDF was detected at lower concentrations if at all. The highly toxic 2,3,4,7,8-P_5CDF contributed

TABLE III

2,3,7,8-T_4CDD TOXIC EQUIVALENCY FACTORS

The 2,3,7,8-T_4CDD toxic equivalency factor (TEF) is a comparison of the toxicity of a particular PCDD/PCDF isomer relative to that of 2,3,7,8-T_4CDD. For example, 1,2,3,7,8-P_5CDD is reported to have a TEF of 0.5. Therefore 10 ng of 1,2,3,7,8-P_5CDD will produce the same toxic effect as 5 ng of 2,3,7,8-T_4CDD.

Compound	2,3,7,8-T_4CDD toxic equivalency factor
2,3,7,8-T_4CDD	1.0
1,2,3,7,8-P_5CDD	0.5
1,2,3,4,7,8-H_6CDD	0.1
1,2,3,6,7,8-H_6CDD	0.1
1,2,3,7,8,9-H_6CDD	0.1
1,2,3,4,6,7,8-H_7CDD	0.01
O_8CDD	0.001
2,3,7,8-T_4CDF	0.1
2,3,4,7,8-P_5CDF	0.5
1,2,3,7,8-P_5CDF	0.01
1,2,3,4,7,8-H_6CDF	0.1
1,2,3,6,7,8-H_6CDF	0.1
1,2,3,7,8,9-H_6CDF	0.1
2,3,4,6,7,8-H_6CDF	0.1
1,2,3,4,6,7,8-H_7CDF	0.1
1,2,3,4,7,8,9-H_7CDF	0.01
O_8CDF	0.001

only approximately 7% of the total P_5CDF concentration. Similarly, the 2,3,7,8-T_4CDF was found to constitute between 9 and 14% of the total level of the T_4CDFs.

In order to estimate the relative toxicities of the oil samples, the 2,3,7,8-T_4CDD toxic equivalency concentrations were calculated using the toxic equivalency factors given in Table III. By multiplying the concentrations of the individual 2,3,7,8-substituted PCDD/PCDF congeners by the appropriate toxic equivalency factor and summing these concentrations for each sample, Table IV was generated. The 2,3,7,8-T_4CDD toxic equivalency concentrations for the five samples were found to range from 130 to 200 ppt. The predominant congeners with respect to the contribution to the total 2,3,7,8-T_4CDD toxic equivalency concentrations were 1,2,3,7,8-P_5CDD, 2,3,7,8-T_4CDD, and 1,2,3,7,8,9-H_6CDD. In all five samples, the contribution of the 2,3,7,8-substituted PCDDs accounted for approximately 90% of the total 2,3,7,8-T_4CDD toxic equivalency concentration.

The total PCDD concentrations were found to range from 8000 to 11 000 ppt while the 2,3,7,8-T_4CDD toxic equivalency concentrations for the PCDDs ranged from 120 to 190 ppt. Similarly the total PCDF concentrations ranged from 770 to 1100 ppt while the 2,3,7,8-T_4CDD toxic equivalency concentrations of the PCDFs were found to be between 10 to 19 ppt. The total concentrations of the PCDDs and PCDFs in the oil are much higher than the estimated 2,3,7,8-T_4CDD toxic equivalency concentrations. The more highly toxic 2,3,7,8-substituted congeners (those having a 2,3,7,8-T_4CDD toxic equivalency of greater than 0.1) are present at relatively low concentrations. Therefore in all cases, the

TABLE IV

2,3,7,8-T_4CDD TOXIC EQUIVALENCY OF OIL SAMPLES

2,3,7,8-T_4CDD toxic equivalency concentrations reported in parts per trillion (10^{-12} grams of 2,3,7,8-T_4CDD equivalents per g of oil).

	Oil A	Oil B	Oil C	Oil D	Oil E
PCDD contribution[a]	191	160	117	140	155
PCDF contribution[a]	10	13	12	19	13
Total 2,3,7,8-T_4CDD toxic equivalency	201	173	129	159	168

[a] PCDD contribution = total toxic equivalents from PCDDs only; PCDF contribution = total toxic equivalents from PCDFs only.

2,3,7,8-T_4CDD toxic equivalency concentrations of the PCDDs and PCDFs are less than 2% of the respective total PCDD/PCDF concentrations.

CONCLUSIONS

It is difficult to estimate the potential impact of this previously unrecognized source of PCDDs and PCDFs. Every year millions of tires are discarded worldwide. Only a very small percentage of these tires are actually recycled for other uses. Incineration is a popular method of reducing the volume of waste material. In some cases tires are actually burned as part of the fuel mixture used to generate heat for industrial operations (for example, cement kilns). Based on the findings of this study, further investigations regarding the formation of PCDDs and PCDFs through the combustion of automobile tires are clearly warranted.

REFERENCES

1 O. Hutzinger, M.J. Blumich, M. v.d. Berg and K. Olie, *Chemosphere*, 14(6/7) (1985) 581.
2 K. Olie, P.L. Vermeulen and O. Hutzinger, *Chemosphere*, 6 (1977) 455.
3 H.Y. Tong and F.W. Karasek, *Chemosphere*, 15 (1986) 1219.
4 R.E. Clement, H.M. Tosine, J. Osborne, V. Ozvacic, G. Wong and S. Thorndyke, *Chemosphere*, 16(8/9) (1987) 1895.
5 T.O. Tiernan, M.L. Taylor, J.G. Solch, G.F. VanNess, J.H. Garrett and M.D. Porter, in J.H. Exner (Editor), *Detoxification of Hazardous Waste*, Ann Arbor Science, Ann Arbor, MI, 1982, p. 143.
6 C. Rappe, S. Marklund, P.A. Bergqvist and M. Hansson, in G. Choudhary, L.H. Keith, and C. Rappe (Editors), *Chlorinated Dioxins and Dibenzofurans in the Total Environment*, Butterworth, Boston, MA, 1983, p. 99.
7 J.H. Southerland, W.B. Kuykendal, W.H. Lamason, II, A. Miles and D.A. Oberacker, *Chemosphere*, 16(8/9) (1987) 2161.
8 B. Jansson, G. Sundstrom and B. Ahling, *Sci. Total Environ.*, 10 (1978) 209.
9 C. Rappe, S. Marklund, H.R. Buser and H.P. Bosshardt, *Chemosphere*, 7 (1978) 269.
10 C. Chui, R.S. Thomas, J. Lockwood, K. Li, R. Halman and R.C. Lao, *Chemosphere*, 12 (1983) 607.
11 K. Olie, M.v.d. Berg and O. Hutzinger, *Chemosphere*, 12 (1983) 627.
12 T.O. Tiernan, M.L. Taylor, J.H. Garrett, G.F. VanNess, J.G. Solch, D.A. Deis and D.J. Wagel, *Chemosphere*, 12 (1983) 595.
13 T.J. Nestrick and L.L. Lamparski, *Anal. Chem.*, 54 (1982) 2292.
14 R.E. Clement, H.M. Tosine and B. Ali, *Chemosphere*, 14 (1985) 815.
15 B.J. Kimble and M.L. Gross, *Science*, 207 (1980) 59.
16 S. Marklund, C. Rappe, M. Tysklind and K.E. Egeback, *Chemosphere*, 16 (1987) 29.
17 M.D. Erickson, C.J. Cole, J.D. Flora, Jr., P.G. Gorman, C.L. Haile, G.D. Hinshaw, F.C. Hopkins, S.E. Swanson and D.T. Heggem, *Chemosphere*, 14 (1985) 855.
18 M.D. Erickson, S.E. Swanson, T.M. Sack and D.T. Heggem, *Chemosphere*, 15 (1986) 1261.
19 G. Addis, *Chemosphere*, 15 (1986) 1265.
20 A. Schecter, *Chemosphere*, 15 (1986) 1273.
21 P.E. des Rosiers, *Chemosphere*, 16(8/9) (1987) 1881.
22 R.R. Barnhart, in M. Grayson (Editor), *Encyclopedia of Chemical Technology*, Vol. 20, Wiley, New York, NY, 3rd ed., 1982, p. 431.
23 R.E. Adams, M.M. Thomason, D.L. Strother, R.H. James and H.C. Miller, *Chemosphere*, 15(9–12) (1986) 1113.
24 H. Hagenmaier and H. Brunner, *Fresenius' Z. Anal. Chem.*, 324(1) 1986) 23.
25 W. Christmann, W. Rotard, A. Lattner, W. Mann, A. Reichert, S. Reiss and V. Schinz, *Chemosphere*, 16(8/9) (1987) 1649.
26 L.L. Lamparski, T.J. Nestrick and R.H. Stehl, *Anal. Chem.*, 51(9) (1979) 1453.
27 D.H. Schellenberg, B.A. Bobbie, E.J. Reiner and V.Y. Taguchi, *Rapid Comm. Mass Spectrom.*, 1(7/8) (1987) 111.
28 E.J. Reiner, D.H. Schellenberg, V.Y. Taguchi, R.S. Mercer, J.A. Townsend, T.S. Thompson and R.E. Clement, *Chemosphere*, 20(10–12) (1990) 1385.

Journal of Chromatography, 648 (1993) 221–232
Elsevier Science Publishers B.V., Amsterdam

CHROM. 25 345

Flame ionization detector responses to ethyl esters of sand eel (Ammodytes lancea) fish oil compared for different gas and supercritical fluid chromatographic systems

A. Staby, C. Borch-Jensen and J. Mollerup*

Department of Chemical Engineering, Technical University of Denmark, DTH, Building 229, 2800 Lyngby (Denmark)

B. Jensen

Technological Laboratory, Danish Ministry of Fisheries, Technical University of Denmark, DTH, Building 221, 2800 Lyngby (Denmark)

(First received December 3rd, 1992; revised manuscript received April 19th, 1993)

ABSTRACT

A fish oil fatty acid ethyl ester mixture derived from the sand eel (Ammodytes lancea) has been analysed using various capillary gas chromatography (GC) and supercritical fluid chromatography (SFC) methods and 39 components including cholesterol have been identified. The results of the analytical SFC and GC experiments are compared showing a good reproducibility within methods and a fair agreement between methods. The advantages and disadvantages of the employment of manual and autosampler split injection, splitless injection, and cold on-column injection in GC as well as the use of polar and non-polar columns in GC and SFC are discussed.

INTRODUCTION

The annual world production of marine oil is about 1.5 billion kg [1]. The predominant part of it is used for the production of margarines and shortenings used to make pastries, bread, cakes, creams, and margarines and emulsifiers for human consumption. Other uses include feed for livestock, pets and fish farming, and industrial products like soaps, fuel oils, lubricants, greases, linoleum, protective coatings, etc. Fish is the most important source of long-chain ω-3 unsaturated fatty acids, specially the polyunsaturated EPA (eicosapentaenoic acid) and DHA (docosahexaenoic acid), which are the most important and valuable of the ω-3 fatty acids. Recent reports indicate that ω-3 fatty acids may have medical effects in treatment of rheumatoid arthritis [2], heart diseases and strokes [3], atherosclerosis by lowering the cholesterol absorption [4], and cancer diseases in the colon region [5], and the use in the pharmaceutical industry may be the most important use of fish oils in the future.

Gas chromatography (GC) is a well-established method for the analysis and separation of fish oil esters [6–33]. Other methods, like high-performance liquid chromatography (HPLC) [18,21,28,29,34,35], and lately supercritical fluid chromatography (SFC) [27,36,37] have also been employed, but the method preferred for the analysis of fish oil esters is the capillary gas liquid chromatography (GLC) method using columns of moderate to high polarity. A standard method

* Corresponding author.

0021-9673/93/$06.00

for determination of fatty acid compositions of fish oil by GLC utilizing the split injection and the flame ionization detection techniques has been proposed [38]. This technique has been used by several authors, see, for instance, refs. 11, 23, and 27. Other choices may include employment of cold on-column injection [15,18,31] or mass spectrometric (MS) detection [29,30,33].

The primary use of HPLC and SFC for the examination of fish oil esters has focused on the separation and fractionation in a semi-preparative or preparative scale, followed by a GLC analysis of the fractions obtained. Recently, attempts to use HPLC [35] and SFC [36] as analytical tools for the fatty acid composition determination of fish oil ester mixtures have been published. However, J.M. Beebe *et al.* [35], using the HPLC method, report only the separation of 7 major compounds combined with a rather poor resolution, while Görner and Perrut [36], using the packed column SFC method, report the separation of 6 (2×3) methyl and ethyl esters present in fish oil. The main purpose of our study is to compare the well-established capillary GLC method with the rather untested capillary SFC method in the analysis of ethyl esters from fish oil using various columns. Although HPLC and SFC methods have less resolution when compared to GLC, they have the advantage of being ideal for on-line analysis coupling to processes like preparative HPLC or supercritical fluid extraction (SFE), where the automatic transfer of a representative sample to on-line coupled GC often is a major problem [39]. The results of this study will show that capillary SFC in many cases is sufficient as the analytical tool, when coupled directly to a continuous SFE process.

Analysis of the fatty acid composition of the sand eel or sand launce (Ammodytes lancea) has previously been presented by Laakso *et al.* [28] and Langholz *et al.* [25], who identified 19 and 14 components, respectively. The second aim of this work is to obtain more information about the fatty acid composition of the sand eel. We have analysed the composition of a sand eel fatty acid ethyl ester mixture using different capillary GC methods including various columns and injection techniques, and 39 components including cholesterol have been identified by retention time comparison. When comparing the fatty acid compositions of this work with compositions obtained by others, one should observe that the composition changes every year and from season to season depending on the feed the fish eat [10].

To sum up, the primary goal of this work was to compare the SFC technique with the GC technique using different columns. Additionally, more detailed information on the sand eel fatty acid composition was obtained, and reliability figures for GC analysis by various injection techniques and stationary phases were compared.

EXPERIMENTAL

Materials

Standards of fatty acid methyl esters were purchased from Sigma (St. Louis, MO, USA). Standard mixtures of methyl esters were purchased from Nu-Chek-Prep (Elysian, MN, USA). A qualitative standard mixture of fish oil methyl esters was from Larodan Fine Chemicals (Malmö, Sweden). *n*-Heptane LiChrosolv used as solvent for the fatty acid esters was obtained from Merck (Darmstadt, Germany). Helium, hydrogen, and atmospheric air were supplied by Hede Nielsen (Ballerup, Denmark). The stated purities are $>99.996\%$ of helium and $>99.8\%$ of hydrogen. Carbon dioxide was supplied by Linde (München, Germany) with a stated purity of $>99.995\%$, and sand eel ethyl esters were supplied by Grindsted Products (Århus, Denmark) with a stated purity of 98%. All materials were used without further purification.

GC methods

Six different gas chromatographic analyses were carried out under various experimental conditions.

Method 1

A Carlo Erba SFC-3000 Instrument (Carlo Erba Instruments, Milan, Italy) was set up as a gas chromatograph. The chromatograph was equipped with a flame ionization detector and a manual cold on-column injection port connected to a retention gap ($1.5\ m \times 0.32$ mm) and a

terephthalic acid (TPA) modified polyethylene glycol HP-FFAP (Hewlett-Packard, Avondale, PA, USA) fused-silica capillary column (25 m × 0.2 mm × 0.33 μm). 1 μl of a 0.05% (w/w) solution of ethyl esters in *n*-heptane was injected. The detector temperature was 270°C. The initial oven temperature of 95°C was held for 2 min, then increased at a rate of 3°C/min to 170°C followed by an increase of 1°C/min to 210°C, where it was held constant for 52 min. Helium carrier gas flow was set at 26 cm/s and the helium make-up gas flow at 30 ml/min. The hydrogen and air gas flows for the FID were 30 ml/min and 230 ml/min, respectively, and secondary cooling pressure (nitrogen or air) of the injection system was 500 kPa. Integration and control of the chromatographic run were carried out via a personal computer with MAXIMA chromatography software (Dynamic Solutions, Ventura, CA, USA).

Method 2

An HP 5880A gas chromatograph was equipped with a manual capillary injection port and a flame ionization detector was used. The split injection mode with a split ratio of 1:100 and a TPA modified polyethylene glycol HP-FFAP fused-silica capillary column (25 m × 0.2 mm × 0.33 μm) was employed. The fast injected volume was 2 μl of a 2.7% mixture of ethyl esters in *n*-heptane. The injection and detection temperatures were 250°C. The initial oven temperature of 140°C was held for 15 min, then increased at a rate of 3°C/min to 170°C followed by an increase of 1°C/min to 240°C, where it was held constant for 10 min. The linear velocity of the helium carrier gas was 53 cm/s. The hydrogen and air flow rates for the FID were 40 ml/min and 500 ml/min, respectively. Integration and control of the chromatographic run were carried out by an HP 5880A Series GC Terminal.

Method 3

The chromatographic runs of this method were carried out as described in Method 2, except for the use of the splitless injection mode with a fast injected volume of 1 μl of a 1.0% mixture of ethyl esters with *n*-heptane, and a different oven temperature program. The initial oven temperature of 80°C was held for 1 min, then increased at a rate of 5°C/min to 200°C followed by an increase of 3°C/min to 230°C, where it was held constant for 15 min.

Method 4

The chromatographic runs of this method were carried out as described in Method 2, except for the use of a dimethylpolysiloxane HP-1 fused-silica capillary column (12 m × 0.2 mm × 0.33 μm), a fast injected volume of 1 μl of a 2.7% solution of ethyl esters in *n*-heptane, and a different oven temperature program. The initial oven temperature of 140°C was held for 1 min, then increased at a rate of 3°C/min to 186°C followed by an increase of 4.5°C/min to 270°C, where it was held constant for 1 min.

Method 5

An HP 5890 gas chromatograph equipped with a capillary injection port, a HP-7673A autosampler and a flame ionization detector was used. The column was a 68% cyanopropyl–phenylpolysiloxane SP-2330 (Supelco Bellefonte, PA, USA) fused-silica capillary column (30 m × 0.32 mm × 0.2 μm). Injection in split mode with a split ratio of 1:50 was used. The injected volume was 0.2 μl of a 4.6% solution of ethyl esters in *n*-heptane. The injection and detection temperatures were 250°C and 240°C, respectively. The initial oven temperature of 140°C was immediately raised at a rate of 3°C/min to 200°C, held for 1 min, and further raised at 3°C/min to 220°C, where it was held for 9 min. The helium carrier gas flow was 21 cm/s, nitrogen make-up gas flow was set at 25 ml/min, and hydrogen and air supplies for the FID were set at 33 ml/min and 500 ml/min, respectively. Integration was carried out by an HP-3396A integrator and the data were transferred to a computer by HP-3393A/3396A contributed file server software.

Method 6

This method differed from Method 5 in the choice of column, which was a polyethylene glycol Omegawax 320 (Supelco) fused-silica capillary column (30 m × 0.32 mm × 0.25 μm).

The split ratio was 1:30, and the injected volume of a 4.1% mixture of ethyl esters in *n*-heptane was 0.2 μl. The temperature program began with an oven temperature of 160°C, immediately followed by an increase at 3°C/min to 200°C, where it was held for 1 min, followed by an increase at 3°C/min to 220°C, where it was held constant for 12 min. The helium carrier gas flow was 30 cm/s, while the other conditions were as for Method 5.

SFC methods

Three different supercritical fluid chromatographic analyses were carried out at different conditions. A Carlo Erba SFC-3000 system equipped with a flame ionization detector and a pneumatic Valco valve with a 0.2 μl sample loop was used in all SFC experiments. The injection temperature was 60°C and the detector temperature was 300°C. Hydrogen and air gas pressures for the FID were 55 kPa and 100 kPa, respectively. Carbon dioxide was employed as the carrier gas. The pump cylinder was thermostatted by circulation of ethylene glycol from a Hetofrig CB 12 cooling bath (Heto Lab Equipment, Birkerød, Denmark) at − 5°C to ensure carbon dioxide flow rate reproducibility. The pressure drop over the chromatographic system was obtained by integral restrictors made of uncoated fused-silica tubing by the method of Guthrie and Schwartz [40] and connected to the chromatographic column. Integration and control of the chromatographic run were carried out via a personal computer with MAXIMA chromatography software.

Method 7

A 50% cyanopropylphenyl–methylpolysiloxane DB-225 (J&W Scientific, Folsom, CA, USA) fused-silica capillary column (20 m × 0.1 mm × 0.1 μm) was employed. The injection time was 0.2 s. The concentration of the samples injected was 0.5% of ethyl esters in *n*-heptane. The chromatographic runs were performed isothermally at 140°C. The initial carbon dioxide density of 0.15 g/ml was held for 25 min, then increased at a rate of 0.001 g/ml/min to 0.225 g/ml followed by an increase of 0.002 g/ml/min to 0.355 g/ml, where it was held constant for 30 min. The initial and final carbon dioxide pressures were 9.8 MPa and 19.3 MPa, respectively, and the initial linear velocity was 1.7 cm/s.

Method 8

A dimethylpolysiloxane CP-Sil 5 CB (Chrompack Instruments, Greve, Denmark) fused-silica capillary column (20 m × 0.05 mm × 0.2 μm) was employed. The injection time was 0.2 s. The concentration of the samples injected was 2.7% of ethyl esters in *n*-heptane. The chromatographic runs were performed isothermally at 70°C. The initial carbon dioxide density of 0.15 g/ml was held for 20 min, then increased at a rate of 0.011 g/ml/min to 0.22 g/ml, followed by an increase of 0.001 g/ml/min to 0.455 g/ml, and then followed by an increase of 0.003 g/ml/min to 0.63 g/ml, where it was held constant for 10 min. The initial and final carbon dioxide pressures were 7.2 MPa and 19.6 MPa, respectively, and the initial linear velocity was 3.6 cm/s.

Method 9

A 5% phenyl–methylpolysiloxane DB-5 (J&W Scientific) fused-silica capillary column (20 m × 0.1 mm × 0.4 μm) was employed. The injection time was 0.1 s. The concentration of the samples injected was 2.5% of ethyl esters in *n*-heptane. The chromatographic runs were performed isothermally at 60°C. The initial carbon dioxide density of 0.65 g/ml was held for 40 min and then increased at a rate of 0.001 g/ml/min to 0.83 g/ml, where it was held constant for 60 min. The initial and final carbon dioxide pressures were 16.4 MPa and 29.9 MPa, respectively, and the initial linear velocity was 1.9 cm/s.

Sample preparation and peak identification

The fish oil ethyl esters were transesterified to the corresponding methyl esters by a base-catalyzed transesterification followed by a boron trifluoride-catalyzed esterification according to the AOCS method Ce 1b-89 [38]. In the transesterification step the molar concentration of methanol was about 300 times that of the ethyl esters, thus minimizing the occurrence of un-

changed ethyl esters in the methyl ester chromatograms.

The methyl ester standards were dissolved in *n*-heptane to a concentration of each component of 0.001% (w/w) for the cold on-column injections, of 0.14% for the GC split injections, and 0.026% for the splitless injections. The fish oil methyl ester standard mixture was dissolved in *n*-heptane to a total concentration of 2.0% for use in the autosampler split injections. For the SFC injections the concentration of each component of the methyl ester standards was 0.14% on the CP-Sil 5 CB and the DB-5 columns, and 0.05% on the DB-225 column.

Comparison of the retention times found in these chromatograms with those of commercially available standard mixtures (*cf.* Materials) formed the basis for peak identification of the ethyl esters derived from the fish oil.

RESULTS AND DISCUSSION

GC

The 39 components found and the experimental peak area% of the gas chromatographic analyses are presented in Table I. Each chromatographic experiment was performed three times, except Method 1 which was performed six times. For each of the six methods the repeatability was quite good. The relative standard deviation of major compounds (>1 area%) was occasionally as large as 2.5%, but generally it was less than 1%, while for minor compounds (<1 area%) in a few instances it was as large as 10%, but usually less than 3%. The elution sequence shown in Table I is as for the FFAP column.

A comparison of the two methods using autosampler split injection and polar columns, methods 5 and 6 in Table I, displays good agreement except for a few compounds. The temperature program used in Method 6 was set so that the components $C_{10:0}$ and $C_{12:0}$ eluted together with the solvent. The amount of $C_{18:1\omega7}$ clearly deviates between the two methods and to some extent also the amounts of $C_{22:6\omega3}$ and $C_{24:1\omega9}$ and their total sum. The amounts of $C_{22:1\omega11}$ and $C_{22:1\omega9}$ differ due to poor separation using both methods, but the total sum of $C_{22:1}$ of the two methods is in balance.

Examining the results of Method 2 using the manual split injection and the polar FFAP column, a rather good agreement with the results of methods 5 and 6 can be seen. The components $C_{16:2}$, $C_{17:0}$, $C_{16:3}$, $C_{18:3\omega6}$, $C_{20:1\omega9}$ and $C_{22:4\omega6}$ show significant differences in peak area%. The differences of the components $C_{16:2}$, $C_{17:0}$ and $C_{16:3}$ could be due to the presence of phytanic acid ethyl ester, which elutes close to or together with $C_{17:0}$ on polyglycol columns [41]. The difference in area% between the components $C_{22:1\omega11}$ and $C_{22:1\omega9}$ is caused by peak overlapping and probably the presence of other $C_{22:1}$ isomers, while the difference between $C_{22:6\omega3}$ and $C_{24:1\omega9}$ is mainly caused by the peak overlapping when using polyglycol columns, methods 2 and 6 [17].

The cold on-column injection operation with the FFAP column, Method 1, demonstrates significant differences in peak area% for the major light and heavy compounds, indicating some kind of discrimination compared to Method 2. Peak area% of light compounds like $C_{16:0}$ and $C_{16:1\omega7}$ are greater than those of Method 2, while of heavy compounds like $C_{20:5\omega3}$ and $C_{22:6\omega3}/C_{24:1\omega9}$ they are less. Traitler [42] has noted that when using the cold on-column injection technique, discrimination of low-volatility compounds is much less pronounced than in heated injection port systems, which is directly contrary to what we experience. Even though on-column injection is considered the method of choice for optimal quantitative analysis of complicated mixtures [43,44], careful optimization of the splitting injector will lead to accurate quantitation [45]. As we find good agreement between results by the three split injection methods, and as for the cold on-column injection method we find the same low relative standard deviations as the other methods, we must assume a systematic, yet unexplained, error of either the cold on-column injection method or of the three split injection methods. A chromatogram of the ethyl ester mixture using Method 1 is presented in Fig. 1. The figure shows the good separation of the isomers $C_{18:1\omega9}$ and $C_{18:1\omega7}$, $C_{22:1\omega11}$ and $C_{22:1\omega9}$, and a partial peak overlap between $C_{22:6\omega3}$ and $C_{24:1\omega9}$ which might be expected [17]. The sepa-

TABLE I

GAS CHROMATOGRAPHIC PEAK AREAS OF THE SAND EEL ETHYL ESTER MIXTURE USING VARIOUS COLUMNS AND INJECTION TECHNIQUES

The experimental conditions are given in the text. The relative standard deviations of each of the six methods are generally less than 1% for major compounds (> 1 area%) and less than 3% for minor compounds, but they may be as large as 2.5% and 10%, respectively. n.a.: not analyzed for, elutes before the integration start. n.d.: not detected.

Method no.	1	2	3	4	5	6
Column	FFAP	FFAP	FFAP	HP-1	SP-2330	SP-320
Injection	on-column, manual	split, manual	splitless, manual	split, manual	split, auto	split, auto
Component	Peak areas (%)					
$C_{10:0}$	0.3	0.3	0.3	0.3	0.3	n.a.
$C_{12:0}$	0.2	0.2	0.2	0.2	0.2	n.a.
$C_{14:0}$	7.1	6.3	6.8	6.2	6.2	6.1
$C_{14:1\omega5}$	0.5	0.3	0.3	n.d.	0.2	0.3
$C_{15:0}$	0.5	0.5	0.5	0.5	0.5	0.5
$C_{15:1\omega5}$	0.1	0.2	0.2	n.d.	0.1	n.d.
$C_{16:0}$	17.9	16.5	17.1	16.3	16.6	16.3
$C_{16:1\omega7}$	12.1	11.1	11.9	11.9	10.9	11.2
$C_{16:2}$	1.4	1.4	1.4	0.6	0.8	0.6
$C_{17:0}$	0.2	0.2	0.2	0.2	0.9	0.4
$C_{16:3}$	0.6	0.6	0.7	0.9	(0.0)[a]	0.4
$C_{16:4\omega3}$	0.8	0.8	0.8	(0.0)[b]	0.9	0.8
$C_{18:0}$	2.1	2.2	2.2	2.2	2.4	2.3
$C_{18:1\omega9}$	10.1	10.0	10.3	9.9	10.2	10.3
$C_{18:1\omega7}$	2.3	2.3	2.3	2.5	2.9	2.4
$C_{18:2\omega6}$	2.9	3.0	3.1	4.3	3.0	3.0
$C_{19:0}$	0.1	0.2	0.2	n.d.	n.d.	n.d.
$C_{18:3\omega6}$	0.4	0.4	0.4	(0.0)[c]	0.2	0.2
$C_{18:3\omega3}$	1.3	1.4	1.4	(0.0)[c]	1.4	1.5
$C_{18:4\omega3}$	3.8	4.0	4.1	4.4	4.2	4.0
$C_{19:1\omega9}$	0.1	0.1	0.1	n.d.	0.1	0.2
$C_{20:0}$	0.2	0.1	0.2	0.1	0.2	0.1
$C_{20:1\omega9}$	4.2	4.4	4.3	4.9	4.8	4.9
$C_{20:2\omega6}$	0.3	0.4	0.3	0.3	0.3	0.3
$C_{21:0}$	0.1	0.1	0.1	n.d.	n.d.	0.0
$C_{20:3\omega6}$	n.d.	n.d.	n.d.	n.d.	0.1	0.1
$C_{20:4\omega6}$	0.3	0.3	0.3	n.d.	0.4	0.4
$C_{20:3\omega3}$	0.1	0.1	0.1	(0.0)[d]	(0.0)[e]	0.2
$C_{20:4\omega3}$	0.7	0.7	0.7	1.2	0.8	0.8
$C_{20:5\omega3}$	10.3	11.2	10.7	11.1	11.1	11.0
$C_{22:1\omega11}$	6.6	7.0	6.3	7.5	6.4	7.4
$C_{22:1\omega9}$	1.1	0.7	0.7	0.2	1.9	0.9
$C_{21:5\omega3}$	0.4	0.5	0.5	0.5	0.5	0.6
$C_{22:4\omega6}$	0.1	0.1	0.1	n.d.	n.d.	0.3
$C_{22:5\omega6}$	0.1	0.1	0.1	n.d.	(0.0)[f]	0.1
$C_{22:5\omega3}$	0.5	0.7	0.6	0.8	0.7	0.7
$C_{22:6\omega3}$	9.2	11.8	9.8	11.3	10.7	11.1
$C_{24:1\omega9}$	0.8	(0.0)[g]	0.6	0.9	0.7	0.9
$C_{27}H_{44}OH$	n.d.	n.d.	n.d.	0.8	n.d.	n.d.
Identified	95.9	96.5	94.6	94.2	94.5	93.4

[a] Possible peak coincidence with component $C_{17:0}$.
[b] Peak coincidence with component $C_{16:3}$.
[c] Peak coincidence with component $C_{18:2\omega6}$.
[d] Peak coincidence with component $C_{20:2\omega6}$.
[e] Peak coincidence with component $C_{20:4\omega6}$.
[f] Possible peak coincidence with component $C_{21:5\omega3}$.
[g] Peak coincidence with component $C_{22:6\omega3}$.

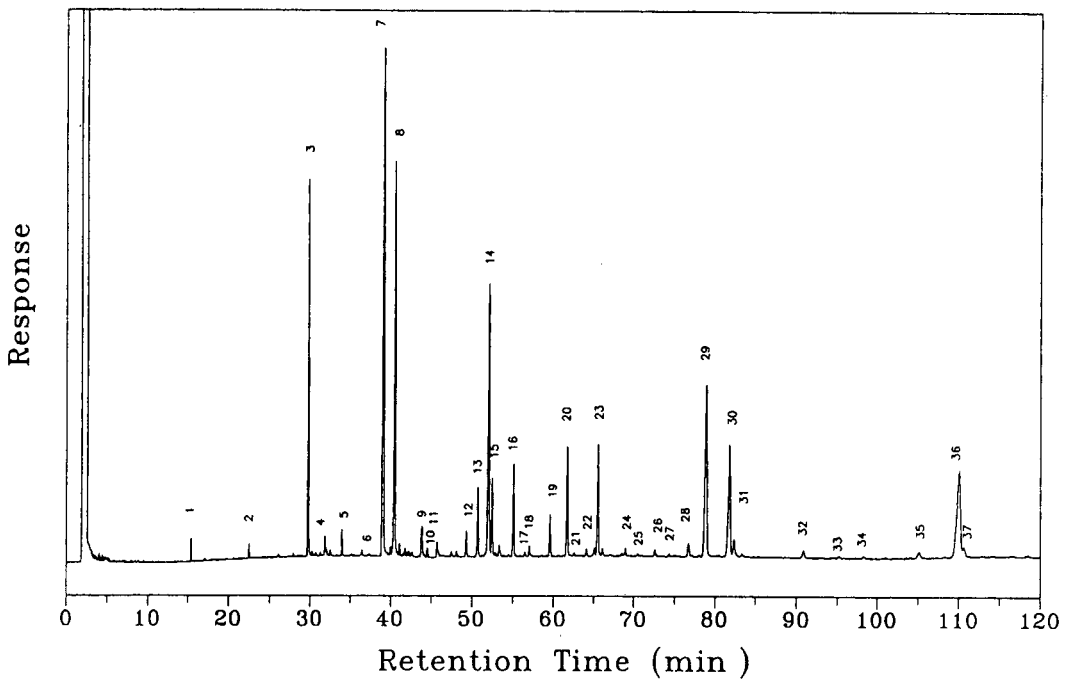

Fig. 1. GLC of sand eel fatty acid ethyl ester mixture. Conditions: column, HP-FFAP (25 m × 0.2 mm × 0.33 μm); injection technique, cold on-column; conditions moreover as in Method 1 of the text. Peaks: 1 = $C_{10:0}$; 2 = $C_{12:0}$; 3 = $C_{14:0}$; 4 = $C_{14:1\omega5}$; 5 = $C_{15:0}$; 6 = $C_{15:1\omega5}$; 7 = $C_{16:0}$; 8 = $C_{16:1\omega7}$; 9 = $C_{16:2}$; 10 = $C_{17:0}$; 11 = $C_{16:3}$; 12 = $C_{16:4\omega3}$; 13 = $C_{18:0}$; 14 = $C_{18:1\omega9}$; 15 = $C_{18:1\omega7}$; 16 = $C_{18:2\omega6}$; 17 = $C_{19:0}$; 18 = $C_{18:3\omega6}$; 19 = $C_{18:3\omega3}$; 20 = $C_{18:4\omega3}$; 21 = $C_{19:1\omega9}$; 22 = $C_{20:0}$; 23 = $C_{20:1\omega9}$; 24 = $C_{20:2\omega6}$; 25 = $C_{21:0}$; 26 = $C_{20:4\omega6}$; 27 = $C_{20:3\omega3}$; 28 = $C_{20:4\omega3}$; 29 = $C_{20:5\omega3}$; 30 = $C_{22:1\omega11}$; 31 = $C_{22:1\omega9}$; 32 = $C_{21:5\omega3}$; 33 = $C_{22:4\omega6}$; 34 = $C_{22:5\omega6}$; 35 = $C_{22:5\omega3}$; 36 = $C_{22:6\omega3}$; 37 = $C_{24:1\omega9}$; 38 = $C_{27}H_{44}OH$.

ration of component $C_{22:6\omega3}$ and $C_{24:1\omega9}$ using Method 2, however, is much poorer, possibly due to the different temperature program.

Method 3 involves the application of a splitless injection with the FFAP column. The use of the splitless injection method is, of course, not the suitable method for the analysis of fatty acid esters, but is usually used for detection and determination of components present in trace amounts [43]. Still, it is included here for reasons of comparison, and when compared to Method 2 it exhibits significant differences in peak area% for the major light and heavy compounds, indicating an expected discrimination of the low-volatility compounds.

The employment of the non-polar HP-1 column and the manual split injection, Method 4, exhibited the expected pattern of peak coincidences between compounds of different degree of unsaturation [17]. The results of Method 4 are in rather good agreement with the results of Method 2 except for components of C_{16} chain lengths and $C_{20:4\omega3}$, but using the HP-1 column it is possible to determine the amount of cholesterol ($C_{27}H_{44}OH$) of the ester mixture in the same chromatographic run. This was not possible with the more polar columns. A chromatogram of the ethyl ester mixture using Method 4 is presented in Fig. 2. The figure shows the peak coincidence of several compounds, indicative of the unsuitability of a non-polar column for the separation of a complex mixture of unsaturated fatty acid ethyl esters. For an uncomplicated mixture, however, this type of column may have some merit as it allows determination of cholesterol simultaneously with the fatty acid ester composition.

All the gas chromatographic experiments showed a good reproducibility and many compounds have been identified, corresponding to

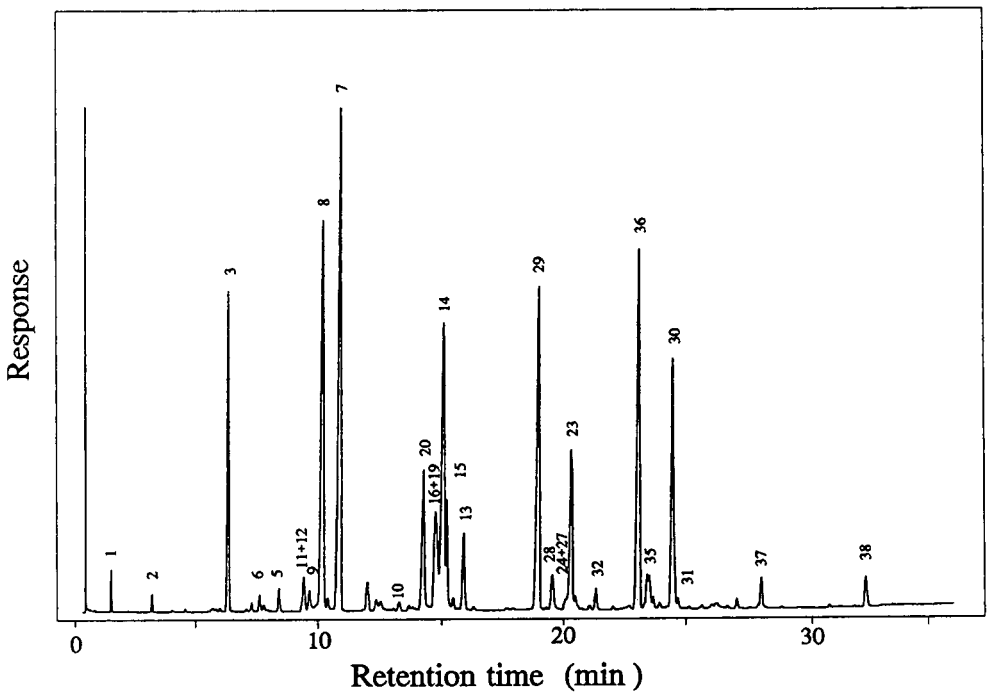

Fig. 2. GLC of sand eel fatty acid ethyl ester mixture. Conditions: column, HP-1 (12 m × 0.2 mm × 0.33 μm); injection technique, manual split; conditions moreover as in Method 4 of the text. Peaks as in Fig. 1.

93–97% of the integrated area. Unidentified components account primarily for various isomers of $C_{16:1}$, $C_{18:1}$, $C_{20:1}$ and $C_{22:1}$.

SFC

The experimental peak area% obtained from the supercritical fluid chromatographic analyses are presented in Table II. Each chromatographic experiment was performed three times. The relative standard deviation for the three methods concerned may be as large as 10%, but generally it is less than 4%. Chromatograms of the methods 6, 7, and 8 are given in Figs. 3, 4, and 5, respectively. The elution sequence shown in Table II is as for the DB-225 column. The fatty acid structures ($\omega - x$) have not been given for some components in Table II due to the peak coincidence of some of the various isomers.

Examining Table II and Figs. 3–5, it can be observed that Method 7, using the polar DB-225 column, separates the ester mixture better than the two other methods, 8 and 9, using the non-polar columns CP Sil 5 and DB-5. The better separation observed of Method 8 using the CP Sil 5 column compared to Method 9 using the DB-5 column is due to the smaller diameter of the CP Sil 5 column, which causes the number of theoretical plates to be higher. Differences in composition obtained by the three methods occurred for some major compounds like $C_{16:0}$, $C_{16:1}$ and $C_{22:6}$, and for peak coincidence of the non-polar columns between polyunsaturated compounds of C_{16} and C_{18} chain lengths. All in all, the optimum choice of column seems to be a polar column like the DB-225 or similar with a diameter of 0.05 mm or less to increase the number of theoretical plates compared to the one employed in this work.

All the supercritical fluid chromatographic experiments showed a good reproducibility with mean relative standard deviations of the identified compounds of approximately 3%. Analysis of cholesterol with all the SFC methods is possible. 95–98% of the integrated area has been identified and unidentified components possibly account for various higher chain length esters.

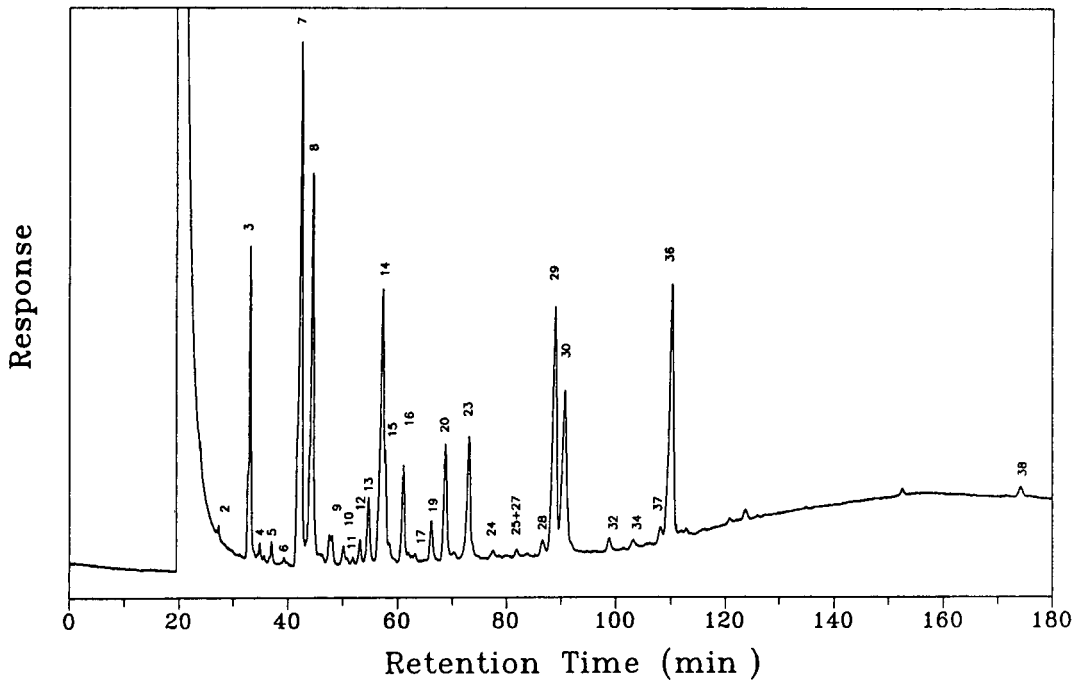

Fig. 3. SFC of sand eel fatty acid ethyl ester mixture. Conditions: column, DB-225 (20 m × 0.1 mm × 0.1 μm); conditions moreover as in Method 7 of the text. Peaks as in Fig. 1.

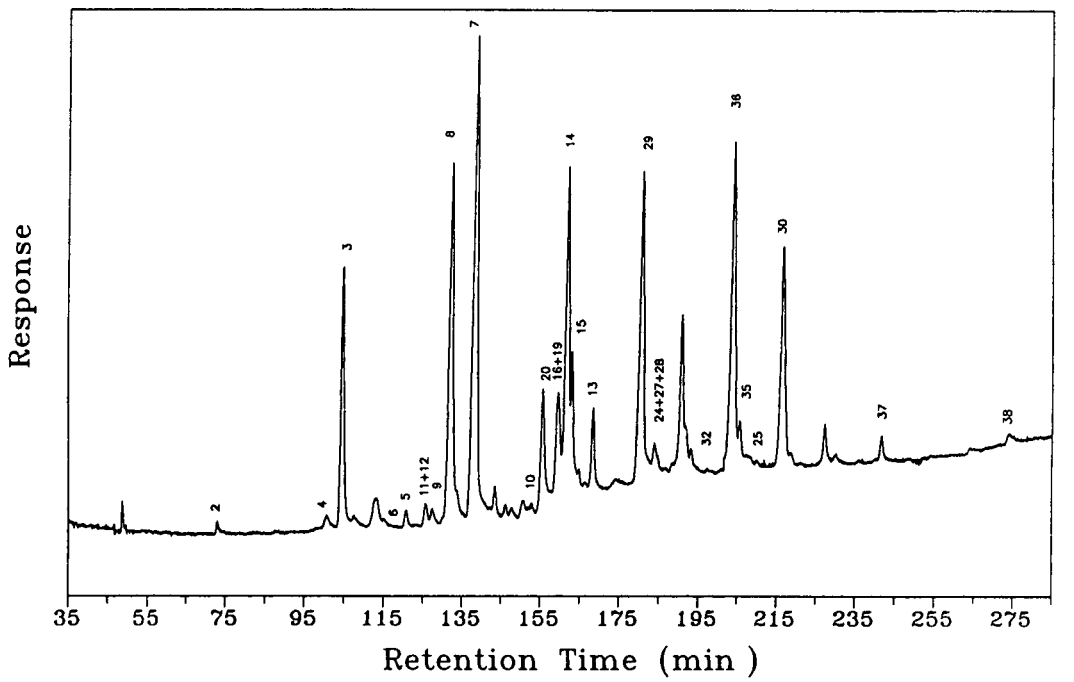

Fig. 4. SFC of sand eel fatty acid ethyl ester mixture. Conditions: column, CP-Sil 5 CB (20 m × 0.05 mm × 0.2 μm); conditions moreover as in Method 8 of the text. Peaks as in Fig. 1.

TABLE II

SUPERCRITICAL FLUID CHROMATOGRAPHIC PEAK AREAS OF THE SAND EEL ETHYL ESTER MIXTURE USING VARIOUS COLUMNS

The experimental conditions are given in the text. The relative standard deviations of each of the three methods are generally less than 4% of each compound, but they may be as large as 10%. n.d.: not detected.

Method no.	7	8	9
Column	DB-225	CP Sil 5	DB-5
Component	Peak areas (%)		
$C_{10:0}$	0.1	0.3	0.3
$C_{12:0}$	0.1	0.2	0.2
$C_{14:0}$	6.2	6.4	6.1
$C_{14:1\omega5}$	0.4	0.4	n.d.
$C_{15:0}$	0.4	0.4	0.5
$C_{15:1\omega5}$	0.2	0.2	0.1
$C_{16:0}$	17.1	17.4	16.2
$C_{16:1}$	12.6	11.8	11.5
$C_{16:2}$	1.3	0.3	1.2
$C_{16:3}$	0.6	0.5	(0.0)[a]
$C_{17:0}$	0.1	0.7	0.4
$C_{16:4\omega3}$	0.6	(0.0)[b]	(0.0)[a]
$C_{18:0}$	1.9	2.2	2.2
$C_{18:1\omega9}$	9.4	9.6	16.6
$C_{18:1\omega7}$	2.6	4.2	(0.0)[c]
$C_{18:2\omega6}$	3.0	3.9	(0.0)[c]
$C_{19:0}$	0.3	n.d.	n.d.
$C_{18:3}$	1.2	(0.0)[d]	4.1
$C_{18:4\omega3}$	4.1	3.8	(0.0)[e]
$C_{20:1}$	4.6	5.2	5.2
$C_{20:2\omega6}$	0.2	1.4	1.0
$C_{20:3}$	0.2	(0.0)[f]	(0.0)[f]
$C_{20:4}$	0.5	(0.0)[f]	(0.0)[f]
$C_{21:0}$	n.d.	0.2	n.d.
$C_{20:5\omega3}$	10.4	10.2	11.0
$C_{22:1}$	8.1	7.6	8.1
$C_{21:5\omega3}$	0.5	0.7	1.1
$C_{22:5}$	0.3	1.3	0.4
$C_{24:1}$	0.5	0.7	0.9
$C_{22:6\omega3}$	11.4	10.5	12.2
$C_{27}H_{44}OH$	0.4	0.4	0.7
Identified	98.4	95.2	96.7

[a] Peak coincidence with component $C_{16:2}$.
[b] Peak coincidence with component $C_{16:3}$.
[c] Peak coincidence with component $C_{18:1\omega9}$.
[d] Peak coincidence with component $C_{18:2}$.
[e] Peak coincidence with component $C_{18:3}$.
[f] Peak coincidence with component $C_{20:2}$.

Comparisons

In this study, the composition of a sand eel fatty acid ethyl ester mixture has been analysed using gas and supercritical fluid chromatography. A comparison of the best SFC method of this work for separation of long chain fatty acid esters, Method 7, with the GC methods 5 and 6, generally displays a good concordance except for a few compounds, especially $C_{16:1}$, $C_{18:1\omega9}$, $C_{20:4}$ and $C_{22:5}$. The results of $C_{10:0}$ and $C_{12:0}$ of Method 7 are less satisfactory due to their presence in the solvent peak. An investigation of Figs. 1 and 3 shows almost the same peak elution order of the FFAP and the DB-225 columns, while Figs. 2, 4 and 5 show a similar pattern of the non-polar columns. The injection technique of the SFC experiments may cause some discrimination of heavy compounds, but the alternatives are few because of the high pressure involved [46].

Not all of the GC and SFC experiments have been optimized regarding the analysis time, but generally the SFC experiments have longer analysis times than the GC experiments. The standard deviation of peak area% of the GC experiments are lower than those of the SFC experiments, and the GC method using a polar column must be the choice of analysis method for the determination of fatty acid ester compositions of fish oils. On the other hand, the SFC method using a polar column offers an easy simultaneous determination of both fatty acid esters and cholesterol and operating temperatures considerably lower than that of the GC methods minimizing the potentiality of irreversible thermal degradation of the polyunsaturated compounds.

The results of this work show that SFC can be used for the analysis of fatty acid esters and legitimate the use of SFC directly coupled on-line to high-pressure equipment for analytical purposes.

ACKNOWLEDGEMENTS

This work has been supported by grants from Nordisk Industrifond and the Danish Research Council. The authors thank Grindsted Products

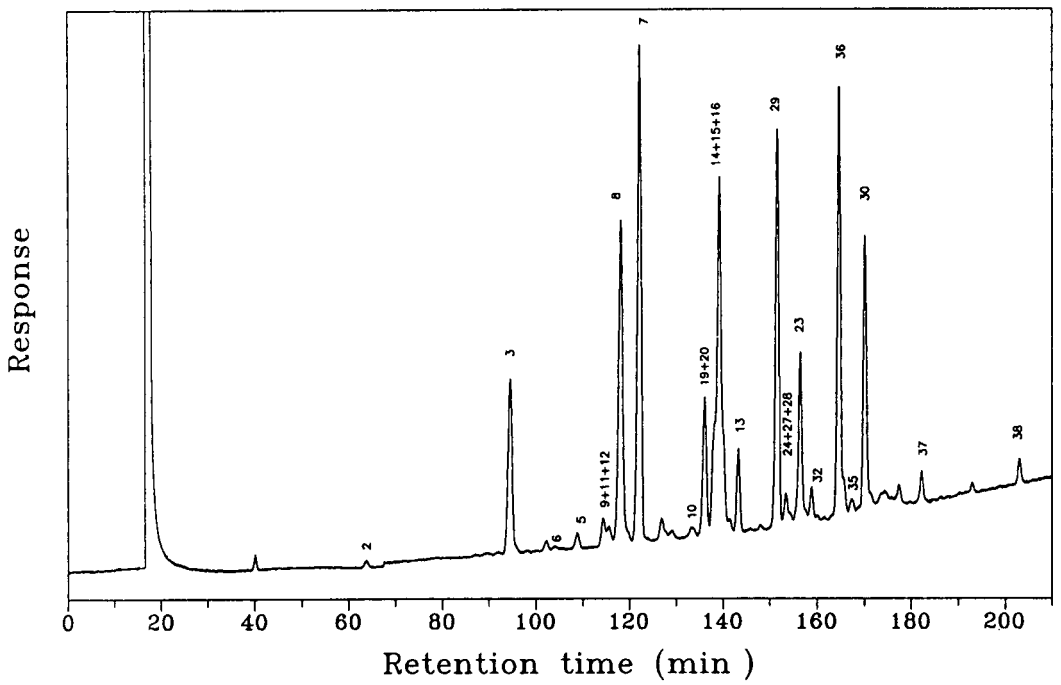

Fig. 5. SFC of sand eel fatty acid ethyl ester mixture. Conditions: column, DB-5 (20 m × 0.1 mm × 0.4 μm); conditions moreover as in Method 9 of the text. Peaks as in Fig. 1.

A/S for the supply of the fish oil ester mixture, M. Sc. Torben Forskov for the set up of the cold on-column injection method, Mr. Ruddy Perriard for performing the GC experiments using splitless injection, and Ms. Trang Thu Vu for performing the GC experiments using autosampler injection.

REFERENCES

1 A.P. Bimbo and J.B. Crowther, *J. Am. Oil Chem. Soc.*, 69 (1992) 221.
2 J.M. Kremer, D.A. Lawrence, W. Jubiz, R. DiGiacomo, R. Rynes, L.E. Bartholomew and M. Sherman, *Arthritis Rheum.*, 33 (1990) 810.
3 A. Hirai, T. Terano, H. Saito, Y. Tamura and S. Yoshida, in W.E.M. Lands (Editor), *Proceedings of the AOAC Short Course on Polyunsaturated Fatty Acids and Eicosanoids, Champaign, IL*, 1987, p. 9.
4 W.E. Connor and S.L. Connor, *Adv. Intern. Med.*, 35 (1990) 139.
5 B.S. Reddy, C. Burill and J. Rigotty, *Cancer Res.*, 51 (1991) 487.
6 E.H. Gruger, Jr., R.W. Nelson and M.E. Stansby, *J. Am. Oil Chem. Soc.*, 41 (1964) 662.
7 R.G. Ackman, J.C. Sipos and P.M. Jangaard, *Lipids*, 2 (1967) 251.
8 R. Hardy and J.N. Keay, *J. Chromatogr.*, 27 (1967) 474.
9 R.G. Ackman, P.J. Ke and P.M. Jangaard, *J. Am. Oil Chem. Soc.*, 50 (1973) 1.
10 R.R. Linko, J.K. Kaitaranta and R. Vuorela, *Comp. Biochem. Physiol.*, 82B (1985) 699.
11 T. Puustinen, K. Punnonen and P. Uotila, *Acta Med. Scand.*, 218 (1985) 59.
12 J.A. Dudek and E.R. Elkins, Jr., in A.P. Simopoulos, R.R. Kifer and R.E. Martin (Editors), *Health Effects of Polyunsaturated Fatty Acids in Seafoods*, Academic Press, Orlando, FL, 1986, Ch. 21, p. 431.
13 J.E. Kinsella, *Food Technology*, 40(2) (1986) 89.
14 M.E. Stansby, in A.P. Simopoulos, R.R. Kifer and R.E. Martin (Editors), *Health Effects of Polyunsaturated Fatty Acids in Seafoods*, Academic Press, Orlando, FL, 1986, Ch. 19, p. 389.
15 D.R. Tocher, A. Webster and J.R. Sargent, *Biotechnol. Appl. Biochem.*, 8 (1986) 83.
16 K. Yamaguchi, M. Murakami, H. Nakano, S. Konosu, T. Kokura, H. Yamamoto, M. Kosaka and K. Hata, *J. Agric. Food Chem.*, 34 (1986) 904.
17 R.G. Ackman, *Acta Med. Scand.*, 222 (1987) 99.
18 H.J. Wille, H. Traitler and M. Kelly, *Rev. Fr. Corps Gras*, 34(2) (1987) 69.
19 R.G. Ackman, W.M.N. Ratnayake and B. Olsson, *J. Am. Oil Chem. Soc.*, 65 (1988) 136.
20 W.B. Nilsson, E.J. Gauglitz, Jr., J.K. Hudson, V.F. Stout and J. Spinelli, *J. Am. Oil Chem. Soc.*, 65 (1988) 109.
21 M. Perrut, *LC·GC International*, 1(6) (1988) 58.

22 W.M.N. Ratnayake, B. Olsson, D. Matthews and R.G. Ackman, *Fat Sci. Technol.*, 90 (1988) 381.
23 R.G. Ackman, W.M.N. Ratnayake and E.J. Macpherson, *J. Am. Oil Chem. Soc.*, 66 (1989) 1162.
24 N. Imanishi, R. Fukuzato, S. Furuta and N. Ikawa, *R&D, Kobe Steel Engineering Reports*, 39 (1989) 29.
25 P. Langholz, P. Andersen, T. Forskov and W. Schmidtsdorff, *J. Am. Oil Chem. Soc.*, 66 (1989) 1120.
26 D. Firestone, *J. Assoc. Off. Anal. Chem.*, 73 (1990) 105.
27 S. Higashidate, Y. Yamauchi and M. Saito, *J. Chromatogr.*, 515 (1990) 295.
28 P. Laakso, W.W. Christie and J. Pettersen, *Lipids*, 25 (1990) 284.
29 T. Řezanka, *LC·GC International*, 3(10) (1990) 46.
30 H. Kallio, T. Vauhkonen and R.R. Linko, *J. Agric. Food Chem.*, 39 (1991) 1573.
31 X. Yan, P.J. Barlow and C. Craven, *Food Chem.*, 40 (1991) 93.
32 J.D. Joseph and R.G. Ackman, *J. Assoc. Off. Anal. Chem. Int.*, 75 (1992) 488.
33 A.S. McGill and C.F. Moffat, *Lipids*, 27 (1992) 360.
34 S. Tokiwa, A. Kanazawa and S.-I. Teshima, *Bull. Jap. Soc. Sci. Fish*, 47 (1981) 675.
35 J.M. Beebe, P.R. Brown and J.G. Turcotte, *J. Chromatogr.*, 468 (1989) 225.
36 T. Görner and M. Perrut, *LC·GC International*, 2(7) (1989) 36.
37 M. Kubota, H. Matsuzaki, S. Takahashi and S. Inoue, *Kagaku Kōgaku Ronbunshu*, 15 (1989) 446.
38 *AOCS Official Method Ce 1b-89*, in D. Firestone (Editor), *The Official Methods and Recommended Practices of the American Oil Chemists' Society*, The American Oil Chemists' Society, Champaign, IL, 1989, p. 1.
39 S.B. Hawthorne, D.J. Miller and M.S. Krieger, *J. Chromatogr. Sci.*, 27 (1989) 347.
40 E.J. Guthrie and H.E. Schwartz, *J. Chromatogr. Sci.*, 24 (1986) 236.
41 R.G. Ackman, in R.G. Ackman (Editor), *Marine Biogenic Lipids, Fats, and Oils*, Vol. 1, CRC Press, Boca Raton, FL, 1989, Ch. 3, p. 103.
42 H. Traitler, *Prog. Lipid Res.*, 26 (1987) 257.
43 K. Grob, *Classical Split and Splitless Injection in Capillary Gas Chromatography*, A. Hüthig Verlag, Heidelberg, Germany, 1986.
44 J.D. Craske and C.D. Bannon, *J. Am. Oil Chem. Soc.*, 64 (1987) 1413.
45 C.D. Bannon, J.D. Craske, D.L. Felder, I.J. Garland and L.M. Norman, *J. Chromatogr.*, 407 (1987) 231.
46 M.R. Andersen, *LC·GC International*, 1(5) (1988) 10.

Journal of Chromatography, 648 (1993) 233–244
Elsevier Science Publishers B.V., Amsterdam

CHROM. 25 361

Electromigration in systems with additives in background electrolytes

II. Ionic admixture

Iva Zusková*, Bohuslav Gaš and Jiří Vacík

Faculty of Science, Charles University, Albertov 2030, 128 40 Prague 2 (Czech Republic)

(First received April 5th, 1993; revised manuscript received June 14th, 1993)

ABSTRACT

A theoretical model is presented for isotachophoretic migration in systems where both the leading and terminating electrolytes contain another common component (admixture) (*e.g.*, a difficult to remove impurity). The effective mobility of the admixture is lower than that of the leading ion and higher than that of the terminating ion. The model system includes a further two samples. The mathematical simulation of the separation dynamics of this system was obtained by solution of basic physico-chemical laws. This facilitated a comprehensive formulation of the principles of the steady state and calculations of the parameters of all zones. Based on the theoretical model, a method for the determination of admixture concentrations in the leading and terminating electrolytes from isotachophoretic measurements and accurate determination of the limiting mobilities of the separated compounds from experimental data affected by the presence of the admixture are described.

INTRODUCTION

Various electrophoretic methods are based on the same separation principle and differ in the initial arrangement or the composition of the electrophoretic system. Real electrophoretic systems frequently cannot be distinguished unambiguously according to the conventional classification of electrophoretic methods. The systems, although designated as isotachophoretic but fulfilling only some demands of classical isotachophoresis (ITP), can be mentioned as examples.

Systems including a mixture of several components instead of one counter ionic species constitute one group [1,2]. The second large group is formed by systems in which the leading electrolyte (LE) or the terminating electrolyte (TE) contains more components migrating in the same direction as the separated substances. So-called combined systems [3,4], where the LE contains some amount of terminating ions or the TE contains some amount of leading ions, are typical examples of this group. A mathematical model was formulated for anionic systems where terminating ions are present in the LE [5] and were denoted as systems with two leading ions. Based on this model, steady-state parameters of separated and terminating zones were calculated. Further, it was shown that at a certain concentration ratio of the two leading ions, also dependent on the effective mobilities of the ions, ITP changes into zone electrophoresis. In contrast, in zone electrophoresis some ions can migrate under certain conditions in the ITP mode [6]. The cationic system, in which a weak or strong acid is used as the LE and the mixture of this

* Corresponding author.

0021-9673/93/$06.00

acid and its salt with a weak or strong base serves as the TE [7], also belongs to the group with mixed background electrolytes. It was shown that the parameters of all zones are affected not only by the composition of the LE but also by that of the TE.

The main effects, *e.g.*, a decrease in the specific resistance and an increase in the zone length of separated components due to the presence of an admixture in their zones originating from the leading or the terminating electrolyte, are well known [5,7–11].

The purpose of this paper is to contribute to the theory of ITP with admixtures in background electrolytes and to the evaluation of the experimental data affected by the admixture.

THEORY

Fundamental characterization of the model system

Let us consider a model system in which both the LE and the TE contain another common ionic component, an admixture. The admixture migrates in the same direction as separated ionic species and its effective mobility is lower than that of the leading ion and higher than that of the terminating ion. Two ionic components, A and B, fulfilling the following relationship of the effective mobilities, m^{ef}, were chosen as samples:

$$m^{ef}_{T,T} < m^{ef}_{B,B} < m^{ef}_{X,X} < m^{ef}_{A,A} < m^{ef}_{L,L}$$

The first subscript indicates the substances: A and B are the samples, L is the leading ion, T is the terminating ion and X is the admixture. The second subscript specifies the zone (see Fig. 1). The arrangement of the model system at the initial state (at time $t = 0$) and at the steady state (at time t) is illustrated schematically in Fig. 1. Not only the classical zones in the separation column (zones L, A, X, B and T) but also the electrolyte in the sampling compartment (zone TS) and the original terminating electrolyte in the electrode compartment (zone TE) are denoted as zones. Zones T and TS differ from each other in the concentration which is determined by the initial state. Zone T is created in the capillary where the leading electrolyte was initially and zone TS is created in the sampling compartment.

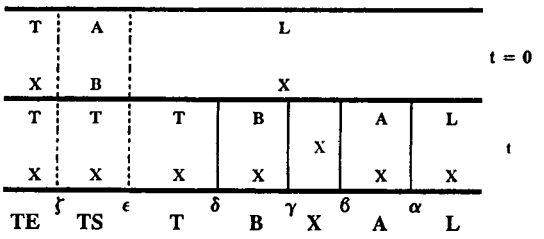

Fig. 1. Schematic illustration of the model system at the initial state (at time $t = 0$) and at the steady state (at time t). The Greek letters denote boundaries and the dashed lines distinguish the stationary boundaries (ϵ, ζ) from the migrating boundaries (α, β, γ, δ). The counter ion R, which is considered identical in all zones, is not marked.

This model system enables one to study the instances where the admixture is separated from the leading and/or terminating electrolyte and creates not only the pure zone itself (zone X) but also the mixed zones with the samples (zones A and B).

In the theoretical model no complex equilibria are taken into account. The temperature changes resulting from the Joule heat and osmotic and convection flows are also omitted. The composition of the TE is maintained constant.

Separation dynamics of the model system

The separation dynamics of the model system were solved by means of the simulation program of electromigration [12]. The graphical depiction of the concentration distribution and of the specific resistance along the capillary are obtained as the result. The algorithm presents the solution in a so-called "observational window", that shifts owing to the migration velocity of the leading ion and shows only the interesting part of the capillary.

The demonstration of the separation dynamics of the anionic model system consisting of uni–univalent strong electrolytes is shown in Fig. 2. It can be clearly seen from Fig. 2b that during the separation the admixture from the LE remains behind the leading ion and the admixture in the TE outruns the terminating ion. Simultaneously, samples A and B separate from each other and their concentrations are changed when they

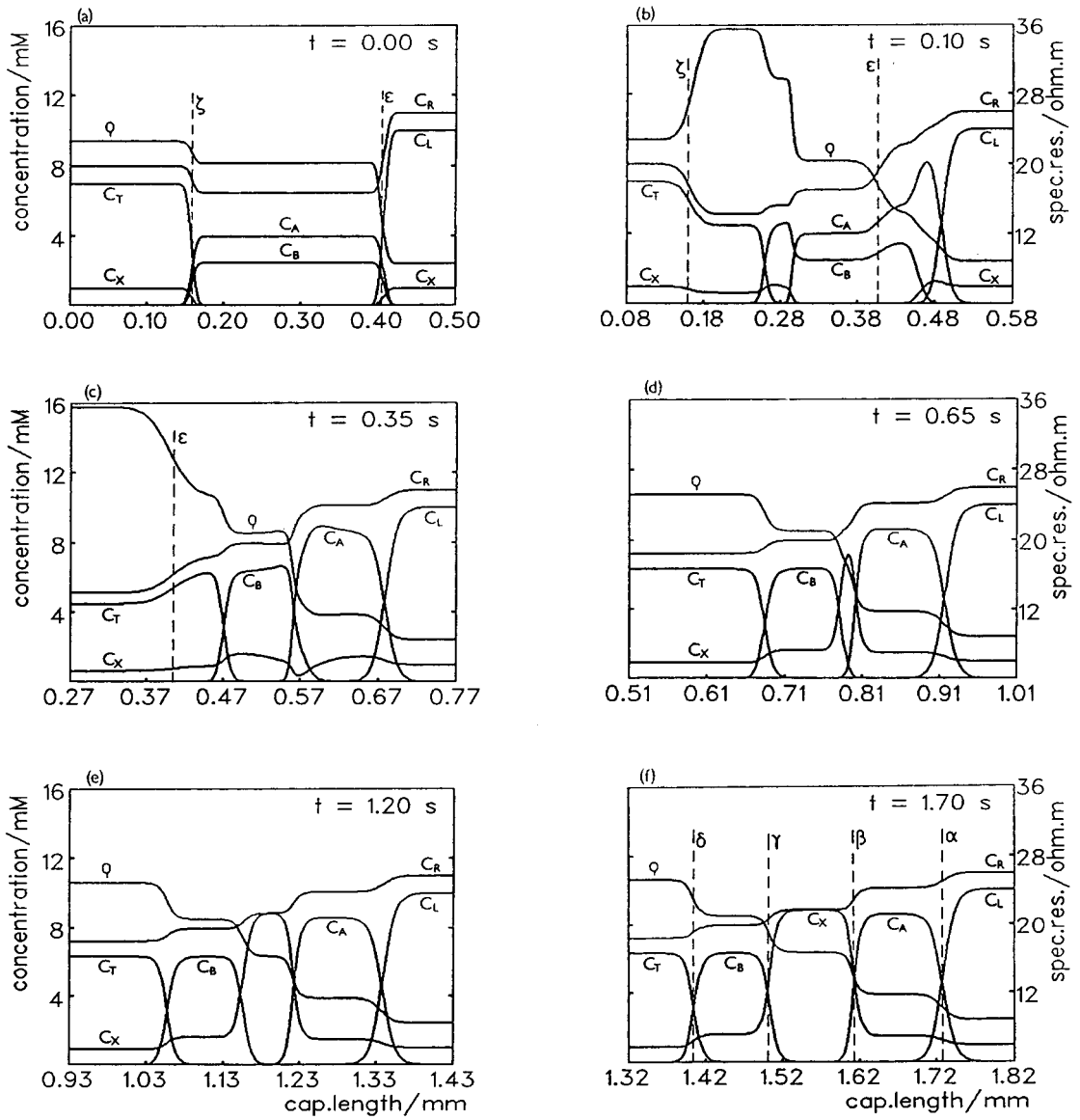

Fig. 2. Separation dynamics of the anionic model system. The mobility of the ions (10^{-9} m^2 V^{-1} s^{-1}) are $m_L = 80$, $m_A = 60$, $m_X = 40$, $m_B = 30$, $m_T = 25$ and $m_R = 30$. The initial concentrations (mM) [see also (a)] are $c_L = 10$ and $c_X = 1$ in both the LE and the TE, $c_A = 4$, $c_B = 2.5$ and $c_T = 7$. The current density is 1100 A m^{-2}. ρ = Specific resistance; α, β, γ, δ = migrating boundaries; ϵ, ζ = stationary boundaries, which demarcate the sampling compartment (see also Fig. 1).

leave the sampling compartment. Similarly, the concentrations of the terminating ion and of the admixture are changed when they migrate into the sampling compartment or when they leave it (see Fig. 2b and c). The admixture further outruns the sample B and remains behind the sample A and so forms its pure zone (see Fig. 2d). After the steady state has been reached (Fig. 2e and 2f), the concentrations of all components in all zones are constant both with time and along the zones. The lengths of zones A and B also do not change with time. On the other hand, the length of zone X increases with time.

Further, it can be concluded that the boundaries α and β migrate at the same velocity equal to the velocity of the leading ion. The

boundaries γ and δ also have the same velocity but different from that of α and β. With the chosen values of the initial concentrations and mobilities, this separation represents a combination of ITP with the method of moving boundaries. The concept of a "steady state", taken over the theory of classical ITP, is understood as the state where the concentrations of all components in all zones are constant.

Steady state of the model system

The mathematical models are formulated for both strong and weak uni–univalent electrolytes. The concentrations of all components in all zones and the zone lengths are obtained as solution of these models.

In the theory of classical ITP, a uniform mathematical description can be used for all separated zones. In the given model system, the zones have different characteristics and, therefore, the mathematical description of every zone must be done separately.

Model system formed by strong uni–univalent electrolytes

In this mathematical model, mobility is considered as a quantity independent on ionic strength. This assumption enables one to acquire the solution in the analytical form.

Zone A includes the ionic species of sample A, the ionic species of admixture X and the counter ionic species R. The concentration of the admixture in the zone A, $c_{X,A}$, can be calculated from the equation describing the mass balance of the admixture for the boundary α:

$$c_{X,L}(m_X E_L - m_L E_L) = c_{X,A}(m_X E_A - m_L E_L) \quad (1)$$

where m is the ionic mobility and E is the potential gradient. The subscripts on m and E denote the ionic species and the zone, respectively. Because the ITP condition

$$m_L E_L = m_A E_A \quad (2)$$

is fulfilled for zone A, eqn. 1 can be expressed in the form

$$c_{X,A} = c_{X,L} \cdot \frac{m_X - m_L}{m_L} \cdot \frac{m_A}{m_X - m_A} \quad (3)$$

The concentration $c_{A,A}$ can be obtained from the Kohlrausch regulating function (KRF) including the electroneutrality condition (EN):

$$c_{A,A} = c_{L,L} \cdot \frac{m_L + m_R}{m_L} \cdot \frac{m_A}{m_A + m_R} + c_{X,L} \cdot \frac{m_X + m_R}{m_X} \cdot \frac{m_A}{m_A + m_R} - c_{X,A} \cdot \frac{m_X + m_R}{m_X} \cdot \frac{m_A}{m_A + m_R} \quad (4)$$

The second term on the right-hand side expresses the increase in the concentration $c_{A,A}$ due to the presence of the admixture in the LE (it is analogous to the first term) and the third term represents the decrease in the concentration $c_{A,A}$ due to the presence of the admixture in zone A.

The simplest is zone X, containing only the ionic species of the admixture and counter ionic species. Therefore, we use the KRF and the EN for expressing $c_{X,X}$:

$$c_{X,X} = c_{L,L} \cdot \frac{m_L + m_R}{m_L} \cdot \frac{m_X}{m_X + m_R} + c_{X,L} \quad (5)$$

If $c_{X,L} = 0$ (so the admixture will be only in the TE), eqn. 5 will be reduced to the form known from classical ITP for a sample.

In zone T, as in the previous instances, the KRF including the EN serves as the first equation for the unknown concentrations $c_{T,T}$ and $c_{X,T}$. The mass balance for the immobile concentration boundaries ϵ and ζ:

$$\frac{c_{T,T}}{c_{X,T}} = \frac{c_{T,TS}}{c_{X,TS}} = \frac{c_{T,TE}}{c_{X,TE}} \quad (6)$$

can be used as the second equation. This mass balance expresses, that all ionic species are diluted or concentrated over the immobile boundary to the same extent. The solution of these two equations leads to

$$c_{T,T} = \left(c_{L,L} \cdot \frac{m_L + m_R}{m_L} + c_{X,L} \cdot \frac{m_X + m_R}{m_X}\right) \times \frac{c_{T,TE}}{c_{T,TE} \cdot \frac{m_T + m_R}{m_T} + c_{X,TE} \cdot \frac{m_X + m_R}{m_X}} \quad (7)$$

A similar relationship can be obtained for the

concentration of the admixture in zone T by combining eqns. 6 and 7. It is clear that the composition of zone T depends not only on the parameters of the LE but also on those of the TE.

An analogous approach to that for zone A can be taken for the expression of parameters of zone B. The concentration $c_{B,B}$ is given by

$$c_{B,B} = c_{L,L} \cdot \frac{m_L + m_R}{m_L} \cdot \frac{m_B}{m_B + m_R} + c_{X,L} \cdot \frac{m_X + m_R}{m_X} \cdot \frac{m_B}{m_B + m_R} - c_{X,B} \cdot \frac{m_X + m_R}{m_X} \cdot \frac{m_B}{m_B + m_R} \quad (8)$$

For the boundary δ the mass balance of admixture can be written as

$$c_{X,B}(m_X E_B - m_T E_T) = c_{X,T}(m_X E_T - m_T E_T) \quad (9)$$

and after rearrangement by means of

$$m_B E_B = m_T E_T \quad (10)$$

we obtain the relationship for the concentration of the admixture in zone B:

$$c_{X,B} = c_{X,T} \cdot \frac{m_X - m_T}{m_T} \cdot \frac{m_B}{m_X - m_B} \quad (11)$$

The parameters of zone B are also dependent on the composition of the TE owing to the concentration $c_{T,T}$ in eqn. 11.

If steady-state concentrations are known, the relationships for the zone length can be derived. Generally, the length of the separated zone k, l_k, is given by

$$l_k = \frac{n_{k,k}}{c_{k,k} S} \quad (12)$$

where S is the inner cross-section of the capillary and $n_{k,k}$ is the amount of component k in the kth zone. The amounts $n_{A,A}$ and $n_{B,B}$ correspond to the sampling amounts $n_{A,0}$ and $n_{B,0}$, respectively. For the admixture the amount $n_{X,X}$ is dependent on time. The following consideration can be applied for its derivation. The admixture goes to zone X from both the leading and the terminating zones. The contribution from the LE (the TE) is given by the amount $n_{X,\alpha}$ ($n_{X,\zeta}$) that passes the boundary α (ζ) during the time t:

$$n_{X,\alpha} = c_{X,L}(m_L - m_X) E_L t S \quad (13)$$

$$n_{X,\zeta} = c_{X,TE} m_X E_{TE} t S \quad (14)$$

These contributions must be deducted by the amount of the admixture contained in the zones A, B, T and TS. These amounts can be generally described as

$$n_{X,k} = c_{X,k} l_k S \quad (15)$$

The following relationship can be derived for the length of the zone T, which is dependent on time:

$$l_T = m_T E_T t - l_{TS} \cdot \frac{E_T}{E_{TS}} \quad (16)$$

Combining the set of eqns. 12–16, we obtain

$$l_X = \frac{c_{X,L}}{c_{X,X}}(m_L - m_X) E_L t + \frac{c_{X,TE}}{c_{X,X}}(m_X - m_T) E_{TE} t - \frac{c_{X,A} n_{A,0}}{c_{X,X} c_{A,A} S} - \frac{c_{X,B} n_{B,0}}{c_{X,X} c_{B,B} S} \quad (17)$$

One important conclusion can be drawn from eqn. 17: the calculation of the zone length of the admixture can be done without a knowledge of the concentrations of the constituents in the zone TS.

Model system formed by weak uni–univalent electrolytes

In this theoretical model, the dependence of ionic mobilities on ionic strength is taken into account. As most of the zones in our model system are mixed zones, the Onsager–Fuoss theory [13], which incorporates also the so-called mixing effect, was used. The McInnes approximation of the activity coefficient was chosen for recalculation of the thermodynamic dissociation constants for a given ionic strength.

The pH and concentrations of ionic forms of given constituents must be calculated in all zones (even in the LE and TE). For the calculation of these unknown parameters, we have the electroneutrality condition and the set of equations describing dissociation equilibria. In the separated zones (zones A, X, B and T) the analytical

concentrations, c^{tot}, are also unknown, so that the equations of the mass balance must be added. The parameters of the LE determine the parameters of the subsequent zones. This is expressed in all zones by the mass balance of the buffer:

$$c^{tot}_{R,k}(m^{ef}_{R,k}E_k + v_{k/k-1}) = c^{tot}_{R,k-1}(m^{ef}_{R,k-1}E_{k-1} + v_{k/k-1}) \quad (18)$$

where $v_{k/k-1}$ represents the velocity of the boundary between the kth and $(k-1)$th zone. For the boundary velocities we can write

$$v_\gamma = v_\delta \quad \text{so} \quad m^{ef}_{B,B}E_B = m^{ef}_{T,T}E_T \quad (19)$$

$$v_\alpha = v_\beta \quad \text{so} \quad m^{ef}_{L,L}E_L = m^{ef}_{A,A}E_A \quad (20)$$

Another equation must give the information about the migration flow of the admixture:

$$c^{tot}_{X,k}(m^{ef}_{X,k}E_k - v_{k/k-1}) = c^{tot}_{X,k-1}(m^{ef}_{X,k-1}E_{k-1} - v_{k/k-1}) \quad (21)$$

Eqns. 18 and 21 together with the EN and the dissociation equilibria are sufficient to describe the five parameters in zone X. Eqns. 19 and 20 must be added to this set for the description of the seven unknown parameters in zones A and B, respectively. In zone T there are also seven unknown parameters. Eqns. 18 and 21 cannot be used for zone T and the closely preceding zone B, because the parameters of zone B depend on zone T and therefore they must be solved subsequently. Considering that the steady state is being described and eqn. 20 is valid, the mass balance of the buffer and the admixture for zones T and X can be used. The dependence of the parameters of zone T on the parameters of the TE is expressed by means of the mass balance of the immobile boundaries ϵ and ζ:

$$c^{tot}_{X,TE}m^{ef}_{X,TE}E_{TE} = c^{tot}_{X,T}m^{ef}_{X,T}E_T \quad (22)$$

The relationships for the zone length are analogous to those for the strong electrolytes:

$$l_k = \frac{n_{k,k}}{c^{tot}_{k,k}S} \quad (23)$$

The considerations leading to the derivation of $n_{X,X}$ are also the same. Nevertheless, for strong electrolytes the mobility of an ionic species is considered to be constant in all zones. Consequently, the zone length l_X is not influenced by the parameters of zone TS. This simplifying assumption is not used for weak electrolytes. Because the calculation of the steady-state parameters of zone TS is feasible only by considering similar assumptions, for the zone length l_X the following approximate relationship is used:

$$l_X = \frac{c^{tot}_{X,L}}{c^{tot}_{X,X}}(m^{ef}_{L,L} - m^{ef}_{X,L})E_L t + \frac{c^{tot}_{X,TE}}{c^{tot}_{X,X}}\left(m^{ef}_{X,TE} - m^{ef}_{T,T}\frac{m^{ef}_{X,TE}}{m^{ef}_{X,T}}\right)E_{TE}t - \frac{c^{tot}_{X,A}n_{A,0}}{c^{tot}_{X,X}c^{tot}_{A,A}S} - \frac{c^{tot}_{X,B}n_{B,0}}{c^{tot}_{X,X}c^{tot}_{B,B}S} \quad (24)$$

The zone length l_k is not experimentally available. The detector records the time during which the zone is passing through. This value, proportional to the zone length, will be called the time zone length, Δt_k. For the time length of the sample zone the following simple equation is valid:

$$\Delta t_k = \frac{l_k}{m^{ef}_{k,k}E_k} \quad (25)$$

For the time length of the admixture zone the calculation is more complicated because the admixture does not migrate at the same velocity as the boundaries that demarcate this zone. As was mentioned above, the length l_X is elongated during passage through the detector. The time length Δt_X can be expressed as

$$\Delta t_X = \frac{l_X}{m^{ef}_{B,B}E_B} \quad (26)$$

where l_X is the zone length of the admixture in time t_β, when the boundary β is missing the detector. For t_β we can write

$$t_\beta = \frac{l_c}{m^{ef}_{L,L}E_L} + \Delta t_A \quad (27)$$

where l_c is the length of the capillary from the sampling compartment to the detector.

An interesting difference exists in the characteristics of the zone of samples and of admix-

tures: the time zone lengths of samples are independent of the capillary inner cross-section, but the time zone length of the admixture is influenced.

Calculation procedure

Various properties of the zone are reflected in the mathematical description, but the procedure of numerical evaluation is the same for all zones. The set of non-linear algebraic equations are solved by the Newton–Raphson iteration method [14]. Another iterative cycle consists of the recalculation of the limiting mobilities and the dissociation constants for the ionic strength in the respective zone. The sequence in which the zones are solved corresponds to their sequence in the capillary only for the first three, *i.e.*, for zones L, A and X. Then zone TE must be computed because the subsequently solved zones T and B are dependent on its parameters.

EXPERIMENTAL

The computational algorithm was programmed in Pascal and runs on PC computers.

A laboratory-made ITP apparatus equipped with a high-frequency contactless conductivity detector [15] was used in all experiments. The electrode compartments and sampling valve were from the commercial apparatus AGROFOR (JZD, Odra Krmelín, Czech Republic). The measuring cell was thermostated at 25°C by means of a water thermostat. Non-linear calibration of the detector was performed without an electric current. A constant current of 30 μA was applied in all experiments. The maximum change of the specific resistance caused by passing the electric current was less than 0.3%.

Chemicals used for the preparation of the leading and terminating electrolytes were of analytical-reagent grade.

RESULTS AND DISCUSSION

Verification of the theoretical model for strong electrolytes

The theoretical model of a steady state for strong electrolytes was verified by means of the simulation program of electromigration that gives information not only about the concentrations of all constituents but also about zone lengths in a given time. The system on which the simulation was demonstrated (input data are given in Fig. 2) was explicitly used for the comparison. The results of the steady-state model together with those obtained by the simulation are presented in Table I.

It can be concluded that both methods of solution afford the same results.

TABLE I

VALUES OF THE STEADY-STATE CONCENTRATION AND THE ZONE LENGTH CALCULATED ON THE BASIS OF THE MATHEMATICAL MODEL OF THE STEADY STATE (1) AND THOSE OBTAINED USING THE SIMULATION PROGRAM OF ELECTROMIGRATION (2)

The input data of the model system are given in Fig. 2. The time $t = 1.7$ s.

Calculation method	Steady-state concentration (mM)						
	$c_{A,A}$	$c_{X,A}$	$c_{X,X}$	$c_{B,B}$	$c_{X,B}$	$c_{T,T}$	$c_{X,T}$
1	8.583	1.500	8.857	6.327	1.627	6.327	0.904
2	8.579	1.500	8.856	6.326	1.627	6.327	0.903
	Zone length (mm)						
	l_A		l_X		l_B		
1	0.0117		0.0109		0.0099		
2	0.0118		0.0110		0.0099		

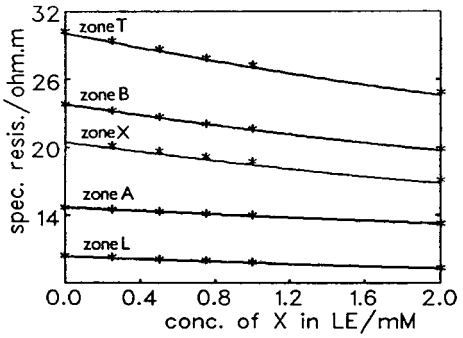

Fig. 3. Calculated (lines) and experimental (asterisks) relationships between the specific zone resistance and the concentration of the admixture in the LE. The concentration of the admixture in the TE is zero.

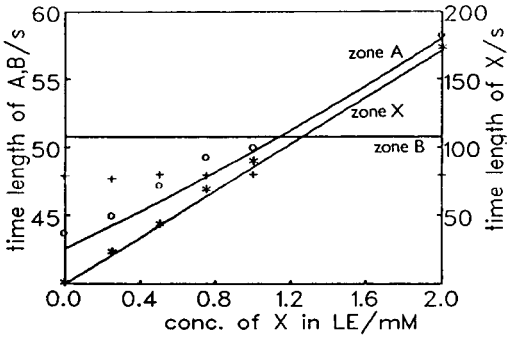

Fig. 5. Calculated (lines) and experimental (points: O = zone A, * = zone X; + = zone B) relationships between the time zone length and the concentration of the admixture in the LE. The concentration of the admixture in the TE is zero.

Verification of the theoretical model for weak electrolytes

The theoretical model for weak electrolytes was verified experimentally. The dependences of the specific resistance and the time length of the zones on the concentration of the admixture in the LE and the TE were both computed theoretically and measured experimentally. The results were processed graphically and are demonstrated in the Figs. 3–6.

The leading electrolyte consists of 0.01 *M* Cl^- as the leading ion, histidine as the buffer counter ion with a total concentration of 0.02 *M* and various concentrations of acetic acid as the admixture X. The terminating electrolyte contains 0.005 *M* glutamic acid, 0.01 *M* histidine and various concentrations of acetic acid. A mixture of formic and propionic acid is used as the sample, both at a concentration of 0.0004 *M*. Formic acid represents sample A in the model system and propionic acid corresponds to the sample B. All ionic limiting mobilities and p*K* values used in the calculation are given in Table II.

As it is clearly seen from Figs. 3 and 4, the agreement between the calculated and measured values of the specific zone resistance is very good. Poorer agreement was achieved between the measured and calculated time zone lengths (see Figs. 5 and 6), but the character of the experimental relationships corresponds to that of the theoretical relationships. For example, in both instances, the time zone length of propionic acid is independent of $c_{X,LE}$ but the measured Δt_B value is *ca.* 5% lower than theoretical value even for zero concentration of the admixture

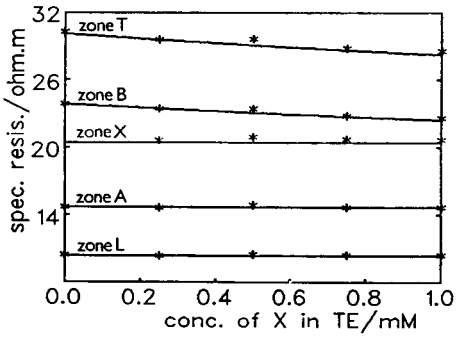

Fig. 4. Calculated (lines) and experimental (asterisks) relationships between the specific zone resistance and the concentration of the admixture in the TE. The concentration of the admixture in the LE is zero.

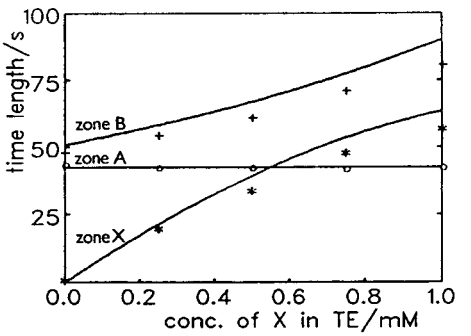

Fig. 6. Calculated (lines) and experimental (points: O = zone A, * = zone X, + = zone B) relationships between the time zone length and the concentration of the admixture in the TE. The concentration of the admixture in the LE is zero.

TABLE II

pK VALUES AND LIMITING MOBILITIES FOR THE IONIC SPECIES USED IN THE CALCULATION

Component	pK	m^0 (10^{-9} m^2 V^{-1} s^{-1})
Acetic acid (−1)	4.76	42.4
Formic acid (−1)	3.75	56.6
Glutamic acid (−1)	4.32	28.9
Histidine (+1)	6.03	29.7
Hydrochloric acid (−1)	−2.00	79.1
Propionic acid (−1)	4.87	37.1

$c_{X,LE}$. The explanation may lie in the inconvenient construction of the sampling valve. The broken shape of the valve gives rise to a "dead space" (the space without a potential gradient) and consequently detains some amount of the sample. This amount can depend on the sample mobility and therefore the differences between the measured and the calculated values can have different magnitudes for different samples.

Determination of admixture concentration in background electrolytes

If the admixture is contained only in the LE or in the TE, the determination is easy on the basis of the known relationships for Δt_X *versus* $c_{X,LE}$ and Δt_X *versus* $c_{X,TE}$, respectively, if no sample is applied.

If the admixture is present in both the LE and the TE simultaneously, then the time length of the admixture zone is given by the sum of the contributions from the LE and the TE. In this more complicated case we can utilize the fact that the parameters of zone A (the zone of the sample with a higher effective mobility than that of the admixture) are influenced only by parameters of the LE. The admixture concentration in the LE, $c_{X,LE}$ is determined from the difference between the time length of zone A with zero concentration of the admixture (computed theoretically) and that with the investigated concentration of the admixture (measured experimentally). From the known concentration $c_{X,LE}$ the contribution of the LE to the time length of the admixture zone is computed and the remainder of this time zone length corresponds to the admixture concentration in the TE.

A computer program for the calculation of the concentrations of the admixture existing simultaneously in the LE and the TE from data from one experiment (the time lengths of zones A and X) was set up. The results of this program together with input experimental data for the three known values of $c_{X,LE}$ and $c_{X,TE}$ are given in Table III.

The principle of the determination utilizes the difference between two values, so the accuracy is lower than that of quantitative ITP analyses. This method can be used (especially if $c_{X,LE}$ is less than 10% of $c_{L,LE}$) only for rough estimations. However, on the other hand it must be realized that if, *e.g.*, $c_{X,LE}$ equals 10% of $c_{L,LE}$

TABLE III

DETERMINED VALUES OF THE CONCENTRATIONS OF THE ADMIXTURE FROM THE EXPERIMENTALLY OBTAINED TIME ZONE LENGTHS FOR THREE KNOWN CONCENTRATIONS $c^{tot}_{X,L}$ AND $c^{tot}_{X,TE}$

The theoretically computed time zone length of sample A (formic acid) for zero concentration of the admixture in the LE is $\Delta t_A = 42.60$ s.

No.	Δt (s)		c (m*M*)			
	Δt_A	Δt_X	$c^{tot}_{X,L}$		$c^{tot}_{X,TE}$	
			Determined	Real	Determined	Real
1	50.15	142.83	1.06	1.00	0.44	0.50
2	49.61	146.49	0.99	0.75	0.53	0.75
3	58.06	199.81	2.01	2.00	0.21	0.25

and is determined within a 20% deviation, we are able to correct the parameters of the LE within an accuracy of *ca.* 2%.

Determination of limiting mobilities

In classical ITP a relative qualitative characteristic R_E (ratio of potential gradients of sample and leading zones) [16] is used for the determination of the limiting mobilities of a sample from experimental ITP data. The advantage of R_E over other relative characteristics used in ITP is given by the ITP condition stating that the R_E is directly equal to the ratio of the effective mobilities of the leading and sample constituents. In our model system, the ITP condition is not generally fulfilled. Nevertheless, it holds that sample A migrates at the same velocity as the leading ion and the migrating velocity of the sample B is equal to that of the terminator in zone T. This means that for the determination of the limiting mobility of sample A (the sample with a higher effective mobility than that of the admixture), the R_E value can be used:

$$R_{E,A} = \frac{E_A}{E_L} = \frac{m^{ef}_{L,L}}{m^{ef}_{A,A}} \tag{28}$$

For expression of the effective mobility of sample B (the sample with a lower effective mobility than that of the admixture) we can analogously introduce a relative qualitative characteristic referred to the adjusted terminating zone T which we shall denote by the symbol R_{ET}:

$$R_{ET,B} = \frac{E_B}{E_T} = \frac{m^{ef}_{T,T}}{m^{ef}_{B,B}} \tag{29}$$

The computing algorithm results from the mathematical description of the model system mentioned above. First the value of $m^{ef}_{L,L}$ is found by the solution of zone L. From the experimentally obtained value of $R_{E,A}$, the effective mobility of substance A is expressed by using eqn. 28. In a similar way, the effective mobility of substance B is determined from $R_{ET,B}$ and $m^{ef}_{T,T}$. For calculation of the $m^{ef}_{T,T}$, the parameters of zones X, TE and T must be known. Then the limiting mobilities of components A and B (approximate values must be given as an initial estimate) are computed from the effective values by iterative calculation of the parameters of the respective zones. It must be emphasized that for the determination of the limiting mobility of sample A, the input data consist only of the parameters of the LE (the limiting mobilities, pK and the total concentrations of the leading ionic species, of the buffer and of the admixture), but for sample B the parameters of the TE must also be known.

The determined values of the limiting mobilities of formic and propionic acid from the experimentally obtained values of $R_{E,A}$ and $R_{ET,B}$, respectively, are given in Table IV for the

TABLE IV

DETERMINED VALUES OF THE LIMITING MOBILITIES (m^0) OF FORMIC AND PROPIONIC ACID FROM THE EXPERIMENTALLY OBTAINED VALUES OF $R_{E,A}$ AND $R_{ET,B}$, RESPECTIVELY, (1) USING THE EXPERIMENTALLY ACQUIRED CONCENTRATIONS $c^{tot}_{X,L}$ AND $c^{tot}_{X,TE}$ (SEE TABLE III) AND (2) SUPPOSING THE CONCENTRATIONS OF THE ADMIXTURE ARE UNKNOWN AND THEREFORE ZERO VALUES WERE USED FOR THEM

The tabulated limiting mobilities are for formic acid $m^0_A = 56.6 \cdot 10^{-9}$ and for propionic acid $m^0_B = 37.1 \cdot 10^{-9}$ V^{-1} m^2 s^{-1}.

Real concentration (mM)		$R_{E,A}$	m^0_A (10^{-9} V^{-1} m^2 s^{-1})		$R_{ET,B}$	m^0_B (10^{-9} V^{-1} m^2 s^{-1})	
$c^{tot}_{X,L}$	$c^{tot}_{X,TE}$		(1)	(2)		(1)	(2)
1.00	0.50	1.421	56.65	56.58	0.794	37.24	37.02
0.75	0.75	1.419	56.72	56.66	0.794	37.23	37.02
2.00	0.25	1.422	56.67	56.54	0.798	37.26	36.85

three different concentrations of acetic acid in the LE and the TE. As can be seen, the differences between the determined and the tabulated values are less than 0.5%. On the other hand, using the $R_{E,B}$ value for calculation of the limiting mobility for propionic acid would give, *e.g.*, for 0.75 m*M* acetic acid in both the LE and TE the value $m_B^0 = 40.22 \cdot 10^9$ V^{-1} m^2 s^{-1}, which means an 8% deviation from the tabulated value.

For the concretely used substances of our model system, the quantities $R_{E,A}$ and $R_{ET,B}$ show an interesting feature. As Figs. 7 and 8 illustrate, their values are hardly influenced by the presence of the admixture in the LE and in the TE. Beckers and Everaerts [5] considered this feature of R_E to be as a consequence of the validity of the ITP condition. However, from the ITP condition it only follows that the quantities R_E and R_{ET} are equal to the ratio of the effective mobilities of the respective pair (see eqns. 28 and 29). Therefore, for uni–univalent electrolytes it can be expected that the quantities R_E and R_{ET} will not be dependent on the presence of the admixture in the LE and the TE if any of the following conditions is fulfilled: (a) the pH of the LE is maintained at a constant value; (b) the effective mobilities of both members of the respective pair do not depend on pH (*e.g.*, it holds for the chloride–formate pair, where HCl is a strong acid and HCOOH is fully dissociated at the pH of the LE); (c) the dependence of the effective mobilities on pH is roughly the same

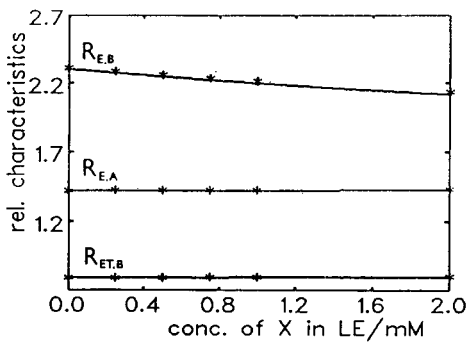

Fig. 7. Calculated (lines) and experimental (asterisks) relationships between the relative characteristics $R_{E,A}$, $R_{E,B}$ and $R_{ET,B}$ and the concentration of the admixture in the LE. The concentration of the admixture in the TE is zero.

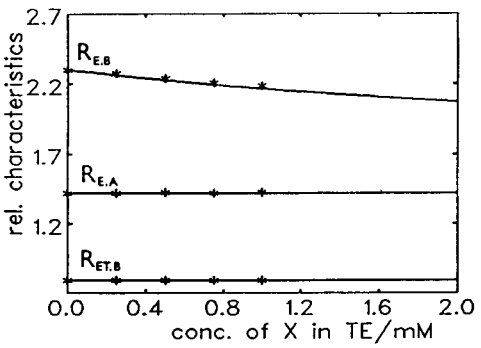

Fig. 8. Calculated (lines) and experimental (asterisks) relationships between the relative characteristics $R_{E,A}$, $R_{E,B}$ and $R_{ET,B}$ and the concentration of the admixture in the TE. The concentration of the admixture in the LE is zero.

for both components (*e.g.*, glutamic and propionic acid, which have similar p*K* values).

The above-mentioned consideration results in an important conclusion. If the LE and the TE can be chosen or prepared in such a way that some of the given demands are fulfilled, the limiting mobilities of samples can be determined without a knowledge of the concentrations of the admixture in the LE and the TE. This is also demonstrated by the results given in Table IV.

CONCLUSIONS

Isotachophoretic migration in systems with an admixture in the background electrolytes has been described. The approach for the determination of the limiting mobilities of separated compounds from experimental data affected by presence of the admixture was introduced. It was shown the attention must be paid to such separated compounds which have effective mobilities lower than that of the admixture. For evaluation of these compounds it is necessary to use the newly established experimental characteristic R_{ET}.

ITP anionic separation at pH > 7, when carbonate anions are an unremovable admixture, is a typical situation when this effect must be considered. The presented mathematical model for uni–univalent electrolytes can be applied to this problem only up to pH 8.5. In forthcoming work this model will be extended to polyvalent electrolytes and used at higher pH for the

accurate determination of anionic limiting mobilities of amino acids and peptides.

REFERENCES

1 P.J. Svendsen and C. Schafer-Nielsen, in B.J. Radola (Editor), *Electrophoresis '79*, Walter de Gruyter, Berlin, 1980, pp. 265–274.
2 C. Schafer-Nielsen, P.J. Svendsen and C. Rose, *J. Biochem. Biophys. Methods*, 3 (1980) 97.
3 C. Schafer-Nielsen and P.J. Svendsen, in B.J. Radola (Editor), *Electrophoresis '79*, Walter de Gruyter, Berlin, 1980, pp. 275–286.
4 C. Schafer-Nielsen and P.J. Svendsen, *Anal. Biochem.*, 114 (1981) 241.
5 J.L. Beckers and F.M. Everaerts, *J. Chromatogr.*, 508 (1990) 3.
6 J.L. Beckers and F.M. Everaerts, *J. Chromatogr.*, 508 (1990) 19.
7 P. Gebauer, L. Křivánková and P. Boček, *J. Chromatogr.*, 470 (1989) 3.
8 F.M. Everaerts, J.L. Bekkers and Th.P.E.M. Verheggen, *Isotachophoresis— Theory, Instrumentation and Applications*, Elsevier, Amsterdam, 1976.
9 Z. Fidler, V. Fidler and J. Vacík, *J. Chromatogr.*, 320 (1985) 175.
10 Th.P.E.M. Verheggen, J.C. Reijenga and F.M. Everaerts, *J. Chromatogr.*, 260 (1983) 471.
11 T. Hirokawa, T. Taka, Y. Yokota and Y. Kiso, *J. Chromatogr.*, 555 (1991) 247.
12 B. Gaš, J. Vacík and I. Zelenský, *J. Chromatogr.*, 545 (1991) 225.
13 L. Onsager and R.M. Fuoss, *J. Phys. Chem.*, 36 (1932) 2689.
14 A. Ralston, *A First Course in Numerical Methods*, McGraw-Hill, New York, 1965.
15 B. Gaš, J. Zuska and J. Vacík, *J. Chromatogr.*, 470 (1989) 69.
16 Y. Kiso and T. Hirokawa, *Chem. Lett.*, (1979) 891.

Journal of Chromatography, 648 (1993) 245–250
Elsevier Science Publishers B.V., Amsterdam

CHROM. 25 371

Capillary zone electrophoresis with time-resolved fluorescence detection using a diode-pumped solid-state laser

Karen J. Miller and Fred E. Lytle*

Department of Chemistry, 1393 Brown Laboratories, Purdue University, West Lafayette, IN 47907-1393 (USA)

(First received May 4th, 1993; revised manuscript received June 17th, 1993)

ABSTRACT

A capillary electrophoresis system with time-resolved fluorescence detection was developed using a diode-pumped solid-state laser. The laser provides 2.5-ns pulses at 349 nm with kHz repetition rates, and the Gaussian-shaped beam can easily be focused to the dimensions of a capillary. The short pulse width makes it possible to achieve nanosecond resolution and time-filtered detection. With this approach, the total signal from one injection can be collected and digitally processed to yield simultaneously "two-channel" data. Instrument capability is demonstrated by resolving short-lived fluorescent interferences in biological sample matrixes from long-lived fluorophores.

INTRODUCTION

Due to high separation efficiency and low sample volume requirements, capillary zone electrophoresis (CZE) has become an established analytical tool in the decade since its introduction [1]. Among the many detection methods used in CZE, laser-induced fluorescence (LIF) has achieved some of the best detection levels. As examples, Yeung *et al.* [2] recently demonstrated a value of 3 p*M* for fluorescein, Wu and Dovichi [3] reported a value of 1.3 p*M* fluorescein isothiocyanate-labeled arginine, and Chen *et al.* [4] constructed a linear calibration curve down to 64 p*M* tetramethylrhodamine isothiocyanate. Additionally, the excellent detectivity of LIF has been used to study the chemical content of individual cells [5].

Attaining low detection limits in capillaries with diameter of 100 μm and smaller presents some unique challenges. It is necessary to not only maximize the collection of the desired signal, but to concomitantly minimize unwanted radiation. Scatter from capillary walls is potentially the largest source of interference. In CZE instruments with LIF detection, the wavelength selection optics are most often comprised of spectral filters to maximize the fluorescence collection efficiency. While highly efficient, spectral filters are often incapable of fully rejecting light at the laser wavelength. As a result, much of the optical design of LIF detectors in CZE systems is geared toward discrimination against scatter. To enhance the performance of spectral filters, a wide variety of spatial filtering or isolation techniques have been used. Sheath-flow cuvettes [3,4] can be used for post-capillary detection and serve to distance the walls of the detection cell from the analyte. Yeung *et al.* [2] place the capillary at 20° with respect to the laser beam to reduce specular reflections. The capillary can also be placed at Brewster's angle to reduce scatter produced at the air–capillary

* Corresponding author.

0021-9673/93/$06.00

interface [6]. Judicious choice of capillary inner and outer diameters may also be important [7].

In addition to spectral and spatial filtering, it has been observed that temporal resolution could provide a third approach to the reduction of background signal in CZE [3,8]. Indeed, time-resolved fluorescence detection has been applied to HPLC for over a decade [9–17]. This strategy has been used to discriminate against background signals [9–12,15–17]. Additionally, the lifetime of the eluent has been employed as an aid to identify peaks [10,12–15]. All but one of the instruments were constructed with either a nitrogen laser or a nitrogen-pumped dye laser. Ref. 17 used a phase fluorometer based on a xenon arc lamp.

A significant difficulty in adapting temporal resolution of CZE has been the lack of pulsed lasers that are both easily focused and user-friendly. None of the sources used in the liquid chromatography studies fit these criteria. Recently a prototype diode-pumped, frequency-tripled, Q-switched neodymium doped yttrium lithium fluoride (Nd:YLF) laser has been developed [18]. This device produces 2.5-ns pulses at 349 nm. The Gaussian-shaped beam (TEM_{00}) can easily be focused to the dimensions of a capillary. The solid-state technology makes operation as simple as turning a key, and the diode provides thousands of hours of use without maintenance. The repetition rate of the laser can be adjusted from 200 Hz to 3 KHz with a maximum average power of 1.9 mW occurring at 2 kHz.

A second limitation to the liquid chromatographic detectors was the universal use of a gated integrator, be it a boxcar integrator of sampling oscilloscope. A much more flexible approach would employ a transient recorder, since it permits software data processing [19]. Examples of possible processing software modules are those emulating oscilloscope presentation, boxcar integration, and photon counting. Additionally, the same data can be reprocessed using an alternative emulation if the first choice does not provide the needed information. An ideal match to the above mentioned ND:YLF laser is a commercially available digital oscilloscope capable of capturing waveforms at 1 Gsample/s and averaging at repetition rates as high as 8 kHz.

In this paper we demonstrate the use of time-resolved fluorescence detection for CZE using the Nd:YLF laser–digital oscilloscope combination. Two thousand fluorescence decays are averaged with the oscilloscope and transferred, via an IEEE-488 bus, to a personal computer. Software data processing permits the construction of two electropherograms from two independently adjustable integration apertures (temporal filters). Performance of the instrument is demonstrated by injection of several biochemically related samples where short-lived interferences are separated from long-lived analytes.

EXPERIMENTAL

Materials

4-Methoxy-β-naphthylamine (4-MBNA) and *l*-isoleucine were obtained from Sigma (St. Louis, MO, USA). 2-Dimethylaminonaphthalene-5-sulfonyl chloride (2,5-Dns-Cl) was obtained from Molecular Probes (Eugene, OR, USA) and used without purification. The supernatant (10 000 *g*) from *E. coli* strain BL21 homogenate was donated by Cheng Chang Wang (Purdue University). Human urine was obtained from a healthy male donor. The *E. coli* supernatant and urine were diluted as needed in the electrophoresis buffer.

The isoleucine was derivatized with 2,5-Dns-Cl using conditions similar to those by Tapuhi *et al.* [20] for the dansylation of amino acids. The 2,5-Dns-Cl solution was prepared to 0.5 m*M* in acetonitrile. Isoleucine was dissolved in 40 m*M* $LiCO_3$ adjusted to pH 9.5 with HCl. The isoleucine concentration was 5 m*M*. An aliquot of 200 μl of the 2,5-Dns-Cl solution was added to 200 μl of the isoleucine solution. The reaction mixture was agitated for 2 min and incubated for 1 h protected from room light. No reaction terminator was used. The sample contained detectable amounts of 2 fluorescent impurities, believed to be 2,5-Dns-OH and 2,5-Dns-NH_2 [20]. The large excess of amino acid used in the derivatization was found to reduce the formation of the 2,5-Dns-OH impurity.

CZE instrumentation

The laser, optics and capillary were placed in a plexiglass box painted flat black on the interior. The door of the box was interlocked to the high-voltage power supply. The box protected the collection optics from room light and protected the user from the high voltage. The highly compact ($30 \times 30 \times 14$ cm) laser was placed in a lower compartment of the plexiglass box below the optics with the laser power supply placed outside the box. The laser repetition rate was set to 2 kHz. The laser is described in the Introduction section and in ref. 18. Fig. 1 shows a block diagram of the instrument. Ultraviolet mirrors were used to direct the beam to a quartz 1.6-mm focal length plano convex lens. The lens focused the laser beam into the capillary. Fluorescence was collected 90° from the excitation beam using a 20× (0.40 numerical aperture) microscope objective. Sample fluorescence was isolated from scatter using an iris, a Corion (Holliston, MA, USA) 450-nm bandpass 40-nm bandwidth interference filter and a Schott (Duryea, PA, USA) KV 399-nm cut-on filter.

The fluorescence signal was detected with a Burle (Lancaster, PA, USA) 931A photomultiplier wired for fast response [21] and biased at −1200 V. A trigger signal was generated by using a quartz window to direct *ca.* 4% of the laser beam to a photodiode. The photomultiplier anode current was monitored by an Analytek (Sunnyvale, CA, USA) Series 2000B digital oscilloscope operated at 1 Gsample/s. Two thousand fluorescence decay waveforms of 200 points each were averaged by the oscilloscope. The averaged waveform was transferred to an IBM PS/2 via an IEEE-488 interface card. A program was written in Microsoft Quick-C to collect and process each averaged waveform.

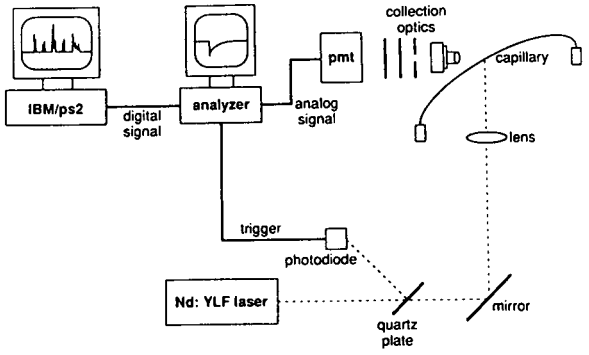

Fig. 1. Block diagram of CZE instrument. Collection optics are described in text. pmt = Photomultiplier tube.

The digitized points from each averaged waveform within the given user-specified integration apertures were summed. The successive sums were saved in an output file along with the elapsed time to create two electropherograms. The successive sums were also plotted to the screen in real time in order to view the peaks as they eluted.

Potential across the capillary was generated using a Glassman (Whitehouse Station, NJ, USA) Series EL high-voltage power supply. The power supply was modified to include the interlock. Polyimide-coated fused-silica capillaries (360 μm O.D. × 75 μm I.D.) were purchased from Polymicro Technologies (Phoenix, AZ, USA). Capillaries were cleaned prior to use by the procedure described by Yeung *et al.* [2].

CZE conditions

A 60-cm capillary was used (50 cm, injection end to detector.) The electrophoresis buffer was 10 m*M* pH 7 sodium phosphate buffer. The electrophoresis potential was 250 V/cm. Samples were injected by raising the sample vial 10 cm above the grounded reservoir for 10 s.

RESULTS AND DISCUSSION

Several difficulties associated with using pulsed lasers in CZE have been discussed in earlier papers [2,3]. Specific problems mentioned are poor spatial quality, fluorescence saturation, photodegradation of the sample, capillary damage, and poor intensity stability. The diode-driven Nd:YLF laser used in this study avoids all but one of these problems. The Gaussian-shaped beam profile (TEM_{00}) easily focusses to a spot size smaller than a 50 μm I.D. capillary. The fluorescent molecules, 4-MBNA and 2,5-Dns-isoleucine, did not show any measurable saturation or photolysis on the chromatographic time scale. This fact was obtained by observing that the fluorescence intensity is proportional to average power as the repetition rate is varied.

Because of the low Joules per pulse, capillary damage has never been observed. Intensity stability has been a significant problem with the prototype Nd:YLF laser. Pulse-to-pulse power variation is high at 18% relative standard deviation. However, when 1000 pulses are averaged, the value is reduced to 1.96%.

Fluorescence decays for the buffer (background signal) and 4-MBNA within the capillary are shown in Fig. 2. The data shown are the average of 2000 waveforms collected at 2 kHz. The blank has a full width at half maximum (FWHM) of 8 ns. This seemingly large value is caused by convolution of the laser pulse, photomultiplier impulse response, oscilloscope rise-time and the fluorescence decays of the capillary and buffer impurities. Due to the width of the blank, fluorophores with lifetimes greater than 16 ns are best suited for quantitation by temporal resolution. Note the lack of radio-frequency noise in the decays, which is an attribute of the low voltages used to drive all laser components.

4-MBNA is a fluorophore commonly used to assay aminopeptidase enzymes. It has an absorbance that is well-matched to the laser ($\lambda_{max} = 338$ nm) but with a marginal molar absorptivity (1060 l cm^{-1} mol^{-1} at 349 nm). The compound is ideal for time-resolved, fluorescence-based aminopeptidase assays primary for its long lifetime (26 ns), and because it is commercially available both as a pure compound and conjugated with several

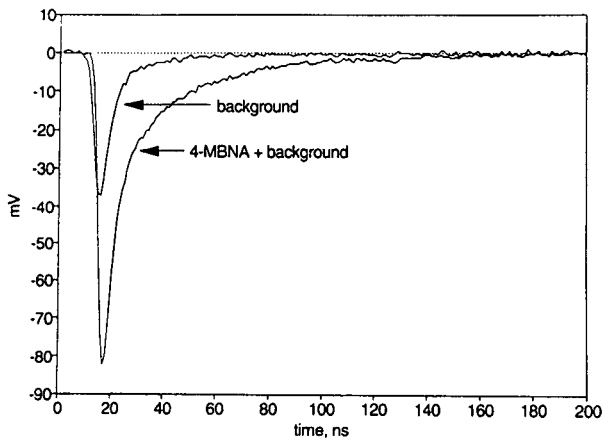

Fig. 2. Fluorescence decay waveforms for 10^{-7} *M* 4-MBNA and the background, collected from within capillary.

amino acids. The CZE detection limit ($S/N = 3$) obtained for 4-MBNA was 10^{-9} *M*, with 1 s of averaging at 2 kHz.

2,5-Dns-Cl, an isomer of the more common reagent dansyl chloride (5-dimethylaminonaphthalene-1-sulfonyl chloride), can be used to assay for amino acids. Conjugates formed with this reagent also have long lifetimes, *e.g.* 24 ns for isoleucine. The absorbance maximum for the isoleucine conjugate ($\lambda_{max} = 359$) is also well matched to the Nd:YLF output. This conjugate also has a low molar absorptivity (3100 l cm^{-1} mol^{-1} at 349 nm). The CZE detection limit obtained for 2,5-Dns-Cl was comparable to that for 4-MBNA. The low purity of the preparation precludes giving a more definitive value.

The poorer detection limits reported above, as compared to the picomolar values mentioned earlier, is attributed almost entirely to the smaller molar absorptivities. Fluorescein, fluorescein isothiocyanate and tetramethylrhodamine isothiocyanate have absorptivities of 90 000 [22], 76 000 [22] and 85 000 [4] l cm^{-1} mol^{-1}, respectively. Unfortunately, these compounds cannot be successfully employed in measurements that involve temporal solution because of short lifetimes at a pH of *ca.* 7, *i.e.* 4.65 ns [23], 3.5 ns [24], and 2.5 ns [24], respectively.

The major advantage of time-resolved detection is the ability to separate short-lived from long-lived components. Biological samples have considerable short-lived fluorescence caused by the native emission from aromatic moieties. The examples used in this feasibility study are urine and *E. coli* supernatant. Fig. 3 shows two electropherograms of a dilute urine sample. Both were simultaneously generated from the same injection using different temporal delays from the excitation maximum, and different integration windows. In the lower electropherogram, generated using a 60-ns time delay, all of the peaks are considerably smaller in amplitude, indicating most of the native fluorescence from the urine has decayed after 60 ns. In Fig. 4 the urine sample has been spiked with $5 \cdot 10^{-7}$ *M* 2,5-Dns-isoleucine. In the upper electropherogram it can be seen that the 2,5-Dns-isoleucine is poorly resolved from one of the components of the urine sample. In the lower electrophero-

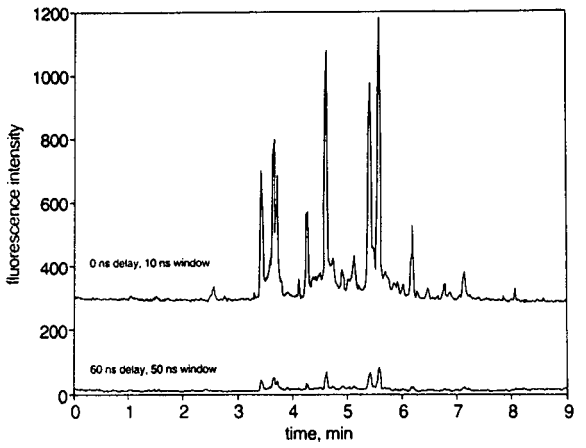

Fig. 3. Electropherograms for human urine sample diluted 1:200. Data were collected simultaneously using different integration delays and windows. Data have been offset for clarity.

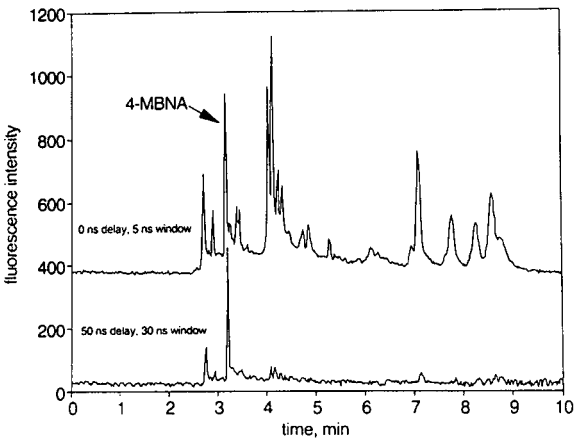

Fig. 5. Electropherograms for *E. coli* supernatant diluted 1:50. Sample was spiked with $3 \cdot 10^{-7}$ *M* 4-MBNA. Data were collected simultaneously using different integration delays and windows. Data have been offset for clarity

gram, collected with a 60-ns time delay, the 2,5-Dns-isoleucine peak has been attenuated less than the native fluorescence peaks. The signal from the interfering peak has been reduced to the extent that it is no longer visible. Similarly, in Fig. 5, a sample of *E. coli* supernatant has been spiked with $3 \cdot 10^{-7}$ *M* 4-MBNA. In the upper electropherogram, collected with no time-delay and a 5-ns integration window, many sample components exhibit native fluorescence, while in the lower electropherogram, the native fluorescence of the sample has been greatly reduced and the 4-MBNA peak is the most prominent feature.

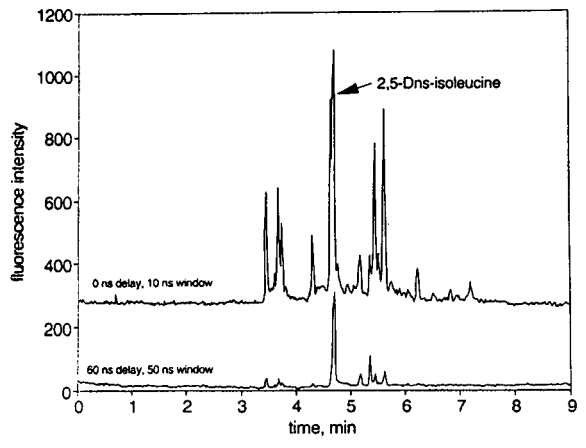

Fig. 4. Electropherograms for human urine sample diluted 1:200 spiked with $5 \cdot 10^{-7}$ *M* 2,5-Dns-isoleucine. Data were collected simultaneously using different integration delays and windows. Data have been offset for clarity.

Future work with this instrument will involve enzyme assays in biological samples, similar to a CZE-based, absorptiometric approach already reported [25]. Our group has a long-standing interest in the identification of bacterial pathogens using aminopeptidase profiling [26,27]. The profile is obtained by measuring enzymatic activity for a suite of amino acids by the hydrolysis of their non-fluorescent, 4-MBNA substrates to produce free 4-MBNA. Converting the published macroscopic analyses into one utilizing CZE should permit identification of fewer than 1000 cells.

The present instrument suffers in two areas. The 18% relative standard deviation associated with the pulse energy appears to be characteristic of the yttrium lithium fluoride (YLF) host crystal. A second generation prototype utilizing a yttrium vanadate host crystal has been built by Continuum. The result was a 1.5% relative standard deviation in the pulse fluctions. Any commercialized version of the diode-driven laser will employ the yttrium vanadate host. This change alone will produce lower detection limits since less noise will need to be averaged. The second change involves switching to OS/2 version 2.0 which permits 32-bit addresses in the C-language. With the attendant ability to com-

pile large data arrays, the entire ensemble of decays transferred to the computer can be stored in memory. Once in memory, post-processing can be used to fine-tune window positions and widths. Additionally, selected data could be processed by non-linear curve fitting routines to deconvolve overlapped peaks. Our ultimate goal is to use the SCSI port of the Analytek digitizer to transfer each decay in real-time to the computer. This will permit much more sophisticated data processing options such as photon counting [19] and computing the fluorescence lifetime of each peak as it elutes.

Future work will also focus on chemically reducing the lower limit of detection (LLD). To some extent this involves conflicting demands upon the fluorescent molecule, *i.e.* long lifetimes are ordinarily produced by transitions with low molar absorptivities. In an attempt to circumvent the problem we are currently searching for classes of molecules that have large molar absorptivities associated with the second, or higher, excited singlet states. This change in strategy should produce a much greater sensitivity combined with a lifetime sufficiently long for temporal rejection of the background interferences. Since the laser wavelength is fixed, an exhaustive examination of many compounds is anticipated.

ACKNOWLEDGEMENTS

The authors gratefully acknowledge Continuum, for the generous loan of the Nd:YLF laser. The authors also thank Dr. Fred E. Regnier for his helpful advice. Cheng Chang Wang's donation of the *E. coli* supernatant is greatly appreciated.

This work was supported by the national Science Foundation Grant CHE-8822878.

REFERENCES

1 J.W. Jorgenson and K.D. Lukacs, *Science*, 222 (1983) 266.
2 E.S. Yeung, P. Wang, W. Li and R.W. Giese, *J. Chromatogr.*, 608 (1992) 73.
3 S. Wu and N.J. Dovichi, *J. Chromatogr.*, 480 (1989) 141.
4 D.Y. Chen, H.P. Swerdlow, H.R. Harke, J.Z. Zhang and N.J. Dovichi, *J. Chromatogr.*, 559 (1991) 237.
5 T.T. Lee and E.S. Yeung, *Anal. Chem.*, 64 (1992) 3045.
6 W.G. Kuhr and E.S. Yeung, *Anal. Chem.*, 60 (1988) 1832.
7 F. Maystre and A.E. Bruno, *Anal. Chem.*, 64 (1992) 2885.
8 L.N. Amankwa, M. Albin and W.G. Kuhr, *Trends Anal. Chem.*, 11(3) (1992) 114.
9 J.H. Richardson, K.M. Larson, G.R. Haugen, D.C. Johnson and J.E. Clarkson, *Anal. Chim. Acta*, 116 (1980) 407.
10 T. Imasaka, K. Ishibashi and N. Ishibashi, *Anal. Chim. Acta*, 142 (1982) 1.
11 N. Furuta and A. Otsuki, *Anal. Chem.*, 55 (1983) 2407.
12 K. Ishibashi, T. Imasaka and N. Ishibashi, *Anal. Chim. Acta*, 173 (1985) 165.
13 S.D. Teet, N. Laurendeau, D.J. Desilets and F.E. Lytle, *Combust. Sci. Technol.*, 52 (1987) 207.
14 D.J. Desilets, P.T. Kissinger and F.E. Lytle, *Anal. Chem.*, 59 (1987) 1830.
15 Y. Kawabata, K. Sauda, T. Imasaka and N. Ishibashi, *Anal. Chim. Acta*, 208 (1988) 255.
16 K. Tsunoda, A. Nomura, J. Yamada and S. Nishi, *Anal. Chim. Acta*, 229 (1990) 3.
17 W.T. Cobb and L.B. McGown, *Anal. Chem.*, 62 (1990) 186.
18 F. Basile, A. Cardamone, K.D. Grinstead, Jr., K.J. Miller, F.E. Lytle, A Caprara, C.D. Clark and J. Heritier, *Appl. Spectrosc.*, 47 (1993) 207.
19 T.L. Campos and F.E. Lytle, *Appl. Spectrosc.*, 46 (1992) 1859.
20 Y. Tapuhi, D.E. Schmidt, W. Lindner and B.L. Karger, *Anal. Biochem.*, 115 (1981) 123.
21 J.M. Harris, F.E. Lytle and T.C. McCain, *Anal. Chem.*, 48 (1976) 2095.
22 R.P. Haugland, *Molecular Probes: Handbook of Fluorescent Probes and Research Chemicals*, Molecular Probes, Eugene, OR, 1992, pp. 22, 85.
23 H. Elmgren, *J. Polym. Sci.: Polym. Lett. Ed.*, 18 (1980) 815.
24 K. Chang and R.K. Forcé, *Appl. Spectrosc.*, 47 (1993) 24.
25 J. Bao and F.E. Regnier, *J. Chromatogr.*, 608 (1992) 217.
26 J.T. Coburn, F.E. Lytle and D.M. Huber, *Anal. Chem.*, 57 (1985) 1669.
27 K.D. Hughes, F.E. Lytle and D.M. Huber, *Anal. Chem.*, 61 (1989) 1656.

Journal of Chromatography, 648 (1993) 251–256
Elsevier Science Publishers B.V., Amsterdam

CHROM. 25 265

Comparison of high-performance liquid chromatography and capillary electrophoresis in the analysis of somatostatin analogue peptides

M. Idei*, I. Mező, Zs. Vadász, A. Horváth, I. Teplán and Gy. Kéri

Semmelweis Medical School, First Department of Biochemistry and Joint Research Organization of Hungarian Academy of Sciences and Semmelweis Medical School, Peptide Research Group, Puskin u. 9, H-1088 Budapest (Hungary)

(First received December 29th, 1992; revised manuscript received May 4th, 1993)

ABSTRACT

HPLC and CE methods were developed for analysis of somatostatin analogue (S-analogue) peptides utilizing triethylammonium phosphate–organic solvent modifier solvents as the CE buffer and HPLC eluent. Acetonitrile, methanol, ethanol and 2-propanol were applied as organic modifiers. The applicability of HPLC and CE systems was evaluated and compared. Optimum conditions for the separation were determined for both methods. Retention (migration) time, elution order and selectivity can be influenced by modifying the composition of the eluent (buffer) with organic solvents not only in HPLC but also in CE. Although the HPLC system reacted to changes in the organic solvent concentration in a much more sensitive way than the CE system did (from the point of view of retention time), CE proved to be a more suitable method for separating the peptides investigated. Baseline separation could be achieved within 6–9 min by CE, a result which was impossible to achieve with HPLC working in the isocratic mode. In CE the effect of the alcohols on migration times proved to be opposite to that of acetonitrile. Whereas ACN decreased, the alcohols increased the migration times in a concentration-dependent way. The results suggest that CE can be applied very advantageously in peptide analysis. Its performance regarding selectivity, resolution, theoretical plate number, duration and cost is comparable or sometimes superior to that of HPLC.

INTRODUCTION

Capillary electrophoresis (CE) is becoming an increasingly important tool in the analysis of widespread range of molecules. High efficiency, versatility and speed of analysis are among the factors that have promoted the application of the method [1–5].

CE offers many opportunities in analysis, and the information obtainable by CE may complement that which can be obtained by various HPLC methods. Similarly to HPLC, the versatility of the separatory process (which is essential from the point of view of widespread applicability) is very important in CE also [5,6].

There are many parameters that can be used to effect separations and manipulate the selectivity in both CE and in RP-HPLC, including the capillary dimensions, chemical character of the wall of the capillary, buffer composition, ionic strength, pH, applied voltage, sample matrix, buffer additives (*e.g.*, organic solvents, ion-pairing reagents, surfactants) and derivatization in CE [7–19]. In RP-HPLC, separation and selectivity can be influenced by altering the buffer composition, ionic strength, pH, concentration and nature of the ion-pairing reagent, stationary phase and derivatization [20,21].

HPLC is a widely established method in the analysis of peptides, although CE is also of increasing importance for the reasons mentioned

* Corresponding author.

0021-9673/93/$06.00

above [8,9,11,22–24]. As a consequence, the analysis of peptides can be accomplished by either HPLC or CE in many instances.

Comparison of CE and HPLC methods, to decide which is the more advantageous in solving a given analytical task, can be made from several points of view, *e.g.*, resolution, selectivity, sensitivity, peak capacity, duration and cost of the analysis, solvent and chemical consumption of the methods can be compared.

In a previous paper [25] we reported a CE method applicable in the analysis of proprietary somatostatin analogue (S-analogue) peptides (synthesized in our laboratory) utilizing triethylammonium phosphate (TEAP)–organic solvent modifier [acetonitrile (ACN), methanol (MeOH), ethanol (EtOH) and 2-propanol (IPA)] mixtures as buffers. The effect of the organic solvents on the separation process was discussed.

In this work, an HPLC method was applied to the analysis of the same S-analogue peptides, in which the composition of the HPLC eluents was identical with that of the buffers applied in our previous CE analysis [25]. In this paper the results obtained by HPLC are reported together with a comparison of the applicability and advantages of the HPLC and CE systems in the analysis of peptides.

EXPERIMENTAL

Materials

Peptides were synthesized and characterized in our laboratory [25,26]. The structures of the peptides used are as follows:

S-218: D-Phe-Cys-Tyr-D-Trp-Lys-β-Ala-Cys-Thr-NH_2

S-220: D-Phg-Cys-Tyr-D-Trp-Lys-Val-Cys-Thr-NH_2

S-228: D-Phe-Cys-Tyr-D-Trp-Lys-Pro-Cys-Thr-NH_2

S-232: D-Phe-Cys-Tyr-D-Trp-Lys-Cys-Thr-NH_2

S-248: β-Asp(indolinyl)-Cys-Tyr-D-Trp-Lys-Val Cys-Thr-NH_2

S-250: D-Phe-Cys-Tyr-D-Trp-Lys-Leu-Cys-Thr-NH_2

where Phg = phenylglycyl.

Chemicals

HPLC-grade acetonitrile, methanol, ethanol and 2-propanol were purchased from Chemolab (Budapest, Hungary) and orthophosphoric acid and triethylamine from Fluka (Buchs, Switzerland). Water utilized to prepare solutions was treated with an Elgastat UHP water-purification system (Elga, Bucks., UK) to obtain deionized water, free from bacteria and organic contaminants.

Peptide samples at a concentration of 1 mg/ml in water were used both in CE and HPLC analyses.

HPLC analysis

The following conditions were used: flow-rate, 1.2 ml/min (BT 8100 pumps, BT 8300 System Controller; Biotronik, Maintal, Germany); detection, 215 nm; sensitivity, 0.32 on Biotronik BT 8200 UV–Vis detector; sample volume, 25 μl in a 10-μl loop (Rheodyne injector); column, Shandon (Astmoor, UK) ODS-Hypersil, 5 μm (250 × 4 mm I.D.); eluents: 0.083 *M* TEAP buffer (pH 2.25) mixed with different concentrations of ACN or MeOH (15, 20, 25, 30, 35, 40, 45 and 50%, v/v).

Capillary electrophoresis

Capillary electrophoretic analyses were performed with an ISCO (Lincoln, NE, USA) Model 3850 capillary electropherograph with the following conditions: capillary, uncoated silica (45 cm × 50 μm I.D.); detection, 215 nm; sensitivity, 0.02; rise time, 0.8 s; voltage, 30 kV; injection volume, 10 μl through a built-in splitter; splitting ratio, 1:1000; buffers, 0.083 *M* TEAP buffer (pH 2.25) modified with different organic solvents (ACN, MeOH, EtOH and IPA) at different concentrations (0, 5, 10, 15, 20, 25 and 30%, v/v).

Digital data collected from CE runs were stored and analysed with an ISCO Chem-Research controlling and data handling system. The data sampling rate was 8 s^{-1}. Four injections were made for each peptide sample at each buffer or eluent composition. HPLC data were collected and processed with a Biotronik C-R6A Chromatopac integrator with paper speed 1 mm/

min, attenuation 4, width 5, slope 2000 and minimum area 10 000.

RESULTS AND DISCUSSION

Results obtained in the CE analysis of S-analogue peptides [migration times (t_m) *versus* concentration of the organic modifiers in TEAP buffer] have been presented and discussed previously [25]. The migration time, elution order and selectivity can be influenced by modifying the composition of the electrophoretic buffer with organic solvents. Applying different organic solvents as modifiers, the elution order of the peptides can be changed in different ways. At a given concentration the effectiveness of the alcohol depends on its nature: the longer the carbon chain of the alcohol, the greater is the increase in the CE migration time of the peptide compared with that obtained with a buffer not containing any organic solvent. At the low pH applied the peptides migrated mainly owing to their electrophoretic mobility and the electroosmotic component of the net mobility was negligible [7,25].

Table I gives the retention times (t_r) of the S-analogue peptides obtained by HPLC as a function of the concentration of ACN and MeOH in TEAP.

The separation could be influenced in both HPLC (Table I) and CE [25] by changing the organic solvent content of the buffer (eluent).

According to well established knowledge regarding the relationship between t_r and solvent strength, the t_r values in HPLC decreased with increasing organic solvent content of the eluent using both ACN–TEAP and MeOH–TEAP buffers. However, in CE the effect of the alcohols on the t_m values proved to be opposite to that of ACN. Whereas ACN decreased, the alcohols increased the t_m values in a concentration-dependent way [25].

Fig. 1 shows the log t_r and log t_m values of S-218 peptide *versus* the percentage of ACN and MeOH in TEAP buffer. This is a representative plot; similar results were obtained for each peptide with both the ACN–TEAP and MeOH–TEAP buffers.

HPLC is more sensitive than CE to changes in the organic solvent content of the eluent. As Fig. 1 shows, the slopes of the lines for HPLC (solid symbols) are much higher than those of the lines for CE (open symbols) with both the ACN–TEAP and MeOH–TEAP buffers.

Although the t_m values obtained in CE could be manipulated in a less sensitive way than the t_r values obtained in HPLC by changing the composition of the buffers (eluents), CE proved

TABLE I

RETENTION TIMES OF THE S-ANALOGUE PEPTIDES

HPLC analysis performed with ACN–TEAP and MeOH–TEAP eluents (for parameters of the analysis and for eluent compositions, see Experimental). Standard deviations for parallel runs ($n = 4$) are not shown for clarity, but were less than 2%.

Modifier	Concentration (%, v/v)	Retention time (min)					
		S-218	S-220	S-228	S-232	S-248	S-250
ACN	15	13.44	11.70	20.62	13.58	48.52	34.25
	20	5.76	5.74	4.66	4.36	28.20	18.21
	25	2.93	3.21	2.96	2.74	7.13	5.84
	30	2.24	3.02	2.42	2.20	5.00	4.17
	35	2.14	2.19	2.15	2.09	3.51	2.39
MeOH	30	19.40	51.50	15.80	7.89	190.83	113.54
	35	13.01	32.27	11.07	6.40	106.01	55.01
	40	9.19	19.66	7.89	6.15	63.51	36.10
	45	4.78	7.76	4.43	3.81	17.92	12.19
	50	3.61	4.94	3.43	3.13	8.85	7.00

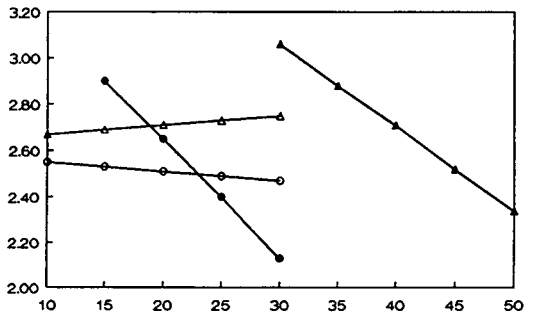

Fig. 1. Log t_r and log t_m values of S-analogue peptide 218 obtained by HPLC and CE analysis *versus* the percentage of ACN or MeOH in TEAP. Abscissa: concentration of ACN or MeOH in TEAP (%, v/v). Ordinate: log t_m and log t_r values. ● = Log t_r obtained by HPLC with ACN–TEAP system; ○ = log t_m obtained by CE with ACN–TEAP system; ▲ = log t_r obtained by HPLC with MeOH–TEAP system; △ = log t_m obtained by CE with MeOH–TEAP system. For data see Table I and ref. 25.

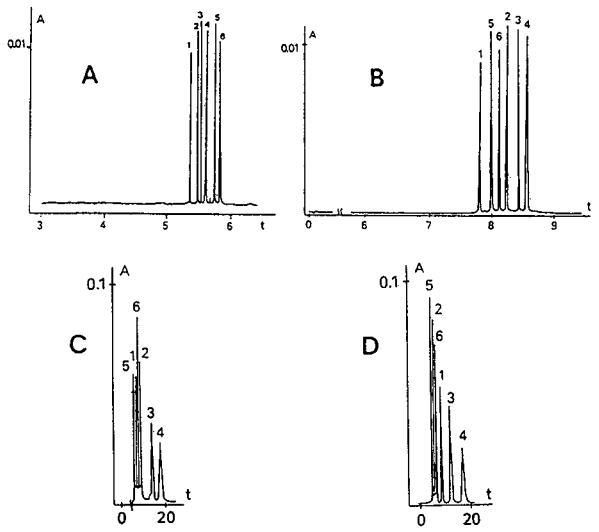

Fig. 2. (A) Electropherogram of the mixture of the six S-analogue peptides obtained with the ACN–TEAP system. Buffer composition: ACN–TEAP (13.2:86.8, v/v). For other parameters, see Experimental. Abscissa: migration time (min). Ordinate: absorbance at 215 nm. Peaks: 1 = S-220; 2 = S-228; 3 = S-250; 4 = S-248; 5 = S-232; 6 = S-218. (B) Electropherogram of the mixture of the six S-analogue peptides obtained with the MeOH–TEAP system. Buffer composition: MeOH–TEAP (9:91, v/v). Other details as in (A). (C) Chromatogram of the mixture of the six S-analogue peptides obtained with the ACN–TEAP system. Eluent composition: ACN–TEAP (23:77, v/v). Other details as in (A). (D) Chromatogram of the mixture of the six S-analogue peptides obtained with the MeOH–TEAP system. Eluent composition: MeOH–TEAP (46.5:53.5, v/v). Other details as in (A).

to be a more suitable method for separating the peptides investigated.

Fig. 2 shows the optimized separation of S-analogue peptides by CE with the ACN–TEAP (13.2:86.8, v/v) and MeOH–TEAP (9:91, v/v) systems and by HPLC with the ACN–TEAP (23:77, v/v) and MeOH–TEAP (46.5:53.5, v/v) systems. Optimization was performed by the simplex grid method [27]. Concentration detection limits based on the analyte peak heights and baseline noise level are 5 and 20 μg/ml for HPLC and CE, respectively.

Neither with the ACN–TEAP nor with the MeOH–TEAP buffers is there a direct relationship between the CE migration order and charge/mass ratio of the peptides investigated. For example, the two peptides with the highest charge/mass ratio (5 and 6 in Fig. 2) migrate with the longest migration times with the optimized TEAP–ACN buffer (the sequence of the peptides in decreasing order of charge/mass ratio is S-232 > S-218 > S-220 > S-228 > S-250 > S-248). Interestingly, the other four peptides migrate in decreasing order of their charge/mass ratio with the same buffer. Similarly, there is no direct relationship between the charge/mass ratio and migration order of the peptides with either the pure TEAP or the optimized MeOH–TEAP buffers.

Baseline separation of the S-analogue peptides could be achieved within 6–9 min by CE, a result which was impossible to achieve by HPLC working in the isocratic mode.

Peptides S-248 and S-250, containing highly hydrophobic moieties [Asp(indolinyl) and Leu moiety, respectively] in addition to the amino acid moieties common in all six peptides, eluted with the ACN–TEAP HPLC system with much higher t_r values than the other four peptides. Baseline separation of the peptide mixture by HPLC could be achieved only by gradient elution of 50 min duration. CE proved not to be sensitive to these hydrophobic moieties of the compounds and similar differences in migration times were not detected.

The net mobility of the analyte in CE is the

sum of the electrophoretic (u_{ep}) and electroosmotic (u_{eo}) mobilities:

$$u_{net} = u_{ep} + u_{eo}$$

$$u_{ep} = e/3 \cdot 10^7 z\eta\sqrt{C}$$

$$u_{eo} = D\zeta_{eo}/4\pi\eta$$

where e is the surface charge density of the analyte, Z the charge of the buffer ion, C the concentration of the buffer ion, η the viscosity of the buffer, D the dielectric constant of the buffer and ζ_{eo} the zeta potential of the capillary wall [7].

Changes in the viscosity and/or the ionic strength of the buffer result in changes in the electrophoretic and electroosmotic mobilities. The alcohols increase whereas ACN decreases the viscosity of the buffer [28,29]. This change in the viscosity could explain the opposite effect of the alcohols and ACN on the net mobilities and therefore on the migration times of the peptides. The higher the viscosity of the alcohol applied, the greater is the increase in the migration time caused at a given concentration.

However, not only the migration times but also the elution order of the peptides can be changed by changing the concentration of the organic solvent [25]. A simple increase or decrease in the viscosity and the ionic strength could only alter proportionately the migration times of each peptide, and could not change their order of elution and their migration times relative to each other.

There is a correlation between the effects of the organic modifiers and their dipole moments (indicating their ability to form associates). ACN decreases the migration times whereas the alcohols increase the migration times (the sequence of the solvents in decreasing order of their dipole moments is ACN > water > MeOH > EtOH > IPA). It cannot be ruled out that the modifiers can interact with the capillary wall and/or can form associates in the buffer.

In CE the effect of the organic solvents cannot be attributed only to the changes in properties of the buffer (viscosity, ionic strength and dipole moment). In addition, organic solvents are able to change the properties of the capillary wall (zeta potential, adsorption–desorption processes between the analyte and the capillary wall) and the properties of the analyte (Stokes radius, mass/charge ratio). These effects may result in changes in the electroosmotic and electrophoretic mobilities of the analyte.

CONCLUSIONS

As in HPLC (where it is a well known and widely applied practice), also in CE the utilization of organic solvents as (eluent) buffer modifiers gives the possibility of manipulating retention (migration) times and selectivity. Utilization of different organic solvents to modify the composition of the electrophoretic buffer in CE even gives the possibility of changing the migration times of the analytes in opposite directions. However, in contrast to HPLC, CE proved not to be sensitive to the hydrophobic moieties of the molecules investigated.

Our results suggest that CE can be applied very advantageously in peptide analysis. Its performance regarding selectivity, resolution, theoretical plate number, duration and cost of the analysis is comparable or sometimes can be superior to that of HPLC.

REFERENCES

1 F.E.P. Mikkers, F.M. Everaerts and T.P.E.M. Verheggen, *J. Chromatogr.*, 169 (1979) 11.
2 J.W. Jörgenson and K.D. Lukács, *Anal. Chem.*, 53 (1981) 1298.
3 S.J. Hjertén, *J. Chromatogr.*, 270 (1983) 1.
4 B.L. Karger, *Nature*, 339 (1989) 641.
5 I.S. Krull and J.R. Mazzeo, *Nature*, 357 (1992) 92.
6 A. Guttman, A. Paulus, A.S. Cohen, N. Grinberg and B.L. Karger, *J. Chromatogr.*, 448 (1988) 41.
7 H.J. Issaq, G.M. Janini, I.Z. Atamina and G.M. Muschik, *J. Liq. Chromatogr.*, 14 (1991) 817.
8 J.K. Towns and F.E. Regnier, *Anal. Chem.*, 63 (1991) 1126.
9 S.A. Swedberg, *Anal. Biochem.*, 185 (1991) 51.
10 J. Frenz, S.-L. Wu and W. Hancock, *J. Chromatogr.*, 480 (1991) 379.
11 M.V. Novotny, K.A. Cobb and J. Liu, *Electrophoresis*, 11 (1990) 735.
12 J.K. Towns and F.E. Regnier, *J. Chromatogr.*, 516 (1990) 69.
13 B.J. Herren, S.G. Shafer, J.v. Alstine, J.M. Harris and R.S. Snyder, *J. Colloid Interface Sci.*, 115 (1987) 46.

14 J.W. Jörgenson and K.D. Lukács, *J. Chromatogr.*, 218 (1981) 209.
15 M.A. Firestone, J.P. Maichaud, R.N. Carter and W. Thorman, *J. Chromatogr.*, 407 (1987) 363.
16 Z. Deyl, V. Rohacek and M. Adam, *J. Chromatogr.*, 480 (1989) 371.
17 H.J. Issaq, G.M. Janini, I.Z. Atamina, G.M. Muschik and J. Lukszo, *J. Liq. Chromatogr.*, 15 (1992) 1129.
18 Q. Wu, H.A. Claessens and C.A. Cramers, *Chromatographia*, 33 (1992) 303.
19 M.E. Schwartz, *J. Liq. Chromatogr.*, 14 (1991) 923.
20 L.R. Snyder and J.J. Kirkland, *Introduction to Modern Liquid Chromatography*, Wiley, New York, 2nd ed., 1979.
21 W.S. Hancock, *Handbook of HPLC for the Separation of Amino Acids, Peptides and Proteins*, CRC Press, Boca Raton, FL, 1985.
22 A. Pessi, E. Bianchi, L. Chiappinelli, A. Nardi and S. Fanali, *J. Chromatogr.*, 557 (1991) 307.
23 J. Frenz, S. Wu and W.S. Hancock, *J. Chromatogr.*, 480 (1989) 379.
24 P.D. Grossman, J.C. Colburn, H.H. Lauer, R.G. Nielsen, R.M. Riggin, G.S. Sittampalam and E.C. Rickard, *Anal. Chem.*, 61 (1989) 1986.
25 M. Idei, I. Mező, Zs. Vadász, A. Horváth, I. Teplán and Gy. Kéri, *J. Liq. Chromatogr.*, 15 (1992) 3181.
26 Gy. Kéri, I. Mező, A. Horváth, Zs. Vadász, Á. Balogh, M. Idei, T. Vántus, I. Teplán, M. Mák, M. Idei, T. Vántus, I. Teplán, M. Mák, J. Horváth, K. Pál and O. Csuka, *Biochem. Biophys. Res. Commun.*, 191 (1993) 681.
27 J. Holderith, T. Tóth and A. Váradi, *J. Chromatogr.*, 119 (1976) 215.
28 J. Timmermann, *The Physico-Chemical Constants of Binary Systems in Concentrated Solutions*, Vol. IV, Interscience, London, 1960.
29 C.D. Hodgman (Editor), *Handbook of Chemistry and Physics*, Chemical Rubber Publishing, Cleveland, OH, 33rd ed., 1951–52.

Journal of Chromatography, 648 (1993) 257–265
Elsevier Science Publishers B.V., Amsterdam

CHROM. 25 388

Separation of neuropeptide Y diastereomers by high-performance liquid chromatography and capillary zone electrophoresis

Dean A. Kirby, Charleen L. Miller and Jean E. Rivier*

Clayton Foundation Laboratories for Peptide Biology, The Salk Institute for Biological Studies, 10010 North Torrey Pines Road, La Jolla, CA 92037 (USA)

(Received April 29th, 1993)

ABSTRACT

Separation of analogues of neuropeptide Y (NPY) in which a single D-amino acid replaced the corresponding naturally occurring residue was performed by chromatographic techniques to ensure the quality of the synthetic peptides to be used for structural and biological studies. Of the 35 compounds, 28 were easily separated ($\alpha = 1.02–2.76$) from native NPY by standard reversed-phase high-performance chromatography (RP-HPLC) methods using a Vydac C_{18} column and a gradient buffer system developed in our laboratory comprised of triethylammonium phosphate (TEAP) at pH 2.25 and acetonitrile at 40°C. The identical diastereomers could be separated on the same solid support and by using 0.1% trifluoroacetic acid (TFA) as the mobile phase modifier, however separation factors were smaller and retention times were longer. Three of the remaining seven unresolved analogues were separated ($\alpha = 1.02–1.96$) by changing the solid-phase support to Vydac diphenyl derivatized silica and a buffer system consisting of 0.1% TFA and acetonitrile. Of the four remaining unresolved analogues, only two could be separated by capillary zone electrophoresis (CZE) in 0.1 *M* sodium phosphate at pH 2.5, but all four were finally resolved by changing the electrophoretic buffer to 0.1 *M* TEAP buffer at pH 2.5. Migration times of the diastereomers differed by 0.2–2.0 min from that of the natural NPY. In addition to confirming the uniqueness of each isomer, this investigation demonstrated the expansive utility and high efficiency of the TEAP buffer system for both RP-HPLC and CZE as well as the difference in selectivity produced by the TEAP and TFA buffers in RP-HPLC. The conditions described here have broad applications for the analysis and preparative separation of synthetic and native peptides.

INTRODUCTION

Neuropeptide Y (**I**) is a 36-residue, C-terminally amidated polypeptide. It is widely distributed in the central and peripheral nervous systems of many species of mammals and fish. It has been implicated in the pathology of many disease states including hypertension and obesity [1,2]. As part of a structure-activity relationships investigation, we synthesized the entire series of D-isomer substitutions to explore the role of backbone modifications at each position in the sequence [3].

1 5

Tyr–Pro–Ser–Lys–Pro–Asp–Asn–Pro–Gly–

10 15

Glu–Asp–Ala–Pro–Ala–Glu–Asp–Leu–Ala–

20 25

Arg–Tyr–Tyr–Ser–Ala–Leu–Arg–His–Tyr–

30 35

Ile–Asn–Leu–Ile–Thr–Arg–Gln–Arg–Tyr–NH_2

I

* Corresponding author.

0021-9673/93/$06.00

The use of racemic mixtures of amino acids in peptide synthesis or epimerization at any one of the many amino acid α carbons during synthesis could lead to the undesired incorporation of D-isomer impurities. Such impurities represent one of the greatest challenges to chromatographic detection systems, since they differ by only a single inversion of a peptide backbone α carbon. Analogues for our studies were assembled by standard solid-phase peptide synthesis (SPPS) methodology, which virtually eliminates the occurrence of epimerization, and were subsequently purified by preparative reversed-phase high performance liquid chromatography (RP-HPLC). Standard characterization of synthetic peptides includes assessment of purity by RP-HPLC, amino acid analysis and determination of molecular mass by mass spectroscopy. Although these three methods allow (in one way or another) the detection of the most common side products in peptide chemistry (adducts and truncations), the latter two techniques will not distinguish diastereomers and thus could not detect racemic contamination that could lead to ambiguous biological results. In this study of a series of NPY analogues we have confirmed both the uniqueness of each derivative differing only by the inversion of a single chiral center and the resolution power of RP-HPLC and that of capillary zone electrophoresis (CZE), especially when combined with the use of the trietylammonium phosphate (TEAP) separation buffer [4].

EXPERIMENTAL

All reagents and solvents were of analytical grade (Aldrich, Milwaukee, WI, USA; Fisher Scientific, Springfield, NJ, USA) and were used without further purification except triofluoroacetic acid (TFA) (Halocarbon, Hackensack, NJ, USA) and triethylamine (TEA) (Aldrich), which were reagent grade and used without further purification for syntheses but were distilled to constant boiling point for use in the chromatographic buffers.

Peptide synthesis

All peptides were assembled using standard SPPS techniques on *p*-methylbenzhydrylamine (MBHA) resin, as previously described, [5,6]. Briefly, *tert.*-butyloxycarbonyl (BOC) was used for N-terminal protection and deblocked with TFA in the presence of ethanedithiol (EDT). Most couplings employed 1,3-diisopropylcarbodiimide (DIC) as primary coupling reagent; more difficult cycles required the use of benzotriazol-1-yl-oxytris (dimethylamino)phosphonium hexafluorophosphate (BOP) in N-methylpyrrolidone (NMP) or dimethylformamide (DMF) in the presence of an excess of diisopropylethylamine (DIPEA). Couplings were generally carried out for 1 h, completion of the couplings was monitored by qualitative Kaiser test [7]. Coupling steps were repeated as necessary. After TFA deprotection, resin washes included 2-propanol (containing 1% EDT), triethylamine [10% in dichloromethane (DCM)] for neutralization, MeOH and DCM. The protected peptide was cleaved from the resin with anhydrous HF in the presence of 10% anisole at 0°C for 90 min. Volatiles were removed *in vacuo*. The crude peptides were precipitated with anhydrous ethyl ether, filtered to remove ether soluble non-peptide materials and extracted in water. After lyophilization, crude peptides were purified by preparative RP-HPLC [8,9] on a Waters DeltaPrep LC 3000 system equipped with a Waters 1000 Prep Pak Module and a Shimadzu SPD-6A variable-wavelength UV detector. The cartridges used were hand packed, in Waters polyethylene sleeves and frits with Vydac C_{18} packing material (15–20 μm particle size, 30 nm pore size). The material was eluted first using a linear TEAP–acetonitrile (40:60) (pH 2.25 or 5.20) buffer system gradient; acceptable fractions were pooled, reloaded onto the preparative cartridge and desalted in 0.1% TFA. Final products were >95% pure by RP-HPLC analysis.

Peptide characterization

Purified peptides were subjected to hydrolysis in 4 *M* methanesulfonic acid at 110°C for 24 h, and analyzed by ion-exchange chromatography with post column derivatization with *o*-phthalal-

dehyde. Liquid secondary ion (LSI)-MS analysis was performed on a Jeol JMS-HX110 double focusing mass spectrometry (Jeol, Tokyo, Japan) fitted with a Cs^+ gun. Samples were added directly to a glycerol–3-nitrobenzyl alcohol (1:1) matrix.

RP-HPLC

Samples for coinjection experiments contained native NPY (0.3 μg/10 μl) and a single diastereomer (1.0 μg/10 μl) dissolved in 0.1% TFA. In addition, each sample contained an analogue of ovine corticotropin releasing factor, [NIe^{21},Tyr^{27}]-oCRF (a 41-peptide) as an internal standard. Coinjection experiments were performed on a Hewlett-Packard Series II 1090 liquid chromatograph with diode array detector and HPLC ChemStation. The Vydac C_{18} and diphenyl columns were from the Separations Group and were 15 × 0.21 cm. Buffer A was 0.1% TFA or TEAP. TEAP was 0.1% phosphoric acid adjusted to the desired pH by addition of TEA. Buffer B (TEAP) was composed of acetonitrile–TEAP A buffer (60:40) while the B buffer (TFA) was 0.1% TFDA in acetonitrile–water (60:40). Analyses were performed at 40°C at a flow-rate of 0.2 ml/min. and detected at 210 nm. Linear gradient conditions were 45–75% B in 30 min. Uniform column characteristics were confirmed by reanalysis of several closely eluting diastereomers following the lenghty C_{18} series.

CZE

CZE was performed on a Beckman P/ACE System 2050 with Spectra-Physics ChromJet SP4400 integrator. Fused silica capillaries from Beckman were 50 cm × 75 μm. The buffer was 100 m*M* phosphoric acid adjusted to pH 2.50 by addition of 2 *M* sodium hydroxide or 100 m*M* phosphoric acid adjusted to pH 2.50 by the addition of TEA. Voltage ranged from 12 to 20 kV and produced from 66 to 100 μA. Detection was at 214 nm and the temperature was maintained at 30°C. Native NPY and the diastereomers were used as prepared for RP-HPLC and applied by pressure injection. After each separation, a 1-min rinse with 0.5 *M* TEAP or sodium phosphate pH 2.50 was performed.

RESULTS AND DISCUSSION

Separation of NPY diastereomers by RP-HPLC

Neuropeptide Y is a relatively large polypeptide (M_r 4252) with 38 chiral centers and a member of the pancreatic polypeptide (PP) family. The tertiary structure of avian PP (aPP) has been elucidated in detail (<1 Å) by X-ray diffraction analysis revealing an intramolecularly stabilized helical structure referred to as the PP-fold [10]. Recent spectral studies as well as molecular dynamics simulation suggest that NPY may have a similar intramolecularly stabilized three-dimensional structure as illustrated in Fig. 1; specifically, a polyproline-type II helix for residues 1–8, a β-turn through positions 9–14, an amphipathic α-helical segment extending from residues 15–32 and a C-terminal turn structure from residues 33–36 [11]. While the α-helical component of the structure of either NPY or NPY C-terminal fragment 18–36 could be demonstrated by NMR [12–14] and circular dichroism (CD) spectroscopy [11,15] other features such as the N-terminal poly-proline helix remain hypothetical or are not substantiated by NMR. Supposing therefore that NPY has a high

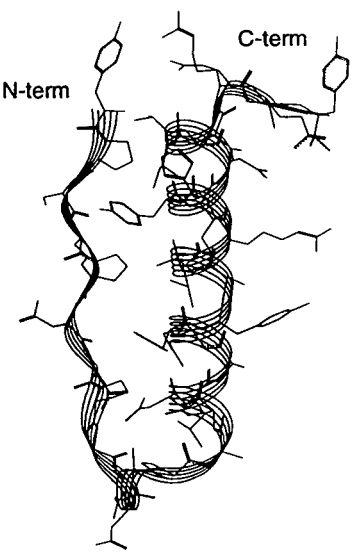

Fig. 1. Ribbon illustration of NPY obtained by modeling of NPY by homology to X-ray crystallographic structure of avian pancreatic polypeptide and tethered minimization to relieve side-chain stretch.

degree of conformational integrity, any modification of the backbone by the introduction of a single D-amino acid was expected to change the solution conformation and thus the chromatographic properties of the resulting diastereomers. Previous attempts at resolving diastereomers of NPY or peptides of similar size by chromatographic techniques have met with only limited success, and have therefore relied heavily on difference in optical rotation or biological activities for complete demonstration of uniqueness such as was the case for bombesin [16], neurotensin [17], somatostatin [18] and CRF [19]. A thorough investigation of retention behavior of the D-series of NPY_{18-36} was recently published, although demonstration of uniqueness of each analogue was not intended [20].

Initially, we obtained retention data for the 35 isomers of NPY in the standard analysis system developed in our laboratory, using a Vydac C_{18} column and mobile-phase composed of TEAP at pH 2.25 at 25°C (Table I). This chromatographic system, which favours basic peptides and amines, was first described by Rivier [4] and has proven to be very useful in the separation of closely associated impurities generated in peptide synthesis (typically fragments or adducts differing from the major component by size and/or charge). As indicated, resolution was achieved for 26 of the 35 analogues yielding separation factors (α) that were greater than 1.03. Centrally modified residues produced the clearest separation with poor resolution of N-terminally modified analogues under the same conditions. These results suggest that a more flexible conformation at the termini may produce few side chain interactions between the peptide and the stationary phase. Since any difference in retention would reflect a difference in the solute's binding affinity to the stationary phase, it is also possible that the N-terminus under these conditions is not exposed to the surface and therefore is prevented from interacting with the stationary ligand. Under the same gradient conditions at 40°C efficiency increased, allowing the separation of three additional N- and C-terminal analogues (Fig. 2 and Table I). Using other supports than the Vydac material reported here, in this case Baker-bond silica, we found that the D-isomer series of NPY_{18-36} displayed maximum retention to a C_8 support at 25°C [20]. Since the magnitude of log k' is a measure of the free energy associated with the binding of the solute to the

TABLE I

COMPARISON OF SEPARATION FACTORS FOR 35 STEREOISOMERS OF NPY UNDER GIVEN RP-HPLC CONDITIONS

A = Vydac C_{18} using TEAP pH 2.25 mobile phase modifier at 40°C; B = Vydac C_{18} using TEAP pH 2.25 mobile phase modifier at 25°C; C = Vydac C_{18} using 0.1% TFA mobile phase modifier at 40°C; D = Vydac diphenyl using 0.1% TFA mobile phase modifier at 40°C.

Isomer	α			
	A	B	C	D
D-Tyr[1]	1.00	1.00	1.00	1.00
D-Pro[2]	1.02	1.00	1.01	1.02
D-Ser[3]	1.00	1.00	1.00	1.00
D-Lys[4]	1.00	1.00	1.00	1.00
D-Pro[5]	1.00	1.00	1.00	1.03
D-Asp[6]	1.03	1.00	1.01	1.02
D-Asn[7]	1.00	1.00	1.00	1.03
D-Pro[8]	1.05	1.03	1.03	1.04
D-Glu[10]	1.07	1.06	1.05	1.09
D-Asp[11]	1.12	1.11	1.08	1.08
D-Ala[12]	1.07	1.06	1.05	1.07
D-Pro[13]	1.05	1.03	1.04	1.06
D-Ala[14]	1.05	1.04	1.03	1.06
D-Glu[15]	1.24	1.18	1.16	1.20
D-Asp[16]	1.06	1.05	1.04	1.05
D-Leu[17]	1.26	1.18	1.16	1.22
D-Ala[18]	1.16	1.09	1.10	1.16
D-Arg[19]	1.34	1.20	1.20	1.32
D-Tyr[20]	1.07	1.14	1.06	1.00
D-Tyr[21]	1.20	1.10	1.13	1.10
D-Ser[22]	1.18	1.07	1.09	1.16
D-Ala[23]	1.39	1.34	1.20	1.27
D-Leu[24]	1.35	1.17	1.19	1.31
D-Arg[25]	2.05	1.56	1.44	1.57
D-His[26]	1.24	1.13	1.12	1.20
D-Tyr[27]	1.41	1.25	1.22	1.32
D-Ile[28]	2.76	1.90	1.62	1.96
D-Asn[29]	1.07	1.04	1.04	1.04
D-Leu[30]	1.46	1.28	1.23	1.32
D-Ile[31]	1.62	1.40	1.31	1.45
D-Thr[32]	1.33	1.19	1.19	1.26
D-Arg[33]	1.15	1.15	1.12	1.10
D-Gln[34]	1.07	1.12	1.06	1.06
D-Arg[35]	1.00	1.00	1.00	1.02
D-Tyr[36]	1.00	1.00	1.00	1.00

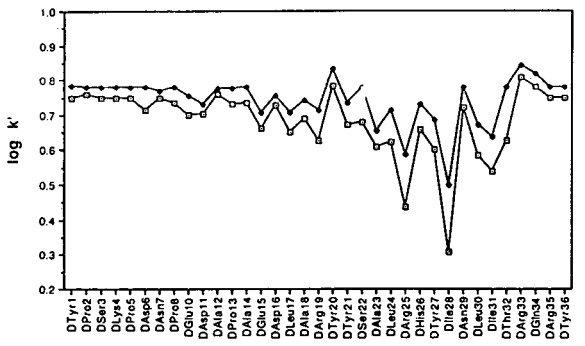

Fig. 2. Plot of log k' *versus* position of D-amino acid substitution in NPY: TEAP pH 2.25–acetonitrile buffer system on Vydac C_{18} at (□) 40°C, and (◆) 25°C. See Experimental section for additional chromatographic details.

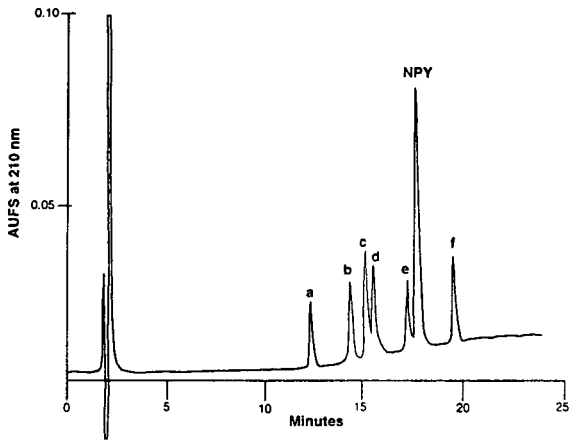

Fig. 3. Coelution of diastereomers of NPY by RP-HPLC using TEAP pH 2.25 buffer at 40°C on Vydac C_{18}. Peaks: a = [D-Ile^{28}]-NPY; b = [D-Ile^{31}]-NPY; c = [D-Leu^{30}]-NPY; d = [D-Thr^{32}]-NPY; e = [D-Asn^{29}]-NPY; f = [D-Arg^{33}]-NPY. See Experimental section for additional chromatographic details.

stationary phase, it is inferred that the interactive behavior of NPY and analogues with the octadecylsilane (Vydac) is stabilized by the presence of N-terminal residues at 25°C. At 40°C, the free energy contribution by each residue was magnified (Fig. 2). Hence, the higher temperature permitted the additional discrimination between D-isomers of [Pro^2]-, [Asp^6]-, and [Arg^{35}]-NPY from the native peptide. At both temperatures, greatest selectivity was exhibited by analogues modified in the region proposed to exist as an alpha helix, as expected since these residues are held in close proximity by hydrogen bonding and hydrophobic interactions and critically depend on the orientation of the side chains to maintain conformational stability. Coinjection of six such centrally modified analogues with NPY is shown in Fig. 3.

When changing the mobile phase modifier to 0.1% TFA, a more hydrophobic counterion, the same 28 isomers were again resolved at 40°C, although α values, in general, were smaller than those obtained with TEAP, and the elution order of two isomers, [D-Pro^2]- and [D-Asp^6]-NPY, was reversed. These observations are not unique to NPY and have been also described for opiate peptides by Zhu *et al.* [21] who used both TFA and phosphate buffers. The decrease in ionic strength of the TFA buffer is implied from the increase in k' values under identical gradient conditions, as graphically illustrated in Fig. 4. The magnitude of the log k' value is a measure of the affinity of the peptide surface to the stationary phase in the absence of the organic modifier. Ion-pairing reagents such as H_3PO_4 and TFA effect changes in peptide retention solely through interaction with positively charged groups on the peptide, with the greater strength of the phosphate counterions reducing the affinity of the peptide to the stationary phase.

Under the acidic conditions of the previous buffer systems, it was expected that the peptide would be partially denatured and all basic residues would be fully protonated. CD and NMR spectroscopy data have indicated that the secondary structural features of NPY, especially α helical content increased as the solution ap-

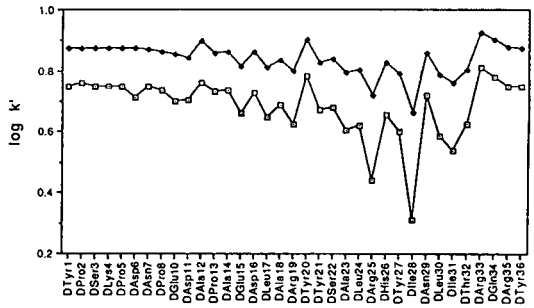

Fig. 4. Plot of log k' *versus* position of D-amino acid substitution in NPY: Vydac C_{18} at 40°C using (□) TEAP pH 2.25 and (◆) 0.1% TFA mobile phase modifiers. See Experimental section for additional chromatographic details.

proached neutral pH [13,14]. Expecting the same effect on the RP-HPLC column, we therefore attempted to separate the four remaining isomers using a Vydac C_{18} stationary phase in a buffer system comprised of TEAP at pH 6.6 and 4.3 [9]. Interestingly, severe band broadening and significantly increased k' of NPY was observed, although the similarly sized and charged corticotropin releasing factor analogue ([Nle^{21},Tyr^{27}]-oCRF), used as an internal standard, eluted as a narrow band indicating no change in H_{eff} (Fig. 5). Since the apparent column efficiency was unchanged, this phenomena alludes to the possibility that NPY may adopt multiple similar transitions or conformations on the C_{18} stationary phase at neutral pH producing a variety of similar surface interactions with the stationary phase. In support of this theory, recently reported structural determination of NPY by NMR spectroscopy using water as the solvent at pH 3.20 and 37°C suggested the exclusive presence of an NPY dimer, though at higher concentrations than those that were used in our studies [14]. Similar effects have been reported for β-endorphin and other related opioid peptides [22] and for NPY and related analogues at elevated temperatures [20].

Of the four unresolved derivatives from the previous stage, we expected that the two terminal D-Tyr analogues (positions 1 and 36) would present the greatest challenge since the physicochemical properties of these derivatives would be expected to be nearly identical to that of the native peptide and the inversion of chirality would assert little effect upon hydrophobicity. Additionally, molecular modeling and other structural investigations [11–13] indicated that the termini display little interaction with neighboring residues. Because of the high content of aromatic residues present in NPY, it was hypothesized that the selectivity of the diphenyl-derivatized column might be more sensitive to the modified orientation at one of these tyrosine residues. Analysis in 0.1% TFA–acetonitrile permitted the resolution of three additional diastereomers, [D-Pro^5]-, [D-Asn^7]- and [D-Arg^{35}]-NPY, but failed to demonstrate increased discrimination of D-tyrosine containing molecules (Table I and Fig. 6). Co-elution of native NPY with the corresponding D-isomers of each of the tyrosines at positions 1, 27 and 36 indicated that the inversion of chirality at these positions was without significant effect on the peptide–diphenyl interaction under the buffer conditions used in these experiments.

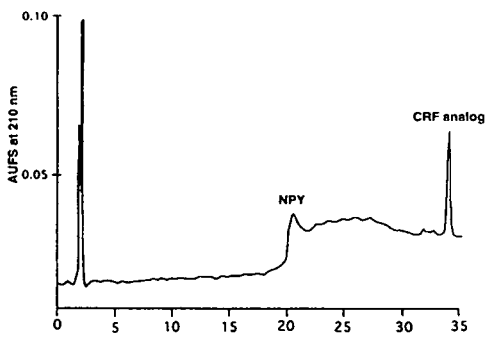

Fig. 5. Chromatogram of NPY and [Nle^{21},Tyr^{27}]-oCRF using TEAP pH 6.50–acetonitrile gradient system on Vydac C_{18} at 40°C. See Experimental section for additional chromatographic details.

The evaluation of data generated by this study of 35 peptide isomers under a variety of separation conditions provides a unique opportunity to discuss trends in chromatographic behavior. First, we have seen that the TEAP buffer system under identical linear gradient conditions produces faster elution of peptide solutes with equal efficiency as the 0.1% TFA buffer system (Fig. 4), long regarded as standard in peptide chemistry. Although the same isomers were resolved from NPY by TEAP, separation factors were greater. Additionally, we have demonstrated improved separation by analysis at 40°C in TEAP (Fig. 2). Second, while the comparison of peptide retention on C_{18} and diphenyl derivatized silica has not proven the advantage of one ligand over the other, concurrent exploitation of both sorbents was shown to be complementary in some cases, with the combination of data producing unequivocal separation of all but four stereoisomers (Table I). Finally, we have recognized the influence of conformation in the variation of peptide retention to a stationary phase. Substitution of NPY by a D-amino acid at positions 22–31 produced analogues with the largest deviations in chromatographic behavior, suggesting that such substitutions were the most disrup-

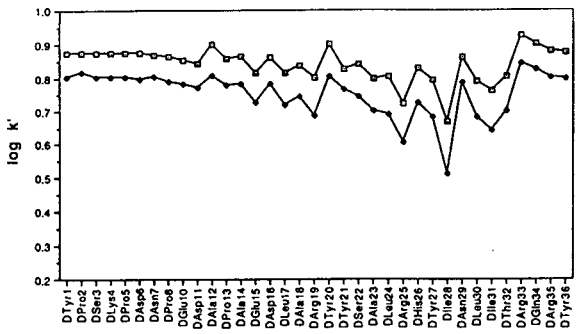

Fig. 6. Plot of log k' *versus* position of D-amino acid substitution in NPY: 0.1% TFA–acetonitrile mobile phase at 40°C using (□) Vydac C_{18} and (◆) Vydac diphenyl. See Experimental section for additional chromatographic details.

tive of NPY's conformation in the buffers used. In all four RP-HPLC analysis conditions, we have seen that the D-amino acid isomer of NPY was overwhelmingly (>80%) the first to elute from the column. This phenomena was independent of particular functional group or position in the sequences. It was also shown that the retention times could vary by as many as 6 min for diastereomers using the identical linear (30 min) gradient conditions, making prediction of peptide retention highly speculative.

Separation of isomers by CZE

As a final approach to separating the remaining isomers, CZE was employed. CZE has been proved to be a very useful analytical tool in our laboratory and that of others [23–25]. The large number of theoretical plates in CZE lends this system the ability to discriminate between small differences in charge densities of peptide molecules and has thus allowed the resolution of species with very subtle differences in structure. The separation mechanism in free solution electrophoresis is based on the differential electrophoretic mobilities of the solutes, which in turn is related to their charge densities [25]. It was expected that, although the global charge of each NPY isomer would be identical, the altered local orientation of a charged group might be exposed, and thus could be expressed by differing migration times. Under the first set of conditions, [D-Ser^3]- and [D-Tyr^{36}]-NPY were resolved from NPY (Fig. 7a) when subjected to the electric field of 12 kV (62 μA) in 0.1 *M* sodium

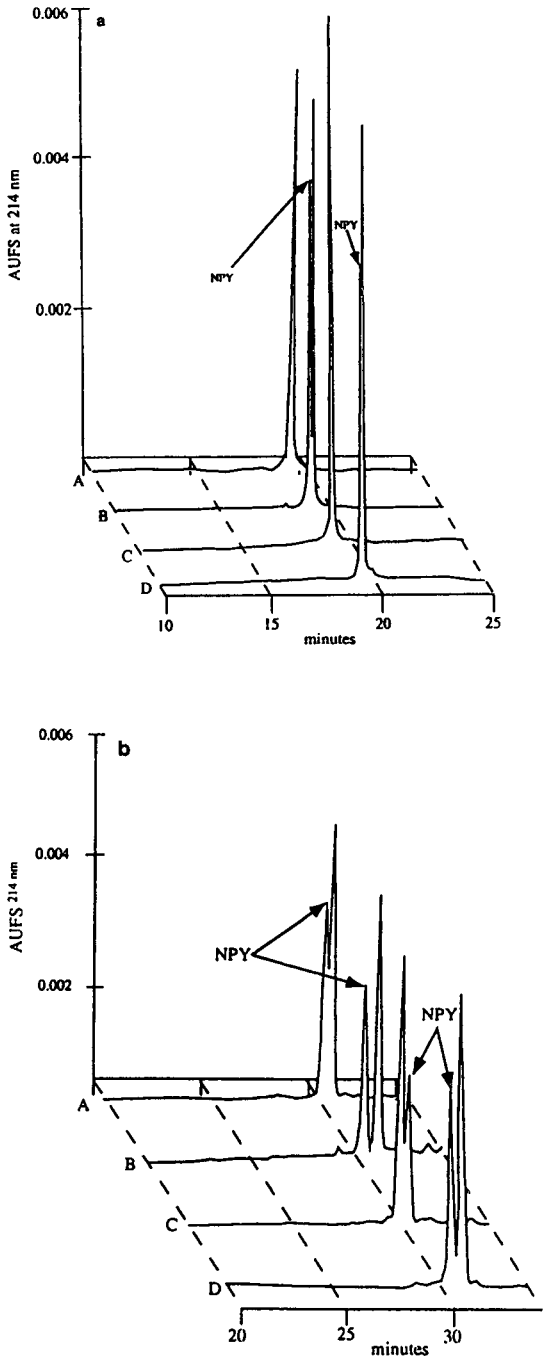

Fig. 7. Coelution of diastereomer pairs of NPY by CZE. (a) Electrophoresis performed at 12 kV, 62 μA using 0.1 *M* sodium phosphate at pH 2.50. (b) Electrophoresis performed at 20 kV, 100 μA using 0.1 *M* TEAP at pH 2.50. For each electropherogram, native NPY was coinjected with one of the following stereoisomers: A = [D-Tyr^1]-NPY; B = [D-Ser^3]-NPY; C = [D-Lys^4]-NPY; D = [D-Tyr^{36}]-NPY.

phosphate at pH 2.5. Migration times differed from that of native NPY by 0.1 min. The other isomers, [D-Tyr[1]]- and [D-Lys[4]]-NPY, were not resolved under the same conditions.

Replacing the sodium cations of the electrolyte with TEA, proven effective in RP-HPLC separations, once again demonstrated the utility of such an acidic TEAP buffer system in another separation system (Fig. 7b). Acidic pH was beneficial in the electrophoretic system as electroosmosis is greatly reduced and solute-silica wall interactions are minimal. As triethylamine replaced sodium as the electrolytic cation the electrophoretic mobility was greatly decreased. This may be due to the increased radius of the TEA cation resulting in an increase in viscosity of the buffer. In order to accelerate analysis times the applied voltage was increased to 20 kV (migration time of the isomers was approx. 30 min) and a current of approximately 100 μA was produced. Under these conditions the entire series of 35 isomers was evaluated and resulted in the separation of 32 out of 35 isomers.

Thus, even those stereoisomeric pairs which could not be resolved by RP-HPLC were clearly separated in this electrophoretic system at an applied voltage of 20 kV. Other contributing factors to a better separation in TEAP as compared to sodium phosphate buffer at the same molar concentration may include such parameters as viscosity, interaction of the triethylammonium ion with the silanols of the capillary walls and/or differences in ionic strength. Migration times, band width and amperage, were highly reproducible in the TEAP system (relative standard deviation = 4%) (Table II). Migration times of each diastereomer did not vary as much as they did under RP-HPLC from that of NPY and in some cases co-elution profiles did not allow unequivocal identification of NPY *versus* its diastereomer. Since the actual charge-to-mass ratio is identical for all diastereomers ($q/M_r^{2/3}$, where q is the calculated charge and M_r is the molecular mass), it was concluded that any separation would be the direct result of intramolecular interactions created by inverting the chirality at a single residue. Because we were able to separate most diastereomers using CZE (see Table II), such an inversion clearly affected the expression of the local charge density. Our conclusion disputes the premise of Rickard *et al.* [24] who proposed that any minor irregularities in solute shape (such as that resulting from inversion of chirality at one center) was likely to

TABLE II

ELECTROPHORETIC MIGRATION TIME DATA FOR 35 STEREOISOMERS OF NPY USING 0.1 *M* TEAP pH 2.50 BUFFER MATRIX

Average migration time (t_m) for NPY was 29.03 min with standard deviation of the mean = 1.31 (n = 35). See Experimental section for additional chromatographic details.

Isomer	First elutant	NPY t_m (min)	D isomer t_m (min)	Δt_m (min)
D-Tyr[1]	L	30.32	30.64	0.32
D-Pro[2]	L	29.94	31.17	1.23
D-Ser[3]	L	30.50	31.12	0.62
D-Lys[4]	D	30.11	29.69	0.42
D-Pro[5]	–	28.19	28.19	0
D-Asp[6]	L	28.86	29.15	0.29
D-Asn[7]	L	26.19	27.33	1.14
D-Pro[8]	L	27.42	27.79	0.37
D-Glu[10]	–	28.39	28.39	0
D-Asp[11]	D	29.04	28.74	0.30
D-Ala[12]	D	27.67	26.30	1.37
D-Pro[13]	D	28.28	28.04	0.24
D-Ala[14]	D	28.03	27.63	0.40
D-Glu[15]	–	28.46	28.46	0
D-Asp[16]	D	28.14	27.68	0.46
D-Leu[17]	L	27.91	28.52	0.61
D-Ala[18]	L	27.87	28.56	0.69
D-Arg[19]	L	27.93	28.66	0.73
D-Tyr[20]	L	28.10	29.58	1.48
D-Tyr[21]	L	28.12	28.66	0.54
D-Ser[22]	L	28.27	28.85	0.58
D-Ala[23]	L	28.17	28.91	0.74
D-Leu[24]	L	28.21	28.59	0.38
D-Arg[25]	D	30.28	29.01	1.27
D-His[26]	D	30.56	28.57	1.99
D-Tyr[27]	D	30.71	30.41	0.30
D-Ile[28]	D	28.61	28.37	0.24
D-Asn[29]	D	30.41	29.96	0.45
D-Leu[30]	L	32.72	33.78	1.06
D-Ile[31]	L	30.84	31.37	0.53
D-Thr[32]	D	30.43	29.03	1.40
D-Arg[33]	D	28.65	28.01	0.64
D-Gln[34]	D	29.28	28.62	0.66
D-Arg[35]	D	29.17	28.71	0.46
D-Tyr[36]	L	30.25	30.72	0.47

be smoothed out by the solvation sphere and ionic atmosphere that surrounds peptide ions in solution.

While 80% of the D-amino acid containing analogues of NPY eluted before NPY under RP-HPLC conditions, we did not discover any obvious trends displayed by the 35 isomers using capillary electrophoresis. Migration times were so close in most cases, that any attempt to draw from such results would likely lead to over-interpretation. There was no pattern to the isomers which failed to be resolved, nor was there any pattern as to which diastereomers displayed the highest electrophoretic mobilities (Table II).

CONCLUSIONS

This study has demonstrated the rapid and effective employment of modern chromatographic techniques for the resolution of diastereomers of NPY. For complete resolution of diastereomers or closely associated impurities in peptides of this size, the challenge presented will likely necessitate the use of several overlapping detection systems to eliminate ambiguity, as in the present study. In this way, many physicochemical properties may be exploited leading to an optimized separation profile. Additionally, we have proven the utility of the TEAP separation buffer system for both RP-HPLC and CZE applications. Although it was proposed that retention times of peptides could be predicted [26] the data presented here clearly indicate that a conformational parameter should be introduced in any such methods. Similarly, although a correlation between q/M_r was suggested by Rickard *et al.* [24] for peptide and proteins using CZE, a conformational component also needs to be introduced as a further refinement of such studies.

ACKNOWLEDGEMENTS

This work was supported by NIH grant HL-43154 and the Hearst Foundation. The authors thank Dr. J. Boublik for synthesis of many NPY analogues, Dr. S. Koerber for the computer-generated illustration of NPY's proposed structure (Fig. 1) and L. Lobnitz for manuscript preparation.

REFERENCES

1 K. Tatemoto, M. Carlquist and V. Mutt, *Nature*, 296 (1982) 659.
2 B.G. Stanley and S.F. Leibowitz, *Proc. Natl. Acad. Sci. U.S.A.*, 82 (1985) 3940.
3 D.A. Kirby, J.H. Boublik and J.E. Rivier, in preparation.
4 J. Rivier, *J. Liq. Chromatogr.*, 1 (1978) 343.
5 M.T. Reymond, L. Delmas, S.C. Koerber, M.R. Brown and J.E. Rivier, *J. Med. Chem.*, 35 (1992) 3653.
6 D.A. Kirby, S.C. Koerber, A.G. Craig, R.D. Feinstein, L. Delmas, M.R. Brown and J.E. Rivier, *J. Med. Chem.*, 36 (1993) 385.
7 E. Kaiser, R.L. Colescott, C.D. Bossinger and P.I. Cook, *Anal. Biochem.*, 34 (1970) 595.
8 J. Rivier, R. McClintock, R. Galyean and H. Anderson, *J. Chromatogr.*, 288 (1984) 303.
9 C. Hoeger, R. Galyean, J. Boublik, R. McClintock and J. Rivier, *Biochromatography*, 2 (1987) 134.
10 T.L. Blundell, J.E. Pitts, I.J. Tickle, S.P. Wood and C.-W. Wu, *Proc. Natl. Acad. Sci. U.S.A.*, 78 (1981) 4175.
11 J. Allen, J. Novotny, J. Martin and G. Heinrich, *Proc. Natl. Acad. Sci. U.S.A.*, 84 (1987) 2532.
12 D.F. Mierke, H. Dürr, H. Kessler and G. Jung, *Eur. J. Biochem.*, 206 (1992) 39.
13 V. Saudek and J.T. Pelton, *Biochemistry*, 29 (1990) 4509.
14 D.J. Cowley, J.M. Hoflack, J.T. Pelton and V. Saudek, *Eur. J. Biochem.*, 205 (1992) 1099.
15 J. Boublik, N. Scott, J. Taulane, M. Goodman, M. Brown and J. Rivier, *Int. J. Peptide Protein Res.*, 33 (1989) 11.
16 J. Rivier and M. Brown, *Biochemistry*, 17 (1978) 1766.
17 J. Rivier, L. Lazarus, M. Perrin and M. Brown, *J. Med. Chem.*, 20 (1977) 1409.
18 J. Rivier, M. Brown and W. Vale, *Biochem. Biophys. Res. Commun.*, 65 (1975) 746.
19 J.E. Rivier, C. Rivier, R. Galyean, A. Miranda, C. Miller, A.G. Craig, G. Yamamoto, M. Brown and W. Vale, *J. Med. Chem.*, in press.
20 S. Mougos, J. Boublik, J. Rivier, M.T.W. Hearn and M.I. Aguilar, *J. Chromatogr.*, (1992).
21 B.Y. Zhu, C.T. Mant and R.S. Hodges, *J. Chromatogr.*, 594 (1992) 75.
22 L.S. Monger and C.J. Olliff, *J. Chromatogr.*, 595 (1992) 125.
23 C. Miller, J.-F. Hernandez, A.G. Craig, J. Dykert and J. Rivier, *Anal. Chim. Acta*, 249 (1991) 215.
24 E.C. Rickard, M.M. Stohl and R.G. Nielsen, *Anal. Biochem.*, 197 (1991) 197.
25 P.D. Grossman, K.J. Wilson, G. Petrie and H.H. Lauer, *Anal. Biochem.*, 173 (1988) 265.
26 C. Chabanet and M. Yvon, *J. Chromatogr.*, 599 (1992) 211.

Journal of Chromatography, 648 (1993) 267–274
Elsevier Science Publishers B.V., Amsterdam

CHROM. 25 330

Chiral separation of basic drugs using cyclodextrins as chiral pseudo-stationary phases in capillary electrophoresis

M. Heuermann and G. Blaschke*

Department of Pharmaceutical Chemistry, University of Münster, Hittorfstrasse 58–62, W-48149 Münster (Germany)

(First received April 19th, 1993; revised manuscript received May 24th, 1993)

ABSTRACT

Capillary electrophoresis was used for the chiral resolution of basic racemic drugs in general and in particular for dimethindene and four possible metabolites. Conditions for optimum enantioselectivity and resolution were determined by changing the cyclodextrin type, cyclodextrin concentration, pH of the run buffer, applied current and capillary temperature.

INTRODUCTION

Enantiomer resolution is an important field in analytical chemistry, especially in pharmaceutical analysis. About 88% of synthetic chiral drugs are sold as racemates [1], and often one of the enantiomers is more active than the other or is responsible for inadvertent side-effects. For the investigation of the metabolism of racemic therapeutic agents, GC [2] and HPLC [3] are widely used. During the last few years, capillary electrophoresis (CE) [4] has developed into a powerful tool, including applications in chiral analysis [5]. Enantiomeric separations can be achieved using chiral buffer additives such as cyclodextrins (CD) [6,7].

The metabolism of dimethindene maleate, N,N - dimethyl - 3 - [1-(2-pyridinyl)ethyl] -1H-indene-2-ethanamine maleate, has been studied by Radler and Blaschke [8] and Prien and Blaschke [9] using protein- and cellulose-based chiral stationary phases for enantiomeric separations by HPLC.

In this work we used CE with run buffers containing different cyclodextrins to resolve dimethindene and four possible metabolites into their enantiomers in one run. A number of parameters influencing the selectivity and resolution of the compounds were investigated. Further, a number of structurally different racemic basic drugs were resolved by CD-containing run buffers.

EXPERIMENTAL

Chemicals and reagents

Dimethindene maleate was obtained from Zyma (Nyon, Switzerland). N-Demethyldimethindene, N-demethyl-6-methoxydimethindene, 6-methoxydimethindene and the enantiomers of dimethindene [(*S*)- (+)- and (*R*)- (−)-] were prepared by Radler and Blaschke [8] and dimethindene-N-oxide was synthesized by Prien and Blaschke [9]. α-, β- and γ-cyclodextrin (α-, β- and γ-CD), methyl-β-cyclodextrin [ME-β-CD, molar substitution (MS) = 1.8], hydroxyethyl-β-cyclodextrin (HE-β-CD, MS = 1.0), hydroxypropyl-β-cyclodextrin (HP-β-CD, MS = 0.9) and hydroxypropyl-β-cyclodextrin (HP-β-

* Corresponding author.

0021-9673/93/$06.00

CD, $MS = 0.6$) were a kind gift from Wacker-Chemie (Munich, Germany). KH_2PO_4, Na_2HPO_4, H_3PO_4, NaOH (all of analytical-reagent grade) were purchased from Merck (Darmstadt, Germany). Other racemic drugs were gifts from the manufacturers.

Apparatus for CE

A Grom (Herrenberg, Germany) capillary electrophoresis System 100, equipped with an HP 3396 A integrator (Hewlett-Packard, Avondale, PA, USA) and a Linear Instruments (Reno, NV, USA) UVIS 200 detector, and a Beckman (Munich, Germany) P/ACE 2100 capillary electrophoresis system were used with an untreated fused-silica capillary (Grom) of 40 cm effective length × 50 μm I.D.

Standard operating conditions, unless stated otherwise, were as follows: effective voltage, 400 V/cm; temperature, 21 ± 1°C; sample introduction, (a) Grom, hydrostatic 10 cm, 30 s and (b) Beckman, low pressure, 10 s; detection, (a) UV at 205 nm and (b) UV at 200 nm; anode and cathode buffers with the same pH and molarity as the run buffer, but containing no CD, were used.

Buffer and sample preparation

Stock solutions of 50 m*M* KH_2PO_4 and 50 m*M* Na_2HPO_4 buffers were prepared in doubly distilled, deionized water, filtered and degassed in an ultrasonic bath before use. The pH was adjusted, if possible, with the stock buffer solutions, otherwise with 50 m*M* H_3PO_4 or 50 m*M* NaOH. Run buffers were prepared accordingly after addition of an appropriate amount of cyclodextrins.

Stock solutions of 1 mg/ml racemic drug were prepared, stored at 4°C and diluted to 60 μg/ml before use.

RESULTS AND DISCUSSION

The endoosmotic mobility was determined using mesityl oxide as a neutral marker. Fig. 1 shows the electroosmotic mobility in the pH range 3–10. The magnitude of the endoosmotic flow (μ_{eof}) was calculated using the equation

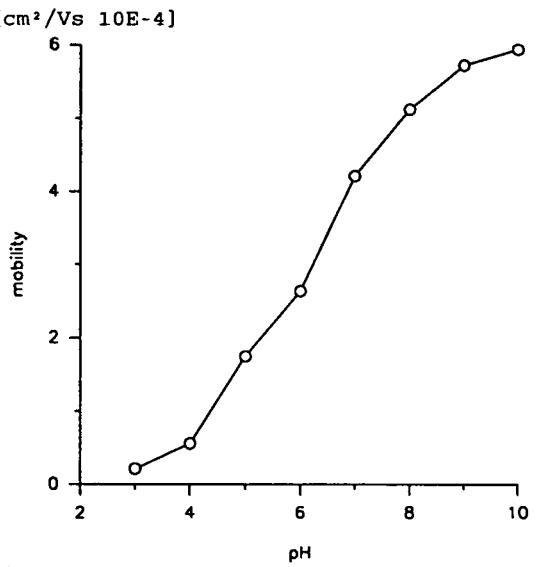

Fig. 1. Endoosmotic flow over the pH range 3–10, determined using mesityl oxide as a neutral marker. Conditions: run buffer, 50 m*M* phosphate buffer; capillary, untreated fused silica, 45 cm length to detector, 62 cm total length.

$$\mu_{eof} + \mu_{eph} = \frac{L}{tE} \quad (1)$$

where L is the capillary length (cm), t the migration time (s) and E the effective voltage (V/cm) [10]. With a neutral marker such as mesityl oxide, no electrophoretic mobility (μ_{eph}) occurs, so that the observed values are due only to the endoosmotic mobility (μ_{eof}).

The separation selectivity (α) in CE can be expressed as the ratio of the effective mobilities using the equation

$$\alpha = \frac{\mu_{eph1}}{\mu_{eph2}} = \frac{\mu_{app1} - \mu_{eof}}{\mu_{app2} - \mu_{eof}} \quad (2)$$

where the subscripts 1 and 2 refer to the earlier and later migrating species, respectively [11]. The effective mobility (μ_{eph}) is calculated as the difference between the apparent mobility (μ_{app}) and μ_{eof}. Because it was not possible to determine the endoosmotic flow (μ_{eof}) under the applied conditions using a run buffer of pH 2 or run buffers with high concentrations of CDs during a period up to 150 min, we calculated α as the relative retention using the equation 3 [12].

$$\alpha = \frac{\mu_{app1}}{\mu_{app2}} = \frac{t_2}{t_1} \quad (3)$$

The resolution (R_s) between the enantiomers can be measured using the equation

$$R_s = 1.18 \cdot \frac{t_2 - t_1}{W_1^{1/2} + W_2^{1/2}} \quad (4)$$

where t_1 and t_2 are the migration times and $W_1^{1/2}$ and $W_2^{1/2}$ are the peak widths at half-height of the first- and second-migrating enantiomer, respectively [13].

Achiral separation of dimethindene and metabolites

Fig. 2 shows the structures of dimethindene (**2**) and the possible metabolites **1** and **3–5**. Their achiral separation was achieved by using 50 m*M* phosphate buffer (pH 3.2) (Fig. 3). According to their basic character, secondary amines show smaller migration times than tertiary amines and weakly basic N-oxide **5** was detected last.

Chiral separation of dimethindene and metabolites

Fig. 4 shows an electropherogram of **1–5** after addition of 30 m*M* HP-β-CD to 50 m*M* phosphate buffer (pH 3.3) [14]. Under these conditions a baseline enantioseparation of **1–5** was achieved. Owing to the different selectivities in the presence of the β-CD derivatives we obtained a change in the elution order of the N-

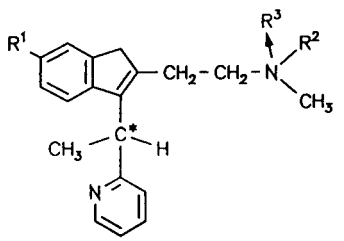

Substance	No.	R^1	R^2	R^3
N-demethyl-dimethindene	1	H	H	
dimethindene	2	H	CH_3	
N-demethyl-6-methoxy-dimethindene	3	OCH_3	H	
6-methoxy-dimethindene	4	OCH_3	CH_3	
dimethindene-N-oxide	5	H	CH_3	O

Fig. 2. Structures of dimethindene and metabolites.

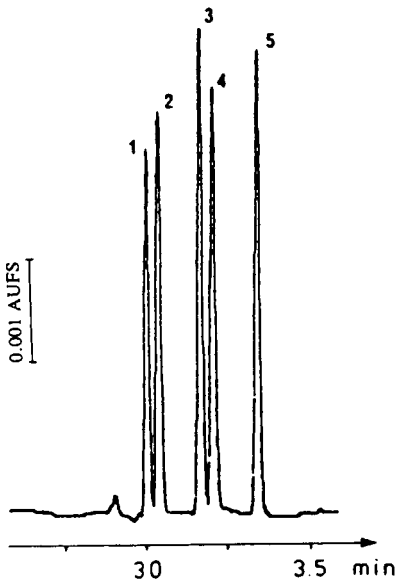

Fig. 3. Achiral separation of **1–5**. Conditions: phosphate buffer (pH 3.2), 500 V/cm, 98 μA, detection at 205 nm, sample concentration 60 μg/ml.

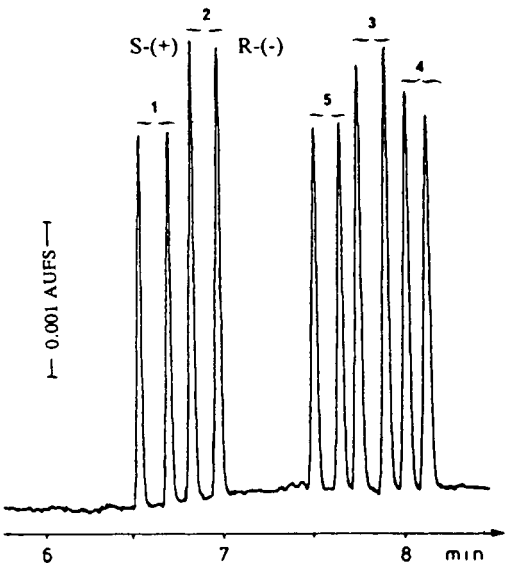

Fig. 4. Chiral separation of **1–5**. Conditions: HP-β-CD 30 μg/ml, 50 m*M* phosphate buffer (pH 3.3), 400 V/cm, 42 μA, detection at 205 nm, sample concentration 30 μg/ml enantiomer.

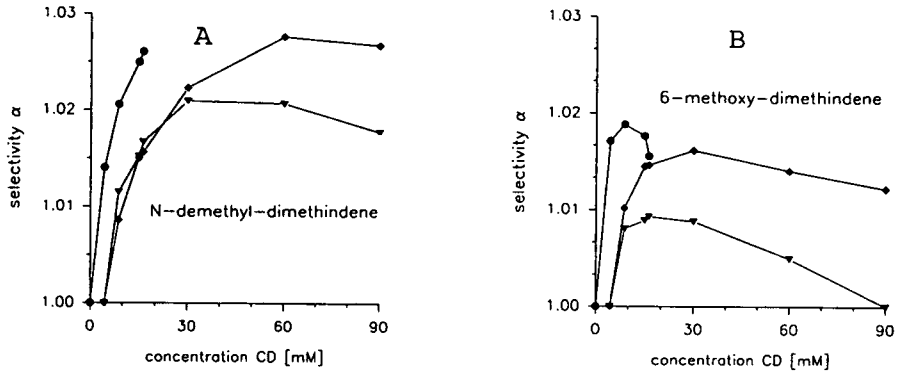

Fig. 5. Selectivity factor (α) of (A) N-demethyldimethindene (**1**) and (B) 6-methoxydimethindene (**5**) as a function of CD type and concentration. ● = β-CD; ◆ = HP-β-CD; ▼ = HE-β-CD.

oxide **5**, which now migrated between **2** and **4** [15,16].

The elution order of the dimethindene enantiomers was determined using enantiomers. (*R*)-(−)-**2** migrates slower, indicating the formation of a stronger diastereomer complex with β-CD derivatives.

Factors affecting chiral separations

Cyclodextrin type and concentration. Seven different CDs were tested for the resolution of **1–5**. It was found that β-CD, HE-β-CD and HP-β-CD showed enantioselectivity with respect to **1–5** (Fig. 5) [17]. Underivatized β-CD possesses the highest selectivity of all the compounds studied up to a concentration of 16.3 m*M*, its limit of aqueous solubility. It is known [7] that urea increases the solubility of β-CD. However, urea was not added because it was found to increase the noise of the detector signal at such high concentrations.

The selectivity of HE-β-CD and HP-β-CD is lower; however, this disadvantage is acceptable in the case of HP-β-CD, because a much higher concentration in water can be achieved owing to its high solubility. As reported for the separations of other compounds [18], an optimum concentration of 60 m*M* is found for **1** and **2** and 30 m*M* for **3–5**. The 6-methoxy substituent of **4** and **5** significantly decreases the α and R_s values (Fig. 5). Especially for **5** a very high HE-β-CD concentration resulted in a complete loss of selectivity. Non-specific hydrophobic associations have been discussed as a reason for this phenomenon [19].

The observed migration times (Fig. 6) of **1–5** in the concentration range 8.8–90 m*M* HP-β-CD exhibited a non-linear increase. This might be explained by the fact that high CD concentrations result in dimerization of CDs [2], leading to a loss of selectivity and hence shorter migration times.

pH of buffer solutions. Chiral separations of **1–5** were investigated separately at pH 2.0, 3.0, 3.3, 3.6, 4.0 and 4.7. Optimum selectivity was

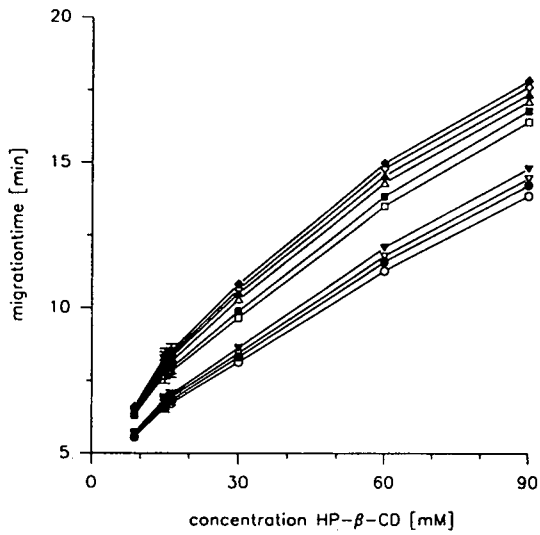

Fig. 6. Plot of the migration times of **1–5** *vs.* concentration of HP-β-CD. ○ = (+)-**1**; ● = (−)-**1**; ▽ = (+)-**2**; ▼ = (−)-**2**; □ = (+)-**3**; ■ = (−)-**3**; △ = (+)-**4**; ▲ = (−)-**4**; ◇ = (+)-**5**; ◆ = (−)-**5**.

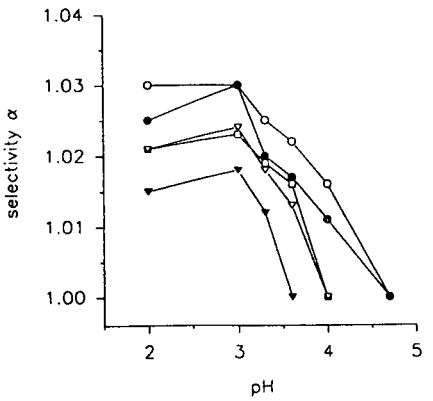

Fig. 7. Plot of selectivity factor (α) *vs.* pH of the run buffer containing 20 m*M* HP-β-CD. ○ = **1**; ● = **2**; □ = **3**; ▽ = **4**; ▼ = **5**.

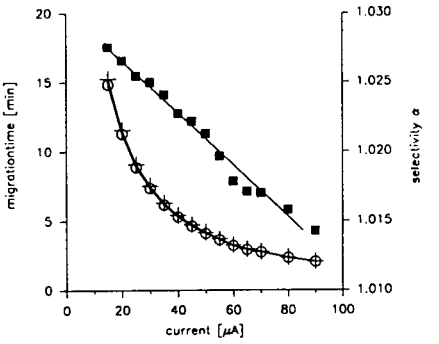

Fig. 8. Dependence of migration time and α values on the effective voltage using different constant currents. Capillary, 47 cm total length, 30 cm effective length. ■ = α for **1**; + = migration time of (−)-**1**; ○ = migration time of (+)-**1**.

found at pH 3.0 in all instances (Fig. 7). However, for the simultaneous analysis of **1**–**5**, pH 3.3 was used in order to avoid overlapping of the enantiomers of **3**, **4** and **5**.

Applied voltage and current. In CE, migration times can be shortened by increasing the applied voltage. Fig. 8 shows the dependence of the migration times and α values of dimethindene (**1**) on the applied voltage. Lower currents result in a higher selectivity with extremely long migration times. With a very high effective voltage of about 640 V/cm, very short migration times are achieved but, owing to Joule heating and ineffective heat dissipation, an extreme decrease in selectivity results. Good resolutions were obtained using a current of 40 μA, corresponding to an effective voltage of about 390 V/cm.

Temperature. An advantage of the Beckman P/ACE instrument over the Grom system is the

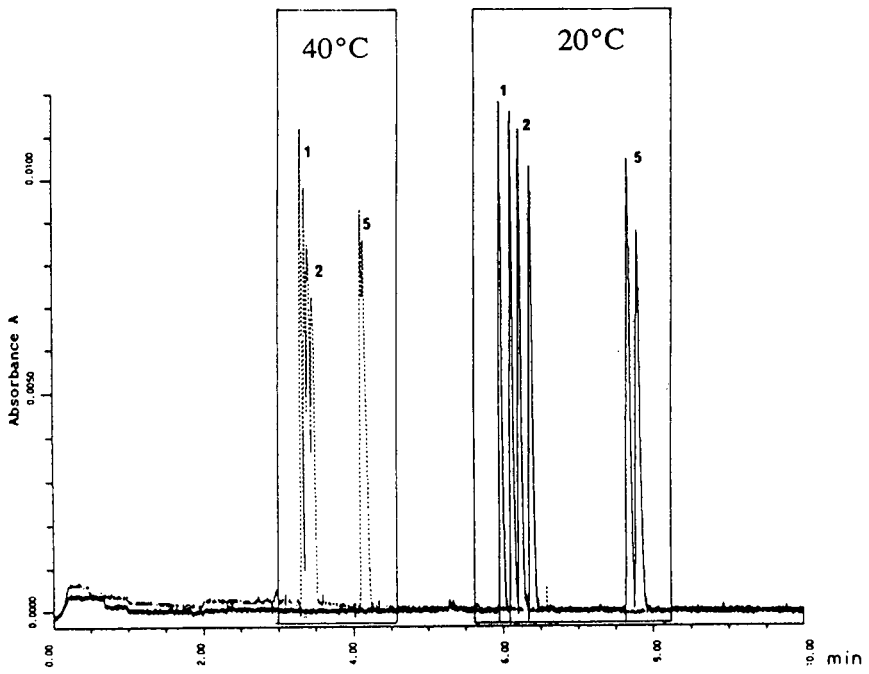

Fig. 9. Superimposition of two electropherograms showing the chiral separations of **1**, **2** and **5** at 20°C and 40°C using 50 m*M* phosphate run buffer (pH 3.3) containing 30 m*M* HP-β-CD.

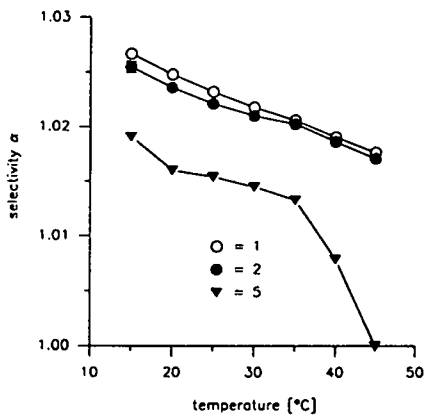

Fig. 10. Effect of the capillary temperature on chiral recognition: selectivity (α) *vs.* temperature. O = **1**; ● = **2**; ▼ = **5**.

use of liquid cooling to dissipate Joule heat. This allows one to work with constant capillary temperatures, independent of changes in the room temperature.

Effects of the temperature on selectivity are generally noticed in chromatography as well as in CE. The influence of temperature on the buffer pH can be used to manipulate the selectivity in CE [20].

We observed that changes in the thermostating temperature between 15 and 45°C had great effects on the migration times and enantioselectivities. Fig. 9 shows an overlay of two electropherograms of **1**, **2** and **5** at 20 and 40°C. The corresponding α values are shown in Fig. 10. The increase in the α values with a decrease in

TABLE I

RESOLUTION OF RACEMIC DRUGS

CD concentrations: α-, β-, γ-CD = 16.3 m*M*, derivatized CDs = 30 m*M* in 50 m*M* phosphate buffer (pH 3.3).

Drug	CD type	t_1 (min)	t_2 (min)	α	R_s
Ambucetamide	HP-β-CD	11.29	11.41	1.010	1.04
Carvedilol	β-CD[a]	8.88	9.05	1.019	1.50
Clenbuterol	HP-β-CL[a]	9.65	10.03	1.039	4.03
Ephedrine	β-CD[a]	7.65	7.73	1.011	0.96
Etilefrine	HP-β-CD[a]	8.35	8.68	1.038	3.82
Imafen	HP-β-CD[a]	9.12	9.28	1.019	1.60
Isoprenaline	ME-β-CD[a]	8.27	8.53	1.031	3.06
Ketamine	β-CD[a]	8.18	8.27	1.010	0.88
Lofexidine	HP-β-CD[a]	8.94	9.32	1.043	3.17
Mefloquine	HP-β-CD	13.19	14.33	1.086	7.96
Methylephedrine	ME-β-CD[a]	8.75	8.87	1.013	1.11
Metomidate	HP-β-CD	14.10	14.99	1.063	4.50
Mianserin	HP-β-CD	12.11	13.08	1.079	4.34
Nefopam	HP-β-CD	15.76	15.9	1.008	0.73
Nomifensine	HP-β-CD	14.77	15.21	1.029	2.45
Norephedrine	ME-β-CD	7.08	7.22	1.019	1.53
Norfenefrine	ME-β-CD[a]	6.79	6.99	1.029	2.59
Octopamine	HP-β-CD	8.81	8.91	1.010	0.80
Pholedrine	HP-β-CD[a]	8.65	8.87	1.026	2.29
Salbutamol	ME-β-CD[a]	7.66	7.74	1.011	1.08
Sotalol	HP-β-CD	13.97	14.13	1.011	1.20
Synephrine	ME-β-CD[a]	7.25	7.41	1.023	3.20
Zopiclone	HP-β-CD[a]	6.00	6.19	1.030	2.86

[a] One or more of the other CDs tested showed lower selectivities: β-CD, ME-β-CD, HE-β-CD and HP-β-CD.

temperature might be explained by a decrease in rotational and/or vibrational energy, increasing the fixation of the enantiomers inside or at the top of the chiral CD and, thus, increasing the enantioselectivity. Separations below 15°C were not possible with the Beckman system.

The optimum run buffer conditions for the separation of dimethindene were found to be 30 m*M* hydroxypropyl-β-cyclodextrin in 50 m*M* phosphate buffer (pH 3.3) with an effective voltage of 400 V/cm at 20°C. This method can be used to determine **1** and **2** in human urine samples after oral administration of dimethindene maleate [17]. The results obtained by this method will be reported elsewhere.

Chiral separation of different drugs

In addition to dimethindene and its possible metabolites, numerous racemic drugs with a basic nitrogen could be resolved by the addition of CDs. Table I summarizes these data, listing only those CDs which resulted in the best resolution of the drugs under the conditions applied. Some of these drugs could be separated with other CDs used in this investigation (β-CD, ME-β-CD, HE-β-CD and HP-β-CD), but with lower efficiency. With α- and γ-CD, none of these drugs could be resolved. Further, the following drugs could not be resolved after the addition of HP-β-CD to the run buffer: alimemazine, atropine, bifonazol, butetamate, camylofin, cetirizine, chlorphenoxamine, clofedanol, fenfluramine, ilmofosine, mazindol, mequitazone, metharaminol, orphenadrine, propafenone and terfenadine.

Mixtures of chiral drugs with different chemical structures can be separated and, additionally, resolved into the enantiomers in a single run, as shown in Fig. 11.

In addition to the high resolution and the

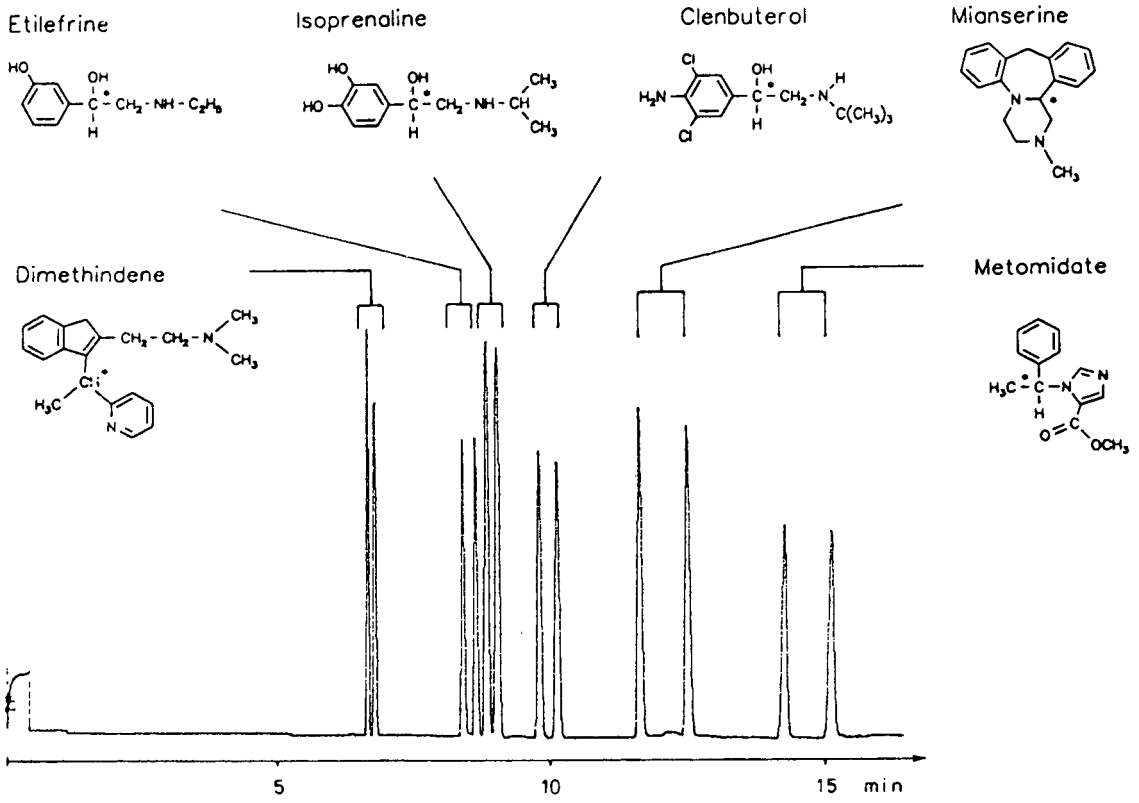

Fig. 11. Electropherogram of a mixture of six chemically different basic racemic drugs using HP-β-CD as a chiral pseudo-stationary phase. Run buffer: HP-β-CD, 30 mg/ml in 50 m*M* phosphate buffer (pH 3.3).

simple chemistry in CE, other advantages are low costs of buffers and pseudo-stationary chiral phases, no or minimum consumption of expensive and harmful solvents and rapidity.

CONCLUSIONS

CE proved to be a powerful tool for resolving the enantiomers of pharmaceutical drugs. The optimum separation conditions depend on the CD type and concentration, the pH of the buffer and the temperature.

ACKNOWLEDGEMENTS

The authors thank Wacker (Munich, Germany) for the supply of cyclodextrins and Zyma (Munich, Germany), the Deutsche Forschungsgemeinschaft and the Fonds der Chemischen Industrie for financial support.

REFERENCES

1 E.J. Ariens, in C. Brown (Editor), *Chirality in Drug Design and Synthesis*, Academic Press, London, 1990, Ch. 2, p. 29.
2 V. Schurig and H.P. Nowotny, *Angew. Chem.*, 9 (1990) 969.
3 D. Sybliska and J. Zukowski, in A.M. Krstulović (Editor), *Chiral Separations by HPLC: Applications to Pharmaceutical Compounds*, Ellis Horwood, Chichester, 1989, Ch. 7, p. 147.
4 J.W. Jorgenson and K.D. Lukacs, *Anal. Chem.*, 53 (1981) 1298.
5 R. Kuhn and S. Hoffstetter-Kuhn, *Chromatographia*, 34 (1992) 505.
6 S. Fanali and P. Boček, *Electrophoresis*, 11 (1990) 757.
7 K.D. Altria, D.M. Goodall and M.M. Rogan, *Chromatographia*, 34 (1992) 19.
8 S. Radler and G. Blaschke, *J. Chromatogr.*, 567 (1991) 229.
9 D. Prien and G. Blaschke, presented at the *3rd International Symposium on Chiral Discrimination, Tübingen, October 1992*, paper No. 130.
10 S.A.C. Wren and R.C. Rowe, *J. Chromatogr.*, 635 (1993) 113.
11 Y.Y. Rawjee, D.U. Staerk and G. Vigh, *J. Chromatogr.*, 635 (1993) 291.
12 A. Guttman, A. Paulus, A.S. Cohen, N. Grinberg and B.L. Karger, *J. Chromatogr.*, 448 (1988) 41.
13 S.A.C. Wren and R.C. Rowe, *J. Chromatogr.*, 609 (1992) 363.
14 M. Heuermann and G. Blaschke, presented at the *4th International Symposium on High Performance Capillary Electrophoresis, Amsterdam, February 1992.*
15 S. Terabe, Y. Miyashita and O. Shibata, *J. Chromatogr.*, 516 (1990) 23.
16 C.P. Ong, C.L. Ng, H.K. Lee and S.F.Y. Li, *J. Chromatogr.*, 588 (1991) 335.
17 M. Heuermann and G. Blaschke, presented at the *3rd International Symposium on Chiral Discrimination, Tübingen, October 1992*, paper No. 122.
18 S.A.C. Wren and R.C. Rowe, *J. Chromatogr.*, 603 (1992) 235.
19 M.J. Sepaniak, R.O. Cole and Clark, *J. Liq. Chromatogr.*, 15 (1992) 1023.
20 C.W. Wang and E.S. Yeung, *Anal. Chem.*, 64 (1992) 502.

Journal of Chromatography, 648 (1993) 275–278
Elsevier Science Publishers B.V., Amsterdam

CHROM. 25 381

Short Communication

Rapid method for the fractionation of nuclear proteins and their complexes by batch elution from hydroxyapatite

A. Zagariya

Department of Biochemistry and Molecular Genetics, University of Alabama at Birmingham, UAB Station, Birmingham, AL 35294 (USA)

S. Khrapunov

Department of General and Molecular Genetics, Kiev University, Vladimirskaya Street 64, Kiev 252601 (Ukraine)

W. Zacharias*

Department of Biochemistry and Molecular Genetics, BHSB 407, University of Alabama at Birmingham, UAB Station, Birmingham, AL 35294 (USA)

(First received February 16th, 1993; revised manuscript received June 15th, 1993)

ABSTRACT

A new procedure for the separation and purification of nuclear proteins and their complexes by batch elution from hydroxyapatite is presented. This method allows to isolate such proteins with different basic character faster and more efficiently than procedures using column chromatography, while showing high selectivity, sensitivity, simplicity, mild conditions of purification, reproducibility and protein stability.

INTRODUCTION

Fractionation and purification of nuclear proteins (histones and non-histones) are among the most versatile tools in modern molecular biology. Here we describe a simple and widely applicable new method for the purification of nuclear proteins and their complexes from mammalian chromatin. Our method is designed to fractionate nuclear proteins bound to hydroxyapatite by batch elution at different ionic strengths instead of the conventional fractionation by hydroxyapatite column chromatography [1]. This method may be used to study the heterogeneity and DNA-binding properties of nuclear proteins. It allows processing of many samples simultaneously and permits the isolation of proteins with different affinities to DNA (histones, their complexes, and non-histone proteins) very efficient-

* Corresponding author.

0021-9673/93/$06.00

ly, compared to previously published procedures using column chromatography [1,2]. These conditions help to avoid redistribution of proteins in the nucleohistone and are accompanied by minimum levels of proteolysis.

EXPERIMENTAL

Chemicals and solutions

The calf thymus nucleohistone material and Sephadex G-100 were obtained from Sigma (St. Louis, MO, USA). DNA 1 kilobase-pair size markers were from Bethesda Research Labs. (Gaithersburg, MD, USA), and total histones from Boehringer Mannheim Biochemicals (Indianapolis, IN, USA). Water was obtained from a Milli-Q system (Millipore, Milford, MA, USA). All other chemicals were analytical grade [Tris, ammonium sulphate, sodium dodecyl sulphate (SDS), acrylamide, bisacrylamide, Coomassie Blue, ethidium bromide, sodium chloride, acetic acid, methanol, boric acid, EDTA] and were obtained from Mallinckrodt (Paris, KY, USA) or Sigma. The 0.5 *M* phosphate buffer (pH 7.5) was prepared by combining 0.5 *M* NaH_2PO_4 and 0.5 *M* Na_2HPO_4 up to pH 7.5.

Hydroxyapatite preparation

Hydroxyapatite was prepared according to Tiselius *et al.* [3], with some modifications [4], by slow mixing (500 ml/h) of 0.5 *M* sodium phosphate (pH 7.5) and 0.5 *M* $CaCl_2$. We measured a protein content of 70% and DNA content of 30% in our calf thymus nucleohistone material. A 100-mg sample of this nucleohistone was mixed with 21 g of hydroxyapatite in 1 m*M* Tris–HCl (pH 7.9). Proteins with different DNA-binding affinities were eluted by washing and centrifugation in 10-ml fractions of different NaCl concentrations in 50 m*M* sodium phosphate buffer (pH 7.5).

Separation of histone complexes

Eluted histone complexes were loaded onto a Sephadex G-100 column (10 cm × 1 cm) equilibrated with 5 m*M* Tris–HCl (pH 8.0). Stepwise elutions of histone dimer by 1 *M* NaCl and tetramer by 2 *M* NaCl were precipitated overnight by $(NH_4)_2SO_4$ at 100 and 80% saturation, respectively. Histone octamer was eluted by 2 *M* NaCl, without previous elutions of histone dimer and tetramer, and was precipitated by $(NH_4)_2SO_4$ at 60% saturation.

Protein and DNA analysis

Protein concentrations were determined with the Bradford protein assay kit (Bio-Rad, Melville, NY, USA) by using a standard curve established with purified total calf thymus histone. DNA concentrations were measured by the UV absorbance at 260 nm (1 AU = 50 μg/ml).

Proteins (10 μg per lane) were analyzed in gels containing 15% acrylamide, 0.5% bisacrylamide, 0.38 *M* Tris–HCl (pH 8.8), 0.1% SDS; staining was done with 0.1% Coomassie Brilliant Blue R250 in acetic acid–methanol–water (10:25:65). Analysis of DNA (0.5 μg per lane) was done in 0.8% agarose gels in 89 m*M* Tris–borate, 2 m*M* EDTA (pH 8.3) at 50 V for 2 h, followed by staining in 10 μg/ml ethidium bromide for 1.5 min and destaining in water overnight.

RESULTS AND DISCUSSION

Fig. 1 shows the results obtained with the batch elution procedure. Hydroxyapatite-absorbed calf thymus nucleohistone complex was equilibrated with 50 m*M* sodium phosphate buffer (pH 7.5), and proteins were batch-eluted with different concentrations of NaCl in the same buffer. A small amount of basic non-histone proteins (NHP) was released in 0.35 *M* NaCl. Histone H1, which has more basic character than the other histones, was released in 0.6 *M* NaCl, histones H2A and H2B (with less basic character than H1) in 1.0 *M* NaCl, and histones H3 and H4 (with the least basic character) were eluted in 2 *M* NaCl (Fig. 1A). The purities of these fractions, as determined by gel electrophoresis (Fig. 1B), were 80–85% for H1, 90% for H2A and H2B, and 80–90% for H3 and H4. A small amount of weakly basic non-histone proteins was released in 5 *M* NaCl. The fractionation procedure could easily be performed in 1 day.

The recoveries of eluted histones were 12.5 mg

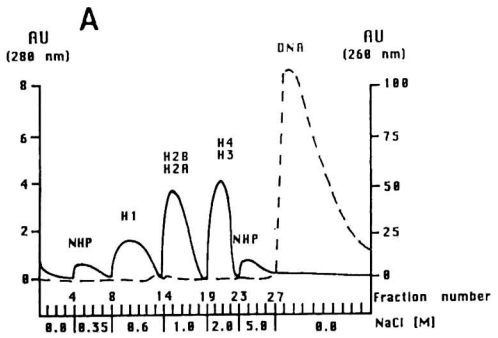

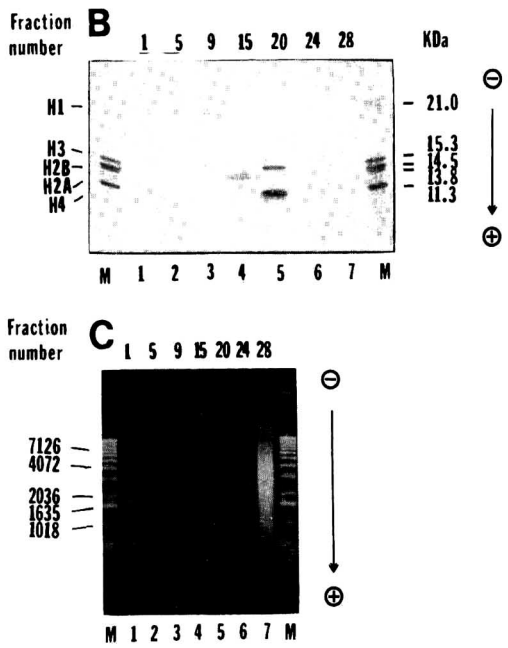

Fig. 1. Fractionation of histones from nucleohistone complex by batch elution from hydroxyapatite. (A) Elution profiles as determined by UV absorbance at 280 nm (protein; solid line) and 260 nm (DNA; dashed line). Fractions 1–27 were obtained at 0, 0.35, 0.6, 1.0, 2.0 and 5.0 *M* NaCl, respectively. Fractions 28–37 were obtained at 0.5 *M* sodium phosphate buffer (pH 7.5) without NaCl. (B) Analysis of eluted proteins by electrophoresis in denaturing polyacrylamide gels. Fraction numbers correspond to the numbers in the elution profile of Fig. 1A. M = Total histones (10 μg) from calf thymus nucleohistone. (C) Analysis of eluted DNA by agarose gel electrophoresis. Fraction numbers correspond to the numbers in the elution profile of Fig. 1A. M = DNA molecular mass marker.

for H1, 19.7 mg for H2A–H2B, and 22.5 mg for H3–H4. The yields of the non-histone proteins eluted by 0.35 *M* NaCl or by 0.5 *M* sodium phosphate (pH 7.5) without NaCl were 5.3 and 3.3 mg, respectively. Because of their low amounts, these non-histone proteins could not be detected in the Coomassie-stained gel (Fig. 1B). Altogether, the recovery of total proteins from 100 mg of nucleohistone complex was 63.3 mg, corresponding to an exellent yield of approximately 90%. For the column chromatography method, recoveries of 66% for H2A and

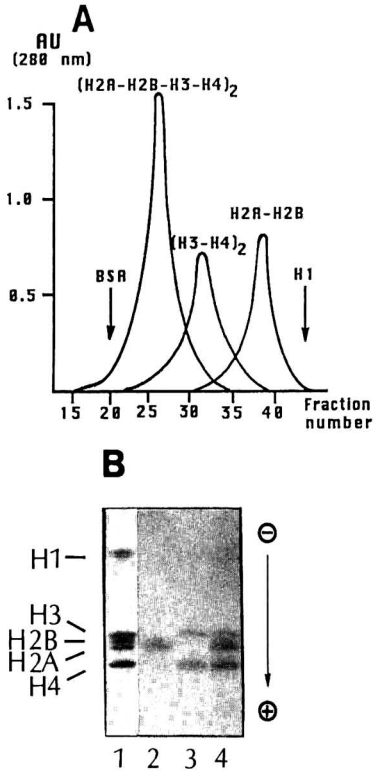

Fig. 2. Separation and identification of histone complexes after batch elution and Sephadex G-100 gel permeation. (A) Elution of histone dimer H2A–H2B by 1 *M* NaCl and tetramer $(H3–H4)_2$ by 2 *M* NaCl. Histone octamer was also eluted by 2 *M* NaCl, but without previous elution of histone dimer and tetramer. BSA = Bovine serum albumin. (B) Analysis of eluted fractions by electrophoresis in denaturing polyacrylamide gels. Lanes: 1 = total histones from calf thymus as marker; 2 = histone dimer; 3 = tetramer; 4 = octamer.

H2B, and 95% for H3 and H4 were reported [1].

Yields of DNA during the elutions up to 5 *M* NaCl (fractions 1–27) were negligibly small (Fig. 1A and C). Approximately 31 mg of free DNA was eluted only in 0.5 *M* sodium phosphate (pH 7.5) without NaCl up to fraction 37. This corresponds to a yield of DNA of approximately 100% from this nucleohistone complex.

The oligomeric complexes of histones were obtained in the following way (Fig. 2). First, a small amount of highly basic non-histone proteins was eluted in 0.35 *M* NaCl, and histone H1 was eluted by 0.6 *M* NaCl. The subsequent fractions were analyzed by Sephadex G-100 gel permeation for the oligomeric nature of the histone complexes (Fig. 2A). Histone dimers (H2A–H2B) were eluted in 1 *M* NaCl, and histone tetramers $(H3–H4)_2$ in 2 *M* NaCl. Histone octamers $(H2A–H2B–H3–H4)_2$ were eluted in a separate batch in 2 *M* NaCl without previous elution of histone dimers and tetramers. The purities of the histone complexes obtained were determined by electrophoresis in denaturing polyacrylamide gels (Fig. 2B). It was shown previously that at reduced ionic strength, histone octamers dissociate into two dimers and one tetramer [4].

CONCLUSIONS

Our data demonstrate some important advantages of protein separation by batch elution: good multiple peak resolution, high purity, excellent yield, and time-saving isolation. Although we have not tried samples of more than 100 mg of nucleohistone complex as starting material, this procedure can certainly be scaled up to larger amounts of nucleohistone. Thus, batch elution from hydroxyapatite can be a valuable and rapid alternative for the purification of nuclear proteins and their complexes, to be used for nucleosome reconstitution, gel shift assays of DNA-protein interactions, for obtaining total histones, and for many other molecular biological applications.

ACKNOWLEDGEMENTS

This work was supported by the General and Molecular Genetics Department, Kiev University, Ukraine (A.Z., S.Kh.), and by a Biomedical Science Grant from the Arthritis Foundation (W.Z.). We thank Dr. N.V. Kalashnikov for reading the manuscript and Dr. L.A. Sitailo for helpful comments.

REFERENCES

1 R.H. Simpson and G. Felsenfeld, *Nucleic Acids Res.*, 6 (1979) 689–696.
2 C. von Holt, W.F. Brandt, H.J. Greyling, G.G. Lindsey, J.D. Retief, J. de A. Rodrigues, S. Schwager and B.T. Sewell, *Methods Enzymol.*, 170 (1989) 431–503.
3 A. Tiselius, S. Hjertén and O. Levin, *Arch. Biochem. Biophys.*, 65 (1957) 132–155.
4 I.B. Dubrovsky and S.N. Khrapunov, *Ukr. Biokhim. J.*, 60 (1988) 8–13.

Journal of Chromatography, 648 (1993) 279–282
Elsevier Science Publishers B.V., Amsterdam

CHROM. 25 374

Short Communication

Isolation of *cis*-$[PtCl(NH_3)_2(H_2O)](ClO_4)$, the monohydrated form of the anti-tumour drug cisplatin, using cation-exchange high-performance liquid chromatography

Florence Gonnet, Damien Lemaire, Jiří Kozelka and Jean-Claude Chottard*

Laboratoire de Chimie et Biochimie Pharmacologiques et Toxicologiques, CNRS, URA 400, 45 rue des Saints Pères, 75270 Paris Cedex 06 (France)

(First received April 29th, 1993; revised manuscript received June 21st, 1993)

ABSTRACT

A novel procedure allowing a quantitative separation of the anti-tumour drug cisplatin and its hydration products, based on cation-exchange high-performance liquid chromatography, is presented. Thanks to this procedure, the monohydrated form of cisplatin, *cis*-$[PtCl(NH_3)_2(H_2O)]^+$, which is possibly the principal species reacting *in vivo* with DNA and thus responsible for the anti-tumour activity, could be isolated and characterized in the pure state for the first time.

INTRODUCTION

The anti-tumour drug cisplatin (*cis*-$[PtCl_2(NH_3)_2]$, **1**) binds to DNA, preferentially cross-linking GpG and ApG dinucleotides [1,2]. This selectivity is not yet well understood. Since the drug's DNA binding is under kinetic control, several groups have investigated the kinetics of the reactions of the hydrolysed, reactive forms of cisplatin, *cis*-$[PtCl(NH_3)_2(H_2O)]^+$ (**2**) and *cis*-$[Pt(NH_3)_2(H_2O)_2]^{2+}$ (**3**), with DNA [3,4] or with oligonucleotides as models for DNA [5,6]. These studies have been hampered by the fact that **2**, which is the initial product of cisplatin hydrolysis and possibly the major species reacting with DNA *in vivo*, could not be prepared in pure form. The principal problem is the relatively rapid disproportionation of **2** in water into **1** and **3**. In this paper, we describe a method based on cation-exchange high-performance liquid chromatography that allows the separation and isolation of the monohydrated complex **2** as a frozen solution with perchlorate counterions from an aqueous solution containing **1**, **2** and **3**.

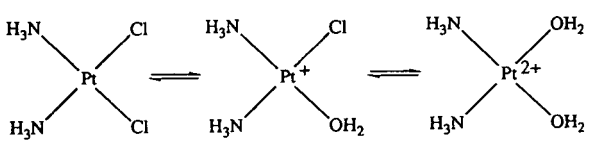

1 2 3

* Corresponding author.

EXPERIMENTAL

cis-$[PtCl_2(NH_3)_2]$ (**1**) was kindly provided by Rhône-Poulenc Rorer, France. Solutions of *cis*-$[Pt(NH_3)_2(H_2O)_2]^{2+}$ (**3**) were prepared by dissolving *cis*-$[Pt(NO_3)_2(NH_3)_2]$ [7] in water. Solutions of *cis*-$[PtCl_2(NH_3)_2]$ were prepared by dissolution of cisplatin in 0.1 *M* NaCl. $NaClO_4 \cdot H_2O$ and $HClO_4$ were purchased from Merck.

The HPLC system consisted of a Shimadzu LC-6A pump (Touzart & Matignon, France), connected to a Rheodyne injector with a 200-μl sample loop, and to a Spectra-Physics Focus diode array detector with a pathlength of 0.6 cm, or to a Shimadzu SPD-6A UV detector with a pathlength of 1 cm coupled to a C-R3A Shimadzu integrator.

The chromatographic conditions were optimized in initial experiments on a 5-μm Nucleosil SA column (250 × 4.6 mm I.D.) (Colochrom, France). For the subsequent separations, a 5-μm Nucleosil SA semipreparative column (250 × 7.5 mm I.D.) (Colochrom) was used. Aliquots of 20 μl (analytical column) or 200 μl (semipreparative column) of approximately 0.1 *M* solutions of the platinum complexes were injected. The mobile phase consisted of aqueous 0.25 *M* $NaClO_4$ (pH adjusted to 4.0 with 0.1 *M* perchloric acid). The flow-rate was 0.7 ml/min in analytical separations and 1.4 ml/min in preparative runs. The detection wavelengths were 302 nm, 265 nm and 254 nm on a Spectra-Physics Focus detector or 265 nm on an SPD-6A UV detector. All separations were done at room temperature.

RESULTS

When **1** is stirred with 1 equivalent of $AgNO_3$ for 24 h in water, the final solution contains an equilibrium mixture of **1**, **2** and **3**. Fig. 1 shows the chromatographic separation of such a solution. Using a semipreparative column, we quenched the fractions containing **2** in liquid nitrogen and stored them at −80°C in order to prevent redisproportionation to **1** and **3**. HPLC analyses showed that the purity of **2** was >99.8% immediately after separation and >96% after 2 weeks at −80°C.

The use of a diode array detector allowed us

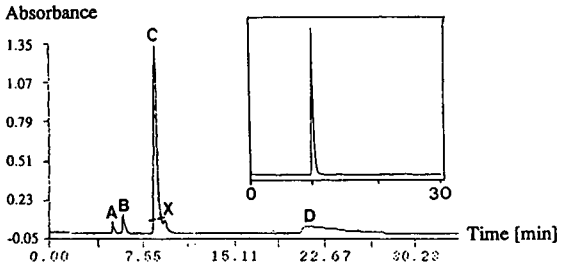

Fig. 1. Typical chromatogram of the equilibrated solution of **1**, **2** and **3** (prepared from **1** and 1 equivalent of $AgNO_3$) using UV detection at 265 nm. A = Anions (Cl^-, NO_3^-); B = **1**; C = **2**; D = **3**; X = impurity. Insert: pure **2** after separation using a semipreparative column (between the two cuts). Conditions are given in the Experimental section.

to record the absorption spectrum of each complex. The spectrum of **2**, which could be measured on a pure sample for the first time here, is shown in Fig. 2. The quantitative determination of the absorbance was carried out based on the "theoretical plates concept" [8]. According to this concept, the molar concentration of a component at the top of its peak, C_{max}, is a function of the "number of theoretical plates", N, and the injected molar fraction Q_0 [9]:

$$C_{max} = \frac{Q_0}{V_R}\sqrt{\frac{N}{2\pi}} \quad (1)$$

V_R is the retention volume, calculated as the product of the retention time t_R and the flow-rate. N is determined for each peak as $N = 5.54(t_R/\delta)^2$, δ being the half-width of the peak, measured in time units. We first recorded the chromatograms of pure authentic solutions of **1** and **3**, in order to determine precisely their quotients between peak area and concentration. Then, we analysed equilibrium mixtures of **1**, **2**

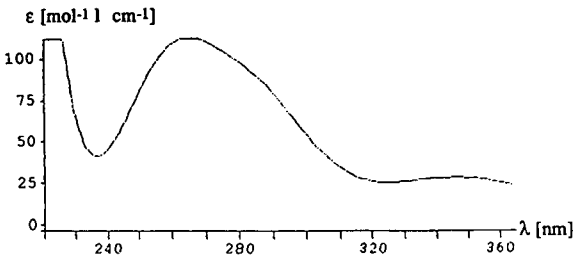

Fig. 2. UV absorption spectrum of **2** recorded at the top of its peak.

and **3** with the three detection wavelengths of 302, 265 and 254 nm, corresponding to the λ_{max} values for the first spin-allowed transition of **1**, **2** and **3**, respectively [10]. The chromatograms recorded at $\lambda_{max}(\mathbf{1})$ and $\lambda_{max}(\mathbf{3})$ were used to measure the molar fractions $Q_0(\mathbf{1})$ and $Q_0(\mathbf{3})$, using the quotients determined in the previous experiment. Since the sum of the molar fractions $Q_0(\mathbf{1}) + Q_0(\mathbf{2}) + Q_0(\mathbf{3})$ is equal to the total injected molar amount of platinum, $Q_0(\mathbf{2})$ and thus $C_{max}(\mathbf{2})$ can be easily calculated, giving, with the absorbance at the top of the peak of **2**, the molar absorption coefficient $\varepsilon(\mathbf{2})$ for the wavelength used. From the chromatogram recorded at $\lambda_{max}(\mathbf{2})$, $\varepsilon(\mathbf{2})$ at 265 nm was determined as $112 \pm 8\ M^{-1}\ cm^{-1}$ (mean value from six experiments).

DISCUSSION

The first step of the reaction between cisplatin (**1**) and DNA is the hydrolysis of **1** to **2** [3,4,11]. Compound **2** reacts with DNA *in vitro* either directly or via further hydration to **3**, the relative proportions of these pathways depending on DNA concentration [3]. Since it is doubtful whether we can regard the cell nucleus with the compactly packed DNA and the surrounding cytoplasm as a diluted system to which we could assign a DNA concentration, it is difficult to extrapolate *in vitro* results to living cells and to predict which pathway will be predominant *in vivo*. Thus, both **2** and **3** have to be considered as possible candidates for the interaction with DNA.

In previous studies on reactions of **2** with DNA, enriched solutions resulting from the reaction of **1** with 1.2 equivalents of $AgNO_3$ in dimethylformamide were used [4]. This method affords about 80% solutions of **2**, with not very precisely defined concentrations of **1** and **3**. The system is further complicated by the presence of the potential ligand dimethylformamide, which is not removed but only diluted with H_2O. Miller and House [12] prepared solutions enriched in **2** by passing an equilibrated solution containing **1**, **2** and **3** in 0.1 *M* $HClO_4$ through an anion-exchange column charged with ClO_4^- ions. The resulting solution contains, as can be calculated from its absorption spectrum (Fig. 2 in ref. 13), approximately 85% **2**, 5% **1** and 10% **3**. Accurate kinetic measurements clearly require well-defined starting concentrations, and, preferably, the pure species whose reactivity is being investigated.

Separation of platinum complexes by high-performance liquid chromatography has been subject to several studies [14–20]. Most commonly, reversed-phase columns were modified with alkylsulphonate salts as ion-pair reagents and phosphate or acetate buffers were used as the mobile phase [14–17]. Sulphonate, phosphate and acetate are potential ligands for platinum, and rapid interconversions between the hydrated complexes **2** and **3** on the one hand and sulphonato, phosphato and acetato complexes on the other hand are expected [21]. These equilibria apparently do not interfere with the analytical procedure. However, since such ions as ligands alter the affinity of the complex for DNA, they would jeopardize kinetic measurements. Brandsteterova *et al.* [20] have used a Separon C_{18} packed glass column with water as mobile phase, allowing the analytical separation of **1**, **2** and **3**. However, the peaks overlapped significantly, rendering their integration inaccurate and making a preparative fractionation incomplete.

The principal idea of this work was to find out whether a cation-exchange column as currently used for the separation of hydrated metal ions would work for covalently bound complex cations as well. In fact, as demonstrated in Fig. 1, our simple system using a sulphonate-packed Nucleosil column does not only allow the separation of the cationic species **2** and **3**, but also elutes the uncharged complex **1**, affording accurate peak integration and complete separation (>99.8%) of **2**. Sodium perchlorate employed as eluent is a non-invasive salt which we used in subsequent kinetic measurements in order to maintain a constant ionic strength.

Compound **2** has been recently used as an intermediate in syntheses of the anti-tumour complexes *cis*-$[PtCl(NH_3)_2(am)]Cl$ (am = aromatic amine) [22]. Enriched solutions of **2** from the reaction between **1** and $AgNO_3$ in dimethyl-

formamide were employed. The use of pure samples of **2** could considerably improve the yield of such preparations.

In conclusion, we have developed a method based on cation-exchange high-performance liquid chromatography allowing a quantitative separation of cisplatin and its hydration products. The absorption spectrum of the pure monohydrated complex **2**, given here for the first time, enables, since the spectra of **1** and **3** are known [13], a rapid determination of the molar fractions of **1**, **2** and **3** in their solution mixtures.

ACKNOWLEDGEMENT

We are indebted to Mr. J.J. Beaurain (Colochrom, France) for the generous gift of an analytical Nucleosil SA column.

REFERENCES

1 A.M.J. Fichtinger-Schepman, J.L. van der Veer, J.H.J. den Hartog, P.H.M. Lohman and J. Reedijk, *Biochemistry*, 24 (1985) 707.
2 A. Eastman, *Biochemistry*, 25 (1986) 3912.
3 N.P. Johnson, J.D. Hoeschele and R.O. Rahn, *Chem.–Biol. Interactions*, 30 (1980) 151.
4 D.P. Bancroft, C.A. Lepre and S.J. Lippard, *J. Am. Chem. Soc.*, 112 (1990) 6860.
5 A. Laoui, J. Kozelka and J.C. Chottard, *Inorg. Chem.*, 27 (1988) 2751.
6 F. Gonnet, J. Kozelka and J.C. Chottard, *Angew. Chem., Int. Ed. Engl.*, 31 (1992) 1483.
7 Y.N. Kukushkin and S.C. Dhara, *Ind. J. Chem.*, 8 (1970) 184.
8 A.J.P. Martin and R.L.M. Synge, *Biochem. J.*, 35 (1941) 1358.
9 R. Rosset, M. Caude and A. Jardy, *Chromatographies en Phases Liquide et Supercritique*, Masson, Paris, 1991, p. 25.
10 J. Chatt, G.A. Gamlen and L.E. Orgel, *J. Chem. Soc.*, (1958) 486.
11 P. Horacek and J. Drobnik, *Biochim. Biophys. Acta*, 254 (1971) 341.
12 S.E. Miller and D.A. House, *Inorg. Chim. Acta*, 161 (1989) 131.
13 S.E. Miller and D.A. House, *Inorg. Chim. Acta*, 166 (1989) 189.
14 W.A.J. de Waal, F.J.M.J. Maessen and J.C. Kraak, *J. Chromatogr.*, 407 (1987) 253.
15 P.J. Parsons, P.F. Morrison and A.F. Leroy, *J. Chromatogr.*, 385 (1987) 323.
16 S. Murakami, K. Saito and A. Muromatsu, *Inorg. Chim. Acta*, 152 (1988) 91.
17 M. Macka, J. Borak and F. Kiss, *J. Chromatogr.*, 586 (1991) 291.
18 R.F. Borch, J.H. Markovitz and M.E. Pleasants, *Anal. Lett.*, 12 (1979) 917.
19 S.J. Bannister, L.A. Sternson and A.J. Repta, *J. Chromatogr.*, 173 (1979) 333.
20 E. Brandsteterova, F. Kiss, V. Chovancova and V. Reichelova, *Neoplasma*, 38 (1991) 415.
21 S.E. Miller and D.A. House, *Inorg. Chim. Acta*, 173 (1990) 53.
22 S.T. Hollis, A.R. Amundsen and E.W. Stern, *J. Med. Chem.*, 32 (1989) 128.

Journal of Chromatography, 648 (1993) 283–288
Elsevier Science Publishers B.V., Amsterdam

CHROM. 25 296

Short Communication

Potentiometric detection in ion chromatography using multi-ionophore membrane electrodes

Sang Hyun Han, Kang Shin Lee and Geun Sig Cha*

Department of Chemistry, Kwangwoon University, 447-1 Wolgye-Dong, Nowon-Ku, 139-701 Seoul (South Korea)

Dong Liu

Department of Chemistry, University of Michigan, Ann Arbor, MI 48109-1055 (USA)

Marek Trojanowicz

Department of Chemistry, University of Warsaw, Pasteura 1, 02-093 Warsaw (Poland)

(First received December 9th, 1992; revised manuscript received April 27th, 1993)

ABSTRACT

The incorporation of ionophores selective for ammonium, potassium, sodium and calcium ions in an appropriate proportion into a plasticized poly(vinyl chloride) membrane provides a potentiometric membrane sensor with similar sensitivity to ammonium, alkali and alkaline earth metal ions. Such a sensor was employed in single-column ion chromatography using the wall-jet flow-cell arrangement, and was shown to exhibit similar detectability to that observed for conductivity detection.

INTRODUCTION

Conductivity is certainly the most commonly used detection method in modern high-performance ion chromatography [1,2]. A possible alternative in some applications is the use of inexpensive potentiometric devices. These can be applied by using two types of electrode [3]. The first type of electrodes are half-cells in which an element (usually a metallic one) is in equilibrium with its ions in solution. In the second type a metallic element and its insoluble salt are in equilibrium with the counter ion of the salt present in the solution. In addition, membrane electrodes employing various types of membranes are very often used. For example it has been shown that sensitive potentiometric pH detection in suppressed ion chromatography can in some cases give better detection limits than conductivity detection [4]. Replacement ion chromatography with in-line Donnan dialysis also allows the potentiometric detection of various ions with a similar sensitivity using selective membrane electrodes with particularly low detection limits for a given ion [5,6].

The direct application of common potentiometric membrane electrodes with plasticized

* Corresponding author.

0021-9673/93/$06.00

polymer membranes containing selective complexing ionophores does not allow the detection of different ions with similar sensitivity [7,8]. One way of achieving similar detectability of different ions is to use a less selective ionophore in a plasticized membrane or to select a suitable plasticizer [3].

This work presents another approach to designing a potentiometric sensor for ion chromatography. A detector with similar sensitivity to several ions can be achieved by incorporating several selective ionophores in suitable proportions in a polymer membrane. The results of the optimization of such a membrane composition and the study of its selectivity in flow-injection measurements have been presented elsewhere [9]. Membrane electrodes containing three different ionophores in different ratios in a polymer membrane were also applied recently in arrays of ion-selective electrodes for the simultaneous determination of sodium, potassium and calcium in a flow-injection system [10].

EXPERIMENTAL

Flow-injection measurements were performed using a system consisting of a Rabbit peristaltic pump from Rainin (Woburn, MA, USA), a Rheodyne Model 5020 injection valve (Cotati, CA, USA), an Accumet Model 925 digital pH meter from Fisher Scientific (Romulus, MI, USA) and a Fisher Recordall Series 5000 strip-chart recorder.

Chromatographic measurements were carried out using a Model 200 pump from Scientific Systems (State College, PA, USA), a Rheodyne Model 7125 injection valve with 250-μl sample loop and an ION-210 cation-exchange column from Interaction Chemicals (Mountain View, CA, USA). Potentiometric detection was with the same instrumentation as described above for the flow-injection measurements.

The composition of the multi-ionophore membrane was as follows: 66 mg of poly(vinyl chloride) (PVC) from Fluka (Milwaukee, WI, USA) or a mixture of 52.8 mg of polyurethane (PU) Tecoflex SG-80A (Thermedies, Woburn, WA, USA) and 13.2 mg of a copolymer of vinyl chloride–vinyl acetate–vinyl alcohol (80:5:15, %, w/w) from Scientific Polymer Products (New York, NY, USA) as the matrix, 132 mg of dioctyl adipate (DOA) as the plasticizer, 0.1 mg of valinomycin (selective ionophore for potassium), 0.16 mg of nonactin (selective ionophore for ammonium ions), 8 mg of calcium ionophore II (N,N,N′,N′-tetracyclohexyl-3-oxapentanediamide), 0.3 mg of sodium ionophore III (N,N,N′,N′-tetracyclohexyl-1,2-phenylenedioxydiacetamide) and 0.12 mg of potassium tetrakis (4-chlorophenyl) borate (KTpClPB) as active components. All ionophores, DOA and KTpClPB were purchased from Fluka. Details of selectivities can be found in ref. 13. All the membrane components (200 mg) were dissolved in tetrahydrofuran and cast into a 22 mm I.D. glass ring placed on a glass plate for evaporation. A piece of 5 mm diameter membrane disc was then cut out of the master membrane and mounted in the Philips ISE-561 electrode body from Glasblaserei Moller (Zurich, Switzerland). A mixture containing 0.02 *M* of each KCl, NH_4Cl, NaCl and $CaCl_2$ was used as internal solution.

The electrode equipped with a wall-jet cup [11] was placed in a beaker, in which a constant level of effluent from the measuring system was maintained and its potential was measured *versus* a double junction reference electrode Model 13-620-47 from Fisher Scientific.

RESULTS AND DISCUSSION

Flow-injection potentiometric response of the multi-ionophore detector

Flow-injection measurement with a non-selective detector and without an on-line analyte separation step cannot be utilized for practical analytical purposes; however, it can be a very useful tool for estimating the usefulness of such a detector for chromatographic detection. In the flow-injection system employed in this study, 50 μl of sample solution were injected into a water carrier stream, which was then merged with a stream of 50 m*M* Tris–HCl buffer solution, pH 7.2, and through the 50-cm mixing coil to the flow-through detector.

In this work we used both electrodes with PVC-based membranes optimized previously [9] and electrodes with PU-based membranes con-

taining the same proportion of ionophores, which are more suitable for producing solid-state sensors [12].

Electrodes with both types of membranes exhibit very similar properties. As one can observe from the flow-injection peaks recorded (Fig. 1), the dynamic response towards monovalent cations is satisfactory, and only in the case of calcium was a much slower return of the electrode potential value to the baseline level found. With PVC-based membrane electrodes, for all monovalent cations except lithium flow-injection peaks are followed by a potential dip below the baseline level, which was not observed with PU-based membranes. As demonstrated by the flow-injection response for various concentrations of ammonium ions (Fig. 2), with a lower concentration of analyte in the injected sample this disturbance disappears and should not affect the chromatographic detection.

The largest signal magnitude was obtained for ions for which selective ionophore was incorporated into a polymer membrane (Table I), although at the proportion of ionophores used the

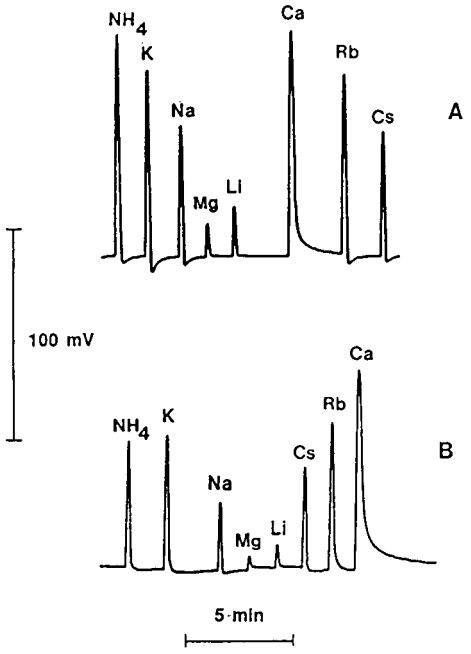

Fig. 1. Flow-injection response obtained for the injection of 50 μl of a 10 mM solution of metal ions with PVC-based (A) and PU-based (B) multi-ionophore membrane electrodes.

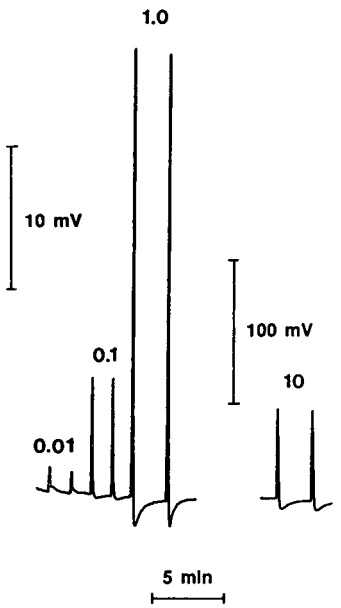

Fig. 2. Flow-injection response obtained for the injection of 50 μl of ammonium chloride solution of the concentration shown in mM with a PVC-based multi-ionophore membrane electrode.

peak height for 1 mM sodium is three times smaller than for the same concentration of calcium. High sensitivity to rubidium and caesium ions can be attributed to the presence of valinomycin in the membrane phase. The sensitivity of valinomycin-based membrane to these cations is known to be relatively high [13]. For the concentration range from 1 to 10 mM analyte in the injected sample, the Nernstian electrode slope was found for calcium only. As in real chromatographic measurements observed potential changes usually do not exceed 15 mV, it is more likely that a linear relationship between the signal magnitude and analyte concentration in injected samples should be expected.

Chromatographic detection with multi-ionophore membrane electrode

For most of cations examined, a larger signal magnitude was obtained with PVC-based membranes, and thus an electrode with such a membrane was employed for all subsequent ion chromatography experiments.

According to the manufacturer, the cation-exchange column ION-210 is most suitable for

TABLE I

FLOW-INJECTION RESPONSE OF MULTI-IONOPHORE MEMBRANE ELECTRODES IN THE SYSTEM SHOWN IN FIG. 1 FOR VARIOUS MATRIX POLYMERS

Sample injection volume 50 μl. Total flow-rate in detector 5.1 ml/min

Cation	PVC-based membrane		PU-based membrane	
	Peak height (mV)[a]	Slope (mV/pM)[b]	Peak height (mV)[a]	Slope (mV/pM)[b]
Li^+	5	19	2	8
Na^+	24	39	7	25
K^+	46	43	25	37
Rb^+	51	34	32	38
Cs^+	28	32	16	30
NH_4^+	58	47	26	32
Mg^{2+}	12	4	4	2
Ca^{2+}	78	30	64	30

[a] For 1 mM concentration of injected solution.
[b] Between 1 and 10 mM concentration of injected solution.

the chromatography of transition metal ions; however, it can also be used to obtain satisfactory results for the chromatography of alkali metals and ammonium ions [4,5]. Of the eluents examined, 10 mM nitric acid, 2 mM picolinic acid, 10 mM citric acid (recommended by Aldrich as eluents for mono- and divalent cations using their universal cation column) and Tris buffer, satisfactory results were obtained with 50 mM Tris–HCl buffer, pH 7.2, as eluent, as used previously for flow-injection measurements (Fig. 3). However, this eluent was not suitable for resolution of rubidium and caesium ions.

The importance of incorporating four different ionophores into the membrane phase is demonstrated by the chromatograms shown in Fig. 4, obtained using conventional ion-selective electrodes for ammonium, potassium and sodium ions with a single, selective ionophore in a PVC-based membrane. However, single-ionophore detectors may serve as very effective selective detectors for some real applications, *e.g.* the determination of ammonia in high-sodium matrices.

From the calibration plots obtained from chromatograms recorded for potentiometric detection with PVC-based multi-ionophore membrane electrodes (Fig. 5) the detection limit for the determined cations was estimated. The amplitude of the baseline noise equal, for the instrumentation used, to 40 μV was compared with the signal magnitude obtained from the injection of 10 μM solutions of the examined metal ions. For a signal-to-noise ratio of 3 and 250 μl sample volume the detection limit was

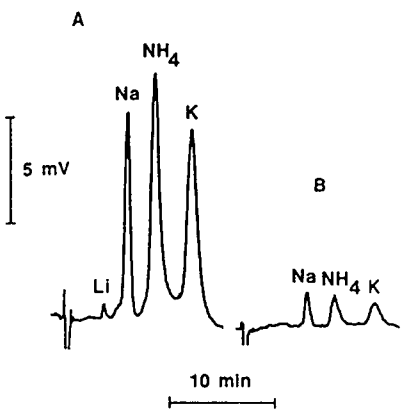

Fig. 3. Ion chromatograms obtained for the injection of 250 μl of a mixture containing 0.25 mM (A) and 25 μM (B) lithium, sodium, ammonium and potassium chlorides at a flow-rate of 2.5 ml/min using 50 mM Tris–HCl buffer, pH 7.2, as eluent with a PVC-based multi-ionophore membrane electrode for detection.

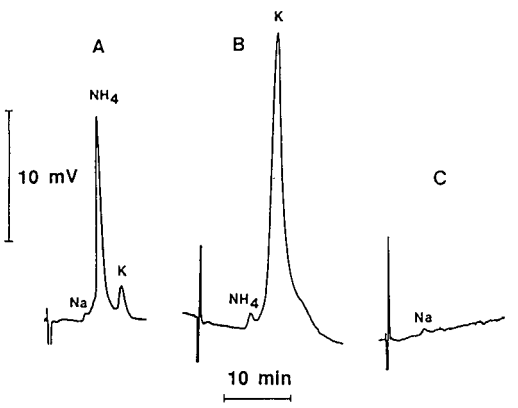

Fig. 4. Ion chromatograms obtained for the injection of 250 μl of a mixture containing 0.25 m*M* lithium, sodium, ammonium and potassium chlorides using as detectors ammonium (A), potassium (B) and sodium (C) ion-selective electrodes at a flow-rate of 2.5 ml/min using the same eluent as in Fig. 3.

estimated to be 0.7, 0.5 and 1.0 μ*M* for sodium, ammonium and potassium, respectively, which corresponds to 4, 2 and 7 ng. This detectability can be further improved by increasing the Tris concentration in the eluent solution, however it is accompanied by the loss of the baseline resolution for concentrations higher than 10 μ*M* in injected solution.

The detectability obtained without any preconcentration step should be considered as satisfactory. It is for all examined ions almost of an order of magnitude better than obtained previously for pH detection in suppressed ion chromatography [4]. The sensitivity of detection of the alkali metal ions studied is similar to the sensitivity of single-column chromatography with conductivity detection [14,15].

Further study on the use of this detection for other columns and simultaneous separations of mono- and divalent ions are in progress, as well as study on development of solid-state sensor with multi-ionophore membranes.

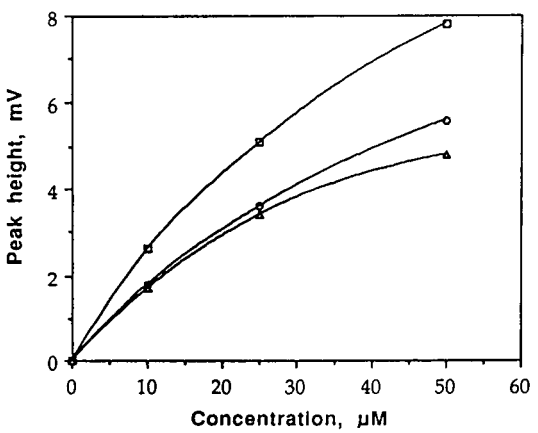

Fig. 5. Calibrations plots obtained for ion chromatography of sodium (○), ammonium (□) and potassium (◇) with a PVC-based multi-ionophore membrane electrode as detector.

ACKNOWLEDGEMENT

The authors thank Professor Mark E. Meyerhoff for helpful discussions and for providing laboratory facilities for performing this study. The research group at Kwangwoon University gratefully acknowledges the Korea Science and Engineering Foundation for supporting this work. The authors also wish to thank Dr. Hai Dong Kim for providing the data acquisition system.

REFERENCES

1 J.G. Tarter (Editor), *Ion Chromatography*, Marcel Dekker, New York, 1987.
2 P.R. Haddad and P.E. Jackson, *Ion Chromatography —Principles and Applications*, Elsevier, Amsterdam, 1990.
3 M. Trojanowicz, A. Ivaska (Editor), *Contemporary Electroanalytical Chemistry*, Plenum Press, New York, 1990, pp. 255–266.
4 M. Trajanowicz and M.E. Meyerhoff, *Anal. Chem.*, 61 (1989) 787.
5 M. Trojanowicz and M.E. Meyerhoff, *Anal. Chim. Acta*, 222 (1989) 95.
6 M. Trojanowicz, E. Pobozy and M.E. Meyerhoff, *Anal. Chim. Acta*, 222 (1989) 109.
7 K. Suzuki, H. Aruga and T. Shirai, *Anal. Chem.*, 55 (1983) 2011.
8 K. Watanabe, K. Tohda, H. Sugimoto, F. Eitoku, H. Inoue, K. Suzuki and S. Nakamura, *J. Chromatogr.*, 566 (1991) 109.
9 Y.S. Park, M.J. Cha, S.H. Han, D.S. Shin, H.D. Kim and G.S. Cha, *J. Korean Chem. Soc.*, 37 (1993) 259.
10 R.J. Forster and D. Diamond, *Anal. Chem.*, 64 (1992) 1721.
11 M. Trojanowicz and W. Frenzel, *Fresenius' Z. Anal. Chem.*, 328 (1987) 653.

12 G.S. Cha, D. Liu, M.E. Meyerhoff, H.C. Cantor, A.R. Midgley, H.D. Goldberg and R.B. Brown, *Anal. Chem.*, 63 (1991) 1666.
13 W.E. Morf and W. Simon, in H. Freiser (Editor), *Ion-Selective Electrodes in Analytical Chemistry*, Vol. 1, Plenum Press, New York, 1978.
14 H. Shintami, K. Tsuji and T. Oba, *Bunseki Kagaku*, 24 (1985) 109.
15 P.E. Jackson, T. Bowser and P.G. Alden, *LC·GC*, 10 (1992) 787.

Journal of Chromatography, 648 (1993) 289–293
Elsevier Science Publishers B.V., Amsterdam

CHROM. 25 405

Short Communication

Determination of chlorinated benzaldehydes and acetophenones in pulp bleaching effluents by gas chromatography

Terrence J. Smith, Ross H. Wearne and Adrian F.A. Wallis*

Division of Forest Products, CSIRO, Private Bag 10, Rosebank MDC, Clayton, Victoria 3169 (Australia)

(First received May 13th, 1993; revised manuscript received June 23rd, 1993)

ABSTRACT

Application of modern sequences involving chlorine, chlorine dioxide and oxygen–alkali to the bleaching of hardwood pulps has led to the formation of chlorinated benzaldehydes and acetophenones as the major chlorinated phenols in the bleaching filtrates. Compounds identified in the filtrates include the chloro derivatives of vanillin, acetoguaiacone, syringaldehyde and acetosyringone. Thirteen of these compounds were converted to their acetates by *in situ* acetylation and were analysed by GC on a J&W DB5 capillary column. Chlorovanillins (2-chlorovanillin, 2,5- and 2,6-dichlorovanillin), chloroacetoguaiacones (2-, 5- and 6-chloroacetoguaiacone) and chloroacetosyringones (2-chloroacetosyringone and 2,6-dichloroacetosyringone) were positively identified as components of filtrates from bleaching of kraft pulps for the first time, along with the five other compounds tested. Satisfactory separation for all analytes was achieved except for 5-chloroacetoguaiacone and 2,5-dichlorovanillin, which co-eluted. Analysis of the latter compounds could be accomplished by mass detection with target ion monitoring. The DB5 column is thus useful for the analysis of the chlorinated benzaldehydes and acetophenones.

INTRODUCTION

The bleaching of wood pulps with molecular chlorine or reagents containing chlorine (chlorine dioxide, hypochlorite) leads to the formation of chlorinated phenols which as components of the effluents have known environmental effects [1]. The chlorinated phenols derive from the residual lignin in the pulps; the major analytes in effluents from bleaching of softwood pulps are chlorophenols, chlorocatechols, chloroguaiacols and chlorovanillins [2], whereas hardwood pulps give, in addition, chlorosyringols and chloro syringaldehydes [3]. Knowledge of the types and amounts of chlorinated phenols in bleaching effluents is an important factor in assessing the environmental quality of the effluents.

In response to the drive to minimise the formation of chlorinated organic compounds in bleaching effluents, continual changes in bleaching technology are taking place. Some of these modifications are oxygen delignification prior to bleaching, the use of chlorine dioxide instead of molecular chlorine in the first bleaching stage, and the reinforcement of the alkali extraction stage with oxygen [4]. These modifications have led to the preponderance of chlorovanillins in

* Corresponding author.

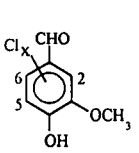

Chlorovanillins

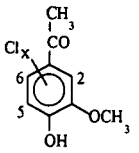

Chloroacetoguaiacones

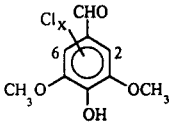

Chlorosyringaldehydes

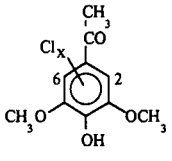

Chloroacetosyringones

the effluents from bleaching of softwood pulps [5,6] and chlorovanillins, chlorosyringaldehydes and chloroacetosyringones with lesser amounts of chloroacetoguaiacones from bleaching of hardwood pulps [7]. Thus the composition of chlorinated phenols in the effluents is changing as the new technology is adopted, and the analytical techniques must be appropriate to accommodate these changes.

The chlorinated phenols in bleaching effluents are usually estimated by the procedure of Voss *et al.* [8] involving *in situ* acetylation GC with electron-capture detection (ECD). The method was assessed in an intercalibration study involving 11 laboratories in Scandinavia [9], and while it was found to be satisfactory for chlorophenols and chloroguaiacols, the precision obtained in the analysis of the chlorocatechols was poor. Lee *et al.* [10] applied a modified *in situ* acetylation procedure to the analysis of a total of 31 chlorinated phenols, and found good recoveries for all compounds including chlorocatechols, with the exception of 4-chlorocatechol. A recent study of the analysis of chlorinated phenols in pulp mill effluents has described a procedure in which acetylation is carried out after extraction [11].

Knuutinen and co-workers have reported the GC separation of the acetates of chlorinated phenols [12], catechols [13] and guaiacols [14], and the three classes of compounds in admixture [15]. In this paper, we describe the GC separation of ring-chlorinated derivatives of vanillin, syringaldehyde, acetoguaiacone and acetosyringone as their acetates after subjecting them to the *in situ* acetylation procedure, and the application of the method to the analysis of pulp bleaching filtrates.

EXPERIMENTAL

Chemicals

1,3-Dichlorobenzene, 2,3,6-trichlorophenol, 2-bromophenol, vanillin, syringaldehyde, acetoguaiacone and acetosyringone were purchased from Aldrich. The remaining compounds were prepared by established techniques. Satisfactory spectral and analytical data were obtained for new compounds.

2-Chlorovanillin was prepared from vanillin via the 2-nitro derivative by the method of Raiford and Lichty [16] as modified by Ross *et al.* [17]. 5-Chlorovanillin was the product of direct chlorination of vanillin [18], and 6-chlorovanillin was prepared by chlorination of benzalvanillin triacetate [16]. Chlorination of 2-chlorovanillin and 6-chlorovanillin yielded 2,5-dichlorovanillin and 5,6-dichlorovanillin respectively, and 2,6-dichlorovanillin was obtained from 6-chlorovanillin through the 2-nitro intermediate [16].

The ring-chlorinated acetoguaiacones, 5-chloroacetoguaiacone and 6-chloroacetoguaiacone, were prepared from the acetates of 5-chlorovanillin and 6-chlorovanillin respectively by reaction with diazomethane and subsequent hydrolysis [19]. Similarly, the hitherto-unknown 2-chloroacetoguaiacone, m.p. 97–98°C, was prepared from the acetate of 2-chlorovanillin.

Chlorination of syringaldehyde and acetosyringone in dioxane with 1 mol.equiv. chlorine in acetic acid gave 2-chlorosyringaldehyde, m.p. 108–109°C, and 2-chloroacetosyringone, m.p. 93–94°C, respectively. Analogously, reaction with 2 mol.equiv. chlorine afforded 2,6-dichloroacetosyringone, m.p. 114–115°C. 2,6-Dichlorosyringaldehyde, m.p. 195–196°C, was obtained by chlorination of syringaldehyde acetate in acetic acid, and subsequent alkaline hydrolysis. These four compounds have not been previously described.

Bleaching of wood pulp

An oxygen-delignified eucalypt kraft pulp was treated with an aqueous solution of chlorine at pH ≈ 2, washed, and was subsequently extracted in a steel autoclave with a sodium hydroxide solution in the presence of oxygen [7]. The filtrate from the alkaline extraction was acidifed to pH 2 with 18 *M* sulphuric acid and stored at −12°C until required for analysis.

Acetylation and extraction of the phenols

Analysis with ECD. To a well-mixed solution of the bleach filtrate (10 ml) in a test tube, an aliquot of 2,3,6-trichlorophenol (25 μl of 25 μg/ml solution in methanol) was added as the internal standard, and 2-bromophenol (25 μl of a 5.0 μl/ml solution in methanol) was added as the surrogate standard. Potassium carbonate solution (72%, 1.0 ml) was added with swirling, followed by acetic anhydride (1.0 ml). The contents of the test tube were mixed on a vortex mixer for 1.0 min, distilled hexane (5 ml) was added, and mixing was continued for a further 0.5 min. Part of the hexane solution which separated (1 ml) was transferred to a sample vial, and 1,3-dichlorobenzene (25 μl of 130 μg/ml solution in methanol) was added as check on the injection prior to the GC analysis.

Analysis with the mass-selective detector (MS). A solution of the bleach filtrate (50 ml) was placed in a 100 ml separating funnel, and an aliquot of 2,3,6-trichlorophenol (250 μl of 25 μg/ml solution in methanol) was added as the internal standard. Potassium carbonate solution (72%, 1.0 ml) was added with swirling, followed by acetic anhydride (1.0 ml), and the mixture was shaken with frequent venting for 1.0 min. Distilled hexane (5 ml) was added, and mixing was continued for a further 0.5 min. The hexane solution was removed, and was concentrated to *ca.* 1 ml by passing a stream of nitrogen over the solution, and was transferred to a sample vial for GC analysis.

Gas chromatography

GC was carried out on a Hewlett-Packard HP5890 series II chromatograph fitted with an autoinjector, an electron-capture detector and an HP5971 mass-selective detector. The column used for the analyses was a J&W bonded phase DB5 fused-silica column (30 m × 0.25 mm I.D.) with a phase thickness 0.25 μm. Additional data were obtained on an SGE bonded phase BP20 fused-silica column (12 m × 0.25 mm I.D.). Purified helium was used as the carrier gas with a linear flow velocity 30 cm/s. Injector and detector temperatures were 300°C. The column temperature was kept at 50°C for 1 min, then programmed at 5°C/min to 250°C, and 20°C/min to 280°C. Injections were splitless, 2.0 μl for analyses using ECD and 4.0 μl for analyses with MS, and a purge delay of 0.75 min was used. For MS, electron impact (70 eV) spectra were obtained for masses 40 to 450 u.

RESULTS AND DISCUSSION

The GC behaviour of a mixture of 46 acetylated chlorinated phenols, catechols and guaiacols on an SE-30 quartz capillary column was studied by Knuutinen and Korhonen [15]. Lee *et al.* [10] tested four capillary columns of different manufacture and polarity, and concluded that the columns with a bonded phase containing 5% phenyl silicone gave the best resolution of their 31 acetylated chlorinated phenols. The column with the same bonded phase, a 30 m J&W DB-5 fused-silica column, was used in the present work.

The *in situ* acetylation technique is satisfactory for the analysis of chlorinated phenols in effluents from pulp bleaching, providing care is taken to ensure the precision of the chlorocatechol analyses. We found that after rendering the solution to be analysed alkaline with sodium carbonate, the recoveries of chlorocatechols were poor unless the extraction with hexane was carried out immediately. As well as the internal standard, 2,3,6-trichlorophenol, a surrogate standard, 2-bromophenol, was added to the solutions before the derivatisation–extraction procedure. An aliquot of 1,3-dichlorobenzene was added to the final hexane solution to check the amount of solution injected into the GC system.

The chromatogram of the mixed acetylated phenols with mass detection is presented in Fig. 1A, and the retention times of the phenols are given in Table I. It can be seen that the

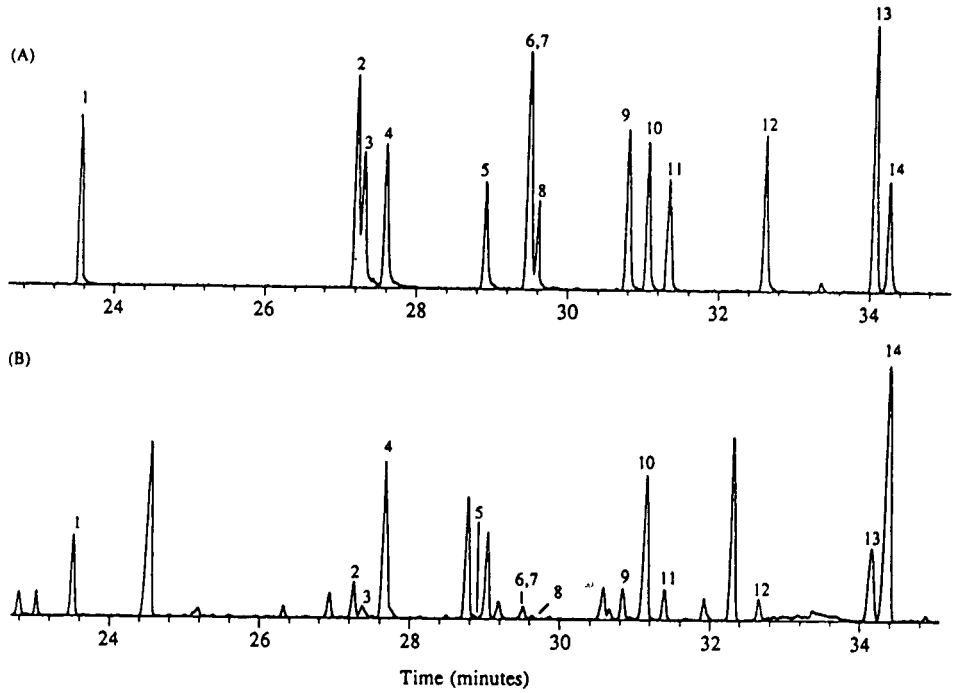

Fig. 1. Gas chromatogram with MS detection of (A) a standard mixture of acetylated phenols (numbers refer to compounds listed in Table I) and (B) a mixture of acetylated chlorinated phenols obtained by *in situ* acetylation of a filtrate from treatment of a chlorinated eucalypt kraft pulp with oxygen-alkali.

TABLE I

GC RETENTION TIMES OF ACETYLATED CHLORINATED PHENOLS

GC conditions as outlined in the Experimental section.

Peak No.	Phenol	Retention time (min)	Relative retention time
1	2,3,6-Trichlorophenol	23.50	1.00
2	2-Chlorovanillin	27.23	1.159
3	5-Chlorovanillin	27.35	1.164
4	6-Chlorovanillin	27.65	1.177
5	2-Chloroacetoguaiacone	28.91	1.230
6	5-Chloroacetoguaiacone	29.48	1.254
7	2,5-Dichlorovanillin	29.51	1.256
8	6-Chloroacetoguaiacone	29.61	1.260
9	5,6-Dichlorovanillin	30.81	1.311
10	2-Chlorosyringaldehyde	31.08	1.323
11	2,6-Dichlorovanillin	31.39	1.336
12	2-Chloroacetosyringone	32.62	1.388
13	2,6-Dichloroacetosyringone	34.11	1.451
14	2,6-Dichlorosyringaldehyde	34.32	1.460

13 acetylated benzaldehydes and acetophenones are separated well, with the exception of 5-chloroacetoguaiacone and 2,5-dichlorovanillin. Attempted separation of these components on a polar SGE BP20 column was not successful, as the analytes were retained on the column. In general, the J&W DB5 column is able to separate most of the chlorinated phenols in the bleaching effluents [10], and its continued use is recommended.

A GC trace with MS detection of an acetylated extract from a typical oxygen-reinforced alkali extraction of chlorinated eucalypt kraft pulp is given in Fig. 1B. The presence of 2,5-dichlorovanillin and 5-chloroacetoguaiacone in the peak at *ca.* 29.5 min may be ascertained by inspection of the mass spectra, and their quantification may be achieved by monitoring the m/z $220^{+\cdot}$ and $185^{+\cdot}$ ions respectively. The chlorovanillins, 2-chlorovanillin, 2,5- and 2,6-dichlorovanillin, the chloroacetoguaiacones, 2-, 5- and 6-chloroacetoguaiacone, and the chloroacetosyringones, 2-chloroacetosyringone and 2,6-dichloroacetosyringone, have not previously been positively identified in the effluents from pulp bleaching [20]. Both 5-chlorovanillin and 6-chlorovanillin have been reported as components of bleach effluents. However, 2-chlorovanillin is present in greater amounts than 5-chlorovanillin in an alkaline extraction filtrate following chlorination (Fig. 1B), and as the retention time of 2-chlorovanillin and 5-chlorovanillin are similar, it is possible that the compound analysed in the earlier studies was the 2-chloro isomer. An additional peak occurring in the acetylated bleaching filtrate at 33.42 min (Fig. 1B) is probably the acetate of 2,5,6-trichlorovanillin. The mass spectrum of the peak was consistent with the acetate of 2,5,6-trichlorovanillin (m/z $[M]^+$ 296).

ACKNOWLEDGEMENTS

Financial support from the National Pulp Mills Research Program is gratefully acknowledged. The authors thank Mr. Luke R. Biltris for his expert technical assistance.

REFERENCES

1 N. Bonsor, N. McCubbin and J.B. Sprague, *Kraft Mill Effluents in Ontario, MISA Report*, Ontario Ministry of the Environment, Toronto, April 1988.
2 R.H. Voss, J.T. Wearing and A. Wong, *Pulp Pap. Mag. Can.*, 82 (1981) T65.
3 R.H. Voss, J.T. Wearing and A. Wong, *Tappi*, 64 (3) (1981) 167.
4 R.M. Berry, C.E. Luthe, R.H. Voss, P. Wrist, P. Axegård, G. Gellerstedt, P.-O. Lindblad and I. Pöpke, *Pulp Pap. Can.*, 92 (1991) T155.
5 N. Liebergott, B. van Lierop, T. Kovaks and A. Nolin, *Tappi J.*, 73 (10) (1990) 207.
6 R.W. Allison, P.N. McFarlane and M.C. Judd, *Pap. Puu*, 74 (1992) 404.
7 T.J. Smith, R.H. Wearne and A.F.A. Wallis, in preparation.
8 R.H. Voss, J.T. Wearing and A. Wong, in L.H. Keith (Editor), *Advances in the Identification and Analysis of Organic Pollutants in Water*, Vol. 2, Ann Arbor Science Publ., Ann Arbor, MI, 1981. pp 1059–1095.
9 B. Starck, P.-O. Bethge, M. Gergov and E. Talka, *Pap. Puu*, 67 (1985) 745.
10 H.-B. Lee, R.L. Hong-You and P.J.A. Fowlie, *J. Assoc. Off. Anal. Chem.*, 72 (1989) 979.
11 A. Morales, D.A. Birkholz and S.E. Hrudey, *Water Environ. Res.*, 64 (1992) 669.
12 I.O.O. Korhonen and J. Knuutinen, *J. Chromatogr.*, 256 (1983) 135.
13 J. Knuutinen, J. Tarhanen and M. Lahtiperä, *Chromatographia*, 15 (1982) 9
14 J. Knuutinen and E. Kolhmainen, *Chromatographia*, 15 (1982) 707.
15 J. Knuutinen and I.O.O. Korhonen, *J. Chromatogr.*, 257 (1983) 127.
16 L.C. Raiford and J.G. Lichty, *J. Am. Chem. Soc.*, 52 (1930) 4576.
17 S.T. Ross, R.G. Franz, J.W. Wilson, R.A. Hahn and H.M. Sarau, *J. Heterocycl. Chem.*, 23 (1986) 1805.
18 G.D. Thorn and C.B. Purves, *Can. J. Chem.*, 32 (1954) 373.
19 J.E. Jayne, *J. Am. Chem. Soc.*, 75 (1953) 1742.
20 L.R. Suntio, W.Y. Shiu and D. Mackay, *Chemosphere*, 17 (1988) 1249.

Journal of Chromatography, 648 (1993) 294–298
Elsevier Science Publishers B.V., Amsterdam

CHROM. 25 320

Short Communication

False results in headspace–gas chromatographic analysis of trihalomethanes in swimming pool water due to elevated headspace temperatures

Karl Cammann and Karl Hübner*

Chair for Analytical Chemistry, University of Münster, Wilhelm Klemm Strasse 8, W-4400 Münster (Germany)

(Received March 30th, 1993)

ABSTRACT

The application of a headspace GC method for the determination of trihalomethanes (THMs) in water is described for the case of swimming pool water. As a consequence of chlorination, swimming pool water contains, besides THMs, many other halogenated compounds. Among these, the trihaloacetic acids may interfere with THM determination because they are decarboxylated to the related THMs at the usually applied headspace temperatures. This disturbing effect was investigated at different temperatures for real swimming pool water samples. It occurs down to 40°C and was found to be avoidable at a headspace temperature of 33°C or less.

INTRODUCTION

Headspace GC (HS-GC) is a common method for the determination of volatile species in water. Since 1991 HS-GC has been a standardized method for the analysis of volatile halogenated hydrocarbons (VHCs) in water in Germany [1]. It is a cleaner and less time-consuming method than, for example, liquid–liquid extraction. Because of the Clausius–Clapeyron equation most applications recommend a HS temperature of 60–80°C to achieve good sensitivity. Higher temperatures should be avoided to keep the amount of vaporized water coming onto the column low (water can destroy the stationary phase of non-polar columns).

The application of this method to water samples from swimming pools can lead to false results in the determination of trichloromethane, which is usually the most interesting VHC in chlorinated swimming pool water [2]. In addition to the trihalomethanes (THMs, including trichloro-, bromodichloro-, dibromochloro- and tribromomethane), which are the most discussed products of water chlorination, more than 100 other halogenated compounds have been identified so far [3]. The brominated species are a consequence of the bromide concentration in the water used [4]. One type of species that occurs is the trihaloacetic acids (THAs). So far mainly the presence of trichloroacetic acid (TCA) has been reported [5,6]. TCA can undergo decarboxylation to trichloromethane and carbon dioxide at high temperature. This fact is used for the determination of TCA in urine by keeping the

* Corresponding author.

0021-9673/93/$06.00

urine sample at 90°C for, *e.g.*, 90 min followed by an HS analysis to quantify the trichloromethane formed, which can be used to determine the original TCA concentration in the urine [7,8]. So far, the temperature above which TCA begins to be decarboxylated has not been reported. Decarboxylation starting at lower temperatures could cause problems in THM determination.

In this paper the influence of the HS temperature on the decarboxylation of TCA will be reported, as well as the maximum temperature that can be applied for the HS analysis to determine trichloromethane in swimming pool water without any interference by trichloromethane formed from TCA. The found concentrations of different THMs and THAs for an investigated swimming pool water will be given.

EXPERIMENTAL

The HS temperature dependence of the THM peak areas of real swimming pool water samples was investigated by measuring at three different temperatures (33, 40 and 60°C) and different dwell times at these temperatures. The results were compared with an aqueous THM standard measured at 60°C HS temperature.

Instrumentation

The gas chromatograph (5890 series II) and HS sampler (19395 A) were from Hewlett Packard. The vial pressure prior to injection was set at 1.1 bar, the sample loop volume was 1 ml and the injection time was 15 s. The vials had a volume of 13 ml, contained 2 ml of sample and were capped with butylgum septa coated with PTFE. The GC injection port temperature was 250°C. The column was an SE 52 (50 m × 0.32 mm I.D.; film thickness = 0.25 μm). The temperature programme was 11 min at 40°C, 8°C/min to 80°C. Detection was accomplished by election-capture detection at 320°C.

RESULTS AND DISCUSSION

Fig. 1 shows the peak areas of trichloromethane found for the three temperatures and the different equilibration times. It can be seen

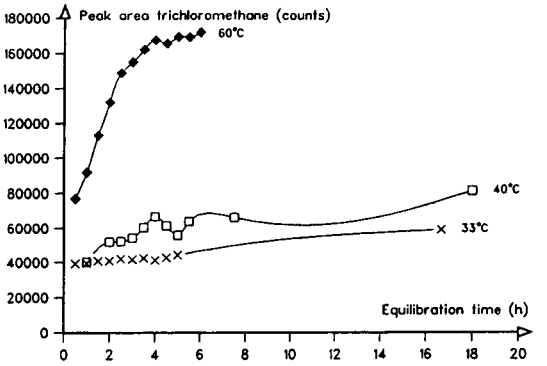

Fig. 1. Influence of HS temperature and equilibration time on the additional formation of trichloromethane in a swimming pool water sample.

that at 60°C the area is increasing continuously. To a lesser extent this pattern was also found at 40°C, whereas at 33°C the peak area was almost constant for several hours. A temperature lower than 33°C was not always practicable and reliably constant owing to the high laboratory ambient temperatures during the summer. The increasing areas at higher HS temperatures were found not to be a consequence of a slow reaching of the equilibrium state between the gaseous and the liquid phase. This is shown in Fig. 2, in which the peak area of trichloromethane in a THM standard in distilled water is plotted against the equilibration time at 60°C. Fig. 2 shows that the equilibrium state in an aqueous matrix is reached after 60 min or even after 30 min. This leads to the assumption of an additional formation of trichloromethane in the pool water sample dur-

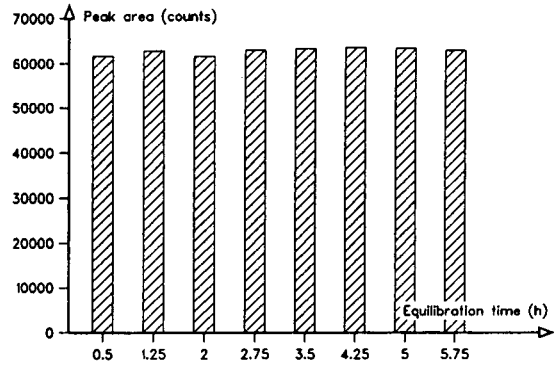

Fig. 2. Influence of the equilibration time at 60°C on the peak area of trichloromethane in an aqueous standard.

ing the equilibration in the HS sampler. Since the chlorine was reduced by sodium thiosulphate at the moment of sampling, the formation of trichloromethane by chlorine could be excluded. Thus, most likely, the presence of TCA in the sample was the reason for the trichloromethane formation. Temperatures of 40 and 60°C seem to be high enough to allow TCA to be decarboxylated to trichloromethane. Fig. 3 shows the decarboxylation rate of TCA at four different temperatures and various dwell times at these temperatures. This experiment was carried out with a TCA standard containing 142 μg/l TCA. Thus 104 μg/l trichloromethane would have meant 100% decarboxylation. At 70 and 90°C, after 1 or 2 h decarboxylation, rates of 80% (90°C) or more than 10% (70°C), respectively, were found. More than 10% can mean tens of μg/l of additional trichloromethane in the case of hundreds of μg/l TCA. This would lead to much increased and therefore false results in the determination of trichloromethane. An investigation at 60°C is missing, but Fig. 1 shows that the contribution of TCA to the formation of trichloromethane cannot be neglected at 60°C. At 50 and 40°C the increase in peak areas was still measurable but not very high. Thus, the error would be smaller but not negligible depending on the quantity of TCA. Even 48 h at 30°C had no influence on the peak area of trichloromethane.

Fig. 4 shows the results for bromodichloro-

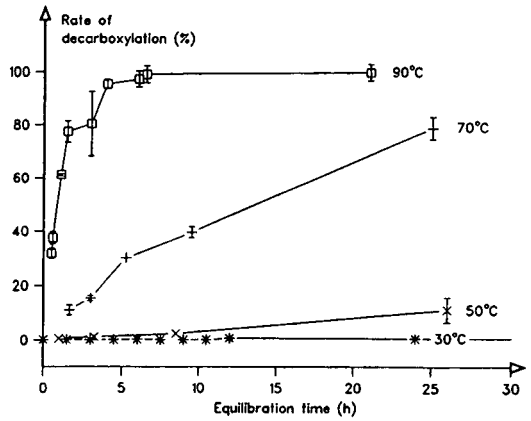

Fig. 3. Influence of temperature and dwell time on the decarboxylation rate of TCA.

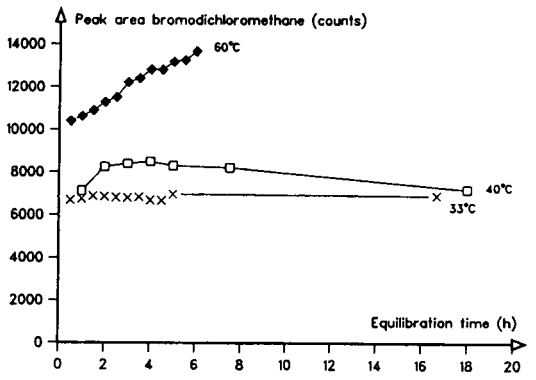

Fig. 4. Influence of HS temperature and equilibration time on the additional formation of bromodichloromethane in a swimming pool water sample.

methane of the same pool water sample. Again an increase in the peak area was found at 60°C but not at 40°C (at least not after 2 h equilibration time) or 33°C. The increase at 60°C indicated the presence of bromodichloroacetic acid in the sample.

The areas of the other trihalomethanes, dibromochloro- and tribromomethane, showed no dependence on temperature, which might be because of the absence of the corresponding THAs or because those decarboxylations only take place at even higher temperatures.

Measured concentrations

Applying a HS temperature of 33°C, the concentrations of THMs were measured by using an external calibration in distilled water. The equilibration time was 90 min, the vial pressure was set at 1.1 bar and the sample volume was 2 ml in 10-ml vials. For the determination of the THAs other vials of the same water samples were kept at 90°C for 6.5 h (less did not lead to a 100% decarboxylation rate according to Fig. 3) and afterwards analysed in the same way as the samples mentioned above. The results from the samples not treated at 90°C were subtracted from the latter ones and thus gave the amounts of THM formed by the decarboxylation of THA. These concentrations could be transformed into the original amounts of THA in the water samples. Table I shows the results for the four THMs, TCA, bromodichloroacetic acid and dibromochloroacetic acid. The concentration of

TABLE I

FOUND CONCENTRATIONS OF THMs AND THAs IN THREE DIFFERENT POOLS OF TWO GERMAN INDOOR SWIMMING POOLS

	Concentration (μg/l)		
	Bath I (swimmers' pool)	Bath I (jumpers' pool)	Bath II (swimmers' pool)
Trichloromethane	22.4 ± 2.64	26.5 ± 3.18	21.4 ± 2.52
Bromodichloromethane	2.60 ± 0.89	2.90 ± 1.01	2.28 ± 0.77
Dibromochloromethane	0.40 ± 0.09	0.36 ± 0.08	0.50 ± 0.12
Tribromomethane	0.06 ± 0.01	0.18 ± 0.04	0.35 ± 0.09
Trichloroacetic acid	199 ± 45.9	175 ± 37.1	245 ± 43.9
Bromodichloroacetic acid	1.59 ± 3.04	0.85 ± 3.04	1.05 ± 2.49
Dibromochloroacetic acid	0.47 ± 0.34	0.08 ± 0.23	0.06 ± 0.31

tribromomethane did not change after the treatment at 90°C and thus no tribromoacetic acid was quantified. More than 6.5 h at 90°C did not lead to higher peak areas and therefore it can be assumed that for all THAs the decarboxylation was completed after 6.5 h, though this was not investigated in detail for THAs other than TCA.

The proportions of THMs are typical of chlorinated water that contains very little bromide. In the investigated pools the concentrations found were less than 0.1 mg/l. Because of this trichloromethane is the main THM and the concentrations of the other THMs decrease with increasing number of bromine atoms per molecule. The THAs behave in the same way, which means that trichloroacetic acid is the dominant representative of this group. The relatively high levels of confidence for the THAs result from the standard deviation of the results after keeping the samples at 90°C, which were quite high (n = 3). The confidence levels of the THAs were obtained by addition of those of the measurements before and after 90°C treatment, also making them higher.

CONCLUSIONS

Since the presence of TCA in swimming pool water seems to be common, the determination of trichloromethane (and thus also of the other VHCs, *e.g.* trichloroethene) by HS-GC should be performed by using an HS temperature of 33°C or even less to avoid any interference by additional THM formation. This considered, the HS method is still a sufficient, clean and time-saving method compared with liquid–liquid extraction methods. Higher temperatures would lead to false results and thus misinterpretations.

By keeping part of the samples at 90°C for at least 6.5 h, the total amount of THM after decarboxylation of the corresponding THA can be measured. Subtracting the values found without treatment at 90°C from those after this treatment gives the amount of THAs in the water samples.

ACKNOWLEDGEMENTS

This work was financially supported by the German Ministry for Research and Technology funding the Projects 325-4007-07 INR-223 and 325-4007-07 INR-245.

The results of this paper will also be part of a master thesis.

REFERENCES

1 *Analyses in Water, Waste Water and Sewage Sludge*, DEV (German Standardized Methods), 1991, prescription 38407 part 5.

2 G. Aggazzotti, G. Fantuzzi, P.L. Tartoni and G. Predieri, *Arch. Environ. Health*, 45 (1990) 175–179.

3 M.P. Italia and P.C. Uden, *J. Chromatogr.*, 449 (1988) 326–330.
4 B. Gabell, *Master Thesis*, University of Bremen, Germany, 1980.
5 M. Clemens and H.F. Schöler, *Zentralblatt Hygiene*, 193 (1992) 91–98.
6 T. Kemmei, N. Takayanagi, Y. Iyama, N. Saito, M. Komori and K. Kitakado, *Toyamaken Eisei Kenkyusho Neup*, 14 (1990) 202–204.
7 V. Senft, *J. Chromatogr.*, 337 (1985) 126–130.
8 J.M. Christensen, K. Rasmussen and B. Köppen, *J. Chromatogr.*, 442 (1988) 317–323.

Journal of Chromatography, 648 (1993) 299–305
Elsevier Science Publishers B.V., Amsterdam

CHROM. 25 397

Short Communication

Separation of the anomers and isomers of 2′-deoxyuridine and thymidine by capillary zone electrophoresis

A. Van Schepdael*, M. Vandewyer, A. Van Aerschot, P. Herdewijn, E. Roets and J. Hoogmartens

Laboratorium voor Farmaceutische Chemie, Instituut voor Farmaceutische Wetenschappen, Van Evenstraat 4, B-3000 Leuven (Belgium)

(First received March 30th, 1993; revised manuscript received July 1st, 1993)

ABSTRACT

Anomerisation and isomerisation take place during acidic degradation of 2′-deoxyuridine (dUrd) and thymidine (Thd) due to the opening and reclosure of the furanose ring. A capillary electrophoretic method was developed which was able to separate dUrd and Thd from their respective anomers and pentopyranosyl isomers. Using a fused-silica capillary (70 cm × 75 μm I.D.) the influence of the type, pH and concentration of the buffer was systematically investigated as well as the effect of voltage and temperature. With a 20 m*M* sodium tetraborate buffer of pH 9.5 and 10 for dUrd and Thd, respectively, good resolution between anomers and isomers was obtained at 20 kV and 50°C.

INTRODUCTION

Degradation studies on 2′-deoxyuridine (dUrd) and thymidine (Thd) necessitated an analytical system that was able to separate all the compounds formed. It has been shown that the hydrolysis of dUrd and Thd is accompanied by the formation of the anomeric and isomeric forms 1-(2-deoxy-α-D-*erythro*-pentofuranosyl)-uracil (αFdUrd), 1-(2-deoxy-α-D-*erythro*-pentopyranosyl)uracil (αPdUrd), 1-(2-deoxy-β-D-*erythro*-pentopyranosyl)uracil (βPdUrd) and 1-(2-deoxy-α-D-*erythro*-pentofuranosyl)thymine (αFThd), 1-(2-deoxy-α-D-*erythro*-pentopyranosyl)-thymine (αPThd), 1-(2-deoxy-β-D-*erythro*-pentopyranosyl)thymine (βPThd) respectively [1]. See Fig. 1 for structures of these compounds. In that paper it was demonstrated that anomerisation and isomerisation of dUrd and Thd take place during degradation, due to the opening and reclosure of the furanose ring. The degradation compounds were at that time separated by two-dimensional thin layer chromatography and quantitated by ^{14}C liquid scintillation counting. To investigate the kinetics of hydrolysis of dUrd and Thd, a liquid chromatographic (LC) method for the analysis of the cold substance was developed previously [2]. Since an LC analysis takes approximately 1/2 hour, the potential of

* Corresponding author.

0021-9673/93/$06.00

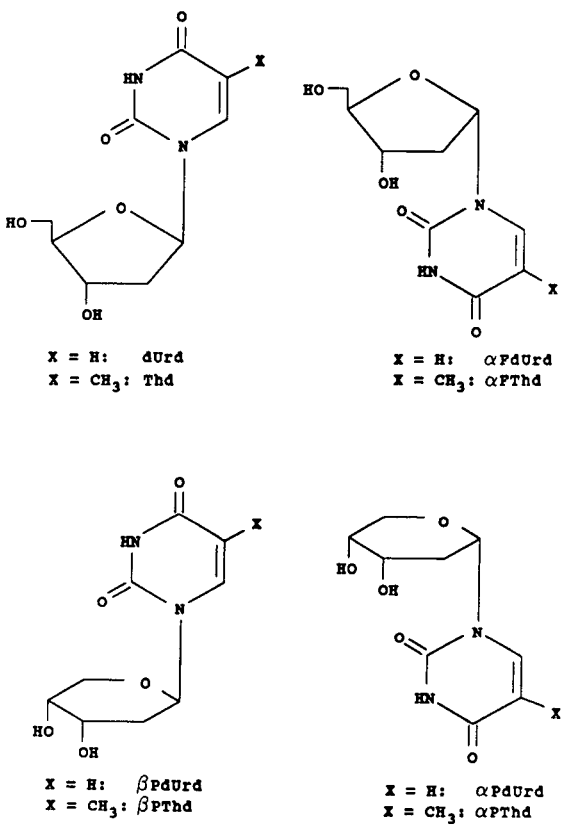

Fig. 1. Structures of dUrd and Thd, and their anomers and isomers.

capillary electrophoresis (CE) was investigated, to speed up the assay. Previous work on CE of nucleosides includes polyacrylamide gel electrophoresis [3], micellar electrokinetic chromatography (MECC) [4–9] and capillary zone electrophoresis (CZE) at pH values ≤ 7 [10–14].

EXPERIMENTAL

Chemicals

dUrd and Thd were purchased from Janssen Chimica (Beerse, Belgium). αFdUrd and αFThd were synthesized according to a previously published procedure [15]. The synthesis of the other compounds is described elsewhere [16]. Reagents were of analytical grade (Merck, Darmstadt, Germany) and Milli-Q water (Millipore, Milford, MA, U.S.A.) was used throughout. The concentration of each of the compounds in the test mixture was approximately 10^{-5} *M* in Milli-Q water.

Capillary electrophoresis

CE was performed on a Spectraphoresis 500 (Spectra Physics, San Jose, CA, USA) coupled to a Model 3396 seriesII integrator (Hewlett-Packard, Avondale, PA, USA). Fused-silica capillaries (70 cm × 75 μm I.D.) were obtained from Spectra Physics. pH adjustments of sodium tetraborate buffer were performed with a 0.1 *M* boric acid solution or a 0.5 *M* sodium hydroxide solution.

RESULTS AND DISCUSSION

To develop a suitable CE method for the resolution of dUrd and its anomer and isomers, the influence of the pH and concentration of the buffer, applied voltage and temperature was successively investigated. Preliminary studies using sodium glycinate buffer of pH 10.8, sodium phosphate buffer of pH 9.3 and sodium tetraborate buffer of pH 9.5 and 20 m*M* each had shown that the latter gave the best separation of the four compounds. The influence of the pH was thus studied using sodium tetraborate buffers and the results of the pH study are summarized in Table I. The separation parameters were calculated following instructions for liquid chromatography in the European Pharmacopoeia [17], for example: resolution = 1.18 × (difference in migration times of the peaks)/(sum of peak widths at half of the peak height). It can be seen that the resolution of αFdUrd and dUrd changes drastically in the neighbourhood of the pK_a of dUrd ($pK_a = 9.3$). Mobility diminishes with a pH increase, because the ionization of the compounds and thus the electrophoretic repulsion from the cathode, increases. The increase in electroosmotic flow velocity is apparently less than the increase in electrophoretic velocity. For subsequent studies a pH of 9.5 was chosen because it yielded a fairly good separation combined with symmetrical peaks. This pH is furthermore obtained when making a 20 m*M* solution of sodium tetraborate in Milli-Q water without any further pH adjustment.

Table II shows the results of experiments in

TABLE I

INFLUENCE OF THE BUFFER pH ON THE SEPARATION CHARACTERISTICS OF dUrd AND ITS ANOMER AND ISOMERS

Electrolyte, 20 m*M* sodium tetraborate adjusted to pH with 0.5 *M* sodium hydroxide or 0.1 *M* boric acid; capillary, fused silica, 70 cm × 75 μm I.D.; temperature, 30°C; voltage, 15 kV; injection, hydrodynamic, 3 s; detection, UV at 262 nm.

pH	Mobility ($cm^2 kV^{-1} min^{-1}$)				Peak symmetry				Resolution		
	αFdUrd	dUrd	αPdUrd	βPdUrd	αFdUrd	dUrd	αPdUrd	βPdUrd	αFdUrd-dUrd	dUrd-αPdUrd	αPdUrd-βPdUrd
8.6	36.5	36.5	35.9	33.7	[a]	[a]	1.0	0.9	0	2.2	6.8
9.1	37.1	36.9	34.2	32.1	[a]	1.1	0.9	1.0	1.2	9.6	5.8
9.5	36.9	36.1	32.4	30.6	1.1	1.0	1.0	1.1	2.7	11.1	4.9
10.0	29.8	29.1	25.2	23.5	1.0	1.0	1.0	1.0	2.9	13.2	5.4
10.5	25.1	24.6	20.9	19.0	1.0	0.9	1.0	1.1	2.1	12.6	5.4
11.0	22.8	22.5	19.0	17.1	[a]	[a]	1.0	1.0	1.1	10.6	4.8

[a] No separation of peaks at one twentieth of the peak height.

which the concentration of the buffer was modified. Since a good overall resolution combined with good symmetry factors and short analysis times was obtained with a 20 m*M* buffer, this concentration was chosen for further work. The analysis is faster with less concentrated buffer. This is consistent with an increase of the electroosmotic flow when ionic strength diminishes, which was also confirmed by the current monitoring method [18].

The influence of the applied voltage is summarized in Table III. A voltage of 20 kV was chosen for further work, because it allowed a fast separation with symmetric peaks and very good resolution. It is apparent that the electroosmotic velocity increases more with increasing voltage than the electrophoretic velocity of the negatively charged compounds, since the overall mobility rises with rising voltage.

Table IV indicates that temperature does not significantly change the separation pattern. Due to a lowering of the viscosity, the separation was speeded up with a temperature increase. A temperature of 50°C was selected for subsequent studies.

Fig. 2 depicts the separation of dUrd from its

TABLE II

ELECTROPHORETIC PARAMETERS FOR THE SEPARATION OF dUrd FROM ITS ANOMER AND ISOMERS USING DIFFERENT CONCENTRATIONS OF SODIUM TETRABORATE BUFFER OF pH 9.5

Other conditions were as described for Table I.

Buffer concentr.	Mobility ($cm^2 kV^{-1} min^{-1}$)				Peak symmetry				Resolution		
	αFdUrd	dUrd	αPdUrd	βPdUrd	αFdUrd	dUrd	αPdUrd	βPdUrd	αFdUrd-dUrd	dUrd-αPdUrd	αPdUrd-βPdUrd
10 m*M*	44.1	43.3	40.5	39.0	0.9	0.9	1.0	0.9	1.9	6.3	2.8
15 m*M*	39.1	38.3	35.0	33.2	0.9	0.9	0.9	0.9	2.4	9.0	4.0
20 m*M*	36.9	36.1	32.4	30.6	1.1	1.0	1.0	1.1	2.7	11.1	4.9
25 m*M*	31.9	31.2	27.3	25.5	1.0	1.0	1.0	1.0	2.9	13.8	5.9
30 m*M*	30.0	29.5	25.4	23.5	1.0	0.8	1.0	0.9	2.0	15.1	6.4

TABLE III

ELECTROPHORETIC PARAMETERS FOR THE SEPARATION OF dUrd FROM ITS ANOMER AND ISOMERS WHEN APPLYING DIFFERENT VOLTAGES

Electrolyte, 20 m*M* sodium tetraborate pH 9.5. Other conditions were as described for Table I.

Voltage	Mobility ($cm^2 kV^{-1} min^{-1}$)				Peak symmetry				Resolution		
	αFdUrd	dUrd	αPdUrd	βPdUrd	αFdUrd	dUrd	αPdUrd	βPdUrd	αFdUrd-dUrd	dUrd-αPdUrd	αPdUrd-βPdUrd
5 kV	34.7	34.0	30.3	28.4	1.0	1.0	1.0	1.0	1.9	9.0	4.5
10 kV	36.3	35.6	31.9	30.1	1.0	1.0	1.1	0.9	2.5	10.8	4.8
15 kV	36.9	36.1	32.4	30.6	1.1	1.0	1.0	1.1	2.7	11.1	4.9
20 kV	37.7	36.9	33.1	31.1	1.0	1.1	1.0	1.0	2.7	10.5	4.6
25 kV	39.4	38.6	34.8	32.9	0.9	0.9	0.8	0.9	2.3	9.3	4.1
30 kV	41.7	40.8	37.0	35.0	1.0	1.0	0.9	1.1	2.0	7.7	3.5

anomer and isomers under the finally chosen conditions. The linearity of the detector was tested in a range of 10^{-3} *M* dUrd (228 μg/ml dUrd) to $3.9 \cdot 10^{-6}$ *M* dUrd (0.89 μg/ml dUrd) using 9 calibration points (27 data points). The following regression curve was obtained: peak area = 1601 + 4481 × concentration (μg/ml); r = 0.9999; standard error of y estimate = 2039; standard deviation of slope = 10.

The limit of detection for a S/N ratio of 3 was approximately 10^{-6} *M* for dUrd using a 3-s hydrodynamic injection. Six injections of this solution showed a R.S.D. of 18.0% on the peak area, which would correspond to a limit of quantification of approximately 2.7 pg (given the apparatus injects approximately 4 nl per s for a 75-μm capillary).

Table V contains the R.S.D. values for repeated hydrodynamic 3-s and 9-s injections within-day and 3-s injections between-day of the dUrd test mixture. The same table also mentions R.S.D. values for a 1-kV 9-s electrokinetic injection of a $1.2 \cdot 10^{-4}$ *M* solution of dUrd in sodium tetraborate electrolyte, which yielded peak areas for dUrd comparable to those for a 3-s hydrodynamic injection. On inspection of the table, one can conclude that within-day repeatability is far better than between-day repeatability and

TABLE IV

ELECTROPHORETIC PARAMETERS FOR THE SEPARATION OF dUrd FROM ITS ANOMER AND ISOMERS AT DIFFERENT TEMPERATURES

Electrolyte, 20 m*M* sodium tetraborate, pH 9.5; voltage, 20 kV. Other conditions were as described for Table I.

T	Mobility ($cm^2 kV^{-1} min^{-1}$)				Peak symmetry				Resolution		
	αFdUrd	dUrd	αPdUrd	βPdUrd	αFdUrd	dUrd	αPdUrd	βPdUrd	αFdUrd-dUrd	dUrd-αPdUrd	αPdUrd-βPdUrd
20°C	29.4	28.7	25.2	23.4	1.1	0.9	1.1	1.0	2.6	11.9	5.1
30°C	37.7	36.9	33.1	31.1	1.0	1.1	1.0	1.0	2.7	10.5	4.6
40°C	39.4	38.5	34.4	32.4	1.1	0.9	0.9	0.9	1.4	9.4	4.0
50°C	43.6	42.5	38.4	36.4	0.9	1.0	0.9	1.0	2.3	8.4	3.8
60°C	48.0	46.8	42.6	40.6	0.9	0.9	1.0	1.0	2.1	7.5	3.4

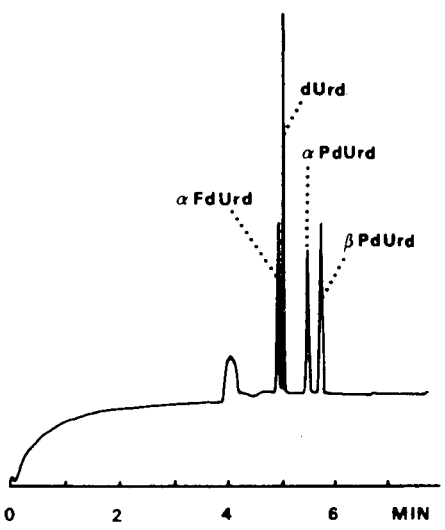

Fig. 2. Capillary zone electrophoresis of a mixture containing dUrd and its anomer and isomers. Electrolyte, 20 m*M* sodium tetraborate, pH 9.5; capillary, fused silica, 70 cm × 75 μm I.D.; temperature, 50°C; voltage, 20 kV; injection, hydrodynamic, 3 s; detection, UV at 262 nm.

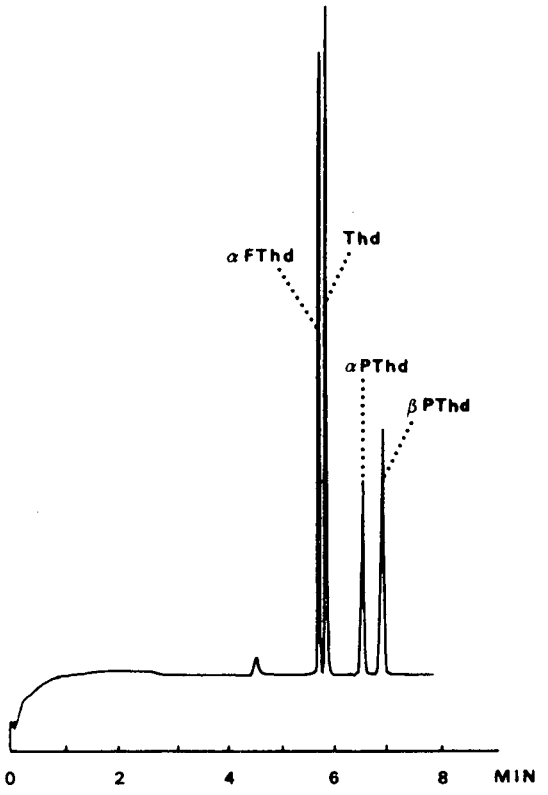

Fig. 3. Capillary zone electrophoresis of a mixture containing Thd and its anomer and isomers. Electrolyte, 20 m*M* sodium tetraborate, pH 10.0; capillary, fused silica, 70 cm × 75 μm I.D.; temperature, 50°C; voltage, 20 kV; injection, hydrodynamic, 3 s; detection, UV at 262 nm.

hydrodynamic injection is preferable over the electrokinetic mode.

The conditions for dUrd were then applied on a mixture of Thd and its anomer and isomers. Since αFdUrd and dUrd were only poorly resolved and since Thd has a slightly higher pK_a value (9.8) than dUrd, it was decided to raise the pH to 10. This yielded the electropherogram shown in Fig. 3.

Moreover, it is possible to obtain a good separation of dUrd and Thd from their main degradation compounds uracil and thymine, respectively. The same conditions can be used as described above, except for temperature which has to be lowered to 30°C. Electrophoretic parameters are given in Table VI, which shows

TABLE V

R.S.D. VALUES OF MIGRATION TIMES AND PEAK AREAS FOR REPEATED INJECTIONS ($n = 9$)

	R.S.D. (migration times) (%)				R.S.D. (peak areas) (%)			
	αFdUrd	dUrd	αPdUrd	βPdUrd	αFdUrd	dUrd	αPdUrd	βPdUrd
Hydrodynamic injection								
within-day, 3 s	0.2	0.2	0.2	0.2	3.0	1.1	1.8	1.0
within-day, 9 s	0.3	0.3	0.4	0.4	1.0	0.2	1.4	1.1
between-day, 3 s	2.1	2.1	2.3	2.4	2.1	1.5	2.8	2.2
Electrokinetic injection								
within-day, 1 kV, 9 s		3.0				3.9		

TABLE VI

ELECTROPHORETIC PARAMETERS FOR THE SEPARATION OF TWO ARTIFICIAL DEGRADATION MIXTURES OF dUrd AND Thd

U = uracil. T = thymine. Electrolyte, 20 m*M* sodium tetraborate pH 9.5 (dUrd) and 10.0 (Thd); capillary, fused silica, 70 cm × 75 μm I.D.; temperature, 30°C (dUrd) and 50°C (Thd); voltage, 20 kV; injection, hydrodynamic, 3 s; detection, UV at 262 nm.

Mobility ($cm^2 kV^{-1} min^{-1}$)					Peak symmetry					Resolution			
αFdUrd	dUrd	U	αPdUrd	βPdUrd	αFdUrd	dUrd	U	αPdUrd	βPdUrd	αFdUrd-dUrd	dUrd-U	U-αPdUrd	αPdUrd-βPdUrd
37.7	36.9	33.8	33.2	31.4	1.0	1.0	[a]	1.0	1.0	2.6	9.1	1.3	4.3
αFThd	Thd	T	αPThd	βPThd	αFThd	Thd	T	αPThd	βPThd	αFThd-Thd	Thd-T	T-αPThd	αPThd-βPThd
35.7	35.0	32.0	30.9	29.1	1.0	1.1	1.0	1.0	1.0	2.2	7.0	2.4	4.1

[a] No separation of peaks at one twentieth of the peak height.

that uracil and thymine migrate between dUrd or Thd and their α-pyranosyl counterparts.

ACKNOWLEDGEMENTS

A. Van Aerschot is a Senior Research Associate and A. Van Schepdaël a Senior Research Assistant of the Belgian National Fund for Scientific Research. The authors thank A. Decoux and I. Quintens for fine secretarial assistance.

REFERENCES

1 J. Cadet and R. Téoule, *J. Am. Chem. Soc.*, 96 (1974) 6517.
2 A. Van Schepdael, A. Van Aerschot, P. Herdewijn, E. Roets and J. Hoogmartens, *Chromatographia*, 33 (1992) 571.
3 S. Hjertén and M.-D. Zhu, *J. Chromatogr.*, 327 (1985) 157.
4 A.S. Cohen, A. Paulus and B.L. Karger, *Chromatographia*, 24 (1987) 15.
5 A.S. Cohen, S. Terabe, J.A. Smith and B.L. Karger, *Anal. Chem.*, 59 (1987) 1021.
6 A.S. Row, W.H. Griest and M.P. Maskarinec, *J. Chromatogr.*, 409 (1987) 193.
7 W.H. Griest, M.P. Maskarinec and K.H. Row, *Sep. Sci. Technol.*, 23 (1988) 1905.
8 M.J. Gordon, X. Huang, S.L. Pentoney, Jr. and R.N. Zare, *Science*, 242 (1988) 224.
9 A.-F. Lecoq, C. Leuratti, E. Marafante and S. Di Biase, *J. High. Resolut. Chromatogr.*, 14 (1991) 667.
10 R.D. Smith, J.A. Olivares, N.T. Nguyen and H.R. Udseth, *Anal. Chem.*, 60 (1988) 436.
11 D.J. Rose and J.W. Jorgenson, *J. Chromatogr.*, 438 (1988) 23.
12 W.G. Kuhr and E.S. Yeung, *Anal. Chem.*, 60 (1988) 2642.
13 V. Suštáček, F. Foret and P. Boček, *J. Chromatogr.*, 480 (1989) 271.
14 R.D. Smith, H.R. Udseth, J.A. Loo, B.W. Wright and G.A. Ross, *Talanta*, 36 (1989) 161.
15 H. Aoyama, *Bull. Chem. Soc. Jpn.*, 60 (1987) 2073.
16 P. Herdewijn, A. Van Aerschot, R. Busson, P. Claes and E. De Clercq, *Nucleosides Nucleotides*, 10 (1991) 1525.
17 *European Pharmacopoeia*, Maisonneuve S.A., Sainte-Ruffine, France, 2nd ed., 1987; V. 6. 20. 4.
18 X. Huang, M.J. Gordon and R.N. Zare, *Anal. Chem.*, 60 (1988) 1837.

PUBLICATION SCHEDULE FOR THE 1993 SUBSCRIPTION

Journal of Chromatography and *Journal of Chromatography, Biomedical Applications*

MONTH	1992	J–A	M	J	J	A	S	O	N	D
Journal of Chromatography	Vols. 623–627	Vols. 628–636	637/1 637/2 638/1 638/2	639/1 639/2 640/1 + 2	641/1 641/2 642/1 + 2 643/1 + 2 644/1	644/2 645/1 645/2 646/1	646/2 647/1 647/2	648/1 648/2		
Cumulative Indexes, Vols. 601–650[a]										
Bibliography Section		649/1		649/2			650/1			650/2
Biomedical Applications		Vols. 612, 613 and 614/1	614/2 615/1	615/2 616/1	616/2 617/1	617/2 618/1 + 2	619/1 619/2	620/1 620/2	621/1 621/2	622/1 622/2

[a] To appear in 1994

INFORMATION FOR AUTHORS

(Detailed *Instructions to Authors* were published in Vol. 609, pp. 437–443. A free reprint can be obtained by application to the publisher, Elsevier Science Publishers B.V., P.O. Box 330, 1000 AH Amsterdam, Netherlands.)

Types of Contributions. The following types of papers are published in the *Journal of Chromatography* and the section on *Biomedical Applications:* Regular research papers (Full-length papers), Review articles, Short Communications and Discussions. Short Communications are usually descriptions of short investigations, or they can report minor technical improvements of previously published procedures; they reflect the same quality of research as Full-length papers, but should preferably not exceed five printed pages. Discussions (one or two pages) should explain, amplify, correct or otherwise comment substantively upon an article recently published in the journal. For Review articles, see inside front cover under Submission of Papers.

Submission. Every paper must be accompanied by a letter from the senior author, stating that he/she is submitting the paper for publication in the *Journal of Chromatography.*

Manuscripts. Manuscripts should be typed in **double spacing** on consecutively numbered pages of uniform size. The manuscript should be preceded by a sheet of manuscript paper carrying the title of the paper and the name and full postal address of the person to whom the proofs are to be sent. As a rule, papers should be divided into sections, headed by a caption (*e.g.*, Abstract, Introduction, Experimental, Results, Discussion, etc.) All illustrations, photographs, tables, etc., should be on separate sheets.

Abstract. All articles should have an abstract of 50–100 words which clearly and briefly indicates what is new, different and significant. No references should be given.

Introduction. Every paper must have a concise introduction mentioning what has been done before on the topic described, and stating clearly what is new in the paper now submitted.

Illustrations. The figures should be submitted in a form suitable for reproduction, drawn in Indian ink on drawing or tracing paper. Each illustration should have a legend, all the *legends* being typed (with double spacing) together on a *separate sheet.* If structures are given in the text, the original drawings should be supplied. Coloured illustrations are reproduced at the author's expense, the cost being determined by the number of pages and by the number of colours needed. The written permission of the author and publisher must be obtained for the use of any figure already published. Its source must be indicated in the legend.

References. References should be numbered in the order in which they are cited in the text, and listed in numerical sequence on a separate sheet at the end of the article. Please check a recent issue for the layout of the reference list. Abbreviations for the titles of journals should follow the system used by *Chemical Abstracts.* Articles not yet published should be given as "in press" (journal should be specified), "submitted for publication" (journal should be specified), "in preparation" or "personal communication".

Dispatch. Before sending the manuscript to the Editor please check that the envelope contains four copies of the paper complete with references, legends and figures. One of the sets of figures must be the originals suitable for direct reproduction. Please also ensure that permission to publish has been obtained from your institute.

Proofs. One set of proofs will be sent to the author to be carefully checked for printer's errors. Corrections must be restricted to instances in which the proof is at variance with the manuscript. "Extra corrections" will be inserted at the author's expense.

Reprints. Fifty reprints will be supplied free of charge. Additional reprints can be ordered by the authors. An order form containing price quotations will be sent to the authors together with the proofs of their article.

Reversed Phase CHIRAL HPLC Column

NEW CHIRALCEL® OD-R

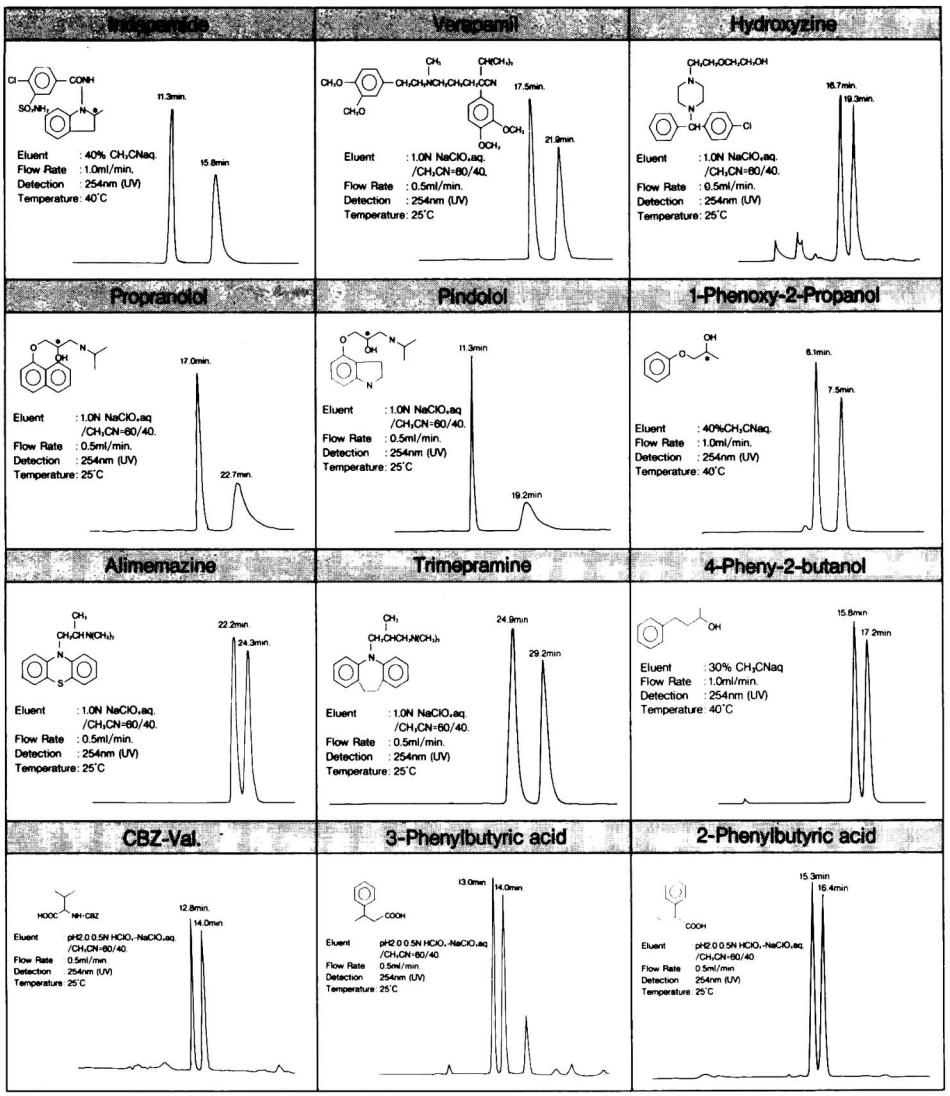

For more information about CHIRALCEL OD-R column, please give us a call.

DAICEL CHEMICAL INDUSTRIES, LTD.

CHIRAL CHEMICALS DIVISION 8-1, Kasumigaseki 3-chome, Chiyoda-ku, Tokyo 100, JAPAN
Phone: +81-3-3507-3151 Facsimile: +81-3-3507-3193

AMERICA
CHIRAL TECHNOLOGIES, INC.
730 SPRINGDALE DRIVE
DRAWER I EXTON, PA 19341
Phone: 215-594-2100
Facsimile: 215-594-2325

EUROPE
DAICEL (EUROPA) GmbH
Ost Street 22
4000 Düsseldorf 1, Germany
Phone: +49-211-369848
Facsimile: +49-211-364429

ASIA/OCEANIA
DAICEL CHEMICAL (ASIA) PTE. LTD.
65 Chulia Street #40-07
OCBC Centre, Singapore 0104.
Phone: +65-5332511
Facsimile: +65-5326454